**Unearthing the molecular mechanisms that govern L-selectin-dependent adhesion and migration**

Newe, Abigail Lucy

*Awarding institution:*
King's College London

# Unearthing the molecular mechanisms that govern L-selectin-dependent adhesion and migration

**Abigail Newe**

This thesis is submitted for the degree of

*Doctor of Philosophy*

(PhD)

from

**King's College London, School of Medicine**

**University of London**

August 2014

*King's College London,*

*School of Medicine,*

*Cardiovascular Division,*

*Denmark Hill Campus,*

*London, U.K.*

Supervisors: Dr Aleksandar Ivetic

Prof. Maria R Conte

# Abstract

L-selectin has been well characterised as a cell adhesion molecule, which plays a role in the recruitment of leukocytes to sites of inflammation and is responsible for the recirculation of lymphocytes to secondary lymphoid organs. Recent evidence has shown that L-selectin also acts as a signalling molecule to activate pathways and regulate the inflammatory response. The cytosolic tail of L-selectin plays a crucial role in regulating its activity through its interaction with binding partners, such as calmodulin (CaM) and the ERM protein family. However, little is known about how the interaction between L-selectin and its binding partners is regulated. The aim of this multidisciplinary PhD project is to use biophysical and cell biological methods to address the role of the interaction between L-selectin and its binding partners during leukocyte recruitment. To this end, the interaction between CaM and the L-selectin cytosolic tail was assessed using isothermal titration calorimetry (ITC) and nuclear magnetic resonance (NMR) spectroscopy. Analysis revealed that phosphorylation of serine residues within the cytosolic tail of L-selectin did not affect CaM binding. To enable the observation of the interaction between L-selectin and CaM whilst leukocytes are undergoing transendothelial migration (TEM), the THP-1 monocytic cell line was engineered to stably express L-selectin-GFP and CaM-RFP so their interaction could be monitored at different stages of TEM. The data showed that phosphorylation of serine 364 in the L-selectin tail is important for regulating CaM interaction. Discrepancies were identified between the biophysical and cell biological results, implying the leukocyte plasma membrane may play a vital role in regulating the interaction between L-selectin and CaM. This highlights the importance of studying transmembrane proteins in the correct context.

# Contents

# List of Figures

10

# List of Tables

# Acknowledgements

I would like to thank my supervisors Aleksandar Ivetic and Sasi Conte for the opportunity to work in their labs and undertake this project. Their expert guidance and support has been invaluable.

My thanks also go to the members of the Ivetic and Conte labs, who have all provided advice along the way, as well as many fun times. Special thanks go to Dr Luigi Martino for teaching me the many complexities of ITC and Dr Angela Rey-Gallardo and Karolina Rzeniewicz for their help with the cell biology work. I would also like to mention Dr Andrew Atkinson for his help with the NMR and Dr Maddy Parsons for carrying out the FRET/FLIM analysis in this thesis. All the biophysical experiments were undertaken at the Centre for Biomolecular Spectroscopy, KCL, except the MST which was carried out by staff at NanoTemper Technologies GmbH, Munich.

I am very grateful to my wonderful friends who have put up with me over the years. Even when I was no fun to be around they have never given up on me!

I owe the biggest thanks to my wonderful family, who have always believed in me. In particular my brothers and sisters-in–law, all of whom have gotten me through some tough times.

Lastly I express my deepest gratitude to my parents. Without their love and support I would not have achieved all I have. Words cannot express how thankful I am for all you have done for me.

Thank you all so much!

# Declaration of Independent Work

I, the author of this thesis, declare that the work presented in this thesis was conducted by me, except where indicated in the text.

……………………………………..

Abigail Newe

# Abbreviations

-TΔS- Entropic contribution

1D- One Dimensional

2D- Two Dimensional

ΔG- Change in Gibbs Free Energy

ΔH- Change in enthalpy

$\Delta H_{ion}$- Enthalpy of Ionisation

ΔS- Change in Entropy

A-Alanine

ADAM- A Disintegrin And Metalloproteinase

APC- Antigen Presenting Cell

ApoCaM- Calcium Free CaM

ApoE-Apolipoprotein E

APS- Ammonium Persulphate

ASF- Asialofetuin

ATCC- American Type Culture Collection

BAPTA- 1,2-bis(o-aminophenoxy)ethane-N,N,N',N'-tetraacetic acid)

BSA- Bovine Serum Albumin

CaM- Calmodulin

CaM-Ca- Calcium Bound CaM

CCL- Chemokine C-C motif Ligand

CD- Circular Dichroism

CD'X'- Cluster of Differentiation, where 'X' denotes the number

Cdc42- Cell division control protein 42

cDNA- Complementary DNA

CIP- Calf Intestine Phosphatase

$C_p$- Heat Capacity

CSF-1- Colony-stimulating Factor-1

CSP- Chemical Shift Perturbations

CSPG- Chondroitin Sulphate Proteoglycan

CV- Column Volume

CVD- Cardiovascular Disease

CXCL- Chemokine C-X-C motif Ligand

D- Aspartate

DAG- Diacylglycerol

DMSO- Dimethyl sulphoxide

DNA- Deoxyribonucleic Acid

DS- Disaccharide

DSPG- Dermatan Sulphate Proteoglycan

E- Glutamate

EBP50- ERM Binding Protein 50

ECL- Enhanced chemiluminescence

ECM- Extracellular Matrix

EDTA- Ethylenediaminetetraacetic Acid

EGF- Epidermal Growth Factor

EGTA-Ethylene Glycol Tetraacetic Acid

ER- Endoplasmic Reticulum

ERK-Extracellular signal-regulated kinase

ERM- Ezrin Radixin Moesin protein family

FACS- Fluorescence-activated cell sorting

F-actin- Filamentous Actin

FBS- foetal bovine serum

FCS- Fluorescence Correlation Spectroscopy

FERM- Four-point-one, ezrin, radixin, moesin

FLIM- Fluorescence Lifetime Imaging Microscopy

FMVEC- Foreskin Microvascular Endothelial Cell

FOXO-1- Forkhead box 1

FRET- Fluorescence Resonance Energy Transfer

FT- Flow Through

G- Glycine

GAG- Glycosaminoglycan

GDI- Guanosine nucleotide Dissociation Inhibitor

GEF-Guanine Exchange Factor

GFP- Green Fluorescent Protein

GlyCAM-1- Glycosylation-dependent Cell Adhesion Molecule-1

GPCR- G-protein Coupled Receptor

Grb- Growth Factor Receptor-bound Protein

GST- Glutathione S-Transferase

GTP- Guanine Triphosphate

HEK- Human embryonic Kidney

HEPES- 4-(2-hydroxyethyl)-1-piperazineethanesulfonic acid

HEV- High Endothelial Venule

His6- Hexa-Histidine

His6-CaM- His6-tagged CaM

His6-moesin-FERM- His6-tagged moesin FERM domain

HIV- Human Immunodeficiency Virus

HRP- Horseradish Peroxidase

HS- Heparan Sulphate

HSPG- Heparan Sulphate Proteoglycan

HSQC- Heteronuclear single quantum coherence

HUVEC- Human Umbilical Vein Endothelial Cell

I- Isoleucine

ICAM- Intercellular Adhesion Molecule

IFN- Interferon

IL- Interleukin

IL-R- Interleukin- Receptor

IMAC- Immobilised Transition Metal Affinity Chromatography

IP$_3$-Inositol Triphosphate

IPTG- Isopropyl β-D-1-thiogalactopyranoside

IR- Infra Red

ITC- Isothermal Titration Calorimetry

JAM- Junction Adhesion Molecule

JNK-c-Jun N-terminal kinase

K- Lysine

K$_b$- Binding Constant

KC- Keratinocyte-derived Chemokine

K$_D$- Dissociation Constant

KO- Knockout

KOD- *Thermococcus kodakaraensis*

L- Leucine

LB- Lysogeny broth

Lck- Leukocyte-specific protein tyrosine Kinase

LDL- Low Density Lipoprotein

LFA-1- Lymphocyte Function Associated Antigen-1

LTR- Long Terminal Repeat

M- Methionine

MAC-1- Macrophage-1 Antigen

MAdCAM-1- Mucosal Vascular Addressin Cell Adhesion Molecule-1

MAPK- Mitogen Activated Protein Kinase

MARKS- Myristoylated alanine-rich C-kinase substrate

mAU- mill Absorbance Unit

MCS- Multiple Cloning Site

MES- 2-(N-morpholino) ethanesulfonic acid

Moesin-FERM- FERM domain of moesin

MOI- Multiplicity of Infection

mRNA- Messenger Ribonucleic Acid

MST- Microscale Thermophoresis

N- Asparagine

n- Stoichiometry

NFAT- Nuclear Factor of Activating T-cells

NHS- N-hydroxysuccinimide

NK- Natural Killer

NMR- Nuclear Magnetic Resonance

NO- Nitric Oxide

NOS- Nitric Oxide Synthase

NP-40- Nonidet P-40 substitute

NSAID- Non-steroidal Anti-inflammatory Drug

NTA- Nitrilotriacetic acid

OD- Optical Density

Oligo- Oligonucleotide

OxLDL- Oxidised LDL

P- Proline

PAGE- Polyacrylamide Gel Electrophoresis

PBS- Phosphate Buffered Saline

PCR- Polymerase Chain Reaction

PDI- Protein Disulphide Isomerase

PECAM- Platelet Endothelial Cell Adhesion Molecule

PEI- polyethylene imine

PFA- Paraformaldehyde

PG- Proteoglycan

PI3K-Phosphoinositide 3-Kinase

$PIP_2$ -Phosphatidylinositol 4,5-bisphosphate

PKC- Protein Kinase C

PLC- Phospholipase C

PLL- Poly-L-Lysine

PMA- Phorbol 12-Myristate 13-Acetate

PRR- Pattern Recognition Receptor

PS- Phosphatidylserine

PSGL- P-selectin Glycoprotein Ligand

PVDF- Polyvinylidene fluoride

Q- Glutamine

R- Arginine

Rac- Ras-related C3 botulinum toxin substrate

RFP- Red Fluorescent Protein

Rho- Ras homolog

RNA- Ribonucleic acid

ROS- Reactive Oxygen Species

Rpm- Revolutions per minute

S- Serine

SCR- Short Consensus Repeat

SDF-1- Stromal cell-Derived Factor-1

SDS- Sodium Dodecyl Sulphate

SDS-PAGE- SDS Polyacrylamide Gel Electrophoresis

SF- Synovial Fluid

SFFV- spleen focus-forming virus

sLe$^x$- Sialyl Lewis X

sL-selectin- soluble L-selectin

SOD- Superoxide Dismutase

Sos- Son of Sevenless

Src- Sarcoma

SPR- Surface Plasmon Resonance

Syk- Spleen Tyrosine Kinase

TACE- TNF-alpha-converting enzyme

TAE- Tris-acetate-EDTA

TBS- Tris Buffered Saline

TBST- Tris Buffered Saline Tween

TCR- T-Cell Receptor

TEM- Transendothelial Migration

TEMED- Tetramethylethylenediamine

TEV- Tobacco Etch Virus

TFE- Tetrafluoroethylene

TGF- Transforming Growth Factor

TNF- Tumour Necrosis Factor

tRNA- Transfer RNA

UV- Ultraviolet

V- Valine

VCAM- Vascular Adhesion Molecule

VLA-4 Very Late Antigen-4

VSMC- Vascular Smooth Muscle Cell

W- Tryptophan

WPRE- Woodchuck Hepatitis Virus Posttranscriptional Regulatory Element

Y- Tyrosine

# Chapter 1: Introduction
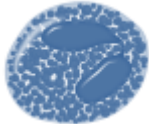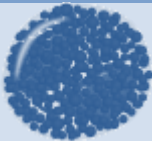
## 1.1 The Inflammatory Response

Inflammation is a natural response to injury, brought about by infection, physical or chemical trauma, allergy or autoimmunity. The inflammatory response is designed to contain and resolve the injurious stimulus and initiate the healing process. Inflammation is characterised by pain, swelling, redness, heat and loss of function (of the organ or tissue) at the sight of insult. These signs of inflammation require the co-ordinated actions of the innate immune and adaptive immune systems.

The inflammatory response can be divided into two components: a vascular arm and a cellular arm. The vascular arm is controlled by endothelial cells, which are activated by leukocyte- and fibroblast-derived cytokines, promoting adhesion molecule expression on the luminal surface of the endothelial cells to actively recruit leukocytes from the microcirculation and the subsequent migration of the leukocytes to the site of insult (8,9). Endothelial cells that are local to a site of inflammation transport stromal-derived chemokines from the abluminal side and deliver them to the luminal side (10). Note that endothelial cells can also produce chemokines (11). This ultimately activates leukocytes that possess the appropriate chemokine receptor. Inflammatory signals also cause vasodilation (through the relaxation of local vascular smooth muscle cells in arterioles) which additionally leads to an increased permeability of the microvasculature (9). This causes a decrease in the velocity of blood flow (as blood is now flowing through dilated vessels), which increases the chance for passing leukocytes to bind to the endothelium that is local to the site of inflammation (12).

The cellular arm of the inflammatory response involves the passage of leukocytes from the circulation into the surrounding tissue. Leukocytes, such as monocytes and neutrophils, originate in the bone marrow. Once mature, they reside in tissues or organs, the blood stream and the lymphatics - ready to respond to inflammatory signals. There are two lineages that define the leukocytes; myeloid cells and lymphoid cells. Myeloid cells are precursors to a majority of cells that partake in the innate immune response, which is the initial stage of the response following an inflammatory insult. Myeloid cells are precursors for granulocytes, mast cells, dendritic cells and monocytes (which differentiate into macrophages after they have migrated in to tissue). These cells remove the injurious stimuli via phagocytosis and release of

granule contents, which activate the adaptive immune system. Lymphoid cells give rise to the cells of the adaptive immune system, which involves the production of pathogen-specific receptors to focus the immune response on a particular pathogen, i.e. B-cells and T-cells. The different cell types have different roles during an inflammatory response, which is summarised in Table 1.1. All subsets of leukocytes are thought to communicate to one another by releasing cytokines and chemokines to activate and attract other immune cells, to amplify the immune response (13,14).

| Type | Diagram | Main Functions |
|---|---|---|
| **Monocytes** |  | Differentiate into macrophages, which phagocytose infectious species and cell debris and act as APCs |
| **Dendritic cells** |  | Act as APCs to present antigens for recognition by T-cells |
| **Neutrophils (also referred to as polymorphonuclear leukocytes (PMNs) due to the presence of the multi-lobe nucleus** |  | Phagocytosis and release cytoxins from granules to destroy bacteria and fungi |
| **Eosinophil** |  | Phagocytosis and release of granule contents to remove larger parasites. Also responsible for allergic reactions |
| **Basophils** |  | Involved in allergic reactions by releasing histamine |
| **Lymphocytes** |  | B-cells: secrete antibodies to label infectious species and target them for destruction. |

Release IgE following exposure to allergen, leading to the activation of basophils and mast cells.

Cytoxic T-cells: release cytotoxins to kill virus-infected cells.

Helper T-cells: produce and release cytokines to activate other lymphocytes. The subset TH2 cells recognise allergens and activate B cells to produce IgE.

Regulator T-cells: produce anti-inflammatory cytokines to supress the immune response.

Natural killer cells: release cytotoxins to kill cells recognised as stressed without requiring antibody labelling.

**Table 1.1: Summary of the leukocyte subsets and their function in inflammatory responses.** The different types of leukocytes are listed, with a representative diagram of each cell type shown. The major role of each cell type in the inflammatory response is described.

Acute inflammation is a fast response to an inflammatory stimulus and is initiated by leukocytes migrating directly to the site of the insult. The inflammatory response normally lasts a few days, after which the stimulus has been removed. However, in certain circumstances inflammation remains unresolved ("non-resolving" inflammation), which is the driver of multiple chronic inflammatory diseases, including atherosclerosis (15), rheumatoid arthritis and lupus (12). Non-resolving inflammation leads to the continued destruction and necrosis of cells. Recent evidence has shown that patients suffering from chronic inflammatory disease have increased susceptibility to cardiovascular disease, such as atherosclerosis, although little is known about how this is initiated and manifested (15). As leukocyte recruitment is a key driver of chronic inflammation, a key goal in the area of inflammation biology is to expose novel therapeutic targets for blocking the chronic recruitment of leukocytes to non-resolving sites of inflammation. Note that "sterile inflammation" refers to an inflammatory

stimulus driven by non-infectious cell necrosis. In Section 1.8.1 the development of atherosclerosis is described, with reference to the role of sterile inflammation.

## 1.2 The Multi-Step Leukocyte Adhesion Cascade.

As stated above, during an inflammatory response leukocytes must exit the bloodstream and enter the surrounding microenvironment. This process is controlled by cell adhesion molecules on both the leukocyte and endothelial cell. The multi-step leukocyte adhesion cascade is a paradigm that has been established through the work of many labs and describes the way in which leukocytes migrate out of the bloodstream through a series of discrete and inter-dependent steps. As shown in Figure 1.1, the multi-step adhesion cascade is broken down in to increasingly adhesive interactions called: capture (or tethering), rolling, slow rolling, firm adhesion and transmigration (10). Note that in order for the adhesion cascade to progress, the previous step in the cascade must be executed correctly. Therefore, firm adhesion cannot proceed without rolling, and rolling without tethering, etc. Each step of the adhesion cascade will be discussed in detail below.
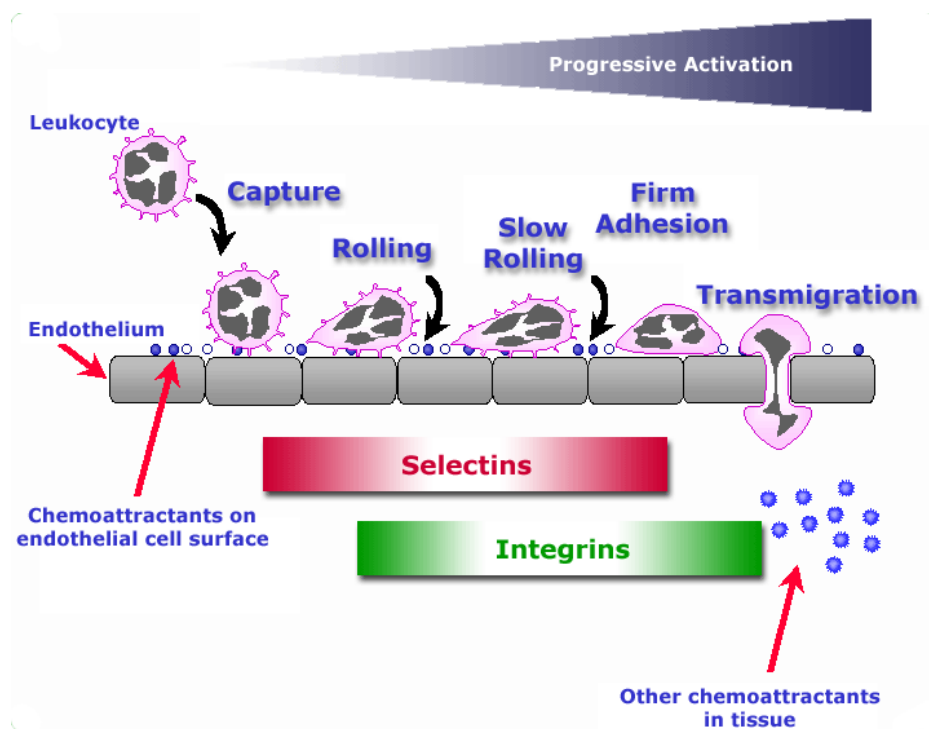


**Figure 1.1: The Multi-Step Leukocyte Adhesion Cascade.** A diagram showing the individual stages of the multi-step leukocyte adhesion cascade. The selectins and the integrins are absolutely essential for successful progression through the adhesion cascade. It should be noted that other cell adhesion molecules are also involved in this process, and some detail of these will be discussed later. Diagram modified from bme.virginia.edu/ley/.

## 1.2.1 Leukocyte tethering and the selectins

Tethers are transient interactions between leukocytes and endothelial cells lining the blood vessels, and are predominantly mediated by members of the selectin family of cell adhesion molecules. There are three selectin family members: E-, P-, and L-selectin. E- and P-selectin are expressed in endothelial cells, P-selectin is expressed specifically in platelets, and L-selectin is expressed on leukocytes (details of the selectins are described in Section 1.3) (10). Following injury, tissue-resident macrophages release the cytokines interleukin-1 (IL-1) and tumour necrosis factor-α (TNF-α), both of which activate endothelial cells causing them to express selectins (see Section 1.2.2 for details of selectin expression on endothelial cells). L- and P-selectin interact with P-selectin glycoprotein ligand-1 (PSGL-1) (16) and other glycoproteins on the plasma membrane of corresponding cells to form the tethers between the leukocyte and endothelium, enabling the leukocyte to adhere to the endothelium from blood flow. The importance of L-selectin in tether formation has been investigated *in vitro,* with L-selectin function blocking antibody reducing the adhesion of lymphocytes, neutrophils and monocytes to the endothelial monolayer under flow conditions (17-19).

Leukocytes can also tether to one another, with L-selectin on a free-flowing leukocyte able to interact with PSGL-1 on the surface of a leukocyte tethered to the endothelium (or vice versa), a process known as secondary tethering, to further amplify the inflammatory response (16).

## 1.2.2 Rolling and regulation of selectin expression

Once tethers have formed between leukocytes and endothelial cells, and if there is sufficient ligand available (i.e. the ligand density is high enough), cells will begin to roll along the endothelium. Rolling is important as it brings the leukocyte into close proximity to the endothelium allowing the leukocyte-derived receptors to recognise apically presented chemokine more readily. This triggers activation of the leukocyte integrins, which can mediate arrest from blood flow (see later in Section 1.2.3). During rolling, bonds between selectins and their counter ligands are formed and broken. Selectins are suited to this process as the interaction between them and their ligands have fast on and off rates (20).

L-selectin has been shown to cause leukocyte rolling both in the recirculation of lymphocytes to secondary lymphoid organs and during inflammation, with the role of L-selectin in these processes discussed in detail in Sections 1.7.1 and 1.7.2. Pre-B-cells transfected with L-selectin were shown to roll in inflamed rat mesenteric venules (21) and inflamed rabbit venules (22). The role of L-selectin in leukocyte rolling has been studied using intravital microscopy and L-selectin function blocking antibodies, with rolling inhibited in rat and rabbit mesenteric venules in the presence of the antibody (21,23). Studies in L-selectin knockout mice have shown a decrease in the rolling of leukocytes in mesenteric venules by 70 % (24). *In vitro* studies of L-selectin-dependent rolling using a flow chamber assay has also revealed that neutrophil (25) and monocyte (26) rolling on Human Umbilical Vein Endothelial Cells (HUVECs) were both inhibited by L-selectin function blocking antibody.

Many potential ligands for L-selectin-dependent rolling have been explored (as discussed in detail in Section 1.3.2). PSGL-1 has been implicated as a possible ligand, as when a function blocking antibody for PSGL-1 was used, L-selectin dependent rolling was blocked in the flow chamber assay and neutrophils treated with L-selectin function blocking antibody no longer rolled on PSGL-1 (27,28). L-selectin-dependent rolling was also lacking *in vivo* with PSGL-1 knockout mice and in wildtype mice treated with PSGL-1 function blocking antibody (29), further highlighting the role of PSGL-1 in L-selectin dependent rolling. However, there has been some dispute over the capability of PSGL-1 to support L-selectin-dependent rolling due to a lack of expression on the endothelium, with Sperandino *et al* (2003)(16) showing no expression of PSGL-1 on resting or inflamed endothelial cells in mice. A study did reveal, however, that HUVECs and foreskin microvascular endothelial cells (FMVECs) both expressed PSGL-1 and could support monocyte adhesion and rolling (30). This clearly shows further research is required to determine if PSGL-1 can act as a ligand for L-selectin-dependent rolling.

P-selectin has been shown to be involved in the early stages of rolling, with no rolling initially observed in the surgically exteriorised cremaster venules of P-selectin deficient mice (31,32). Neutrophil recruitment to the peritoneum after an inflammatory stimulus is delayed by 2-4 hours in P-selectin knockout mice (31), suggesting a role for P-selectin in the early steps of the adhesion cascade. P-selectin is produced and stored in α-granules and Weibel-Palade bodies, which are secretory storage granules that contain different substances for rapid release upon cell

activation. Once the cell is activated, these granules fuse with the plasma membrane to deliver P-selectin to the surface (33,34), with the protein detectable within minutes of cell activation (31), allowing P-selectin to play a role in early rolling. PSGL-1 is the main leukocyte-restricted ligand for P-selectin. Using antibodies against PSGL-1 blocks the rolling of neutrophils, monocytes and eosinophils on P-selectin *in vitro* (27).

Unlike P-selectin, E-selectin expression is controlled by transcriptional activation only. It was shown using COS7 cells transfected with E-selectin that expression was induced by the cytokines IL-1 and TNF-α, with the protein present at the cell surface two to four hours after activation (35). Expression was also assessed in HUVEC cells activated with TNF-α, with peak expression observed three to six hours after stimulation (36). As there is a delay in surface expression of E-selectin, rolling becomes dependent on E-selectin binding its ligands after this time (37). The capability of E-selectin to support leukocyte rolling has been assessed both *in vitro* and *in vivo* (31), with neutrophils able to roll on E-selectin in the flow chamber (38,39) and E-selectin-dependent rolling evident in murine mesenteric venules activated with Interleukin-1β (IL-1β) (40). However, blocking E-selectin with antibodies or knocking out E-selectin in mice does not affect rolling (31). This is due to the co-expression of P-selectin compensating for the loss of E-selectin.

All types of selectin-dependent rolling have been shown to depend on a threshold of shear stress, which is the force applied to the cells due to the flow of the blood through the vessel (41,42). Shear stress is required for the rolling of the HL-60 human promyelocytic leukaemia cells on P- and E-selectin and without flow, gravity causes the detachment of the cells when the flow chamber is placed upside down (41). Different cell types have been transfected with either PSGL-1 or L-selectin and in all cases rolling was only seen under shear stress conditions (41), showing that this requirement is neither molecule nor cell type specific. It is likely this mechanism exists to prevent the aggregation of leukocytes at sites of low blood flow (42). How the increase in shear stress increases the adhesion between selectins and their ligands remains unclear. It has been proposed that selectins form catch-bond interactions with their ligands (reviewed in (43)), where the increase in force causes the straightening of the L-selectin molecule, enhancing its ability to interact with the ligand pocket of its binding partner. However, due to experimental limitations it is not possible to monitor

the conformational rearrangement of L-selectin under flow, so this has yet to be confirmed.

### 1.2.3 Slow rolling and the three integrin activation states

The slow rolling step of the adhesion cascade is important for initialising arrest of the leukocyte through the activation of integrins. The process has recently been revealed to occur through E-selectin, which can bind to PSGL-1, CD44 and CD43 on the leukocyte (37). The rolling velocity of leukocytes from E-selectin knockout mice were much higher than that of wildtype mice (44), showing its importance in initialising slow rolling.

$\beta_1$- and $\beta_2$-integrins are expressed on the surface of leukocytes and upon activation they switch from the low-affinity bent state to a high-affinity extended state, which leads to the opening of the ligand pocket, via the intermediate state (Figure 1.2) [1]. Three integrins are expressed on leukocytes, namely Lymphocyte function-associated antigen-1 (LFA-1), Macrophage-1 (MAC-1) and Very Late Antigen-4 (VLA-4). They bind cell adhesion molecules (CAMs) expressed on endothelial cells. LFA-1 interacts with endothelial Intercellular Adhesion Molecule-1(ICAM-1) and the endothelial Intercellular Adhesion Molecule-2 (ICAM-2), MAC-1 interacts with ICAM-1 and the VLA-4 interacts with Vascular Cell Adhesion Molecule-1 (VCAM-1) [1].

Both the integrins LFA-1 and MAC-1 become activated to an intermediate state following E-selectin-dependent rolling. In fact clustering of PSGL-1 and CD44 is sufficient to activate integrins to the intermediate state, which results in weak binding to their cognate ligands (32). When E-selectin and the integrin ligand ICAM-1 were co-immobilised the number of cells engaged in slow rolling increased (45). Antibody blocking of $\beta_2$-integrins increases the rolling velocity of lymphocytes on endothelial cells in flow chamber assays (46), showing integrin ligand binding promotes slow rolling. Studies of the role of integrins in slow rolling have been assessed *in vivo* using knockout mice and assessing leukocyte rolling in the cremasteric muscle venules by intravital microscopy. The velocity of rolling in LFA-1$^{-/-}$ and MAC-1$^{-/-}$ mice was higher compared to wildtype mice, with the double knockout having an even higher rolling velocity (47). VLA-4 has also been shown to support rolling, with lymphocytes shown to roll on VCAM-1 via VLA-4 *in vitro* (10,48).

During slow rolling chemokine signalling activates integrins, which leads to the arrest of the cell on the surface of the endothelium (10). One example of this is the interaction between VLA-4 and VCAM-1. Chemokines up-regulate this interaction by increasing the affinity of VLA-4 for VCAM-1, leading to an increase in adhesion and monocyte arrest (49).
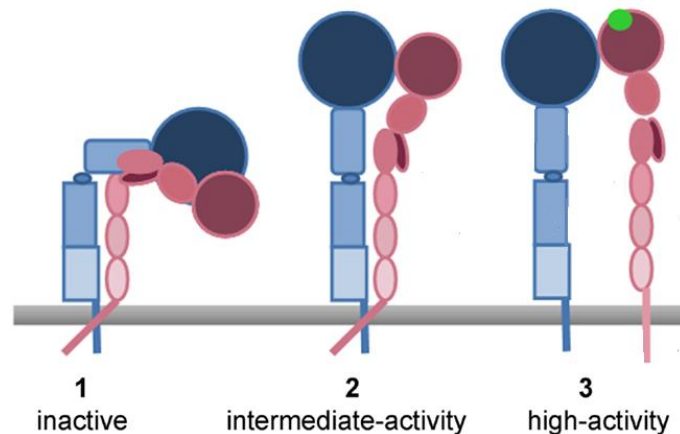


**Figure 1.2 Conformations of integrins.** A schematic showing the different conformational states of $\alpha_4\beta_1$-integrin during cell activation. The α domain is shown in blue and the β domain is shown in pink. In resting cells integrins exist in a bent inactive state (1). After the first stage of activation the integrins are in an extended closed intermediate state (3). The high activity state is achieved when the integrins become extended and open, exposing the ligand binding site (shown in green). Figure modified from Johansson, M. W., and Mosher, D. F. (2013) Integrin activation states and eosinophil recruitment in asthma. *Frontiers in Pharmacology* **4** (4).

## 1.2.4 Leukocyte arrest and chemokine-induced integrin activation

Binding of the integrins to their ligands causes leukocytes to arrest under flow conditions. Chemokines presented by endothelial cells increase the avidity and affinity of integrins to promote leukocyte arrest (10). It has been shown *in vitro* that chemokines trigger the extension of the bent form of LFA-1. ICAM-1 then binds to LFA-1 fully activating it and causing high affinity binding, leading to arrest (50). Chemokines also induce the mobility of integrins to sites that enhance the frequency of binding, which increases the likelihood of arrest. Phosphatidylinositide 3-kinase (PI3K) inhibition has been shown to block the mobility of LFA-1 and as a result prevents the firm adhesion to ICAM-1 immobilised at low densities (51).

The signalling pathways behind chemokine-induced leukocyte arrest have been investigated. Chemokines bind to G Protein Coupled Receptors (GPCRs) on the surface of the leukocyte, which leads to phospholipase C (PLC) activation (10). VLA-4-

dependent arrest is blocked when an inhibitor to PLC is added to neutrophils (52). PLC cleaves the phospholipid phosphatidylinositol 4,5-bisphosphate ($PIP_2$) into diacyl-glycerol (DAG) and inositol 1,4,5-trisphosphate ($IP_3$), both of which act as secondary messengers. DAG activates PKCs and $IP_3$ binds to receptors on the endoplasmic reticulum (ER) to cause the release of calcium into the cytosol. With the use of inhibitors against these two molecules it was found that the release of calcium was required for VLA-4-dependent arrest (52). Calcium release from the ER induces the influx of extracellular calcium via activation of calcium ion channels. Using and inhibitor of these channels also blocked VLA-4 binding (52), showing that it is this influx that leads to the conformation change of VLA-4 and firm adhesion. The calcium binding protein calmodulin (CaM) was also implicated in this pathway, as blocking this protein with the CaM specific inhibitor W7 inhibited firm adhesion (52). It is possible that release of calcium from the ER binds to CaM enabling it to interact with the calcium channels, leading to their opening, though how calcium influx causes a change in affinity of VLA-4 remains unclear.

It is possible that activation of signalling pathways lead to the binding of partners to the cytosolic tail of integrins, affecting their binding affinity. Talin has been shown to bind to $\beta_3$-integrins and this interaction either induces or stabilises the high affinity conformation of the adhesion molecule (10,53,54).

Activation of integrins by chemokines also initiates signalling in the leukocytes. Studies have revealed that a lack of integrin signalling accelerates the detachment of neutrophils (10,55). The Src family kinase members Fgr and Hck have been shown to be involved in integrin signalling. When these kinases were knocked out in neutrophils the cells were able to adhere to co-immobilised ICAM-1 and P-selectin under flow at the same rate as wildtype cells, but detached much quicker (55), showing that integrin signalling is required for the sustained arrest of leukocytes.

## 1.2.5 Leukocyte crawling

After leukocyte arrest, cells must transmigrate across the endothelial monolayer. The first step of this process is the crawling of the leukocytes on the luminal surface of the endothelium in order to seek a preferred site of transmigration (10,56,57). This process has been shown to be dependent on the integrin MAC-1, as

blocking this integrin on monocytes *in vitro* (56) or analysis of neutrophils in MAC-1 knockout mice (57) showed that crawling did not occur. Blocking of ICAM-1 also inhibited crawling *in vitro* (56), showing it is the ligand for MAC-1. Inhibition of crawling in monocytes led to the cells spinning in circles where they became arrested (56), thus the cells were unable to undergo directive movement. Neutrophils from MAC-1 knockout mice would transmigrate more slowly at the site of arrest, with more cells using the transcellular pathway (see later in Section 1.2.6.2) (57). This shows the importance of crawling in facilitating rapid transmigration.

## 1.2.6 Transmigration

The movement of leukocytes across the endothelial monolayer is known as transendothelial migration (TEM) or diapedesis. Leukocytes can either transmigrate between the junctions formed by opposing endothelial cells (paracellular route) or through an individual endothelial cell (transcellular route).

### *1.2.6.1 Paracellular Route*

For leukocytes to pass between endothelial cells, the tight junctions between the cells must be disrupted. It is thought that ligation of adhesive molecules on the endothelial cells leads to activation of signalling pathways that disrupt the inter-endothelial contacts to facilitate migration. Clustering of VCAM-1 on endothelial cells has been shown to cause the disruption of adherens junctions (58,59). VE-cadherin is found in tight junctions and binds to β-catenin to form contacts between endothelial cells. The presence of VE-cadherin in junctions blocks the migration of leukocytes. Using function-blocking antibodies against VE-cadherin accelerates the migration of neutrophils in to the inflamed peritoneum – a commonly used mouse model of acute inflammation (60). It has been shown that VE-cadherin is cleaved during TEM (58) and as a result is removed from the junctions. Neutrophil binding causes the production of fragments of VE-cadherin and the proteases elastase and cathespin G on the surface of neutrophils were found to be responsible for this production (58).

Members of the RhoGTPase family have been implicated in regulating signalling pathways that promote paracellular migration. Rac1 is activated by VCAM-1 and is thought to be responsible for the disruption of adherens junctions (58). ICAM-1

clustering has been shown to activate RhoA leading to the contraction of adjacent endothelial cells, and the opening of the junctions (58).

A number of junctional proteins are involved in the paracellular route of migration, such as Platelet Endothelial Cell Adhesion Molecule-1 (PECAM-1) and Junctional Adhesion Molecules (JAMs). PECAM-1 is involved with homophilic interactions whereas JAMs can form homotypic interactions and interact with integrins. Studies have shown the importance of these molecules in transmigration (61,62). PECAM-1 is expressed on the surface of all types of leukocytes and endothelial cells (63) and has been shown to mobilise to the surface of the endothelial cell after neutrophil interaction (58), presumably to enable the interaction between PECAM-1 on the leukocyte and endothelial cell. Blocking PECAM-1 with antibodies blocks paracellular migration *in vitro* (60). There are three different JAMs: JAM-A, JAM-B and JAM-C. JAM-A and JAM-C are expressed on leukocytes and endothelial cells and JAM-B is expressed on endothelial cells (64). LFA-1 interacts with JAM-A on endothelial cells. Blocking JAM-A with antibodies inhibited transmigration of monocytes *in vitro* and also reduced the recruitment of monocytes and neutrophils to sites of inflammation (64). This shows the importance of the interaction between adhesion molecules on leukocytes and endothelial junctions in paracellular transmigration.

### *1.2.6.2 Transcellular Route*

Transcellular migration accounts for only 5-20% of transmigration in activated HUVECs (65). Vesiculo-vacuolar organelles are continuous membrane-associated channels present at the sites of leukocyte adhesion, suggesting they act as the site for leukocytes to pass through the body of the endothelial cell (10,66). Structures containing junctional cell adhesion molecules have been observed just below the plasma membrane and it is possible that these facilitate transcellular migration (10). Cross-linking of ICAM-1 with monoclonal antibody translocates it to caveolin-rich membrane domains and is subsequently transcytosed to the basal plasma membrane (67). Similarly, as leukocytes bind ICAM-1, their protrusions meet with sites within the endothelium that are enriched in caveolin and F-actin, which form a passage for the leukocyte to pass through (67). This suggests that ICAM-1 internalisation within caveolin-rich sites initiates the formation of a channel for transcellular migration. Using

RNA interference (RNAi) to reduce the expression of caveolin decreased the number of cells undergoing transcellular migration (67), showing the importance of this protein in the process.

### 1.2.6.3 Migration through the Basement Membrane and Pericyte Sheath

Once the leukocyte has transmigrated across the endothelium it must penetrate the basement membrane and the pericyte sheath. The basement membrane is made up of laminins and collagen type IV (68). Studies have determined that certain areas of the basement membrane contain less of these molecules, with 60% less laminin 10, collagen IV and nidogen-2 at these sites compared with the average content of these proteins in the basement membrane (69), and these sites are where most neutrophils migrate through. Interestingly, these sites are also co-localised with gaps between pericytes, which loosely surround post-capillary venules. So, it seems that neutrophils migrate through areas of least resistance (10,69). Interestingly, these areas have been shown to be enlarged after stimulation with the cytokine IL-1β and this increase in size was dependent on neutrophil elastase (69). Inhibition of neutrophil elastase caused a reduction in transmigration (69).

Integrins also play a role in migration through the basement membrane to the site of inflammation. $\alpha_6$-integrin is activated by the engagement of PECAM-1 and is able to bind to the laminin molecules in the basement membrane, therefore facilitating the migration through the basement membrane (10). Antibodies blocking $\alpha_6$-integrins binding inhibited the migration of neutrophils across inflamed cremasteric venules (70).

Now that all of the individual steps of the adhesion cascade have been discussed, the next section will focus on more detailed aspects of cell adhesion molecules that relate to this PhD project, namely L-selectin, it's binding partners and their involvement in signal transduction.

## 1.3 L-selectin form and function

The selectin family of proteins are a group of three adhesion molecules which have been shown to be critical in leukocyte trafficking. The members of the family are named after the location of their first discovery. P-selectin was first classified by expression on platelets, but has since been shown to be expressed on endothelial cells,

E-selectin is expressed on endothelial cells and L-selectin is expressed on most circulating leukocytes. There are many similarities between the three family members, including their structural similarity and ligand specificity, which is discussed below.

## 1.3.1 Structure of the Selectins

All members of the selectin family have a C-type lectin domain, followed by an epidermal growth factor (EGF) like domain, two to nine short consensus repeat (SCR) domains, a single transmembrane domain and a cytoplasmic tail (Figure 1.3). The number of SCR domains varies between the selectins and different species, with L-selectin containing two SCR domains in all species studied and E- and P-selectin having between four and nine SCR domains (31). The homology between the extracellular domains between the different selectins is high, with around 52% homology amongst the lectin domains, 35-40% amongst the SCR domains and 47% amongst the EGF domains (31). Interestingly, there is no conservation in the transmembrane domain and the cytoplasmic tail across the three selectins, but these two domains for each individual selectin is well conserved between species, for example the L-selectin cytosolic tail in human and mouse share 78 % identity. This suggests they may play an important role in regulating selectin-specific properties.

### 1.3.1.1 C-type Lectin Domain

The C-type lectin domain is a carbohydrate binding domain 'C' indicates that carbohydrate binding is dependent on calcium. It has been shown that the interaction between the C-type lectin domain and carbohydrate moieties is required for the binding of lymphocytes to lymph node high endothelial venules (HEVs). The addition of carbohydrate mimetics inhibited this interaction *in vitro* (71), as did the addition of the enzyme neuraminidase (72), which cleaves the carbohydrate moiety sialic acid from the surface of the HEVs. The importance of calcium in regulating the interaction between selectins and their ligands was assessed by chelating calcium with ethylene glycol tetra-acetic acid (EGTA) (73). This blocked selectin adhesion under flow, clearly showing adhesion occurs in a calcium-dependent lectin-like fashion. Mutagenesis studies have mapped the carbohydrate-binding site to near the calcium-binding site, with positive amino acids surrounding the calcium binding site responsible for

recognising carbohydrate moieties (74). The carbohydrate ligands of selectins are discussed elsewhere in more detail (see Section 1.3.2).

### 1.3.1.2 EGF-like Domain

Deletion of the EGF-like domain has been shown to abolish adhesion (31). It is thought that this is due to an alteration in the structure of the selectin protein, affecting its ability to interact with carbohydrate moieties (75). Further evidence that the EGF-like domain plays a structural role and does not specifically interact with selectin ligands is provided by domain swapping studies. When the EGF-like domains of the L-selectin and P-selectin were swapped with one another, there was no effect on L-selectin-dependent adhesion of lymphocytes to HEVs of the lymph nodes and mesenteric venules *in vivo* (76). Similarly, when the EGF-like domain of E-selectin was swapped with that of protein factor IX, cell adhesion was not affected (74). Interestingly, when the EGF-like domain of P-selectin was swapped with one of the other EGF-like domains, interaction with P-selectin specific ligands was suboptimal (76), showing both the lectin and EGF-like domains of P-selectin are required for optimal interaction with its ligands and suggests the P-selectin EGF-like domain does play a role in ligand specificity.

### 1.3.1.3 SCR Domain

Deletion mutagenesis of the SCR domains reveal an impairment in ligand binding under flow (75). Further evidence of the importance of the SCR domains in ligand recognition has been shown by antibody studies. The addition of an antibody against the SCR domain inhibited the adhesion of both L- and E-selectin, with lymphocyte adhesion to HEVs and neutrophil adhesion to E-selectin respectively blocked (77). However, the swapping of the L- and P-selectin SCR domains had no effect on adhesion (76), showing the SCR domains do not play a role in ligand specificity. This has led to the hypothesis that the SCR domain could be important in controlling the distance of the C-type lectin domain from the membrane, which could be important for ligand interaction. For example, L-selectin is anchored to microvilli (78) and, as such, is less likely to require many SCR domains during tethering and rolling events (as it stands head and shoulders above other molecules that reside on

the planar part of the plasma membrane). In contrast, P-selectin contains 9 SCR domains and is thought not to localise to microvilli.

L-selectin contains a unique membrane proximal cleavage domain (shown as a pentagon in Figure 1.3) located below the SCR domains. This allows the regulation of L-selectin surface levels via the cleavage of the extracellular domain, as will be explained in detail in Section 1.3.4.
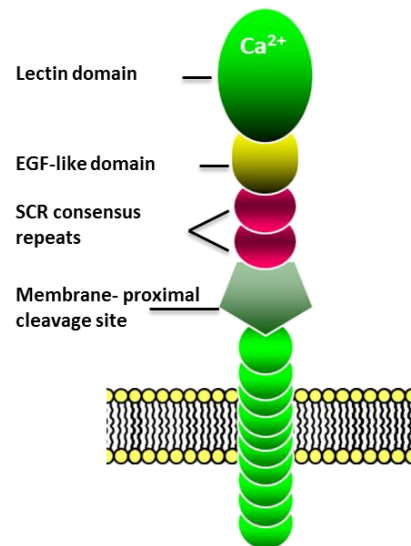


**Figure 1.3: Structure of selectins.** A diagram showing the different domains of the selectins, including the C-type lectin ectodomain, epidermal growth factor (EGF)-like domain, short consensus repeat (SCR) domains, a single transmembrane region and a C-terminal 17 amino acid cytoplasmic tail. The structural domains are similar for all family members, except the number of SCR domains varies and the sequence of the transmembrane and cytosolic domains is not conserved between family members. L-selectin also contains a membrane proximal cleavage site, allowing it to be cleaved from the cell surface.

## 1.3.2 Selectin Ligands

As stated, the C-type lectin domain of selectins is responsible for interacting with carbohydrate moieties on the surface of corresponding cells. The carbohydrate moieties required for binding are sialyl Lewis X (sLe$^x$)-based tetrasaccharides. This is a sialofucosylated glycan with a terminal sialic acid linked to a galactose and a fucose, both linked to N-acetyl-glucosamine (Figure 1.4) (79,80). Selectin ligands are also often sulphated (81). Studies have been carried out in order to decipher which components are required for selectin binding. The loss of sialic acid from sLe$^x$ by the addition of sialidase abolishes the interaction between lymphocytes and HEVs, therefore inhibiting lymphocyte homing to the lymph node (82). The role of fucose was assessed in

fucosyltransferase knockout mice. This resulted in HEV cells with no ligand activity, resulting in the loss interaction between lymphocytes and the cells of HEV (82). The addition of the sulphation inhibitor sodium chlorate also led to a reduction in the binding between the selectins and their ligands (82).

Although the carbohydrate moiety sLe$^x$ is capable of acting as the ligand for selectins, highlighted by the fact it can support leukocyte rolling, the number of ligands required is two-three orders of magnitude higher than physiologic selectin ligands (83). This shows that other components are required to enhance the selectin/ligand interaction. The protein backbone upon which sLe$^x$ is attached is important for displaying the carbohydrate moiety in the correct orientation for presentation to selectins (31,80). The glycoprotein also plays important roles in ensuring correct posttranslational modifications, initiating outside-in signalling and sorting of the ligand to the correct location (31).
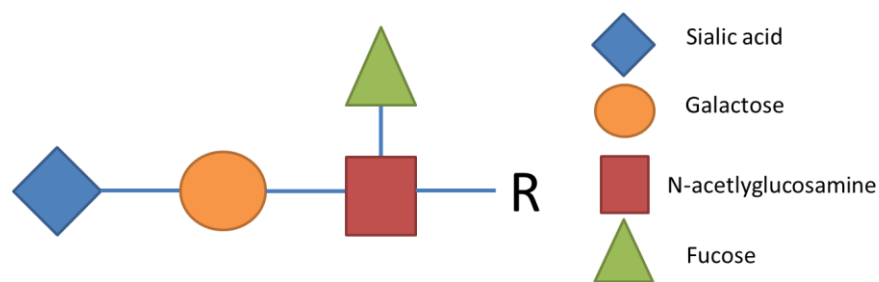


**Figure 1.4: Sialyl Lewis X.** A diagram showing the composition of sLe$^x$ and the attachments between them. R represents any glycoprotein to which sLe$^x$ is attached.

### 1.3.3 Regulation of L-selectin expression

L-selectin is constitutively expressed on the surface of a majority of circulating leukocytes, including monocytes, neutrophils, naïve T- and B-cells (31). The expression of L-selectin is controlled both at the mRNA and the protein level. Analysis of the DNA sequence upstream of the L-selectin start codon has revealed several transcription factors are capable of binding to the promoter region. Site-directed mutagenesis and chromatin immunoprecipitation experiments have shown that Mzf1, Klf2, Sp1, Fts1, Irf1 bind to and activate the murine L-selectin promoter (84). The role of these transcription factors was further assessed by over expressing them in EL4 cells, which led to an increase in L-selectin mRNA levels (84). It was also shown that when Sp1

expression was silenced using siRNA, the expression of L-selectin mRNA was decreased (84), further highlighting the ability of this transcription factor to promote L-selectin expression. The analysis of the promoter region also found a potential Forkhead box 1 (FOXO1) binding sequence upstream of the L-selectin start codon (85). Studies have shown FOXO1 is capable of activating expression of L-selectin in several different cell lines. A constitutively active form of FOXO1 expressed in Jurkat T-cells led to an up-regulation of L-selectin expression, as did overexpression of FOXO1 (85). FOXO1 has been reported to control L-selectin expression in naïve T-cells (86,87) and in B-cells, where a lack of FOXO1 has been shown to lead to lower L-selectin expression and as a result fewer B-cell populating peripheral lymph nodes (88).

Although the transcription factors responsible for promoting L-selectin expression have been deciphered, the signalling pathways leading to their activation remain unclear. Several pathways have been shown to regulate L-selectin mRNA levels in T-cells. Activation of T-cells through the T-cell receptor (TCR) has been shown to down-regulate L-selectin within a few hours through an acceleration of L-selectin cleavage (see Section 1.3.4) (89). Over the next few days L-selectin levels increase then decrease once again via regulation of mRNA levels (89), though how mRNA levels are regulated is unclear. It has also been shown that the PKC pathway is capable of up-regulating L-selectin mRNA levels in Jurkat T-cells (90). In this study PMA was used to activate PKCs, which initially causes shedding of L-selectin (see Section 1.3.4), followed by a progressive increase in the surface expression of L-selectin and an increase in mRNA levels (90). It is possible that the increase in L-selectin expression is in response to the induction of shedding and further research is required to assess the role of PKC signalling in inducing L-selectin expression in T-cells.

In B-cells, L-selectin mRNA levels are increased by the cytokine interferon (IFN)-α (91), although again the signalling pathway remains unclear. The role of nitric oxide (NO) synthase (NOS) in regulating L-selectin expression has also been investigated. It has been reported that when rats were treated with the NOS inhibitor L-NAME, the expression of L-selectin was reduced and this was due to an overall reduction in L-selectin mRNA (92). The cytokine IL-7 has been shown to negatively regulate L-selectin expression. IL-7 is a regulator of T-cell development and as T-cells enter the lymph node they encounter IL-7 (93). IL-7 regulates Cdc25A, a phosphatase that activates cyclin-dependent kinases and actively promotes T-cell proliferation (93).

High doses of IL-7 promote low-level L-selectin expression and a higher level of nuclear-localised Cdc25A causing T-cell proliferation (93). This causes the sequestration of FOXO1 in the cytosol, therefore blocking the promotion of L-selectin expression (93).

L-selectin is down-regulated from the surface by cleavage at an extracellular site, leading to soluble L-selectin present in the plasma. Details of how L-selectin shedding is regulated can be found in Section 1.3.4.

## 1.3.4 Shedding of L-selectin

The biological significance of shedding of L-selectin remains unclear, although it is likely to rapidly halt L-selectin-dependent adhesion and signalling events, as discussed below. Shedding of L-selectin from the plasma membrane occurs rapidly, following several different stimuli including: phorbol 12-myristate 13-acetate (PMA) (94), antibody cross-linking (6), thrombin, IL-8 (95), TNF-α (6) and mechanical force due to rolling (96). Shedding has been shown to occur rapidly after activation of both neutrophils and lymphocytes (97,98), suggesting that it plays a role in rapidly shutting down signalling from this molecule.

The process of shedding is regulated by metalloproteases, such as a disintegrin and metalloprotease domain 17 (ADAM17) (also known as TNF-α converting enzyme (TACE)) (99). This is a transmembrane protein with an extracellular metalloproteinase domain (100) that cleaves L-selectin at an extracellular membrane-proximal site (Figure 1.5A). Over 70 different substrates for ADAM17 have been identified, with ligands involved in development and inflammation characterised (101,102). These ligands can broadly be grouped in 3 categories: 1) membrane-anchored ligands, such as growth factors and cytokines that are synthesised and attached to the membrane and ADAM17 cleavage forms an active soluble protein, for example TGF-α and TNF-α (99), 2) receptors, whose cleavage may either block signalling or induce an alteration in signalling, with the membrane retained fragment capable of inducing different signals, for example Notch (103) and ErbB4 and 3) cell adhesion molecules, with ADAM17 cleavage blocking adhesion, for example ICAM-1 (104) and VCAM-1 (105). It must be noted that many adhesion molecules also act as signalling receptors, and therefore cleavage by ADAM17 will also impact signalling events. ADAM17 is expressed in all cell

types, including endothelial cells and leukocytes, with inflammatory stimuli shown to increase its expression (101). Surface expression of ADAM17 is also induced by translocation of stored protein to the plasma membrane (100). This is controlled by threonine phosphorylation of ADAM17 by the p38 MAPK or ERK (106,107). The activity of ADAM17 is controlled at the protein conformation level. It exists in a closed inactive conformation, maintained by intramolecular disulphide bonds, which in turn is regulated by the activity of extracellular protein disulphide isomerases (PDIs) (108,109). Upon stimulation with PMA, reaction oxygen species (ROS) are produced, which inactivate PDI and thereby activate ADAM17 (108).

Initial analysis of the role of ADAM17 in inflammation was attempted with knockout mice, however, the loss of ADAM17 was embryonic lethal (99). For that reason lymphocytes lacking ADAM17 were adoptively transferred in to wildtype mice. Results showed that survival against bacterial infection was improved, with a greater number of neutrophils infiltrating to the site of infection to aid bacterial clearance (110), suggesting ADAM17 has a protective role in curbing infection. However, evidence also points to ADAM17 being pro-inflammatory, with the risk of septic shock reduced when ADAM17 was lacking in lymphocytes (101). It was also observed that the number of ADAM17$^{-/-}$ neutrophils recruited to the lung was reduced compared to wildtype cells following inflammation (111). ADAM17 is also up-regulated in chronic inflammatory diseases (112), including atherosclerosis (101). These differences are most likely down to the different targets of ADAM17 cleavage being involved in different processes during inflammation.

The role of ADAM17 in negatively regulating L-selectin expression is highlighted in ADAM17-null neutrophils, where it is 10-fold higher than in wildtype cells (113). The location of the cleavage site in L-selectin is located between residues K321 and S322 (114,115). Studies focusing on site specificity found that the sequence of amino acids surrounding the cleavage site was not important, but the actual distance of the cleavage site from the plasma membrane is vital (114,116-118). This suggests that the ADAM17 active site is poised on a fixed stalk, and lacks flexibility when cleaving its substrates. Mutants of L-selectin, where the extracellular domain adjacent to the membrane has been truncated by eight amino acids (a mutation referred to as ΔM-N in humans and ΔK-N in mice), showed a blockage of shedding (98,119) (Figure 1.5B).

The cytoplasmic tail has also been shown to play an important role in regulation of shedding of L-selectin. Truncating the entire tail of L-selectin leads to just 44% shedding (114,118), suggesting that there are critical elements within the tail that are sufficient to drive the shedding response. As explained in a later section in this thesis, the binding of CaM to L-selectin has been shown to be involved in regulating L-selectin shedding (Section 1.3.7.3). It is also possible that PKC phosphorylation of the cytosolic tail of L-selectin is important in regulating shedding, as inhibitors of PKCs also block shedding (120).

Experiments where L-selectin cleavage is inhibited have been undertaken in order to decipher the role of shedding. Results showed that rolling velocities are reduced, with a velocity of 59 μm/s before inhibition and 39 μm/s velocity when shedding was inhibited, and this leads to an increase in the accumulation of leukocytes attached to endothelial cells (121,122). Similarly, ADAM17-null neutrophils roll slower and adhere more readily to endothelial cells, with a greater number of neutrophils being recruited to the site of inflammation (113). Mouse models expressing "sheddase resistant" L-selectin have been produced to study the effect of shedding in the whole organism. The expression of sheddase resistant L-selectin in neutrophils leads to the prevention of neutrophil migration into tissue following activation (114,123). Sheddase resistant L-selectin also leads to activated T-cells re-entering the lymph nodes (114,124).

Cleavage of L-selectin results in the creation of a soluble extracellular fragment of L-selectin, which is able to bind to its ligand and therefore competes for binding sites on both the leukocyte (e.g. PSGL-1) and the endothelium, antagonising further recruitment of leukocytes (125). As L-selectin is a signalling molecule (see Section 1.3.6), shedding will presumably halt the activation of L-selectin-dependent signalling pathways. This is highlighted by the fact that shedding limits the activation of integrin molecules (114,126). Therefore L-selectin cleavage may be required to limit L-selectin-dependent signalling. All these factors suggest shedding is important for limiting the inflammatory response by ensuring that the number of leukocytes recruited to the sight of infection is controlled and limit the activation of the cells by halting L-selectin signalling.

Shedding of L-selectin also creates a membrane-retained fragment, often referred as the "stump". It is possible that this fragment of L-selectin is able to induce

different signalling pathways to the full length L-selectin, however, this has not been studied in any detail. The stump remains intact for 30 minutes after cleavage before being degraded (127), giving it ample time to activate signalling pathways. One possible pathway is the activation of PKC isozymes. PKCs have been shown to bind phosphorylated L-selectin cytosolic tail (see Section 1.3.7.2 for details), possibly after L-selectin has been cleaved. However, further research is required to determine if this is the case. There are several other examples of the stump of transmembrane proteins produced by ADAM17 cleavage acting as signalling molecules (102,128). The stump of CD44 is susceptible to γ-secretase cleavage, which is an intramembrane protease that cleaves transmembrane proteins at residues within the transmembrane domain. This produces a fragment of the protein, which enters the nucleus and induces protein expression (129). It is possible that the same mechanism also occurs with L-selectin. The importance of the stump formation may be highlighted by an *in vivo* chemotaxis assay using L-selectin knockout and ΔK-N-L-selectin mice. In both cases, leukocytes failed to chemotax towards the keratinocyte-derived chemokine (KC) (123,130). The similarity in both cases is the lack of the formation of the stump, implying it may be responsible for inducing signalling pathways that allow chemotaxis.
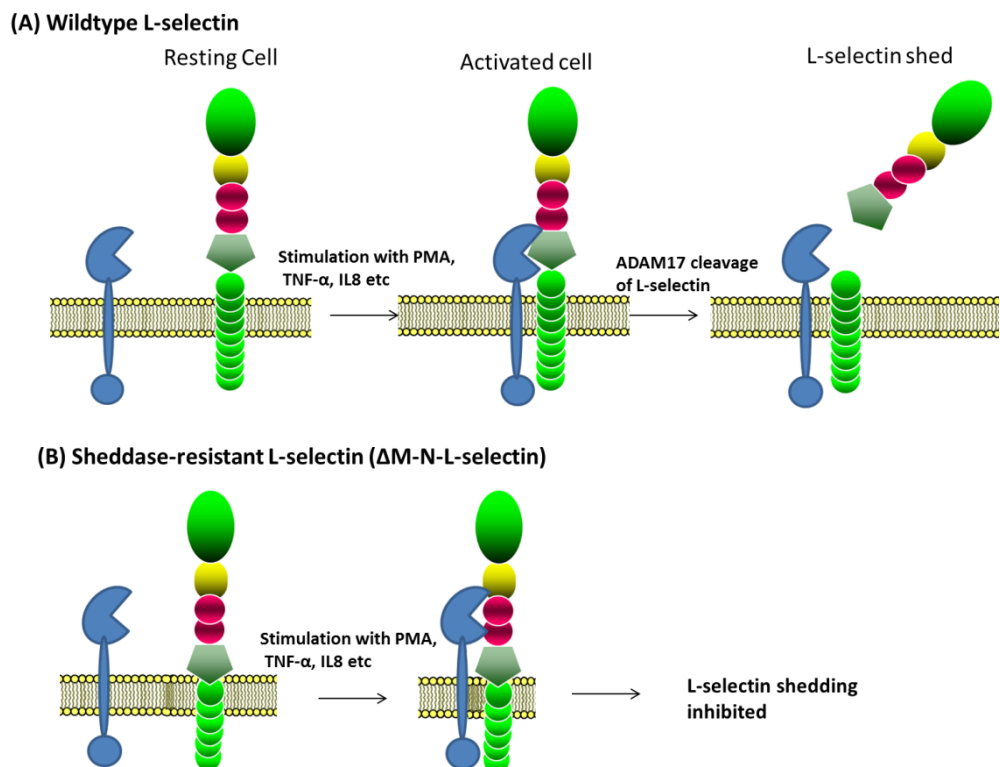
**Figure 1.5: The shedding of L-selectin by ADAM17.** (A) In cells expressing wildtype L-selectin, upon stimulation with PMA etc., ADAM17 (shown in blue) comes into close proximity to L-selectin and can access the cleavage site (shown by the hexagon), leading to shedding of L-selectin from the cell surface. (B) In cells expressing sheddase resistant L-selectin (known as ΔM-N-L-selectin in humans), 8 amino acids proximal to the cleavage site have been deleted resulting in a cleavage site being closer to the plasma membrane. When the cell is activated ADAM17 can no longer access the cleavage site and so L-selectin is not shed.

It has been observed that non-steroidal anti-inflammatory drugs (NSAIDs) induce shedding of L-selectin (131). NSAIDs inhibit the interaction between neutrophils and endothelial cells, leading to a reduction in the number of neutrophils migrating to the site of inflammation (132,133). Experiments have been carried out to try to decipher the mechanism by which NSAIDs induce L-selectin shedding. Inhibiting the protease ADAM17 blocks the induction of L-selectin shedding (134), showing this protease is responsible for shedding L-selectin in response to NSAIDs. How NSAIDs activate ADAM17 remains unclear, although studies have revealed that ROS are involved. NSAIDs have previously been shown to induce the production of ROS. When neutrophils were incubated with both antioxidants and NSAIDs, the capability of NSAIDs to reduce the basal expression of L-selectin was diminished (135), showing NSAID-induced shedding requires a high oxidative status. Analysis of the ROS required has shown that superoxide is responsible, as the presence of superoxide dismutase (SOD), which catalyses the conversion of superoxide to oxygen and hydrogen peroxide, abrogates NSAID induced shedding almost entirely (135). Further investigation is required to fully decipher the mechanism behind NSAID induced shedding of L-selectin.

### 1.3.5 L-selectin Ligands

As stated above, L-selectin ligands normally consist of glycoproteins decorated with sLe[x] moieties, although glycolipids can also act as ligands. It has also been shown that sulphation of sLe[x] is required for L-selectin interaction with ligands expressed by HEVs, as mice deficient in the enzyme capable of sulphating sLe[x], namely N-acetlyglucosamine 6-O-sulfotransferase-1, results in a reduction of lymphocyte homing to peripheral lymph nodes, mesenteric lymph nodes and Peyer's Patch (136). Many potential L-selectin ligands have been identified, though the specific role of each

individual ligand remains unclear. Several of the ligands whose role, to a certain extent, has been deciphered are described below, with further examples shown in Table 1.2, though this is not an exhaustive list.

The ligands can be broadly classed in two categories, those found on the luminal side of the endothelial (Figure 1.6A) and those primarily found in the ECM beneath the endothelium (Figure 1.6B). A majority of those on the luminal side are glycoproteins decorated with sLe$^x$, whereas those within the ECM lack sLe$^x$ and instead L-selectin adhesion depends on highly sulphated proteoglycans. Another interesting difference is the fact the L-selectin binds to luminal ligands under shear flow, which is required for the interaction (see Section 1.2.2), whereas shear flow is obviously lacking subluminally. It is therefore possible that the binding mechanisms are different in both cases, though further research is required to understand this difference. The fact that the L-selectin encounters the different subsets of ligands in distinctive microenvironments may be fundamental in fine-tuning L-selectin signalling in these very different locations.


### *1.3.5.1 L-selectin ligands expressed on the luminal surface*

PSGL-1 is the best-characterised luminal ligand of L-selectin and is expressed on leukocytes and endothelial cells as a homodimer, with two subunits linked together by a disulphide bond (137). It has been demonstrated that L-selectin binding depends on sialylation, fucosylation (138) and sulphation of at least one of three tyrosine residues of PSGL-1 (139). Mutating one or two of the tyrosine residues to phenylalanine, and therefore blocking sulphation, led to a lowering in the binding affinity between L-selectin and PSGL-1 (137). This is likely to be due to a loss of charge on PSGL-1 preventing the formation of electrostatic interactions between L-selectin and PSGL-1 (137). As stated above (Section 1.2.2) PSGL-1 is able to support L-selectin dependent rolling. Mutating either the tyrosine residues or the threonine residue to which sLe$^x$ is attached abrogated rolling (140). The interaction between L-selectin and PSGL-1 has been implicated in secondary tethering, as described in Section 1.2.1.

Glycosylation-dependent cell adhesion molecule-1 (GlyCAM1) has also been shown to bind to L-selectin, with the interaction requiring the sialylation and sulphation of GlyCAM-1 (141). It is expressed by HEVs and lacks a transmembrane

domain, so is secreted as a soluble protein (142). As GlyCAM-1 is secreted it may not play a role in cell-cell interactions and instead be involved in initiating L-selectin dependent signalling. In fact, studies have demonstrated that treatment of naïve T cells with GlyCAM-1 stimulates adhesion via $\beta_2$-integrins (142,143). It is also possible that GlyCAM-1 is immobilised on to the luminal surface of the endothelial cells, likely through electrostatic interactions. If this is the case then it is possible that GlyCAM-1 is capable of supporting leukocyte attachment to the endothelium through its interaction with L-selectin. The levels of GlyCAM-1 found in the plasma after an inflammatory stimulus has been shown to increase (144), suggesting a role in inflammatory induced signalling.

Another luminal ligand of L-selectin is mucosal vascular addressin cell adhesion molecule 1 (MAdCAM-1). MAdCAM-1 is a member of the immunoglobulin superfamily expressed on the surface of the endothelium of venules, including HEVs in Payer's Patch and mesenteric lymph nodes (145). It has been shown that MAdCAM-1 can be post-translationally modified with sLe$^x$ to enable L-selectin binding (145). Studies have divulged that lymphoid cells transfected with L-selectin are capable of adhering to MAdCAM-1 isolated from mesenteric lymph nodes under shear flow (146) and rolling of the lymphoid cells was observed (146). This shows that MAdCAM-1 may play a role in recruitment of lymphocytes to the secondary lymph nodes.

Members of the CD34 family of glycoproteins have also been implicated as L-selectin ligands. CD34 is a single pass transmembrane sialomucin protein, which is expressed on endothelial cells. CD34 can be decorated with sulphated sLe$^x$ and is then able to bind L-selectin (147) and mediate lymphocyte extravasation (148). In fact, antibodies against CD34 are capable of blocking T cell binding to lymph node and Peyer's Patch HEVs and therefore block T cell extravastion from the blood into secondary lymphoid tissue (149). Blocking CD34 with antibody has also been shown to inhibit the recruitment of neutrophils and monocytes to the peritoneum following an inflammatory stimulus (150). Interestingly, studies carried out with CD34-deficient mice have shown that lymphocytes homed to the secondary lymphoid organs more frequently than wildtype mice (151). Analysis showed that lymphocytes were twice as likely to tether, roll and adhere in peripheral lymph nodes when CD34 was lacking (151). This suggests that CD34 may interfere with L-selectin dependent recruitment of lymphocytes and it is possible plays a dual role in regulating lymphocyte recruitment to

secondary lymph nodes. Other members of the CD34 family have also been shown to be capable of acting as L-selectin ligands, with podocalyxin presenting sulphated sLe$^x$ to enable L-selectin binding (152) and endoglycan interacting with L-selectin through sulphated tyrosine residues and sLe$^x$ (152).

Proteoglycans (PGs) expressed on the cell surface form a part of the glycocalyx in addition to the extracellular matrix (ECM) and collectively act as L-selectin ligands. Heparan sulphate proteoglycans (HSPGs) are one class of proteoglycans that make up the glycocalyx and can bind L-selectin. Interestingly, it is thought that the glycocalyx acts as an anti-inflammatory sheath by repelling leukocytes and masking underlying binding molecules (153). The thickness of the glycocalyx differs in different vessel types, with large arteries, such as the aorta, having a significantly thicker glycocalyx than post capillary venules (154). In fact, it was shown that segments of the post capillary venules in both rat and mouse almost completely lacked the glycocalyx (154). As a majority of leukocytes exit the blood vessels in post capillary venules, these areas lacking glycocalyx may act as areas where leukocyte-endothelium interactions can occur, with the presence of the thicker glycocalyx blocking leukocyte adhesion in the arteries. Upon an inflammatory stimulus the glycocalyx is shed allowing leukocyte adhesion to occur. Degradation of heparan sulphate, by treatment with heparitinase I, causes an increase in the number of adherent leukocytes (155).

Several different studies have shown that L-selectin is able to bind to HSPGs in several different vessels including the kidney and spleen (156-158). A role for HSPGs in monocyte binding to bovine aortic endothelial cells has also been demonstrated, as heparanase treatment inhibited approximately 80% of monocyte attachment to the aortic endothelium under flow (159). The importance of heparan sulphate in the interaction between L-selectin and HSPGs is highlighted by the inactivation of N-deacetylase-N-sulfotransferase-I, an enzyme responsible for the addition of the sulphate group to the heparan sulphate chains. When this enzyme is inactive, the binding between L-selectin and its ligands is much weaker, leading to reduced neutrophil infiltration following an inflammatory stimulus (160).

### 1.3.5.2 Potential L-selectin ligands beyond the vessel lumen

As stated above, HSPGs expressed in the ECM may potentially act as L-selectin ligands. Potential HSPG L-selectin ligands were identified by staining frozen tissue

samples with L-selectin-Ig and then using carbohydrate-degrading enzymes in order to classify the ligand type. Using this method it was revealed that L-selectin interacted with the HSPG collagen XVII, with cells transfected with L-selectin able to bind to wells coated with collagen XVII (156). A similar method was used to identify chondroitin sulphate proteoglycans (CSPGs) and dermatan sulphate proteoglycans (DSPGs) that were also capable of binding to L-selectin (157), with versican (157,161) and biglycan (162) both shown to be potential L-selectin ligands. Although the above method was able to show that L-selectin is capable of binding glycoproteins expressed in the basement membrane, it remains to be investigated if L-selectin is capable of interacting with these ligands in this microenvironment.

The importance of the L-selectin interaction with ECM components is highlighted in a model of kidney interstitial inflammation. It was revealed that the sulphated glycolipid sulphatide was able to act as a ligand for L-selectin (163) in the peritubular capillaries and interstitium following infection (164). It was revealed that the infiltration and migration of monocytes to the interstitium following an inflammatory stimulus was reduced in mice lacking sulphatide (164). It is possible that other components of the ECM may be important for migration of leukocytes into other tissue types.

It is thought that PGs in the ECM have to be cleaved to enable leukocyte migration (153). It is possible that fragments of PGs bind to L-selectin and promote cell signalling in leukocytes to enhance directional migration. T-cells produce heparanase to degrade HS to sulphated disaccharides (DSs) (165,166). Treatment of T-cells with DS induces the adhesion of the cells to ECM components via integrins (166) and inhibits the production of TNF-α following an inflammatory stimulus (165). Both biglycan and versican have been shown to interact with toll-like receptors (TLRs) on T-cells to induce inflammatory responses, including production of TNF-α and IL-6. To date it is unclear if the L-selectin interaction with components of the ECM is capable of inducing signalling pathways. Further investigation is required to decipher the importance of the L-selectin interaction with glycoproteins in the ECM.
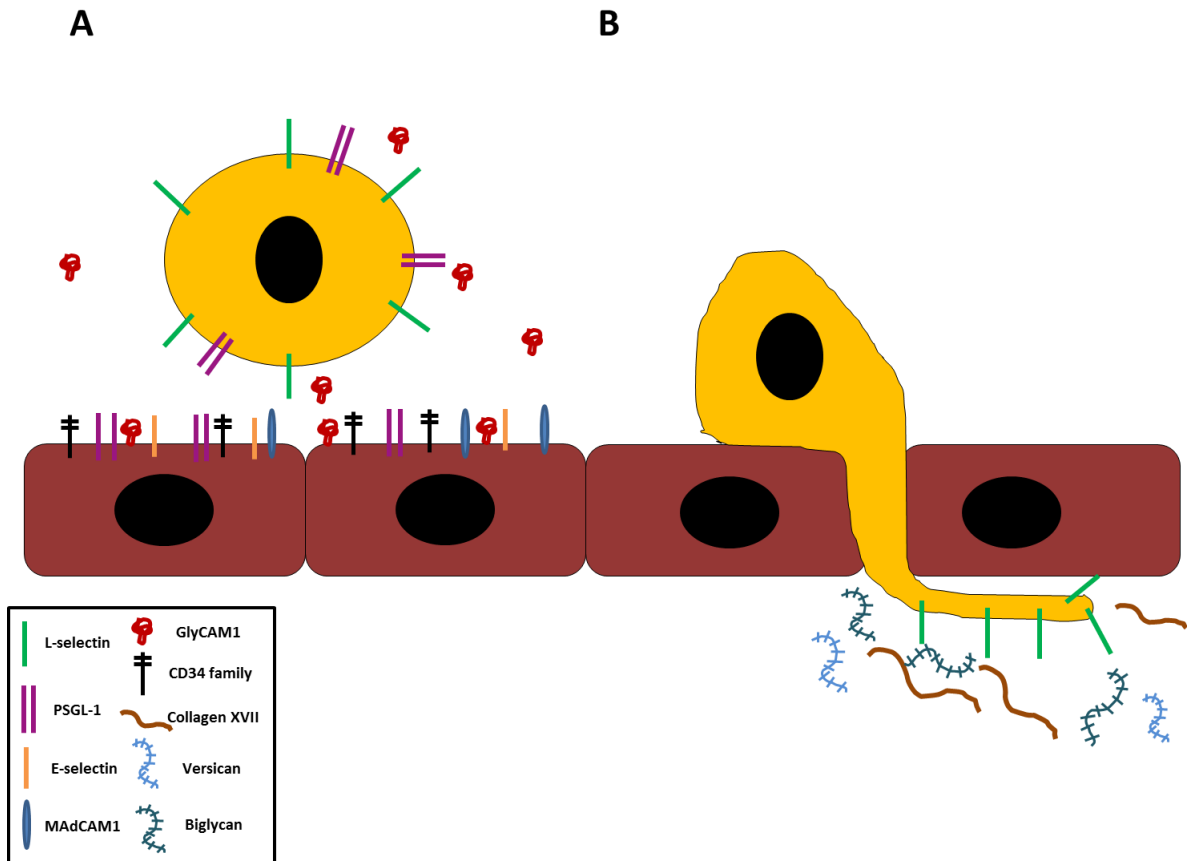
**Figure 1.6: Ligands of L-selectin.** A depiction of the location of different L-selectin ligands found on the luminal side of the endothelium (A) and in the ECM (B). It is worth noting that GlyCAM-1 is a secretory protein, but may be attached to the endothelium by a yet undiscovered mechanism.

| Ligand | Expression | Role of Interaction | Reference |
|---|---|---|---|
| **PSGL-1** | Leukocytes | Secondary tethering | (137-139) |
| **GlyCAM1** | Secreted by HEVs | Initiation of L-selectin-dependent signalling, leukocyte-endothelium interaction? | (141-143) |
| **MAdCAM1** | HEVs | Recruitment of lymphocytes to secondary lymph organs? | (145,146) |
| **CD34** | Endothelial cells | Regulation of lymphocyte recruitment to secondary lymph nodes. Recruitment of neutrophils and monocytes to sites of inflammation. | (147,149-151) |
| **Podocalyxin** | Pancreatic cancer | Metastasis of cancer cells | (152,167) |

| | | | |
|---|---|---|---|
| | cells | | |
| **Podocalyxin-like-protein** | Colon carcinoma and HEVs | Metastasis of colon carcinoma cells and lymphocyte binding to HEVs | (168,169) |
| **Endoglycan** | Vascular endothelial cells, B cells, T cells and peripheral blood monocytes | Leukocyte-endothelial and leukocyte-leukocyte interactions *in vitro* | (152,170) |
| **Endomucin** | Vascular and lymphatic endothelial cells, including HEVs | Shown to support L-selectin-dependent tethering and rolling *in vitro* | (171,172) |
| **Sgp200** | HEVs | Support lymphocyte-HEV interactions? | (173,174) |
| **Nucleolin** | Leukocytes | Leukocyte-leukocyte interactions *in vitro* | (175) |
| **E-selectin** | Endothelial cells | Supports L-selectin-dependent adhesion *in vitro* | (176) |
| **Collagen XVIII (HSPG)** | ECM | Link between L-selectin dependent adhesion and chemokine signalling? | (156,177) |
| **Versican (CS/DSPG)** | ECM | Leukocyte trafficking into the kidney during disease conditions? | (161,178) |
| **Biglycan (DSPG)** | ECM | Tethering and rolling of CD16- NK cells on endometrial microvascular endothelial cells | (162) |
| **Lubrican** | Synovial fluid (SF) | Recruitment of polynuclear granulocytes to SF during rheumatoid arthritis | (179) |

**Table 1.2: L-selectin Ligands.** A summary of glycoproteins identified as ligands for L-selectin. Note: this is not an exhaustive list.

### 1.3.5.3 The role of multivalent ligands in L-selectin function

Studies reveal an important role for multivalent ligands in regulating L-selectin function; for example, multivalent ligands are capable of inducing L-selectin shedding (114,180). Experiments using glycopolymers with sulphated sLe$^x$ moieties showed these multivalent ligands bind to L-selectin molecules and not only cause L-selectin shedding, but, as a result, inhibit L-selectin-dependent rolling (180,181). Further analysis of the requirements of the multivalent ligands to induce shedding revealed that the spacings of the ligands on the polypeptide was important, as shedding occurred when the ligands are 17-35 Å apart, but not when they were 35-50 Å apart (182). This suggests that clustering of L-selectin, induced by multivalent ligands, is a prerequisite for L-selectin shedding (Figure 1.7). The mechanism underlying this shedding response remains unclear, although it is likely that signalling through clustering of L-selectin may activate a signalling cascade to kick-start the process.
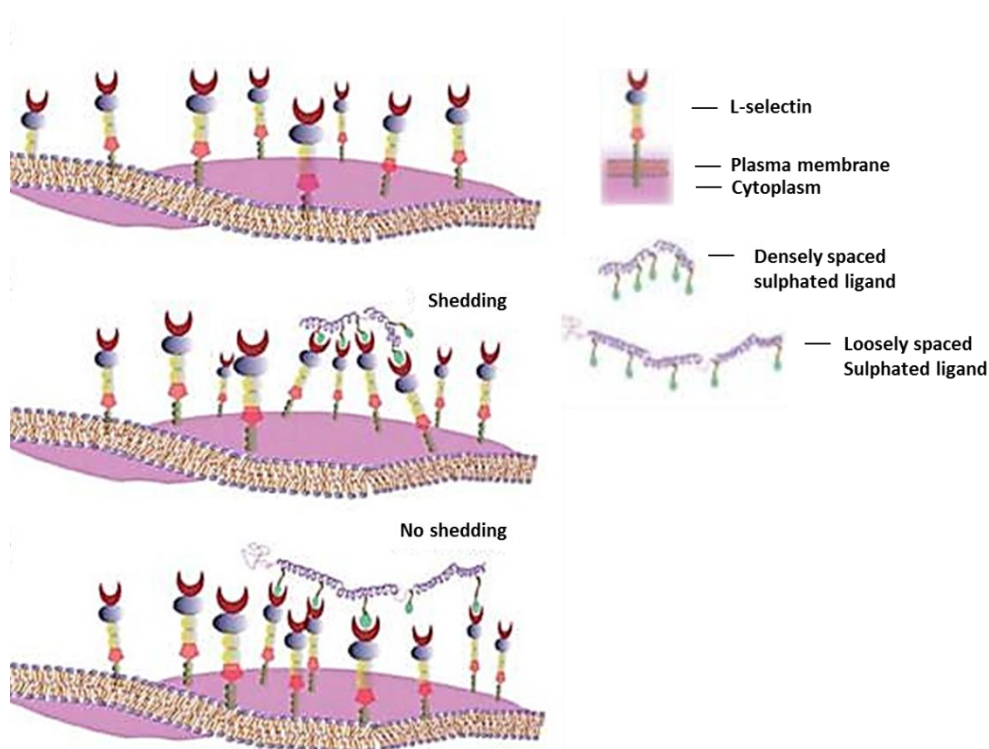


**Figure 1.7: Multivalent ligand induced clustering of L-selectin causes L-selectin shedding**. In resting cells L-selectin is distributed at the plasma membrane as a monomer. When a densely packed multivalent ligand is bound by L-selectin molecules clustering occurs, leading to L-selectin shedding. Engagement of a loosely spaced multivalent ligand by L-selectin does not induce clustering and therefore shedding does not occur. Figure taken from Liu, S., and Kiick, K. (2011) Architecture effects on L-selectin shedding induced by polypeptide-based multivalent ligands. *Polymer chemistry* **2**, 1513-1522 (2).

## 1.3.6 L-selectin-dependent Signalling

L-selectin has been described as a signalling receptor, with many studies undertaken in an attempt to decipher the pathways triggered upon ligand binding of L-selectin. Although many effectors of L-selectin stimulation have been identified, the signalling pathways underlying them remain elusive. Those that have been deciphered are shown in Figure 1.8.

Many examples of L-selectin signalling have been observed in neutrophils. In these cells, signalling downstream of L-selectin using sulphatide or antibody to cluster L-selectin increases the free cytosolic concentration of calcium (Figure 1.8, 2) (183-185). An increase in superoxide production for use in the oxidative burst in neutrophils was also observed using these methods (Figure 1.8, 2) (183,184). L-selectin has also been shown to promote the activation of integrins and therefore facilitating the transition from rolling to firm adhesion and arrest of leukocytes. Clustering of L-selectin activates both $\beta_1$ and $\beta_2$-integrins in both neutrophils and lymphocytes (Figure 1.8, 2) (186-188). Interestingly, it is thought that L-selectin signalling induces a change in the integrin conformation leading to their activation, as opposed to mobilisation of internal stores of integrins, due to the rapid increase in adhesiveness observed not allowing a time for the mobilisation to occur (188). The pathway behind L-selectin-dependent integrin activation in neutrophils has been investigated, in conjunction with PSGL-1. It has previously been shown that PSGL-1 was responsible for the activation of integrins through its interaction with and activation of Spleen tyrosine kinase (Syk) and Sarcoma (Src) family kinases (189,190). L-selectin and PSGL-1 are in close proximity in neutrophils and upon ligation of E-selectin this becomes more apparent with co-localisation on microvilli and tethers evident on cells rolling on P-selectin, as shown by proximity ligation assay and FRET analysis (191). PSGL-1 knockout mice lack LFA-1-dependent slow rolling (Section 1.2.3), as do L-selectin knockout mice (191), suggesting both molecules are required for the extension of LFA-1. Both Syk and the Src Kinase family members Fgr, Hck and Lyn were shown to interact with the L-selectin/PSGL-1 complex in neutrophils, as shown by co-immunoprecipitation experiments with peptides representing the cytosolic tails of PSGL-1 and L-selectin (191). The activation of these kinases was assessed in neutrophils under shear stress by lysing adherent cells, immunoprecipitating the kinases and assessing their phosphorylation state (191). The kinases Fgr, Lyn, Hck and Syk were all phosphorylated following the interaction of

the cell with P- and E-selectin, but not in cells lacking L-selectin (191). Taken together these results suggest that both L-selectin and PSGL-1 are required for the activation of LFA-1 in neutrophils through their activation of Syk and Src family kinases.

Antibody ligation of L-selectin in neutrophils has been shown to phosphorylate and therefore activate several tyrosine kinases, such as MAPK (192). In fact, activation of the p38 MAPK by L-selectin stimulation has been shown to be required for L-selectin-dependent priming of degranulation in neutrophils (Figure 1.8, 3) (193). Another signalling pathway activated in neutrophils upon L-selectin stimulation leads to the activation of the transcription factor NF-κB. Using the L-selectin ligand sulphatide and by crosslinking L-selectin with antibodies this transcription factor becomes activated (194). It has previously been shown that NF-κB induces the transcription of TNF-α in the monocyte cell line Mono Mac 6 and Human Embryonic Kidney (HEK) cells (195,196) and sulphatide ligation of L-selectin in neutrophils also leads to expression of TNF-α (185). It is therefore possible that L-selectin induction of TNF-α expression in leukocytes involves the activation of NF-κB (Figure 1.8, 4).

Studies using T-cells have also been undertaken to gain insight into signalling pathways activated upon L-selectin stimulation. The most clearly defined pathway involves the tyrosine kinase p56lck, which is activated upon L-selectin cross-linking (197,198). It has been shown, following the activation of p56lck, that the Growth factor receptor-bound protein (Grb)/Son of sevenless (Sos) complex becomes associated with L-selectin (197) and this in turn leads to the activation of the Ras-MAPK signalling pathway (197). Through the activation of this pathway superoxide generation (197) and cytoskeletal reorganisation (shown by a tenfold increase in actin polymerisation) both occur (Figure 1.8, 7) (199). Activation of p56lck is also involved in the activation of JNK via the Rac proteins (Figure 1.8, 8) (200), though the function of this kinase in L-selectin signalling remains unclear. L-selectin stimulation causes the translocation of the transcription factor family nuclear factor of activated T-cells (NFAT) (201). The Ras-MAPK pathway has been implicated in this process (201). The role of NFAT in L-selectin signalling is still being investigated, though it has been shown that L-selectin regulation of the cytokine colony-stimulating-factor-1 (CSF-1) expression is controlled through the translocation of NFAT (Figure 1.8, 6) (202). L-selectin stimulation also leads to the increase in sphingomyelinase activity, which in turn leads to a release in ceramide (Figure 1.8, 5) (203). Ceramide is a secondary

messenger shown to modulate inflammatory responses by mediating TNF-α and IL-1 activity (204) (205). Ceramide is also capable of stimulating the transcription factors c-Myc and NF-κB (206,207), and thus may play a role in activating the adherent cell. The signalling pathway behind the sphingomyelinase activity remains unclear, though it is known that tyrosine kinase signalling is not involved (203).

L-selectin signalling plays a role in chemokine signalling in lymphocytes. Ligation of L-selectin through antibody cross-linking and engagement of the ligands fucoidin and sulphatide has been shown to increase the surface expression of the chemokine receptor CXCR4 in T-cells (208) and natural killer (NK) cells (209). Analysis revealed that the increase in surface expression of this receptor was due to the mobilisation of internal stores of CXCR4 to the plasma membrane (Figure 1.8, 1) (208,209). It was also revealed that L-selectin ligation inhibited stromal cell-derived factor-1 (SDF-1) induction of the internalisation of CXCR4 (208), further increasing the surface levels of the receptor and its potential responsiveness to the chemokine. The higher levels of CXCR4 results in an increase in the adhesion and TEM of lymphocytes (208). Further evidence of the role of L-selectin in chemokine signalling was demonstrated by the fact that L-selectin ligation enhances the chemotaxis of murine T- and B-cells in response to the chemokine CCL21 (210). However, the mechanism behind this enhancement remains elusive, with results showing it is not a result of an increase in the expression levels of the receptor for the chemokine (CCR7), though the PKCs, MAPKs and the Syk family of kinases have been implicated in the chemotaxis mechanism (210).

The examples above show the many different signalling roles of L-selectin, however, the molecular mechanisms of these processes remain elusive and more research is required to unearth the details of these pathways. Previous work by the Ivetic group has shown that, despite its short size, the cytoplasmic tail of L-selectin can accommodate both CaM and ERM in resting cells (3). This trimeric assembly is thought to play an important role in mediating signal transduction. Section 1.6 will discuss what is known about the formation of this complex, with the role of each individual protein in L-selectin function described in Sections 1.3.7.3 and 1.3.7.4.
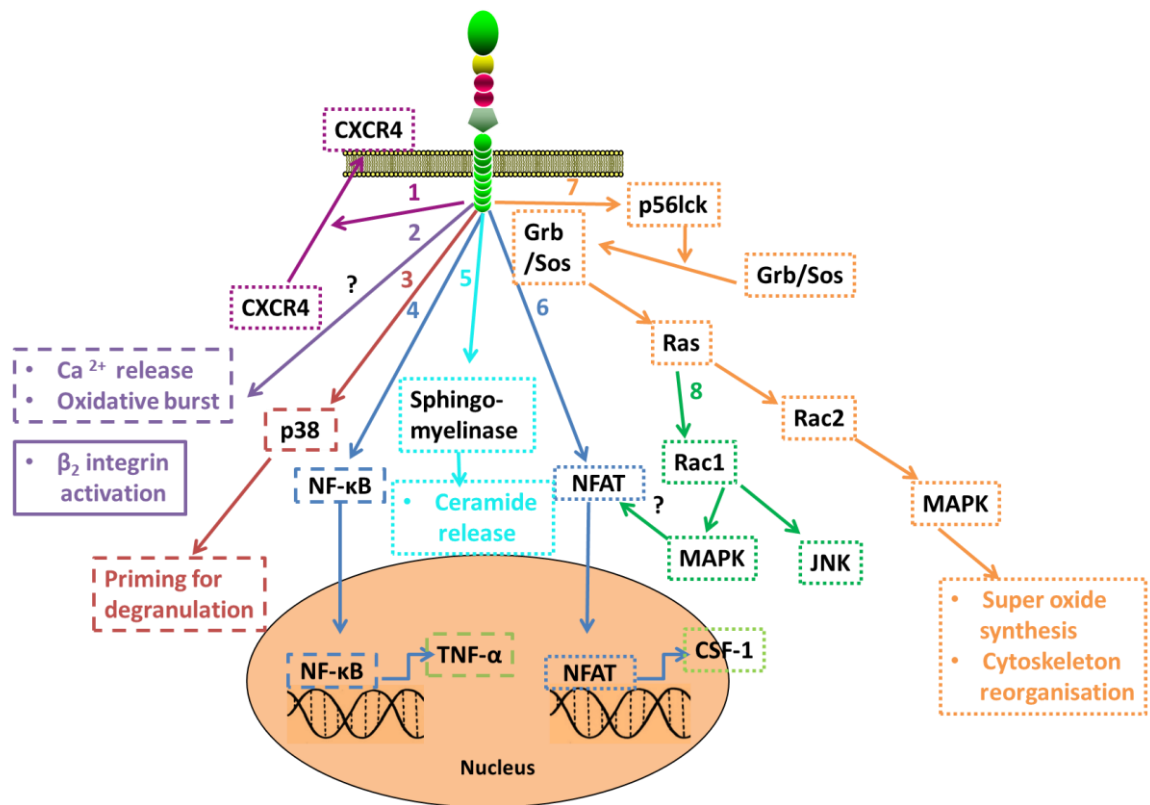
**Figure 1.8: Signalling pathways induced by L-selectin stimulation.** A depiction of signalling pathways shown to be initiated upon L-selectin ligation. Pathways found in lymphocytes are indicated by a dotted boarder, those studied in neutrophils is highlighted by a dashed boarder and those in both are shown with a solid line. Numbers indicate the different pathways and are referred to in the text where the specific pathway is described. Where the components of the pathway are unknown a "?" is used.

## 1.3.7 L-selectin binding partners

The cytosolic tails of E-, P- and L-selectin are the most divergent sub-domains, suggesting they may play unique roles in downstream signalling events. The tail of L-selectin is composed of seventeen amino acids, with many basic residues (Figure 1.9). It has been reported that the tail is able to interact with several proteins, including α-actinin, Calmodulin (CaM), the ezrin-radixin-moesin (ERM) family of cytoskeletal proteins (211,212) and PKC isozymes. In the following sections, each binding partner will be discussed individually in the context of how it might be involved in regulating L-selectin function. As this thesis will focus on the interaction between L-selectin, CaM and moesin, these binding partners will be discussed in more detail in Sections 1.4 and 1.5, with an emphasis on structure and binding mechanisms.
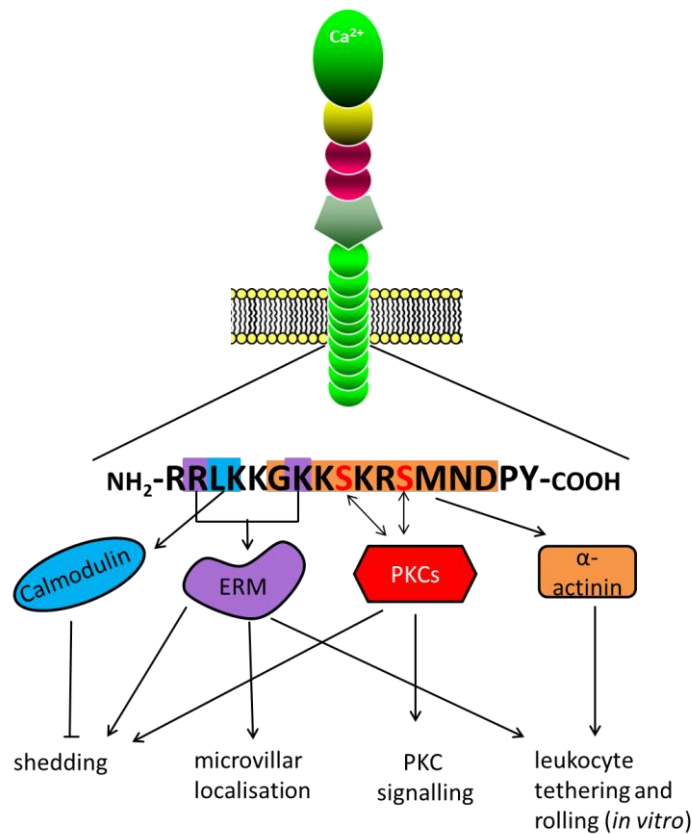
**Figure 1.9: Cytosolic tail of L-selectin.** The seventeen amino acids that constitute the cytosolic tail of L-selectin are shown. Residues involved in the interaction with the different L-selectin binding proteins are highlighted, with residues important for CaM binding shown in blue, for ERMs shown in purple and α-actinin in red. The major functions of the interaction between L-selectin and the proteins is shown, with CaM inhibiting L-selectin shedding, ERMs controlling localisation of L-selectin as well as having a role in shedding and tethering and α-actinin shown to control leukocyte tethering *in vitro*. PKC isozymes are capable of phosphorylating and interacting with the two serine residues within the cytosolic tail of L-selectin. PKC interaction/phosphorylation of L-selectin has been implicated in shedding of L-selectin and activation of signalling pathways.

### *1.3.7.1 α-actinin*

Studies have shown that α-actinin interacts with the last 11 amino acids of the cytosolic tail of L-selectin (213). Using the pre-B cell line 300.19, transfected with either full length or a truncated form of L-selectin lacking the last 11 residues of the cytosolic tail (213), it was shown through immunoprecipitation that α-actinin was co-precipitated with full length but not the truncated form of L-selectin (213). When α-actinin is not able to bind to L-selectin, reduced tethering and rolling were observed. α-actinin is an actin-binding protein, so may be involved in connecting L-selectin to the cytoskeleton, which could be important for tethering and rolling (211,212). It is worth noting, however, that truncation of the last 11 amino acids of the L-selectin cytosolic tail may affect the interaction of the other binding partners. It is therefore possible

that the tethering defect observed with the truncated form of L-selectin is due to other L-selectin binding partners not interacting. By narrowing down the residues required for α-actinin binding specifically, the role of the interaction between this protein and L-selectin can be fully investigated.

### 1.3.7.2 PKC Isozymes

Following the observation that the cytosolic tail of L-selectin was phosphorylated upon activation of the cell, Kilian *et al* (2004)(214) investigated which protein kinases were capable of interacting with and phosphorylating L-selectin. Using Glutathione S-transferase (GST)-tagged L-selectin cytosolic tail peptides to pull-down proteins from T cell lysates it was revealed that PKCs co-precipitated with the L-selectin peptide and exhibited kinase activity. Analysis of which PKC isozymes were capable of interacting with L-selectin was undertaken by Western blot with isozymes specific antibodies. It was determined that PKCθ and PKCι interacted with L-selectin and were responsible for its phosphorylation (Figure 1.10) (214). Using serine to alanine mutated peptides, it was shown that these PKC isozymes were capable of phosphorylating both S364 and S367, however, there was a preference for phosphorylating S364 (214). Kilian *et al* (2004) further investigated whether phosphorylation of the L-selectin tail affected its ability to bind to PKCs, with the results showing that PKCθ binding was enhanced after phosphorylation and PKCα binding was induced (Figure 1.10) (214). It is therefore possible that phosphorylation of L-selectin by PKCs activates other PKC signalling pathways.

### 1.3.7.3 Calmodulin (CaM)

Several studies have shown that CaM is able to interact with the L-selectin cytosolic tail (215,216). Kahn et al (1998)(215) investigated the role of CaM binding to L-selectin using several CaM inhibitors, such as calmidazolium and trifluoperazine. They showed that L-selectin-dependent adhesion of lymphocytes to HEVs was disrupted in the presence of the inhibitors (215). It was determined that the disruption of adhesion was due to the down-regulation of L-selectin from the surface of lymphocytes and that this cleavage of L-selectin was caused by metalloproteases, as shown by the co-treatment of cells with metalloprotease inhibitors blocking the down-regulation (215). This has led to the hypothesis that CaM binding prevents the cleavage

of L-selectin (211). However, how this is achieved remains unclear. A possible mechanism of regulation is phosphorylation of serine residues located in the cytosolic tail of L-selectin (Figure 1.10), a theory that is investigated in this thesis. Interestingly, CaM has been shown to bind to several different transmembrane domains and protect them from extracellular cleavage. Examples include PECAM-1 (217), ACE2 (218), GPIb-IX-V (219,220), GPVI (221) and TIM-2 (222), clearly highlighting a role for CaM in regulating transmembrane protein shedding.
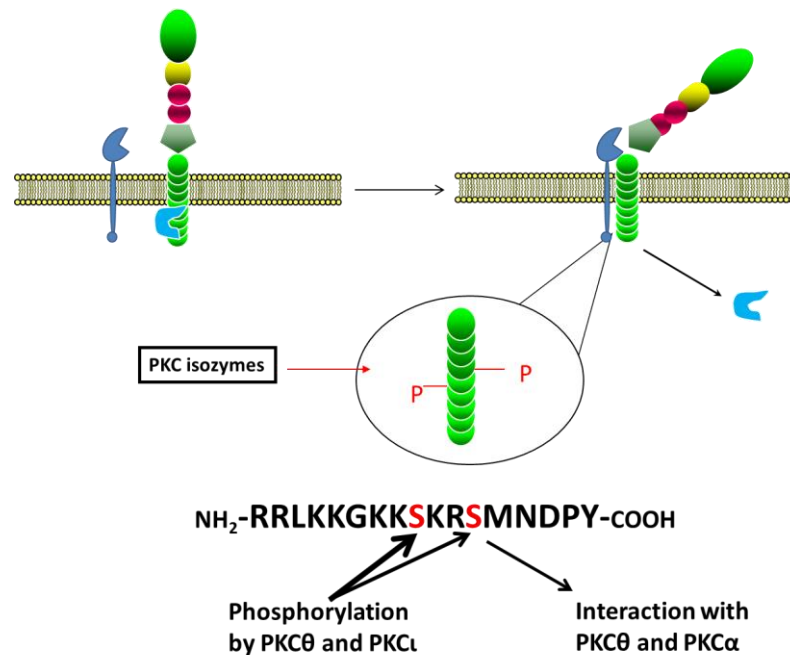


**Figure 1.10: Hypothesis of CaM regulation of L-selectin shedding.** In resting cells CaM interacts with L-selectin and protects it from shedding. Upon cell activation CaM dissociation occurs and L-selectin is cleaved by ADAM17 at the extracellular cleavage site. A possible mechanism of CaM dissociation is phosphorylation of serine residues within the cytosolic tail of L-selectin by PKC isozymes, which have been shown to be activated upon leukocyte activation. The PKC isozymes θ and ι are able to phosphorylate the serine residues in the tail, with a preference for S364 (shown by the thicker arrow). Phosphorylation of the tail also leads to the binding of PKCα and PKCθ.

An interesting study undertaken by Deng *et al* (2011)(216) investigated the interaction between L-selectin and CaM in the presence of a lipid bilayer to identify the role of the plasma membrane in regulating the interaction. To carry out these experiments a peptide consisting of L-selectin transmembrane and cytosolic domains was synthesised and inserted into liposomes containing different phospholipid species. It was revealed that the cytosolic tail of L-selectin was in closer proximity to the surface of the membrane when the negatively charged phospholipid

phosphatidylserine (PS) was present (216), presumably due to electrostatic interactions between positive amino acids in the tail and the negative charge of PS. This interaction was shown to block CaM association with the L-selectin cytosolic tail (Figure 1.11A) (216). Further investigation showed that ERM binding desorbs the L-selectin cytosolic tail from the lipid bilayer and allows CaM to bind (Figure 1.11B, described in detail in Section 1.6) (223). It would be interesting to determine if this also occurred with intact cells as it could be a possible method of regulation.
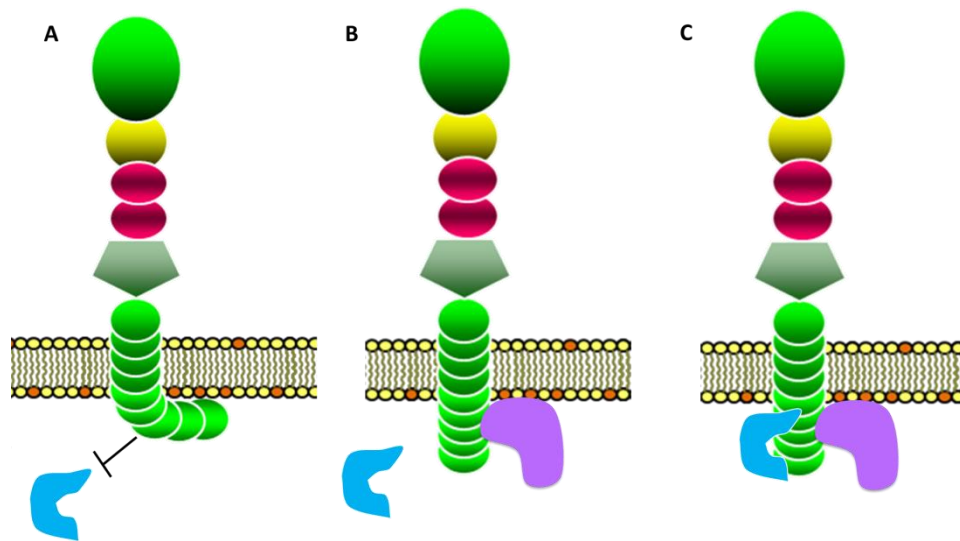


**Figure 1.11: The cytosolic tail of L-selectin interacts with phosphatidyl serine (PS) in the plasma membrane.** A study has shown that when PS is present in the plasma membrane the cytosolic tail of L-selectin interacts with the plasma membrane (A) through electrostatic interactions between negatively charged PS and positively charged amino acids in the tail. This interaction inhibits CaM binding to the tail. The FERM domain of ERMs is able to interact with the cytosolic tail of L-selectin and desorb it from the plasma membrane (B). This in turn allows CaM to bind (C).

### *1.3.7.4 ERM Proteins*

Previous work in the Ivetic lab showed that moesin is able to interact with the tail of L-selectin, although the nature of this interaction was not defined. Affinity chromatography, using an L-selectin cytosolic tail peptide conjugated to sepharose, revealed moesin and ezrin were purified from lymphocyte extracts (224). The N-terminal domain of the protein was found to be required for this interaction (224). The interaction between moesin and L-selectin was also studied in phospholipid-containing liposomes to assess the effect of the presence of the lipid bilayer on the interaction (223). Analysis revealed that moesin and L-selectin were capable of interacting when L-

selectin was embedded into the liposomes (223). Studies have shown that residues R357 and K362 within the L-selectin tail are involved in the interaction with the FERM domain of moesin (211,225). Mutation of these amino acids in pre-B cells causes a reduction in microvillar localisation and tethering efficiency (225).

## 1.4 CaM form and function

CaM is a calcium binding protein, which acts as a cytosolic calcium receptor. It binds four calcium ions in response to extracellular signals, causing a conformational change and enables calcium bound CaM (CaM-Ca) to bind and activate its target proteins by causing further conformational changes in the target (226).

### 1.4.1 Structure of CaM

The structure of CaM with and without $Ca^{2+}$ has been solved by NMR and X-ray crystallography (227-229). The crystal structure of CaM-Ca reveals a dumbbell shaped molecule, approximately 65Å in length (Figure 1.12A) (226). The N- and C-terminal domains are globular lobes made up of two EF hands, each of which is able to bind one calcium ion. The two globular domains are separated by an eight turn α-helix (226). NMR structures showed that the central helix is highly flexible and that the tumbling of the two lobes is effectively independent of one another (230). Structural studies of the calcium free CaM (ApoCaM) showed a more compact structure compared with the Ca-bound form, with a loss of the central helix (Figure 1.12B). In agreement with this CD spectroscopy showed that calcium binding causes CaM to become more helical (231). Structural rearrangements upon calcium binding causes hydrophobic surfaces on the globular domains to form on the surface and allow it to bind to target proteins (226). The exposure of these hydrophobic groups results in a release of energy, which can be transduced as a change in affinity for the CaM effector and/or an alteration in effector function (232).

NMR and several spectroscopy methods have been used to elucidate the changes to CaM upon calcium binding. These studies determined that there is a two-step conformational change observed and this shows that the binding domains have different affinities for calcium, with the C-lobe EF hands having a three-fivefold higher affinity for calcium compared to the N-lobe (232,233). Analysis has also revealed that

target protein binding also affects the affinity of calcium, with the $K_D$ for $Ca^{2+}$ increasing in the presence of target peptides (226).

## 1.4.2 CaM-Binding Proteins

CaM is able to bind to and regulate the activity of many different proteins. Studies of several CaM-binding proteins have shown that the CaM-binding domain is made up of fourteen to twenty six residues that are able to form a basic amphiphilic α-helix. Interestingly, there is no consensus sequence to which CaM binds. Instead, varying motifs exist with several hydrophobic anchor residues which are embedded into the hydrophobic pockets of CaM-Ca (234). The nature of the binding motif is based on the spacing of the hydrophobic anchor residues (Table 1.3), with the spacing dictating the compaction of the structure of the complex. Many different spacings of the hydrophobic anchors can be accommodated due to the flexibility of the linker between the two lobes of CaM-Ca (234).

The canonical mechanism of CaM binding is highly conserved: both globular domains interact with the target peptide and end up in close proximity to each other, with the central helix being disrupted, forming a hydrophobic channel which is occupied by the helical target peptide. An example of this recognition mechanism is shown in Figure 1.12C. Analysis of the interactions in the complex showed that the binding is mainly driven by hydrophobic interactions with some salt bridges also contributing to complex formation (226). Several protein kinases, phosphatases and secondary messenger generators have been shown to interact with CaM in this manner, including CaMKII, MLCKs (235), calcineurin (236), $Ca^{2+}$-ATPase (237) and NO synthase (238) (though different spacings of the hydrophobic anchors are observed). CaM acts as a calcium sensor to activate these proteins. In the absence of $Ca^{2+}$ the target proteins are unable to bind to their substrates as the binding site is blocked by an inhibitory domain. An influx of $Ca^{2+}$ will lead to CaM-Ca interacting with the target protein and a conformational change is induced, which relieves the auto-inhibition and promotes activation (226). Phosphorylation has been shown to be important in switching off the target protein again. Many kinases are able to phosphorylate residues in the CaM-binding site and reduce the affinity of CaM for the site and inhibit activation of the target protein.
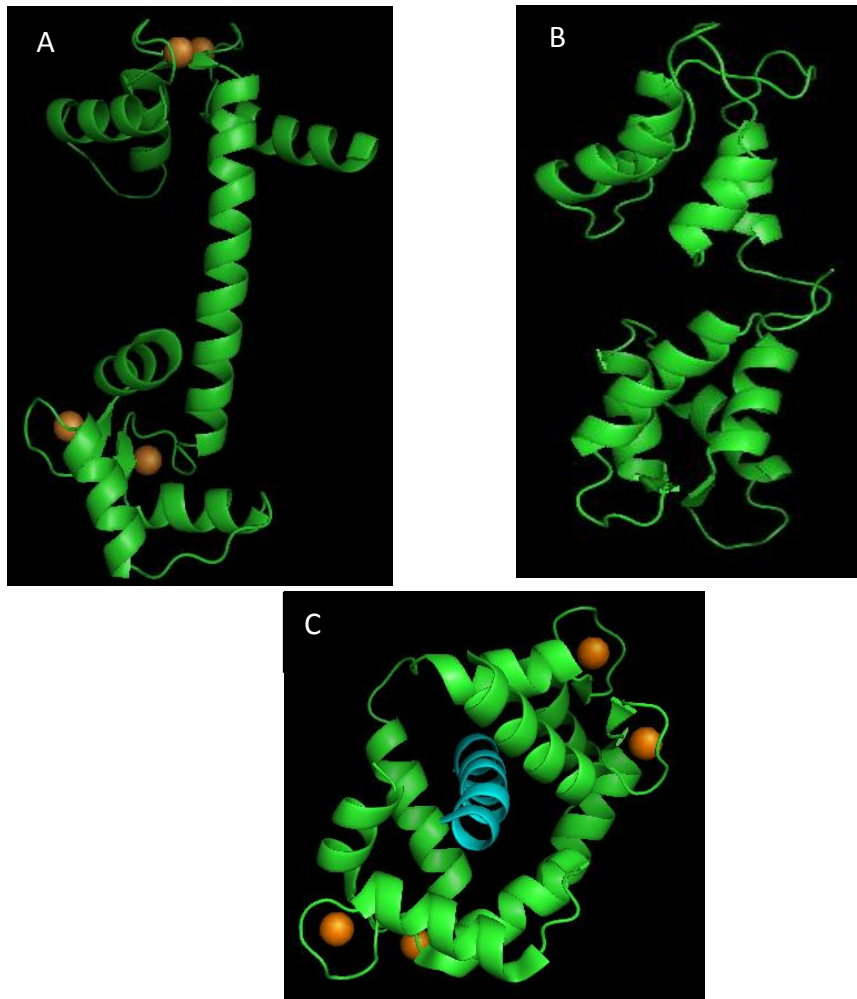
**Figure 1.12: Structure of CaM.** (A) The X-ray structure of calcium bound CaM, calcium ions shown in orange. (B) The structure of Apo-CaM. (C) An example of the canonical binding method of CaM, with both lobes wrapped around the binding peptide (shown in cyan) (in this case MLCK). Structures are downloaded from the Protein Data Bank (PDB) (A id is 3CLN, B id is 1CFC and C id is 2LV6).

Variations of this canonical binding mechanism have been observed, involving an extended conformation of CaM. The crystal structure of CaM-Ca bound to calcineurin showed that CaM was in an extended conformation of 63 Å. Interestingly, it also showed that the complex was formed in a 2:2 manner, with two CaM molecules associating head to tail with each peptide bound between the N-terminal domain of one molecule and the C-terminal of the other (236). Munc13-1 was also shown to interact with extended CaM, but in this case with a 1:1 stoichiometry: here an amphiphilic helix of munc13-1 interacts with the C-terminal domain of CaM and a tryptophan residue is embedded in the hydrophobic cleft of the N-terminal domain, rather than the peptide sitting in a channel (239). Other examples of CaM binding in an

extended conformation include Bacillus anthracis edema factor (240), small-conductance $Ca^{2+}$-activated $K^+$ channel (241) and NaV1.5 (shown in Figure 1.13) (242).
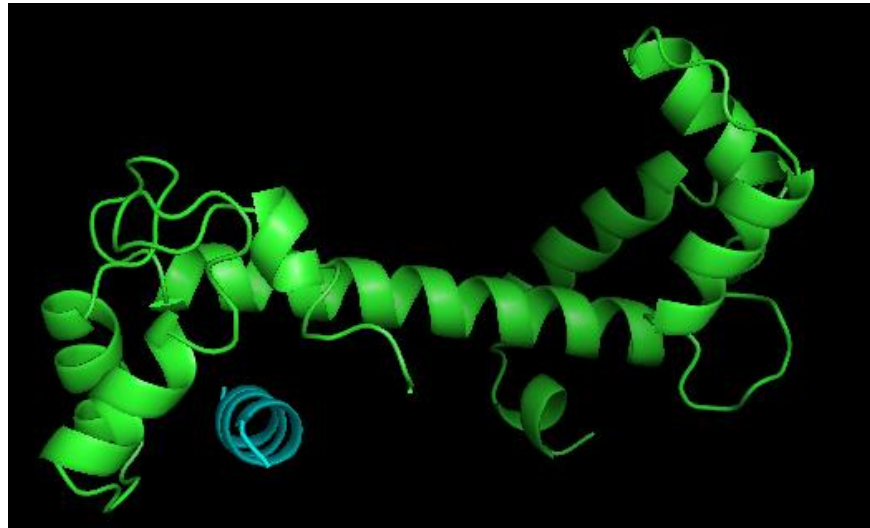


**Figure 1.13: Non-canonical binding mode of CaM.** An example of CaM binding to a target protein in a non-canonical mode. The example shown is CaM-Ca binding to a NaV1.5 peptide (shown in cyan), with the C-lobe of CaM-Ca on the left. In this example, only the C-lobe of CaM-Ca interacts with the target peptide. PDB id 4DJC.

It has been observed that CaM is also able to bind proteins in the absence of calcium, but this interaction is sensitive to $Ca^{2+}$ concentration. One example of this is neuromodulin, which binds CaM with a higher affinity in the absence of $Ca^{2+}$ and dissociates in the presence of $Ca^{2+}$ (232). It is suggested that neuromodulin acts as a CaM-trap which releases CaM into the cytosol when the $Ca^{2+}$ concentration increases (243), though further investigation is required to confirm this. There are many examples of different CaM binding mechanisms that highlight the plasticity of CaM function, allowing it to regulate a vast array of proteins.

CaM is capable of interacting with the FERM domain of several proteins. The FERM domain of erythrocyte protein band 4.1R was shown to interact with CaM (244), having two CaM binding domains, one calcium-independent and one calcium-sensitive and that binding to both sites is required for regulation of 4.1R binding to its membrane protein targets (245). The kinase CAKβ contains a FERM domain which inhibits the kinase activity. CaM has been shown to bind the FERM domain and requires calcium for the interaction. The site of interaction was shown to be an α-helix present in the F2 lobe of the FERM domain. Binding of CaM-Ca causes activation of the

kinase domain by promoting the formation of a CAKβ homodimer, which leads to trans-phosphorylation of CAKβ (245). Sequence alignment of the FERM domain of 4.1R with ERM proteins showed that the CaM binding sequence was not highly conserved, so it was thought that CaM would not be able to bind to ERMs (245). However, comparing the structures of the proteins show this site is structurally conserved, so CaM could interact with the ERM proteins, which was shown to be true and will be discussed later in Section 1.6.

| CaM Binding Motif Spacing | Example of Binding Partner | Reference |
|---|---|---|
| 1-14 | Myosin light chain kinase | (246,247) |
| 1-5-10 | CaM-dependent protein kinase II | (248) |
| 1-10-16 | CaM-dependent protein kinase | (249) |
| 1-(10)-14 | Death-associated protein kinase-1 | (234) |
| 1-(8)-14 | Olfactory CNG channel 2 | (250) |
| | Alpha-II spectrin | (251) |
| 1-7-10 | Calcineurin A1 | (252) |
| | NMDA receptor | (253) |
| 1-5-11 | TNF receptor 16 | (234) |
| 1-18 | Plasma membrane $Ca^{2+}$-ATPase | (254) |
| 1-10 | CaV1.1 | (255) |
| | TNF receptor 6 | (234) |
| | TRPV1 | (256) |
| 1-17 | Ryanodine receptor 1 | (257) |
| 1-(5)-10 | CaV1.2 | (258) |
| | CaV2.1 | (234) |
| | CaV2.3 | (234) |

**Table 1.3 CaM binding motifs for the canonical binding method.** A list different CaM binding motifs for the canonical binding method of CaM, where both lobes of CaM-Ca interact with the binding target. The motifs are defined by the spacings of the hydrophobic residues within the motif. Examples of proteins with the specified binding motif spacing are listed.

## 1.5 ERM proteins – form and function

The ERM family of proteins has three members: <u>e</u>zrin, <u>r</u>adixin and <u>m</u>oesin. All ERMs are structurally similar and have redundant and non-redundant functions. They are composed of three domains, an N-terminal FERM domain, an extended alpha-helical domain and a charged C-terminal domain. The FERM domain is responsible for interactions with proteins the plasma membrane. The C-terminal domain binds F-actin, enabling ERMs to link the cytoskeleton with the plasma membrane (259,260). This means that ERMs play a crucial role in regulating alterations in shape, which often involve changes in the plasma membrane protrusions and the underlying actin-based cytoskeleton, as discussed later (Section 1.5.3).

## 1.5.1 Structure and Regulation of ERMs

ERMs transition between active and inactive states. The FERM domain interacts with the C-terminal domain, which adopts an auto-inhibited conformation and renders the molecule inactive (Figure 1.14A). Phosphorylation of a conserved threonine residue in the C-terminal domain, T558 in the case of moesin, disrupts this interaction and activates the protein (Figure 1.14B and C) (1,259,261). Many different kinases have been suggested to be responsible for the phosphorylation, including Rho kinase (262), PKC$\alpha$ and PKC$\theta$ (1,263). It is thought that these kinases may act in a cell-type and stimulus-specific manner. The FERM domain is capable of binding phosphatidylinositol bisphosphate (PIP$_2$) in the plasma membrane and this binding has also been implicated in playing a role in activating ERMs (264). PIP$_2$ binding between the F1 and F3 lobes is thought to induce a conformational change that renders the threonine residue more accessible for phosphorylation, which will inhibit the C-terminal domain from re-binding to the FERM domain, allowing both terminal domains to bind to their target partners (1).

The FERM domains of the three ERM proteins share around 75% identity and are thought to be isoforms with both redundant and non-redundant functions (259). This was thought to be the case as moesin knockout mice had no discernable phenotype (265), possibly due to the other ERMs compensating for the loss (259). However, it is worth noting that the expression profile of ERM differs in different cell types, for example ezrin is abundantly expressed in epithelial cells. This means that,

although the ERMs do have redundant functions, they may possess tissue specific expression, in which case they play non-redundant roles in specific cell types. This is evident in ezrin knockout mice, where intestinal villi formation is impaired due to the lack of ezrin in intestinal epithelial cells, with these mice not able to survive past weaning (266), with a similar defect in microvilli formation on retina cells also observed when ezrin was lacking (267). Moesin has also been shown to be essential for lung alveolar structure preservation following lung injury (268) and for efficient B- and T-cell egression from the primary lymph organs (269).

The crystal structure of the FERM domain has been solved for all three members and has shown they are all very similar (259,270). The F1 domain is made up of a five-stranded mixed β-sheet packed against an α-helix with a short linker helix between β-strand 3; a structure resembling ubiquitin. F2 contains five α-helices with a long loop and short α-helix between B and C and this lobe resembles acyl CoA-binding protein. The F3 lobe is a sandwich of two orthogonal antiparallel β-sheets connected by a loop containing small helix, followed by a long helix. This is a phosphotyrosine-binding (PTB)-like domain (259,270).

The crystal structure of inactive moesin has been solved, confirming the site of the interaction between the FERM and the C-terminal domains (Figure 1.14A) (259,270). The data showed that the C-terminal domain is made up of a β-strand and four α-helices that adopt an extended structure which binds to the FERM domain covering a large surface of the F2 and F3 lobes (as shown in Figure 1.14A), which is the area responsible for binding to the cytoplasmic tails of cell adhesion molecules (see later) (259,270). Multiple contact sites form between the FERM and C-terminal domains, which collectively strengthen the auto-inhibited interaction (259,261). The threonine, which regulates the auto-inhibition, is located on the helix C of the C-terminal domain and is in contact with the FERM domain. This means that phosphorylation of this residue will likely disrupt the interaction due to steric clashes as well as electrostatic effects (259,270). Crystal structures also show that the α-helical linker (shown in yellow in Figure 1.14) between the FERM and C-terminal domains sits between the F1 and F3 lobes. This has been shown to be the site occupied by $PIP_2$. This means that $PIP_2$ may be able to displace the linker, which may cause the conformational change required for phosphorylation of the C-terminal domain threonine (270).
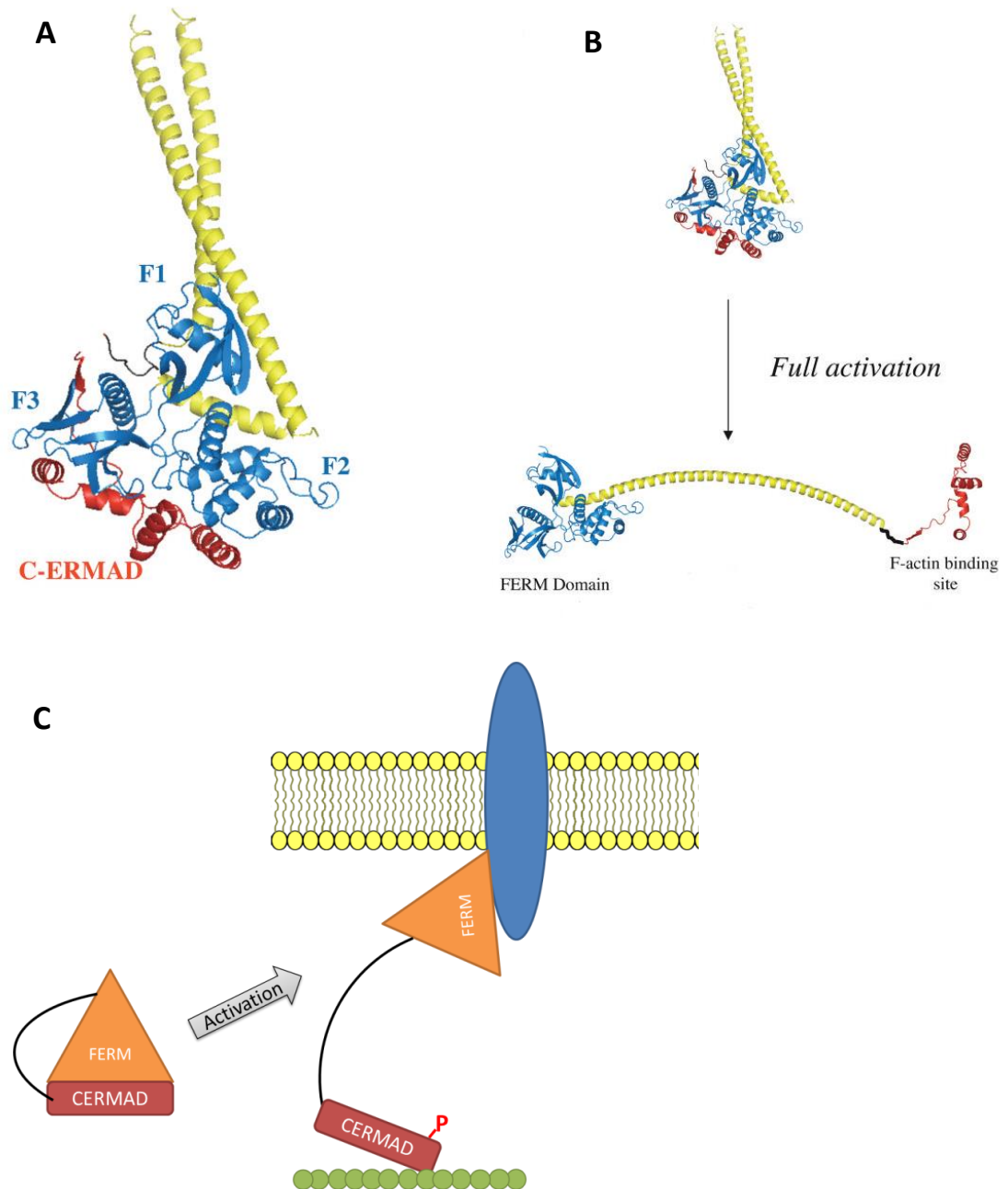
**Figure 1.14: Structure of ERMs.** (A) Shows the crystal structure the inactive structure of ERMs, with the C-terminal domain (also referred to as COOH-ERM associated domain (CERMAD)) (red) bound to the FERM domain (blue). (B) The structural change that occurs upon activation of ERMs, with the bottom diagram showing the extended active protein structure. Images are taken from Fehon, R. G., McClatchey, A. I., and Bretscher, A. (2010) Organizing the cell cortex: the role of ERM proteins. *Nat Rev Mol Cell Biol* **11**, 276-287 (1).(C) Depicts the activation mechanism of ERM proteins. Upon activation, the C-terminal domain is phosphorylated (shown by the red P), causing dissociation of the two domains. This allows the FERM domain to interact with plasma membrane associated proteins (shown in blue) and the C-terminal domain to interact with actin filaments (shown in green).

## 1.5.2 ERM-binding proteins

Many proteins have been shown to bind to the FERM domain of ERM proteins. Many of these have been observed to be transmembrane proteins, with the FERM domain interacting with their cytosolic tails. L-selectin (see later), CD44 (271), CD43 (272), ICAM-1, ICAM-2 (273) ICAM-3, and PSGL-1 (274) are all examples of this. The crystal structures of the FERM domain of radixin in complex with the cytosolic tails of ICAM-2, CD44 and PSGL-1 have all been solved. They showed that all three peptides bind at the same site, namely the groove between the β-sheet and the α-helix of F3 (271,273,274). This provides us with a possible site for the interaction between FERM domain and the tail of L-selectin. Interestingly, analysis of the function of ERM interaction with CD43 (272) and PSGL-1 (275,276) showed the interaction was required for normal tethering, rolling and trafficking of leukocytes, similarly to observations made with L-selectin and ERMs (Section 1.3.7.4).

Other non-transmembrane proteins have also been shown to interact with ERMs FERM domain. The protein ERM binding protein 50 (EBP50) (which acts as a linker between ERMs and membrane proteins) (277), and protein kinases such as sodium-hydrogen exchanger 3 (NHE3) kinase A have been shown to interact with ERMs. Studies have revealed that ERMs are able to interact with proteins that control the Rho GTPase pathway, such as several guanidine nucleotide exchange factors (GEFs) (278) and GDP dissociation inhibitors (GDIs) (279), though analysis has found both an activating and inhibiting role of ERMs in this signalling pathway, suggesting the relationship is very complex and is reviewed elsewhere (280). Briefly, ERM proteins interact with RhoGDI and sequester it away from interacting with RhoGTPases, leading to their activation (280). Dbl is a RhoGEF which has been shown to interact with ezrin, facilitating the activation of the Rho family member Cdc42 (281). ERMs also interact with Sos, a GEF that activates members of the Ras family of small GTPases, implicating ERMs in activating Ras signalling pathways (282).

## 1.5.3 Role of ERMs in Leukocyte Function

Studies have been undertaken to understand the role of ERM proteins in leukocyte function. ERM-deficient lymphocytes show defects in homing to lymphoid organs (283), with a decrease in resident B- and T-cells in the lymph nodes (269). Analysis suggests this is due to impairment in the egression of T-cells from the thymus

and B-cells from bone marrow (269). The role of L-selectin in lymphocyte recirculation is well established (see Section 1.7.1) and it is therefore possible that this requires the interaction with ERMs. Studies have also been carried out with constitutively active ezrin, which has been mutated to mimic phosphorylation of the threonine residue required for activation of the protein. These results also showed a reduction in the number of T-cells in the lymph nodes (284). This was accompanied with a reduction in T cell shape change in response to cytokines and reduced migration (284). This shows that dephosphorylation of ezrin is required for migration of leukocytes. This is likely due to the fact that dephosphorylation of ERMs has been shown to precede the retraction of trailing uropods (285), so by blocking ezrin dephosphorylation the uropod cannot retract and migration is impaired.

## 1.6 The L-selectin/ERM/CaM Complex

Following the discovery that L-selectin was capable of binding to CaM and ERM proteins, it was of interest to decipher whether both proteins were capable of interacting with L-selectin simultaneously. Deng *et al* (2013)(223) showed in two separate reports that CaM and moesin were capable of interacting with a peptide representing the cytosolic tail of L-selectin ((216) and (223) respectively). As explained in Section 1.3.7.3 they also found that CaM could not interact with L-selectin when it was embedded in liposomes containing PS. Deng *et al* (2013) revealed that the moesin FERM domain (moesin-FERM) was able to interact with L-selectin embedded in liposomes even in the presence of PS and that this interaction increases the distance between the lipid bilayer and the L-selectin cytosolic tail (223). It was then shown that this desorption allowed CaM to bind and therefore moesin-FERM binding to L-selectin primed it for CaM binding (223).

The trimeric complex was also studied using L-selectin cytosolic peptide attached to sepharose, preloaded with one of the proteins and results revealed the other was still able to bind (3). Further study in COS7 cells revealed that FRET was observed between CaM-RFP and ezrin FERM-GFP upon clustering of L-selectin (3). This led to molecular modelling of the complex, depicted in Figure 1.14 (taken from (3)), showing all three were capable of interacting with one another, with CaM and moesin-FERM contacting specific residues within the cytosolic tail of L-selectin. The model also

predicted that significant contacts between CaM and moesin-FERM were present, independently of L-selectin, which was confirmed biochemically (3). Interestingly, the site of interaction predicted between CaM and moesin shows similarities with the site of interaction between CaM and band 4.1R, namely CaM forming contacts with α-helix one of F3 in the FERM domain of both moesin (3) and band 4.1R (245). The predicted binding site for L-selectin within the moesin-FERM structure was very similar to the binding site for the other transmembrane proteins shown to bind to ERM family members, as described in Section 1.5.2. This shows that the model of the predicted structure of the tertiary complex provides a good representation of the possible interaction; however, further experiments are required to prove that the predicted interactions occur.

Killock *et al* (2009) postulated that the formation of the complex is likely to be important for controlling L-selectin-dependent signalling. The importance of the individual binding partners in regulating L-selectin function is highlighted above. It is possible that CaM and moesin interact with other proteins as well as L-selectin and therefore lead to the activation of signalling pathways. Intriguingly, as stated above, ERMs are able to bind to the Ras activator Sos. As explained in Section 1.3.6, L-selectin activation has been shown to activate the Ras-MAPK signalling pathway. It is therefore possible that ligand binding of L-selectin promotes the formation of a complex with ERM and Sos to activate Ras. This hypothesis becomes more appealing as CaM is able to bind to K-Ras (286) and it is therefore plausible that activation of L-selectin leads to the formation of the L-selectin/CaM/ERM complex and enables the activation of Ras by bringing Sos and K-Ras into close proximity.
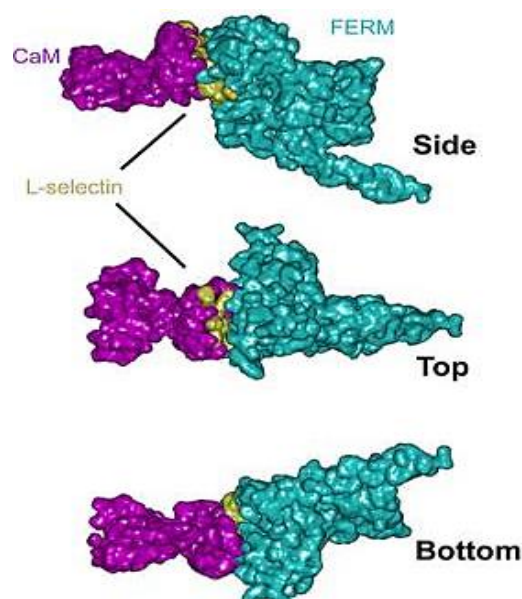
**Figure 1.15: Model of the tertiary complex between L-selectin, CaM and the FERM domain of moesin.** A computer generated model predicting the possible complex of L-selectin (yellow), CaM (purple) and moesin-FERM (cyan). The image is taken from Killock, D. J., Parsons, M., Zarrouk, M., Ameer-Beg, S. M., Ridley, A. J., Haskard, D. O., Zvelebil, M., and Ivetic, A. (2009) In Vitro and in Vivo Characterization of Molecular Interactions between Calmodulin, Ezrin/Radixin/Moesin, and L-selectin. *Journal of Biological Chemistry* **284**, 8833-8845 (3).

## 1.7 L-selectin-dependent trafficking

### 1.7.1 The role of L-selectin in Lymphocyte Recirculation

L-selectin is exclusively responsible for the recirculation of T- and B-cells through secondary lymphoid organs. Naïve lymphocytes are produced in the primary lymphatic organs (i.e. the thymus and bone marrow) (287). The cells then circulate through the blood and home to secondary lymphoid organs to patrol specific zones for antigen (287). For the cells to exit the bloodstream and enter the lymphoid organs requires the interaction between lymphocytes and specialised post-capillary HEVs (287). Studies using L-selectin function blocking antibodies have shown that when L-selectin adhesion is inhibited, the interaction between lymphocytes and HEVs is blocked and lymphocyte migration does not occur (31). *In vitro* analysis revealed that lymphocytes lacking L-selectin were not able to bind HEVs (24). The role of L-selectin in the accumulation of lymphocytes in lymph nodes was assessed *in vivo* by comparing L-selectin deficient and wildtype mice. Results showed that the number of lymphocytes in the peripheral lymph nodes was decreased by 99 % in mice lacking L-selectin (24). L-selectin knockout mice also present decreased lymphocyte trafficking to mesenteric lymph nodes (88 %) and Payer's Patches (50 %) (24). Taken together, these results clearly show the importance of L-selectin in lymphocyte homing.

### 1.7.2 The role of L-selectin in the Recruitment of Leukocytes during the Inflammatory Response

*In vivo* experiments using L-selectin function-blocking antibodies showed a reduction in neutrophil recruitment to peritoneum (288), skin (289) and lung (290) after the induction of inflammation. The role of L-selectin in migration of leukocytes during inflammation was further confirmed in L-selectin knockout mice, with a marked

reduction in the accumulation of neutrophils (56-62%), macrophages (72-78%) and lymphocytes (70-75%) in inflamed peritoneum relative to wildtype mice (24,291). The role of L-selectin in TEM following inflammatory stimuli has been assessed in post capillary venules in the cremaster muscle of mice superfused with the inflammatory mediators platelet-activating factor and keratinocyte-derived chemokine and monitoring TEM with intravital microscopy. The results revealed that the recruitment, rolling flux and adhesion of leukocytes was similar for both wildtype and L-selectin [-/-] mice (130). However, the emigration was lower for L-selectin^{-/-} and the directional migration was reduced (130), showing L-selectin plays a role in migration towards inflammatory stimuli. It is also worth noting that L-selectin has also been implicated in sterile inflammation. An example of this is atherosclerosis and the contribution of L-selectin in the development of this condition is described in Section 1.8.3.

## 1.8 L-selectin in Disease States

L-selectin has been implicated in the development of several disease states, including atherosclerosis (292), rheumatoid arthritis (179) and ischemia reperfusion injury (293). In a majority of cases L-selectin-dependent recruitment of leukocytes is involved in exacerbation of the disease. This has been shown to be the case for IR injury, where induction of shedding of L-selectin by activating ADAM17 with hydrogen sulphide led to a reduction in the recruitment of neutrophils to ischemic tissue (293). Other examples of L-selectin involved in disease development include ileitis, where T-cells expressing L-selectin have been shown to enhance disease development compared to L-selectin[- /-] T-cells (294) and in allogeneic skin graft rejection, with rejection shown to be delayed in L-selectin deficient mice due to a reduction in the recruitment of lymphocytes to the graft site (295). The role of L-selectin in development of type 1 diabetes was assessed using the non-obese diabetic (NOD) mouse model. Treatment of these mice with an antibody against L-selectin prevented the development of the disease (296,297). This is due to a reduction in the infiltration of lymphocytes to β islets (296). L-selectin has also been implicated in the metastasis of tumour cells (298). With L-selectin deficient mice, metastasis of tumour cells was attenuated (299,300). Leukocytes can interact with cancer cells in the bloodstream and anchor them on the endothelium, thereby enabling their metastatic spread (301). It is

therefore likely that the interaction between leukocytes and cancer cells is in some part regulated by L-selectin on leukocytes interacting with ligands on cancer cells.

## 1.8.1 Atherosclerosis

Cardiovascular diseases (CVDs), such as atherosclerosis, have become highly prevalent in the developed world, causing an economic burden on society. Research has revealed that inflammation is a major driver of disease progression in atherosclerosis, with L-selectin-dependent recruitment of leukocytes shown to play a role (see below). The development of atherosclerosis (depicted in Figure 1.15) and the evidence of the involvement L-selectin in disease development are described below.

### *1.8.1.1 Development of Atherosclerosis*

Atherosclerosis is the thickening of the arterial walls caused by the accumulation of lipoproteins in the vessels. The first stage of atherosclerosis is the formation of fatty streaks, which are caused by the accumulation of lipid-rich macrophages and T cells in the intima; the inner most layer of the arterial wall (302). The fatty streaks develop into intermediate plaques or lesions, which are defined by layers of macrophages and vascular smooth muscle cells (VSMCs) (302). Complex lesions then develop, which are larger in size and project into the lumen. They are composed of a lipid and necrotic debris core overlaid with VSMCs and have a dense fibrous cap formed by components of the connective tissues, such as collagen (302). These plaques are unstable and often rupture, causing occlusion of blood vessels to feed oxygen-rich blood to the brain or heart, leading to stroke or myocardial infarction.

Lesions form in large and medium sized elastic arteries, which contain large amounts of elastin and collagen, and muscular arteries, which contain layers of VSMCs (303). They are also most often found at branch points in vessels, where the shear flow is disturbed (304). This disturbance leads to a reduction in the generation of NO (304). NO production can protect against the development of atherosclerosis by inhibiting leukocyte adhesion to the endothelium (305,306) and inhibiting VSMC proliferation and migration, both of which contribute to atherogenesis.

Many different processes and cell types are involved in the development of atherosclerosis. Endothelial injury leading to dysfunction is thought to be an early step

in atherogenesis. Oxidized low density lipoproteins (oxLDL) deposited on the surface of the endothelium cause injury to the cells. This leads to the up-regulation of adhesive glycoproteins on the luminal surface (302), leading to the recruitment of leukocytes to the area. VCAM-1 expression has been observed in early atheroma and mice deficient for VCAM-1 show reduced plaque development (304), showing the role of this molecule in atherogenesis. The role of leukocytes in the development of atherosclerosis is described below. In brief, monocytes recruited to the area differentiate into macrophages, which then engulf oxLDL and differentiate into foam cells, causing them to secrete cytokines and chemokines that recruit other monocytes and leukocytes, such as T-cells, to the site and exacerbate the inflammatory response. Endothelial cells also release growth factors that promote VSMC proliferation and migration (303), which leads to the formation of more complex plaques. VSMC change from a contractile phenotype to a synthetic phenotype, which enables them to respond to growth factors, proliferate and deposit ECM components such as collagen that contributes to the formation of a fibrous cap (302).

Other processes apart from lipoprotein deposition are thought to enhance atherogenesis, either by causing endothelial dysfunction or promoting inflammation. Homocysteine is toxic to the endothelium and degrades structural components of the artery, such as collagen (303). High plasma levels of homocysteine have been linked to an increase the development of atherosclerosis (303). Hypertension can increase the risk of atherogenesis. Angiotensin II (AngII) levels are elevated in hypertension (303,304). AngII stimulates VSMC growth (303) and also increases the expression of VCAM-1 (304), both of which promote atherogenesis. Hyperglycaemia in diabetes leads to the release of pro-inflammatory cytokines, which potentially can induce atherogenesis (304). Diabetes also increases oxidative stress, which can lead to an increase in the formation of oxLDL and therefore enhance atherogenesis (304). Infection has also been implicated in atherogenesis. Herpes viruses and *Chlamydophila pneumonia* have both been found in lesions (303), though their role in atherogenesis remains unclear as the presence of these molecules alone does not induce the formation of atherosclerotic plaques (303). It is possible that infections accelerate atherogenesis by causing release of cytokines and activating leukocytes at the site of plaques (304). Further investigation is required to decipher the role of infectious agents in atherogenesis.
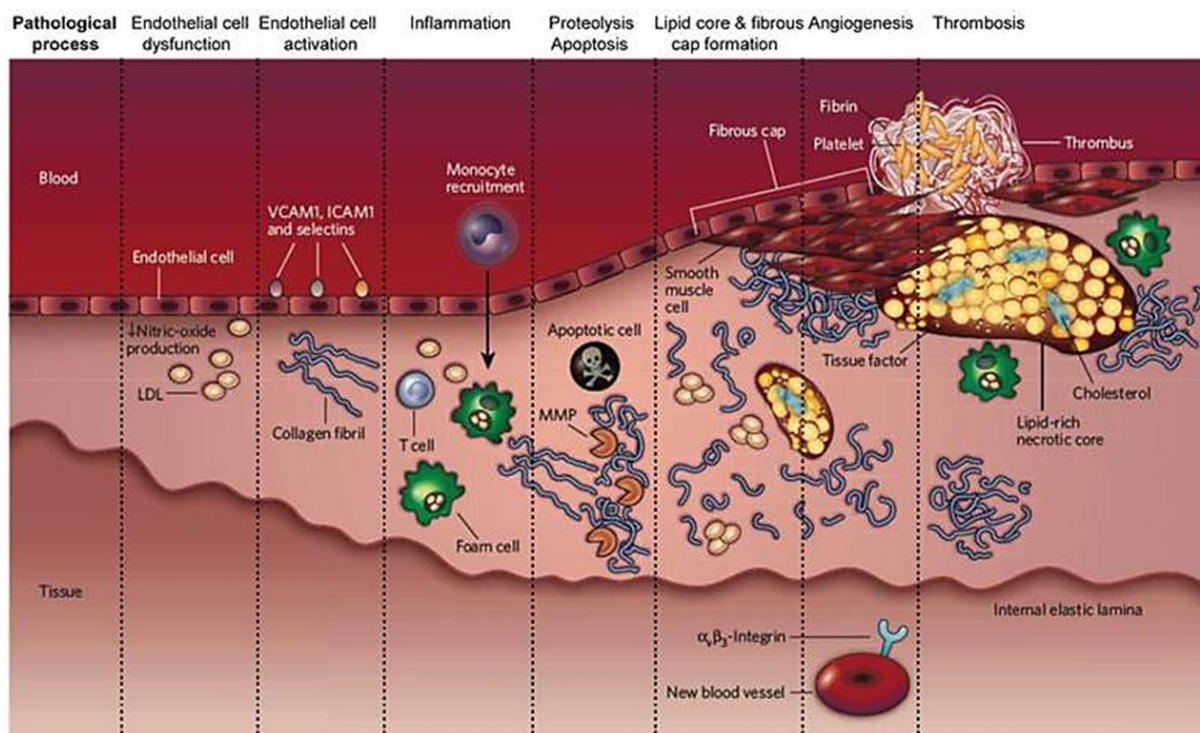
**Figure 1.16: Development of atherosclerosis.** A schematic showing the stages of atherogenesis. OxLDL deposition leads to endothelial dysfunction and the recruitment of monocytes to the vessel wall. The monocytes differentiate into macrophages that ingest the LDL, become foam cells and, overwhelmed with lipid, die through the process of necrosis. Vascular smooth muscle cells proliferate and migrate to form a fibrous cap, along with components of the connective tissues, such as collagen, over the necrotic cells. During plaque development angiogenesis occurs to form microvessels within the plaque. As atherosclerosis progresses the lesion grows in size, becomes unstable and ruptures. This leads to a rapid block in the vasculature, blocking the vital supply of oxygen to the heart and/or the brain, which will lead to myocardial infarction and/or stroke. Figure taken from Orbay, H., Hong, H., Zhang, Y., and Cai, W. (2013) Positron emission tomography imaging of atherosclerosis. *Theranostics* **3**, 894-902 (5).

### 1.8.1.2 Role of Leukocytes in Atherosclerosis

Atherosclerosis is characterised by chronic inflammation and abundant immune cells are found in atherosclerotic plaques, especially macrophages and T-cells, implicating these cells in the development of atherosclerosis. Due to lipid accumulation and other stimuli, monocytes are allowed to cross the endothelium and differentiate to macrophages (307-310). Pattern recognition receptors (PRRs) expressed by macrophages recognise oxLDL, which leads to its uptake (307,311). As lipid accumulates in macrophages they transform in to foam cells (called according to their appearance), many of which will die (307). Lipid accumulation also induces macrophages to release netrin-1, which blocks the migration of macrophages out of the lesion (307,312). When netrin-1 is deleted smaller plaques develop (312). Macrophages also enhance atherosclerosis development by secreting cytokines that

attract other leukocytes, disturbing VSMC function and producing proteinases that digest the ECM, which can cause thinning of the fibrous cap covering the lesion and leads to plaque rupture (304) (307).

T-cells have also been found in atherosclerotic plaques and have been shown to account for 10-20% of the total leukocyte population (310). Different subsets of T-cells are believed to have different roles in atherosclerosis. Both $T_H1$ and $T_H17$ have been shown to be atherogenic and $T_H2$ and $T_{reg}$ cells are protective (307,313,314). Recent research showed that T-cells produce heparan-binding epidermal growth factor-like growth factor (HB-EGF) *in vitro* and these proteins act as mitogens to stimulate VSMC proliferation (315). This may have a role in VSMC proliferation in atherosclerosis.

B-cells have also been implicated in atherosclerosis. They produce natural antibodies that recognise oxLDL (310) and this is thought to be atheroprotective as it is suggested that these antibodies mark lipids for removal (307). Neutrophils have been shown to be atherogenic by releasing proteins that contribute to oxidative stress, which leads to endothelial dysfunction and the growth of the plaque (307). Mast cells have been shown to accumulate at sites of plaque rupture (310,316). They are capable of producing proteases that degrade the ECM and it is possible that this contributes to plaque rupture and progression of atherosclerosis (316).

The information above shows the role of different leukocytes in the development and protection against atherosclerosis. This shows how important understanding their function in this process is and studying their roles further will provide targets for the prevention of atherosclerosis development.


### 1.8.1.3 Implication of L-selectin in atherosclerosis

The role of L-selectin in the development of atherosclerosis has been disputed. A report has shown that advanced plaques contain "lesional microvessels", produced in response to hypoxic necrosis. These microvessels promote lesion growth by providing a nutrient supply and also contribute to plaque rupture by causing haemorrhage within in the plaque, increasing the lipid core and increases plaque development (317). Microvessels act as important entry sites for leukocytes to gain access to the plaque. Rolling within these microvessels was observed and studies showed that L-selectin was required for recruitment. Interestingly, PSGL-1 was found

to be the primary ligand on the endothelium (292), and shows a direct link between L-selectin-dependent trafficking of leukocytes to a developing atheromatous plaque. It has also been observed that L-selectin-dependent secondary tethering (see Section 1.2.1 on secondary tethering) occurs in atherosclerotic plaques in the aorta of mice (318). It is possible that this secondary tethering increases the leukocyte recruitment to atherosclerotic plaques and therefore enhances plaque development. A study using L-selectin$^{-/-}$ mice revealed that recruitment of both B-cells and T-cells to atherosclerotic plaques in the aorta was reduced by around 50% (319). This shows that L-selectin is partially responsible for the recruitment of leukocytes to atherosclerotic plaques.

The above results showed that L-selectin played a role in the development of atherosclerosis, however, another study has shown that the deletion of L-selectin in ApoE$^{-/-}$ mice increased the development of atherosclerosis (320). It was observed that more plaques were present in ApoE$^{-/-}$ L-selectin$^{-/-}$ compared to ApoE$^{-/-}$ mice (320), suggesting L-selectin does not play a role in plaque formation and rather acts to limit plaque burden. When analysis was carried out to decipher the reason for the increase in plaque formation, it was found that there was no difference in leukocyte capture, rolling or accumulation in plaques between the two groups (320), suggesting the other selectins are capable of maintaining the leukocyte-endothelial interaction. There was, however, an increase in the number of lymphocytes found in the blood in the ApoE$^{-/-}$ L-selectin$^{-/-}$ mice, likely due to impaired migration into tissues (320). It is argued that this increase in circulating pro-atherogenic lymphocytes promotes the enhanced atherogenesis (320), though the exact mechanism by which this occurs remains elusive. It is worth noting that location of the plaque size measurement and the cellular composition of the plaques are measured in different locations, with them being measured in the descending aorta and aortic sinuses respectively (320). Ideally these two characteristics would be measured in the same location before firm conclusions for the role of L-selectin in atherogenesis can be made.


## 1.9 Selectins as therapeutic targets

The well-defined role of selectins in leukocyte recruitment and the evidence of their involvement in disease states made them attractive prospects for possible anti-

inflammatory targets. To this end, several clinical trials have been undertaken using function blocking antibodies and synthetic ligands. Early analysis revealed that anti-L-selectin antibodies reduced inflammation and myocardial necrosis in murine models (321). However, a clinical trial using an L-selectin function blocking antibody, named aselizumab, had limited success against recovery from trauma, with no significant benefit with the administration of the drug in Phase II trials (322). sLe$^x$ mimics have also been utilised as a way of inhibiting all three selectins (323). Promising results have been observed with the treatment of asthma (324) and psoriasis (325), but had no effect on IR injury in infants in phase III trials (323), showing different roles of selectins in different diseases. A soluble form of recombinant PSGL-1 conjugated to IgG1 (PSGL-1-Ig) has been developed as a potential inhibitor of selectins. PSGL-1-Ig is capable of inhibiting leukocyte rolling in a murine model on all three selectins (326). It has also been shown to inhibit inflammation in rat and mouse models of inflammation, including trauma, haemorrhagic shock and IR (327-329). However, clinical trials were discontinued due to the cost and the limited efficacy of PSGL-1-Ig (330). Several small molecules have also been tested as possible therapeutic inhibitors of selectins. Heparin is able to bind to P- and L-selectin and inhibit their interactions (331). A study has shown that heparin blocks selectin-dependent cancer metastasis (331).

The limited success of clinical trials using selectin antagonists may suggest the complex role of selectins in disease states. Further understanding the mechanisms that regulate selectin function during recruitment may provide more targets for the development of more potent therapies. This thesis will endeavour to explore the regulation of L-selectin in order to add insight to such approaches.

## 1.10 Original Hypothesis

Interaction between the L-selectin tail and its binding partners plays a critical role in regulating L-selectin-dependent adhesion and signalling. Specifically, CaM binding protects L-selectin from being shed and interaction with ERM regulates L-selectin-dependent tethering and shedding. Although these interactions have been addressed during tethering and rolling, very little is known about how these interactions are co-ordinated during TEM. It is therefore hypothesised that monocyte TEM is regulated at the level of L-selectin and its interaction with CaM and ERM.

Understanding how these interactions are co-ordinated may identify novel mechanisms for therapeutic targeting chronic inflammation.

## 1.11 Aims of the Project

The aims of this thesis are as follows:

1) Produce recombinant soluble CaM and FERM domain of moesin proteins in order to study the interaction between these proteins and L-selectin cytosolic tail peptide *in vitro*.

2) Use biophysical techniques to characterise the interaction between the L-selectin tail and its binding partners, and assessing the role of serine phosphorylation in modulating the interaction.

3) Generate monocytic cell lines to co-express GFP/RFP-tagged forms of CaM and L-selectin, so that their interaction can be analysed in resting cells.

4) Characterise the interaction between CaM-RFP and L-selectin-GFP during TEM and determine: (i) the sub-cellular distribution of L-selectin-GFP and CaM-RFP interaction specifically during TEM; (ii) the effect of blocking phosphorylation at one or both serine residues within the cytosolic tail of L-selectin on the L-selectin-GFP/CaM-RFP interaction during TEM; (iii) if changes in cell morphology during TEM are directly affected when specific residues within the L-selectin tail are mutated.

# Chapter 2: Materials and Methods

## 2.1 Chemicals and Reagents

A list of the chemicals and reagents used in this thesis is shown in Table 2.1

|  | Chemical/Product | Supplier |
|---|---|---|
| Cell Culture | RPMI media | Life technologies |
|  | M199 media | Life technologies |
|  | Penicillin/Streptomycin | Life technologies |
|  | FBS | Sigma Aldrich |
|  | B-Mercaptoethanol | Sigma Aldrich |
|  | Trypsin-EDTA | Sigma Aldrich |
| *E.coli* growth | LB media | Sigma Aldrich |
|  | LB agar | Sigma Aldrich |
|  | Ampicillin | Sigma Aldrich |
| Buffers and Solutions | Nuclease Free Water | Ambion |
|  | PBS | Severn Biotech Ltd |
|  | HEPES | Life Technologies |
|  | BSA | Sigma Aldrich |
|  | MES 20X | Invitrogen |
|  | Transfer Buffer 10X | Life Technologies |
|  | Tris-Glycine Native running buffer 10X | Life Technologies |
|  | Protein Ladder | Life Technologies |
|  | Native Protein Ladder | Life Technologies |
|  | ECL | Perkin Elmer |
| Chemicals | PFA | BDH Laboratory Supplies |
|  | Glutaraldehyde | VWR international |
|  | NP-40 | Fluka, Sigma Aldrich |
|  | Tween 20 | Sigma Aldrich |
|  | Protease inhibitor cocktail | Roche Diagnostics GmbH |
|  | DMSO | Sigma Aldrich |
|  | CytoBuster Protein Extract | Novagen |

| | Reagent | |
|---|---|---|
| | Sodium Borohydride | Sigma Aldrich |
| | Nitrogen$^{15}$NH$_4$Cl | Goss Scientific, Manufacturer Cambridge Isotope Laboratories Inc. |
| | D$_2$O | Goss Scientific, Manufacturer Cambridge Isotope Laboratories Inc. |
| | Calyculin A | Sigma Aldrich |
| | Bisindolylmaleimide | Calbiochem |
| | Alexa Fluor 633 Phalloidin | Invitrogen |

**Table 2.1: List of Reagents used during the project.** Table shows the reagents and chemicals used in this thesis. The supplier of each reagent is listed. The concentrations used are stated in the specific sections in the Material and Methods.

## 2.2 Antibodies

A list of the primary and secondary antibodies used in this thesis is provided in Table 2.2, along with the concentration at which each is used.

| Antibody | Species | Dilution Factor | Company |
|---|---|---|---|
| **Anti-CaM** | mouse | 1:1000 | Millipore |
| **Anti-GFP** | rabbit | 1:500 | SantaCruz |
| **CA21:anti- L-selectin tail** | mouse | 1:1000 | |
| **Anti-Actin** | goat | 1:1000 | Santa Cruz |
| **Goat-anti-mouse-HRP** | goat | 1:1000 | DAKO |
| **Goat-anti-rabbit-HRP** | goat | 1:1000 | DAKO |
| **Rabbit-anti-goat-HRP** | rabbit | 1:1000 | DAKO |

**Table 2.2: Antibodies used during this project.** Table shows the primary and secondary antibodies used in this thesis. The source, concentration used and the company that supplies each antibody is listed.

## 2.3 Peptides and plasmids

Peptides were synthesized at the department of Biochemistry, University of Bristol. For *E. coli* production of proteins the pET duet-1 vector was used (Figure 2.1).

Wildtype cDNA of full length CaM was cloned into multiple cloning site (MSC) 1 of the pETduet-1 vector. SalI and NotI restriction sites were engineered at the 5' and 3' ends using PCR for the Hexa Histidine (His6)-tagged CaM with a Tobacco Etch Virus (TEV) protease cleavage site engineered between the coding sequence of CaM and the His6-tag. The His6-tagged moesin-FERM domain was cloned in the same way. Untagged moesin-FERM was also cloned into pET duet-1 vector at MSC 2 using the restriction enzymes NdeI and XhoI. A vector containing untagged CaM was a kind gift from Antonio Villalobo. CaM was also purchased from Enzo. The N and C lobes of CaM were cloned into pET duet-1 vector at MSC 2 using NdeI and XhoI restriction sites.

The pET46 Ek/LIC vector (Figure 2.2) containing the Trp-Cage sequence (Figure 2.2Aiii) was a gift from Dr Pete Simpson, Imperial College London. The L-selectin cytosolic tail was cloned into the vector using EcoRI and BaMHI restriction sites.

For lentiviral vector production, the pHR'SIN-SEW vector, which was a gift from Prof. Adrian Thrasher (Institute of Child Health, UCL), was used with either GFP or RFP C-terminal tag (Figure 2.3). For CaM cloning into the vector, BaMHI and XhoI restriction sites were engineered at the 5' and 3' ends using PCR. Moesin was cloned with XhoI and KpnI restriction sites at the 5' and 3' ends. Ezrin was cloned with either XhoI and SalI or XhoI and KpnI restriction sites at the 5' and 3' end depending on the method of cloning (see Section 5.3.3). The primers used for all the cloning are summarised in Table 2.3.

**A (i)**

**A (ii)**

pETDuet-1 cloning/expression regions
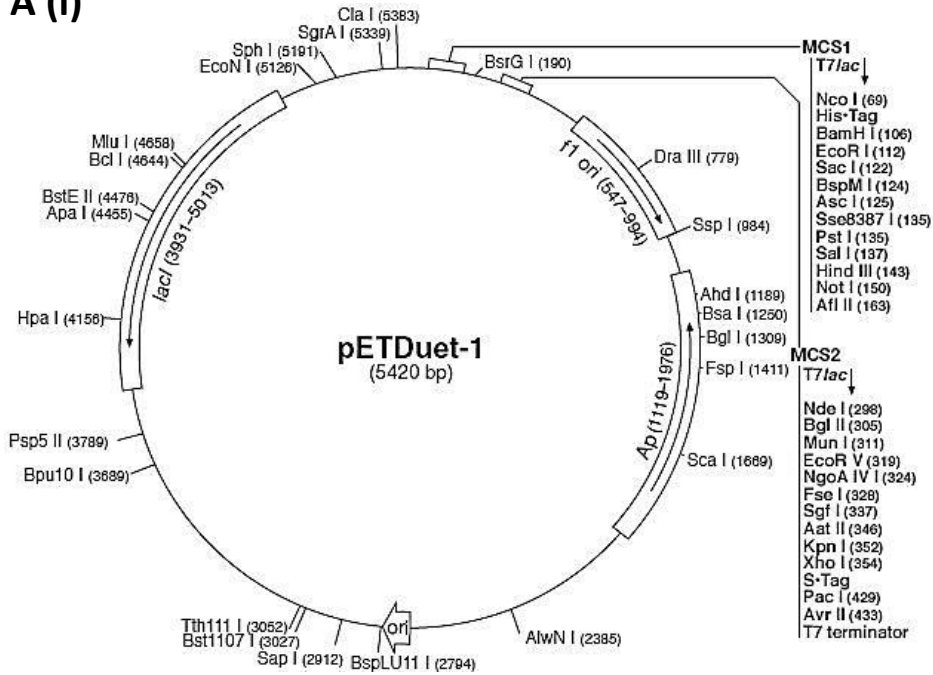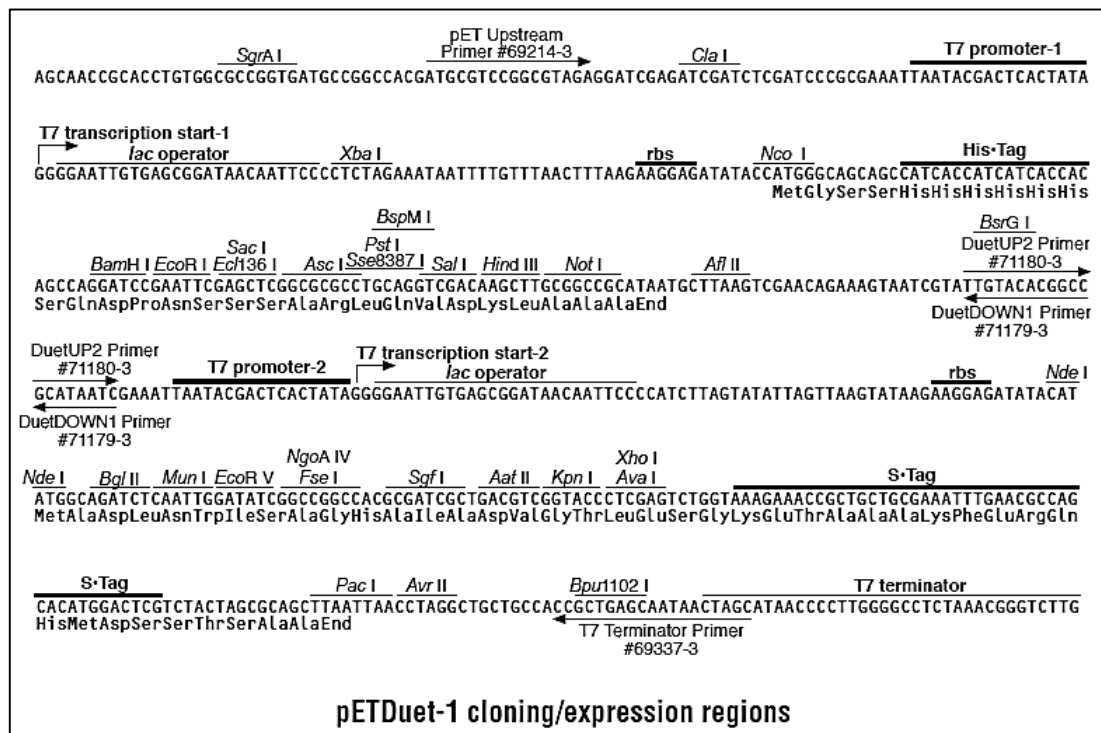
**Figure 2.1: Vector Maps of the Plasmids used for Cloning of Recombinant Proteins.** (Ai) Vector map of pETDuet-1 showing the two multiple cloning sites (MCS) and the restriction sites found in each, with the details of the cloning site shown in (Aii). There is also Ampicillin resistant gene and lacI gene.

**A (i)**
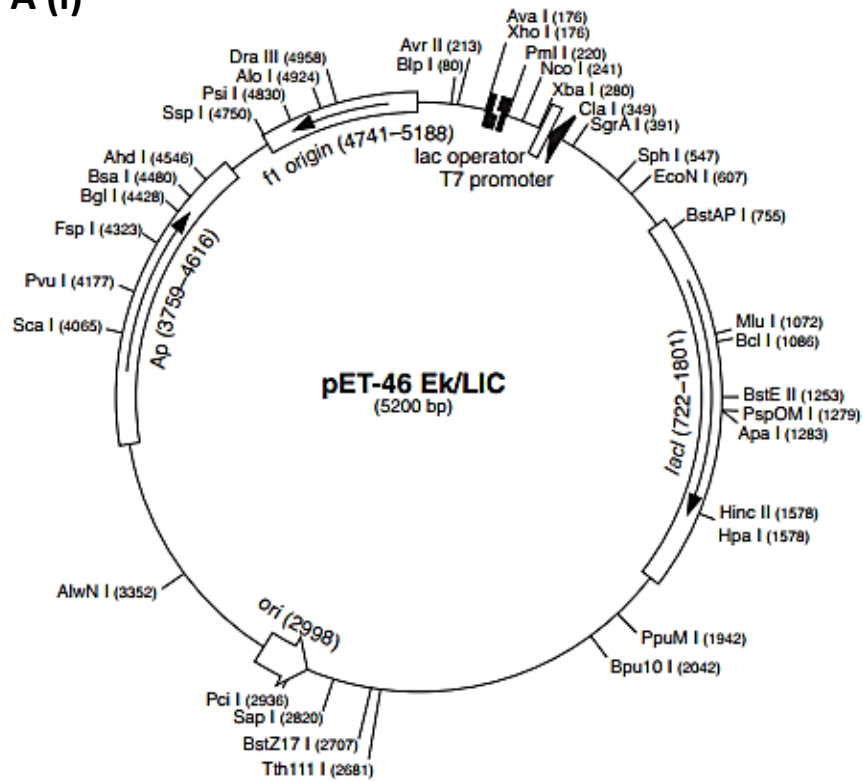
**A (ii)**
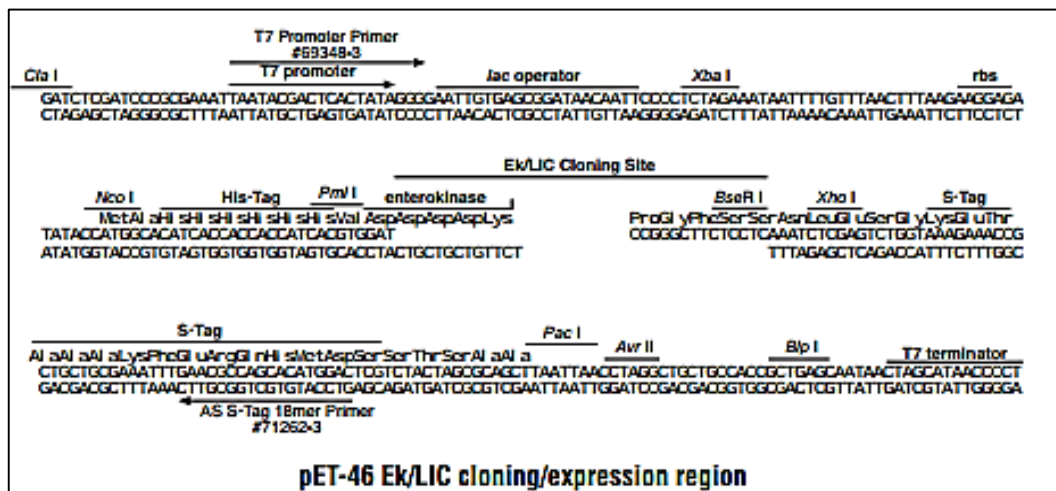
**A (iii)**
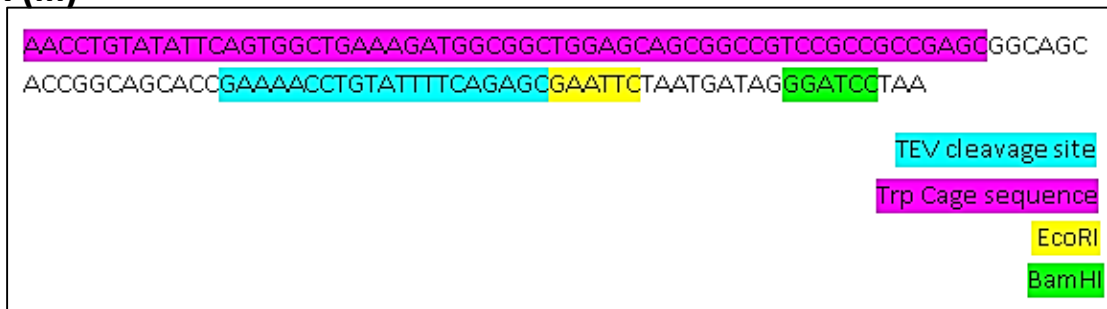
**Figure 2.2: Vector Map of the Plasmid used to Clone Trp-Cage-L-selectin**. (Ai) The vector map of pET-46 EK/LIC vector with the ampicillin resistant gene (Ap) and lacI gene shown. (Aii) shows the detail of the cloning site into which the Trp Cage was cloned, with (Aiii) showing the sequence cloned into the site, including the Trp Cage, a TEV cleavage site and the restriction sites EcoRI and BamHI, which can then be used for further cloning.
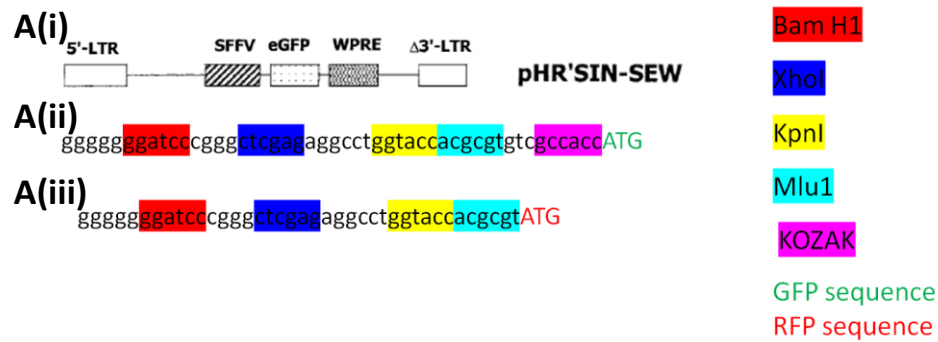
**Figure 2.3: Vector Maps of the Plasmids used for Cloning of Lentiviral Vectors.** (A) Vector Map of pHR'SIN-SEW showing the cloning site for either GFP containing vector or RFP containing vector. (Ai) shows the cloning site of the vector with the GFP sequence and (Aii) shows the cloning site for the vector containing RFP. The restriction sites are highlighted in different colours, with BamHI shown in red, XhoI shown in blue, KpnI shown in yellow and MluI shown in cyan. The KOZAK sequence is shown in magenta.

## 2.4 *E.coli* Strains

KRX *E.coli* cells (genotype F´, [traD36, ΔompP, proA$^+$B$^+$, lacI$^q$, Δ(lacZ)M15] ΔompT, endA1, recA1, gyrA96 (Nal$^r$), thi-1, hsdR17 (r$_K^-$, m$_K^+$), e14$^-$ (McrA$^-$), relA1, supE44, Δ(lac-proAB), Δ(rhaBAD)::T7 RNA polymerase) were used for cloning of the DNA vectors. The strains BL21(DE3)pLysS (genotype F$^-$ ompT hsdS(rB$^-$ mB$^-$) gal dcm λ(DE3) pLysS (Cam$^r$ ) ( λ(DE3): lacI, lacUV5-T7 gene 1, ind1, sam7, nin5 )) and Rosetta2(DE3) (genotype F$^-$ompT hsdS$_B$(r$_B^-$ m$_B^-$) gal dcm (DE3) pRARE2 (Cam$^R$))were used for protein expression. For proteins found to be insoluble with BL21(DE3)pLysS and Rosetta2(DE3) cells, expression was carried out using *E.coli* ArcticExpress cells (genotype F$^-$ompT hsdS(r$_B^-$ m$_B^-$) dcm$^+$ Tet$^r$ gal (DE3) endA Hte [cpn10 cpn60 Gent$^r$]). All the *E.coli* strains used for protein expression contain the DE3 bacteriophage γ lysogen, which encodes for T7 RNA polymerase under the control of a lacUV5 promoter and the lacI gene. This allows provides a system for the control of expression of the recombinant protein, through the addition of IPTG (see Section 3.2 for details).

## 2.5 PCR

PCR amplification of the desired DNA was carried out using the following method for *Pyrococcus furiosus* (Pfu) DNA polymerase: 1 µl of each primer (10 µM), 100 ng of template, 1 µl dNTPs, 5 µl of Pfu polymerase buffer and 1 µl of Pfu

polymerase, made up to a final volume of 50 µl and placed in a thermo cycler (Perkin Elmer, GeneAmp 34 PCR System 2400) using the following conditions: hot-start denaturation 95°C 5 min, followed by 25 cycles of denaturation 95°C 30 seconds, annealing 55°C 40 seconds, elongation 72°C (30 seconds per 500 bp), with 72°C 2 min end. For *Thermococcus kodakaraensis* (KOD) polymerase: 1.5 µl of each primer, 0.5 µl of template and 25 µl KOD polymerase mix made up to 50 µl and placed in a thermo cycler using the following conditions: hot-start denaturation 95°C 5 min, followed by 25 cycles of denaturation 95°C 20 seconds, annealing 55°C 14 seconds, elongation 75°C (15 seconds per 1kb). PCR products were run on a 0.8-1% agarose gel, cut out and purified using QIAquick Gel Extraction kit (Qiagen) or Wizard® SV Gel and PCR Clean-Up System (promega) according to manufacturer's protocol. All primers used are summarised in Table 2.3.

| | Forward Primer | Reverse Primer |
|---|---|---|
| His-tagged CaM | GAGAGAGTCGACATGGCTGACCAACTGACTGAA | GAGAGAGCGGCCGCTCACTTTGCTGTCATCATTTG |
| His-tagged moesin FERM domain | GAGAGAGTCGACATGCCGAAGACGATCAGTGTG | GAGAGAGCGGCCGCTCACTTGCGCCGACGCATGTACAG |
| Untagged moesin FERM domain | GAGAGACATATGATGCCGAAGACGATCAGTGTG | GAGAGACTCGAGTCACTTGCGCCGACGCATGTACAG |
| C-lobe of CaM | GAGAGACATATGATGAAAATGAAAGACACAGACAG | GAGAGACTCGAGTCACTTTGCTGTCATCATTTG |
| N-lobe of CaM | GAGAGACATATGATGGCTGACCAACTGACTGAA | GAGAGACTCGAGTCATGTGTCTTTCATTTTTCTTGCC |
| CaM lentivirus | GAGAGAGGATCCATGGCTGACCAACTGACTGAA | GAGAGACTCGAGCTTTGCTGTCATCATTTG |
| Moesin lentivirus | GAGAGACTCGAGATGCCGAAGACGATCAGTGTG | GAGAGAGGTACCCATGGACTCAAACTCATCAATG |
| Ezrin lentivirus | GAGAGACTCGAGATGCCGAAACCAATCAATGTC | GAGAGAGGTACCCAGGGCCTCGAACTCGTCGAT |

**Table 2.3: Primers for cloning of Recombinant and Lentiviral Proteins.** Table showing the primers used for the PCR of CaM and moesin-FERM for cloning into pET duet-1 vector and cloning CaM, moesin and ezrin into the lentiviral vector pHR'SIN-SEW.

## 2.6 Restriction Digest and Ligation

The clean PCR product and the vector were cut with the appropriate restriction enzymes for 2 hours at 37 °C. The vector was also treated with Calf Intestinal Alkaline Phosphatase (CIP) for one hour at 37 °C and the DNA was purified using QIAquick Gel Extraction kit (Qiagen) or Wizard® SV Gel and PCR Clean-Up System (promega) according to manufacturer's protocol. The ligation was carried out with a molar vector to insert ratio of 1:3 with T4 DNA ligase (Promega) in a 10 µl reaction at 15°C overnight and was then used to transform KRX *E.coli* cells.

### 2.6.1 Partial Digestion of Ezrin Insert

After the ezrin PCR reaction, 10 µl of the product was digested with the restriction enzyme which does not cleave in the ezrin sequence as described above. Once the first digestion was completed the reaction was diluted up to 100 µl using dH$_2$O and the appropriate restriction enzyme buffer. The solution was then aliquoted into five tubes. The second restriction enzyme was added to the first tube and a serial dilution using this solution was carried out into the other tubes. All the tubes were then incubated at 37 °C for 3 minutes. The tubes were then pooled and purified using the QIAquick column system. The purified DNA was run on an agarose gel and the band corresponding to the correct weight for the desired product was excised and purified using QIAquick Gel Extraction kit (Qiagen). The purified DNA was then used for ligation as described above.

## 2.7 Transformation and plasmid detection

50 µl of bacteria was incubated with 1 µl of plasmid DNA or 5 µl of ligation reaction for 45 mins on ice. The bacteria were then heat shocked at 42 °C for 45 secs. 500 µl of LB was added and the cells were incubated for one hour at 37 °C shaking. The cells were then plated on LB plates with the appropriate antibiotic and incubated overnight at 37 °C. Colonies were picked for colony PCR, to test if the insert is present, and grown for plasmid isolation using PureYield™ Plasmid Miniprep Kit (Promega) according to the manufacturer's protocol. The plasmid was then sent for sequencing by Geneservice to confirm the presence of the insert.

## 2.8 Glycerol Stock Generation of Transformed E.coli Cells

To produce frozen stocks of the *E.coli* cells expressing the recombinant proteins, 3 ml of *E.coli* cells were cultured overnight. The overnight culture was mixed 1:1 with 100 % sterile glycerol and kept on ice. The vials were then transferred to -80 °C for long time storage and could be used for inoculating future growth cultures.

## 2.9 Agarose Gel Electrophoresis

0.8-1% agarose Tris-acetate-EDTA (TAE) gels were made with 1:1000 ethidium bromide. DNA samples were mixed with loading buffer (0.25% bromophenol blue, 0.25% xylene cyanol FF, 30% glycerol) and loaded on the gel. The gel was run at 120 V until bands were separated. DNA was visualized by UV transillumination.

## 2.10 Oligonucleotide Kinase Treatment and Annealing

Oligonucleotides (oligos) for the L-selectin cytosolic tail were designed with EcoRI and BamHI sticky ends (Table 2.4). The oligos were treated with polynucleotide kinase in the following reaction: 1 µl kinase buffer, 1 µl 10 mM ATP, 2.5 µl kinase, 2 µg oligo. The reaction was incubated at 37 °C for 1 hour and then heated to 75 °C for 10 minutes to deactivate the kinase. The kinase treated oligos were mixed in a 1:1 molar ratio in annealing buffer (10 mM tris, 1 mM EDTA, 100 mM NaCl, pH 7.5) the mixture was heated to 95 °C for 5 minutes then left to cool to room temperature overnight. The annealed oligos were then used for ligation into the restriction digested vector.

| | Forward oligo | Reverse oligo |
|---|---|---|
| **L-selectin cytosolic tail** | GAATTCCGTCGTCTGAAAAAAGGC AAAAAAAGCAAACGTAGCATGAAC GATCCGTATTGAGGATCC | GGATCCTCAATACGGATCGTTCATGCTA CGTTTGCTTTTTTTGCCTTTTTTCAGACG ACGGAATTC |

**Table 2.4: Oligonucleotides used to clone L-selectin Cytosolic Tail.** Oligos were annealed together (see Section 2.10 for experimental details) and used for ligation as described in Section 2.6.

## 2.11 Mutagenesis of L-selectin cytosolic tail

pHR'SIN-SEW vectors containing the cDNA of human wildtype L-selectin, or the sheddase-resistant mutation ΔM-N-L-selectin, fused with GFP were used as the templates for generating mutations in the cytosolic tail of L-selectin at residue L358 to L358E. PCR was carried out using primers engineered to contain the mutation (see Table 2.5), followed by digestion with DpnI for one hour at 37 °C, to remove the methylated parental DNA which did not contain the mutation. The digested PCR product was then used to transform BL21 competent *E. coli*. Colonies were picked and cultured overnight. Minipreps were carried out and DNA was sent for sequencing to confirm the presence of the mutation. Once this was confirmed the vector was used for lentivirus production (see Section 2.19).

| | Forward primer | Reverse primer |
|---|---|---|
| **L358E mutagenesis** | CTGGCAAGGAGAGAAAAAAAGGCAAG | CTTGCCTTTTTTTTCTCTCCTTGCCAG |

**Table 2.5: Primers used for mutagenesis of L-selectin.** The primers used to produce the L358E mutant. These were used in PCR experiments using Wildtype L-selectin-GFP as the template.

## 2.12 Production of Recombinant Proteins

### 2.12.1 Overexpression of Recombinant Proteins

CaM, moesin-FERM and the N and C lobes of CaM were expressed in either BL21 strain (Stragene) or Rosetta II strain (Novagen) *E.coli* cells and moesin and C-CaM were also expressed in arctic cells (Agilent Technologies). For large scale production of the proteins, two litres of bacteria were cultured. For the starter culture a colony was picked from an agar plate or cells were taken from glycerol frozen stocks and diluted in 3 ml of lysogeny broth (LB) with the appropriate antibiotics. The starter culture was then grown overnight at 37 °C with agitation. The next morning 1 ml of the starter culture was used to inoculate 1 L of LB. The cells were then grown at 37 °C under agitation until an optical density measured at

600 nm (OD600) of 0.6 was reached. At this point 1 ml of 1 M isopropyl β-D-1-thiogalactopyranoside (IPTG) was added to the 1 L of bacterial culture, so a final concentration of 1 mM IPTG was achieved, in order to induce expression of the recombinant protein. The bacterial growth and protein expression conditions for each recombinant is summarised in Table 2.6.

| Recombinant Protein | Growth Temperature/°C | Length of Induction/hrs |
| --- | --- | --- |
| CaM | 37 | 4 |
| Moesin-FERM | 37 | 4 |
| | 18 | 12-16 |
| | 13 | 24 |
| N-CaM | 37 | 4 |
| | 18 | 12-16 |
| C-CaM | 37 | 4 |
| | 18 | 12-16 |
| | 13 | 24 |

**Table 2.6: Growth and expression conditions of *E.coli* cells expressing recombinant proteins.** A table summarising the temperature and length of time used for the induction of the recombinant proteins.

## 2.12.2 Production of Soluble Protein

After growth and induction, the cells were pelleted by centrifugation (Beckman Avanti J-26XP centrifuge with a JLA-8.1000 rotor) at 2500xg for 20 minutes. The pellet was re-suspended in the appropriate buffer (depending on the purification method to be used). The solution was then sonicated for three minutes, amplitude 30%, pulsing five seconds on five seconds off, repeated twice. The soluble and insoluble fractions were separated by centrifugation at 20000xg using a Beckman Avanti J-26S centrifuge with a JA-18 rotor for one hour.

To improve the amount of soluble protein, the Sarkosyl method was used on the insoluble fraction produced after sonication and centrifugation. This method uses a detergent known as sarkosyl to solubilise proteins found in inclusion bodies

(see Section 3.3.2 for an explanation). The pellet was re-suspended in 2 ml of 10 % sarkosyl solution and was left on ice for one hour. The sarkosyl solution was then diluted to 1 % with the appropriate buffer required for protein purification up to 20 ml. The solution was centrifuged at 20000xg for 45 minutes. The supernatant was then collected and used for purification.

## 2.12.3 Hexahistidine-tag (His6-tag) Purification

For the recombinant proteins expressed with a His6-tag, purification was carried out using a nickel column attached to an AKTA system. The *E.coli* cells were suspended in nickel buffer A (20 mM Tris pH 8, 10 mM imidazole, 300 mM NaCl, 5% glycerol) prior to sonication and centrifugation. The soluble fraction was then loaded onto a 5 ml nickel column pre-equilibrated with nickel buffer A. The column was washed with thirty column volumes (CV) of nickel buffer A and proteins were eluted using a concentration gradient of nickel buffer B (20 mM Tris pH 8, 500 mM imidazole, 300 mM NaCl, 5% glycerol) from 0 to 100% in 25 CV. Fractions containing the protein of interest identified using sodium dodecyl sulphate polyacrylamide gel electrophoresis (SDS-PAGE) gel (see Section 2.16.1 for details) were collated and underwent TEV protease cleavage, to remove the His6-tag, during dialysis in TEV cleavage buffer (50 mM Tris pH 8, 1 mM EDTA, 1 mM DTT, 50 mM NaCl) and the protein solution was passed through the nickel column once again to remove the His6-tagged TEV protease, the His6-tag and any uncleaved product. CaM was then dialysed in NMR buffer (20 mM Tris, 100 mM KCl, 1 mM DTT, and 1 mM EDTA pH 7.25) or the same buffer plus 5 mM $CaCl_2$ for $Ca^{2+}$ bound CaM (CaM-Ca). The protein was then concentrated to the desired concentration.

## 2.12.4 Hydrophobic Interaction Chromatography Purification of CaM and CaM lobes

Untagged CaM and the lobes of CaM were purified using a phenyl sepharose column. The soluble fraction was prepared as before except the *E.coli* pellet was re-suspended in 50 mM Tris pH 7.5 and 2 mM EDTA prior to sonication, with 5 mM $CaCl_2$ added after centrifugation. A 5 ml phenyl sepharose column attached to the AKTA system and pre-equilibrated with 50 mM Tris pH 7.5, 5 mM $CaCl_2$, 0.1 M NaCl

(known as pre-equilibration buffer). The supernatant containing the recombinant protein was loaded onto the column, after which the column was washed with 1$^{st}$ wash buffer (50 mM Tris pH 7.5, 0.1 M $CaCl_2$, 0.1 M NaCl) until UV absorption at 280 nm was constant. It was then washed with 2$^{nd}$ wash buffer (50 mM Tris pH 7.5, 5 mM $CaCl_2$, 0.5 M NaCl) again, until a constant UV absorption at 280 nm was observed. CaM was eluted from the column with 50 mM Tris pH 7.5 and 1 mM EGTA (elution buffer). Fractions containing CaM were dialysed in either NMR buffer with 5 mM $CaCl_2$ or NMR buffer with 5 mM EGTA, then NMR buffer.

## 2.12.5 Purification of untagged Moesin-FERM

The soluble fraction of *E.coli* expressing moesin-FERM domain was produced as above, except the bacteria pellet was re-suspended in hydroxyapatite buffer A (200 mM potassium phosphate pH 7) prior to sonication. The soluble fraction was loaded onto a hydroxyapatite column pre-equilibrated with hydroxyapatite buffer A. The column was then washed with 10 CV of buffer A and the protein was eluted with 5 CV hydroxyapatite buffer B (600 mM potassium phosphate buffer pH 7). The protein was the dialysed in potassium phosphate buffer (17.4 mM $KH_2PO_4$, 27 mM $Na_2HPO_4$ at pH 7) or 100 mM sodium acetate buffer and then concentrated to the desired concentration.

## 2.13 Purification of Peptides

The peptides purchased from Bristol University were purified using PD MidiTrap G-10 desalting columns. The column was equilibrated with 16 ml $dH_2O$, then 1 ml of peptide dissolved in $dH_2O$ was loaded onto the column, followed by 0.7 ml of $dH_2O$ and this was allowed to completely enter the packed bed. The peptide was eluted in 1.2 ml of distilled $H_2O$. The solution was then freeze dried and the peptide was weighed and dissolved in the appropriate buffer to the desired concentration.

## 2.14 Concentrating Proteins

Proteins were concentrated using Amicon Ultra-15 Centrifugal filter units (cellulose membrane) with a molecular weight cut off of either 3 kDa or 10 kDa, depending on the size of the protein. The concentrators were centrifuged at 4 °C with a speed of 1200xg using the JA-18 rotor until the desired concentration of protein was achieved.

## 2.15 Determination of Protein Concentration

The protein concentration was determined using the Beer Lambert law: $A = \varepsilon cl$ where A is the absorbance at 280 nm, ε is the molar extinction coefficient of the protein (determined using Protparam (332)), c is the concentration and l is the path length. The absorbance was measured using a Nanodrop spectrophotometer, with the protein buffer used to set the baseline.

## 2.16 Protein Analysis

### 2.16.1 SDS-PAGE

SDS-PAGE is a method used to separate proteins based on their size. SDS is an anionic detergent which when added to the protein sample removes the high order structure of the protein, forming an unstructured linear chain, and imparts a negative charge to the linearized protein. This means that separation of proteins in the sample depends on molecular weight only.

12.5% SDS-PAGE resolving gel was made by diluting polyacrylamide in protogel resolving buffer with APS and TEMED following the manufacturer's protocol. Once the resolving gel had set, the stacking gel was made in the same way, except protogel stacking buffer was used. Precast NuPAGE 4-12% Bis-Tris gels were also purchased (Novex). The protein samples were mixed with loading buffer (63 mM Tris-HCl, pH 6.8, 10% (w/v) glycerol, 2% (w/v) SDS and 0.0025% (w/v) bromophenol blue) and loaded on the gel. The gel was run with Tris-glycine running buffer at 200V for around 45 minutes. Gels were stained with 0.25% (w/v) Coomassie Brilliant Blue R-250 in 45% (v/v) methanol, 10% (v/v) acetic acid and de-

stained in 45% (v/v) methanol, 10% (v/v) acetic acid, or the proteins were transferred to nitrocellulose membrane for western blot analysis.

## 2.16.2 Western Blot Analysis

Polyvinylidene difluoride (PVDF) Immobilon-P (Millipore) transfer membrane was equilibrated in 100% methanol followed by transfer buffer (Invitrogen). Polyacrylamide gels were transferred to the membrane using the NuPAGE transfer module (Invitrogen) and run for 35V for 1 hour 45 minutes. After transfer the membrane was fixed in 0.3% glutaraldehyde for 15 minutes at room temperature. The membrane was then washed three times in tris-buffered saline (TBS) (150 mM NaCl, 15 mM Tris-HCl pH 7.4) supplemented with 0.05% Tween20 (TBST), each wash lasting 10 minutes. The membrane was then blocked in 5% milk in TBST for 1 hour with agitation. The primary antibody was added at the desired concentration in blocking solution and the membrane was incubated overnight at 4 °C with agitation. The next day the membrane was washed three times with TBST as described above. Horseradish peroxidise (HRP)- conjugated secondary antibody was then added at a dilution of 1:1000 in blocking solution and incubated for 1 hour at room temperature with agitation. The membrane was washed with TBST as described above. Protein detection was performed using Western Lightning chemiluminescent reagent, with 500 µl of the two solutions being mixed together and incubated with the membrane for 1 minute. The membrane was then exposed with SuperRX X-ray film (Fuji) and films were developed using a compact X4 automatic X-ray film developer (X-ograph imaging systems).

## 2.16.3 Densitometric Analysis of Western Blot Images

Western blot X-ray films were scanned using a conventional scanner (EPSON Perfection 2400). The scanned images were analysed using ImageJ software. Differences in protein levels were assessed by measuring the intensities of the selected bands. The intensities were first normalised against a loading control (actin) and then compared to the control or baseline value for each experiment.

## 2.17 Biophysical Techniques

## 2.17.1 Isothermal Titration Calorimetry (ITC)

### 2.17.1.1 Theory

Isothermal titration calorimetry (ITC) is a technique used to characterise the interaction between two molecules in solution, by measuring any heat either absorbed or generated during the association. From the resultant ITC thermogram the binding constant, thermodynamic profile and stoichiometry of the interaction can be deduced.

The calorimeter is made up of a syringe, which injects one molecule into the other and two cells surrounded by an adiabatic jacket, which controls the temperature of the cells (Figure 2.3A). Temperature sensitive circuits monitor temperature differences between the two cells and switches on heaters, located on the cells or jacket, to maintain a constant temperature between the cells (333,334). One cell is the reference cell and contains buffer or water and the other cell is the sample cell, in which one molecule of interest will be placed.

Prior to the start of the experiment a constant power is applied to the reference cell. This causes the feedback circuit to activate the heater of the reference cell (334). This represents the baseline. During the experiment the amount of power required to maintain the same temperature between the two cells is measured (2,335) and this information provides the amount of heat associated with the interaction between the two molecules (333,334).

As the molecule in the syringe is titrated into the sample cell heat is absorbed or evolved depending on the type of interaction (333). For an exothermic reaction the temperature of the reference cell will increase, so the feedback power will be deactivated to maintain the same temperature as the reference cell (334). For an endothermic reaction heat will be taken up, meaning the feedback power must increase to maintain the temperature. The heat absorbed or evolved during the titration of one molecule into the other is proportional to the fraction of bound molecules (334,335). For the initial injections all of the injected molecules are bound to the molecules in the cell, which will cause a large change in heat and therefore a large signal. Later as the system becomes saturated, less change in heat

is observed and the signal is smaller. This produces a typical profile of peaks that decrease in size as the experiment proceeds (Figure 2.3B) (335), with the area under each peak corresponding to the heat associated with the interaction at that injection point (2).

From this profile the binding constant, stoichiometry and thermodynamic profile can be found. The area under each peak is integrated and plotted against the molar ratio of the two molecules. This will produce a sigmoidal curve for experiments with one binding site. From this curve the heat of binding ($\Delta H$) is observed as the height of the curve, the binding constant ($K_b$) is measured from the slope of the curve (following curve fitting) and the stoichiometry (n) is observed as the middle point of the slope (Figure 2.3C). From this the Gibbs free energy ($\Delta G$) and entropy ($\Delta S$) can be calculated using the following equation:

$$\Delta G = -RT \ln K_b = \Delta H - T\Delta S$$

Where R is gas constant and T is temperature.

This means that from one experiment all the information about the interaction can be deciphered by simple manipulations.

There are some important considerations to take into account when setting up ITC experiments. It is important to ensure the concentrations of both molecules of interest are accurately measured. As the binding curve is produced using the molar ratio, any inaccuracies in the concentration will affect the binding curve and therefore the stoichiometry. It is also important to ensure that the buffer for both molecules is the same. This is ensured by dialysing both molecules in the same buffer for an extended period of time. If there are differences in the buffers when the two molecules are mixed, the mixing of the buffer components will also induce a change in heat. This will mean the heat due to the interaction will not observed accurately. It is also important to ensure all air bubbles are removed from the system. Air bubbles will affect the baseline and interfere with the feedback circuit, leading to abnormal peak profiles (334).

A potential problem with using this method to study interactions between two molecules is that it depends on measuring the $\Delta H$ associated with the interaction. If the $\Delta H$ of an interaction is small it is possible that it will not be seen

through the heat of dilution noise of the experiment or potentially will be too small to be measured by the equipment. Therefore this may lead to the incorrect assumption that no interaction occurred, whilst it is possible that the two molecules interact without large changes in enthalpy (in the particular experimental conditions used), in cases where the reaction is largely driven by changes in entropy. In the event that ΔH of a given interaction is close to zero, it is essential to optimise the experimental conditions of the interaction by changing the concentration of the molecules, the temperature at which the interaction is measured or the buffer in which the interaction is measured, aiming at increasing the ΔH to values that may be above the sensitivity threshold of the instrument.

The change in ΔH as the temperature changes is described by Kirchhoff's Law. This temperature dependence is due to the heat capacity ($C_p$) of the interaction, which is calculated using the following equation:

$$\Delta C_p = \frac{\Delta H}{\Delta T}$$

By measuring ΔH across a temperature range and plotting a graph of ΔH versus temperature, the $\Delta C_p$ of the interaction can be calculated by the slop of the straight line profile produced (333,335). This graph can then be used to predict the ΔH at different temperatures so a temperature where ΔH should be measurable can be found.

The buffer conditions will also affect ΔH, with the composition, concentration, pH and ionic strength having an affect (333). Of particular importance is the enthalpy of ionization of the buffer ($\Delta H_{ion}$). Protons are taken up or released during the complex formation and the equivalent number of protons will be taken up or released from the buffer components (334), leading to the $\Delta H_{ion}$. The measured enthalpy will reflect the $\Delta H_{ion}$ as well as the complex formation (334). Different buffers have different $\Delta H_{ion}$, with sodium phosphate having a low $\Delta H_{ion}$ and Tris-HCl having a high $\Delta H_{ion}$ (334). By carrying out experiments in buffers with different $\Delta H_{ion}$ the measured enthalpy will also be different and this will help to find conditions in which ΔH is measurable.

### 2.17.1.2 Experimental Procedure

ITC experiments were carried out using a MicroCal ITC200 instrument at 20 or 10 °C. CaM was used at a concentration of 0.38 mM in the syringe (40 μl) and L-selectin tail peptides at 0.04 mM in the cell (220 μl). CaM was titrated into the cell in twenty injections of 2 μl each with 180 seconds spacing between them and constant stirring at 1000 rpm. The heat of dilution was obtained from the heat of the last injections and was subtracted from the other peaks to obtain the heat of the interaction. The data was fit to a single site binding model using Origin7. This gave the stoichiometry, $K_b$ and ΔH. The dissociation constant ($K_D$) was calculated using the equation:

$$K_D = \frac{1}{K_b}$$

The ΔG and the entropic contribution (-TΔS) were calculated using the equation:

$$\Delta G = -RT \ln K_b = \Delta H - T\Delta S$$

Where R is the gas constant (1.986 cal K-1mol-1) and T is the absolute temperature.
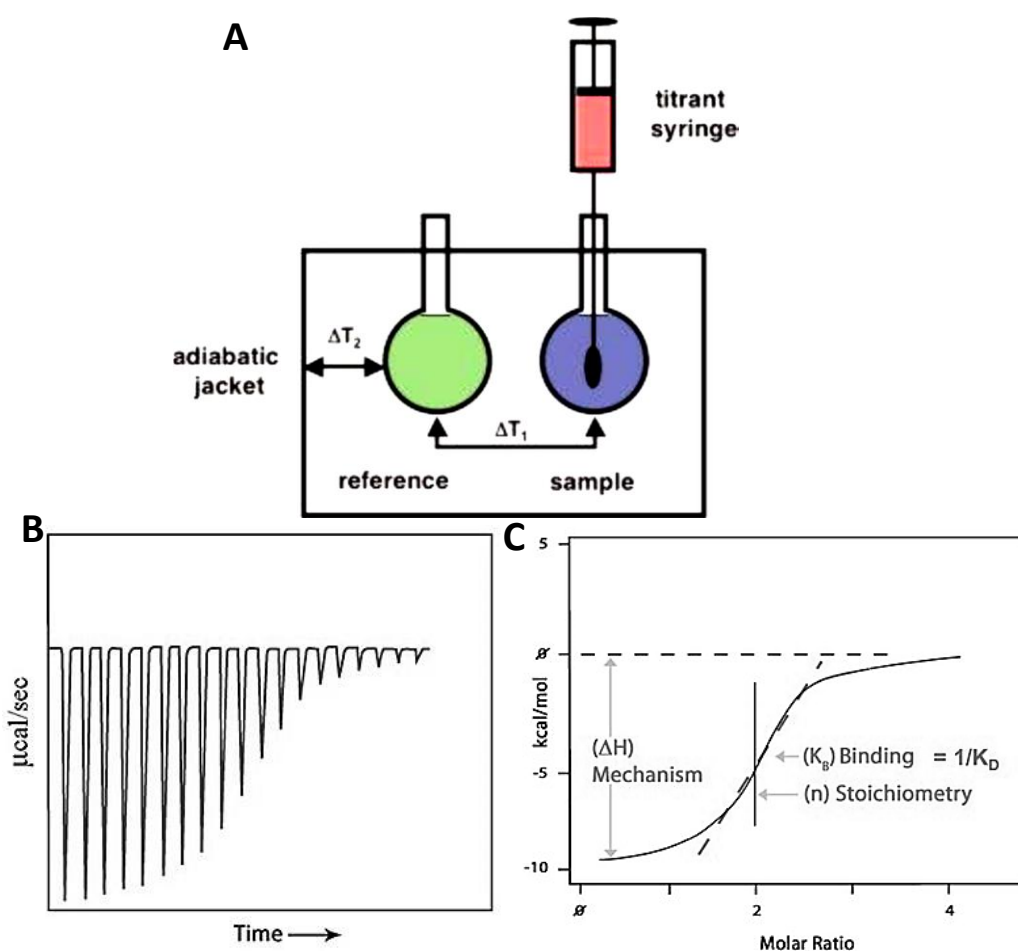
**Figure 2.4: ITC equipment and example of data produced.** (A) Schematic showing the ITC machine. The instrument is made up a reference cell, sample cell containing one molecule of interest and a syringe containing the other molecule of interest. The cells are surrounding by an adiabatic jacket to control the temperature. Image taken from Feig, A. L. (2007) Applications of isothermal titration calorimetry in RNA biochemistry and biophysics. *Biopolymers* **87**, 293-301 (2). (B) A typical profile of the peaks of heat generated by each injection of the experiment. (C) A representation of the binding curve produced by integrating the area under the peaks. The affinity is calculated by the slope of the curve, the enthalpy is represented by the height of the curve and the stoichiometry is found by finding the middle of the slope. Images B and C were taken from: http://www.huck.psu.edu/facilities/calorimetry-up/guides/itc.

## 2.17.2 Nuclear Magnetic Resonance (NMR) Spectroscopy

### 2.17.2.1 Theory

NMR spectroscopy is a method used to gain structural information of molecules by exploiting the physical properties of active nuclei to absorb electromagnetic radiation when placed in a magnetic field and the dependence of their resonance frequency on the environment of the nuclei.

NMR is based on spin angular momentum, also known simply as spin, which is a property of all particles including nuclei (336). This spin will generate a magnetic moment. When the nuclei are placed in a magnetic field the nuclei exist in two spin states: one that aligns with the external magnetic field and the other that opposes it. The Boltzmann distribution for thermal equilibrium dictates that in a sample of molecules a majority of spins will be in the lower energy level, meaning that a bulk of the magnetization will be in the direction of the external magnetic field (336). A radio frequency pulse is applied to the system to rotate the magnetization of the nuclei, usually by 90° or 180°. When a 90° pulse is applied to the system, the magnetization of the nuclei will be perpendicular to the external magnetic field and this is known as transverse magnetization (336). The transverse magnetization will rotate around the static field, in a process known as precession (336). The precession of the magnetic field induces a current in a receiver coil, which is the signal (free induction decay or FID) which is measured (336). The Fourier transform is applied to produce the spectrum of intensity as a function of frequency (13).

The shell of electrons surrounding the nuclei has an effect on its resonance frequency, as they produce a local magnetic field opposing the applied magnetic

field (336). This causes a reduction in the magnetic field sensed at the nucleus, known as shielding. The degree of shielding depends on the electron density surrounding the nucleus. The different environment surrounding the nucleus will change the resonance at slightly different radiation frequencies. This difference in frequency can be measured in the NMR spectrum, a property known as chemical shift. This can be used to decipher structural properties of the molecule, as different local environments will lead to different chemical shifts. Therefore, each nucleus within a molecule with different chemical shifts will produce peaks at different frequencies. Protons within the molecule that are in the same chemical environment will have the same chemical shift value. This will mean the peak on the spectra representing that particular chemical shift will increase in area to represent the multiple protons.

$^1$H is the most common nuclei used in NMR. As the size of the molecule increases the $^1$H 1D spectrum becomes overcrowded and assigning individual peaks becomes too difficult (336). To analyse the structures and the properties of more complex molecules, such as proteins, 2D NMR experiments are carried out, where two nuclei are analysed and the data is plotted in a space defined by two frequency axes rather than one (337). 2D experiments consist of four consecutive time periods: preparation, evolution ($t_1$), transfer and acquisition ($t_2$) (336). After the preparation time transverse magnetization has been generated and this is allowed to evolve during $t_1$. During the transfer time the magnetization is transferred to the other nucleus and the signal from the second nucleus is measured during $t_2$. The 2D data are obtained from a series of 1D measurements with $t_1$ increased between each one (336). To produce the spectra two Fourier transformations are performed, one with respect to $t_2$, and one with respect to $t_1$ (336).

For protein structure analysis, the protein must be labelled with $^{13}$C and $^{15}$N as the naturally occurring $^{12}$C and $^{14}$N will not produce an NMR signal as they do not have spin. To produce proteins labelled with $^{13}$C and/or $^{15}$N, *E.coli* are grown in media with a source of these isotopes. [$^1$N-$^{15}$N] Heteronuclear single quantum coherence (HSQC) spectroscopy is a 2D experiment that correlates hydrogen and nitrogen nuclei that are separated by one covalent bond thereby producing a spectrum with one peak for each pair of coupled nuclei representing the chemical

shift of those nuclei. For proteins this means one peak is present for every amino acid corresponding to the backbone NH groups (336). Peaks will also be generated for side chains that contain amino or amide groups. The spectrum produced is known as the fingerprint of the protein. [$^1$N-$^{15}$N] HSQC spectra are extensively used for studying the interaction between proteins and ligands, by titrating a ligand into the $^{15}$N-labelled protein of interest and following any changes in chemical shifts of the NH groups, indicating a change in the chemical environment. If the protein backbone has been fully assigned, this allows quick identification of amino acids whose chemical shift have been altered during the titration, suggesting an involvement in the molecular interaction or a conformational change upon binding (336). The [$^1$N-$^{15}$N] HSQC spectra for CaM, with and without calcium, have previously been assigned (for ApoCaM BMRB ID 5353 (338)and for CaM-Ca BMRB ID 1634 (339)), so this information can be used to assign the spectra produced in this study.

### 2.17.2.2 Experimental Procedure

*E.coli* transformed with the protein of interest was grown in minimal media (Na$_2$HPO$_4$ 6 g/L, KH$_2$PO$_4$ 3 g/L, NaCl 0.5 g/L, $^{15}$NH$_4$Cl 1 g/L, CaCl$_2$ 0.1 μM, MgSO$_4$ 2 μM, glucose 2.5 % (v:v), thiamine 1 μM, 10 ml *E.coli* trace elements (100 mM FeCl$_3$·6H$_2$O, 10 mM ZnCl$_2$·4H$_2$O, 15 mM CoCl$_2$·6H$_2$O, 10 mM Na$_2$MoO$_4$·2H$_2$O, 7 mM CaCl$_2$·2H$_2$O, 5 mM CuCl$_2$·6H$_2$O and 8 mM H$_3$BO$_3$)) and purified as before. Prior to experimentation, D$_2$O was added to the purified protein to a final concentration of 10%. 1D and 2D [$^1$H-$^{15}$N] HSQC spectra were recorded on a Bruker 500 NMR spectrometer at 25°C equipped with a cryoprobe. For analysis of the interaction between L-selectin and CaM, L-selectin cytoplasmic tail peptide was titrated in from 0.2:1 to 1.2:1 concentration with respect to CaM. This was carried out in the presence and absence of calcium. Spectra were processed using NMRPipe and analysed using NMRView. Peaks were assigned by comparing to other assigned spectra (from Biological Magnetic Resonance Data Bank, for ApoCaM BMRB ID 5353 for ApoCaM (338)and BMRB ID 1634 for CaM-Ca (339)).

_2.17.2.2.1 Chemical Shift Perturbation (CSP) Calculation and Mapping onto Structural Models_

Once the [$^1$H-$^{15}$N] HSQC spectra were assigned the peaks that shifted with titration of L-selectin were found. For each amino acid the chemical shift perturbation (CSP) was calculated using the formula:

$$\Delta\delta_{AV} \sqrt{\left((\Delta\delta H)^2 + (0.2 \times \Delta\delta N)^2\right)}$$ (340)

Where ΔδH is the difference in the proton chemical shift of the amide and ΔδN is the difference in the chemical shift of the nitrogen amide. The CSPs were then divided into categories depending on their size and colour coordinated, with red representing the largest CSPs (Δδ$_{AV}$≥0.03), orange representing moderate CSPs (0.01≤Δδ$_{AV}$≥0.03), yellow representing small CSPs (0.005≤Δδ$_{AV}$≥0.01) and white representing little or no CSPs (Δδ$_{AV}$ ≤0.005). The colour of each amino acid was then plotted on the structure of the protein obtained from the RSCB protein data bank (id 3CLN for CaM-Ca and 1CFC for ApoCaM).

## 2.17.3 Circular Dichroism (CD) Spectroscopy

### 2.17.3.1 Theory

Circular dichroism (CD) spectroscopy is a form of spectroscopy used to analyse the secondary structure of proteins and peptides. When circular polarised light hits a protein or peptide the electronic structure of the molecule of interest will cause characteristic bands on the CD spectrum (341). This means that different secondary structures within the protein or peptide will give distinct spectral bands. This information can then be used to calculate the proportion of the different secondary structures within the protein and therefore indirectly provide information of the overall structure of the protein (342).

Circular polarised light is produced by superimposing two linearly polarised beams of light of the same magnitude that are oscillating perpendicular to one another, one right polarised and one left polarised (341). This light is passed through a solution of molecules of interest. If the left and right polarised light are not absorbed or equally absorbed the radiation generated will be polarised in the

same plane, so no signal will be seen on the spectrum (343). If the solution contains chiral (asymmetric) molecules then the right and left polarised light will be refracted differently (343), the two beams will travel at different speeds and will be absorbed to different extents at each energy (341). The difference in absorption between right and left polarised light is measured and plotted against the wavelength to produce the CD spectrum (341). There are several different methods used to measure the difference in absorbance: a) modulation where the incident radiation is continuously switched between left and right polarised light, b) direct subtraction where the absorbances of left and right polarised light are measured separately and subtracted from one another and c) ellipsometric where elliplicity of the transmitted radiation is measured. Modulation is the most common method used (343).

There are several different causes of chirality: a) a molecule can be intrinsically chiral such as molecules contain carbon atoms that have different groups attached at each bonding site, b) if the moiety is covalently attached to a chiral centre within a molecule and c) the asymmetric environment the moiety is in due to the 3D structure of the molecule (343). In proteins there are several different species that contribute to chirality. These include the peptide bond, aromatic amino acid side chains and disulphide bonds. Information on the secondary structure of the molecule comes from the peptide bond, which produces bands on the spectrum from 240 nm and below (343). Figure 2.4 shows the typical spectra for alpha helix, beta sheet and random coil.
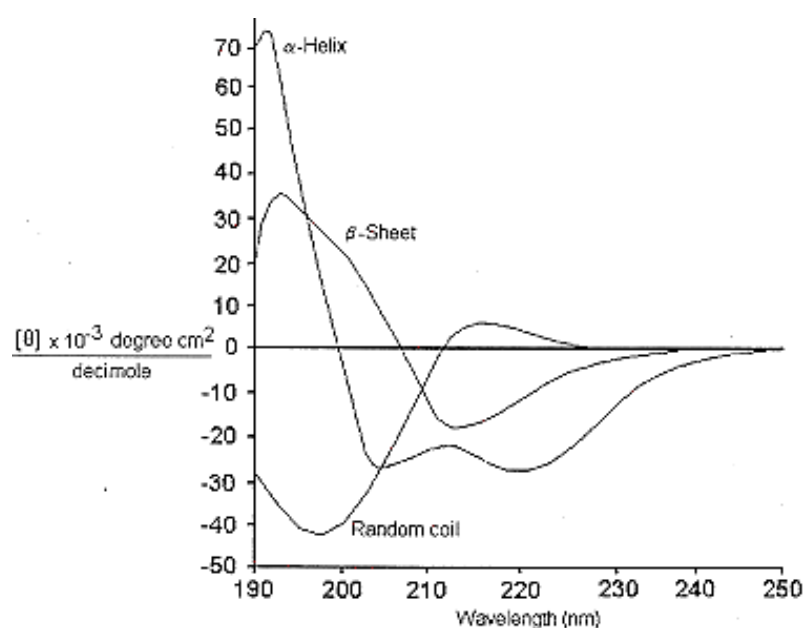
**Figure 2.5: CD Spectra of Secondary Structure.** A graphic representation of CD spectrum for different secondary structures, showing the difference in absorption at different wavelengths for α-helix, β-sheet and random coil. Figure taken from http://www.chemistry.nmsu.edu/Instrumentation/CD1.html

The electronic structure of the molecule produces characteristic bands in specific regions in the spectrum. As the different secondary structures have different electronic structures they will produce the different spectra seen in Figure 2.4 (341).

In this report CD was used to assess the secondary structure of L-selectin cytosolic tail peptides in solution.

### 2.17.3.2 Experimental Procedure

Purified lyophilised peptides were dissolved in NMR buffer or potassium phosphate buffer at a concentration of 0.2 mg/ml. CD spectra were measured by Dr Tam T.T. Bui (Biomolecular Spectroscopy Centre, King's College London) using Chirascan Plus spectrometer (Applied Photophysics Ltd). The CD spectra were measured between 260-190 nm in a 0.5 mm rectangular cell. The instrument was flushed continuously with pure evaporated nitrogen throughout the measurements. Spectra were recorded with a 1 nm step size, a 3 s measurement time-per-point and a spectral bandwidth of 1 nm.

## 2.17.4 Microscale Thermophoresis (MST)

### 2.17.4.1 Theory

Microscale thermophoresis (MST) is a biophysical technique used to analyse the interaction between two molecules. It has been observed that a temperature gradient in an aqueous solution of molecules induces a flow of molecules, an effect known as thermophoresis (344,345). The thermophoretic effect is controlled by the charge of the molecule, the size of the molecule and the interaction with the solvent environment (344). When two molecules interact with one another, one or more of these properties will be altered. This allows the binding event to be analysed and the binding constant measured.

One of the molecules of interest is labelled with a fluorescent probe. This is then added to a serial dilution of the other molecule of interest and placed in capillaries (344). An infrared (IR) laser is then focused on the sample to heat it with high precision at a specific spot, allowing a localised temperature increase over a few hundred micrometres (344,345). The fluorescence of the heated area is measured to assess the movement of the molecules in the heated area. This is repeated for all dilutions then fluorescence is plotted against the concentration of the titrated molecule to produce the binding curve, from which the binding constant can be found.

Figure 2.5 depicts a typical MST signal for one capillary (344). It shows the five stages of the signal. The initial fluorescence is the fluorescence of the sample prior to laser heating. The temperature jump is the fluorescence change induced by heating the sample and is prior to the thermophoretic molecule transport. This temperature jump represents the change in fluorescence yield of the dye due to the temperature increase (344). This is not necessarily influenced by the binding event but can be affected in some cases as the local environment will affect the temperature dependence of the dye (344). This means that if the molecule binds in close proximity to the dye or induces a conformational change close to the dye the temperature dependence of the fluorescence will change and be detected in the temperature jump. The next stage of the signal is thermophoresis, which is the change in fluorescence due to the thermophoretic movement of the molecules. This is a diffusion limited transport process and reflects any changes that have an effect on the thermophoretic mobility of the labelled molecule (344). Both the temperature jump and thermophoresis can be affected by the binding event, temperature jump is affected if binding alters the internal state of the labelled molecule, whereas size, charge and hydration shell changes from the binding event affects the thermophoresis signal (344). Analysis can include temperature jump as well as thermophoresis if desired. After a steady state is reached the laser is turned off and an inverse temperature jump is observed, as the reduction of temperature affects the fluorescent dye as before, after which back-diffusion is seen (345), where fluorescence increases as the labelled molecule diffuses back to the area heated.

To produce the binding curve the normalised fluorescence ($F_{norm}$) is plotted against the concentration of the titrated molecule (344). In principle normalised fluorescence can be calculated by: $F_{(hot)}/F_{(initial)}$, however, this does not take into consideration the change in the fluorescence due to the temperature jump. It is possible to separate the contribution of temperature jump and thermophoresis to the MST signal by choosing different times to calculate the $F_{norm}$, with temperature jump occurring less than one second after the temperature increase and thermophoresis occurring after one second (344). For analysis of just thermophoresis the $F_{norm}$ is calculated by comparing the fluorescence after thirty seconds to fluorescence after one second. The change in fluorescence will depend on the binding of the labelled molecule and can is given by:

$$F_{norm}= (1-x)\, F_{norm}\,(unbound) +xF_{norm}\,(bound)$$

where x is the fraction of labelled molecules bound to their target, $F_{norm}$ (unbound) is the normalised fluorescence of unbound labelled molecules and $F_{norm}$(bound) is the normalised fluorescence of complexes (344). From this equation differences in the normalised fluorescence of the bound and unbound state allows the determination of the fraction of molecules bound at different known concentrations of binding partners, and from this the dissociation constant can calculated.

There are many advantages to using this method to analyse the binding event between two molecules; it is quick, with each measurement only taking around 20 minutes, and requires very little material, with concentrations of low micromolar used and very small volumes required to fill the capillaries. The main disadvantage is that as it depends on measuring changes in fluorescence one molecule must be labelled, contrary to ITC, which is a label-free technique, and this labelling may affect the binding. Fluorescent dyes are covalently attached to cysteine residues using a dye attached to a maleimide group, or covalently attached to lysine residues using a dye attached to an N-hydroxysuccinimide (NHS) ester group. If the residues labelled are located in the binding site for the ligand of interest, the binding could be altered or even blocked. The cost of labelling is also a consideration.

Thermodynamics of the binding can be calculated by carrying out experiments at different temperatures and plotting $lnK_b$ against inverse temperature to obtain $\Delta H$ from the slope of the straight line graph and the intercept is $\Delta S/R$ (346), but this requires a higher number of experiments than ITC.
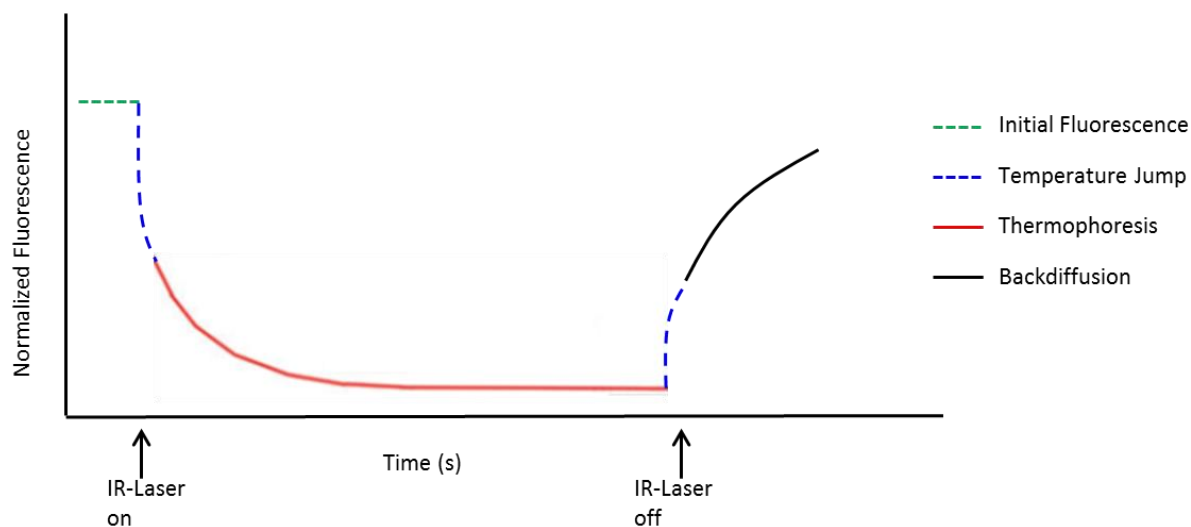


**Figure 2.6: A typical profile of the fluorescence during an MST experiment**. At the start the solution is homogeneous and fluorescence is constant. When the IR laser is switched on fluorescence changes are observed, first due to the temperature jump and then due to thermophoretic movement of the molecule. The IR laser is then switched off and there is an inverse temperature jump followed by back diffusion.

### 2.17.4.2 Experimental Procedure

Samples for MST analysis were sent to NanoTemper Technologies GmbH for experimentation. Both CaM and the peptides were sent in NMR buffer with 5 mM CaCl$_2$, with 0.05% TWEEN-20 added at NanoTemper Technologies GmbH. CaM was labelled with NT-647 dye (Lys-coupling technology) at NanoTemper Technologies using Nanotemper's protein labelling kit RED (Nanotemper Technologies) and mixed with the unlabelled peptide. CaM was kept at a concentration of 20 nM, with peptide concentration starting at 262.2 µM for wildtype and 375 µM for S364phos, S367A and S364A, and diluted down to 1:1, with 16 dilutions carried out and incubated at room temperature for 30 minutes. Each different dilution was loaded into an enhanced gradient standard treated MST-grade glass capillary using capillary force and the ends of the capillary were sealed with wax. The capillaries were placed into the instrument tray in concentration order and the tray was

transferred to the instrument. Analysis of each capillary was carried out using a Monolith NT.115 instrument with 15 % LED power and 20 % IR power.


## 2.18 Cell lines and Culturing

All cell lines used were cultured at 37 °C in a 5 % $CO_2$ incubator.

### 2.18.1 Human Embryonic Kidney (HEK) 293T Cells

HEK cells were a gift from Dr Yolanda Calle (Cancer Division, King's College London). The cells were cultured in RPMI-1640 media (Life Technologies) supplemented with 10 % FBS, 1 % antibiotics (penicillin/ streptomycin). The media was changed every 2 days and once confluent, cells were passaged with a sub-cultivated ratio of 1:6.

### 2.18.2 THP-1 cells (Acute Monocytic Leukaemia, Human)

THP-1 cells were purchased from American Type Culture Collection (ATCC) and those containing wildtype L-selectin or the mutants ΔM-N, S364A, S367A, and SSAA all tagged with GFP were produced by Karolina Rzeniewicz (Cardiology, King's College London). Cells were cultured in RPMI-1640 media supplemented with 10 % FBS, 1 % antibiotics (penicillin/ streptomycin) and 0.05 mM β-mercaptoethanol. Cells were seeded at a density of $0.5 \times 10^6$ cells/ml and split every 2-3 days.

### 2.18.3 Human Umbilical Vein Endothelial Cells (HUVECs)

HUVECs were purchased from Lonza and cultured in M199 media supplemented with 10 % FBS, 1 % antibiotics (penicillin/ streptomycin) and endothelial cell growth supplement in fibronectin (10 µg/ml) coated plates. Cells were grown to confluence then used in experiments.

### 2.18.4 Cryopreservation of Cells

For cryopreservation, around $10 \times 10^6$ cells were collected by centrifugation and re-suspended in 1 ml 90% FBS 10% DMSO. The cells were immediately transferred to pre-chilled Corning freezing vials and placed on ice prior to being stored at -80 °C. After 48 hours the vials were transferred to liquid nitrogen for long term storage. For re-culturing, vials were rapidly thawed in a 37 °C water bath.

After thawing the cells were added to 9 ml of fresh media and the cells were harvested by centrifugation. The cell pellet was then re-suspended in fresh media and placed in a flask for culturing.

## 2.19 Lentiviral Production and Generation of Stable Cell lines

### 2.19.1 Lentivirus Production

Lentiviral particles were produced using HEK cells as the packaging cell line. Cells were plated one day before transduction at a density of 10-15 x $10^6$ cells per 14 cm dish. On the day of transduction 30 µg Pax2, 10 µg pMD.G helper vectors and 40 µg of the vector of interest were added to 4 ml of OPTIMEM media. 1 µl of 10 mM polyethylene imine (PEI) was added to 4 ml of OPTIMEM in a separate tube (all quantities are correct for one dish; if more than one dish is required the reagents were adjusted accordingly). The two tubes were mixed and left at room temperature for 15 minutes. The culture media was aspirated from the HEK cells and the transduction media was added to the cells in a drop wise manner. The cells were incubated at 37 °C for 4 hours, after which the transduction media was removed and fresh media was added to the cells. Cell supernatant containing lentiviral particles was collected 48 and 72 hours after transduction. The lentiviral particles were concentrated by ultracentrifugation using a SORVALL® Discovery ultracentrifuge with a TH641 rotor, spinning at 19900 rpm, at 4 °C for 2 hours. After ultracentrifugation the supernatant was decanted and 50 µl of RPMI was added to each tube and incubated on ice for 20-40 minutes. The lentivirus pellets were re-suspended, pooled together, aliquoted in 25 µl fractions and stored at -80 °C until used.

### 2.19.2 Titration of Lentivirus

In order to establish lentiviral titres, HEK cells were transduced with different dilutions of the concentrated lentivirus. HEK cells were plated in 24-well plates at a density of 150-200x$10^5$ cells/well. A serial dilution was carried out with the lentivirus ($10^{-1}$ to $10^{-6}$) in HEK cell media, and added to the cells. The next day

the media was changed and two days later the cells were collected by trypsinisation and re-suspended in PBS. The expression of GFP/RFP was analysed using FACs to identify the percentage of GFP/RFP positive cells. The virus titre was established from cells that were 1-20% transduced. The titres were calculated using the following equation:

$$T = \frac{P \times N}{D \times V}$$

where T=titer, P=GFP/RFP positive cells, N= number of cells, D=dilution and V=volume. The volume of lentivirus required for the transduction of the target cells was calculated based on the desired multiplicity of infection (MOI) using the following equation:

$$Volume(ml) = \frac{no.cells \times MOI}{titre}$$

### 2.19.3 Production of THP-1 transduced cells

The lentivirus produced was used to transduce either THP-1 ATCC cells or THP-1 cells that had previously been transduced with different L-selectin-GFP lentiviruses. $1 \times 10^6$ THP-1 cells were collected and re-suspended in THP-1 media containing the volume of lentivirus required for the desired MOI. The media was changed the next day and the cells were grown until $10 \times 10^6$ cells were produced. The cells were then sorted using a Beckman Coulter cell sorter at a core funded FACs sorting facility, to produce a population expressing the fluorescent protein required. The sorted cells were then cultured for use in experiments.


## 2.20 Parallel Plate Flow Chamber Assay

Transmigration of THP-1 cells through TNF-α activated HUVECs was carried out using a parallel plate flow chamber assay. Coverslips were covered with fibronectin (10 µg/ml) in PBS and incubated for 2-4 hours at 37 °C. The fibronectin solution was removed and HUVECs were plated onto the coverslips. The HUVECs were left to reach confluence (3-5 days) and were then stimulated with TNF-α for between 4 hours and overnight. The coverslip of HUVECs was attached to the flow chamber using a vacuum pump and was placed on the microscope (Figure 2.6).

THP-1 cells were re-suspended in THP-1 media with 25 mM HEPES at a density of 0.5 x 10$^6$ cells/ml. The cells were then perfused over the HUVECs at a flow rate of 0.25 ml/min, applied using a Harvard syringe pump. Experiments were carried out at 37 °C. Experiments were visualized using an Olympus IX81 time-lapse inverted fluorescence microscope attached to a Hamamatsu C10600 ORCA-R2 video camera. For short transmigration experiments cell were perfused for 5-7 minutes, and images were recorded at three random fields of view with three time points per minute. For long transmigration experiments cells were perfused for 5 minutes then media only was perfused over the HUVECs for a further 20 minutes, with images recorded at three random fields of view with one time point per minute. All experiments were recorded using a 10x objective. Images were acquired into video files using Volocity imaging software.
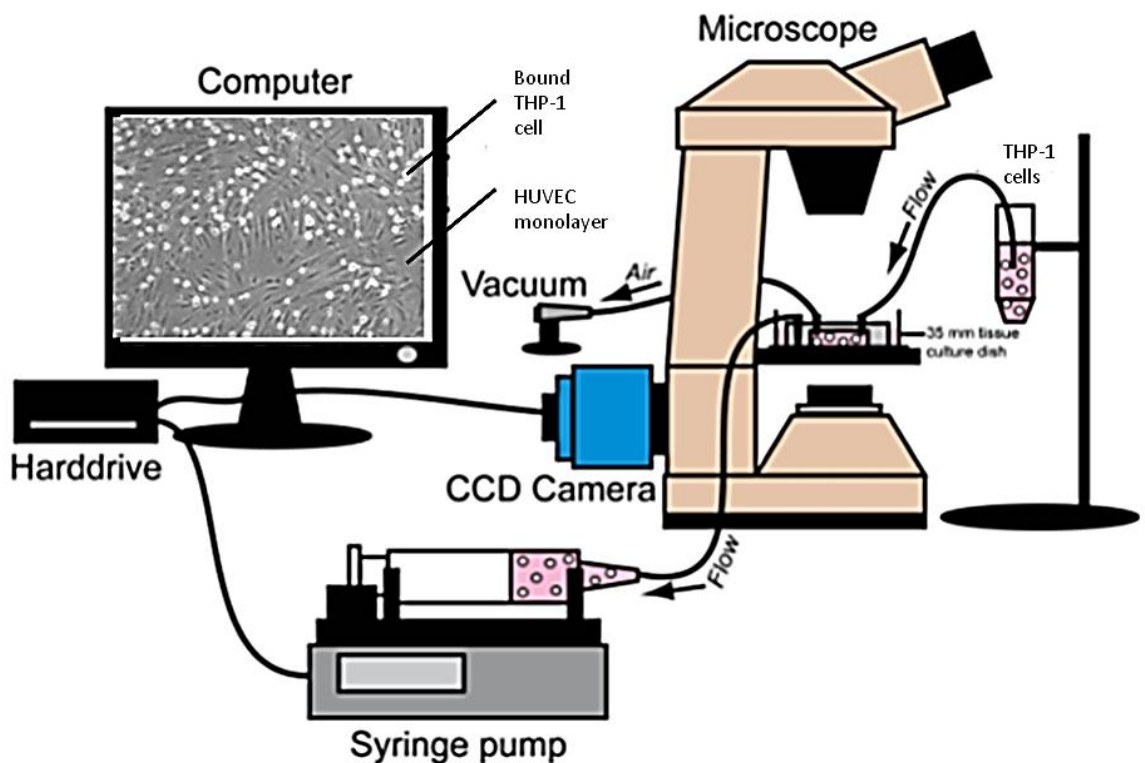


**Figure 2.7: Parallel plate Flow Chamber system.** Diagram illustrating the system used for the parallel plate flow chamber assay. The chamber is attached to a coverslip with a monolayer of HUVECs grown over it using the vacuum force and placed over the objective of an inverted microscope. A syringe pump is used to draw THP-1 cells suspended in media through the chamber with a set flow rate (set by a syringe refill rate). The footage is recorded by the CCD camera connected to the computer. The data is visualised and analysed Volocity. Image modified from Wiese, G., Barthel, S. R., and Dimitroff, C. J. (2009) Analysis of physiologic E-selectin-mediated leukocyte rolling on microvascular endothelium. Journal of visualized experiments : JoVE (7).

## 2.21 Preparation of Coverslips for FRET/FLIM Analysis

### 2.21.1 Poly-L lysine (PLL) coated coverslips

Coverslips were placed in the bottom of the wells in a 24-well plate and 100 µl of PLL was added to each well. The plate was incubated at room temperature for twenty minutes, after which time the PLL was aspirated and the coverslips were allowed to dry overnight. The next day $0.1 \times 10^6$ THP-1 cells were suspended in 100 µl of PBS, placed on top of the coverslips and left for ten minutes. After this time the coverslips were aspirated and fixed with 4 % paraformaldehyde (PFA) for ten minutes at room temperature. The coverslips were then washed with PBS several times and permeabilised with ice cold 0.1 % Nonidet P-40 (NP-40) substitute for a maximum of three minutes. The NP-40 was then aspirated and the coverslip was washed several times with PBS. Sodium borohydride (1 mg/ml) was added to the coverslips for ten minutes and they were left in the dark. This is a reducing agent used to decrease the background fluorescence. The sodium borohydride was aspirated and the coverslips were washed several times in PBS. The coverslips were then mounted on glass slides and stored in the dark at 4 °C until analysis was carried out by Dr Maddy Parsons, KCL.

### 2.21.2 Coverslips from flow chamber assay experiments

Once flow chamber assay experiments were completed, the coverslips were removed and placed in 4 % PFA for ten minutes at room temperature to fix the cells. The coverslips were washed several times in PBS and then permeabilised with ice cold 0.1 % NP-40 substitute for no more than three minutes. The NP-40 solution was then aspirated and the coverslip was washed several times with PBS. Sodium borahydride (1 mg/ml) was then added for ten minutes and the coverslips were placed in the dark. After aspiration of the sodium borohydride, the coverslips were washed several times in PBS. The coverslips were then blocked with 5 % BSA in PBS for 20 minutes at 4 °C, after which time they were placed in a humidifying chamber on top of phalliodin-Alexa633 diluted 1:300 in 5 % BSA in PBS. The chamber was

placed at 4 °C in the dark overnight. The next day the coverslips were removed from the chamber and washed several times with PBS. They were then mounted on slides and stored in the dark at 4 °C until analysed. All FRET/FLIM analysis was carried out by Dr Maddy Parsons, KCL.

## 2.22 Analysis of cell characteristics during TEM

The videos produced during the parallel plate flow chamber assay were used to analyse the protrusion number, cell area and circularity of the THP-1 bound to the HUVEC monolayer. The videos were paused at 7, 15 and 25 minutes and the THP-1 cells within the field of view were characterised as having no, one, two or multiple protrusions. ImageJ software was then used to draw around each cell, including any protrusions that were visible. The cell area and circularity were then calculated by the ImageJ software. For each experiment three fields of view were analysed at each time point, with between 20 and 100 cells being assessed.

## 2.23 GFPTrap Immunoprecipitation Assay

### 2.23.1 Cells in suspension

GFPTrap beads were purchased from chromotek. Cell lysate was produced by collecting $2 \times 10^7$ cells, which were washed with PBS. The cells were then re-suspended in 200 µl lysis buffer (10 mM Tris-HCl pH 7.5, 150 mM NaCl, 0.5 mM EDTA, 0.5% NP40, 1 x protease inhibitor cocktail, 50 nM calyculin, 1 µM bisindolylmaleimide). The lysis solution was placed on ice for thirty minutes with vigorous mixing every ten minutes. The lysate was then spun at 20000 xg for ten minutes at 4 °C using an eppendorf 5417R microcentrifuge. The supernatant was collected and 550 µl of wash buffer (10 mM Tris-HCl pH 7.5, 50 mM NaCl, 0.5 mM EDTA, 1 x protease inhibitor cocktail, 50 nM calyculin, and 1 µM bisindolylmaleimide). 25 µl of GFPTrap beads were re-suspended in 500 µl of wash buffer and spun down at 2700 xg for two minutes at 4 °C. The supernatant was discarded and the wash steps were repeated twice more. The cell lysate was added to the beads and incubated at 4 °C overnight with constant mixing. The next day the

beads were spun down at 2700 xg for two minutes at 4 °C and the supernatant was discarded. The beads were washed three times with cold wash buffer (500 µl). After washing, the beads were re-suspended in 2x SDS protein loading buffer and boiled for ten minutes at 95 °C. The beads were collected by centrifugation at 2700 xg for two minutes at 4 °C. The supernatant was used for SDS-PAGE and Western blot analysis was carried out to detect CaM and GFP.

Experiments were also carried out as above, except 1% ovalbumin was added to the lysis and wash buffers.

## 2.23.2 THP-1 cell co-culture with TNF-α activated HUVECs

HUVECs were plated in six well plates and left to grow until confluent. Once confluent, the HUVEC were activated with TNF-α for 4 hours. $2 \times 10^6$ THP-1 cells were re-suspended in 1.5 ml of media and added on top of the activated HUVECs. The cells were incubated at 37 °C for five minutes, then the media was aspirated and 400 µl of lysis buffer or lysis buffer supplemented with 1% ovalbumin was added and the plate was placed on ice for thirty minutes, with mixing every ten minutes. The lysate was then spun down as before and the supernatant collected and diluted with 1 ml of wash buffer or wash buffer containing 1% ovalbumin. The immunoprecipitation was then carried out as described above (Section 2.23.1).

## 2.24 Co-Culture of THP-1 cells with HUVECs for Shedding Analysis

HUVECs were grown in six well plates until confluent and were then activated with TNF-α overnight. $0.75 \times 10^6$ THP-1 cells were re-suspended in 1 ml of THP-1 media and added to each well of the plate. Each well was allocated a time point: 0, 5, 10, 20, 30 or 60 minutes. At the corresponding time point the media from that well was collected as the unbound fraction and the bound fraction was collected from the well using a cell scraper. CytoBuster (Novagen) supplemented with protease inhibitors was used to lyse the cells using the manufacturer's protocol. Protein loading buffer was added to the cell lysate and the samples were

run on SDS-PAGE and Western blot analysis was carried out as described in Section 2.16 to detect L-selectin-GFP.

## 2.25 Statistical Analysis

Quantitative data was collated and analysed using Microsoft Excel 2010, which was also used to produce all bar and line graphs, except for those produced by the analysis of the ITC, which were produced by Origin7. To determine significant differences between data an independent two-tailed Student's T test or a One-way Anova followed by a Tukey's post-hoc test were carried out where mentioned in the text.

# Chapter 3: Production and Characterisation of Recombinant Proteins for Biophysical Assays

## 3.1 Introduction

L-selectin has a 17 amino acid cytosolic tail, which has been reported to bind several proteins, including CaM and the ERM family of proteins (215,216,223,224). The binding of such proteins is thought to mediate numerous functions of L-selectin function, which includes downstream signalling (Section 1.3.6). Study of the interaction between L-selectin, CaM, and moesin was carried out *in vitro* using a peptide corresponding to the cytosolic tail of L-selectin coupled to sepharose beads. The results showed that both CaM and moesin were able to interact with the peptide and when the beads were preloaded with one of the proteins, the other was still capable of interacting, suggesting that a tertiary complex was formed (3). The interaction was then studied *in vivo* using COS-7 cells transfected with ezrin-FERM-GFP, CaM-RFP and wildtype full-length L-selectin. The FRET efficiency between ezrin-FERM-GFP and CaM-RFP increased when all three proteins were co-expressed and L-selectin was clustered using antibody, providing further proof that the three proteins form a tertiary complex (3). Although it has been shown that this interaction occurs, little is known about the mechanism or the regulation of this process.

To gain further insight into the interaction between the cytoplasmic tail of L-selectin, CaM and moesin, a detailed characterisation was performed using complementary *in vitro* biophysical techniques, such as NMR, ITC and MST. The details of these methods are described in Section 2.17 of Materials and Methods. Peptides representing the 17 amino acid cytosolic tail of L-selectin, either wildtype, phosphorylated or alanine-mutated versions were commercially sourced. Recombinant CaM and the FERM domain of moesin (moesin-FERM) were produced in an *E.coli* system to produce large quantities of the protein. Recombinant proteins expressed in *E.coli* have been successfully purified, using a number of chromatography procedures. This chapter describes in detail the methods that

were used to clone and express CaM and moesin-FERM so that these could be used in the following chapter.

## 3.2 Experimental Design

When large quantities of recombinant protein are required for experimentation, genetically modified expression systems are used. There are several different expression systems available, including *E.coli*, yeast and mammalian systems, all with different advantages and disadvantages. The most commonly used system is the *E.coli* expression system. This involves cloning recombinant genes into vectors used to transform *E.coli* cells, which will then produce the protein under the control of an induction system. A common induction method employs the T7 RNA polymerase to over-produce the recombinant protein. This polymerase is often used for recombinant protein expression due to its ability to rapidly transcribe mRNA. The *E.coli* cells used to produce recombinant proteins all encode the T7 RNA polymerase under the control of a lacUV5 promoter (347). The cells also contain the *lacI* gene, which encodes the lac repressor that binds to the lacUV5 promoter, inhibiting transcription of the T7 RNA polymerase. Addition of the lactose analogue IPTG blocks this inhibition by binding to the lac repressor, causing allosteric alterations to the lac repressor and therefore promoting the release of the repressor from the promoter, allowing transcription of T7 RNA polymerase and therefore production of the recombinant protein of interest, which has been cloned downstream of a T7 promoter, allowing tight control of the expression of the recombinant protein of interest (347,348). There are several advantages to using the *E.coli* expression system, which include: easy growth conditions and the ease in which production can be scaled up. The major disadvantage of this system is that it is estimated that only 10 % of mammalian proteins expressed by *E.coli* are soluble and proteins larger than 60 kDa are more likely to be insoluble (349). Solubility can be improved by altering growth conditions (348), or by the co-expression of chaperone proteins. It is also possible to purify insoluble proteins by controlled denaturation, followed by refolding the proteins after purification; however, this is time consuming and the success is again very dependent on the protein.

In this thesis, an *E.coli* expression system was chosen for the production of recombinant proteins due to the simple transformation and growth of the cells and the quick production of large quantities of protein possible. This method has previously been utilised to successfully produce recombinant CaM (350), which was employed in the first instance.

Many different *E.coli* cells have been engineered to replicate the vector and enhance the production of recombinant proteins, with several of these different strains being used in this thesis. The KRX *E.coli* strain (which will be referred to as KRX cells) was used to replicate the vector containing the recombinant protein. It has been engineered to lack the nuclease endoA (351), which co-purifies with plasmid DNA and will therefore contaminate the vector containing the recombinant protein. KRX have a mutated version of the RecA gene (351), which encodes a recombination protein, and therefore undesirable recombination events are minimized. It also contains a partially defective restriction modification system (351), limiting the degradation of the vector containing the recombinant protein gene. KRX cells have also been modified to enhance protein production, including mutations of the protease genes OmpT and OmpR to minimize proteolysis of the recombinant protein (351). The cells contain a copy of the T7 RNA polymerase controlled by a rhamnose promoter. Using a rhamnose promoter enables tight control of the expression of the protein (351). In this study KRX cells were not utilised for protein production as the presence of glucose in the growth media inhibits the rhamnose promoter. This means that $^{13}$C-labelled glucose cannot be added to minimal media for the production of labelled protein required for NMR studies. It is possible to use $^{13}$C-labelled glycerol as an alternative; however this is much more costly. For this reason two other *E.coli* strains were utilised for protein production in this thesis. The first is the BL21-DE3-pLysS strain, which is deficient in the proteases Lon and OmpT (348,352). The pLysS gene encodes a plasmid for T7 lysozyme. This lowers the background of recombinant protein expression prior to induction, but has no effect after protein expression has been induced, therefore reducing the leakiness of the expression (353). The second *E.coli* strain used was the Rosetta 2 strain (referred to as Rosetta cells). This strain contains a plasmid

containing tRNA for seven codons rarely used by *E.coli* strains. This allows for quick translation that would otherwise be delayed by the *E.coli* codon use (354,355). Due to the advantages of using both these strains of *E.coli* for recombinant protein production, both strains are used for different proteins in this report. A third *E.coli* strain was utilised for the production of proteins that had been produced in the insoluble fraction by the other *E.coli* strains. This strain is known as "Arctic cells", as it has been engineered to produce proteins at very low temperatures. The alterations that have been made to these cells to promote protein expression are described below (Section 3.3.2).

Once the *E.coli* expression system has been used to produce large quantities of recombinant protein, the protein must be isolated from the cell lysate to very high purity. The most efficient way to purify recombinant proteins is via affinity chromatography, which requires the protein to be cloned as a fusion protein with an affinity tag. Affinity chromatography is very efficient in separating the desired protein from other contaminant proteins. Several different tags have been engineered to aid purification of recombinant proteins, including a glutathione S-transferase (GST) and Hexa Histidine tag (His6-tag), all with advantages and disadvantages. An advantage to using the GST-tag is that it provides some protection from proteolysis, leading to increased protein yield (356). There are several disadvantages to using this tag however, including a time-consuming purification (357). The tag can also promote oxidative aggregation (358), leading the recombinant protein becoming insoluble. Due to its large size, NMR analysis of the recombinant protein is not possible with the GST-tag attached (359), meaning it has to be removed prior to experimentation.

In this study recombinant proteins were tagged with a His6-tag, which allowed for purification using immobilised metal affinity chromatography (IMAC). This method involves histidine interacting with immobilised transition metal ions, in this case nickel ions. The electron donor groups within the imidazole ring of histidine coordinate bonds with the nickel ions. The recombinant protein can be eluted by altering the pH, salt concentration or adding imidazole to the buffer to act as a direct competitor for the nickel ions. The nickel resin is formed by using a

chelator, such as nitrilotriacetic acid (NTA), to attach the nickel ions to an agarose matrix, therefore the resin is known as Ni-NTA (356). The advantage of using this resin for purification is that it is capable of withstanding a wide range of buffer conditions, including detergents, it is also inexpensive and can be regenerated for repeated use. A possible disadvantage is that the resin will interact with any protein containing clusters of histidine residues, which means that endogenous proteins often interact with the resin, causing contaminants to the recombinant protein (360). An advantage to using the His6-tag is that NMR studies can be carried out with the tag present due to its small size. Indeed studies have been carried out on proteins with and without the tag and have shown the resulting 3D structures were roughly equivalent (348).

As the addition of affinity tags can pose problems, purification procedures without the addition of tags has been developed for several proteins. In this thesis, methods for purifying untagged CaM and moesin are also described. These methods take advantage of intrinsic chemico-physical properties of the protein to facilitate purification.

In addition to recombinant proteins, the production of $^{15}$N/$^{13}$C-labelled L-selectin cytoplasmic tail was attempted. Peptides and small proteins that are intrinsically unfolded are often degraded when produced by *E.coli* cells (361,362). To help protect against degradation, the peptide was expressed with a tag. The scaffold protein Trp-Cage was chosen as the tag as it has previously been utilised as a tag for NMR studies, so has been characterised already and the method used can be followed here.

## 3.3 Results

### 3.3.1 Production of recombinant CaM protein

In order to produce recombinant CaM, a vector containing the cDNA for CaM was produced. The pETDuet vector (Figure 2.1A in Materials and Methods) was chosen as the expression vector. It contains two multiple cloning sites (MCS): MCS1 and MCS2, both of which contain a T7 promoter to allow for the control of the expression of the recombinant protein (as described in section 3.2). MCS1

enables proteins to be cloned with a His6-tag attached to aid purification of the recombinant protein. To enable the removal of the His6-tag after purification, CaM was cloned with primers that contained an N-terminal tobacco etch virus (TEV) protease cleavage site, positioned between the tag and the start of CaM. TEV protease is a highly specific cysteine protease from the tobacco etch virus. It recognises the amino acid sequence ENLYQS, cleaving between Q and S. The high specificity for this sequence is endowed by the presence of a binding tunnel for the substrate. This means that there is a large contact area between the TEV protease and the target sequence, allowing for high specificity (363) and therefore the use of this protease in removing protein tags is desirable, as it is highly unlikely that it will cleave within the sequence of the recombinant protein.

PCR was carried out using full length human CaM cDNA, a gift from Donald C. Chang (Hong Kong, China), as the template and primers containing restriction sites for SalI and NotI to allow the insertion of the CaM cDNA into MCS1 of the pETDuet vector. A PCR reaction was carried out as previously described (Section 2.5) to amplify the CaM cDNA with the restriction sites required for cloning. The purified PCR product was then digested with appropriate restriction enzymes and a ligation of the CaM insert and the pETDuet vector was carried out as described in Section 2.6. The ligation reaction mixture was then used to transform KRX cells and the bacteria were grown on LB agar containing ampicillin, for the selection of colonies that had successfully been transformed with the pETDuet vector. Single colonies were picked, cultured overnight, and the plasmid DNA was isolated using the "mini prep" protocol, following the manufacturer's instructions. The isolated plasmids were sent for sequencing to ensure the DNA sequence for CaM had been successfully cloned in frame with His6-tag and that no mutations had occurred during the cloning procedure. A plasmid containing the correct sequence was then used to transform Rosetta cells for protein expression.

After cloning had been successfully achieved, expression of His6-tagged CaM (His6-CaM) by Rosetta cells had to be tested as well as whether any His6-CaM produced was soluble, and therefore could be purified. To assess this, an expression test was carried out at 37 °C inducing cells with 1 mM IPTG for six hours, taking

samples every hour. Expression of His6-CaM was clearly observed from one hour induction onwards, with a peak of expression observed at four hours (Figure 3.1A). The solubility of His6-CaM was tested by sonication followed by separating the insoluble fraction from the soluble fraction by centrifugation, then analysing both samples by SDS-PAGE. The results showed that the protein was found in the soluble fraction (Figure 3.1B). As the protein was soluble and highly expressed, large quantities of His6-CaM could be produced and purified.
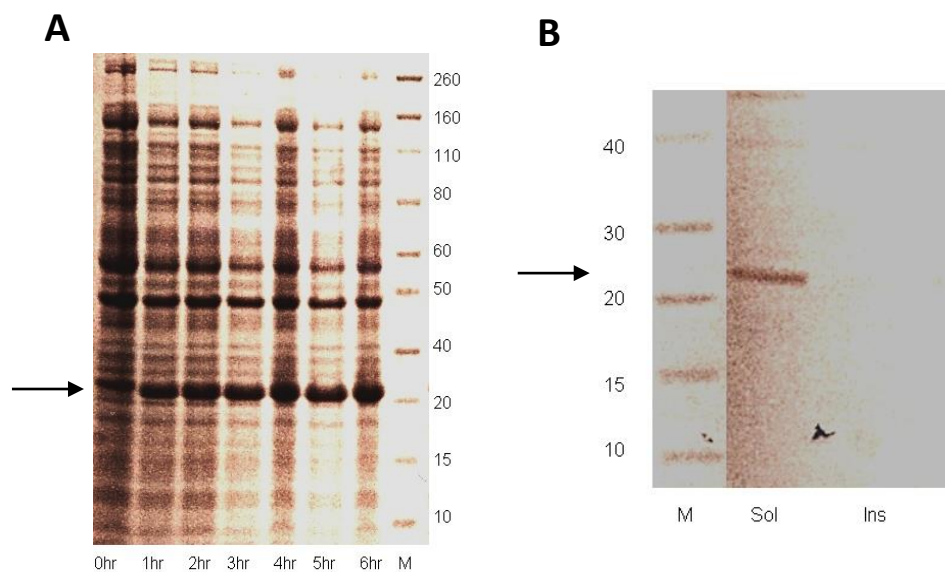


**Figure 3.1: Expression test of His6-CaM in BL21-DE3-pLys cells.** (A) Test expression of His6-CaM in BL21-DE3-pLys *E.coli* cells showing the protein present between 0 and 6 hours post induction. (B) The solubility of His6-CaM was assessed by sonicating the cells and fractionating the lysate in to insoluble and soluble entities and analysing the fractions by SDS-PAGE. Arrows indicates His6-CaM. M= Protein marker, with molecular weights shown in kDa, Sol= soluble fraction, Ins= insoluble fraction.

Large scale production of recombinant His6-CaM was carried out by growing two litres of bacteria culture using the conditions shown to be favourable for protein production in the expression test, namely 37 °C and induction with 1 mM IPTG for four hours. The bacteria were harvested and sonicated to disrupt the cell membrane and release the soluble proteins produced by the cell. The soluble proteins were separated from the cell debris by centrifugation at high speed. An AKTA system was used for the purification of His6-CaM. A 5 ml nickel ($Ni^{2+}$) affinity

column was attached to the system and equilibrated with 10 column volumes of Ni$^{2+}$ buffer A (see Section 2.12.3 for the buffer recipe). The soluble proteins were loaded onto the column, which was pre-equilibrated with 10 column volumes of Ni$^{2+}$ buffer A to remove any unbound proteins. His6-CaM was eluted from the column using a gradient of Ni$^{2+}$ buffer B (see Section 2.12.3 for a recipe), which contains a high concentration of imidazole to compete with the His6-tag for Ni$^{2+}$ binding sites, causing His6-tag dissociation from the Ni$^{2+}$ resin and therefore elution of His6-CaM from the column. The AKTA purification system measures the absorbance of ultraviolet (UV) light of wavelength 280 nm. As proteins contain amino acids with aromatic rings, ultraviolet light of this wavelength will be absorbed. This allows one to follow the purification experiment with an absorbance profile, so that the elution of proteins can be observed by a change in the absorbance (Figure 3.2A). After the purification experiment was completed any fractions that were shown to contain protein by the 280 nm absorbance profile were analysed by SDS-PAGE (Figure 3.2B). This allowed for the selection of fractions that contained only His6-CaM.

TEV protease was produced in-house as a His6-tag fusion protein to enable the easy removal of the protease from the recombinant protein of interest after His6-tag cleavage was carried out. Fractions eluted from the Ni$^{2+}$ column shown to contain His6-CaM, were dialysed with TEV protease in TEV cleavage buffer (see Section 2.12.3) overnight to remove the His6-tag. The untagged CaM was then purified from the TEV protease, the cleaved tag and any CaM that remained tagged, by passing it once again through the Ni$^{2+}$ affinity column, with cleaved CaM being present in the flow through (Figure 3.2C).  The yield of pure recombinant CaM fllowing these purification steps was around 12 mg/l.
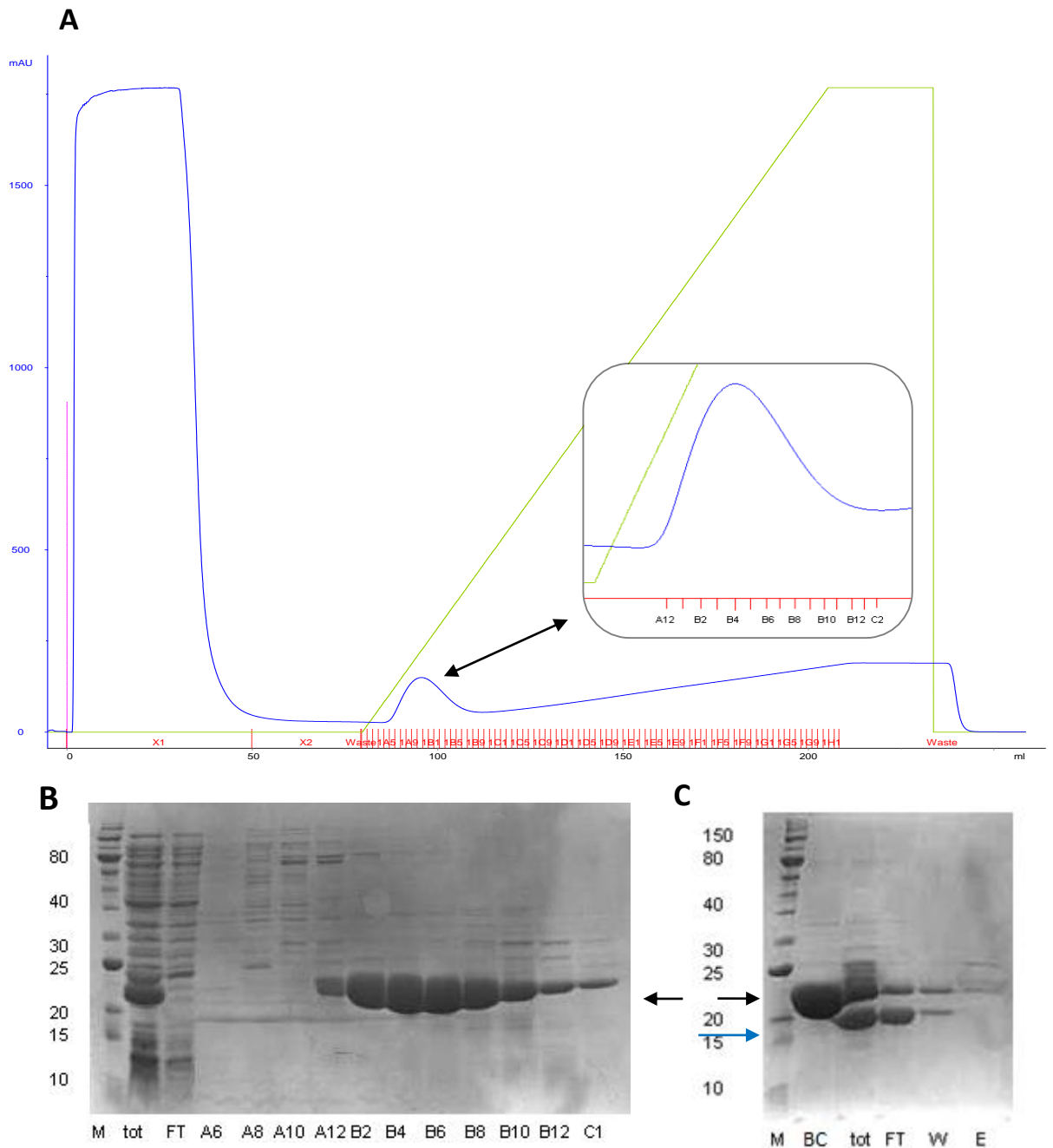
**Figure 3.2: Purification of His6-CaM.** (A) The purification profile for CaM passed through the nickel affinity column attached to the AKTA system. The blue trace represents the UV280 absorbance measured in milli-absorbance units (mAU), green represents the concentration of buffer B, injection of the lysate onto the column is shown by the pink marker and collection fractions are shown in red. The zoom insert shows the elution peak for His6-CaM, with the fractions collected for analysis by SDS-PAGE shown. (B) Fractions from the purification were run on SDS-PAGE gel and those fractions shown to contain CaM were taken for TEV protease cleavage. (C) After TEV cleavage solution was passed through a nickel column to attempt to separate cleaved CaM from the His6-tag, uncleaved His6-CaM and the His6-tagged TEV protease. M=marker, with the molecular weight shown in kDa, tot=total lysate, FT= flow through, BC= before cleavage, W= wash with $Ni^{2+}$ buffer A, E= elution with $Ni^{2+}$ buffer B. Cleaved protein is shown with the blue arrow, whereas uncleaved protein is indicated with the black arrow.

Problems were encountered when separating the tagged CaM from the untagged. After TEV cleavage was carried out, and the solution was passed through the nickel column once again, both untagged and tagged proteins were found in the flow through. The flow through was then passed through the nickel column once more in an attempt to re-capture some of the unbound protein, and though some of the tagged CaM was removed, a proportion was still visible in the flow through (Figure 3.3). This meant that the His6-tag of the tagged CaM was not interacting efficiently with the $Ni^{2+}$ affinity column. A possible explanation for this behaviour could be that CaM may be interacting with, and therefore masking, the His6-tag of tagged CaM molecules. If this was the case, the interaction may well affect subsequent binding studies. To avoid this potential problem, an *E.coli* vector containing an untagged CaM sequence was obtained (364) so untagged-CaM protein could be produced in-house and in the short term pure recombinant untagged-CaM protein was commercially sourced (see Section 2.3).
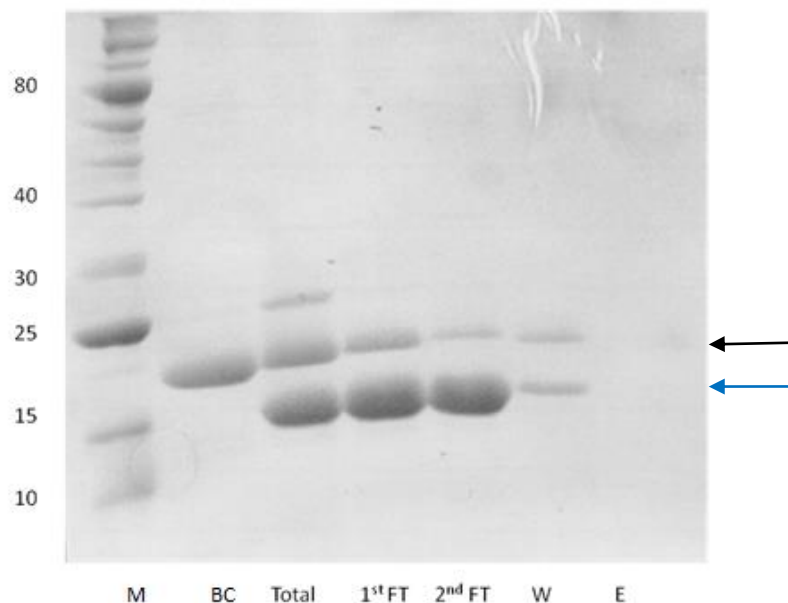


**Figure 3.3: Separation of His6-CaM from TEV protease cleaved CaM.** TEV cleavage was carried out on His6-CaM and the solution was passed through nickel column. The flow through was collected (1st FT) and found to contain both cleaved and uncleaved protein. The 1st FT was then passed through the column once again in an attempt to further separate cleaved CaM from uncleaved CaM and fractions collected for analysis by SDS-PAGE. Both cleaved and uncleaved CaM was once more found in the flow through (2nd FT). The marker is shown on the left, with molecular weights shown in kDa, BC= before cleavage, Total = total after incubation with TEV, W=wash with $Ni^{2+}$ buffer A and E=elution with $Ni^{2+}$ buffer B. Cleaved protein is shown with the blue arrow, whereas uncleaved protein is indicated with the black arrow.

128

The vector encoding for untagged CaM was used to transform Rosetta cells and, as before, an expression test was carried out to ensure that CaM was produced in a soluble form. As soluble protein was observed at 37°C inducing cells with 1 mM IPTG for four hours for His6-CaM, these conditions were also used to test the expression of soluble untagged CaM. Analysis of the solubility of untagged CaM by SDS-PAGE revealed that the protein was in fact soluble (Figure 3.4A) and so therefore large quantities of the protein could be produced and purified.

Production of untagged CaM was scaled-up by culturing two litres of *E.coli* using the growth conditions found to be favourable for the production of soluble protein in the expression test and the soluble fraction was obtained as described previously (Section 2.12.2). The method used to purify untagged CaM altered slightly on the basis that the protein must be in its calcium loaded form (CaM-Ca). For this reason 5 mM $CaCl_2$ was added prior to purification. CaM was then isolated using a phenyl sepharose column for hydrophobic affinity purification (350). When calcium is bound to CaM it causes structural rearrangements that leads to the exposure of hydrophobic surfaces on CaM (365). When this was passed through the column the two hydrophobic surfaces interact and CaM remained bound to the column. Other proteins are removed from the column by several washing steps (see Section 2.12.4 for experimental details). CaM was then eluted from the column by the addition of buffer containing a high concentration of the chelating agent EGTA. The removal of calcium from the binding sites on CaM causes structural rearrangements of the protein, which leads to the hydrophobic surfaces of CaM becoming hidden within the protein and reversing the interaction with the hydrophobic column. The purification was also carried out using the AKTA system, and therefore the presence of protein was monitored by measuring the absorbance of ultraviolet light of 280 nm wavelength (Figure 3.4B). Fractions thought to contain protein were analysed by SDS-PAGE to assess if CaM was present (Figure 3.4C). Fractions containing CaM were collected, dialysed and concentrated for use in future experiments. The yield of pure CaM produced using this method of purification was found to be around 16 mg/l.

**A**

U I | I Ins | I S | M

250
80
50
40
25
20

**B**

mAU

**C**

M  tot  sol  FT  W1  W2  A7  A8  A9  A10 A11 A12 B1  B2  B3

80
40
25
20
15

130
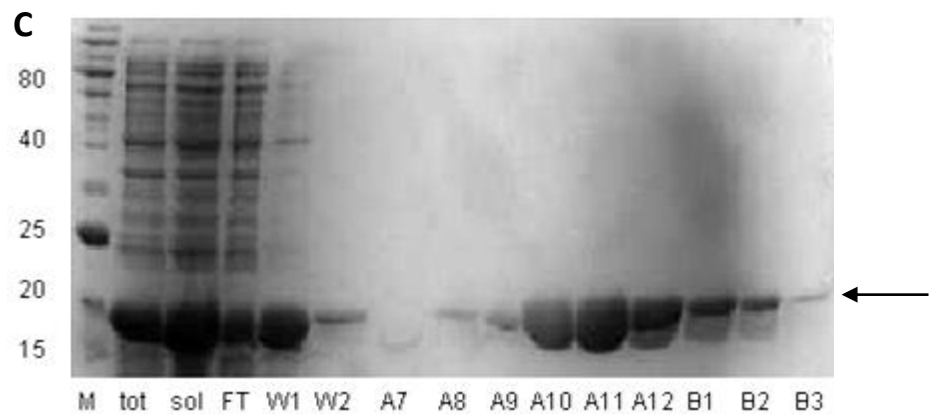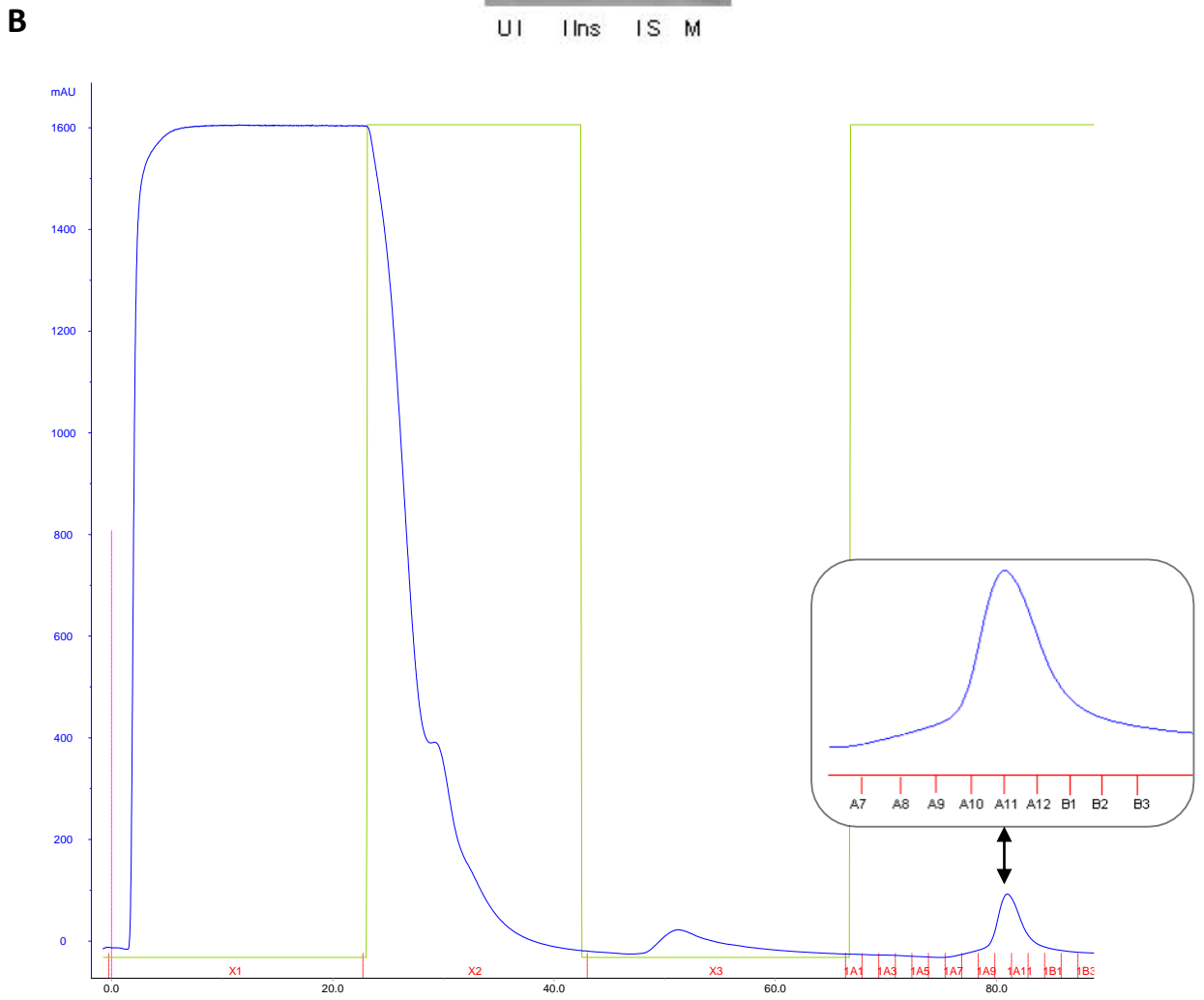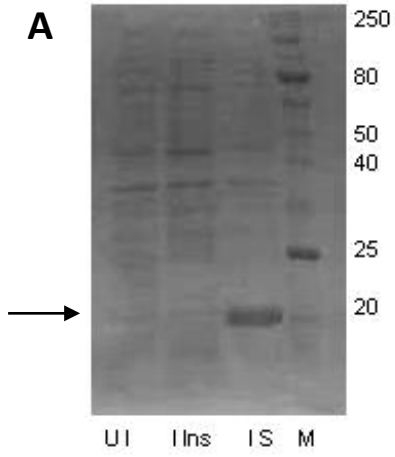
**Figure 3.4: Expression and purification of untagged CaM.** (A) *E.coli* cells were transformed with the vector encoding untagged CaM. Expression was tested using same conditions as His6-CaM. The soluble and insoluble fractions were separated by centrifugation and analysed by SDS-PAGE. The black arrow indicates CaM. M= marker, with protein molecular weight shown in kDa, UI= Uninduced, I Ins= Induced insoluble fraction, I S= Induced soluble fraction. (B) Purification profile of untagged CaM passed through phenyl sepharose column. The blue trace represents the UV280 absorbance measured in milli-absorbance units (mAU), green represents the concentration of buffer, the injection of the protein onto the column is shown by the pink marker and collection fractions are shown in red. The zoom insert represents the elution peak of CaM with the fraction collected for SDS-PAGE analysis labelled. (C) Fractions from the purification were analysed by SDS-PAGE and those containing CaM were collected for dialysis. Arrow shows CaM. M= marker, with protein molecular weight shown in kDa, FT= flow through. W1= wash with first wash buffer, W2= wash with second wash buffer.

## 3.3.2 Production of N and C-lobes of CaM

In Killock et al (2009)(3), molecular modelling was used to look at the possible interaction between the L-selectin cytosolic tail, CaM and FERM domain of moesin. The model predicted that, in the ternary complex, only the C-lobe of CaM was involved in the interaction with L-selectin (3). To prove this experimentally, individual lobes of CaM were cloned separately to assess the ability of each domain to bind to the cytosolic tail of L-selectin.

The boundary domains for the two individual lobes of CaM (N-CaM and C-CaM) were taken from published data (366). N- and C-CaM were cloned into MCS2 of pETDuet using NdeI and XhoI restriction sites. This meant that both lobes were cloned without a tag. After ligation, KRX cells were transformed with the vector using the method described in Section 2.7. Positive colonies were tested for the presence of the correct insert, using colony PCR. Several positive colonies were observed and these were sent for sequencing to confirm the incorporation of the correct insert.

The vector encoding N-CaM was used to transform Rosetta cells and small scale growth was carried out at 37°C and 18°C to test for expression of soluble protein. It was not obvious if soluble N-CaM was produced following induction (data not shown). This may have been because of the small size of the protein making it difficult to visualise on the SDS-PAGE gel. For this reason 1 L of culture

was grown to produce a larger amount of N-CaM and purification was attempted using the same method as untagged CaM. The results showed that at 37°C no protein eluted from the column (Figure 3.5A), whereas at 18°C protein was eluted from the column with a molecular weight corresponding to that of N-CaM (Figure 3.5B), meaning soluble N-CaM was successfully produced at 18 °C. These growth conditions could now be used for large-scale production of N-CaM for future experiments.
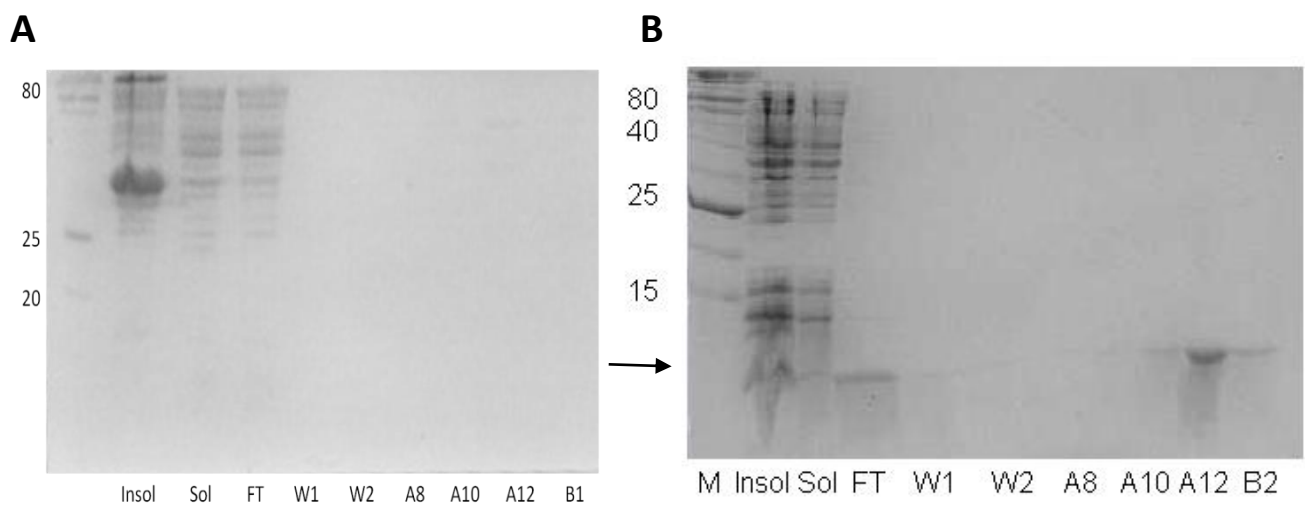


**Figure 3.5: Expression and purification of N-CaM.** N-terminal domain of CaM was expressed in Rosetta *E.coli* cells either at 37 °C (A) or at 18°C (B). Soluble and insoluble proteins were separated by sonication and centrifugation. N-CaM was separated from other soluble proteins using a HIC column attached to the AKTA system. M= marker, with protein molecular weight shown in kDa, Insol=insoluble proteins, sol= soluble proteins, FT= flow through, W1= wash with first wash buffer, W2= wash with second wash buffer, A8-B2= elution fractions. The arrow shows N-CaM.

As with N-CaM, the C-CaM vector was used to transform Rosetta cells and small-scale expression tests were performed at different growth temperatures in an attempt to produce soluble protein. The expression tests revealed that no soluble protein was produced when expression was induced at 37°C (Figure 3.6A) or 18°C (Figure 3.6B). In an attempt to obtain soluble protein the Sarkosyl method was used. This is a method that uses the detergent Sodium lauroyl sarcosinate, known as sarkosyl, to solubilise proteins found in inclusion bodies (367,368). During

bacterial expression of recombinant proteins many become packaged in inclusion bodies or co-aggregate with bacterial proteins. By using sarkosyl detergent these inclusion bodies are disrupted and recombinant proteins can be solubilised. The major advantage of using this method is that it does not entail denaturing the protein. Proteins solubilised by denaturing require renaturing, which can be time consuming, costly and may result in incorrectly folded proteins, therefore avoiding denaturation is desirable. The sarkosyl detergent was used to re-suspend the pellet produced after sonication and centrifugation. After incubation on ice the solution was diluted and centrifuged once again. The supernatant was collected and analysed to decipher if the protein of interest was now found in the soluble fraction. The soluble and insoluble fractions produced using this method with Rosetta cells expressing C-CaM were analysed by SDS-PAGE, showing C-CaM remained in the insoluble fraction even after the Sarkosyl method (Figure 3.6C).

A further attempt to produce soluble C-CaM was undertaken using Arctic cells to express the protein. These cells are engineered to increase the yield of folded, active proteins at lower temperatures. Standard *E.coli* cells contain chaperonins, such as GroEL and GroES, that help process and fold the recombinant proteins, but these chaperonins have a reduced activity when the temperature is lowered (369). Arctic cells contain the chaperonins Cpn10 and Cpn60 which have high refolding activity at lower temperatures (370). These cells were transformed with C-CaM and induced at 13°C with 1 mM IPTG for twenty four hours. The results showed that although most of the protein remained insoluble, a small amount was observed in the soluble fraction (Figure 3.6D). Further experiments are required to determine if this method is viable for the large-scale production of C-CaM.
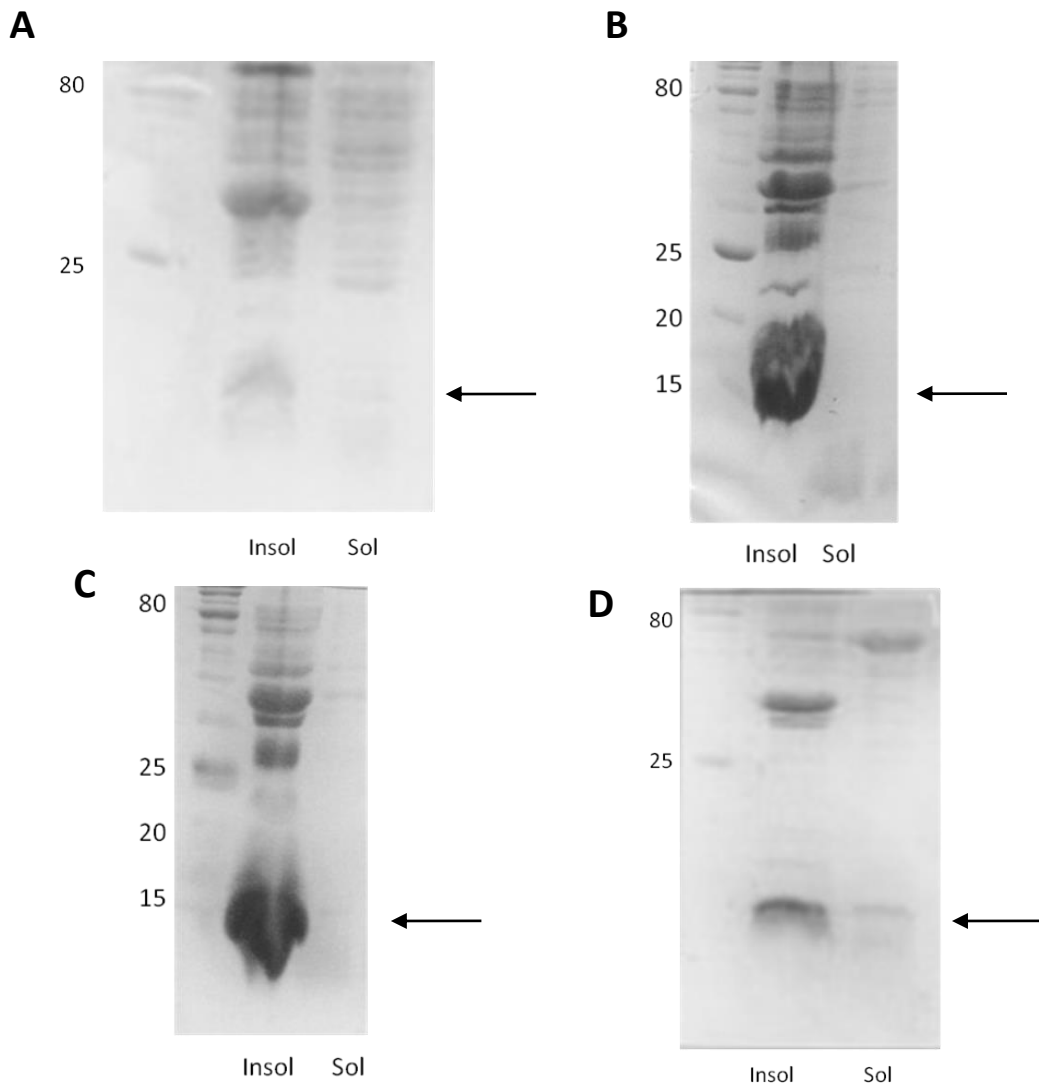
**Figure 3.6: Expression tests of C-CaM.** Expression tests were carried out for the C-lobe of CaM using different conditions to produce soluble protein. After induction the cells were sonicated and the soluble and insoluble fractions were separated by centrifugation. The different fractions were analysed by SDS-PAGE. (A) Induction carried out at 37 °C for 4 hours, (B) at 18 °C overnight. (C) Sarkosyl method was used on the insoluble protein produced after induction at 18 °C overnight. (D) Expression of C-CaM was also assessed using Arctic cells induced at 13 °C for 24 hours. Insol=insoluble fraction, sol=soluble fraction. The marker is shown on the left of each gel, with protein molecular weights shown in kDa. The black arrow indicates C-CaM.

### 3.3.3 Production of Moesin FERM domain

It has previously been shown that ERM proteins can bind to the cytosolic tail of L-selectin and play a role in locating it to microvilli (3,225). It was found that the FERM domain of moesin is responsible for interacting with L-selectin and other transmembrane proteins (223,371-373). For that reason, this domain was cloned and produced to further study the interaction between L-selectin and moesin.

Moesin-FERM was cloned into MCS1 of pETDuet using the same restriction sites as full length CaM, so would therefore be expressed with a His6-tag. A TEV protease cleavage site was engineered between the His6-tag and the protein sequence. The cloning was carried out as described before for CaM. The plasmid DNA from several colonies was isolated and sent for sequencing to confirm the presence of the correct insert. The vector with the correct sequence was then used to transform BL21-DE3-pLyS cells.

An expression test for His6-tagged moesin-FERM (His6-moesin-FERM) was carried out to assess protein expression and solubility and this showed that cells cultured at 37°C and induced with 1 mM IPTG for six hours produced His6-moesin-FERM in the insoluble fraction (Figure 3.7A and B). For the expression at 18°C overnight, some soluble protein was seen, albeit the majority remained insoluble (Figure 3.7C). The Sarkosyl method was attempted to increase the amount of soluble protein, as previously described (Section 3.3.2). After incubation with Sarkosyl detergent, the solution was passed through a $Ni^{2+}$ affinity column and fractions containing His6-moesin-FERM was determined by SDS-PAGE. A small amount of His6-moesin-FERM was eluted from the column, however a majority of the protein was found in the flow through (Figure 3.8A), showing it did not interact with the $Ni^{2+}$ affinity column. One possible explanation for this is that the His6-tag is unable to bind to the column through partial folding, or non-specific interactions between the protein and the tag. There have been previous reports where the His6-tag did not interact with the resin, which similarly hypothesise concealment of the tag (356). The His6-moesin-FERM eluted from the column was collected and TEV digestion was carried out as described earlier. After overnight cleavage, precipitation was observed in the digestion reaction. The solution was centrifuged

at 4000 rpm for five minutes to remove the precipitate and the soluble fraction was passed through the Ni$^{2+}$ affinity column to separate tagged from untagged moesin-FERM, the His6-tag and TEV protease. Fractions analysed by SDS-PAGE (Figure 3.8B) indicated that no moesin-FERM was observed in the flow through or elution fractions. A sample of the precipitate formed overnight was also analysed by SDS-PAGE, showing that moesin-FERM was indeed precipitated (Figure 3.8B), indicating overnight aggregation. Taken together these results showed that the Sarkosyl method was not successful in improving the yield of soluble moesin-FERM.
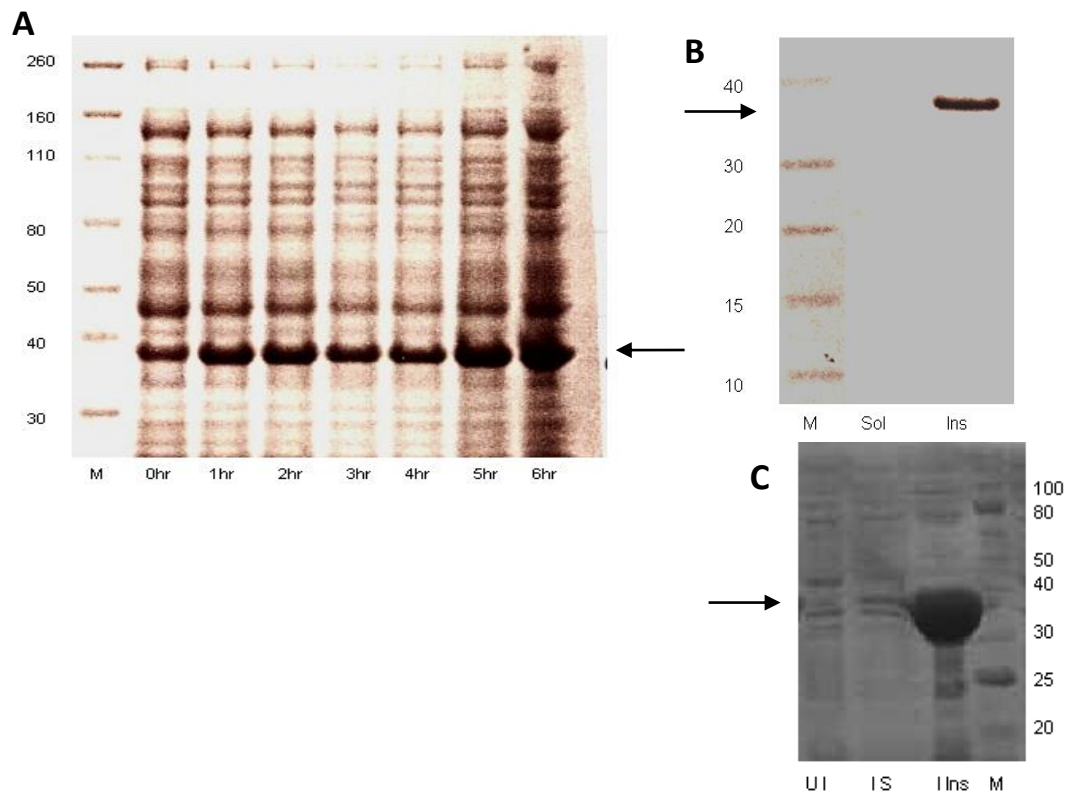


**Figure 3.7: Expression of His6-moesin-FERM.** (A) Expression of His6-moesin-FERM was tested at 37°C with IPTG induction over six hours. Samples were collected once every hour and analysed by SDS-PAGE. (B) Solubility at 37°C was tested by sonicating the cells and separating the soluble and insoluble fraction by centrifugation and analysing the fractions by SDS-PAGE. Sol= soluble fraction and Ins= insoluble fraction. (C) An expression test was carried out at 18°C overnight in an attempt to produce soluble protein. The soluble and insoluble fractions were analysed by SDS-PAGE. UI= Uninduced, IS= Induced soluble, I Ins= Induced insoluble. The marker (M) is shown on the left of each gel, with the molecular weights shown in kDa. The arrows show His6-moesin-FERM.
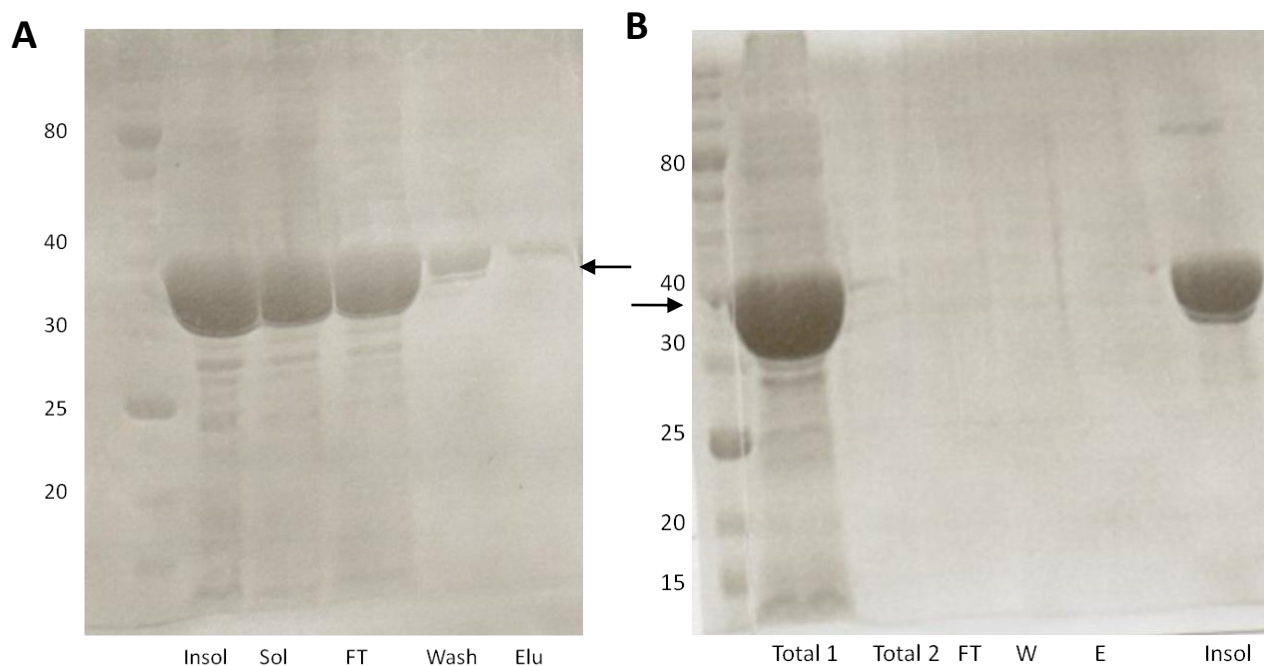
**Figure 3.8: Purification of Moesin FERM domain after Sarkosyl treatment.** (A) The insoluble fraction produced after protein induction at 18 °C was treated with sarkosyl reagent and the soluble fraction produced was passed through a $Ni^{2+}$ affinity column. The flow through, wash and elution fractions were collected and analysed by SDS-PAGE. (B) The elution collected in (A) was digested with TEV protease overnight (Total 1). A precipitation was observed in the digestion solution the next day and centrifugation was carried out to separate the soluble from insoluble fractions. Soluble fraction (Total 2) was passed through the nickel column once again, with fractions collected for analysis by SDS-PAGE. However, moesin-FERM was found to be insoluble. Insol= insoluble fraction, sol= soluble fraction, FT= flow through, W= wash, E= elution. The marker is shown on the left of the gels, with the molecular weights shown in kDa. The arrow shows moesin-FERM.

Large-scale production of His6-moesin-FERM was carried out using 18°C induction overnight. The soluble fraction was produced as explained previously (see Section 3.3.1) and His6-moesin-FERM was purified with a $Ni^{2+}$ affinity column using the protocol previously described (see Section 3.3.1). Fractions were collected from the column and those shown to contain protein by changes in the 280UV trace (Figure 3.9A) were analysed by SDS-PAGE (Figure 3.9B). His6-moesin-FERM then underwent TEV cleavage. Although the removal of the tag was successful, this caused precipitation of the protein (Figure 3.9C). This meant that this method could not be used to produce soluble untagged moesin-FERM.
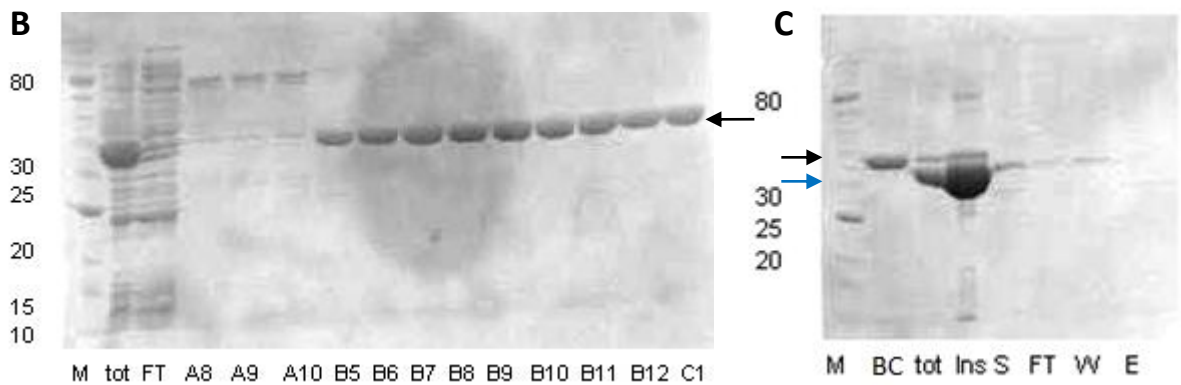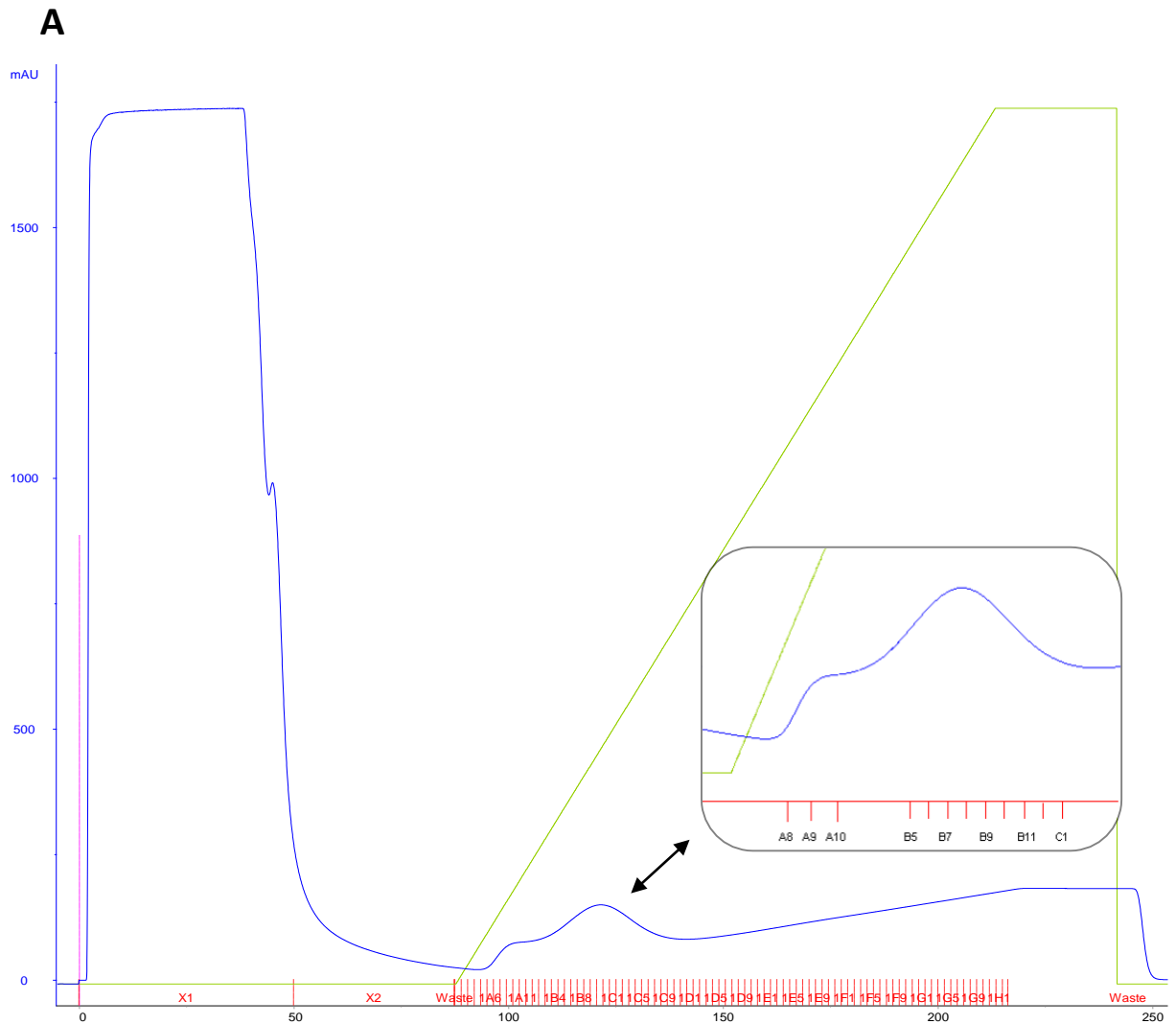
**Figure 3.9: Purification of His6-moesin-FERM.** (A) Purification profile of His6-moesin-FERM using a Ni$^{2+}$ affinity column attached to the AKTA system. The blue trace represents the UV280 absorbance measured in milli-absorbance units (mAU), green represents the concentration of buffer B, injection onto the column is shown by the pink marker and collection fractions are shown in red. The zoom insert shows the elution peak of His6-moesin-FERM, with the fractions collected for SDS-PAGE shown. (B) Fractions thought to contain protein were analysed by SDS-PAGE and those found to contain His6-moesin-FERM were subjected to TEV protease cleavage. (C) After cleavage the solution was passed through a nickel column and fractions were analysed by SDS-PAGE. Moesin-FERM was found to be insoluble after cleavage. Black arrow shows uncleaved His6-moesin-FERM and blue arrow shows cleaved moesin-FERM. tot=total lysate, FT= flow through, BC= before cleavage, Ins= Insoluble fraction after cleavage, S= soluble fraction after cleavage, W= wash with Ni$^{2+}$ buffer A, E= elution with Ni$^{2+}$ buffer B. The marker (M) is shown on the left of each gel, with the molecular weights shown in kDa.

The His6-tag was attached to the N-terminus of moesin-FERM, which was predicted to be the binding site for CaM. This meant that it was possible that the tag might interfere with the binding between CaM and moesin-FERM. For that reason moesin-FERM was re-cloned into MCS2 of the pETDuet vector, so it would be expressed without a His6-tag. NdeI and XhoI restriction sites were used to clone moesin-FERM domain into the vector. After transformation, colony PCR was carried out to confirm the presence of the insert, revealing that the insert was present in the colonies tested. The vector was sent for sequencing confirming that the moesin-FERM sequence was correct.

The vector with the correct sequence was used to transform Rosetta cells. Expression of moesin-FERM was assessed at 37°C and the SDS-PAGE analysis showed that the protein was present in the insoluble fraction (Figure 3.10A). At 18°C some of the protein was seen in the soluble fraction but a majority of it was still insoluble (Figure 3.10B). In an attempt to improve the solubility further, Arctic cells were transformed with the vector and induced for twenty four hours at 13°C. This resulted in an increase in the amount of soluble protein produced (Figure 3.10C) and so Arctic cells were used for future expression of moesin-FERM.

Untagged moesin-FERM was purified using hydroxyapatite resin, using a previously described protocol (261,274). The resin has the chemical formula $Ca_{10}(PO_4)_6(OH)_2$ and forms crystals with pairs of calcium ions (C-sites), clusters of six oxygen atoms from phosphate groups (P-sites) and hydroxyl groups, which are all arranged in a fixed pattern on the surface of the crystal (374-376). Amino groups of the protein are attracted to P-sites but repelled by C-sites, with the opposite being true for carboxyl groups. Phosphoryl groups interact with C-sites more strongly than carboxyl groups, therefore the proteins are loaded onto the column with a buffer of low potassium phosphate concentration and proteins are eluted by increasing the potassium phosphate concentration (376-379). Cell lysate from Arctic cells expressing moesin-FERM was added to the resin, which was then washed with hydroxyapatite buffer A (see Section 2.12.5 for a recipe) and then hydroxyapatite buffer B (the recipe is shown in Section 2.12.5) to elute the protein. Fractions were collected after each wash stage and analysed by SDS-PAGE, showing that moesin-

FERM was located in the elution fraction with no impurities (Figure 3.10D). This method was therefore successful in producing pure recombinant moesin-FERM, with a yield of approximately 0.95 mg/l being produced.

The protein was then dialysed in tris buffer, phosphate buffer and sodium acetate buffer to determine which was best for stabilising the protein. It was found that sodium acetate buffer allowed the protein to be concentrated to the highest level, with a low micromolar concentration reached in this buffer, whereas the protein precipitated earlier in the other buffers. However this concentration was not high enough to carry out NMR or ITC experiments successfully.
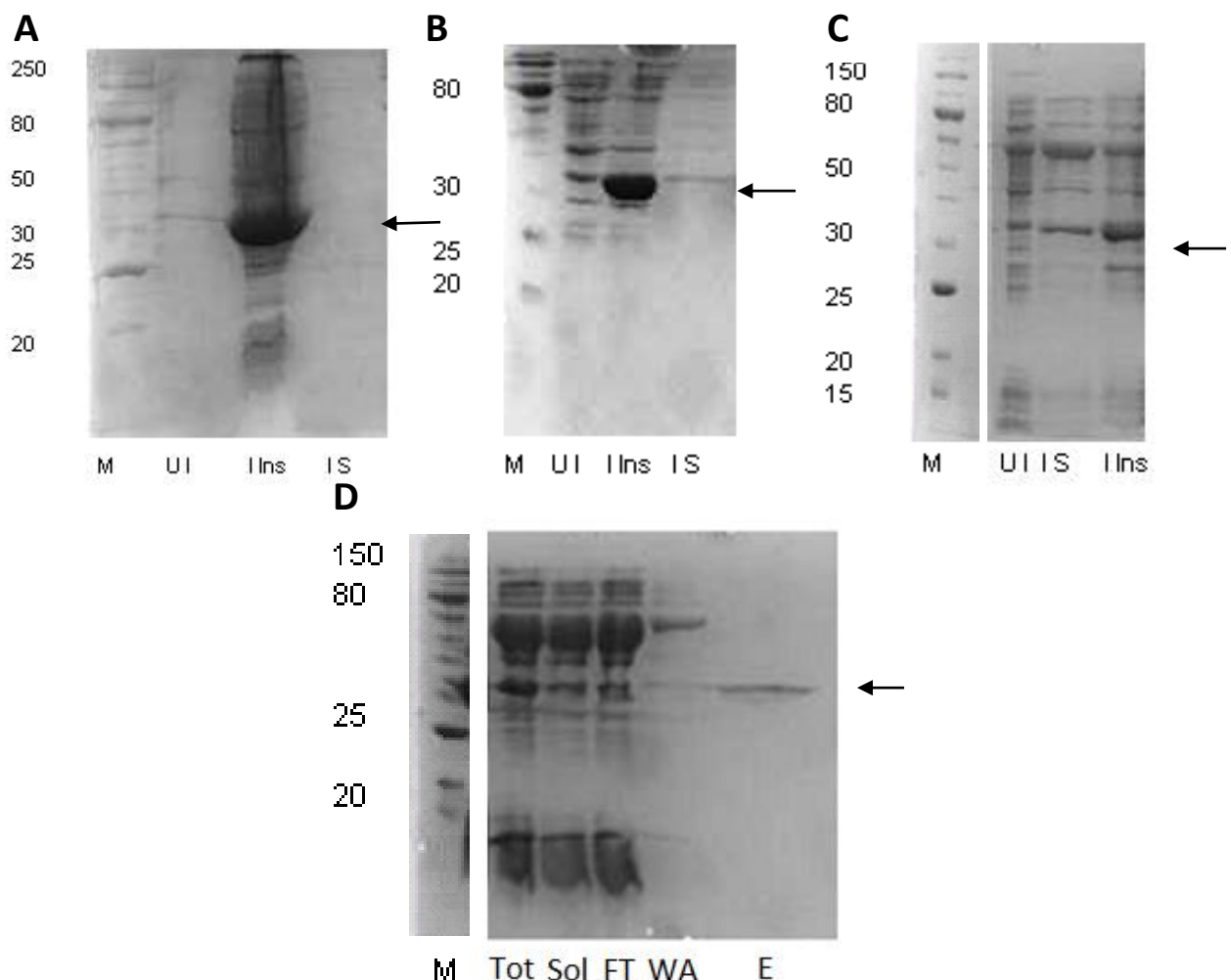


**Figure 3.10: Expression and purification of untagged moesin-FERM.** Expression of untagged moesin-FERM was tested at different conditions in an attempt to produce soluble protein, first at 37°C (A) then at 18°C (B) and 13°C (C). UI= Uninduced, IS= induced soluble, Ins= Induced insoluble fraction. (D) As soluble protein was produced at 13°C, purification of the protein produced under these conditions was attempted using a hydroxyapatite column. Arrow shows the location of FERM. Tot= total lysate, Sol= soluble fraction, FT= flow through, WA= wash with hydroxyapatite buffer A, E= elution with hydroxyapatite buffer B. Arrows shows the location of FERM. The marker (M) is shown on the left of each gel, with the molecular weights shown in kDa.

### 3.3.4 L-selectin Peptides

L-selectin peptides, wildtype, alanine mutations and serine phosphorylated peptides, were purchased from the University of Bristol. They were purified using desalting columns to remove any impurities and salt that would interfere with ITC experiments. The peptides were then lyophilised and weighed to accurately calculate the concentrations required for biophysical techniques.

### 3.3.5 Production of Trp-Cage-L-Selectin

One possible method to pinpoint the residues involved in specifically interacting with CaM would be to carry out NMR experiments with $^{15}$N/$^{13}$C-labelled L-selectin cytosolic tail peptides. To purchase labelled peptides is expensive; therefore it was desirable to produce peptides in-house using *E.coli* expression. However, production of recombinant peptides and unstructured proteins in *E.coli* cells is often unsuccessful because of degradation of the desired product by contaminating bacterial proteases (361,362). To circumvent this, peptides can be tagged with fusion partners that help protect against degradation (380). One of the possible tags is Exendin-4, a 39 residue peptide isolated from the saliva of the Gila monster (381). The NMR structure was solved and it showed that residues 21-38 of the C-terminus formed a stable tertiary structure, designated a Trp-Cage motif (382). The motif is a hydrophobic cluster with tryptophan residue 25 buried in the centre of the structure. Several proline residues, 31 and 36-38, form a cage around Trp-25 to shield the hydrophobic core from solvent exposure (383). Mutational studies have been carried out on the Trp Cage motif to produce the folded structure with the fewest possible amino acids. The studies showed that the 20 amino acids of the C-terminus are adequate for the formation of the Trp-Cage motif. Further mutations were carried out to improve the formation of the motif in water and the stability of the structure. The optimized sequence was found to be NLYIQWLKDGGWSSGRPPPS and known as TC5b (381), which is the sequence used in this study (known as Trp-Cage hereafter).

The vector containing the Trp-Cage construct with an N-terminal His6-tag and a TEV cleavage site between the Trp-Cage and the cloning site was a gift from Dr Pete Simpson, Imperial College London. The L-selectin cytosolic peptide was cloned using primer oligonucleotides designed to span the entire sequence for the cytosolic tail of L-selectin and containing overhangs for the restriction enzymes EcoRI and BamHI to allow ligation of the insert into the vector cleaved with these restriction enzymes. The L-selectin insert was made by annealing the oligonucleotides together by heating the mixture to 95°C then allowing the solution to cool slowly. The insert was then treated with a kinase to phosphorylate the ends and enable ligation to occur, as the vector was treated with calf-intestinal alkaline phosphatase (CIP) after restriction digestion. The ligated vector was then used to transform *E.coli*. Several colonies were sent for DNA sequencing to confirm the presence of L-selectin, with results showing the correct sequence was present.

After transformation of Rosetta cells with the vector containing the correct sequence, expression of Trp-Cage-L-selectin was carried out at 20°C overnight, using a protocol provided by Dr Pete Simpson (Imperial College London). Analysis revealed that the Trp-Cage-L-selectin appeared to be soluble (Figure 3.11A). The protein was purified using $Ni^{2+}$-NTA resin as described before, with a protein band visible on the SDS-PAGE gel corresponding to the molecular weight of the Trp-Cage-L-selectin apparent in the elution fraction (Figure 3.11B). The presence of intact L-selectin was confirmed by western blot analysis using antibody CA21, which recognises the tail of L-selectin (Figure 3.11C).

TEV cleavage was carried out to separate the Trp-Cage from L-selectin. The flow through was collected from the $Ni^{2+}$ column following cleavage and samples were analysed by SDS-PAGE, but L-selectin was not visible on the gel due to its small size. UV analysis did suggest the presence of the peptide in the flow through so this was desalted into water then lyophilised. Analysis of the lyophilised product is required to assess if the cytosolic tail of L-selectin peptide is indeed present.
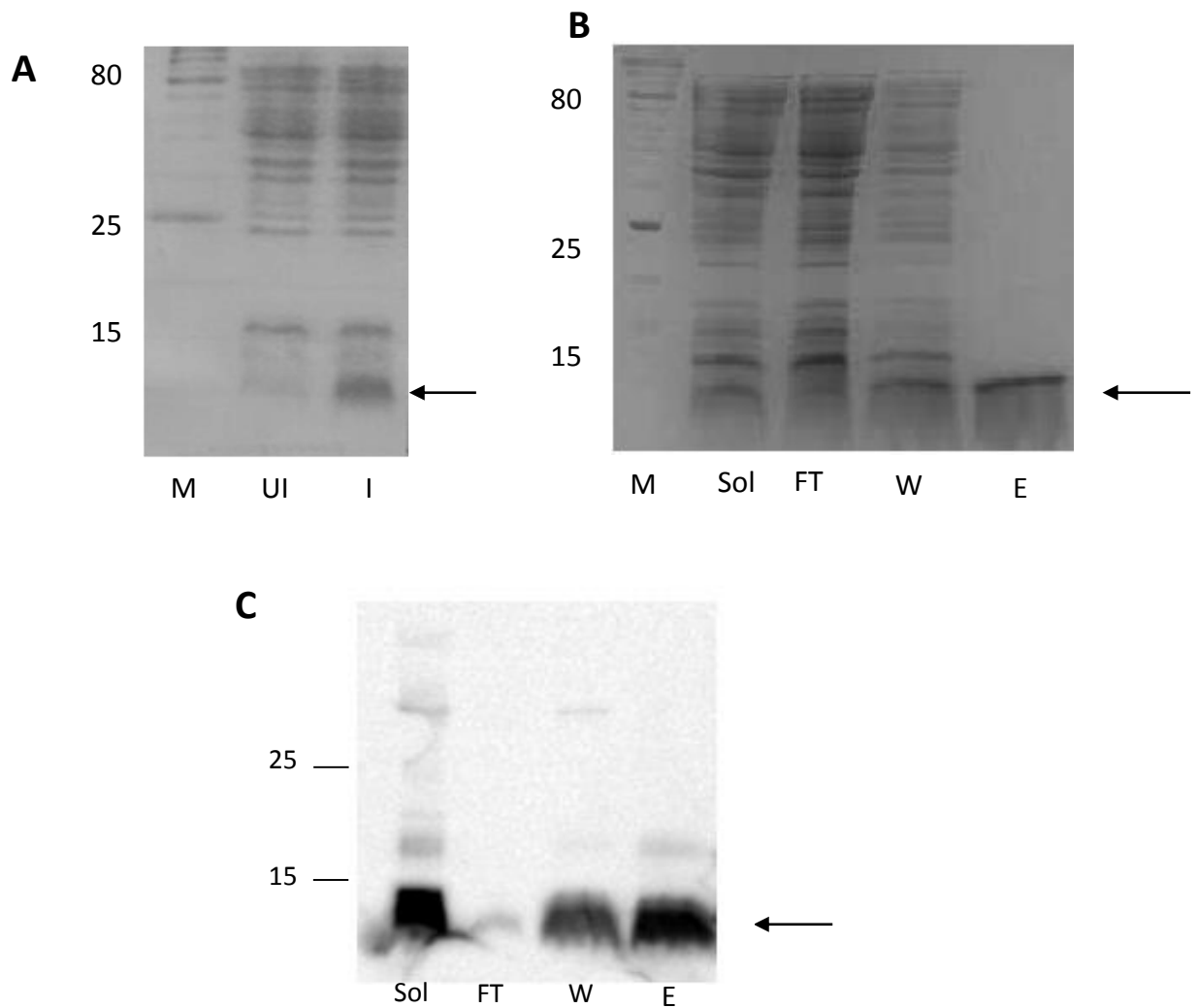
**Figure 3.11: Expression and purification of Trp-Cage-L-selectin.** (A) Rosetta cells were transformed with Trp-Cage-L-Selectin vector and expression was induced at 20 °C overnight. The soluble and insoluble fractions were produced by sonication and centrifugation and were analysed by SDS-PAGE. (B) Trp-Cage-L-Selectin was purified from the cell lysate using nickel resin, with fractions collected and analysed by SDS-PAGE. (C) Western blot was carried out using CA21 antibody specific for the L-selectin tail to confirm the presence of L-selectin. Sol= total soluble fraction, FT= Flow through, W= wash, E= elution. The arrow shows the Trp-Cage-L-Selectin. The marker (M) is shown of the left side of the gels, with the molecular weights shown in kDa.

## 3.3.6 Characterisation of Recombinant CaM

To check that the purified recombinant CaM protein was folded and to confirm its calcium-loaded state, 1D $^1$H NMR experiments were carried out on CaM samples thought to be calcium bound (CaM-Ca) (Figure 3.12B) and calcium free (ApoCaM) (Figure 3.12A). The 1D $^1$H spectrum shows the resonance signals for every proton in the protein (see Section 2.17.2.1 in Material and Methods for an explanation). Due to the difference in the structures of ApoCaM and CaM-Ca, the proton chemical shifts will be different for each one, producing clear differences in the proton spectrum. As there are many protons in the protein, there is much overlap within the spectrum, so these differences can only be seen at the periphery. These peripheral areas represent the methyl groups at around 0 ppm (red circle) and the NH groups around 10 ppm (blue circle). The spectra of CaM with and without calcium show clear differences that are consistent with spectra published in the literature (365,384). These differences can be used as a diagnostic tool to assess CaM where the calcium content is unknown.

**A**
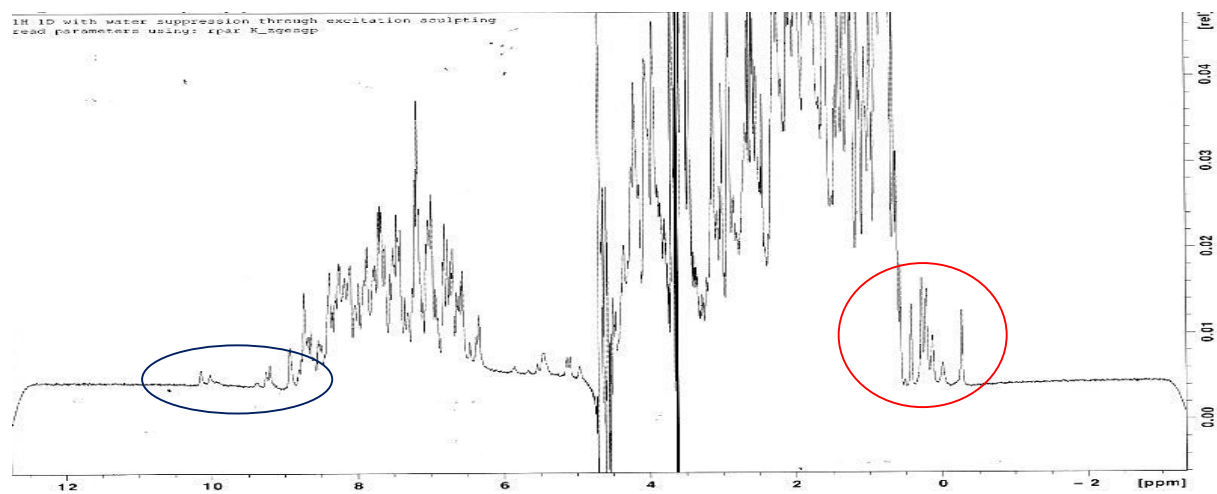


**B**
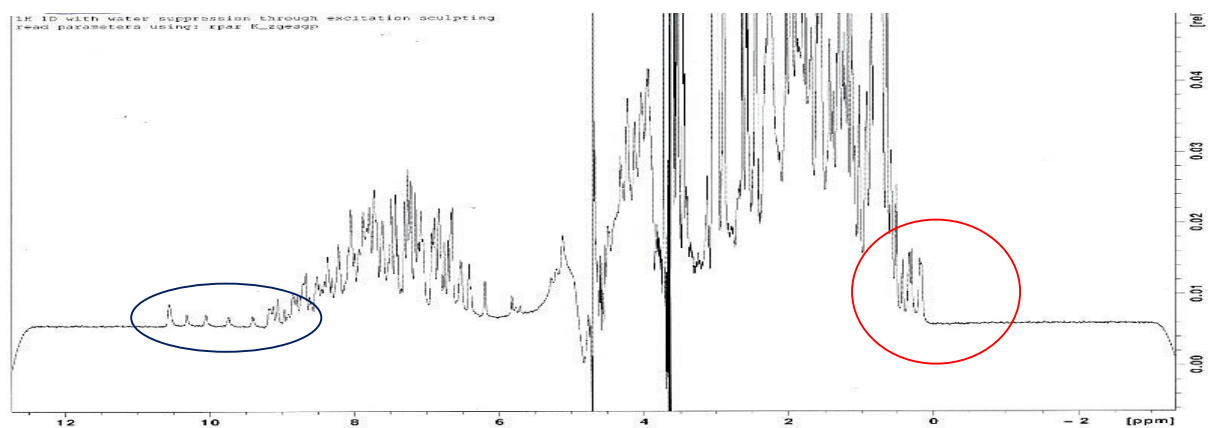


**Figure 3.12: 1D ¹H NMR of CaM.** (A) Spectra for Apo CaM and (B) CaM-Ca. The differences in the chemical shifts of the methyl groups and NH groups are shown in red and blue respectively. Spectra were recorded using a Bruker 700 MHz at 25 °C in NMR buffer (see Section 2.12.3) with and without 5 mM $CaCl_2$.

The folding of CaM was also assessed using 2D NMR with proteins labelled with $^{15}$N and carrying out [$^1$H-$^{15}$N] HSQC experiments, where each peak on the spectrum represents one NH group (therefore one amino acid) of CaM. The experiments were carried out in the presence and absence of calcium as before, to check the differences in the spectrum between the two (Figure 3.13). The spectrum showed that both CaM-Ca and Apo-CaM were folded and there were clear differences between the spectra. 2D [$^1$H-$^{15}$N] HSQC spectra have previously been published and were used to assign the spectra produced here (for ApoCaM BMRB ID 5353 was used (338) and for CaM-Ca BMRB ID 1634 was used (339)).

**A**
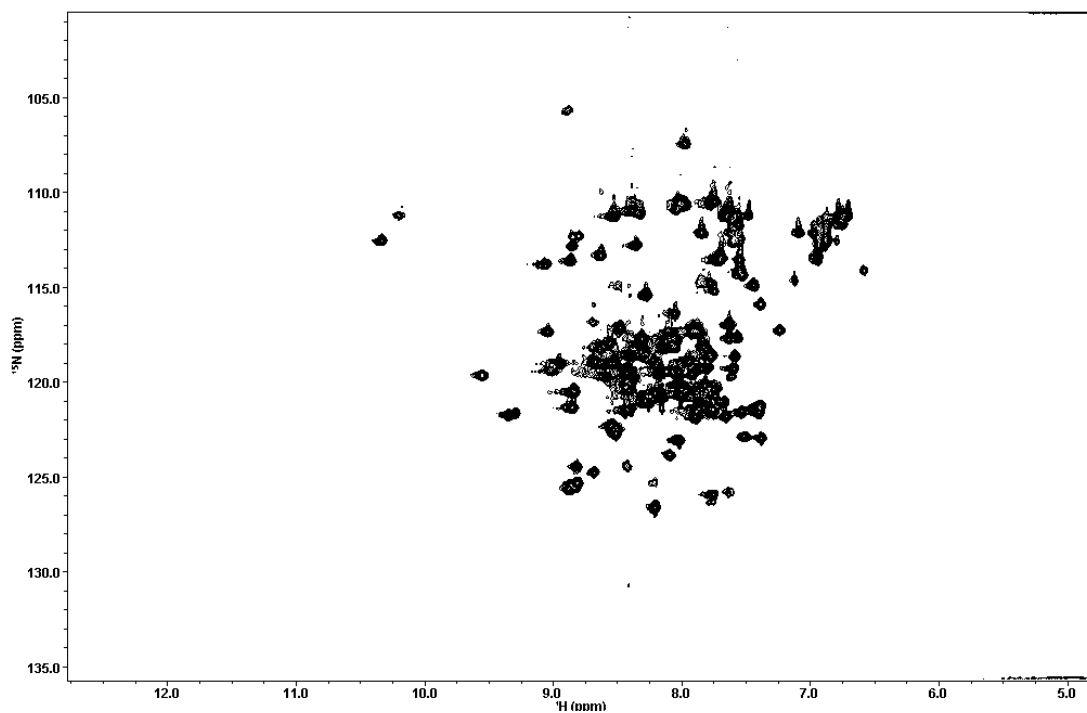


**B**
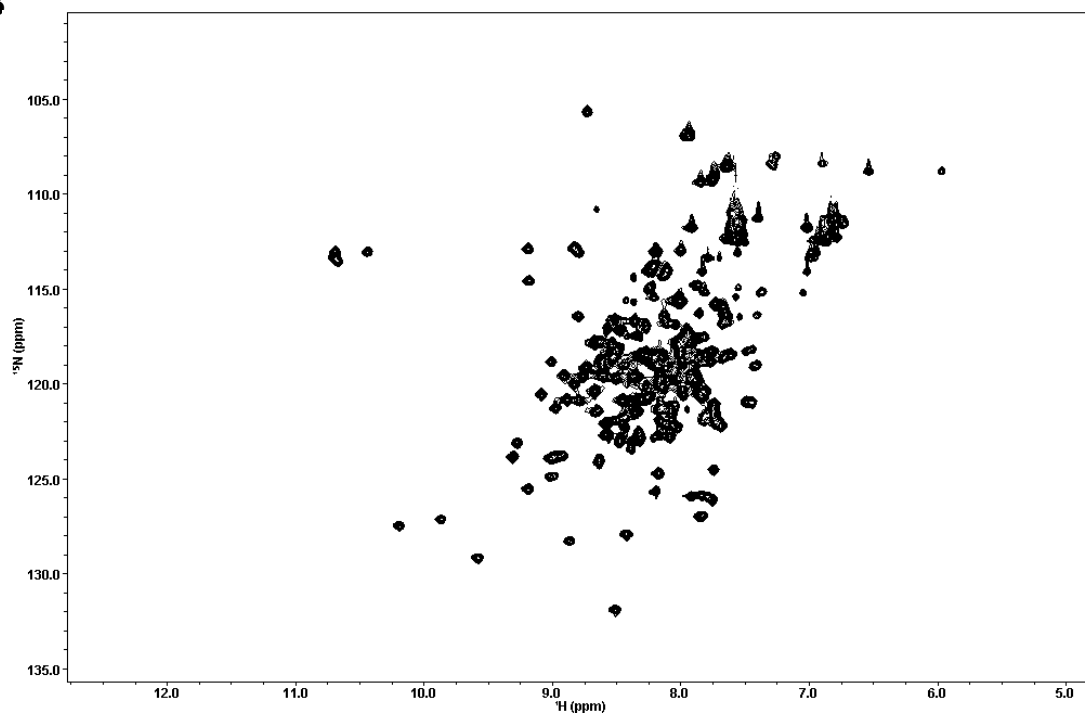


**Figure 3.13: 2D [$^1$H-$^{15}$N] HSCQ of CaM.** (A) Spectra of ApoCaM and (B) CaM-Ca. Spectra were recorded using a Bruker 700 MHz at 25 °C in NMR buffer (see Section 2.12.3) with and without 5 mM CaCl$_2$.

### 3.3.7 Characterisation of L-selectin Peptides

To assess the secondary structure of wildtype L-selectin in solution, CD experiments were carried out. Several buffers were used to see if different conditions affected the structure. The results showed that the peptide formed a random coil structure in both tris (Figure 3.14A) and phosphate buffer (Figure 3.14B) and the addition of 0.05% TWEEN had little effect on the structure of the peptide (Figure 3.14C).

CD experiments carried out on peptides with the serine to alanine mutations S364A and S367A indicated that these peptides also form random coils in the different buffers tested; no different to wildtype L-selectin. This shows that the alanine mutations did not affect the secondary structure of the peptide in solution.
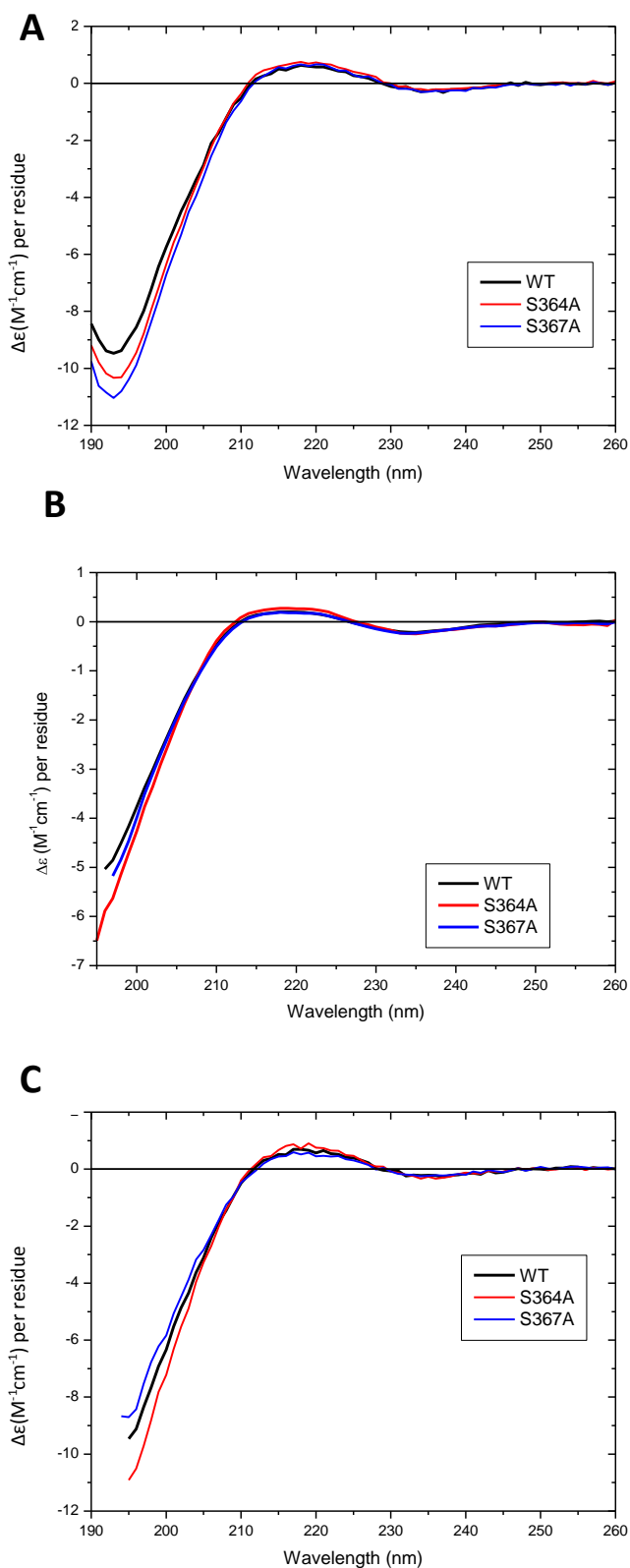
**Figure 3.14: CD of L-selectin peptides.** (A) CD spectra of peptides in 150 mM Tris buffer, (B) phosphate buffer and (C) 150 mM Tris with 0.05% TWEEN. Experiments were carried out by Tam Bui, Kings College London using an Applied Photophysics Chirascan Plus spectrometer (Leatherhead, UK).

### 3.3.8 Characterisation of Trp-Cage-L-selectin

$N^{15}$-labelled Trp-Cage-L-selectin was produced using the protocol described in Section 2.17.2.2. Once purity of the protein was confirmed by SDS-PAGE analysis, the protein was concentrated to 124 µM and NMR experiments were performed. A 1D $^1$H experiment was carried out (Figure 3.15A) and the spectrum was compared to a previous Trp-Cage spectrum produced by Imperial College London (unpublished data). The spectra were very similar and the protein was mainly folded, shown by the presence of sharp narrow peaks. A 2D [$^1$H-$^{15}$N] HSQC experiment (Figure 3.15B) was undertaken to further assess the folding of the protein. Once again there were signs that the protein was folded, as well-dispersed and distinct peaks were observed. There were however, also signs of degradation or unfolding of the protein, as highlighted by a cluster of overlapping peaks in the centre of the spectra. Comparison of the spectra produced here and previous spectra (unpublished data, Imperial College London), showed some similarities but, as there were signs of unfolding, further analysis is required to decipher whether the labelled version of the cytosolic tail of L-selectin can be used for binding studies.

**A**
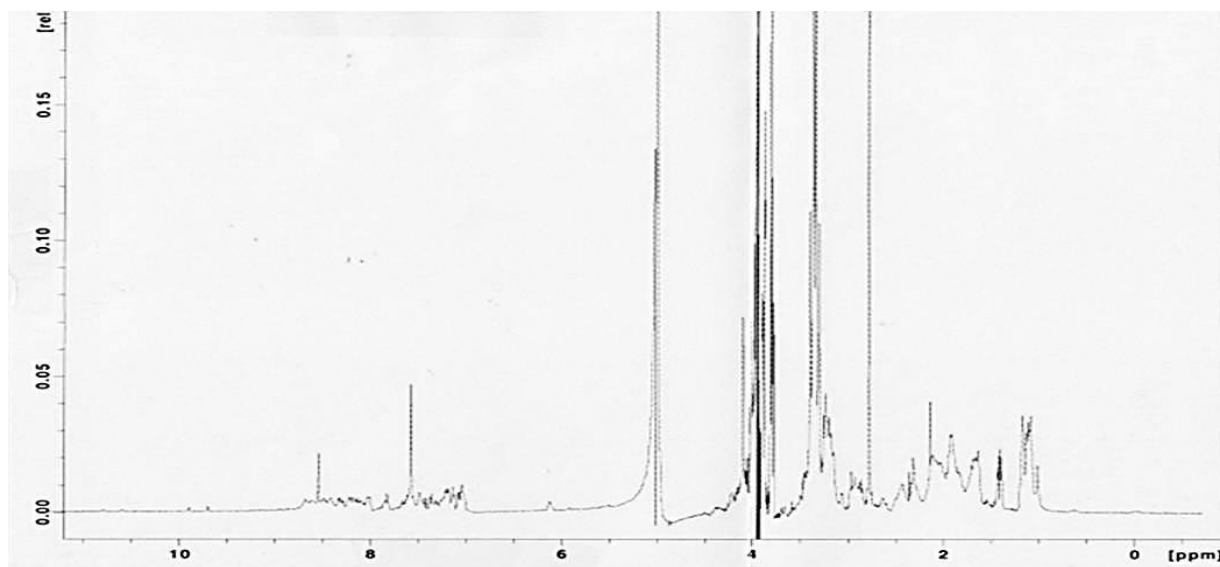


**B**
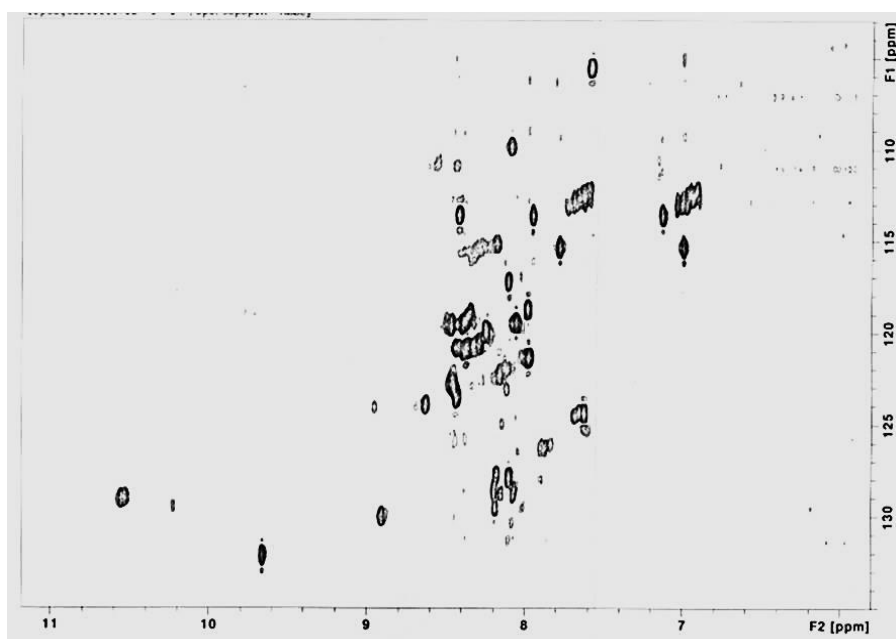


**Figure 3.15: NMR studies of Trp-Cage L-selectin.** (A) A 1D ^{1}H spectrum of Trp-Cage L-selectin and (B) a 2D [^{1}H-^{15}N] HSQC spectrum of Trp-Cage L-selectin. Both spectra were recorded using a Bruker 700 MHz at 25 °C in NMR buffer (see Section 2.12.3).

## 3.4 Discussion

### 3.4.1 Production of CaM

CaM was originally produced with an N-terminal His6-tag to aid purification. However, as mentioned above, removal of the tag became problematic. ITC experiments were attempted with His6-CaM and wildtype L-selectin peptide. Binding was seen but the results were different from those seen with untagged CaM (see Chapter 4), in particular the stoichiometry was much lower than 1. This may have been caused by the presence of the tag, affecting the binding characteristics or the structure of CaM. This is in agreement with previous studies in which the His6-tag was found to interfere with protein-protein interactions (356,385). For this reason CaM without a tag was used. This untagged CaM was purified using a protocol previously described by Hayashi et al (1998)(350) and has been widely used in the literature. Using this method not only removed the problem with the tag but also reduced the time required for production of the protein, as only one purification step was required.

Once CaM was produced, NMR experiments were carried out to check that the protein was folded. Both The 1D $^1$H NMR and the 2D [$^1$H-$^{15}$N]-HSQC spectra showed that the protein was folded and looked similar to spectra previously reported. This meant that CaM could be used for further experiments, confirming that it was correctly folded.

### 3.4.2 Protein expression of the Individual Lobes of CaM

To be able to understand if one or both terminal domains of CaM are required for the interaction with L-selectin, each lobe was cloned separately. The N-terminal lobe of CaM was successfully produced and purified. The method described here can now be used to produce large quantities of the N-lobe for biophysical studies. Production of the C-lobe was more problematic, as several different growth conditions were tested and only a small amount of soluble protein was yielded using Arctic cells. Further experiments are required to determine the possibility of purifying this domain of CaM with high efficiency. To facilitate

increased production of this domain may require altering the boundary used for the C-lobe, either extending the N-terminus or removing residues from the C-terminus, as this may somehow promote the production of soluble protein, as shown in many examples (348,386). It is also possible that the addition of a fusion partner may promote solubility. Several fusion partners have been shown to increase solubility, including maltose-binding protein and GST (356). Persechini (1996) (387) used a slightly different method to study the role of the different lobes of CaM. They produced mutants with one of the lobes "swapped out", so CaM was made up of either two N-lobes (CaMNN) or two C-lobes (CaMCC) (387). They were then able to use these recombinant proteins to assess their ability to activate skeletal muscle myosin light chain kinase, known to become activated through CaM binding. A similar study could be employed here if it is not possible to clone the lobes separately; CaMNN and CaMCC could be produced and used to assess if there is a difference in their capacity to bind to the L-selectin cytosolic tail.

### 3.4.3 Production of moesin FERM domain

A majority of the His6-moesin-FERM produced was found in inclusion bodies, especially when produced at 37 °C. This was likely due to insufficient time for correct folding (356). To improve the solubility, the temperature was decreased in an attempt to slow down the production of protein expression and increase the time available for correct folding to occur. This did improve the amount of soluble protein produced and more protein could be purified. However when the His6-tag was removed the protein precipitated. This may be due to an increase in protein stability or solubility in the presence of the His6-tag and once it was removed the protein aggregated/precipitated. Due to the concern that the His6-tag may interfere with the interaction between moesin-FERM and L-selectin or CaM, it was decided that production of moesin without a tag was a better approach to purify the protein using hydroxyapatite resin (261,274). This enabled the production of purified soluble protein. However, when this protein was concentrated it began to precipitate. ITC experiments were attempted with this purified protein, but the results were inconsistent. This was most likely due to the instability of the protein,

and having to use very low concentrations of moesin (results not shown). Therefore it was not possible to use ITC to study the interaction between moesin, L-selectin and CaM. There are no examples of moesin FERM domain being used for studies using ITC. In a recent study using recombinant ezrin FERM, the protein was purified in the same way that moesin was produced and purified in this chapter (261). It is possible that the ezrin FERM domain is slightly more stable and as it is likely to bind in the same way as moesin, it could be used to study the interaction between L-selectin and the FERM domain. MST requires much lower concentrations of protein, so it is possible this technique could be attempted to study the interaction between moesin, L-selectin and CaM in the future.

### 3.4.4 Production of Trp-Cage L-selectin

By using the Trp-Cage motif as a scaffold protein, it was possible to produce $^{15}N$ labelled L-selectin cytosolic tail peptide. However, further study is required to assess the stability of this construct. This means that future NMR studies could be carried out by titrating in CaM to observe which amino acids in the L-selectin tail undergo chemical shift perturbations (CSPs), upon CaM binding. This will provide useful information on which residues in the cytosolic tail of L-selectin are responsible for the interaction with CaM. The same method can be used to produce mutated labelled peptides to assess if they have an effect on the binding between CaM and L-selectin. For example aspartic acid can be substituted for serine residues to act as a phosphomimetic to see if this affects the binding.

# Chapter 4: *In vitro* Analysis of the Interaction between CaM and L-selectin

## 4.1 Introduction

The binding of CaM to the cytosolic tail of L-selectin in resting cells is thought to negatively regulate L-selectin's cleavage by the metalloprotease TACE (114). Leukocyte activation results in CaM dissociation and subsequent cleavage of L-selectin (215). It is not known what causes the dissociation of CaM from the tail; although it is hypothesised that phosphorylation within the L-selectin cytosolic domain may play a key role. The cytosolic tail of L-selectin contains two serine residues, whose phosphorylation may potentially regulate the binding of CaM and moesin, and several PKCs isozymes have been shown phosphorylate L-selectin upon leukocyte activation (95,214). There are many examples in which phosphorylation at sites within CaM binding domains regulate CaM binding, for example in β-adducin, which is a subunit of the heteromeric adducin protein involved in the assembly of the spectrin-actin network (226). Myristoylated alanine-rich C-kinase substrate (MARCKS), a membrane associated protein that interacts with actin, is another example where the CaM-binding domain contains phosphorylation sites that, when phosphorylated, result in a markedly reduced binding affinity for CaM (226).

In the previous chapter the production of recombinant CaM was described. This protein can now be used to study its interaction with L-selectin. As previously described, peptides corresponding to the cytosolic tail of L-selectin were synthesised commercially. Along with the wildtype sequence, peptides with alanine mutations and phosphorylated serines were used to assess which residues within the cytosolic tail of L-selectin contributed to the interaction and whether serine phosphorylation affected CaM binding.

## 4.2 Experimental Design

A variety of biophysical methods can measure the strength of interaction between molecules. These include isothermal titration calorimetry (ITC) (388),

mircoscale thermophoresis (MST) (344), surface plasmon resonance (SPR) (389) and fluorescence correlation spectroscopy (FCS) (390) and they all have advantages and disadvantages which must be considered when designing the experimental strategy to use. The advantages of SPR include the fact that labelling is not required, which is advantageous as the presence of a label could affect the binding between the molecules. Experiments can be carried out on crude cell lysates, meaning that purification of the protein of interest may not be necessary in all cases. The major disadvantage of this method is it requires the immobilisation of one of the molecules of interest onto a support metal surface, which could seriously affect its ability to bind to its partner (391). FCS does not require immobilisation but does require fluorescently labelling one of the molecules of interest.

The primary method chosen in this study to investigate protein-peptide interaction was ITC, on the basis that the molecules do not need to be labelled or immobilised, therefore there was a lower chance of binding interference. Furthermore a major advantage of this technique is that the thermodynamic profile of the interaction, the constant of binding and the stoichiometry can be analysed from a single experiment, providing further information about the mechanism of interaction beyond affinity strength. MST was used in parallel with ITC, not only to verify the results from ITC experiments but also to provide a valid alternative when ITC proved inconclusive. MST was chosen because it is relatively straightforward to implement and uses little material, although it does require the labelling of the protein.

To map the regions of CaM involved in L-selectin binding, NMR spectroscopy was utilised. [$^{1}$H-$^{15}$N] HSQC titration experiments were carried out to assess the residues within CaM which experienced chemical shift perturbations upon addition of L-selectin, giving a more detailed picture of the potential surface of molecular interaction. As described previously, a chemical shift perturbation will result from a change in the chemical environment of the nuclei (see Section 2.17.2.1), therefore, the analysis of any residues within CaM that are affected by the presence of L-selectin may provide information on CaM's interacting surface, as well as conformational changes induced by the interaction. In this report the changes in

the chemical shifts, chemical shift perturbations (CSPs), were identified and quantitatively measured.

In this chapter, the analysis of the interaction between CaM and L-selectin by ITC, NMR and MST is described. As CaM is a calcium-binding protein, the first question was whether calcium was required for L-selectin interaction. This was assessed by comparing the results from ITC experiments carried out in the presence and absence of calcium. The next key question was whether phosphorylation of serine residues within the tail of L-selectin affected the ability of CaM to bind and therefore decipher whether phosphorylation regulates CaM binding to L-selectin during leukocyte recruitment. To address this point, ITC and MST experiments with CaM and phosphorylated peptides were undertaken. A similar approach was used to assess whether mutating residues within the cytosolic tail of L-selectin affected the ability of CaM to bind and provide information about residues within the cytosolic tail of L-selectin that contribute to CaM interaction.

## 4.3 Results

### 4.3.1 Assessing the interaction between CaM and Wildtype L-selectin Cytosolic Tail

To determine the ability of CaM to bind to the L-selectin cytosolic tail, ITC was carried out using recombinant purified CaM and commercially purchased L-selectin tail peptide. Prior to CaM/L-selectin experiments being carried out, a negative control was undertaken, injecting CaM into NMR buffer to observe the heat of dilution. The results in Figure 4.1 represent an example of this control experiment and shows the ITC profile for CaM-Ca/buffer experiment. Small peaks of very similar in size are observed throughout the experiment. The last peak of the CaM/L-selectin experiments was seen to be similar to the peaks observed in the buffer experiment. For this reason it was decided that the final peak to the L-selectin titrations could be used as a heat of dilution.
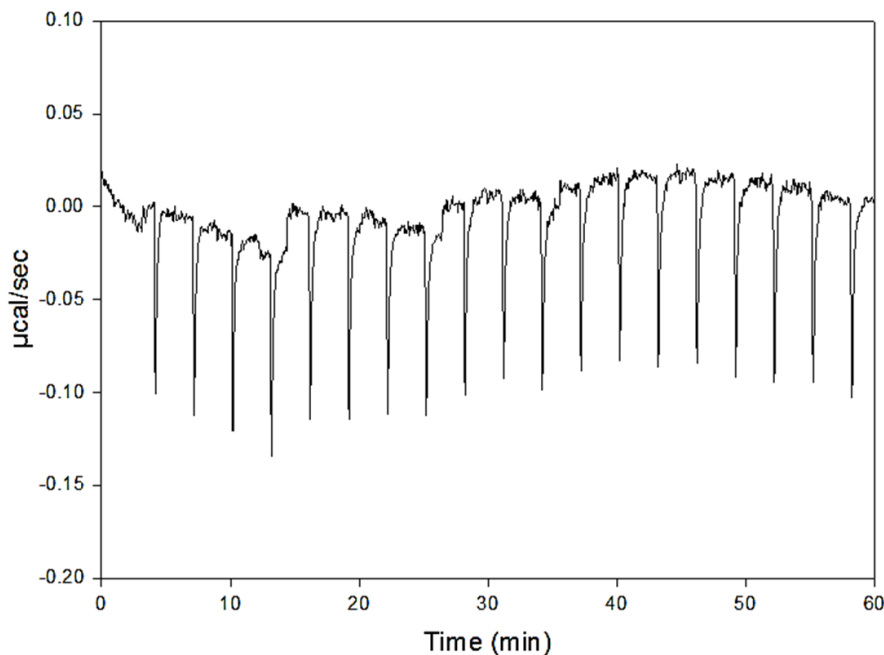
**Figure 4.1: ITC results for CaM injected into buffer.** Raw data for NMR buffer injected into CaM-Ca injected into NMR buffer. The experiment was carried out using a microcalorimeter, with CaM present in the syringe at a concentration of 0.38 mM (see Section 2.17.1.2 for experimental details), with the temperature set to 20 °C.

CaM is a calcium binding protein and a number of its interactions have been reported to depend on the presence of $Ca^{2+}$ (234,392,393). To understand whether this was the case for CaM binding to L-selectin, ITC experiments were carried out with wildtype L-selectin cytosolic tail peptide in the sample cell of the ITC equipment with calcium-bound CaM (CaM-Ca) or calcium-free CaM (ApoCaM) titrated into the cell from the syringe (see Section 2.17.1.1 for a schematic of the ITC equipment). For both experiments the integrated heat data showed that the binding process was composed of one clear event centred on a molar ratio of one (Figure 4.1). The binding isotherm curves have been interpolated using an independent-site model, revealing that at 20 °C CaM protein interacted with L-selectin with a dissociation constant ($K_D$ ) of 1.6±0.3 µM, with an enthalpy change ($\Delta H$) of -416±110 cal/mol and an entropic contribution (defined as -T$\Delta S$) of -6967±393 cal/mol in absence of calcium and a $K_D$ of 4.0±2.1 µM, a $\Delta H$ of 1430±341 cal/mol and a -T$\Delta S$ of  -8528±108 cal/mol in presence of calcium (Table 4.1). Although binding occurred with similar affinities, interestingly, the thermodynamic profiles of the two interactions were different (Figure 4.1C and F): CaM-Ca/L-selectin interaction was described by an exothermic reaction (i.e. had a negative

change in enthalpy) and was both enthalpically and entropically driven (with a dominant entropic contribution); the binding of ApoCaM to L-selectin is an entropically driven endothermic reaction.

For an interaction to occur spontaneously, the change in Gibbs free energy ($\Delta G$) of the interaction must be negative (394). $\Delta G$ has both enthalpic ($\Delta H$) and entropic ($\Delta S$) contributions, which reflect different aspects of the protein-protein interaction. Enthalpy represents the strength of the interactions between the two molecules, such as Van der Waals interactions and hydrogen bonds (335,394). When binding between two proteins occur, new bonds and interactions will form between the two molecules and there will be a change in energy, such as heat being released or absorbed. In addition to bond formation, bonds are also broken during the interaction. These can come in the form of intramolecular interactions or intermolecular interactions – either with the other protein or the surrounding solvent. These processes all contribute to the $\Delta H$ (335,394). $\Delta S$ reflects the change in solvation and conformation during the interaction. When binding occurs, water is released from the binding site causing a gain in solvent entropy (333). There is also a loss in conformational freedom when two molecules interact, resulting in a negative change in conformational entropy (394). $\Delta S$ is the sum of the $\Delta S$ of solvation and $\Delta S$ of conformation.

In the case of CaM-Ca interaction with L-selectin peptide, the reaction was both enthalpically and entropically driven, as both $\Delta H$ and $-T\Delta S$ were negative and therefore contributed to the favourable negative $\Delta G$. The interaction between Apo-CaM was entropically driven, as $-T\Delta S$ was negative whereas $\Delta H$ was positive, so only the $\Delta S$ contributed to a favourable negative $\Delta G$. Different enthalpic and entropic contributions for CaM-Ca and Apo-CaM binding to the L-selectin cytosolic tail could either reflect different mechanisms of binding or could be linked to a different solvation state of Apo-CaM and CaM-Ca.

159
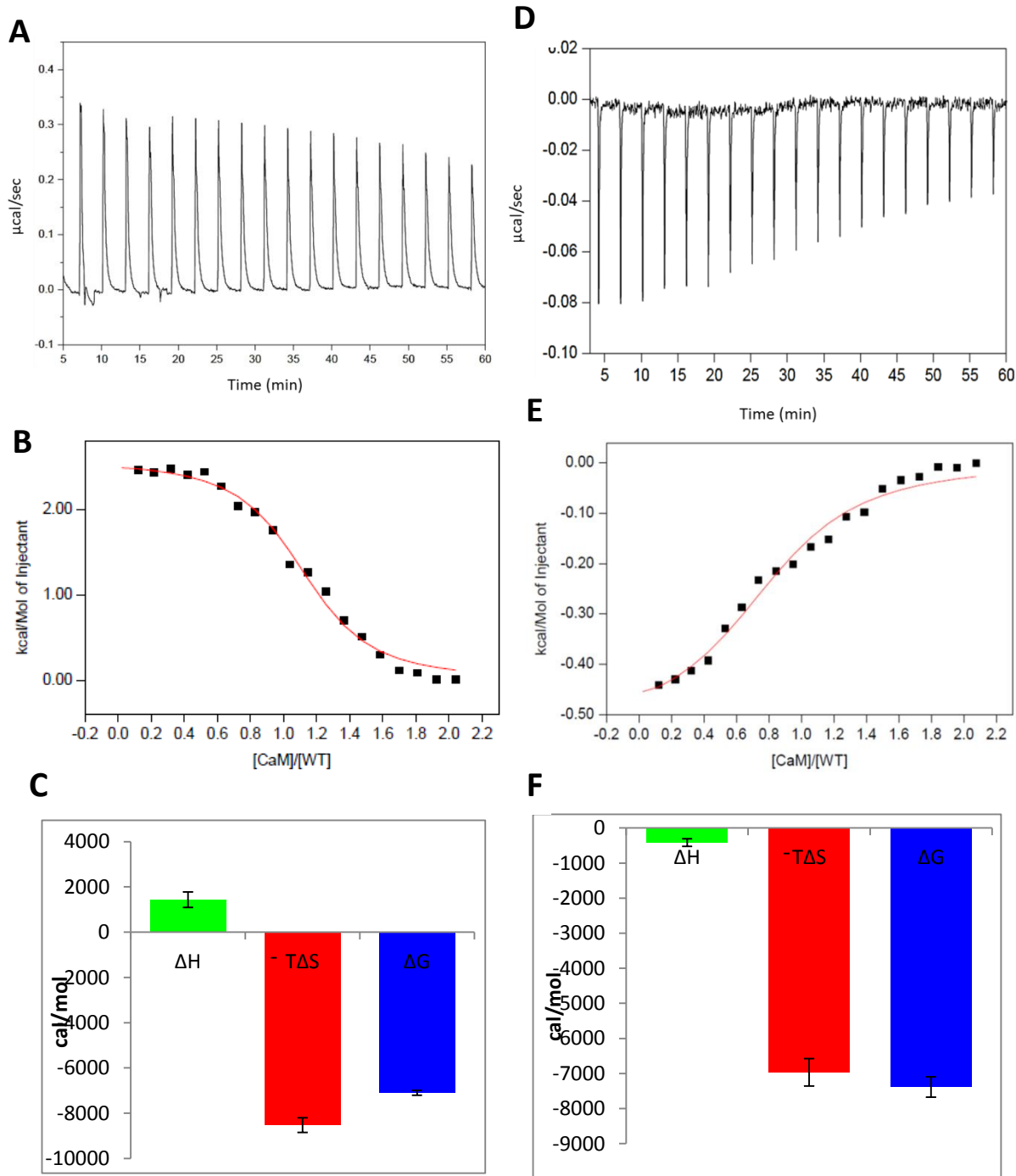
**Figure 4.2: ITC results for CaM binding to wildtype L-selectin tail peptide.** Raw data for ApoCaM (A) and CaM-Ca (D) binding to wildtype L-selectin tail. (B and E) the normalised heat of interaction (the ΔH caused by the interaction of CaM and the L-selectin peptide) was obtained by integrating the raw data and subtracting the heat of dilution from each point. The red line represents the best fit obtained by a non-linear least-squares procedure based on one independent binding site model using origin 7.0. The thermodynamic profile for the interaction between L-selectin and ApoCaM (C) and CaM-Ca (F) is shown, with the ΔH, -TΔS and ΔG for each interaction. Results are representative of three independent experiments.

|  | CaM-Ca | ApoCaM |
|---|---|---|
| **Stoichiometry (N)** | 0.97±0.12 | 1.21±0.15 |
| **K$_D$ (µM)** | 4.01±2.15 | 1.6±0.3 |
| **ΔH (cal/mol)** | -416±110 | 1430±341 |
| **-TΔS (cal/mol)** | -6967±393 | -8528±108 |
| **ΔG (cal/mol)** | 7383±291 | -7028±246 |

**Table 4.1: Thermodynamic parameters of the association of L-selectin and ApoCaM or CaM-Ca.** Measurements were taken using a MicroCal ITC200 instrument at 20 °C in NMR buffer (see Section 2.12.3 for recipe). Results shown represent the mean and standard deviation of three experiments.

To investigate further the interaction between CaM and the L-selectin cytosolic tail and to gain insight into the binding mechanisms for both CaM-Ca and ApoCaM, a series of 2D [$^1$H-$^{15}$N] HSQC NMR experiments were carried out with $^{15}$N-labelled ApoCaM or CaM-Ca kept at a constant concentration whilst titrating in wildtype L-selectin peptide. Changes in amide $^{15}$N and $^1$H chemical shifts (Δδ$_{AV}$), namely chemical shift perturbations (CSP), were calculated for all peaks that showed perturbation using the formula: $\Delta\delta_{AV} = \sqrt{\left((\Delta\delta H)^2 + (0.2 \times \Delta\delta N)^2\right)}$ (340), where ΔδH is the change in the chemical shift of the amide proton and ΔδN is the change in the chemical shift of the amide nitrogen. As described above, CSPs provide information about which residues of CaM may be involved in the interaction (Section 4.2). The CSPs were then colour coded depending on the extent of the perturbation, with red representing the largest CSPs (Δδ$_{AV}$≥0.03), orange representing moderate CSPs (0.01≤Δδ$_{AV}$<0.03), yellow representing small CSPs (0.005≤Δδ$_{AV}$<0.01) and white representing little or no CSPs (Δδ$_{AV}$<0.005). Given that the 3D structures of both Apo-CaM and CaM-Ca are available and that the 2D [$^1$H-

161

[15N] HSQC NMR spectra for CaM-Ca and Apo-CaM have been previously assigned, the residues showing CSPs can easily be identified and mapped onto the structure of the respective protein.

The results showed that with both CaM-Ca (Figure 4.2) and ApoCaM (Figure 4.3) most of the CSPs were observed in the C-terminal lobe of CaM, suggesting that this lobe was largely responsible for binding to L-selectin cytosolic tail. Interestingly, this suggests that CaM did not bind to L-selectin with the classical binding mechanism where both lobes are involved and wrap around the target binding site (see Section 1.4.2, Figure 1.12C). The large conformational rearrangement required for both lobes to interact with L-selectin would result in large CSPs across the entire structure of CaM, as observed in previous studies (254,395,396) but it is not seen here. This was also consistent with the small enthalpy changes observed from the ITC experiments for both CaM-Ca and ApoCaM binding to the L-selectin cytosolic tail peptide. If large structural rearrangements were taking place, larger changes in enthalpy would be expected, as found previously with several examples of canonical binding of CaM to its targets (396,397).

Although both CaM-Ca and ApoCaM show a majority of the CSP in the C-lobe of the protein, there were differences in the amino acid residues affected in one or the other experiments. This may suggest a difference in binding between L-selectin and the two forms of CaM, although this remains to be confirmed through further investigation.
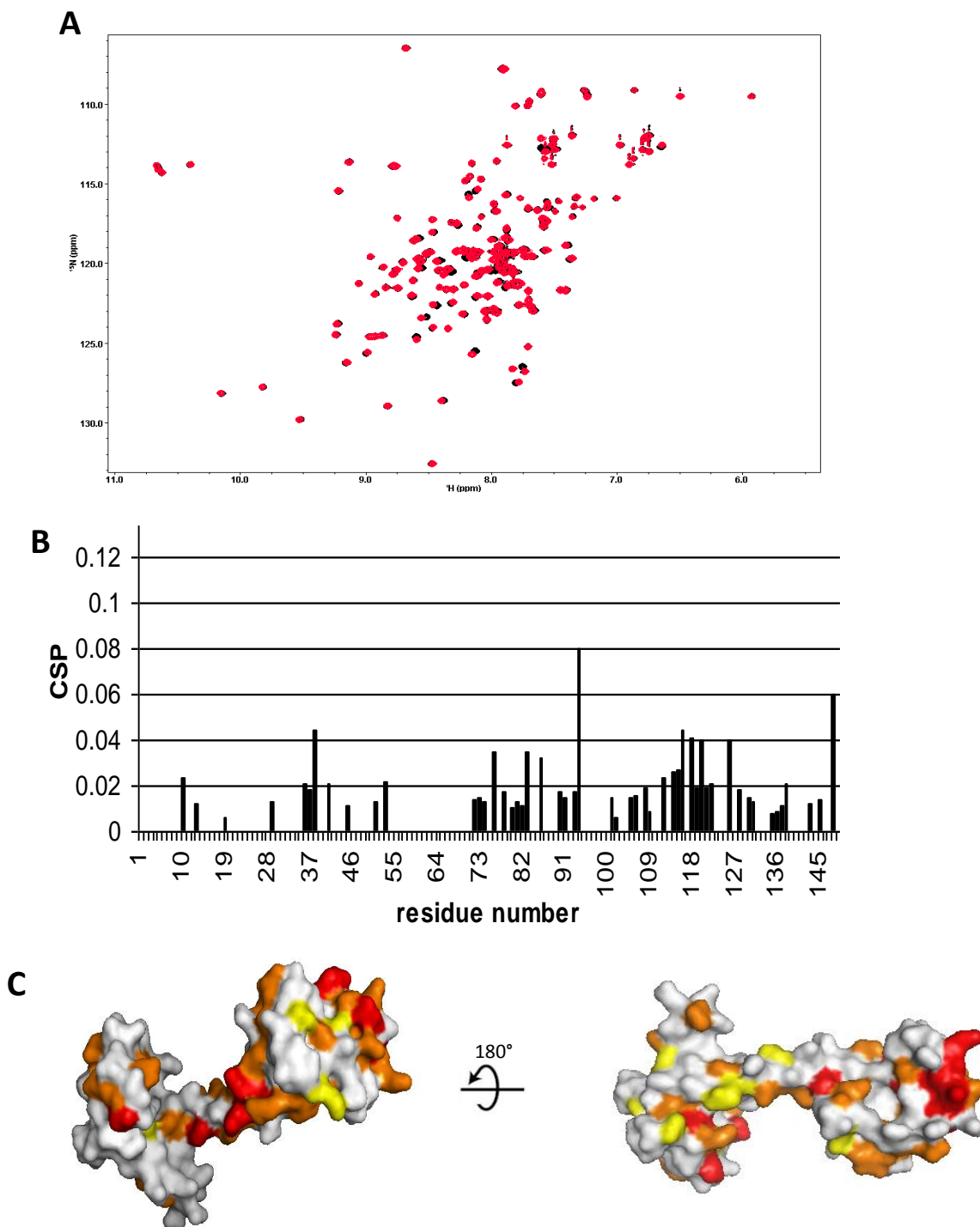
**Figure 4.3: Chemical shift perturbation analysis of CaM-Ca/L-selectin interaction.** (A) [$^1$H-$^{15}$N] HSQC of CaM-Ca (black) and CaM-Ca in the presence of 1.2 equivalent of the peptide (red). $^{15}$N chemical shifts are shown on the Y axis and $^1$H chemical shifts shown on the X axis, both in part per million (ppm). Chemical shifts were assigned from the Biological Magnetic Resonance Bank (BMRB) ID 1634. Spectra were recorded using a Bruker 700 MHz at 25 °C in NMR buffer (see Section 2.12.3 for recipe) with 5 mM CaCl$_2$. (B) Chemical shift perturbations were calculated using the method described in Section 2.17.2.2.1 and (C) plotted on the structure of CaM-Ca, Protein Data Bank (PDB) id 3CLN. Residues coloured red represent CSPs of $\Delta\delta_{AV}\geq0.03$, orange represent CSPs of $0.01\leq\Delta\delta_{AV}<0.03$, yellow represents CSPs of $0.005\leq\Delta\delta_{AV}<0.01$ and white represents CSPs of $\Delta\delta_{AV}<0.005$.
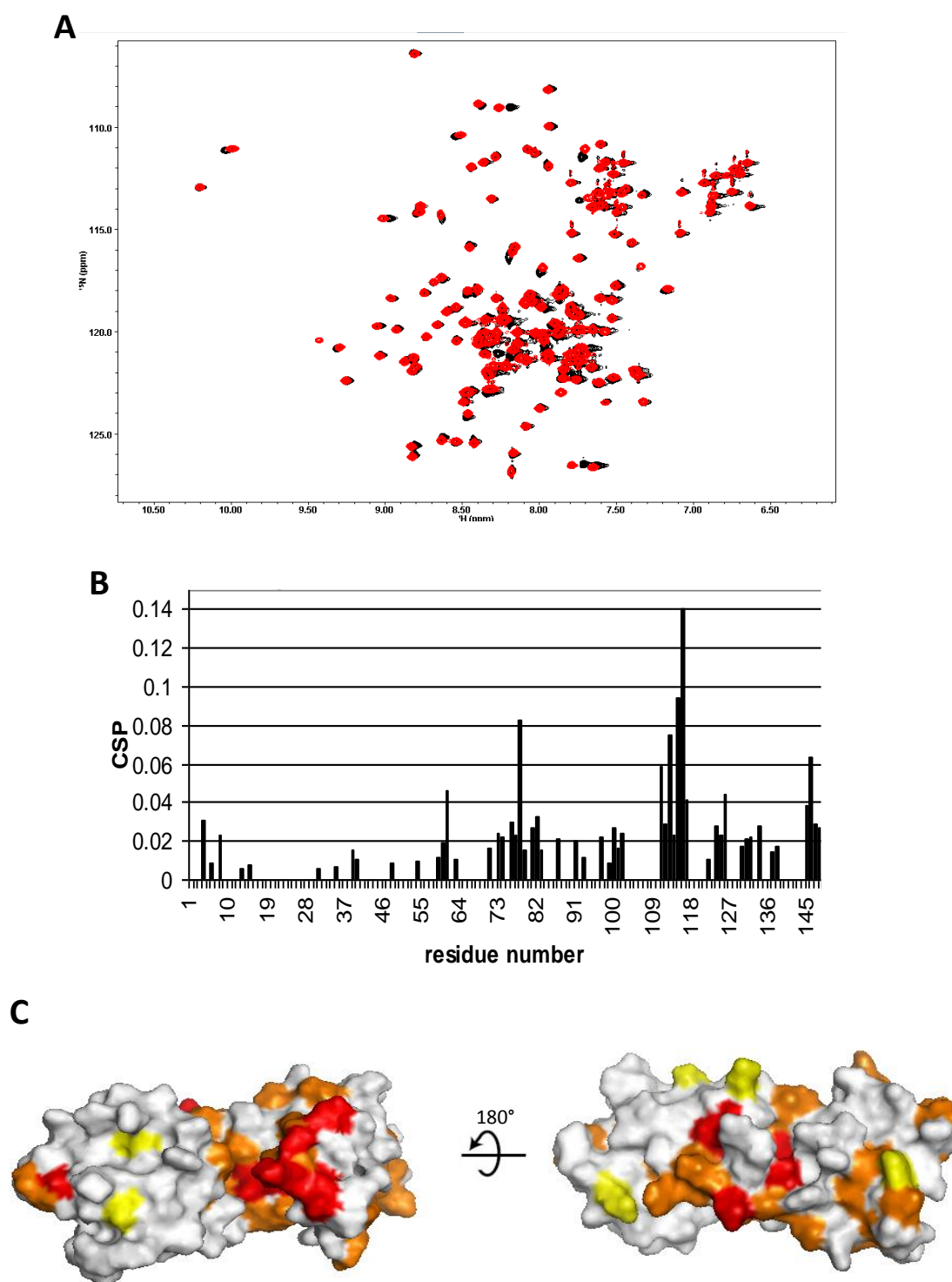
**Figure 4.4: Chemical shift perturbation analysis of ApoCaM/L-selectin interaction.** (A) [$^1$H-$^{15}$N] HSQC of ApoCaM (shown in black) and ApoCaM in the presence of 1.2 equivalent of the peptide (shown in red). $^{15}$N chemical shifts are shown on the Y axis with $^1$H chemical shifts shown on the x axis both measured in ppm. Chemical shifts were assigned from BMRB ID 5353. The spectra were recorded using a Bruker 700 MHz at 25 °C in NMR buffer (see Section 2.12.3 for recipe). (B) Chemical shift perturbations were calculated using the method described in Section 2.17.2.2.1 and (C) plotted on the structure of ApoCaM, PDB id 1CFC. Residues coloured red represent CSPs of $\Delta\delta_{AV}\geq0.03$, orange represent CSPs of $0.01\leq\Delta\delta_{AV}<0.03$, yellow represents CSPs of $0.005\leq\Delta\delta_{AV}<0.01$ and white represents CSPs of $\Delta\delta_{AV}<0.005$.

164

## 4.3.2 Monitoring the binding of CaM to phosphorylated L-selectin peptides

To assess the importance of phosphorylation of two serine residues (S364 and S367) within the cytosolic tail of L-selectin to the binding of CaM, phosphorylated L-selectin cytosolic tail peptides were sourced commercially, with either one of the serines (i.e. S364phos or S367phos) or both (hereafter termed: 'doublephos') phosphorylated. These peptides were tested for CaM binding using ITC experiments.

As with the wildtype L-selectin cytosolic peptide, ITC experiments were carried out with and without calcium in the same conditions used previously (in NMR buffer at 20°C). Integration of the heat of binding for the interaction of ApoCaM with S367phos, S364phos and doublephos peptides revealed that one binding event occurred with each peptide, with a molar ratio of around one. The data was fit to a one independent binding site model, which revealed $K_D$s of 5.0±1.1 µM for S364phos, 5.6±1.7 µM for S367phos and 4.1±1.1 µM for doublephos (Figure 4.4 and Table 4.2). When these $K_D$s were compared to that found with wildtype L-selectin (1.6±0.3 µM), there was a difference of between 2.5 and 3.5 fold (3.5 fold for S364A, 3.1 fold for S367A and 2.5 fold for doublephos), which was not considered significant (see Discussion, Section 4.4.1). The ΔH of the interaction between ApoCaM and wildtype L-selectin (1430±341 cal/mol) was less than the ΔH with the mutated peptides (2236±680 cal/mol for S364phos, 2437±807 cal/mol for S367phos and 2227±380 cal/mol for doublephos, Table 4.2). Although the ΔH and –TΔS were slightly larger with the phosphorylated peptides, this was not considered significant as the errors were quite large (between 17% for doublephos and 33% for S367phos) and ΔH remained endothermic.

The experiments in presence of calcium however, were less straightforward because the changes in enthalpy observed here were particularly small and close to the limit of what can be rigorously measured by ITC (see below). The interaction between CaM-Ca and S367phos or doublephos peptides could barely be measured, but one binding event was observed and the data could be fit to the one independent binding site model. The comparison of the $K_D$s, ΔH and –TΔS between

these peptides and wildtype L-selectin showed no differences that were considered significant (Figure 4.5 and Table 4.2). However, the ΔH values in the ITC experiment with S364phos were even smaller (Figure 4.5A), too small to obtain a clear fitting of the curve and therefore for the experiment to be conclusive.
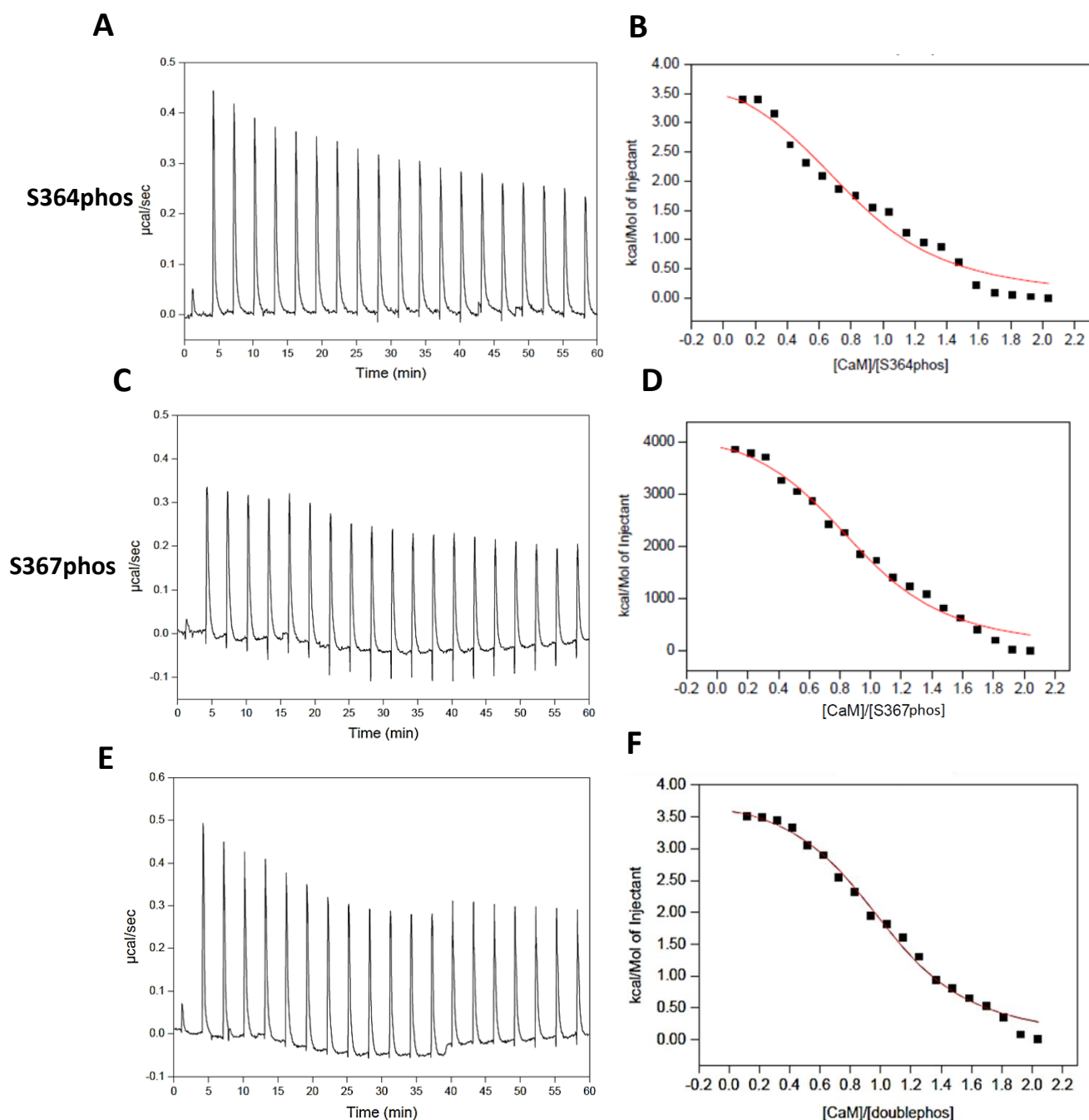


**Figure 4.5: Interaction between ApoCaM and phosphorylated L-selectin peptide.** ITC experiments studying the interaction between ApoCaM and either S364phos (A and B), S367phos (C and D) or doublephos (E and F). The normalised heat of interaction was obtained by integrating the raw data and subtracting the heat of dilution from each point. The red line represents the best fit obtained by a non-linear least-squares procedure based on one independent binding site model using origin 7.0. These results are representative of three independent experiments.
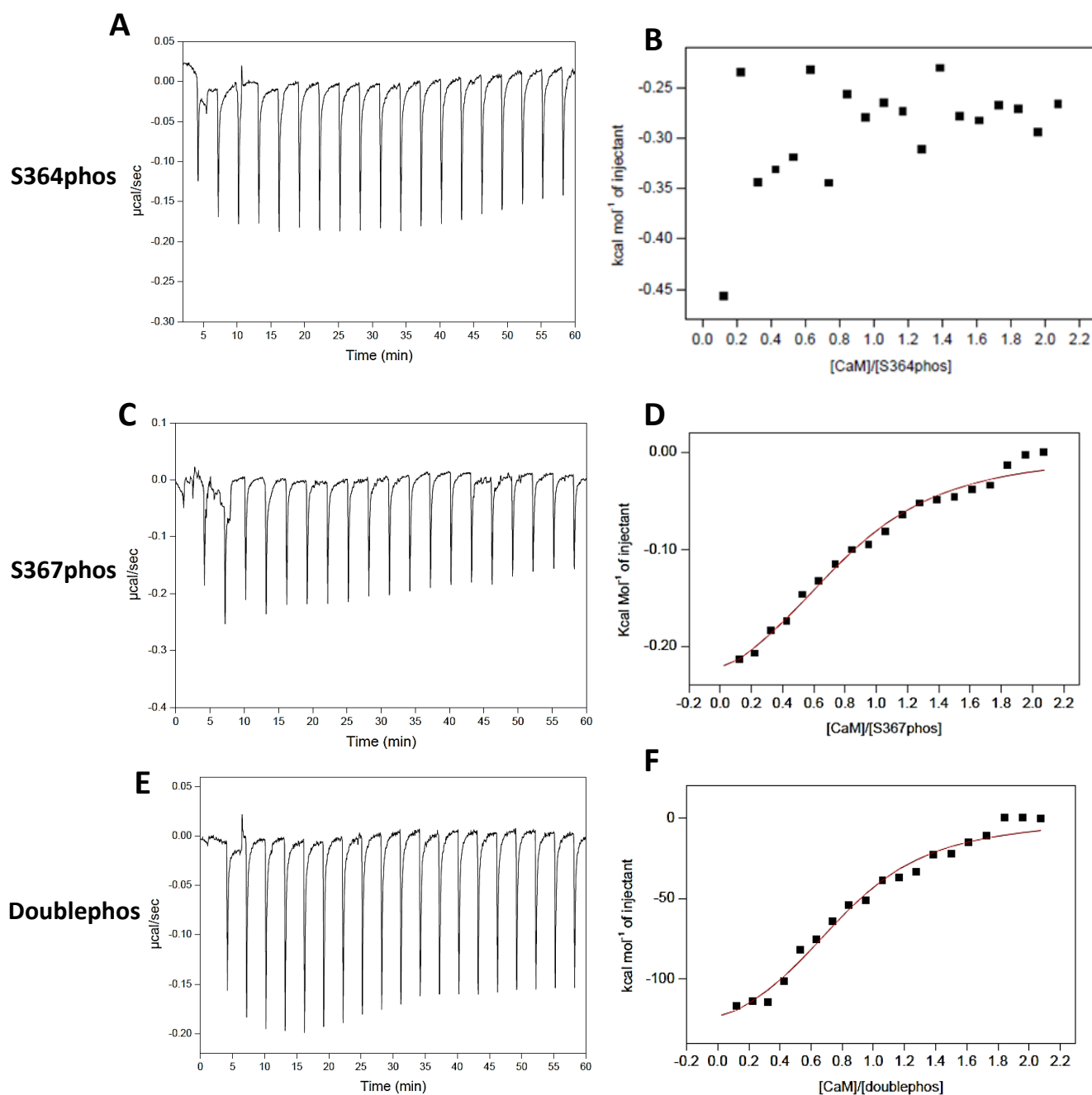
**Figure 4.6: Interaction between CaM-Ca and phosphorylated L-selectin peptide.** ITC experiments of CaM-Ca interacting with either S364phos (A and B), S367phos (C and D) or doublephos (E and F). The normalised heat of interaction was found by integrating the raw data and subtracting the heat of dilution from each point. The red line represents the best fit obtained by a non-linear least-squares procedure based on one independent binding site model using origin 7.0. The results shown here are representative of three independent experiments.

| Proteins | | Stoichiometry (n) | $K_D$ (µM) | ΔH (cal/mol) | -TΔS (cal/mol) | ΔG (cal/mol) |
|---|---|---|---|---|---|---|
| ApoCaM | **Wildtype** | 1.21±0.15 | 1.63±0.33 | 1430±341 | -8528±108 | -7028±246 |
| | **S364phos** | 0.99±0.22 | 5.03±1.02 | 2236±680 | -9441±560 | -7204±120 |
| | **S367phos** | 0.89±0.07 | 5.63±1.72 | 2437±807 | -9583±991 | -7146±183 |
| | **Doublephos** | 0.92±0.18 | 4.12±1.10 | 2227±380 | -9553±540 | -7326±159 |
| CaM-Ca | **Wildtype** | 0.97±0.12 | 4.01±2.15 | -416±110 | -6967±393 | -7383±291 |
| | **S364phos** | Binding could not be measured* | | | | |
| | **S367phos** | 0.81±0.11 | 7.58±3.09 | -443±141 | -6544±113 | -6987±234 |
| | **Doublephos** | 0.89±0.09 | 5.31±2.09 | -248±109 | -6946±192 | -7195±227 |

**Table 4.2: Thermodynamic parameters of the association of CaM and phosphorylated L-selectin peptide**. Measurements were taken using ITC200 instrument at 20 °C in NMR buffer (see Section 2.12.3 for recipe) with and without 5 mM CaCl$_2$. Results shown represent the mean and standard deviation of three independent experiments. *binding could not be measured either because no binding occurred or because the ΔH of interaction was too small to be detected in an ITC experiment.

The determination of binding affinity using ITC relies on a ΔH value measurable above the heat of dilution (the heat associated with the dilution of the buffer components in the syringe into the sample cell) and, most importantly, above the limits of detection of the instrument: the ITC200 is not capable of measuring power compensation changes below 0.05 µcal/sec (388). Considering that the enthalpy changes for the interaction between CaM-Ca and wildtype L-selectin were at the limit of the instrument sensitivity, the inconclusive outcome of the measurement with S364phos did not exclude the possibility that an interaction was indeed occurring between CaM-Ca and S364phos peptide in the experimental conditions used. In this scenario, the reaction would generate a ΔH smaller than the

one observed with wildtype L-selectin tail binding to CaM-Ca and therefore below what could be reliably measured by ITC. To find out conclusively whether CaM-Ca was indeed capable of binding to the S364phos peptide, a different biophysical technique was needed, which would not rely on the changes of enthalpy generated during the reaction but measured a different biophysical parameter. MST was therefore chosen on the basis that the parameter followed in a titration-dependent experiment (the thermophoresis, see Section 2.17.4.1) was independent of enthalpy changes.

Initial MST experiments, carried out during a demonstration of the MST Monolith NT.115 instrument at King's College London, established that this method was competent in measuring the interaction between CaM-Ca and L-selectin cytosolic tail; hence samples were sent to NanoTemper Technologies GmbH for further tests and repeats. CaM was labelled with NT-647 dye, which uses hydroxysuccinimide (NHS)-ester to covalently couple the dye to lysine residues. A serial dilution of CaM (at constant concentration) with the peptide was then performed and the solutions were loaded into glass capillaries. The experiments were carried out in the presence of 0.05% TWEEN: detergents such as TWEEN are often added to the buffer in MST experiments in order to avoid molecular aggregation and to favour sample stability (344,398), given that this technique fails in the presence of even small aggregates. TWEEN also minimises adsorption of the protein to the glass capillary (399). The MST experiments showed that CaM-Ca bound to both wildtype and S364phos peptides with similar affinity (binding constant of 68 µM and 46 µM respectively, Figure 4.6 and Table 4.6), though, due to time constraints, only two experiments were carried out for each interaction and as a result further repeats are required for a statistical analysis to be performed.

The outcome of MST experiments would indicate that CaM-Ca is capable of binding to all the phosphorylated peptides with comparable affinities, adding support to the hypothesis that the initial ITC experiments were unable to detect the interaction between CaM-Ca and the S364phos peptide in the conditions used. However, the experimental conditions used in the MST experiments were slightly different from the ITC tests, in that the buffer used in the former measurements

contained TWEEN, albeit in very small concentration (0.05%). TWEEN is a detergent and it cannot be excluded that it may have an effect on altering the conformation of the protein or peptide, thereby influencing the outcome of the experiment. It has in fact been shown that peptides can easily form helices in the presence of detergents, such as SDS and Tetrafluoroethylene (TFE), though concentrations higher than 0.05% are often required (400-402). This required further investigation.

**A**

**B**
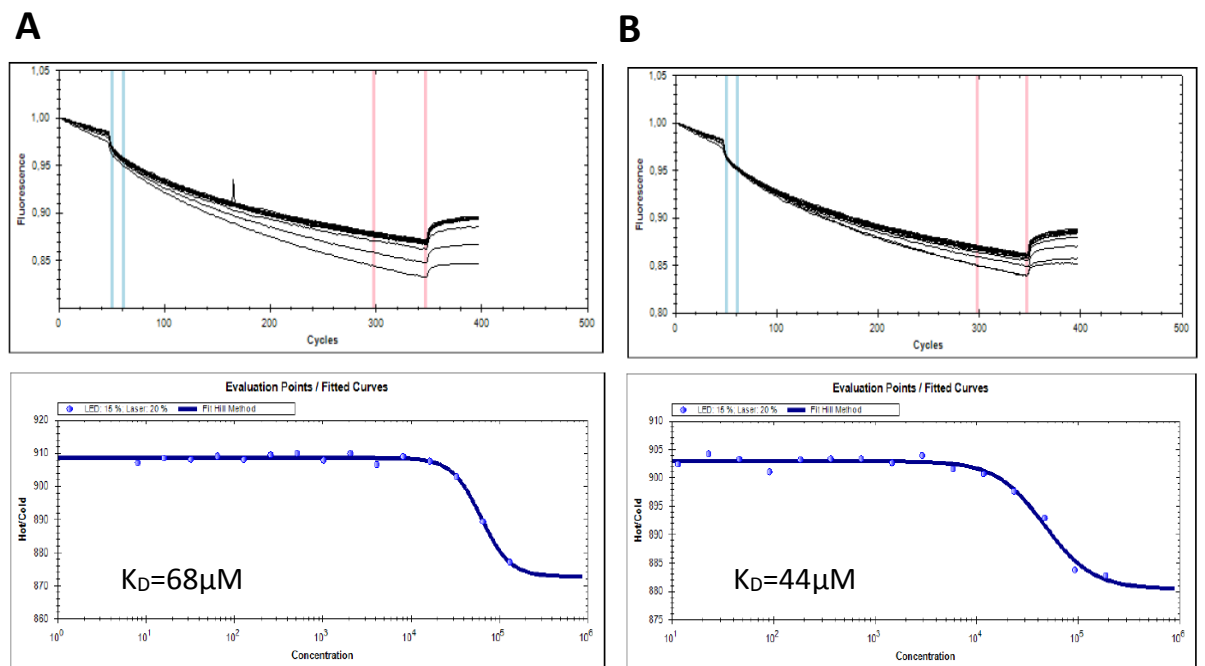


**Figure 4.7: Microscale thermophoresis showing the interaction of CaM-Ca and L-selectin peptides**. Experiments were carried out with (A) wildtype and (B) S364phos. Experiments were carried out by Nanotemper technologies. CaM-Ca was labelled with NT-647 dye (Lys-coupling chemistry) using NanoTemper's Protein Labelling Kit RED (#L001, Nanotemper Technologies). The concentration of the labelled protein was kept constant at 20 nM, whereas for the peptides a 1:1 series of dilution was carried out, starting at a highest concentration of 262 µM for S364phos and 375 µM for wildtype. The samples were loaded into enhanced gradient standard treated MST grade glass capillaries after a short incubation period and an MST analysis was performed using the Monolith NT.115. Concentrations of the unlabelled peptide are in nM (shown on the x axis). n=2 for all experiments. Experiments were carried out by a third party at Nanotemper Technologies GmbH, Munich.

The analysis of the effect of TWEEN on the L-selectin secondary structure was described in the previous chapter (Section 3.3.7), showing that the peptides remained in a random coil formation in a buffer containing 0.05% TWEEN (Figure

3.14). Next, the effect of TWEEN on the conformation of CaM-Ca was assessed by carrying out a 2D [$^1$H-$^{15}$N] HSQC experiment of CaM-Ca in NMR buffer with 0.05% TWEEN and comparing the spectra with that in NMR buffer alone. Figure 4.7A shows that CaM-Ca was folded in the presence of TWEEN; however, the chemical shift of a majority of the residues was altered (Figure 4.7B). Changes in buffer conditions have been shown to affect the [$^1$H-$^{15}$N] HSQC spectrum of proteins (403,404); nonetheless a significant buffer-induced conformational rearrangement of the protein could not be totally excluded from this NMR analysis.

In parallel to the analysis of the effect of 0.05% TWEEN on the conformation of the individual molecular species, its effect on the interaction between CaM-Ca and L-selectin was also investigated by repeating ITC experiments using the MST buffer. Experiments were undertaken with both wildtype and S364phos peptides to allow a direct comparison. Interestingly, the enthalpy of the interaction between CaM-Ca and wildtype L-selectin cytosolic tail peptide increased in these experimental conditions, and, accordingly, a detectable ΔH value was now observed for the interaction between CaM-Ca and the S364phos peptide. A dissociation constant for this interaction could therefore be derived from the curve fitting to the one independent binding site model and was found to be similar to that observed with wildtype L-selectin peptide (Table 4.3). Time constraints prevented further repeats to be carried out for each interaction and therefore a statistical analysis could not be undertaken. For this reason, these experiments were used to compare qualitatively the binding profiles of wild-type selectin and mutant rather than provide a quantitative assessment of the parameters of the interactions.

Considering that the ΔH values increased across the board, a plausible explanation was that 0.05% TWEEN in the buffer could account for the shift of the ΔH values to measurable pulses above the ITC detection limits (see Section 2.17.1.1 for a description of the dependence of ΔH on buffers, temperature etc.). Nonetheless, the changes in chemical shifts observed for CaM-Ca in presence of TWEEN prompted additional experiments to be undertaken to confirm this supposition. In particular, in support of the hypothesis that addition of TWEEN caused ΔH to change to a measurable value without altering any other parameters,

ITC experiments were performed with CaM-Ca and the L-selectin peptides at a different temperature (but without TWEEN), as temperature can also affect ΔH (Kirchhoff's law of thermochemistry, see Section 2.17.1.1 for an explanation). The experiments (Figure 4.8) showed that at 10 °C the ΔH of the interaction between CaM-Ca and the S364phos peptide once again became detectable by ITC200 instrument (compare Figure 4.5A and B with Figure 4.8C and D). The thermogram could be fitted to the one independent binding site model and the resultant $K_D$ for this interaction was found to be similar to that of the CaM-Ca wildtype L-selectin peptide interaction (Table 4.4), though only two experiments were undertaken for each interaction, so further repeats will be required to enable a proper statistical analysis.

It should be noted that MST required covalent modification of primary amine groups derived from lysine residues within CaM, specifically for the attachment of the NT647 dye. Due to time constraints, chemical modification of CaM by the addition of the dye was not controlled for, but is discussed below (in Section 4.4.1).

Taken together all these data support the hypothesis that phosphorylation of the L-selectin cytosolic tail did not affect CaM-Ca binding in a binary *in vitro* system. However, further work will be required to definitively understand the role of phosphorylation of L-selectin in regulating CaM binding.

| Peptide | Stoichiometry (N) | $K_D$ (μM) | ΔH (cal/mol) | -TΔS (cal/mol) | ΔG (cal/mol) |
|---|---|---|---|---|---|
| **WT** | 0.8±0.02 | 11.4 | -1038±32 | -5679 | -6717 |
| **S364phos** | 0.9±0.04 | 6.5 | -405±20 | -6638 | -7043 |

**Table 4.3: Thermodynamic parameters of the association of CaM and L-selectin peptides in the presence of 0.05% TWEEN.** Measurements were taken using ITC200 instrument at 20 °C in NMR buffer (see section 2.12.3 for recipe) with 5 mM $CaCl_2$ and 0.05% TWEEN. Results are from one experiment; with the error associated with fitting the data to the model shown (calculated by Origin 7.0 software).

**A**

**B**
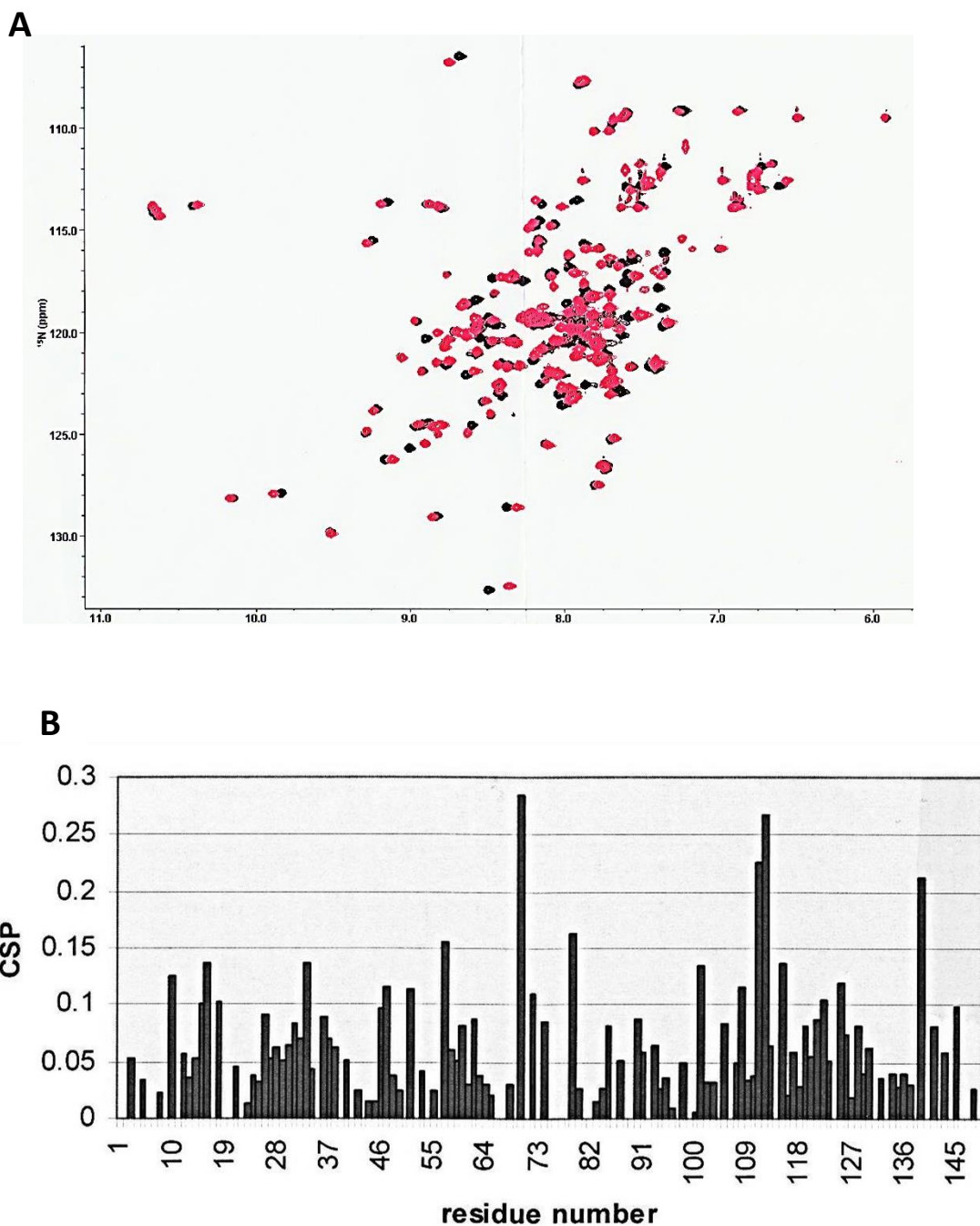
Figure 4.8: Effect of 0.05% TWEEN 20 on CSP of CaM-Ca. (A) [$^1$H-$^{15}$N] HSQC of CaM-Ca (black) and CaM-Ca with 0.05% TWEEN 20 (red). Chemical shifts taken from BMRB ID 1634. Spectra were recorded using a Bruker 700 MHz at 25 °C in NMR buffer with 5 mM CaCl$_2$. (B) Chemical shift perturbations were calculated and plotted against residue number.
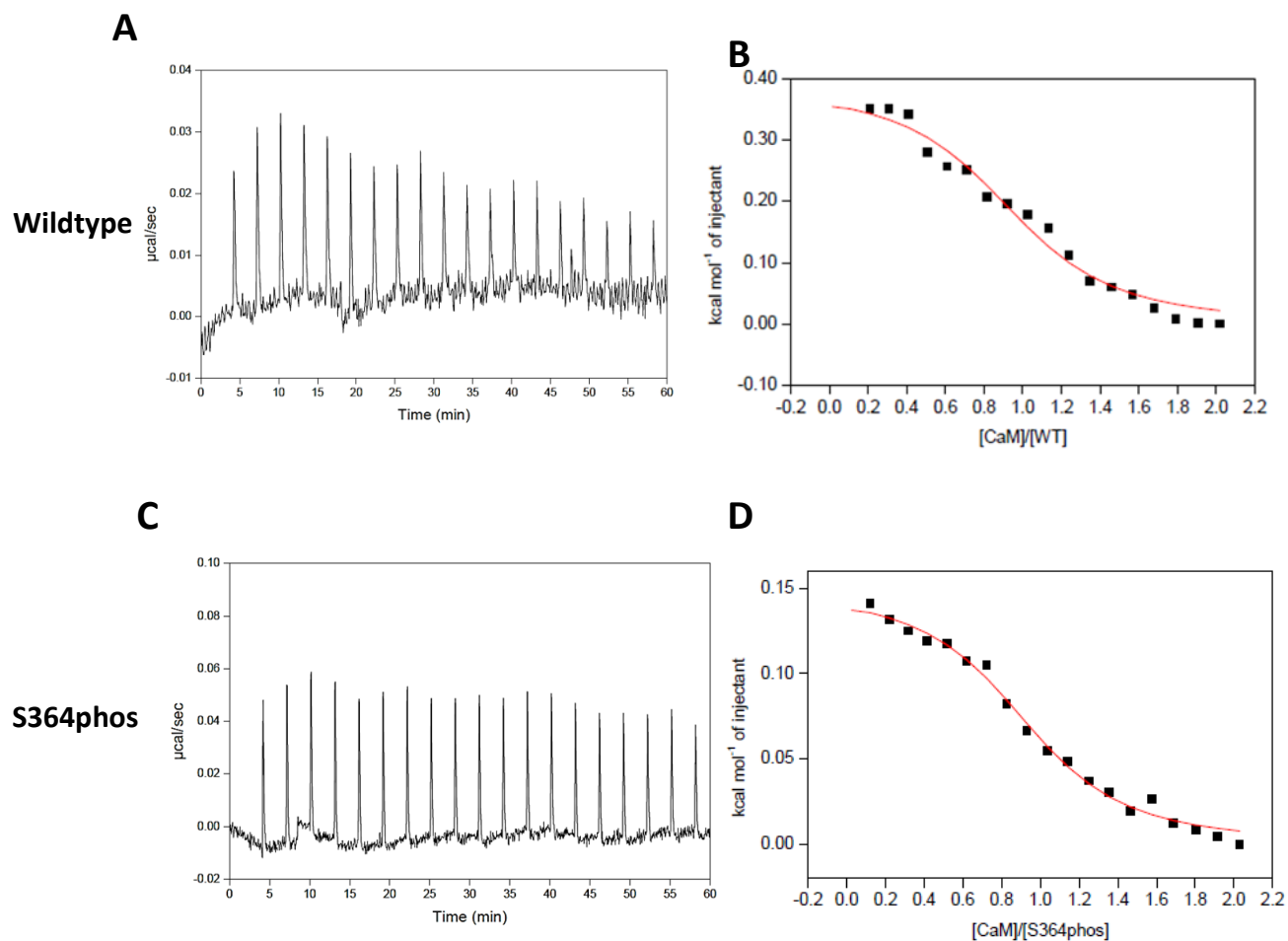
**Figure 4.9: Interaction between CaM-Ca and L-selectin peptides.** ITC experiments for CaM-Ca with wildtype (A and B), S364phos (C and D) at 10 °C. The normalised heat of interaction was obtained by integrating the raw data and subtracting the heat of dilution from each point. The red line represents the best fit obtained by a non-linear least-squares procedure based on one independent binding site model using origin 7.0. Results are representative of two independent experiments.

| Peptide | Stoichiometry (N) | $K_D$ (µM) | ΔH (cal/mol) | -TΔS (cal/mol) | ΔG (cal/mol) |
|---|---|---|---|---|---|
| WT | 1.04±0.09 | 3.90±0.29 | 306±111 | -7285±67 | -6978±43 |
| S364phos | 0.86±0.13 | 6.04±3.04 | 141±10 | -6912±304 | -6771±294 |

**Table 4.4: Thermodynamic parameters of the association of CaM and L-selectin peptides carried out at 10°C.** Measurements were taken using ITC200 instrument at 10 °C in NMR buffer with 5 mM $CaCl_2$. Results represent the mean and standard deviation of two experiments.

NMR was also used to confirm the association between CaM-Ca and S364phos, whilst at the same time gaining further insight into the binding mechanism *via* the chemical shift perturbation analysis. The S364phos peptide was added to a solution containing $^{15}$N labelled CaM-Ca and a series of 2D NMR [$^{1}$H-$^{15}$N] HSQC experiments were carried out to follow the titration. The spectra showed changes in the chemical shifts of CaM-Ca amino acids upon S364phos peptide addition, implying that binding occurred (Figure 4.9). These CSPs were compared to those observed with wildtype peptide and were seen to be very similar, albeit some differences were observed (Figure 4.10), for example detectable CSPs for residues E54, K55 and A57 and higher CSPs for residues S101, L105, V108 and L116. Although this remains to be confirmed, the current working hypothesis is that differences in Ca-CaM CSPs induced by the wild-type peptide and the S364phos mutant interaction are likely to have arisen from local chemical environment perturbations due to the close proximity of some of the CaM residues to the phosphate group of S364phos.

Overall the NMR experiments positively confirm that phosphorylation of S364 does not affect the ability of CaM-Ca to bind to the tail of L-selectin *in vitro* and that the binding mechanisms between CaM-Ca and S364phos or non-phosphorylated full-length L-selectin peptide appeared to be not significantly dissimilar. Further experiments will be required to elucidate the precise point of contacts between the protein and peptides.
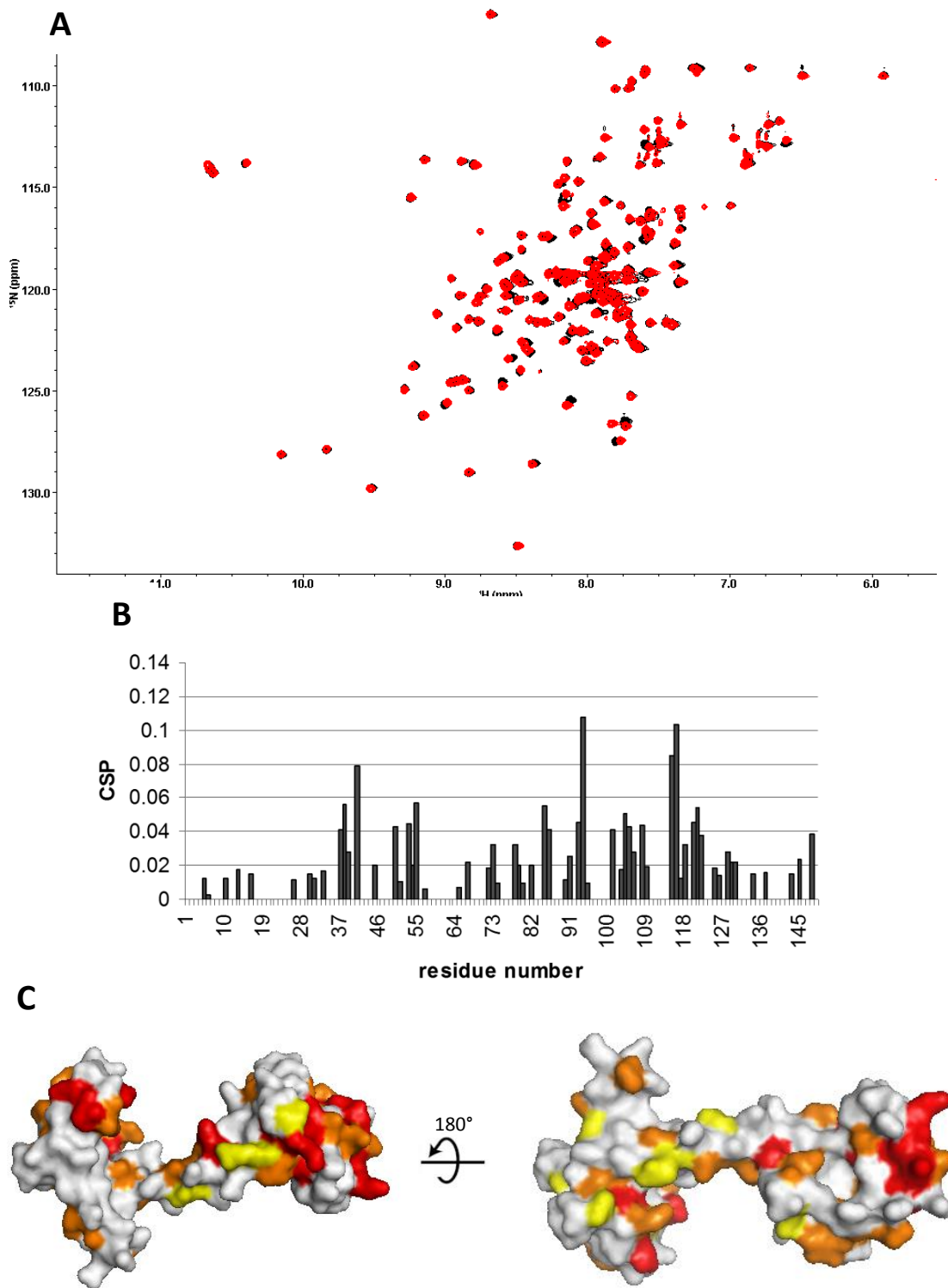
**Figure 4.10: Chemical shift perturbation analysis of CaM-Ca/S364phos-L-selectin interaction.**
(A) [$^1$H-$^{15}$N] HSQC of CaM-Ca (black) and CaM-Ca in the presence of 1.2 equivalent of the peptide
(red). $^{15}$N chemical shifts are shown on the Y axis and $^1$H chemical shifts shown on the X axis,
both measured in ppm. Chemical shifts were assigned from BMRB ID 1634. Spectra were
recorded using a Bruker 700 MHz at 25 °C in NMR buffer with 5 mM CaCl$_2$. (B) Chemical shift
perturbations were calculated using the method described in Section 2.17.2.2.1 and (C) plotted
on the structure of CaM-Ca, PBD id 3CLN. Residues coloured red represent CSPs of $\Delta\delta_{AV} \geq 0.03$,
orange represent CSPs of $0.01 \leq \Delta\delta_{AV} < 0.03$, yellow represents CSPs of $0.005 \leq \Delta\delta_{AV} < 0.01$ and white
represents CSPs of $\Delta\delta_{AV} < 0.005$.

**A**

**B**

**Figure 4.11: Comparison of the CSPs of CaM-Ca with wildtype and S364phos L-selectin peptides.** CSPs for CaM-Ca upon the addition of wildtype (A) or S364phos (B) L-selectin peptide were calculated and plotted against residue number to allow comparison of the CSPs with both peptides.

### 4.3.3 Monitoring the Interaction between CaM and Alanine Mutations of the L-selectin Cytosolic Tail

Much of the work carried out in the Ivetic lab uses cell lines that possess alanine mutations within the L-selectin tail. They have been used to better understand if shedding of L-selectin can be altered, using for example non-phosphorylatable serine-to-alanine residues. To elucidate which residues within the L-selectin cytosolic tail were important for the binding of CaM, several peptides with different alanine mutations were purchased, namely K362A, S364A, S367A and Y372A. The two serine to alanine mutants were chosen to complement the experiments carried out in cell lines (see Chapter 5 and 6). A previous study investigated the role of basic residues in the cytosolic tail of L-selectin in the interaction with moesin (225). K362A was one of the mutations used and it was shown that it strongly inhibited the interaction between L-selectin cytosolic tail peptide and moesin (225) and it was therefore of interest to see its effect on CaM binding. In the same study the Y372A mutant was used as a control peptide with an alanine mutation in a non-basic position (225). The results showed this mutation had little effect on the interaction between moesin and the peptide (225). To understand if the same was true for the interaction between CaM and this peptide was analysed in this section.

ITC experiments were carried out with these peptides as described above, with measurements taken at 20 °C in NMR buffer with or without $CaCl_2$. The experiments with ApoCaM showed a binding process for all the peptides, with one event observed and a molar ratio of around one for each peptide. This allowed the data to be interpolated into binding curves using a one independent binding site model, from which the $K_D$, $\Delta H$ and $-T\Delta S$ for the binding of each peptide could be elucidated (Figure 4.11 and Table 4.5). The $K_D$s were found to be 3.6±1.6 µM for K362A, 4.1±2.0 µM for S364A, 6.3±0.5 µM for S367A and 2.7±0.3 µM for Y372A. As with the phosphorylated peptides, the differences between these $K_D$ values and that observed with wildtype L-selectin were not considered significant. The same was true for the comparison between the $\Delta H$ and $-T\Delta S$ for each peptide.

Results with CaM-Ca showed that binding occurred between CaM-Ca and S367A and Y372A peptides and binding curves could be produced by integrating the heat of interaction of each peak and fitting the data to the one independent binding site model. The $K_D$s extrapolated from the binding curves (2.7±0.5 µM for S367A and 5.0±4.5 µM for Y372A) were compared to that found with wildtype L-selectin peptide (4.0±2.1 µM) and no significant difference was observed, showing the strength of binding was similar with all three peptides. The ΔH for the interaction between CaM-Ca and each peptide were also compared (-416±110 cal/mol for wildtype, -391±73 cal/mol for S367A and -341±225 for Y372A) revealing no significant difference. Experiments with K362A and S364A were inconclusive as no measurable ΔH was produced (Figure 4.12 and Table 4.5). Similarly to previous experiments with the S364phos peptide, the enthalpies of interaction were very close to zero in the above experimental conditions used, thereby rending the experiments inconclusive.
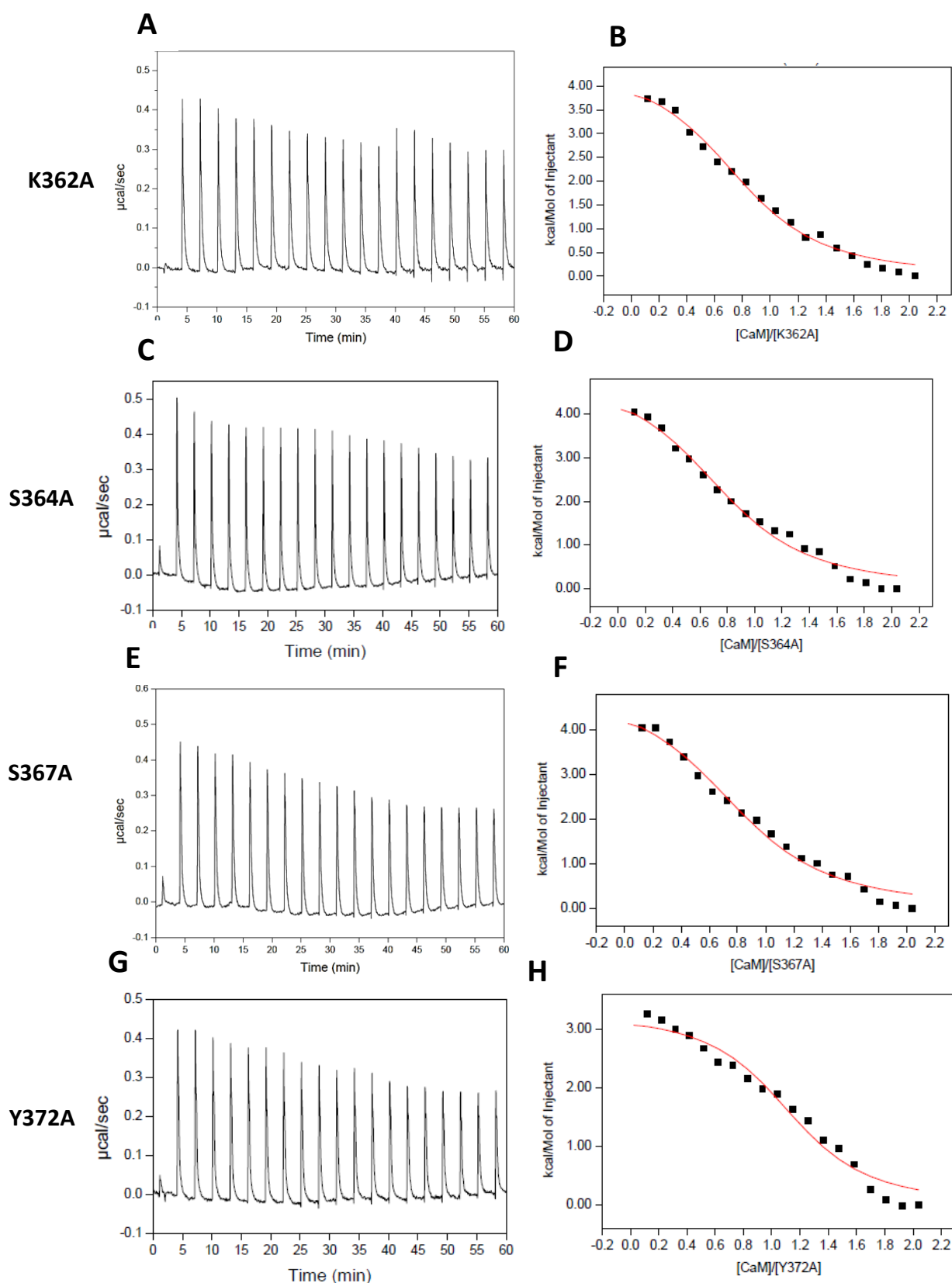
**Figure 4.12: Interaction between ApoCaM and alanine mutant L-selectin peptides.** ITC experiments for ApoCaM with K362A (A and B), S364A (C and D), S367A (E and F) and Y372A (G and H). The normalised heat of interaction was obtained by integrating the raw data and subtracting the heat of dilution from each point. The red line represents the best fit obtained by a non-linear least-squares procedure based on one independent binding site model using origin 7.0. Results are representative of three independent experiments.
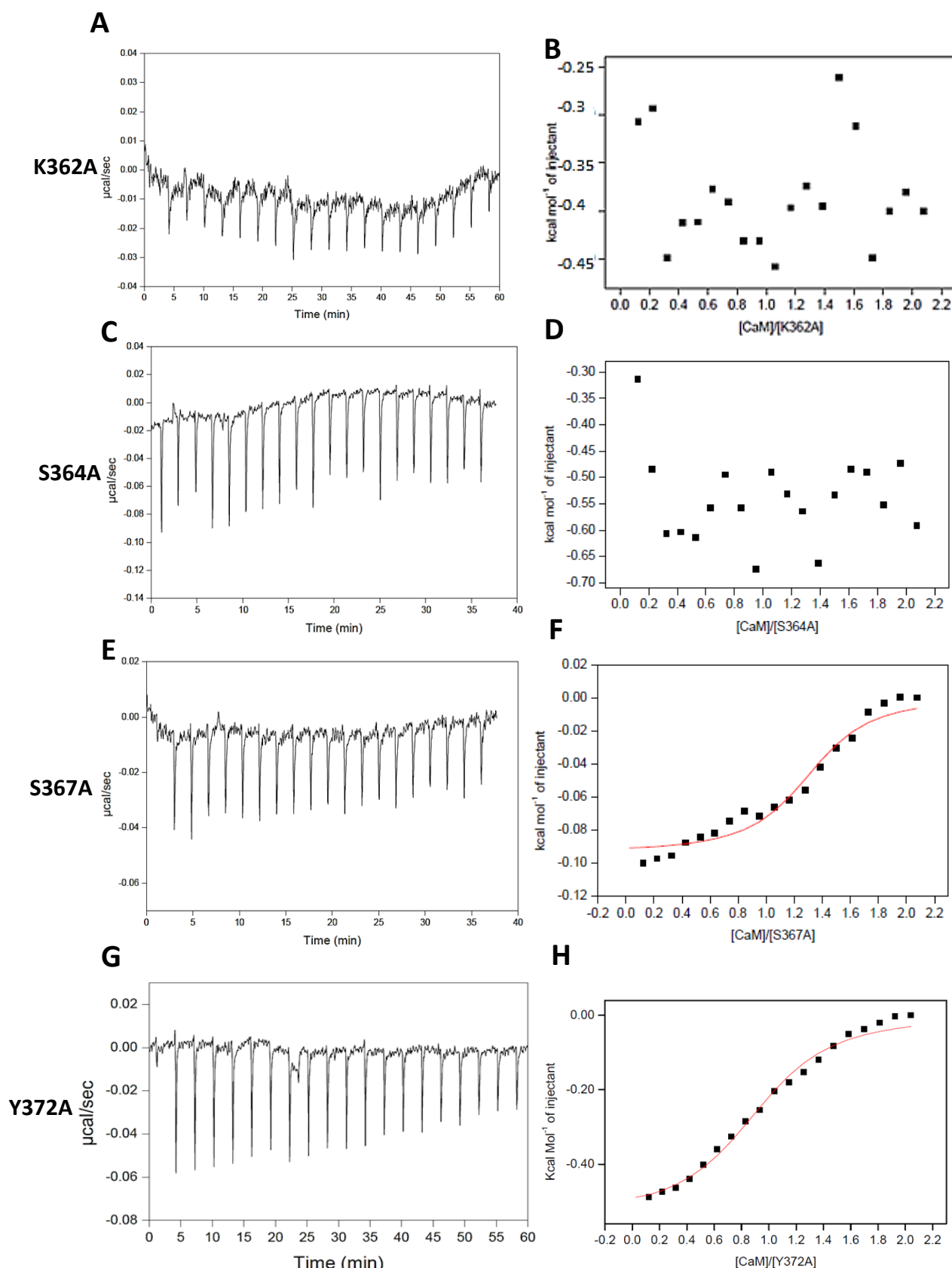
**Figure 4.13: Interaction between CaM-Ca and alanine mutant L-selectin peptides.** ITC experiments for CaM-Ca with K362A (A and B), S364A (C and D), S367A (E and F) and Y372A (G and H). The normalised heat of interaction (change in ΔH associated with the interaction between CaM and the L-selectin peptide) was obtained by integrating the raw data and subtracting the heat of dilution from each point. The red line represents the best fit obtained by a non-linear least-squares procedure based on one independent binding site model using origin 7.0. Results are representative of three independent experiments.

181

| Proteins | | Stoichiometry (N) | $K_D$ (µM) | ΔH (cal/mol) | -TΔS (cal/mol) | ΔG (cal/mol) |
|---|---|---|---|---|---|---|
| ApoCaM | **Wildtype** | 1.21±0.15 | 1.63±0.33 | 1430±341 | -8528±108 | -7028±246 |
| | **K362A** | 0.84±0.010 | 3.62±1.64 | 2428±823 | -9853±546 | -7425±277 |
| | **S364A** | 0.99±0.14 | 4.2±2.0 | 2350±218 | -9719±203 | -7369±357 |
| | **S367A** | 0.92±0.11 | 6.29±0.58 | 1976±556 | -9049±601 | -7074±55 |
| | **Y372A** | 0.99±0.22 | 2.79±0.28 | 2052±721 | -8767±960 | -7549±58 |
| CaM-Ca | **Wildtype** | 0.97±0.12 | 4.01±2.15 | -416±110 | -6967±393 | -7383±291 |
| | **K362A** | Binding could not be measured* | | | | |
| | **S364A** | Binding could not be measured* | | | | |
| | **S367A** | 1.02±0.19 | 2.72±0.53 | -391±73 | -7176±126 | -7567±120 |
| | **Y372A** | 0.93±0.27 | 5.01±4.59 | -341±225 | -7032±709 | -7373±558 |

**Table 4.5: Thermodynamic parameters of the association of CaM and alanine mutant peptides.** Measurements were taken using ITC200 instrument at 20 °C in NMR Buffer with 5 mM $CaCl_2$ for CaM-Ca or NMR alone for Apo-CaM Results represent the mean and standard deviation of three independent experiments. *binding could not be measured either because no binding occurred or because the ΔH of interaction was too small to be detected in an ITC experiment.

The inconclusive ITC results between CaM-Ca and S364A were reminiscent of what was observed with S364phos at 20 °C in NMR buffer. For this reason, the same experimental steps were undertaken to ascertain whether CaM-Ca was binding to the S364A peptide. MST experiments were carried out to test the CaM-Ca and S364A association, using S367A peptide as a positive control because CaM-Ca interaction with this peptide was already characterised by ITC. The MST experiments, performed in the presence of 0.05% TWEEN, revealed a clear interaction between CaM-Ca and S364A peptide, with a similar $K_D$ to that found with wildtype (Figure 4.13A and Table 4.6), though once again, statistical analysis was not possible, as only two experiments were carried out for each interaction. Interestingly, the $K_D$ value of the interaction between CaM-Ca and the S367A peptide obtained from MST was smaller than that of the other peptides (Figure 4.13B and Table 4.6), indicating a stronger interaction between CaM-Ca and S367A in the experimental conditions used. However, the results from MST were the mean

of only two experiments and therefore further repeats are required in order to carry out a comprehensive quantitative analysis on the different $K_D$ values obtained with this technique.

**A**

**B**
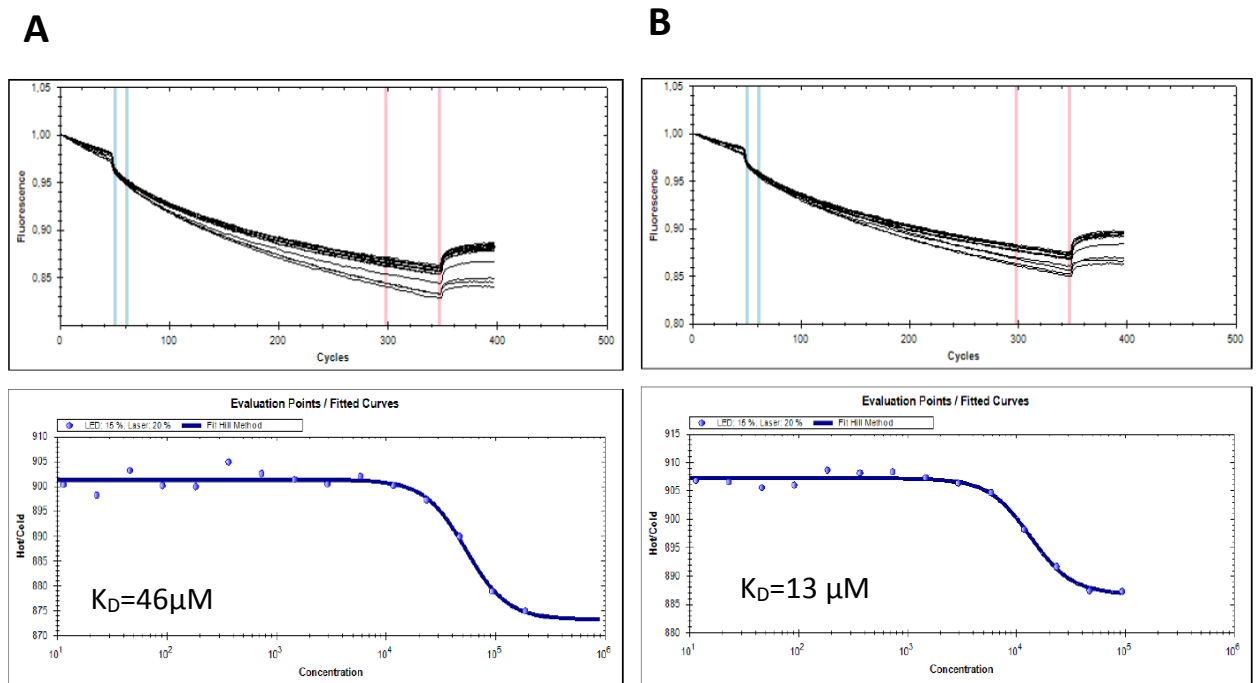


**Figure 4.14: Microscale thermophoresis with CaM-Ca and L-selectin peptides**. Experiments were carried out with (A) S364A and (B) S637A. CaM-Ca was labelled with NT-647 dye (Lys-coupling chemistry) using NanoTemper's Protein Labelling Kit RED (#L001, Nanotemper Technologies). The concentration of the labelled protein was kept constant at 20nM, while a serial dilution of the peptide was carried out, with a starting concentration of 375 μM and diluting down to 1:1. The samples were loaded into enhanced gradient standard treated MST grade glass capillaries after a short incubation period and an MST analysis was performed using the Monolith NT.115. Concentrations of the unlabelled peptide (shown on the x axis) are in nM. N=2 for all experiments. Experiments were carried out by a third party at Nanotemper Technologies GmbH, Munich.

|  | $K_D$ (µM) |
| --- | --- |
| Wildtype | 68 |
| S364phos | 48 |
| S364A | 46 |
| S367A | 13 |

**Table 4.6: Summary of dissociation constants of Cam-Ca and L-selectin peptides calculated by MST analysis.** Measurements were taken with a Monolith NT.115 instrument by a third party at NanoTemper Technologies GmbH, Munich. Results shown are the mean of two independent experiments.

Akin to the S364phos analysis, ITC experiments were repeated with 0.05% TWEEN supplemented to the binding buffer to confirm the results seen with MST. Binding of CaM-Ca was observed with the S364A peptide giving a $K_D$ (12.2 µM), a ΔH (-772 cal/mol) and –TΔS (-5905 cal/mol) (Table 4.7). This indicated that CaM-Ca was capable of interacting with S364A, although only one experiment for each interaction was undertaken because of time restraints. As for before, ITC experiments were also carried out at 10 °C (without TWEEN) to be able to measure ΔH values without the use of TWEEN in the buffer, and this confirmed that CaM-Ca was capable of binding to S364A peptide with similar $K_D$ to wildtype (Figure 4.14. and Table 4.8). These results together confirm that CaM-Ca is able to bind to S364A peptide.

The same experimental conditions were used to assess the binding of CaM-Ca to the S367A peptide, following the differences in the $K_D$s measured with ITC at 20 °C and MST. Binding was observed both in buffer supplemented with 0.05% TWEEN and at 10 °C in NMR buffer and the $K_D$s measured were similar to those for wildtype L-selectin peptide, but due to time limitations, the necessary repeats could not be carried out and therefore the extent of the similarity between wildtype and S367A could not be assessed by statistical analysis.

| Peptide | Stoichiometry (N) | $K_D$ (µM) | ΔH (cal/mol) | -TΔS (cal/mol) | ΔG (cal/mol) |
|---|---|---|---|---|---|
| WT | 0.8±0.03 | 11.4 | -1038±31 | -5679 | -6717 |
| S364A | 0.8±0.06 | 12.2 | -772±28 | -5905 | -6677 |
| S367A | 0.9±0.02 | 7.3 | -560±18 | -6418 | -6978 |

**Table 4.7: Thermodynamic parameters of the association of CaM and L-selectin peptides in the presence of 0.05% TWEEN.** Measurements were taken using ITC200 instrument at 20 °C in NMR buffer with 5 mM $CaCl_2$ and 0.05% TWEEN. Results are from one experiment, with the error in fitting the data to the model (calculated by Origin 7.0) shown.
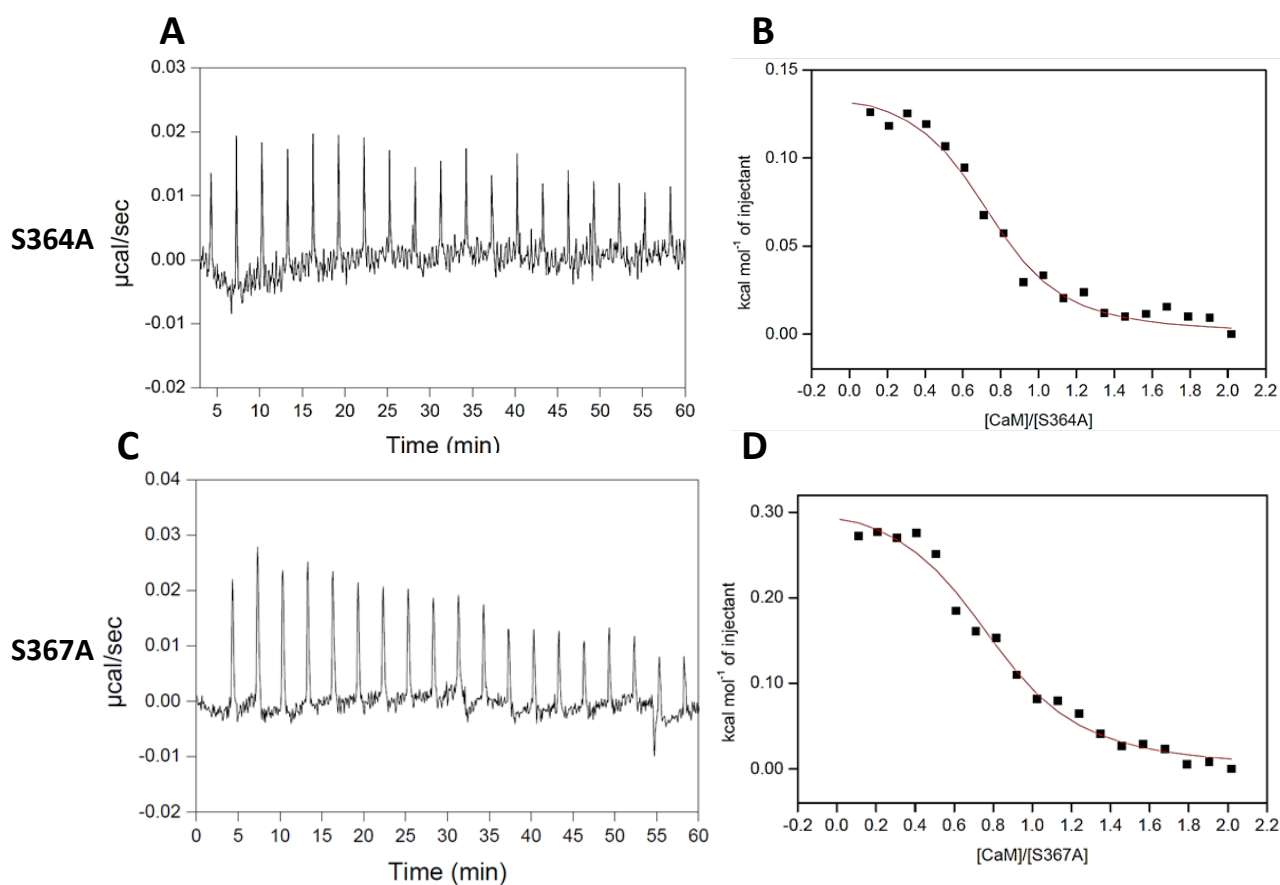


**Figure 4.15: Interaction between CaM-Ca and L-selectin peptides.** ITC experiments for CaM-Ca with S364A (A and B), S367A (C and D) at 10 °C. The normalised heat of interaction was calculated by integrating the raw data and subtracting the heat of dilution from each point. The red line represents the best fit obtained by a non-linear least-squares procedure based on one independent binding site model using origin 7.0. Results are representative of two independent experiments.

185

| Peptide | Stoichiometry (n) | K$_D$ (μM) | ΔH (cal/mol) | -TΔS (cal/mol) | ΔG (cal/mol) |
|---------|-------------------|------------|--------------|----------------|--------------|
| WT | 1.04±0.09 | 3.90±0.29 | 306±111 | 7285±67 | 6978±43 |
| S364A | 0.92±0.25 | 2.72±0.13 | 119±30 | 7302±2 | 7182±27 |
| S367A | 0.89±0.12 | 3.84±0.02 | 358±54 | 7347±52 | 6988±2 |

**Table 4.8: Thermodynamic parameters of the association of CaM-Ca and L-selectin peptides carried out at 10°C.** CaM-Ca binding to L-selectin peptides. Measurements were taken using ITC200 instrument at 10 °C in NMR buffer with 5 mM CaCl$_2$. Results shown represent the mean and standard deviation of two experiments.
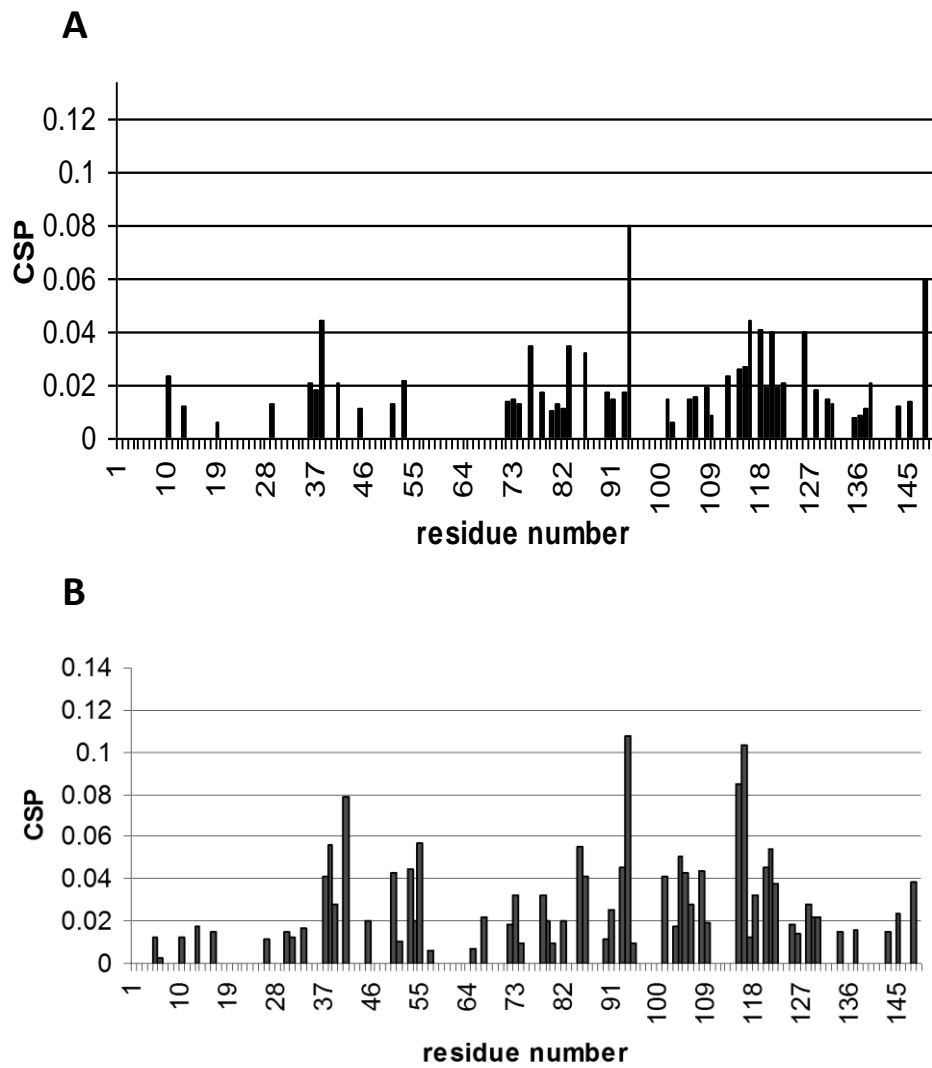
### 4.3.4 ITC Experiments with Trp-Cage L-selectin

In the previous chapter the Trp-Cage L-selectin construct was made in order to produce in-house L-selectin peptides (and mutants), in particular ^{15}N-labelled peptides to be used in NMR investigations aimed at elucidating details of L-selectin interaction with CaM. It was therefore critical to test whether the presence of the Trp-Cage had any effect on the binding of the L-selectin peptide to CaM. To this aim, ITC experiments were used to probe the interaction of Trp-Cage-L-selectin and CaM-Ca and compared with L-selectin peptide alone.

The ITC experiments showed association between CaM-Ca and Trp-Cage-L-selectin, with the interaction being fit to the one independent site model to produce the binding curve, from which the parameters associated with the interaction could be obtained. Comparison of the results for CaM-Ca with Trp-Cage-L-selectin and L-selectin peptide showed a similar binding affinity, however, the thermodynamic profile was very different, with Trp-Cage-L-selectin having a large positive enthalpy (Figure 4.15) compared to a small negative enthalpy for L-selectin peptide (Figure 4.1D and Table 4.1). This may suggest that the Trp-Cage had an effect on the interaction and therefore it is vital to test whether the Trp-Cage motif alone can bind to CaM-Ca. The Trp-Cage motif was obtained from *E.coli* cells following the same protocols used for Trp-Cage-L-selectin (section 3.3.5). Soluble

protein was observed on a SDS-PAGE gel (data not shown), however, when purification of the Trp-Cage motif was attempted using a $Ni^{2+}$ affinity column, a band on the gel corresponding to its expected molecular weight was observed in the flow through fraction, suggesting that the protein did not interact with the affinity column. Lack of time prevented further pursuit of this.
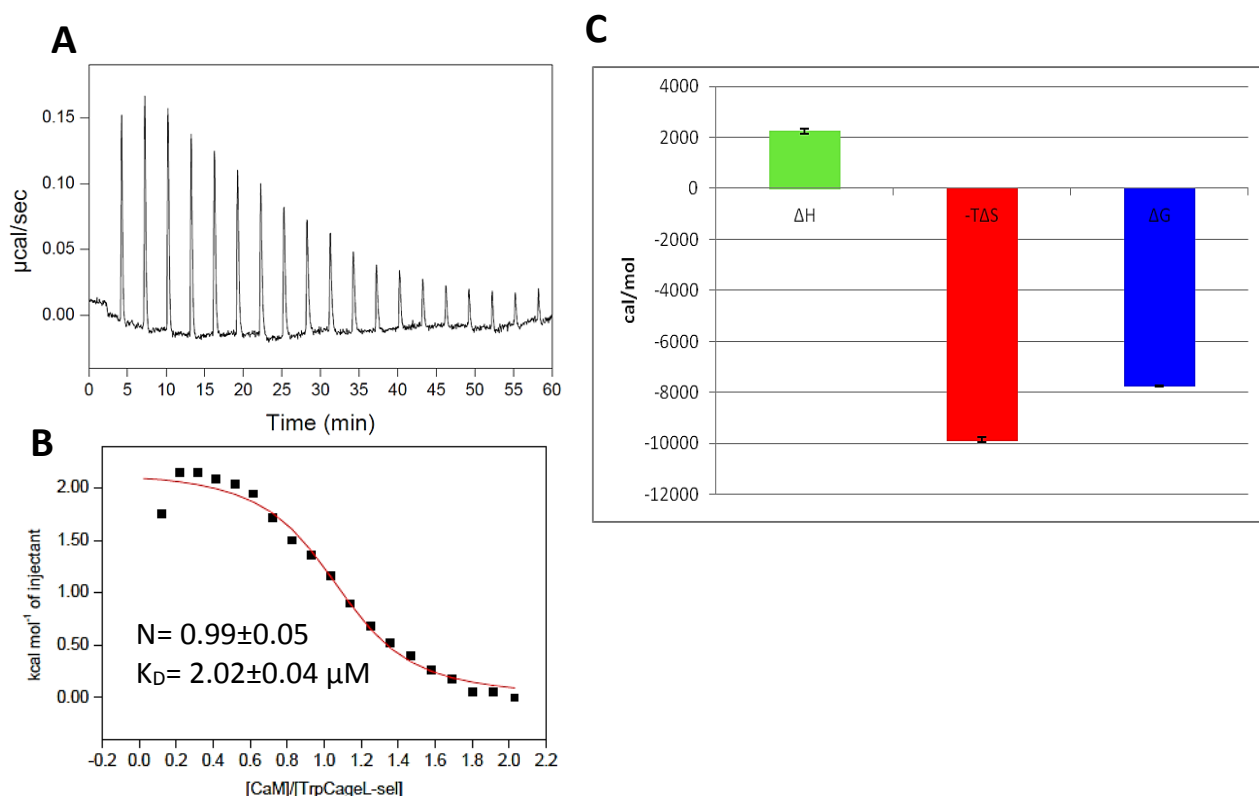


**Figure 4.16: ITC data of CaM-Ca binding to Trp-Cage L-selectin.** (A) ITC raw data profile of Trp-Cage L-selectin titrated into CaM-Ca. (B) binding curve produced by integrating the heat of interaction of each point and fitting the data to the one independent binding site model, with the stoichiometry (N) and dissociation constant( $K_D$) shown. (C) The thermodynamic profile of the interaction, with the ΔH, -TΔS and ΔG for the interaction shown. Measurements were taken using ITC200 instrument at 20 °C in NMR buffer with 5 mM $CaCl_2$. Results are representative of two independent experiments, with standard deviations shown bar the error bars.

## 4.4 Discussion

Previous work showed that L-selectin was capable of interacting with both CaM and ERM proteins at the same time to form a 1:1:1 complex (3). It is thought that this interaction regulates several functions of L-selectin, including localisation of L-selectin to microvilli and extracellular cleavage of L-selectin. Little is known about the mechanism behind the binding and how it is regulated. To study this, recombinant proteins were produced (Chapter 3) and biophysical techniques were used to assess the interaction of CaM to different L-selectin peptides and investigate possible regulation mechanisms of binding, particularly focussing on the requirement for calcium and the effect of L-selectin phosphorylation.

### 4.4.1 Determining what is considered a significant difference between binding constants

In this chapter, ITC and MST have been used to measure the binding constants of CaM with L-selectin peptides. Differences in binding affinities between CaM with wildtype L-selectin peptide and CaM with the mutant L-selectin peptides in any of the conditions tested were found to be fivefold or less with both methods. A fivefold difference in $K_D$s obtained by ITC is generally not considered significant because of the limitations of the technique, as it has been reviewed in previous studies (405-408). In our case this evaluation is justified because of the large error associated with several of the measured $K_D$s, in particular for experiments involving CaM-Ca, which are likely to derive from the small ΔH of interaction. A poor signal-to-noise ratio will inevitably be associated with sizeable experimental errors.

Several of the $K_D$s for the interaction between CaM-Ca and the different L-selectin cytosolic tail peptides measured using MST were also slightly different, with the largest difference being between wildtype and S367A L-selectin peptides, where a fivefold difference was observed (68 μM for wildtype and 13 μM for S367A). It is possible that this difference is significant, but due to time constraints only two experiments were carried out for each interaction and therefore a proper statistical comparison of the $K_D$s could not be undertaken.

In these studies, the $K_D$s for the CaM-Ca/L-selectin interaction measured using ITC and MST showed around a tenfold difference, 4.0±2.1 μM and 68 μM respectively. The exact reason for this difference remains unclear, though it is possible that it is linked to the different techniques used to measure the $K_D$s and different conditions, including the temperature and buffer in which the interaction was measured. It would be useful to compare the $K_D$s measured by ITC and MST in the same buffer (with TWEEN) directly, but further experiments are required for this. It is worth noting that there are several other examples reported in literature where MST and ITC have produced different binding constants for the same interaction (409), for example synaptotagmin binding to calcium (410,411) and riproximin interacting with asialofetuin (ASF) (412). Another consideration is the fact that CaM-Ca is labelled in the MST experiments. It is possible that the presence of the dye affects the interaction between L-selectin and CaM. There are several lysine residues within the C-lobe of CaM (the predicted binding site of L-selectin), such as K94, K115 and K148, with the possibility of the addition of the dye to these residues affecting the interaction, leading to a decrease in strength of binding. To test if this is the case, ITC experiments could be carried out with CaM with the dye covalently attached and comparing the $K_D$ measured with that without the dye and/or conducting MST using an N-terminal or C-terminal labelled protein (413).

## 4.4.2 Calcium is not required for CaM interaction with L-selectin cytosolic tail in vitro, but may affect the mechanism of interaction

ITC measurements conducted in this study show that CaM is capable of binding to L-selectin cytosolic tail peptide in the absence and presence of calcium with comparable affinity. It has been disputed whether calcium is required for the interaction between CaM and L-selectin. Work by Matala et al (2001)(414) showed that CaM could be immunoprecipitated with anti-L-selectin antibodies in resting neutrophils and that this was abrogated when EDTA was present, suggesting a requirement of calcium for the interaction in resting cells. Conversely, Killock et al (2009) (3) reported that the L-selectin cytosolic tail peptide conjugated to sepharose beads was capable of pulling down purified recombinant CaM even in

the presence of 5 mM EGTA, implying CaM interacted with L-selectin in the presence and absence of calcium. Deng et al (2011)(216) also investigated this interaction using an L-selectin cytosolic tail peptide and modified CaM covalently attached to a fluorescent probe. The change in fluorescence was monitored as the peptide was titrated in a solution containing CaM, with or without calcium, revealing that binding occurred in both cases with similar dissociation constants. Furthermore they performed ITC experiments to confirm the fluorescence data, but the experiment was only carried out with calcium. Importantly, the dissociation constant found by Deng et al (2011) for CaM-Ca/L-selectin interaction was consistent with what was found in this chapter. Notably, this report provides for the first time a quantitative measure of the dissociation constants with and without calcium, indicating that CaM can bind to the L-selectin cytosolic tail peptide with similar affinities when calcium bound or calcium free. It is worth noting that the possible discrepancy between the study of Matala et al (2001) and the other studies may be due to different requirements *in vivo* and *in vitro*. All examples where binding appears independent of calcium entailed the use of the L-selectin tail peptide *in vitro*, whereas Matala et al (2001) carried out the experiment using neutrophils with full length L-selectin. This implies that the requirement of calcium for the interaction may be dependent on L-selectin being in its full length form or could highlight differences in the interaction depending on the context in which it is studied, i.e. *in vitro* compared to *in vivo*. Immunoprecipitation requires cellular disruption by non-ionic detergents, which produces a cell lysate and ultimately destroys the cellular architecture and compartmentalisation. As will be seen in the subsequent results chapters of this thesis, assessing L-selectin/CaM interaction *in vivo* may be the best way forward in determining these presumably simple binary interactions occurring in complex cellular systems.

It remains to be defined how similar the binding mechanisms of L-selectin for CaM-Ca and ApoCaM are. The thermodynamics data here suggests that the binding mechanisms may be somewhat different. It is possible in the complex cellular environment that this change may have larger repercussions *in vivo*, whereby calcium influx into the cell, i.e. upon leukocyte activation (185), may lead

to CaM dissociation from L-selectin. One hypothesis may envisage that in resting leukocytes ApoCaM is bound to the tail of L-selectin, but once the leukocyte is activated, the calcium influx will result in CaM dissociation from L-selectin due to the conformational rearrangement of CaM upon calcium binding. It is also possible that cell activation exposes CaM-Ca to more abundant and higher affinity binding sites, which may sequester CaM-Ca away from L-selectin. For example both calcineurin and the CaM kinase family are up-regulated upon leukocyte activation (396) and could be other potential binding sites for CaM-Ca. Further experiments are required to establish the calcium content of CaM at different stages of cell activation to pinpoint the importance of calcium in regulating CaM binding to L-selectin in leukocytes.

The CSPs measured from the analysis of the 2D [$^1$H-$^{15}$N] HSQC NMR titrations suggests that CaM, either in the CaM-Ca or ApoCaM form, interacts with L-selectin predominantly via the C-lobe, with very few perturbations seen in the N-lobe. This suggests that the "wrap-around" mechanism of binding commonly seen with CaM binding to its target sequences does not occur with L-selectin. It is worth noting that the molar ratio of peptide to CaM used in these experiments was 1.2:1. This ratio was used as there was very little difference in the CSPs between this ratio and a ratio of 1:1, suggesting all binding events had occurred by this ratio. It is however, possible that CaM is not saturated in the results shown here. It maybe worth carrying out further titrations, increasing the amount of peptide added to ensure CaM is saturated. The NMR results observed in this thesis are consistent with molecular modelling of the CaM/ERM/L-selectin complex (3). Intriguingly, some of the residues of CaM predicted by this model to be involved in hydrogen bonding with L-selectin have been found in this study to exhibit some experimental CSPs. The majority of these residues are located within the C-lobe of CaM: I100, E114, L112, G134 and D131 are all predicted to form hydrogen bonds with L-selectin and all experience moderate CSPs in the titration of CaM with L-selectin (Figure 4.16). Other residues in CaM surrounding those predicted to form hydrogen bonds have been found to have large CSPs, in particular N111, G113, K115 and L116, consistent with a close proximity to L-selectin. However, residues E127 and

E140 which are predicted to form hydrogen bonds with L-selectin showed no CSPs in the NMR analysis. There are also several residues with large CSPs that are distant from the predicted L-selectin binding site, namely M76, D78 and E82. Though there is a correlation between the residues predicted to be in the vicinity of the L-selectin binding site and those that show large CSPs, there are also some significant differences. This implies that the molecular model produced by Killock et al (2009)(3) may serve as a good starting point in the analysis of a structure of the complex between CaM and L-selectin, but further NMR experiments are required to solve the structure of CaM bound to L-selectin to confirm if the model is correct.

**A**



**B**
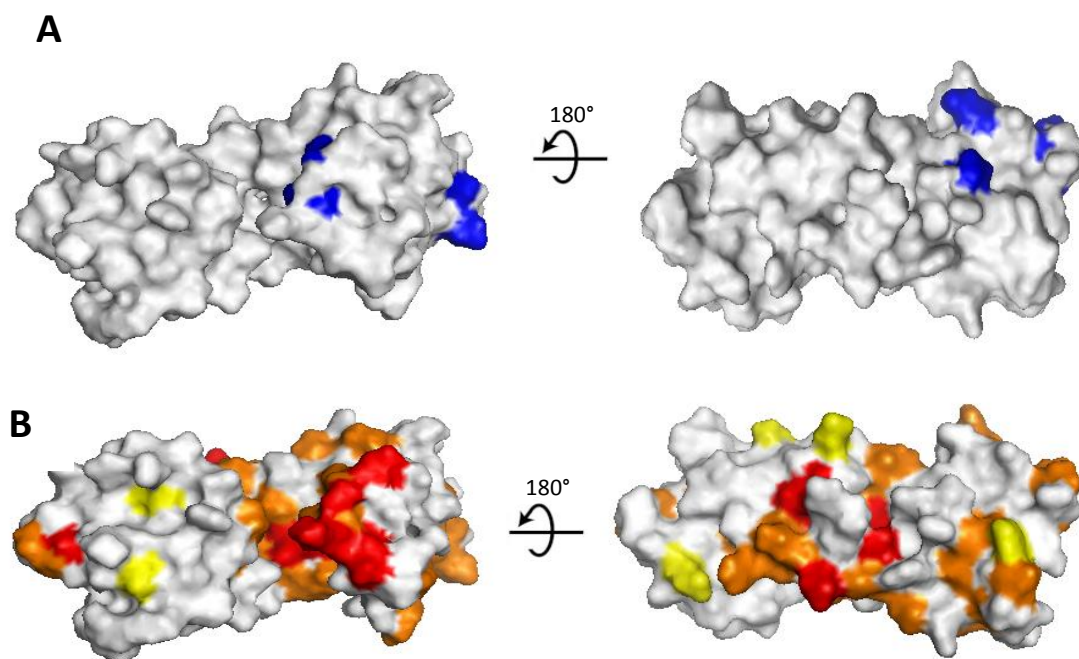


**Figure 4.17: Comparison of predicted residues of CaM involved in Hydrogen bonding with CSP of CaM with L-selectin peptide.** (A) The sites of the predicted Hydrogen bonds were mapped on the CaM structure (shown in blue). When compared to the CSP caused by binding to L-selectin peptide (B) it can be seen that several of the residues that have large CSP match those thought to hydrogen bond to L-selectin.

The model of the tertiary complex of CaM, ERM and L-selectin predicts that the binding sites of CaM and ERMs on L-selectin are very close to one another, with some overlap predicted (3). It therefore seems unlikely that this seventeen amino acid domain would be able to accommodate both lobes of CaM and the FERM

domain of ERMs. Although not as common as both lobes interacting with the CaM binding peptide, there are some examples of one lobe interacting with the target protein. Chagot et al (2011)(242) studied the interaction between ApoCaM and the IQ motif of human cardiac sodium channel NaV1.5 and found that only the C-lobe of CaM interacted with the CaM binding motif of NaV1.5, with several amino acids implicated in the binding overlapping with those that show CSPs in the CaM/L-selectin interaction, including G113, L116 and M145. This so called extended conformation of the CaM-peptide complex was also confirmed by x-ray crystallography of the complex (415).

Structural studies with CaM and the HIV-1 matrix protein Gag showed that when a short peptide, residues 11-28, was used to study the interaction, only the C-lobe of CaM was involved in the interaction (416). ITC experiments also revealed this interaction had a binding constant similar to CaM-Ca/L-selectin peptide interaction (4.4±0.2 μM and 4.0±2.1 μM respectively), though ΔH was larger (-8760±100 cal/mol versus -416±110 cal/mol) (416). When a longer peptide was used, residues 11-46, however, both lobes were found to interact with the peptide. The dissociation constant measured with the longer peptide was also much lower, showing the interaction was stronger (416). This is particularly interesting because when the L-selectin amino acid sequence was analysed for CaM binding domains, the sequence that was predicted to be a CaM binding site included part of the peptide studied here, but also several residues to the N-terminal side of this peptide, which are predicted to be located in the transmembrane domain of L-selectin (Figure 4.17A). Gifford et al (2012) (396) carried out ITC experiments looking at the interaction between CaM and a peptide of L-selectin that contained the cytosolic tail plus seven N-terminal residues located in the transmembrane domain. They found that the binding of CaM to the longer peptide was stronger than the shorter peptide and this increase in affinity was dependent on calcium (396). Furthermore, NMR analysis showed that larger CSPs in CaM were seen with the longer peptide. Gifford et al (2012)(396) also determined the structure of the complex showing that CaM wrapped around the longer peptide, with both domains interacting with the peptide in the canonical CaM binding fashion. However, the

question remains whether CaM is able to access residues located in the transmembrane domain in the cell. Gifford et al (2012)(396) argue that CaM must perturb the membrane bilayer structure to gain access to the site or pull L-selectin down to remove this section from the plasma membrane. This is an interesting point, as it is known that shedding of L-selectin can be inhibited by moving the extracellular cleavage site closer to the plasma membrane by amino acid deletion mutagenesis (117), thus CaM binding in the cell may be responsible for pulling the extracellular cleavage site towards the plasma membrane. When calcium binds to CaM it causes structural rearrangements, which expose hydrophobic regions in both lobes and these are the sites of binding for most target sequences. It is possible that the hydrophobic regions of CaM-Ca can then interact with hydrophobic residues found in the transmembrane domain of L-selectin, forming a favourable environment for these residues when L-selectin is pulled down. But if L-selectin is pulled down then presumably extracellular residues must move into the transmembrane domain. The extracellular amino acids that are proximal to the transmembrane domain consist of several hydrophilic residues (Figure 4.17B), which would make the insertion of these into the lipid bilayer energetically unfavourable. Clearly, more work is required to unearth this interesting hypothesis.

Interestingly, several other examples of CaM binding to transmembrane proteins, including PECAM-1 (217) and ACE-2 (218) have been reported. CaM has been shown to interact with cytoplasmic domain of both these proteins and this interaction protects the protein from extracellular cleavage (217,218). Bioinformatics analysis of the amino acid sequence of these proteins shows a CaM binding motif extending into the transmembrane domain, similar to L-selectin (396).

An attempt to study the interaction in a more biologically significant setting was carried out by Deng et al (2013)(417). CaM was fluorescently labelled with a donor in one lobe and a non-fluorescent acceptor in the other lobe. If both lobes interact with L-selectin they will become closer to one another and quenching of the fluorescence probes could be measured as a function of their binding proximity. An L-selectin peptide containing the cytosolic and transmembrane domains was

inserted into liposomes and the binding of the doubly-labelled CaM was assessed. The results showed that no quenching was observed when the L-selectin embedded liposomes were mixed with doubly-labelled CaM, suggesting the two lobes remained apart (417). This implies that CaM interacts with L-selectin in an extended conformation, with only one lobe participating in the interaction when the transmembrane domain is present in a lipid bilayer. The discrepancy in the results shows the complexities encountered when studying protein interactions and that the environment (as well as the appropriate experimental conditions) can have a dramatic effect on the outcome.

**A**

```
Minimum score for sequence: 0 Maximum score: 10

....1 MGCRRTREGP SKAMIFPWKC QSTQRDLWNI FKLWGWTMLC CDFLAHHGTD
..... 0000000000 0000000000 0000000000 0000000000 0000000000

...51 CWTYHYSEKP MNWQRARRFC RDNYTDLVAI QNKAEIEYLE KTLPFSRSYY
..... 0000000000 0000000000 0000000000 0000000000 0000000000

..101 WIGIRKIGGI WTWVGTNKSL TEEAENWGDG EPNNKKNKED CVEIYIKRNK
..... 0000000000 0000000000 0000000000 0000000000 0000000000

..151 DAGKWNDDAC HKLKAALCYT ASCQPWSCSG HGECVEIINN YTCNCDVGYY
..... 0000000000 0000000000 0000000000 0000000000 0000000000

..201 GPQCQFVIQC EPLEAPELGT MDCTHPLGNF SFSSQCAFSC SEGTNLTGIE
..... 0000000000 0000000000 0000000000 0000000000 0000000000

..251 ETTCGPFGNW SSPEPTCQVI QCEPLSAPDL GIMNCSHPLA SFSFTSACTF
..... 0000000000 0000000000 0000000000 0000000000 0000000000

..301 ICSEGTELIG KKKTICESSG IWSNPSPICQ KLDKSFSMIK EGDYNPLFIP
..... 0000000000 0000000000 0000000000 0000000000 0000000000

..351 VAVMVTAFSG LAFIIWLARR LKKGKKSKRS MNDPY
..... 0000112345 6789999999 9999876543 21100
```

**B**

```
      ******
325 MIKEGDYNPLFIPVAVMVTAFSGLAFIIWLARRLKKGKKSKRSMNDPY 372
```

**Figure 4.18: Analysing the predicted CaM binding site of L-selectin.** (A) Bioinformatic analysis shows the predicted location of the CaM binding site to be located towards the C-terminal end of L-selectin. The binding site contains juxtamembrane region as well as residues located in the transmembrane domain. Results produced by http://calcium.uhnres.utoronto.ca/ctdb/ctdb/sequence.html. (B) The location of the CaM binding site (red residues) and the transmembrane domain (blue box) are shown on the amino acid sequence of L-selectin, showing the residues within the predicted CaM binding site that are located in the transmembrane domain. Hydrophilic amino acids located extracellularly to the transmembrane domain are shown (*).

### 4.4.3 Phosphorylation of the L-selectin cytosolic tail does not inhibit CaM binding in vitro

As phosphorylation has been shown to occur upon leukocyte activation, it was hypothesised that this was the mechanism by which CaM dissociation from L-selectin was initiated. Nonetheless, the results in this chapter suggest this is not the case, with CaM association observed with both S364phos and S367phos peptides. Dr Ivetic has previously shown that phosphorylation, specifically at S364, abrogates L-selectin binding to CaM (Figure 4.18, unpublished data). In his experiments, decreasing concentrations of L-selectin peptide were mixed with a fixed amount of recombinant CaM and a chemical cross-linker. The cross-linked reactions were then resolved on SDS-PAGE and subsequently stained with Coomassie blue staining. At high concentrations of peptide, a higher molecular weight band could be observed above the unbound CaM, representing an electrophoretic mobility shift that corresponded to a complex of CaM and L-selectin peptide. When S364phos peptide was used the band representing the complex decreased in intensity, showing that less complex was formed in the presence of the phosphate group located on S364 (Figure 4.18). Interestingly, the same experiment using the S367phos peptide revealed that the formation of the cross-linked complex was less affected when S367 was phosphorylated, though there was still less complex formation than with the wildtype peptide.
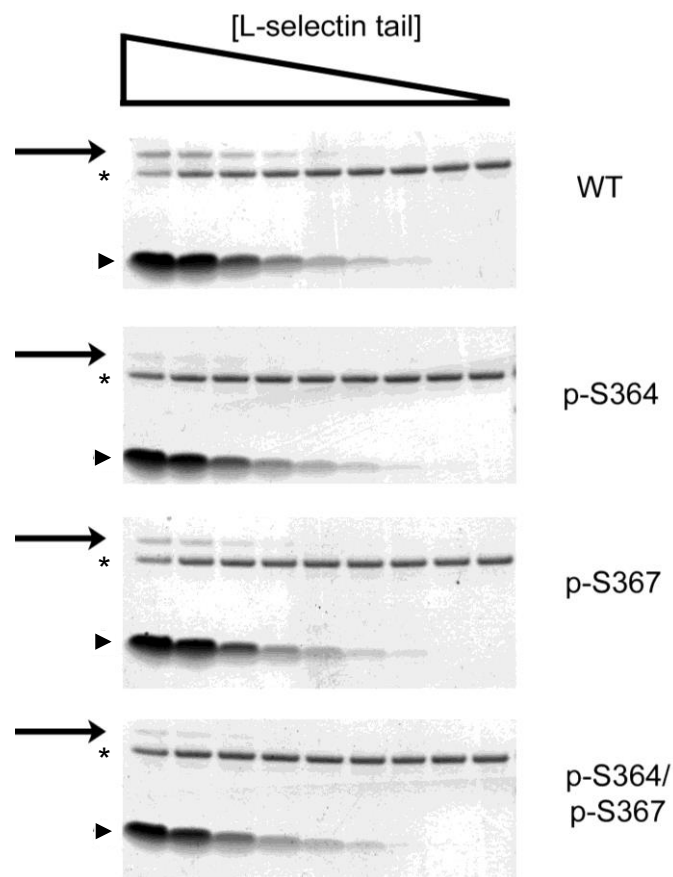
**Figure 4.19: DSS cross-linking reveals that phosphorylation of serine-364 mediates CaM/L-selectin tail complex formation**. Recombinant CaM was incubated with increasing concentrations of phosphorylated or non-phosphorylated L-selectin tail peptides and a fixed concentration of the DSS. Proteins were resolved by SDS PAGE and visualised by Coomassie staining. A reduction in the electrophoretic mobility of CaM was observed upon crosslinking to the L-selectin tail peptide resulting in an obvious band shift to a higher molecular weight (arrow). The amount of protein in the higher molecule weight band was drastically reduced by placing a phosphate group on serine-364, but was not significantly changed by serine-367 phosphorylation. Bands corresponding to monomeric CaM and L-selectin peptide are indicated by asterix and arrowheads respectively. Gels are representative of three independent experiments. Results taken from Dr Ivetic, and previously presented in Dr Killock's PhD thesis.

The results produced in this chapter by employing a range of diverse biophysical techniques, such as ITC, MST and NMR, are all in agreement that phosphorylation of L-selectin on either S364 or S367 had no effect on the binding affinity of either CaM-Ca or ApoCaM. The discrepancies observed in the results with the S364phos peptide could be due to differences in methodology used.

If the Gifford et al (2012)(396) model of binding is correct, then it would be unlikely that phosphorylation of the serine residues in the tail would affect CaM binding. The structure of the CaM-L-selectin complex Gifford et al (2012)(396) produced showed that both serine residues were not comprised within the CaM binding site and furthermore phosphorylation was shown to have no effect on the [$^1$H-$^{15}$N] HSQC spectrum of the complex. The [$^1$H-$^{15}$N] HSQC spectrum of CaM-Ca complexed with S364phos peptide studied in this thesis (Figures 4.9 and 4.10) showed that although overall the CSPs were similar, some differences were observed with the S364phos peptide compared with wildtype L-selectin cytosolic tail peptide. This could be compatible with the phosphate group being located within the binding site, having a local effect on the chemical shift environment for a number of CaM residues. Although unlikely, lacking a validated structural model, it is not possible to exclude that the conformation of the CaM/L-selectin complex would not be different from wild-type - due to the presence of the phosphate group on S364.

It has been shown that several CaM-binding sites can be phosphorylated, but that this does not necessarily affect the binding of CaM (226). For example, calcineurin A can be phosphorylated within its CaM-binding domain, but phosphorylation prior to incubation with CaM did not affect the binding of CaM to calcineurin A, as revealed by mobility shift assays (418). On the other hand, CaM bound to calcineurin A inhibited the phosphorylation within the CaM binding site to occur. The site of phosphorylation of calcineurin A is a serine which is predicted to be located towards the C-terminal boundary of the CaM-binding site; therefore it may be possible to argue that modification to this peripheral position may not have an effect in blocking the interaction with CaM. Nevertheless, the presence of CaM prevents its phosphorylation, counter arguing that this serine is likely to be

positioned within the binding region occupied by CaM or close enough to the binding region to suffer from steric hindrance. Interestingly, bioinformatics predictions of the CaM binding site of L-selectin suggest that S364 is also towards the C-terminal boundary of the site of interaction, and, consistent with what was found with calcineurin A, its phosphorylation does not block binding of CaM to L-selectin as demonstrated by the biophysical experiments carried out in this chapter. The fact that serine phosphorylation does not affect CaM binding to L-selectin according to the biophysical results does not exclude the possibility that in a complex cellular environment, with more players involved in an interplay of interactions, phosphorylation may cause CaM dissociation.

## 4.4.4 Alanine mutation of K362 within the cytosolic tail of L-selectin may affect the interaction with CaM-Ca

The ITC experiments in this chapter could not detect an interaction between CaM-Ca and the L-selectin cytosolic tail peptide containing the K362A mutation when experiments were carried out at 20 °C. It is possible that, as with the S364A mutation, this is due to the small ΔH of interaction, which could not be measured by ITC. However, it cannot be excluded that the K362A mutation is capable of blocking the interaction between L-selectin and CaM-Ca. The molecular model produced by Killock et al (2009)(3) predicted that K362 was involved in forming a salt bridge with residue E114 of CaM, therefore postulating that mutating this residue could disrupt the molecular interaction. On the other hand if the structural model produced by Gifford et al (2012)(396), using the longer L-selectin peptide, is correct, residue K362 would be exposed to the solvent upon CaM binding and would be therefore available to interact with moesin FERM domain upon the formation of the tertiary complex. Immunoprecipitation experiments have previously been undertaken using 300.19 pre-B-cells expressing K362A-L-selectin (225). The results showed that CaM was co-precipitated in these cells, therefore implying CaM was able to bind to L-selectin in the presence of this mutant. Further experiments are required to investigate whether K362 is involved in the interaction with CaM-Ca, i.e. ITC in different experimental conditions, as well as MST and NMR

experiments that were successful in clarifying the first inconclusive ITC results obtained with S364A and S364phos.

## 4.4.5 ITC analysis of Trp-Cage L-selectin and CaM

The feasibility of producing in-house recombinant L-selectin peptide as a Trp-Cage fusion protein was tested by NMR analysis (Section 3.3.8). The rationale for attempting this was to be able to produce $^{15}$N-labelled peptides in a cost effective manner so NMR experiments can be carried out with the aim of elucidating details of L-selectin interaction with CaM. Whether this could be used for investigating the interaction between CaM and L-selectin was probed by ITC experiments conducted using Trp-Cage-L-selectin, to test the influence of the Trp-Cage on CaM association. An interaction between CaM and Trp-Cage-L-selectin could be measured by ITC, but the thermodynamic parameters turned out to be different to those seen with L-selectin peptide alone, raising suspicions that the presence of the Trp-Cage may somehow alter the binding. ITC experiments with CaM and the Trp-Cage alone will therefore be required as a control experiment to ensure that CaM does not interact with the Trp-Cage motif *per se*. Purification of the Trp-Cage motif was attempted once, but was unsuccessful and lack of time prevented this being taken further.

If the Trp-Cage was found to be interfering with CaM interaction, then it could theoretically be cleaved away from the peptide prior to ITC and NMR experiments. A TEV protease cleavage site is indeed present between the Trp-Cage and the L-selectin peptide in the construct used. Such cleavage was attempted (Section 3.3.6) but no analysis was carried out on the peptide produced by this reaction due to time constraints. 2D [$^1$H-$^{15}$N] HSQC titration experiments with $^{15}$N labelled Trp-Cage-L-selectin and CaM would be extremely valuable as they would enable the analysis of the CSPs within the L-selectin cytosolic tail and the consequent identification of residues involved in establishing interactions with CaM. Further investigations will be needed to understand the feasibility of this method.

### 4.4.6 Devising a cell-based model of analysing CaM/L-selectin interaction

In conclusion, the experiments outlined in this chapter attempted to model a binary interaction between L-selectin and CaM with some interesting results. The following two results chapters will focus on the generation of monocyte-like cell lines to model the interaction between CaM and L-selectin in a more complex cellular setting. As the focus of this thesis is centred on understanding the contribution of CaM/L-selectin interaction during inflammation, the analysis is addressed specifically on monocytes undergoing transendothelial migration under flow conditions.

# Chapter 5: Generation and characterisation of a cellular model to explore the in vivo interaction between CaM and L-selectin in monocytes during TEM.

## 5.1 Introduction

After exploring *in vitro* techniques to study the interaction between L-selectin and its binding partners, the next step was to study the interaction *in vivo*. The role of L-selectin in monocytes has previously been studied. It has been shown that L-selectin-dependent adhesion is required for monocyte recruitment, with function blocking antibodies against L-selectin inhibiting monocyte recruitment to endothelial cells (17,18,419). *In vivo*, L-selectin has been shown to be responsible for monocyte recruitment to the skin (420), the interstitum of the kidney (421), the arterial endothelium (159) and the peritoneum (422) following an inflammatory stimulus. L-selectin dependent recruitment of monocytes has also been implicated in several chronic inflammatory disease states, including rheumatoid arthritis (423) and atherosclerosis (292).

As the literature clearly highlights an importance for L-selectin in monocyte adhesion, the interaction between L-selectin and its binding partners, using the THP-1 monocytic cell line as a leukocyte model, could be assessed. These cells were transduced with lentivirus expressing L-selectin tagged with GFP and the binding partners of L-selectin tagged with RFP. This allowed the study of the interaction by using fluorescence-lifetime imaging microscopy (FLIM) to measure the extent of fluorescence resonance energy transfer (FRET) between the tags. Increases in FRET efficiency would translate directly in to protein-protein interaction (see Section 5.2). The FRET efficiency in this thesis was measured by exciting the donor fluorophore, in this case GFP, and then measuring its fluorescence lifetime, which will depend on the proximity of the acceptor fluorophore, i.e. RFP (see Section 5.2).

## 5.2 Experimental Procedure

Lentivirus transduction uses the properties of human immunodeficiency-1 (HIV-1) virus to deliver a transgene to cells and insert it into the genome, therefore ensuring the transgene will be passed on to the cell progeny. The HIV-1 genome is modified so that it contains only the genes necessary for delivery of the transgene but is not capable of replicating itself, so there is no risk of infection (see Section 5.3.1 for details). There are several advantages to using lentiviruses to deliver transgenes to target cells over other methods. Lentiviral vectors are very efficient at transduction (424) and are also able to transduce non-dividing cells, compared with retroviral vectors where the cells must divide within two hours of transduction to successfully deliver the transgene (425). Lentiviruses have previously been used to successfully modify monocyte cell lines (426), showing there is a precedence for using this method.

THP-1 cells are a monocytic cell line originating from an acute monocytic leukaemia. It has previously been shown that minimal levels of L-selectin was observed in this cell line (427); this allows for the transduction of L-selectin-GFP to study the role of L-selectin in these cells without endogenous L-selectin interference. Previously in the lab THP-1 cells had been transduced with L-selectin tagged with GFP (L-selectin-GFP). Cells expressing wildtype L-selectin, the mutants S364A, S367A, SSAA and the sheddase resistant mutant ΔM-N were all produced with a C-terminal GFP tag. The ΔM-N mutant involves the deletion of eight amino acids in the membrane-proximal region, which has been shown to resist shedding (98,116,117,119) and is appropriately called a "sheddase-resistant" mutant of L-selectin (see Section 1.3.4 in Introduction). Analysis of wildtype L-selectin-GFP expressing cells showed that L-selectin was correctly located to the microvilli of the THP-1 cells and increased the binding of these cells to TNF-activated HUVECs under flow (Karolina Rzeniewicz, unpublished data). This means that the L-selectin-GFP was functioning correctly and the GFP tag was not affecting its function. Several other cell biological characterisations were also performed, such as rolling velocity, shedding in response to TNF, PMA and Calyculin A, as well as the sub-cellular localisation of L-selectin-GFP to microvilli (as judged by scanning electron

microscopy). These analyses all demonstrated that the GFP tag did not interfere with L-selectin function. Although noteworthy to mention, the exact experiments will not be discussed in this thesis as they formed a major part of another PhD student's thesis in the Ivetic lab (Karolina Rzeniewicz). In this study CaM and moesin were cloned as RFP-tagged chimerae and lentivirus particles were produced. These were used to transduce cell lines stably expressing L-selectin-GFP. The interaction between L-selectin and its binding partners could then be assessed by studying the FRET efficiency between the two fluorescent tags.

FRET is a method used to assess the proximity of two molecules to one another. It measures the transfer of energy between two fluorophores, one known as the donor and one the acceptor (428). The donor molecule is excited using light at the excitation wavelength. The donor will then transfer the energy to the acceptor through long range dipole-dipole coupling and the donor will return to its ground state (429). For the transfer of energy to occur the emission wavelength of the donor must overlap with the excitation wavelength of the acceptor (Figure 5.1A) (428). The FRET efficiency depends on the distance between the two molecules, with FRET occurring between two molecules less than 10 nm apart (428). The closer the two molecules are to one another the higher the FRET efficiency.  As a result, this method can provide information about the interaction of two molecules. In this thesis the FRET efficiency is measured using fluorescence lifetime imaging microscopy (FLIM). With FLIM the fluorophore is excited and the decay of the fluorophore from the excited state to the resting state is measured (430). The fluorescence lifetime is the time the molecules spends in the excited state (430) and is dependent on the local environment of the molecule, including the presence of an acceptor molecule (431,432).  The presence of the acceptor will lead to a decrease in the lifetime of the donor (Figure 5.1B) (432,433). The fluorescence lifetime of the donor is calculated at each pixel in the image and is displayed as a pseudo-colour image (Figure 5.1C) (431,432,434,435). This allows for visualisation of the sub-cellular distribution of the fluorescence lifetime of the donor within a single cell and therefore the location of the interaction between the donor and acceptor within the cell.

Fluorescent proteins can be tagged to the proteins of interest to study their interaction. As previously stated, the fluorescent proteins GFP and RFP are used in this thesis as the donor and acceptor fluorophores, respectively. The emission wavelength of GFP overlaps the activation wavelength of RFP, meaning they act as a FRET pair (Figure 5.1A).

This chapter details the generation of cell lines used in this study to monitor the interaction between L-selectin and its binding partners during TEM. The ability of L-selectin to bind to CaM was then assessed in more detail, with specific reference to residues within the L-selectin tail that were required to support binding of CaM during TEM.

**A**

GFP excitation
GFP emission
RFP excitation
RFP emission

**B**

483 nm

GFP — >10 nm — RFP    No FRET

Protein A    Protein B

Short Fluorescence Lifetime

483 nm

GFP — <10 nm — RFP

Protein A    Protein B    FRET

**C**

T1    T3    T2    T1

Decay time (T) different for the areas

Lifetime

Fluorescence lifetime for each pixel calculated and pseudo-colour image produced
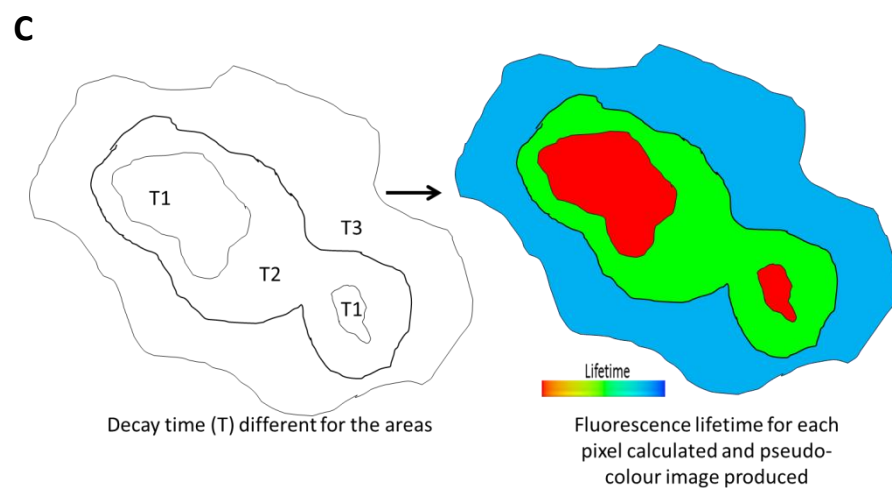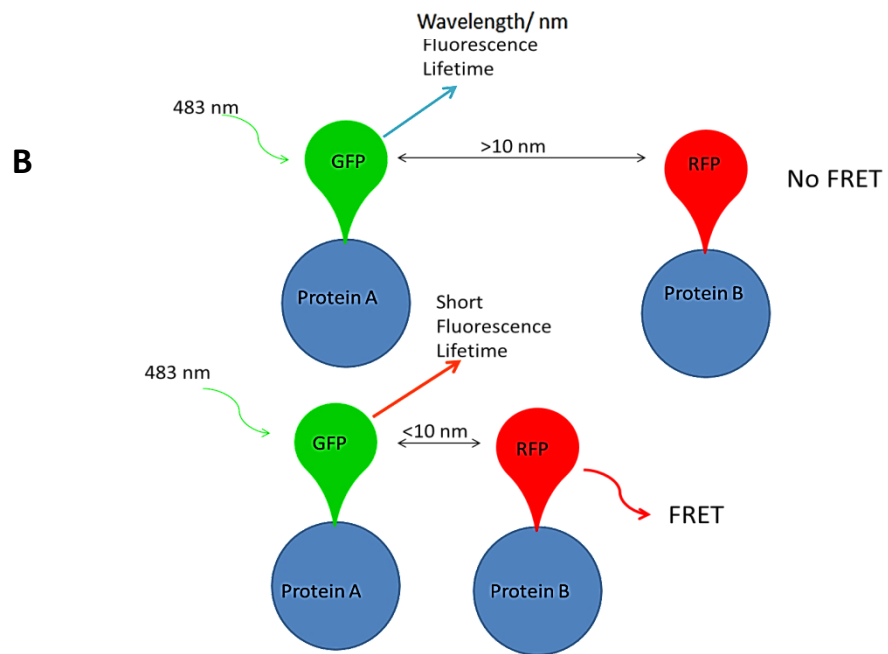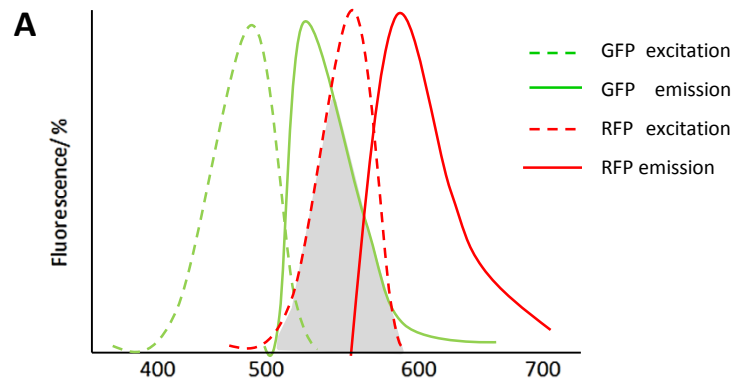
**Figure 5.1: Diagram of FRET/FLIM between GFP and RFP.** (A) Graph showing the excitation and emission spectra of GFP and RFP. The overlap between GFP emission and RFP excitation is shown in grey. (B) A diagram showing the FRET between GFP and RFP. GFP is excited and light is emitted. If the proteins are close to one another FRET will occur and the fluorescent lifetime of the donor emission will decrease (green arrow) and acceptor emission increases (red arrow). This decrease in donor emission is measured during FLIM. (C) Depiction of how FLIM is used to produce images. The decay time of the donor fluorophore is measured throughout the whole cell and found to be different in three areas (T1, T2 and T3). The fluorescence lifetime is calculated for all areas and a pseudo-colour range is used to depict the difference in fluorescence lifetime. In reality the fluorescence lifetime of every pixel is measured, so images are produced with a range of colours to represent the differences between the individual pixels.

## 5.3 Results

### 5.3.1 Generation of Lentivirus particles to deliver CaM-RFP to THP-1 cells expressing L-selectin-GFP

CaM was cloned into the vector pHR'SIN-SEW (see Figure 2.2 in Materials and Methods), which was a gift from Prof. Adrian Thrasher (Institute of Child Health, UCL). The vector contains a spleen focus-forming virus (SFFV) promoter to initiate transcription, followed by the sequence encoding for red fluorescent protein (RFP) and a Woodchuck Hepatitis Virus (WHP) post transcriptional regulatory element (WPRE), which helps to enhance the expression of the gene of interest and stabilize the transcript. Two long terminal repeat (LTR) sequences are also present at the 5' and 3' ends of the cloning site. The 5' LTR is able to act as a promoter for RNA polymerase II and the 3' LTR terminates transcription. LTRs are also responsible for the insertion of the transgene into the host genome. CaM was cloned into the vector at the 5' end of the RFP sequence using the restriction sites BamHI and XhoI, so CaM would be produced with RFP at the C-terminus. PCR was carried out and the product of the correct size was observed, cleaved from the gel and purified (Figure 5.2).



1Kb

0.5Kb

1        2
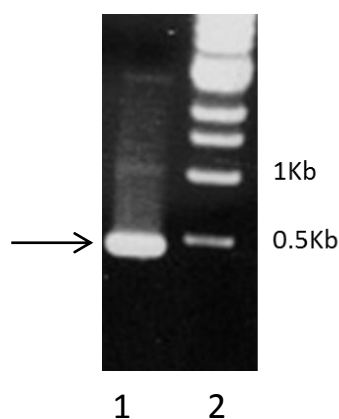
**Figure 5.2: Visualisation of CaM PCR product following the PCR reaction.** PCR was carried out to produce a CaM sequence with XhoI and BamHI restriction sites at the 5' and 3' termini respectively. After the PCR reaction was completed, the reaction solution was analysed by agarose gel electrophoresis and visualizing the DNA bands with ethidium bromide. The band corresponding to the CaM product was cut from the gel and purified. The product was then cleaved with restriction enzymes and used for ligation into the vector. Lane 1 represents the PCR reaction solution and lane 2 is the DNA marker. The arrow shows the CaM PCR product.

A restriction digestion with the appropriate restriction enzymes was carried out on the purified PCR product and the vector as previously described (see Section 2.6 for experimental procedure). The ligation of the CaM insert into the lentiviral vector was undertaken and the vector was then used for transformation of *E.coli* cells. To examine the presence of the CaM insert, *E.coli* colonies were selected and used to inoculate small scale cultures. These were grown overnight and the plasmid DNA was isolated using "mini-prep" kits. The plasmid DNA was then digested with restriction enzymes for one hour. The products of the digestion were analysed by agarose gel electrophoresis. The results showed that plasmid DNA from all the colonies tested produced a DNA band of around 0.5 Kb after digestion, which corresponded to the molecular weight expected for the CaM insert (Figure 5.3). This suggested that all the colonies contained the CaM insert. In parallel, the vector was also sent for sequencing to confirm the presence of the insert and ensure no spontaneous mutations had occurred. To enable the production of lentiviral particles, large quantities of the CaM-RFP lentiviral vector were required. *E.coli* cells expressing the CaM-RFP vector were grown on a large scale and the plasmid DNA was isolated using a "maxi-prep" kit.
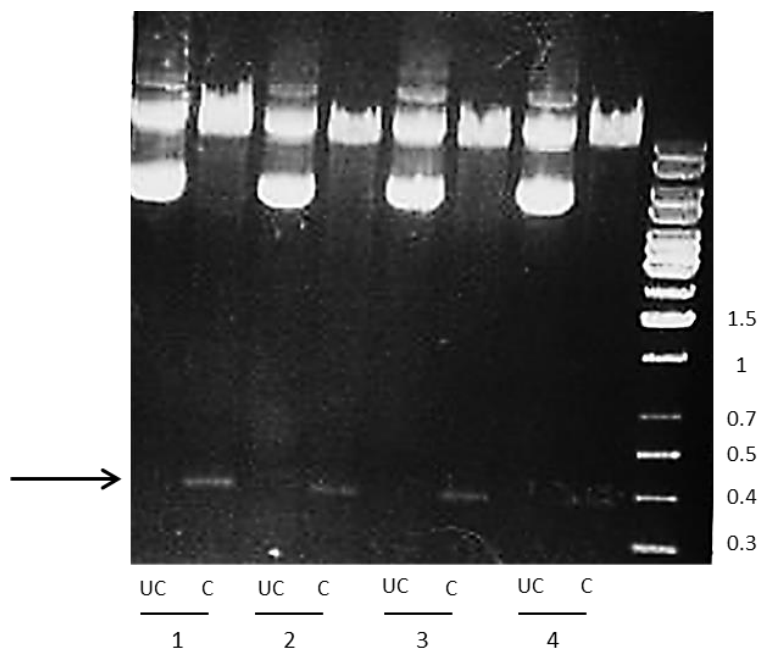
**Figure 5.3: Restriction digest of CaM-RFP lentiviral vector.** Four colonies (labelled 1-4) were picked after transformation of *E.coli* with the lentiviral vector ligated with the CaM PCR product and the plasmid DNA was isolated using "mini-prep" kit. The isolated vector was cleaved with the restriction enzymes XhoI and BamHI to assess the presence of CaM. The digestion products were analysed by agarose gel electrophoresis using a 0.8% agarose gel and ethidium bromide for DNA visualisation. The cleaved vector (labelled C) was run next to the uncleaved vector (labelled UC) for comparison of the DNA bands produced. The arrow shows CaM cleaved from the vector.

Using lentivirus to insert transgenes into the genome of target cells is efficient and enables stable integration of the transgene; therefore the progeny of the transduced cell will also express the gene. This means that the generated cell lines can be used multiple times. There is however, a potential risk with using lentiviruses. It is possible that replication-competent viruses could be generated. To minimize the risk of this, first the viral genes not required for lentivirus production are removed (436,437), and second the genes that are required are split into multiple vectors, each encoding the different genes required (438). In this report three vectors were used, the transfer vector containing the transgene which will be inserted into the cell genome, and two helper vectors containing the genes required for the assembly of the lentiviral particles. Only the transfer vector has the ability to integrate into the genome of the cell, whereas the helper vectors are not integrated. This means that the lentivirus produced does not contain the genes encoded by the helper vectors and therefore the host cells cannot produce functional lentivirus.

The first helper vector used here was the lentiviral packaging vector Pax2. This carries the HIV genes gag, pol, rev and tat which all encode different components required for lentiviral production. The gag gene encodes four structural proteins that make up the core viral structure (438). The pol gene encodes virus specific enzymes that are required for the formation of double-stranded DNA and integration of the DNA into the host genome (438). rev encodes a post translational regulator required for the efficient expression and production of the other viral genes and tat encodes a protein which enhances the efficiency of transcription of viral mRNA (438). The second helper vector was pMD2.G lentiviral

vector, which encodes the viral envelope protein vesicular stomatitis virus (VSV) G protein. The two helper vectors were mixed with the transfer vector containing CaM-RFP and were used to transduce HEK cells for the production of the lentivirus. After 48 and 72 hours transduction the assembled lentiviral particles were collected from the tissue culture supernatant and concentrated by ultracentrifugation.

To optimize the transduction of the target cells, the titre, the number of infectious units per millilitre (i.u./ml), was calculated. To calculate the titre a serial dilution of the concentrated lentiviral particles was carried out and added to HEK cells. Fluorescence-activated cell sorting (FACS) was used to assess the percentage of HEK cells expressing CaM-RFP. The first step in calculating the titre was to plot the percentage of RFP positive cells against the dilution of lentiviral particles (Figure 5.4). The dilutions corresponding to between 1-20% transduction efficiency were then used for the titration calculation. These dilutions were used as they fall within the linear range of transduction and using dilutions in this range means multiple lentiviral integrations into the genome are avoided in the calculation. The titre for each of the dilutions within the linear range was calculated using the equation: $T = \dfrac{PN}{DV}$ , where T is the titre, P is the percentage of transduced cells, N is the number of cells on the day of transduction, D is the dilution of the lentivirus stock added to the cells and V is the volume of lentivirus added to the cells. The final titre was found by calculating the average of the titres of the dilutions within the linear range (Table 5.1). For CaM-RFP this was found to be $4.31 \times 10^9$ i.u./ml.
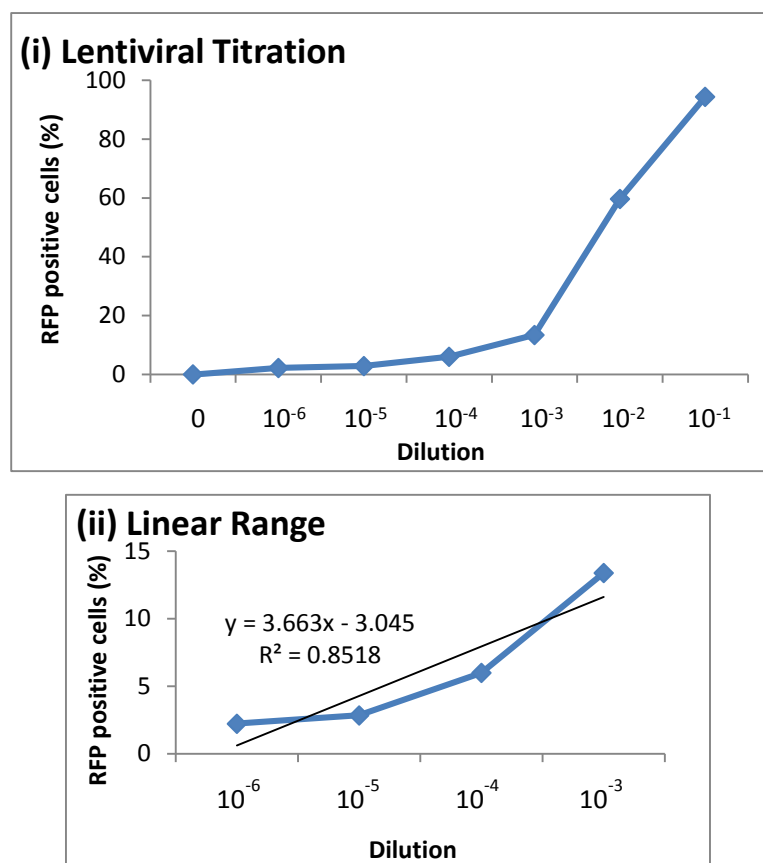
**Figure 5.4: Transduction of HEK cells with lentivirus carrying the lentiviral vector for CaM-RFP.** HEK cells were transduced with CaM-RFP lentivirus using a serial dilution (0, $10^{-6}$, $10^{-5}$, $10^{-4}$, $10^{-3}$, $10^{-2}$, $10^{-1}$) of the concentrated lentiviral particles. (i) The percentage of RFP positive cells was assessed using FACS and plotted against the lentiviral dilution. (ii) Low dilutions, in the linear range were used to calculate the titre to avoid multiple integrations.

| Dilution | % RFP | Titre |
|---|---|---|
| $10^{-6}$ | 2.23 | $14.87 \times 10^9$ |
| $10^{-5}$ | 2.84 | $1.89 \times 10^9$ |
| $10^{-4}$ | 6.04 | $0.41 \times 10^9$ |
| $10^{-3}$ | 13.44 | $0.089 \times 10^9$ |
| | average titre | $4.31 \times 10^9$ i.u./ml |

**Table 5.1: Calculation of viral titre of CaM-RFP from dilutions within the linear range of transduction.** The titre for dilutions with a transduction efficiency of between 1-20 % was calculated using the equation: $T = \dfrac{PN}{DV}$. The final titre was found by calculating the mean of the titres for the dilutions within the linear range.

To ensure that similar levels of protein expression were observed between the different cell lines infected with the CaM-RFP lentivirus, the multiplicity of infection (MOI) was used. The MOI is a measure of the infectious units (lentiviral particles) delivered to each target cell. This was calculated using the equation:

$$MOI = \frac{VT}{N}$$, where V is the volume of lentivirus added, T is the titre of the lentivirus and N is the number of cells to be transduced. Once the MOI of choice has been decided upon, the equation can be rearranged to find the appropriate volume of lentivirus required for that particular MOI. As CaM-RFP was being transduced into THP-1 cells to act the FRET acceptor for GFP tagged to L-selectin, it was decided to use an MOI of 20 for the transduction with CaM-RFP, as it was desirable for the expression of the acceptor to be in excess of the donor to cause saturation of the donor. This meant that for the transduction of 1 x 10$^6$ THP-1 cells, the volume of CaM-RFP lentivirus required was 4.6 μl.

The required amount of lentivirus particles was added to THP-1 cells stably expressing L-selectin-GFP. Several L-selectin mutants tagged with GFP were also transduced with CaM-RFP. The serine to alanine mutants S364A, S367A and SSAA, where both serines are mutated to alanines, were chosen to assess the effect these mutations have on CaM binding to L-selectin. By mutating the serine residues to alanine, phosphorylation can no longer occur at these sites in the cytosolic tail of L-selectin. As a result these mutants enable the assessment of the role of phosphorylation in regulating CaM binding. The sheddase resistant mutant ΔM-N was also transduced with CaM-RFP to assess the effect of blocking shedding on CaM/L-selectin interaction. The MOI of L-selectin-GFP in these cells was 5; meaning CaM-RFP expression should be greater than L-selectin-GFP and saturation of GFP should be achieved. After transduction, the cells were maintained in cell culture until several million were present. At this point samples of each cell line were taken for the analysis of fluorescent protein expression by fluorescence microscopy (Figure 5.5). Images were taken to assess the number of cells expressing both GFP and RFP. The images showed that all the cells were expressing L-selectin-GFP. This was to be expected as the cells had previously been sorted to select GFP positive

cells only. The percentage of cells also expressing CaM-RFP was calculated from three different fields of view for each of the cell lines. The results showed that transduction varied between the cell lines, with SSAA having the highest level of transduction (45%) and S364A having the lowest level (14.3%, Table 5.2).

For future experiments with these cells it was important that all the cell lines had similar levels of expression of the CaM-RFP transgene to enable fair comparison between them. For this reason the cells were sorted to produce populations with uniform expression of CaM-RFP. If unsorted cells were used for future experiments the difference in the number of cells and the expression levels of CaM-RFP could lead to misinterpretation of results.

The cell lines were taken to a core-funded FACs sorting facility for sorting into uniform-expressing populations. The cells were first gated for GFP expression and then within that population cells which expressed similar or higher levels of RFP were selected. The wildtype L-selectin-GFP/CaM-RFP cells were sorted first and the same gating was then used for the other cell lines to ensure the expression levels were similar between them all. Images of the sorted cells are shown in Figure 5.6. Once sorting was completed the cell lines were maintained in cell culture.
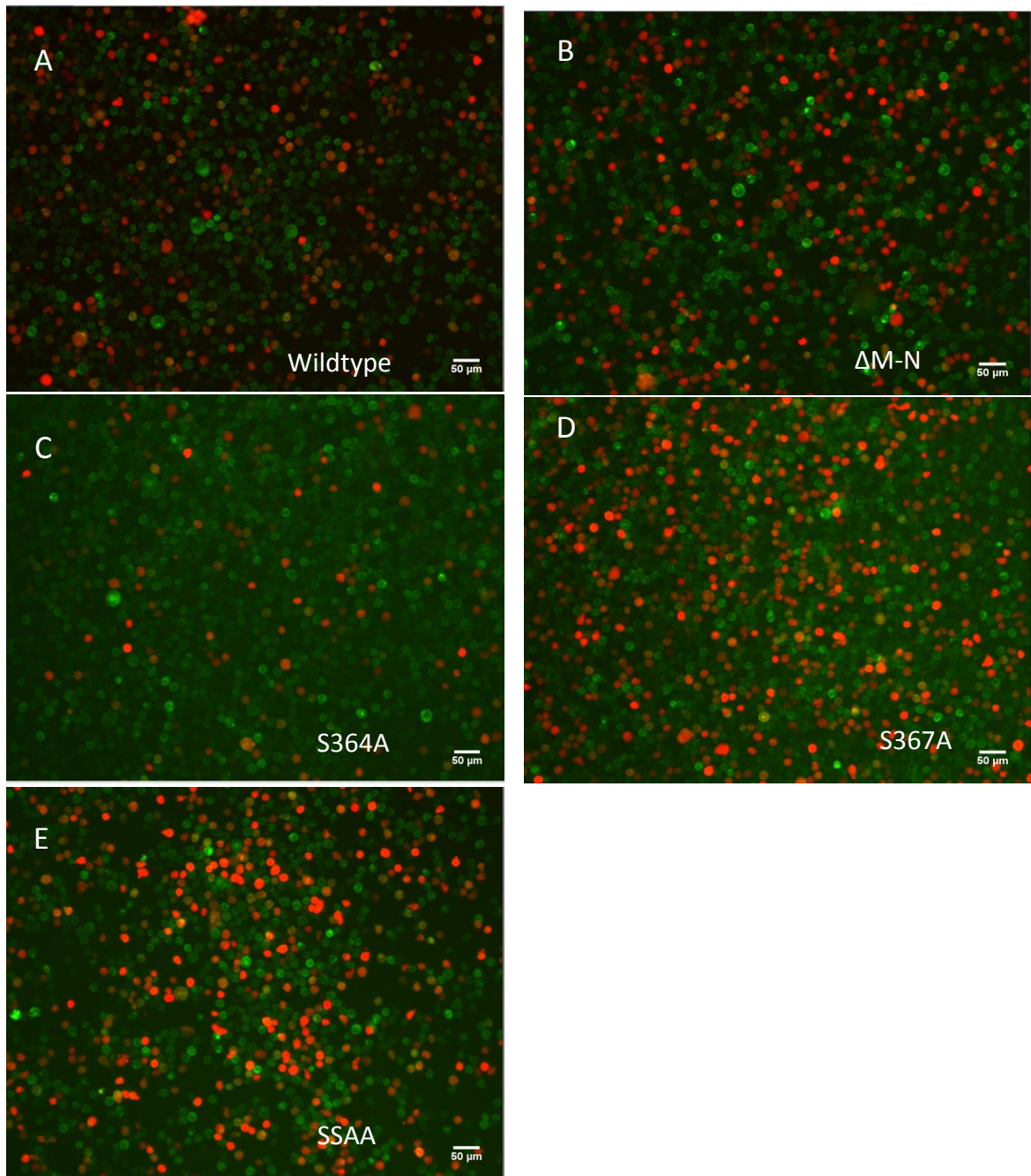
**Figure 5.5: Fluorescence images of THP-1 cell lines transduced with L-selectin-GFP and CaM-RFP prior to cell sorting.** Cells expressing wildtype L-selectin-GFP (A) and the mutants ΔM-N- (B), S364A- (C), S367A- (D) and SSAA-L-selectin-GFP (E) were transduced with lentivirus carrying the lentiviral vector for CaM-RFP and maintained in cell culture until several million cells were present. Images were taken of the THP-1 cell lines with the GFP and RFP channel and the images were subsequently merged. Images were taken using an Olympus IX81 time-lapse inverted fluorescence microscope attached to a Hamamatsu C10600 ORCA-R2 video camera and analysed using Volocity imaging software. All images were acquired using a 10x objective.

| | RFP positive cells (%) |
|---|---|
| Wildtype | 27.5 |
| DM-N | 39.5 |
| S364A | 14.3 |
| S367A | 38 |
| SSAA | 45.5 |

**Table 5.2: Percentage of RFP positive THP-1 cells after transduction with lentiviral particles carrying the lentiviral vector for CaM-RFP.** The percentage of RFP positive cells were calculated for the L-selectin-GFP THP-1 cell lines after CaM-RFP lentiviral transduction by analysis of three fields of view for each cell line and finding the mean of the three.
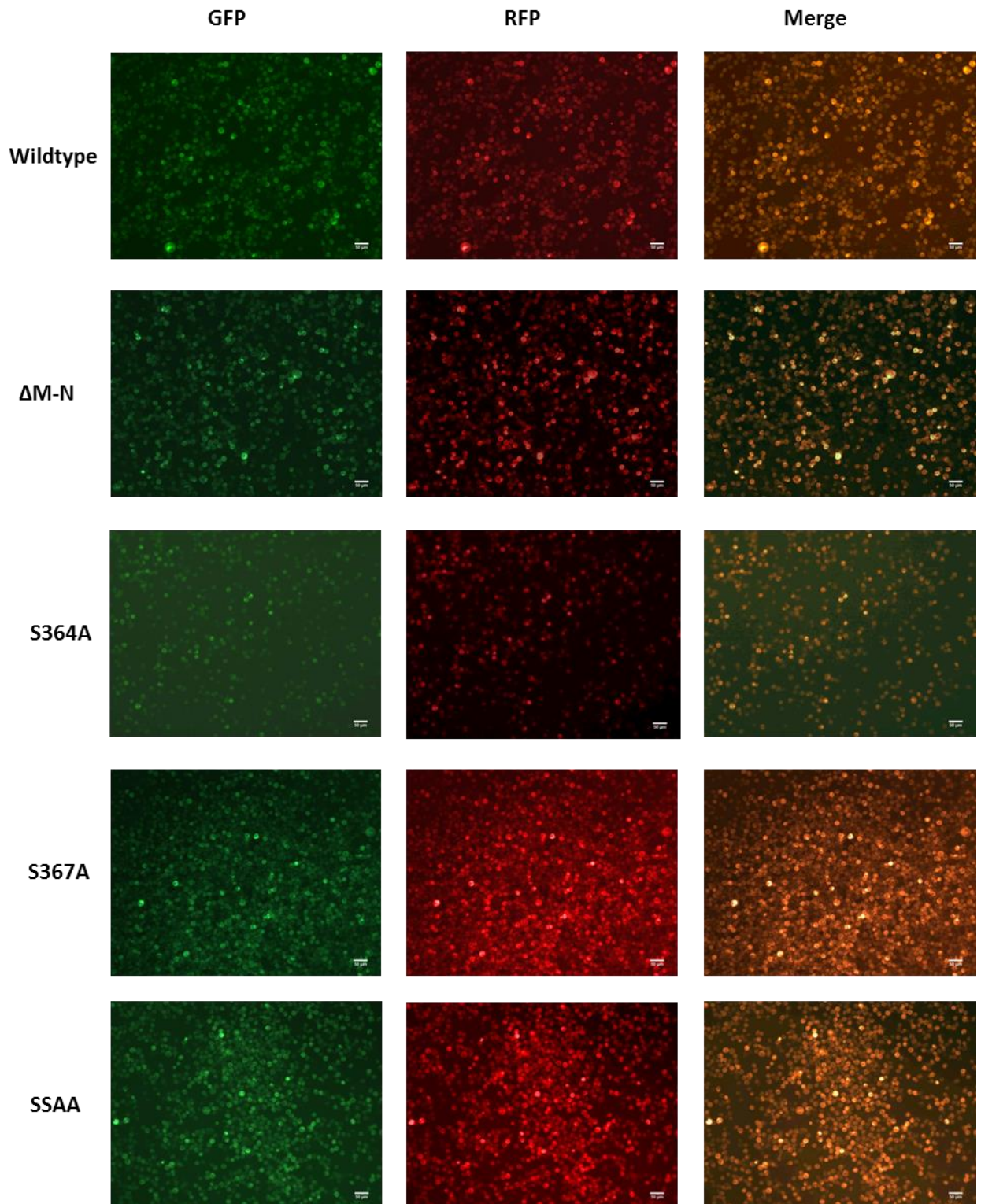
**Figure 5.6: Fluorescence images of THP-1 cell lines transduced with L-selectin-GFP and CaM-RFP after cell sorting.** Cells expressing wildtype L-selectin-GFP and the different L-selectin mutants were sorted using FACs to produce a population of cell expressing L-selectin-GFP and CaM-RFP. After sorting images were taken of the THP-1 cell lines with the GFP and RFP channel and the images were subsequently merged. Images were taken using an Olympus IX81 time-lapse inverted fluorescence microscope attached to a Hamamatsu C10600 ORCA-R2 video camera and analysed using Volocity imaging software. All images were acquired using a 10x objective.

## 5.3.2 Generation of Lentivirus carrying the lentiviral vector encoding Moesin-RFP for the Transduction of THP-1 cell lines expressing L-selectin-GFP

Moesin was cloned into the lentiviral vector pHR'SIN-SEW using the same method described above (see Section 5.3.1) except the restriction sites XhoI and KpnI were used for the insertion of the moesin sequence into the lentiviral vector. Once the correct sequence of the lentivirus was confirmed, lentiviral particles were formed using HEK cells (the same method as in Section 5.3.1 was used). A titration with the lentivirus was carried out and the percentage of RFP positive cells was calculated by FACs (Figure 5.7). From this information the titre was calculated and found to be $1.19 \times 10^9$ i.u./ml (Table 5.3). As with CaM-RFP, the expression levels of moesin-RFP required must be in excess of L-selectin-GFP to cause saturation of the GFP, so an MOI of 20 was used to transduce the L-selectin-GFP cell lines. This meant that a volume of 17 µl was required for the transduction of $1 \times 10^6$ cells.
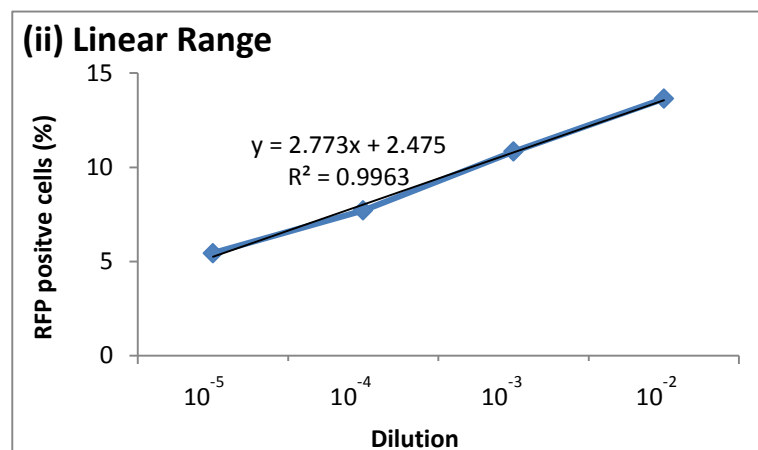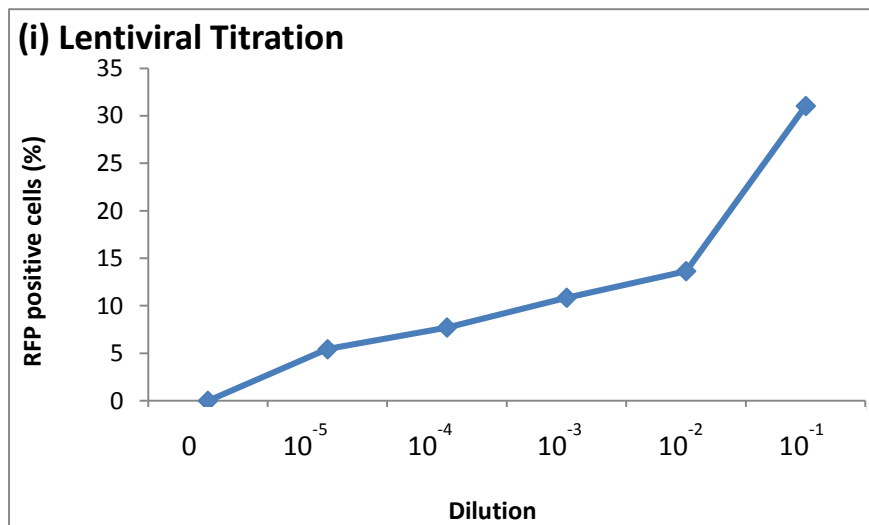
**Figure 5.7: Transduction of HEK cells with lentivirus carrying the lentiviral vector for moesin-RFP.** HEK cells were transduced with moesin-RFP lentivirus using a serial dilution (0, $10^{-5}$, $10^{-4}$, $10^{-3}$, $10^{-2}$, $10^{-1}$) of the concentrated lentiviral particles. (i) The percentage of RFP positive cells was assessed using FACS and plotted against the lentiviral dilution. (ii) Dilutions in the linear range of transduction were used to calculate the lentiviral titre to avoid multiple integrations.

| dilution | RFP positive (%) | titre |
|---|---|---|
| $10^{-5}$ | 5.44 | $4.08 \times 10^9$ |
| $10^{-4}$ | 7.71 | $0.58 \times 10^9$ |
| $10^{-3}$ | 10.84 | $0.081 \times 10^9$ |
| $10^{-2}$ | 13.64 | $0.011 \times 10^9$ |
| | **Average titre** | $1.19 \times 10^9$ i.u./ml |

**Table 5.3: Calculation of viral titre of moesin-RFP from dilutions within the linear range of transduction.** Dilutions with a transduction of between 1-20 % were taken and the titre for each was calculated using the equation: $T = \dfrac{PN}{DV}$. The final titre was found by calculating the mean of the titres for all the lentivirus dilutions within the linear range.

The moesin-RFP lentivirus was used to transduce the THP-1 cell lines stably expressing L-selectin-GFP, either wildtype or the mutations ΔM-N, S364A, S367A and SSAA. The cell lines were maintained in cell culture after transduction until several million cells were present, at which point samples were taken from each cell line for analysis of the transduction efficiency using fluorescence microscopy (Figure 5.8A-E). The percentage of RFP positive cells was calculated for each cell line using three fields of view. The results for all the cell lines showed that the percentage of cells transduced with the moesin-RFP lentiviral vector was between 10 and 5% (Table 5.4). The images also showed that the RFP signal was strongest at one region within the THP-1 cell, close to the plasma membrane (Figure 5.8F) and this was observed in all the different cell lines. As the cells were in suspension it was not possible to see if this region was located at the leading edge or the uropod. It was also possible that this high intensity region represents an accumulation of moesin-RFP within the Golgi apparatus or the endoplasmic reticulum. Due to the low magnification used to acquire the images it was not possible to discern the precise sub-cellular location of the moesin-RFP signal.

As with the THP-1 cell lines transduced with CaM-RFP, the cell lines transduced with moesin-RFP were taken to the core funded FACs sorting facility for the selection of cells expressing both L-selectin-GFP and moesin-RFP. The cells were first gated for cells expressing GFP and then cells within that population that expressed similar or higher levels of RFP were selected. The cells remaining after sorting were collected and maintained in cell culture.
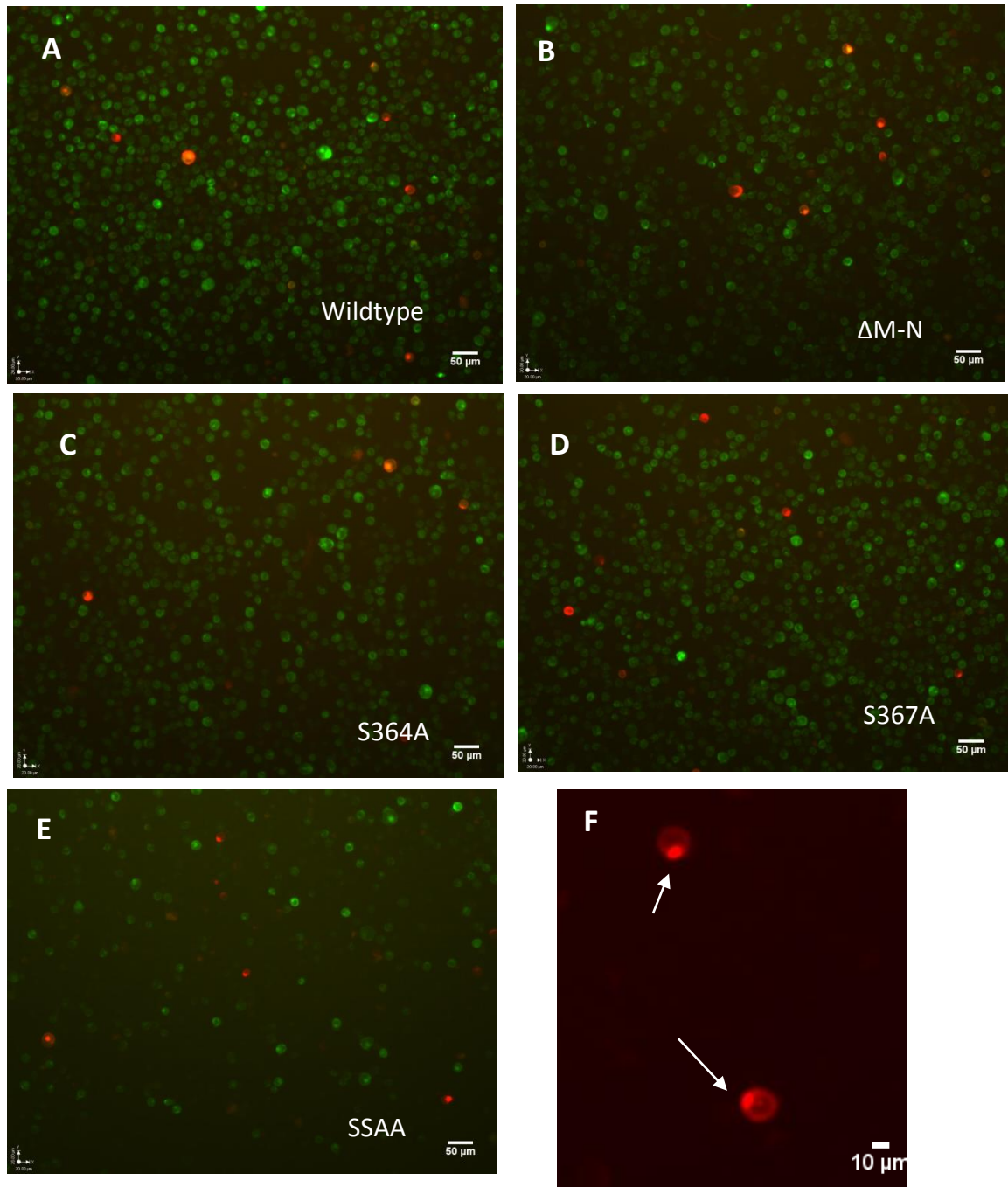
**Figure 5.8: Fluorescence images of THP-1 cell lines expressing L-selectin-GFP and transduced with moesin-RFP acquired prior to sorting.** Images of the THP-1 cell lines expressing wildtype (A), ΔM-N- (B), S364A- (C), S367A- (D) or SSAA-L-selectin-GFP and transduced with lentiviral particles containing moesin-RFP. Images are merged from acquiring individual stills from the GFP and RFP channels. (F) Digital zoom of THP-1 cells expressing moesin-RFP. The arrow shows the sub-cellular location of a high-intensity signal corresponding to moesin-RFP. Images were taken using an Olympus IX81 time-lapse inverted fluorescence microscope attached to a Hamamatsu C10600 ORCA-R2 video camera and analysed using Volocity imaging software. All images were taken at 10x objective.

| | RFP positive cells (%) |
|---|---|
| **Wildtype** | 5.5 |
| **DM-N** | 7.5 |
| **S364A** | 5 |
| **S367A** | 6.4 |
| **SSAA** | 10 |

**Table 5.4: Percentage of RFP positive THP-1 cells after transduction with lentivirus carrying the lentiviral vector for moesin-RFP.** The percentage of RFP positive cells were calculated for the L-selectin-GFP THP-1 cell lines after moesin-RFP lentiviral transduction by analysing three fields of view for each cell line and calculating the mean.

### 5.3.3 Cloning of Lentiviral Vector Expressing Ezrin-RFP

The cloning of ezrin into the pHR'SIN-SEW vector was problematic due to the fact that all the restriction sites in the vector, except XhoI, were also found in the sequence of ezrin, meaning they could not be used for conventional cloning as they would also cleave the ezrin sequence. For this reason ezrin was cloned with an XhoI site at the 3' end and a SalI site at the 5' site. The nucleotide base overhang produced by digestion with SalI is complimentary to that produced by digestion with XhoI, meaning that the two overhangs will interact (Figure 5.8). This meant that the vector was only cut with XhoI prior to ligation of the vector and ezrin insert. One disadvantage of using this method is that the ezrin insert can ligate in both the forward and reverse directions (Figure 5.8). After ligation of the cleaved insert and vector, *E.coli* cells were transformed with the ligation mixture. Colonies were then picked and used to inoculate small scale cultures, and the plasmid DNA was purified using the 'mini-prep' kit. Sequencing was used to check the orientation of ezrin. Several different colonies were tested but were found to either not contain ezrin or contain ezrin in the wrong orientation.
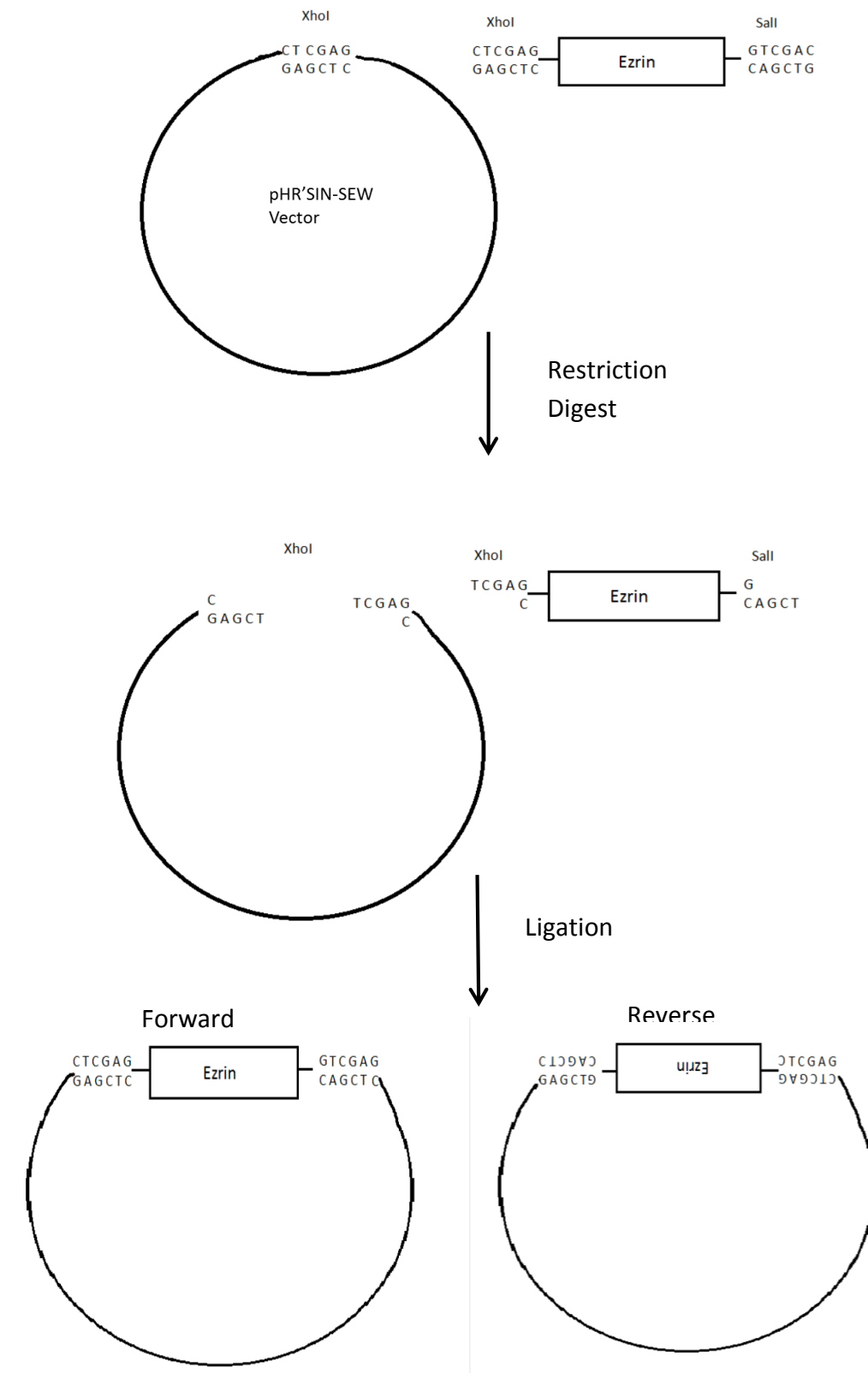
**Figure 5.9: Cloning of Ezrin into pHR'SIN-SEW vector using one cloning site.** Ezrin was cloned with XhoI restriction site at the 3' end and SalI restriction site at the 5' end. Ezrin was then digested with both XhoI and SalI, which produces the same overhang sequence, whilst the lentiviral was digested with XhoI only. When ligation was carried out the ezrin insert could either ligate in the forward or reverse direction.

As using one restriction site was not successful, cloning using a partial digest was attempted. The restriction enzyme KpnI cleaves ezrin in the middle of the DNA sequence. Ezrin was cloned with an XhoI site at the 3' end of the sequence and a KpnI sequence at the 5' end. The PCR product was then fully digested with XhoI followed by the partial digest with KpnI (see Section 2.6.1 for experimental details). The digest mixture was purified and run on an agarose gel. The band corresponding to KpnI cleaving at the 5' end only was cut from the gel and purified to use for the ligation with the vector. Sequencing results of vectors created using this method found that although ezrin was present, the first few amino acids of the sequence were missing. This could be due to a mistake with the PCR reaction or the protein being cleaved at a location at the 3' end. This requires repeating to produce the lentiviral vector for ezrin.

## 5.3.4 Production of THP-1 cells expressing L-selectin CaM-binding Mutants

It has previously been shown that mutating residue L358 to glutamate in the cytosolic tail of L-selectin inhibits CaM binding (215). By mutating this residue the hydrophobic face of the cytosolic tail of L-selectin is disrupted. Kahn et al (1998)(215) showed that when this mutation was present CaM could no longer co-precipitate with immunoprecipitates of L-selectin (215). For this reason, it was decided to use this mutation in THP-1 cells transduced with CaM-RFP to see if the interaction was blocked in this system.

The QuickChange site-directed mutagenesis protocol was used to introduce the mutation into wildtype L-selectin-GFP and the sheddase resistant mutant ΔM-N-L-selectin-GFP. With this method primers are designed to contain the desired mutation with complimentary sequences present either side. The primers must bind to the same site on opposite strands of the vector. During the thermal cycling the primers bound to their complimentary sequences on the parental DNA and are extended by DNA polymerase. Once the thermal cycling reaction is completed the parental DNA is digested using DpnI endonuclease. This enzyme only cleaves

methylated and hemimethylated DNA. As the parental DNA has been isolated from *E. coli* cells, it will be dam methylated and so is digested by DpnI. The newly formed DNA containing the mutation is not methylated so remains un-cleaved. The DNA containing the mutation is then used to transform *E. coli* and the DNA can be isolated.

The lentiviral vector pHR'SIN-SEW containing either wildtype L-selectin-GFP or ΔM-N L-selectin-GFP were used for the mutagenesis of residue 358. Plasmid DNA was isolated from bacterial colonies observed after transformation with the DpnI digested PCR reaction and sequencing was carried out to verify that the appropriate mutation was successfully introduced. These vectors were then used to produce lentivirus as described previously and a titration was carried out with the lentiviral particles produced (see Section 5.3.1).

The titre for lentiviral particles containing L358E-L-selectin-GFP was found to be $5.04 \times 10^9$ i.u./ml (Figure 5.9, Table 5.5). ATTC THP-1 cells were transduced with MOI5 and MOI20 to represent a low and high MOI. The cells were allowed to propagate for two weeks, until several million cells were present. The expression of L358E-L-selectin-GFP was assessed using fluorescence microscopy and images were taken (Figure 5.10). The percentage of GFP positive cells was calculated and the results are summarized in Table 5.6. The results showed that the number of GFP positive cells was 5.3% for MOI5 and 13.7% for MOI20. Due to the low percentage of GFP positive cells produced with MOI5, it was decided to use the MOI20 cells for future experiments. CaM-RFP and moesin-RFP lentiviruses were added to a sample of these cells using the MOI stated above to produce L358E-L-selectin-GFP/CaM-RFP and L358E-L-selectin-GFP/moesin-RFP cell lines. These cell lines were maintained in cell culture ready for cell sorting to select the cells expressing both L358E-L-selectin-GFP and CaM-RFP/moesin-RFP.

**(i) Lentiviral Titration**

**(ii) Linear Range**

$$y = 3.423x - 3.11$$
$$R^2 = 0.8945$$
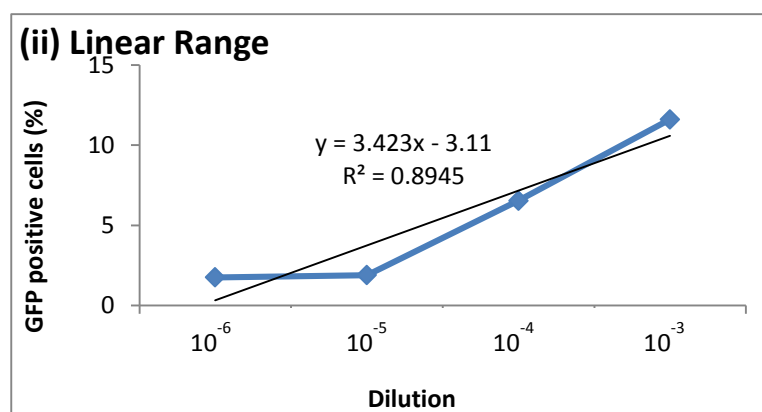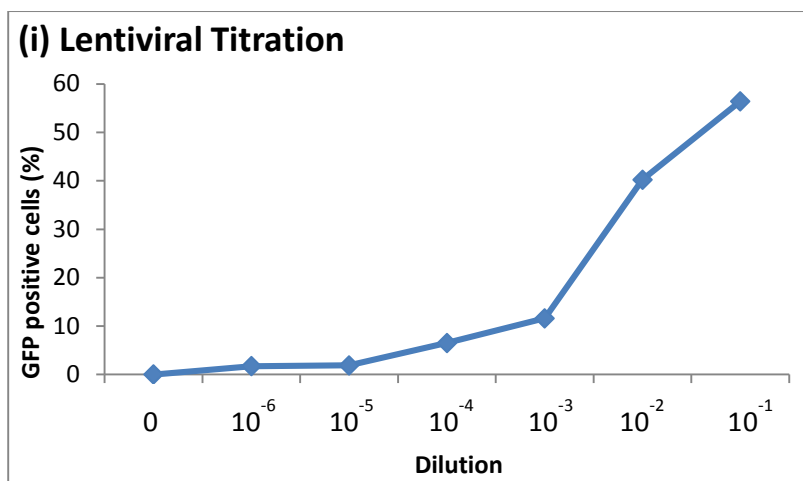
**Figure 5.10: Transduction of HEK cells with lentivirus carrying the lentiviral vector for L358E-L-selectin-GFP.** HEK cells were transduced with L358E-L-selectin-GFP lentivirus using a serial dilution (0, $10^{-6}$, $10^{-5}$, $10^{-4}$, $10^{-3}$, $10^{-2}$, $10^{-1}$) of the concentrated lentiviral particles. (i) The percentage of GFP positive cells was assessed using FACS and plotted against the lentiviral dilution. (ii) Those dilutions found in the linear range of transduction were used to calculate the lentiviral titre to avoid multiple integrations.

| dilution | GFP positive (%) | Titre |
|----------|------------------|-------|
| $10^{-6}$ | 1.75 | $17.50 \times 10^9$ |
| $10^{-5}$ | 1.89 | $1.89 \times 10^9$ |
| $10^{-4}$ | 6.54 | $0.65 \times 10^9$ |
| $10^{-3}$ | 11.61 | $0.12 \times 10^9$ |
| | Average titre | $5.04 \times 10^9$ i.u/ml |

**Table 5.5: Calculation of viral titre of L-selectin-L358E-GFP from dilutions within the linear range of transduction.** Lentiviral dilutions with a transduction efficiency of between 1-20 % were taken and the titre for each dilution was calculated using the equation: $T = \dfrac{PN}{DV}$. The final titre was found by calculating the mean of the titres for the dilutions within the linear range.

**Phase**                    **GFP**
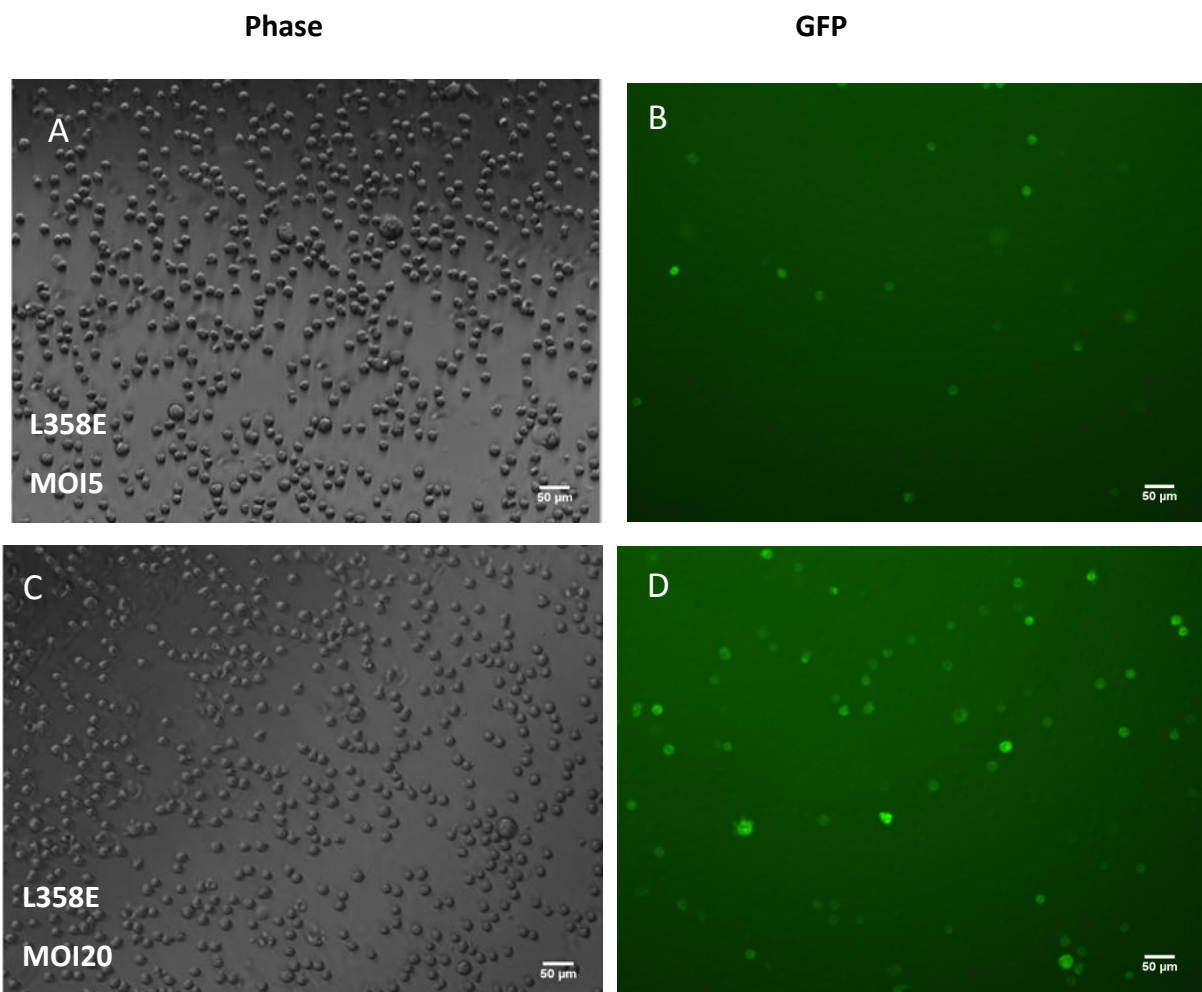
**Figure 5.11: Images of THP-1 cells transduced with L358E-L-selectin-GFP.** ATTC THP-1 cells were transduced with lentivirus encoding L358E-L-selectin-GFP with MOI5 (A and B) or MOI20 (C and D). Images were taken with both the phase and GFP channels using an Olympus IX81 time-lapse inverted fluorescence microscope attached to a Hamamatsu C10600 ORCA-R2 video camera, with analysis undertaken using Volocity imaging software. All images were taken at 10x objective.

| L-selectin L358E-GFP | GFP positive (%) |
|---|---|
| MOI5 | 5.3 |
| MOI20 | 13.7 |

**Table 5.6: Percentage of GFP positive THP-1 cells after transduction with lentivirus carrying the lentiviral vector for L358E-L-selectin-GFP.** The percentage of GFP positive cells was calculated for the THP-1 cell lines after L358E-L-selectin-GFP lentiviral transduction by calculating the mean of three fields of view.

226

The titre for L358E-ΔM-N-L-selectin-GFP was found to be $0.155 \times 10^9$ i.u./ml (Figure 5.11, Table 5.7). ATTC THP-1 cells were transduced with MOI5 and MOI20. The cells were left to propagate for two weeks, at which point the transduction efficiency was assessed using fluorescence microscopy. Images were taken (Figure 5.12) and the percentage of GFP positive cells was calculated for cells transduced with each MOI. The results showed that for MOI5 59.7% of the cells were GFP positive and for MOI20 the percentage of GFP positive cells was 88.5% (Table 5.8). Due to the high levels of expression it was decided that cells transduced with MOI5 would be used for future experiments. CaM-RFP and moesin-RFP lentiviruses were added to a sample of these cells using an MOI of 20 to produce L358E-ΔM-N-L-selectin-GFP/CaM-RFP and L358E-ΔM-N-L-selectin-GFP/moesin-RFP cell lines. These cell lines were maintained in cell culture in preparation of cell sorting, so the cells expressing both GFP and RFP could be selected.
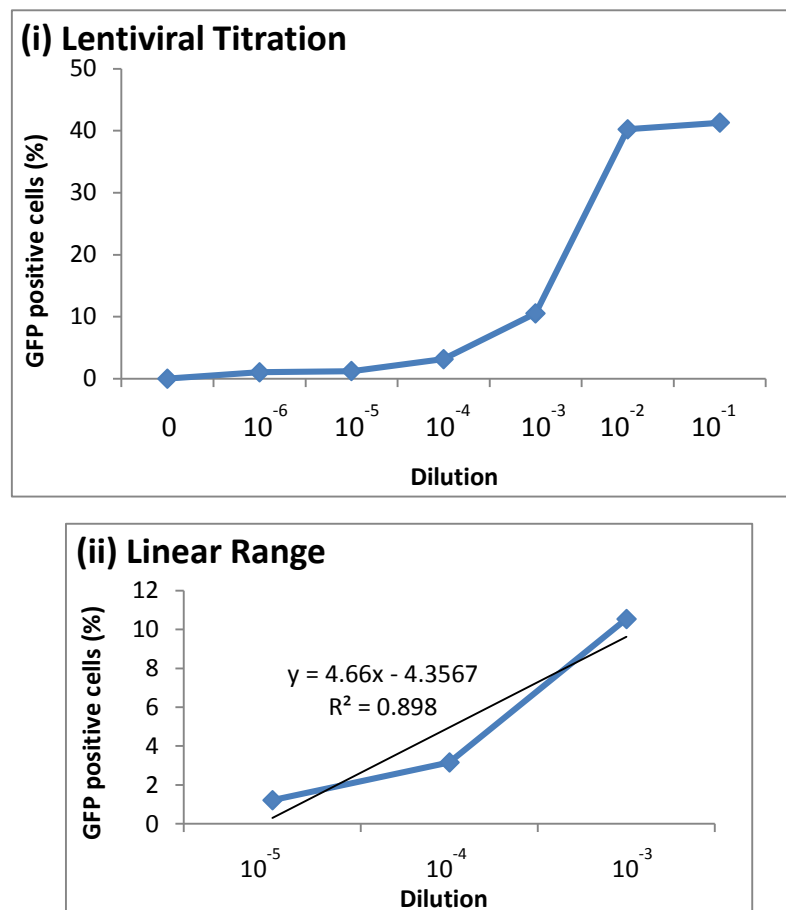


**Figure 5.12: transduction of HEK cells with lentivirus carrying the lentiviral vector for L358E-ΔM-N-L-selectin-GFP.** HEK cells were transduced with L358E-ΔM-N-L-selectin-GFP lentivirus using a serial dilution (0, $10^{-6}$, $10^{-5}$, $10^{-4}$, $10^{-3}$, $10^{-2}$, $10^{-1}$) of the concentrated lentiviral particles. (i) The percentage of GFP positive cells was assessed using FACS and plotted against the lentiviral dilution. (ii) In order to avoid multiple integrations, lentiviral dilutions in the linear range were used to calculate the lentiviral titre.

| dilution | GFP positive (%) | Titre |
|----------|------------------|-------|
| $10^{-5}$ | 1.21 | $1.21 \times 10^9$ |
| $10^{-4}$ | 2.15 | $0.22 \times 10^9$ |
| $10^{-3}$ | 9.53 | $0.095 \times 10^9$ |
| | **average titre** | $0.51 \times 10^9$ u/ml |

**Table 5.7: Calculation of viral titre of L358E-ΔM-N-L-selectin-GFP from dilutions within the linear range of transduction.** Dilutions of the lentivirus with a transduction efficiency of between 1-20 % were taken and the titre for each dilution was calculated using the equation: $T = \dfrac{PN}{DV}$. The final titre was found by calculating the mean of the titres for the dilutions within the linear range.

| **Phase** | **GFP** |
|-----------|---------|
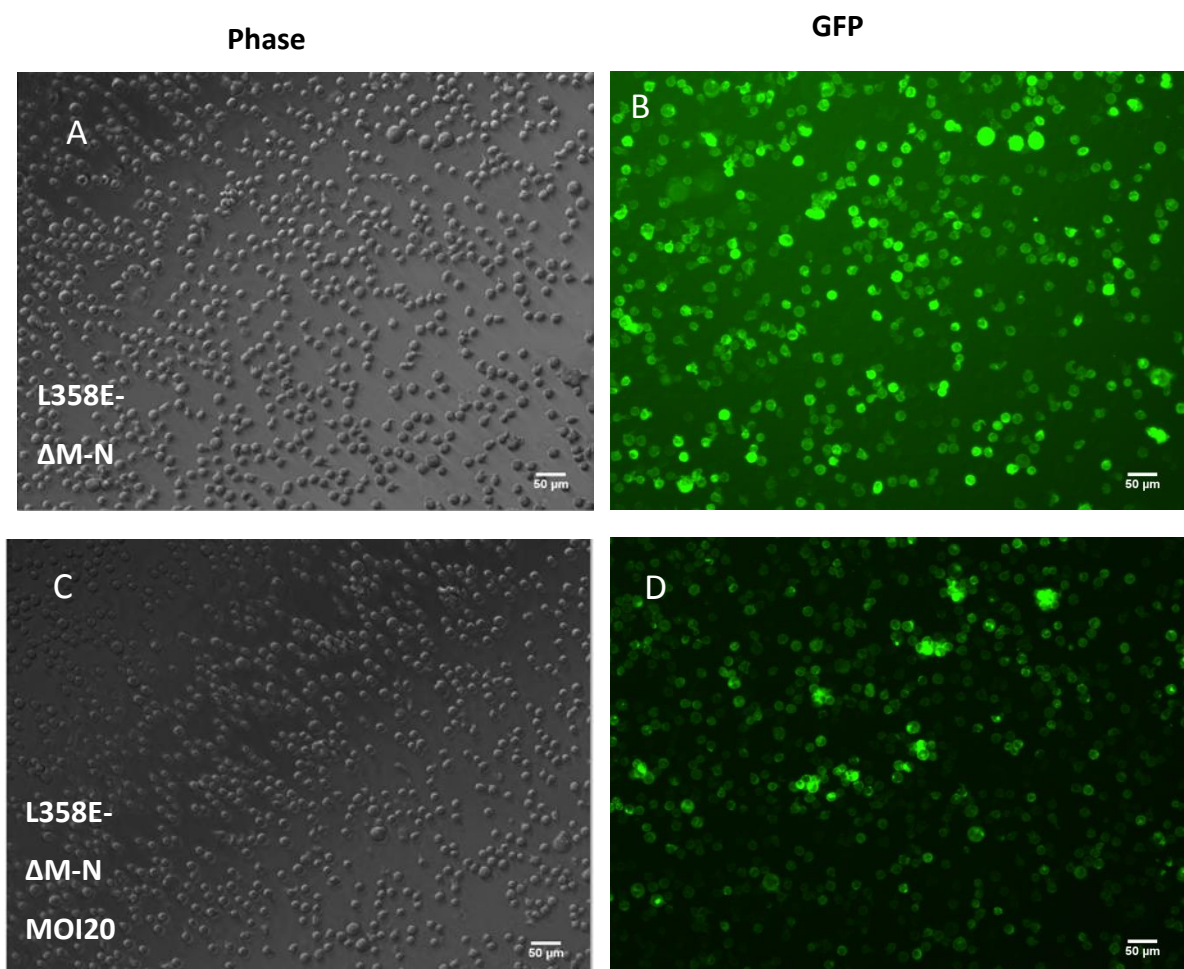


**Figure 5.13: Images of THP-1 cells transduced with L358E-ΔM-N-L-selectin-GFP.** ATTC THP-1 cells were transduced with lentivirus expressing L358E-ΔM-N-L-selectin-GFP with MOI5 (A and B) or MOI20 (C and D). Images were taken using an Olympus IX81 time-lapse inverted fluorescence microscope attached to a Hamamatsu C10600 ORCA-R2 video camera and analysed using Volocity imaging software. All images were taken at 10x objective with both the phase and GFP channels.

| ΔM-N-L358E-L-selectin-GFP | GFP positive (%) |
|---|---|
| MOI5 | 59.7 |
| MOI20 | 88.5 |

**Table 5.8: Percentage of GFP positive THP-1 cells after transduction with lentivirus carrying the lentiviral vector for L358E-ΔM-N-L-selectin-GFP.** The percentage of GFP positive cells were calculated for the THP-1 cell lines after L358E-ΔM-N-L-selectin-GFP lentiviral transduction as the mean of three fields of view for each cell line.

## 5.3.5 Analysis of the Protein Expression Levels of CaM-RFP in THP-1 cell lines

To assess the levels of CaM-RFP expressed in the different THP-1 cell lines, cell lysates were produced and analysed by Western blot, using an anti-CaM antibody. As a negative control THP-1 cells transduced with GFP protein were used, as this cell line would not express CaM-RFP. The results showed that a band with molecular weight of around 50 kDa was observed in all the cell lines except THP-1 cells expressing GFP alone (Figure 5.13A, blue arrow). This molecular weight was consistent with that expected for CaM tagged with RFP (18 KDa for CaM and 27 KDa for RFP). The protein expression levels of CaM-RFP between the different cell lines was analysed using endogenous CaM as a loading control and comparing the CaM-RFP expression levels of all the L-selectin mutant cell lines to wildtype L-selectin-GFP. It was found that the expression levels were very similar, with SSAA having slightly higher levels compared to the others (Figure 5.13B). As all the cell lines expressed CaM-RFP at similar levels, comparison of the interaction between L-selectin-GFP and CaM-RFP across the cell lines could be carried out without the concern of misinterpretation of results due to different protein expression levels.

The anti-CaM antibody also recognised the endogenous CaM expressed in the THP-1 cell lines. A band with a molecular weight between 20 and 15 kDa was present in all the cell lines, corresponding to endogenous CaM, and the protein expression levels of endogenous CaM was similar between the cell lines (Figure

5.13A, back arrow). When the levels of endogenous CaM were compared to CaM-RFP it was clear that endogenous CaM was expressed at a higher level than CaM-RFP. Densitometric analysis was performed to analyse the extent of the difference in the protein expression levels between endogenous CaM and CaM-RFP. Analysis revealed that the expression levels of CaM-RFP were around a quarter of that of endogenous CaM for all the cell lines (Figure 5.13C).
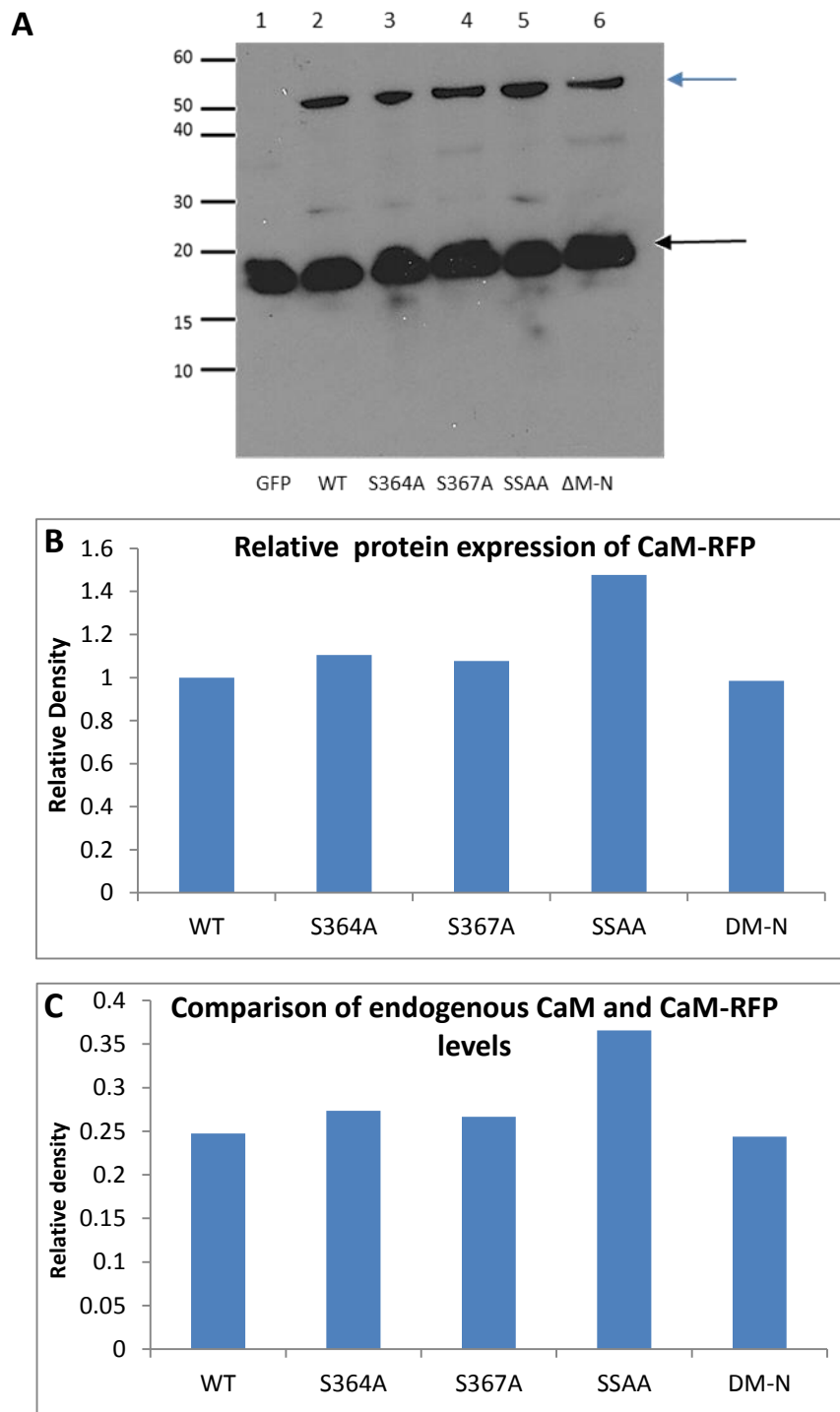
**Figure 5.14: Protein expression levels of CaM in the different THP-1 cell lines.** (A) Cell lysates for the THP-1 cell lines expressing L-selectin-GFP and CaM-RFP were analysed to assess the levels of CaM by western blot using an anti-CaM antibody (The blue arrow shows CaM-RFP and the black arrow shows endogenous CaM). (B) The protein expression levels of CaM-RFP were compared between the cell lines by densitometric analysis, using endogenous CaM as a loading control and comparing the mutants to wildtype L-selectin. (C) Densitometric analysis was used to compare the difference between CaM-RFP and endogenous CaM in the different cell lines. Densitometric analysis was carried out using ImageJ software.

## 5.3.6 Monitoring the biochemical interaction of L-selectin-GFP with endogenous CaM and CaM-RFP

To study the interaction between L-selectin and CaM, a GFP-Trap assay was performed. This entails using a GFP-binding protein coupled to agarose beads to immunoprecipitate GFP (see Section 2.23 in Materials and Methods). When THP-1 cell lysate was added to the GFP-Trap beads, L-selectin would be immunoprecipitated, as L-selectin was tagged with GFP. Any proteins that were interacting with L-selectin will co-precipitate, allowing for the identification of binding partners of L-selectin.

GFP-Trap assays were carried out on cell lysates derived from THP-1 cells expressing wildtype and mutant L-selectin-GFP to determine if any of the mutations had an effect on CaM binding. THP-1 cells expressing GFP were used as a negative control, to ensure that any protein co-precipitated with L-selectin-GFP is due to the interaction with L-selectin and not due to the presence of the GFP tag. Following incubation with the GFP-Trap beads the immunoprecipitated proteins were analysed by Western blot, using anti-CaM antibody to visualise CaM bound to L-selectin. Anti-GFP antibody was also used to assess the quantity of L-selectin immunoprecipitated in the different cell lines, so comparison of CaM binding to L-selectin between the cell lines could be carried out.

Initial experiments showed that endogenous CaM was co-precipitated in all the cell lines (Figure 3.14A, black arrow), with SSAA and ΔM-N showing the greatest amount of co-precipitation (Figure 3.14A, lanes 5 and 6 respectively). CaM-RFP could also be observed as a faint band in the S364A, SSAA and ΔM-N cell lines, but

was not visible in wildtype or S367A cell lines (Figure 3.14A blue arrow). However, a band corresponding to the molecular weight of endogenous CaM was visible in the immunoprecipitation of the THP-1 cells expressing GFP (Figure 3.14A, Lane 1). This suggested that there was nonspecific binding occurring between CaM and the GFP-Trap beads. In an attempt to remove any nonspecific interactions, 1% ovalbumin was added to the lysis and wash buffers, which has been previously used in immunoprecipitation experiments to limit any nonspecific interactions with L-selectin (3). When the experiment was repeated in these conditions, CaM was no longer observed in the lane corresponding to THP-1 cells expressing GFP (Figure 3.14C, Lane 1). Endogenous CaM was still present in the pull-down of all the cell lines (Figure 3.14C, black arrow), however, under these conditions wildtype L-selectin bound best to CaM (Figure 3.14C, Lane 2), with all the mutants co-precipitating much less CaM, suggesting that mutating the tail of L-selectin affected its ability to effectively co-precipitate CaM. The extent of this difference was assessed using densitometric analysis, using the level of full length L-selectin-GFP for each cell line as the loading control (Figure 3.14D) and comparing all the mutant cell lines to the results observed with wildtype L-selectin-GFP. The results clearly showed that wildtype L-selectin-GFP immunoprecipated the greatest amount of CaM, with the mutants having similar levels of CaM (Figure 3.14E). It is worth noting that, due to time constraints this experiment was only undertaken once and therefore further repeats are required in order to carry out statistical analysis of this result. CaM-RFP was no longer visible in the pull-down from the lysate of any cell line. This was likely due to the fact that the levels of CaM-RFP were much lower than endogenous CaM, so was less likely to be bound to L-selectin, meaning less would be present in the immunoprecipitate.
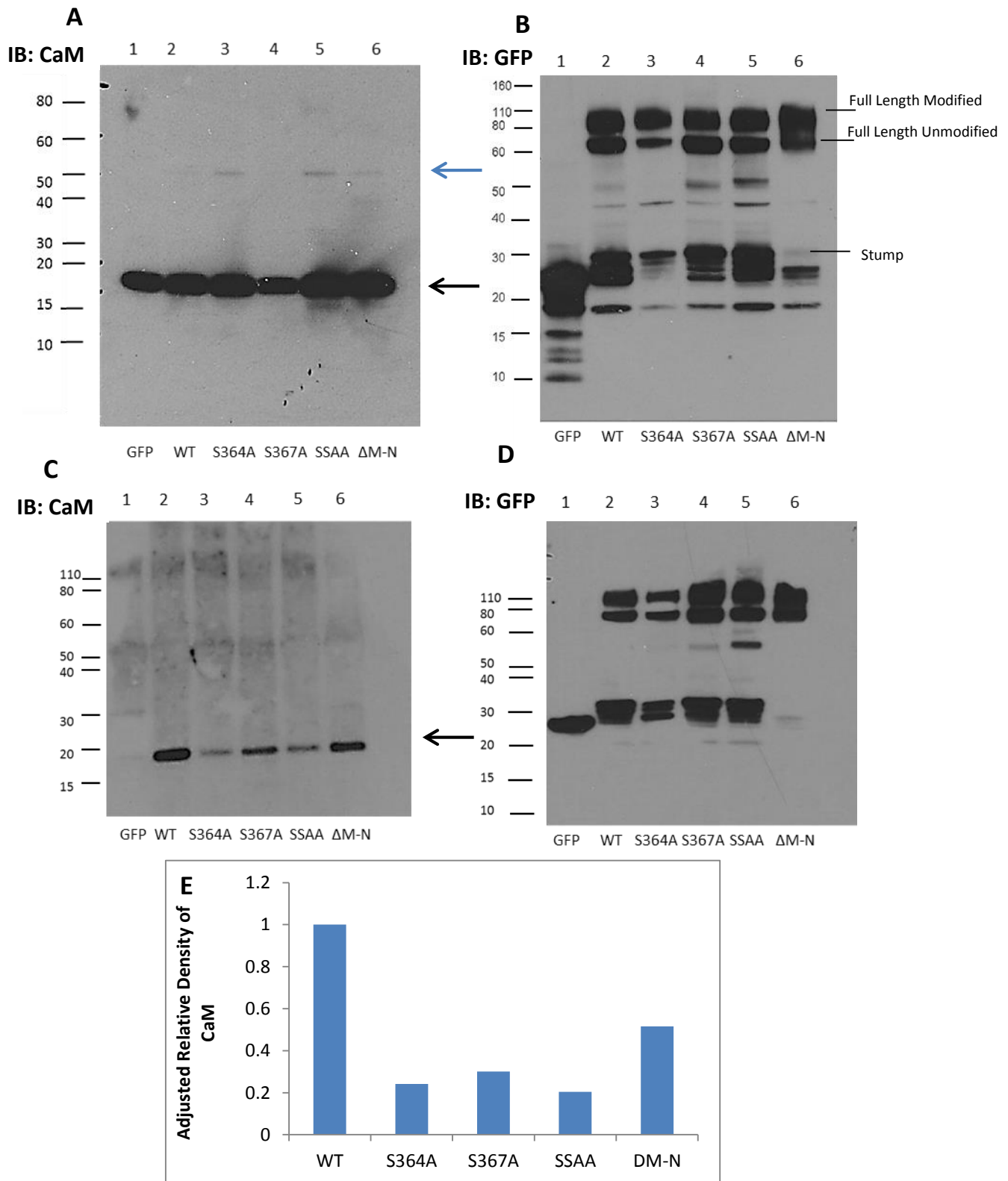
**Figure 5.15: GFP-Trap assay for the analysis of CaM interaction with L-selectin in THP-1 cell lysates.** GFP-Trap assay was carried out to assess the ability of CaM to bind to L-selectin-GFP in either wildtype cells or L-selectin mutants. For each experiment 2x10$^7$ THP-1 cells were collected by centrifugation and the cells were lysed. The lysate was then incubated with pre-equilibrated GFP-Trap beads and any proteins interacting with the beads were precipitated by centrifugation. The precipitated proteins were analysed by Western blot using anti-CaM and anti-GFP antibodies. Initial pull-down was carried out without ovalbumin and levels of CaM (A) and GFP (B) were assessed. 1% ovalbumin was then added to the lysis and wash buffer to block nonspecific interactions and Western blots for CaM (C) and GFP (D) were carried out. (E) The amount of

233

endogenous CaM immunoprecipitated was analysed, using full length L-selectin-GFP to adjust the density of CaM, with the levels compared to wildtype L-selectin-GFP, for the experiment with ovalbumin present. The black arrow endogenous CaM and the blue arrow shows CaM-RFP.

## 5.3.7 FRET/FLIM analysis of CaM and L-selectin in THP-1 cells plated on poly-L-lysine

As explained in Section 5.2, GFP and RFP can act as a donor and acceptor pair for FRET. As the THP-1 cell lines produced here express L-selectin-GFP and CaM-RFP, FRET/FLIM analysis was carried out to gain an insight into the interaction between these two proteins in intact cells. To study the interaction in resting cells, without any activation, cells were taken from suspension and plated onto poly-L-lysine (PLL)-coated glass coverslips and fixed in 4 % paraformaldehyde (PFA) prior to FRET/FLIM analysis. Analysis showed that the FRET efficiency between wildtype L-selectin-GFP and CaM-RFP was very low (Figure 5.15A and F), showing there was no interaction between the two proteins. The same analysis was carried out with cells expressing L-selectin-ΔM-N-GFP and CaM-RFP and the results showed the FRET efficiency was similar to that observed with wildtype L-selectin-GFP, suggesting as with wildtype L-selectin, there was no interaction between ΔM-N-L-selectin-GFP and CaM-RFP in resting cells (Figure 5.15B and F).

The interaction between L-selectin and CaM was also assessed with the serine to alanine mutants in resting cells. The results showed that the FRET efficiency in cells expressing S367A-L-selectin-GFP was similar to that in cells expressing wildtype L-selectin-GFP (Figure 3.15D and F). This suggests that there was little or no interaction between S367A-L-selectin-GFP and CaM-RFP, as with the wildtype cells. However, the FRET efficiency for S364A-L-selectin-GFP/CaM-RFP (Figure 3.15C) and SSAA-L-selectin-GFP/CaM-RFP (Figure 3.15E) was significantly higher than that observed with wildtype L-selectin-GFP, showing an interaction between L-selectin-GFP and CaM-RFP in these cell lines, with the greatest amount of interaction occurring with S364A (Figure 3.15F). This implies that mutating S364 to alanine enhances the interaction of CaM with L-selectin in resting cells. As this mutation blocks the phosphorylation of this residue it is possible that phosphorylation of S364 is involved in abrogating the binding of CaM to L-selectin under resting conditions.
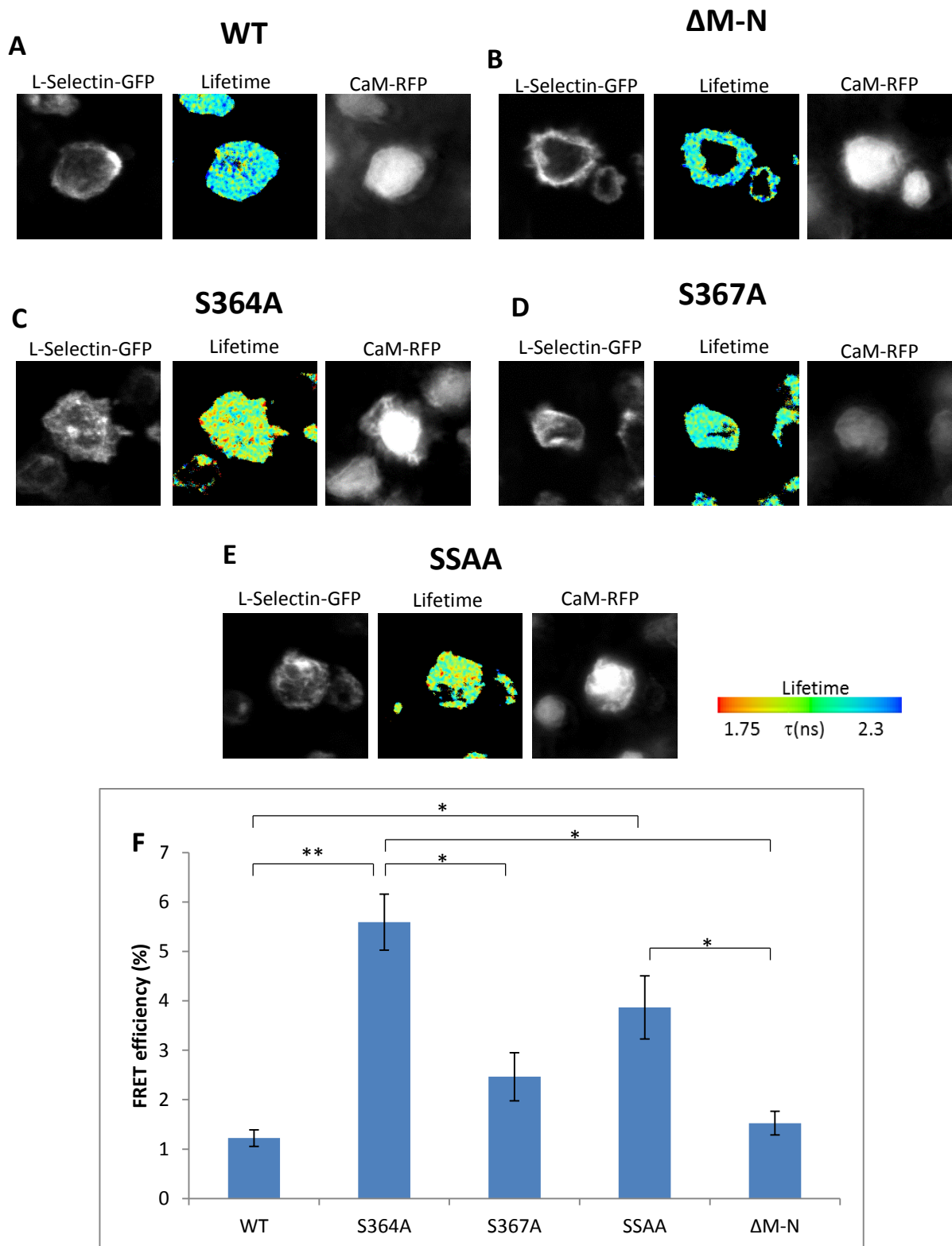
**Figure 5.16: FRET efficiency between CaM-RFP and L-selectin-GFP in resting THP-1 cell lines**. THP-1 cells were plated on PLL covered coverslips, fixed with 4% PFA and mounted on slides ready for FRET/FLIM analysis. Images showing the FRET efficiency between CaM-RFP and L-selectin-GFP in resting cells were taken for wildtype L-selectin (A), S364A (B), S367A (C), SSAA (D) and ΔM-N (E), with the left panel showing the GFP signal, the middle panel showing the fluorescence lifetime and the right panel showing the RFP signal. (F) The FRET efficiency for the cell lines was measured and statistical analysis was carried out using a One-way Annova followed by a Tukey's post-hoc test. Images and measurements were taken by Dr Maddy Parsons, King's College London.  *=p<0.05, **=p<0.01.

235

## 5.4 Discussion

### 5.4.1 Generation of Stably Transduced THP-1 Cell lines

THP-1 cells expressing CaM-RFP and different mutants of L-selectin-GFP were successfully produced for use in future studies of the interaction between the two molecules. Analysis of the lysate of these cells showed that the level of CaM-RFP was much lower than endogenous CaM. This could lead to misinterpretation of results from FRET analysis of the interaction between L-selectin and CaM, as binding of endogenous CaM to L-selectin-GFP would block the binding sites for CaM-RFP, leading to no FRET being observed even though CaM binding was occurring and therefore inaccurate conclusions. In the future it may be advantageous to knock out endogenous CaM before introducing CaM-RFP to ensure this is not a problem. Additionally, overexpressing CaM-RFP in THP-1 cells could confirm if the results were due to a dilution effect of exogenous CaM-RFP versus endogenous CaM. By shifting the pool of available CaM towards the exogenous CaM-RFP may lead to increased co-precipitation of CaM-RFP with L-selectin-GFP.

It is worth noting that some of the Western blot bands corresponding to endogenous CaM are saturated and bleeding into one another (Figure 5.13). This is a problem with using x-ray film to detect bands of different intensities, where the long exposure required to visualise the lower levels of protein expression causes over exposure of bands representing higher protein expression levels. This can be overcome by using a digital Western blot scanner, which is capable of detecting all protein bands at once without causing saturation of the higher intensity bands. This will mean a more accurate densitometric analysis can be undertaken.

Moesin-RFP was also successfully expressed in THP-1 cell lines expressing L-selectin-GFP, both wildtype and the mutants. Images of these cells showed that the distribution of moesin-RFP was found at the membrane, with areas of high expression observed. It has previously been shown that moesin is located primarily at the cell membrane in both neutrophils (439) and differentiated THP-1 cells (440). This is to be expected as it is known that ERM proteins interact with the plasma

membrane (264). It is possible that the high intensity fluorescence signal represents the uropod of the cell. Several proteins, including CD43, CD44 and PSGL-1 are concentrated at the uropod and these molecules have been shown to interact with ERM proteins (271,274,441,442). It was shown that ezrin did co-localize with these molecules in the uropod of T-cells (443). It is therefore feasible that moesin also accumulates to the uropod in THP-1 cells through its interaction with these transmembrane proteins. These transmembrane proteins could be used to decipher the location of moesin within the THP-1 cells. Fluorescently tagged antibodies against CD43, CD44 or PSGL-1 could be used to indicate their location within the cell and it would be possible observe if this signal co-localises with the high intensity RFP signal observed with moesin-RFP. Work in the Ivetic lab is currently underway to address such questions.

Cloning of ezrin-RFP has so far been unsuccessful. Using a partial digest to carry out the cloning can be repeated. If this is still unsuccessful it may be useful to obtain a different lentiviral vector containing RFP with different restriction sites that are not present in the ezrin sequence. This would enable the use of conventional cloning for the production of ezrin-RFP.

## 5.4.2 Monitoring the discrepancies between FRET and biochemical approaches.

To study the interaction between CaM and wildtype L-selectin-GFP in THP-1 cells two methods were used: GFP-Trap assay to detect L-selectin-GFP and any of its binding partners, and FRET/FLIM analysis to observe the interaction in intact cells. The results of these two experiments produced very different results, with the GFP-Trap assay showing an interaction between wildtype L-selectin-GFP and CaM and the FRET/FLIM analysis showing no interaction. It is possible that this is due to endogenous CaM binding to L-selectin and blocking CaM-RFP from binding. It is also possible that the interaction between the cell and PLL affects the interaction between L-selectin and CaM. PLL coats the surface of the glass coverslip with cationic sites which are capable of interacting with anionic sites on the surface of

the cell (444). This process often results in the flattening of the cell to a degree which is not physiological (444). It is possible that this flattening alters signalling within THP-1 cells, leading to CaM dissociation from L-selectin. To test if PLL affects the interaction, THP-1 cells could be fixed prior to immobilization on PLL.

Another reason for these differences is likely to be due to the different methodology used. GFP-Trap pull-down experiments involve creating cell lysates and studying the interaction of the proteins in solution. Whereas the FRET analysis is carried out on intact cells fixed to PLL-coated cover slips. One major difference between these two methods is the presence of an intact plasma membrane with the FRET/FLIM analysis. As L-selectin is a transmembrane protein it is conceivable that the plasma membrane may play a role in regulating the binding of its partners. Deng et al (2011)(216) studied the interaction between CaM and the cytosolic tail of L-selectin by embedding the L-selectin tail and transmembrane domain into liposomes. They found that when a negatively charged phospholipid, phospohotidylserine (PS), was embedded in to liposomes the cytosolic tail of L-selectin was located closer to the surface of the membrane compared to liposomes that did not contain PS and CaM binding was not observed (216). This difference was due to an electrostatic interaction between the negatively charged PS and the positively charged amino acids of the L-selectin tail, which directly competed for CaM binding (216,417). Leukocyte plasma membranes, such as monocytes, contain approximately 7.5% PS (445), with the majority being located within the inner leaflet of the lipid bilayer (446,447). This makes it likely that the mechanism observed by Deng et al (2011) with liposomes may also occur inside the cell. This would explain why CaM binding to L-selectin is not seen when FRET/FLIM analysis is carried out in resting cells. The binding was observed with the GFP-Trap assay, however, as the plasma membrane was disrupted by the lysis, the cytosolic tail of L-selectin is free in solution and so is capable of interacting with free CaM.

To test if PS in the plasma membrane of THP-1 cells is responsible for blocking the interaction between L-selectin and CaM, the cells could be transduced with the protein annexin A5, which binds to PS with a high affinity (448). Annexin A5 binding to PS could potentially block the interaction between L-selectin and PS

and therefore promote the interaction with CaM. It is also possible to force the movement of PS from the inner membrane to the outer using a synthetic PS scramblase (449). If CaM binding was observed after treatment with this scramblase it would suggest that PS in the cell membrane is responsible for blocking the interaction between L-selectin and CaM in resting cells.

The role of the membrane in the regulation of CaM binding to L-selectin raises the question of how CaM association occurs to protect L-selectin from shedding. It has been shown that when CaM was inhibited using the CaM specific inhibitors calmidazolium, trifluoperazine and W7, L-selectin was down-regulated (215), leading to the hypothesis that CaM binding in resting cells protects L-selectin from cleavage. However, the FRET data shown here suggests that CaM is unable to bind to L-selectin in resting cells, possibly due to L-selectin interacting with the plasma membrane. It is possible that there is an early activation step that leads to CaM binding, before dissociation occurs at a later time point. There are several potential mechanisms that could lead to CaM association. It has been shown in Jurkat T cells that a subpopulation of L-selectin is located in lipid rafts (450). The L-selectin antibody Dreg56 was used to crosslink L-selectin, simulating ligand binding, and this led to an increase in the amount of L-selectin found in the lipid rafts (450). It was also found that the L-selectin located in the lipid rafts was tyrosine phosphorylated, suggesting this could be a possible signal that leads to the re-localisation of L-selectin after cell activation. It is possible that this movement to the lipid raft will lead to L-selectin no longer interacting with the cell membrane and allow CaM to bind to the cytosolic tail (Figure 5.16(i)).

It is also possible that other binding partners of L-selectin may enable CaM to bind. It has been shown that the FERM domain of moesin is able to bind to L-selectin embedded in liposomes containing up to 20% of PS (223). It has long been established that the FERM domain is able to interact with the plasma membrane (264). It was also observed that binding of moesin-FERM domain to L-selectin caused it to separate from the membrane surface by interacting with the positive amino acids within the cytosolic tail of L-selectin and blocking their interaction with the anionic membrane surface and this allowed CaM binding (223). This means that

it is possible that early activation of the cell leads to moesin association with L-selectin, which in turn allows CaM to bind (Figure 5.16(iii)).

As was mentioned in Sections 1.3.6 and 4.4.2, upon leukocyte activation an influx of calcium is induced and it is possible that this affects the interaction between CaM and L-selectin, especially given the fact that CaM is a calcium binding protein. As has been explained in Chapter 4, *in vitro* biophysical experiments showed both ApoCaM and CaM-Ca were capable of interacting with L-selectin cytosolic peptide, though it was possible there were differences in the binding mechanisms. It is therefore possible that in the cell only CaM-Ca is able to interact with L-selectin and leukocyte activation and the resultant calcium influx is required for the initiation of the interaction between CaM-Ca and L-selectin (Figure 5.16(v)). The FRET experiments cannot allow one to determine if the CaM-RFP that is binding to L-selectin-GFP is loaded with $Ca^{2+}$ or not. However, using ionophores to increase intracellular $Ca^{2+}$ levels could be one possible way of addressing if the interaction between L-selectin-GFP and CaM-RFP in resting cells is altered by controlling intracellular $[Ca^{2+}]$ levels. Drugs, such as 1,2-bis(o-aminophenoxy)ethane-N,N,N',N'-tetraacetic acid (BAPTA), that prevent intracellular increases in $[Ca^{2+}]$ can also be used. Interestingly, studies have shown that treatment of leukocytes with calcium ionophores induces rapid down regulation of L-selectin (451,452). The exact mechanism by which calcium ionophores cause loss of L-selectin remains unclear, though the addition of PKC inhibitors did not block the effect (452). It is therefore possible that CaM plays a role the down regulation of L-selectin in response to calcium influx.

Another possibility is that activation of the cell leads to the redistribution of PS within the plasma membrane. The externalisation of PS has previously been shown to be an apoptotic signal for the recognition of cells to be removed by phagocytosis (447). It has also been found in non-apoptotic cells. A population of activated/memory CD4$^+$ T-cells were found to have high levels of external PS and were found to be healthy (453). It was found that this redistribution of PS occurs after activation of the P2X$_7$ receptor (453-455). The P2X$_7$ receptor has been shown to be  expressed in THP-1 cells (454), so it is possible that activation of this receptor

causes the externalisation of PS in these cells, which leads to L-selectin no longer interacting with the plasma membrane and allows CaM binding (Figure 5.16(ii)). It would be possible to visualise if PS is externalized after THP-1 cells are activated by using a fluorescent probe which binds to PS. Lactadherin is a milk glycoprotein which binds to PS. it has previously been tagged with GFP and expressed in several different cell types (456). It was shown that in wildtype yeast cells the lactadherin-GFP was localised at the plasma membrane but in cells deficient for PS the protein was cytosolic (456). By comparing THP-1 cells expressing lactadherin-GFP before and after activation it will be possible to see if the distribution of this protein was altered.

Interestingly, it has also been shown that $P2X_7$ receptor activation leads to shedding of L-selectin in several different leukocyte cell types (453-455,457). Inhibitors of PS translocation also inhibited the shedding of L-selectin induced by $P2X_7$ receptor activation (453), showing a clear link between PS redistribution and L-selectin shedding. Although both processes have been shown to occur it is not known if they happen at the same time or are sequential. It is possible that PS redistribution occurs first, allowing CaM binding to take place and regulate the shedding of L-selectin. Further experiments are required to decipher if there is a link between PS distribution and CaM regulation of L-selectin shedding.
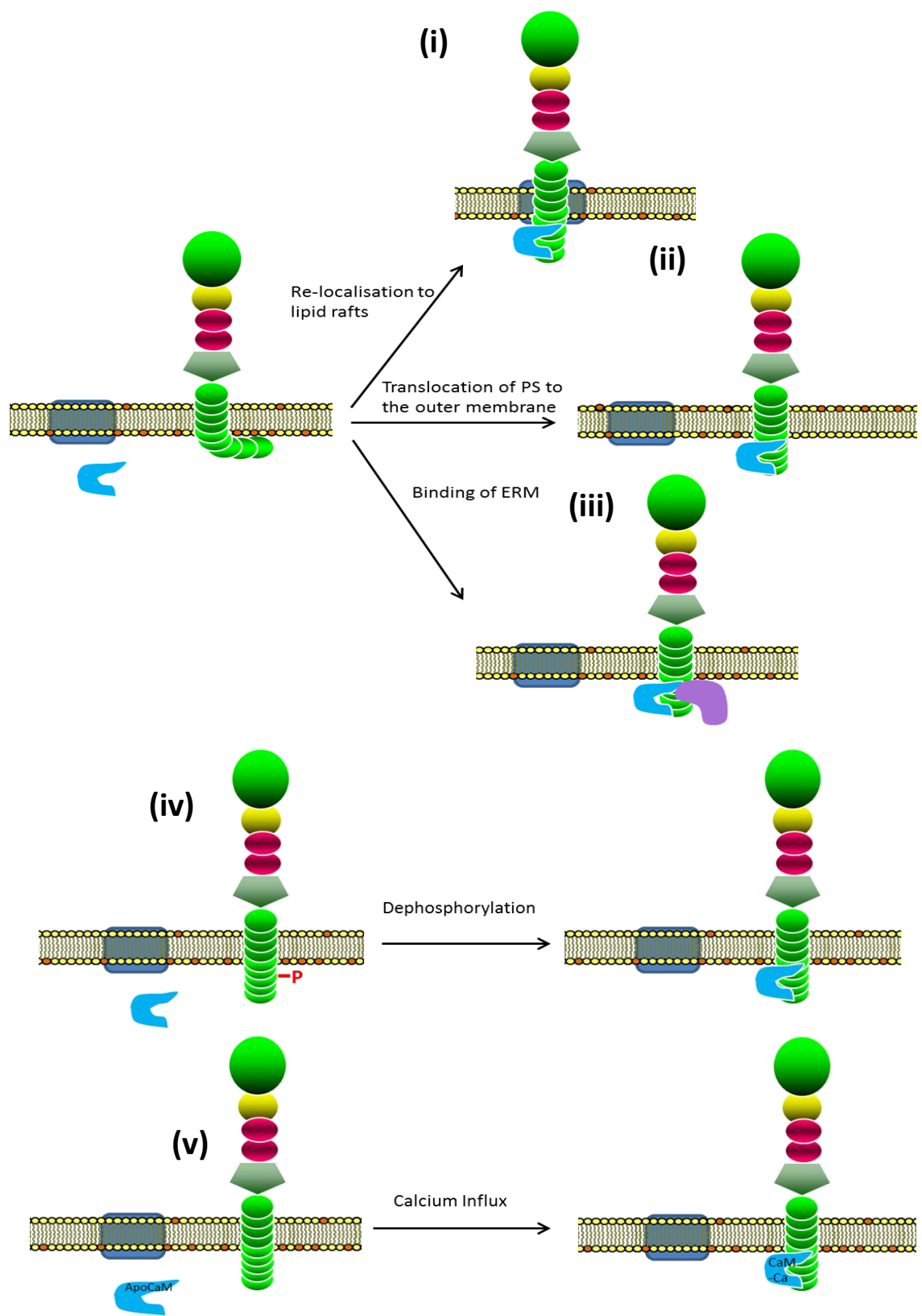
**Figure 5.17: Potential Mechanisms of the initiation of CaM binding to L-selectin upon leukocyte activation.** There are several potential mechanisms that regulate CaM (shown in light blue) association to L-selectin. It is possible that in resting cells the cytosolic tail of L-selectin interacts with PS (shown in orange) in the plasma membrane. Upon activation L-selectin could be re-localised to lipid rafts (shown in dark blue)(i), PS could be translocated to the outer membrane (ii) or ERM could bind to the cytosolic tail of L-selectin(shown in purple), all of which could lead to dissociation of the L-selectin cytosolic tail from the plasma membrane and allow CaM interaction. (iv) It is also possible that phosphorylation of residue S364 (shown in red) in the tail of L-selectin

blocks CaM binding in resting cells. Upon activation, dephosphorylation occurs and CaM is able to bind to L-selectin. (v) Another possibility is that in resting cells CaM is in its Apo form and is not able to interact with L-selectin. Upon activation there is an influx of calcium, which will bind to CaM and lead to the association of CaM-Ca to L-selectin.

### 5.4.3 Mutating the Cytosolic tail of L-selectin affects CaM binding

When GFP-Trap beads were used to immunoprecipitate L-selectin and its binding partners it was found that the sheddase resistant mutant ΔM-N did not bind as effectively to L-selectin when compared to wildtype L-selectin. This difference may be due to the fact that ΔM-N cells do not produce the transmembrane and cytosolic domain, known as the "stump". It is possible that CaM binds to a greater exent to the stump of L-selectin, as this contains the binding site without the large extracellular domain, which may interfere with the binding. The FRET data showed that in resting cells CaM did not interact with ΔM-N-L-selectin, as with the wildtype L-selectin. This shows that if L-selectin does interact with the plasma membrane, as described above, blocking the cleavage of L-selectin does not affect this interaction.

Serine to alanine mutants were used to assess the affect of blocking phosphorylation on the interaction between L-selectin and CaM. The GFP-Trap immunoprecipitation results showed that all the serine to alanine mutants co-precipitated less CaM. This is not consistant with *in vitro* data that showed CaM was able to bind to the serine to alanine mutant peptides with similar affinities as wildtype (see Section 4.3.3 and Table 7.1 for a summary of the results). This highlights how the methodology and context in which the interaction is measured affects the result. With the single serine to alanine mutants, S367A and S364A, it is possible that by blocking phosphorylation of one residue promotes the phosphorylation of the other. This increase in phosphorylation at one site may affect CaM binding. It is not known what the phosphorylation state of the tail of L-selectin is in resting cells. The development of antibodies that can differentiate between the different possible phosphorylation states would provide useful information.

The FRET data for S364A and S367A showed that S367A behaves similar to wildtype L-selectin, with no interaction observed, but the interaction does occur in the S364A mutant cell line. This suggests there maybe a role for S364 phosphorylation in blocking the interaction between L-selectin and CaM in resting cells, and furthermore suggests that S364 may be constitutively phosphorylated in resting THP-1 cells (Figure 5.16(iv)). This may be the method of regulation in place of L-selectin interacting with the cell membrane as described above, or it could be a mixture of the two. Deciphering the phosphorylation state of the tail at different stages may show that it is very dynamic, with phosphorylation and dephosphorylation occuring at several different stages to control the complex mechanism of CaM binding and regulation of L-selectin shedding. It has been shown that basal shedding of L-selectin occurs and this turnover of L-selectin is at a slower rate than activated shedding (458). It is therefore possible that phosphorylation and dephosphorylation is responsible for basal shedding in resting cells.

The GFP-Trap assay results for the SSAA-L-selectin mutant showed that lower levels of CaM were pulled down. It is possible that the double mutation of the tail leads to the disruption of the overall secondary structure of the tail, leading to CaM not binding as tightly as with wildtype L-selectin. CaM normally binds to alpha helical structures and it is possible that the double serine to alanine mutation affects the capability of the tail to form a helix and therefore will affect CaM binding. The FRET data however, shows that CaM is capable of binding to the SSAA mutant in the cell, with a greater interaction observed with this mutant compared to wildtype L-selectin-GFP. This again shows that phosphorylation of S364 may be responsible for blocking the interaction in wildtype L-selectin-GFP cells. This data shows how complex the regulation of the interaction between L-selectin and CaM is. It is also possible that the mutants studied here affect the binding of other proteins, such as moesin or ezrin, to L-selectin and by affecting this interaction it may also affect the interaction with CaM. By studying the interaction between the L-selectin mutants and moesin and ezrin this may help provide information about the importance of these residues in regulating the interaction, which in turn may provide information about the interaction between CaM and L-selectin. It will also be useful to study the interaction of all three *in vivo*.

# Chapter 6: Monitoring L-selectin/CaM interaction during Leukocyte Transendothelial Migration

## 6.1 Introduction

In Chapters 4 and 5 the interaction between L-selectin and CaM was studied both *in vitro* and in resting cells, with an emphasis on deciphering the role of serine phosphorylation in regulating the interaction. The results revealed that CaM was able to interact with L-selectin both when the serine residues were mutated to alanine and when they were phosphorylated *in vitro*. Interestingly, analysis of the interaction in resting THP-1 cells, by GFPTrap assay and FRET/FLIM analysis, suggested that mutating serine residues within the cytosolic tail did affect the interaction between L-selectin and CaM. The GFPTrap assay implied that L-selectin mutations S364A, S367A and SSAA abrogated the binding of CaM to L-selectin (Section 5.3.6). Whereas the FRET/FLIM analysis showed that mutating S364, S367 or both serine residues to alanine promoted the interaction between L-selectin-GFP and CaM-RFP under resting conditions (Section 5.3.7). The differences in these results suggested that the context in which the interaction was studied plays a pivotal role in the regulation of the interaction.

Following the results from the previous chapters, it was important to investigate the interaction between L-selectin-GFP and CaM-RFP during transendothelial migration (TEM). It is well known that direct binding between CaM and L-selectin protects L-selectin from shedding (215). However, much of our understanding that relates to shedding is on leukocytes activated purely in suspension. Static transmigration assays (i.e. without flow) have previously shown that L-selectin is shed during recruitment, suggesting that the CaM/L-selectin interaction is lost at some point during TEM, however, exactly at what stage the dissociation occurs remains unclear. Furthermore, the sub-cellular distribution of the CaM/L-selectin interaction could be different within any given leukocyte. In other words, although L-selectin is expressed in many different leukocyte subsets, it could be regulated very differently within any given cell. By using FRET/FLIM analysis to study the interaction between L-selectin and CaM during TEM, it is

possible to pinpoint where and when the CaM/L-selectin interaction is lost. This will provide an important insight into L-selectin shedding during TEM.

In this chapter the interaction between CaM-RFP and L-selectin-GFP was assessed in THP-1 cells undergoing TEM under flow conditions. Analysis was undertaken with both wildtype and mutant L-selectin-GFP cells to assess whether mutating L-selectin affected this interaction at any stage of the transmigration process. Western blotting of the GFP tag was used as a measure of L-selectin shedding during TEM, which was also used to correlate CaM dissociation from the L-selectin tail. The formation of pseudopod-like protrusions by THP-1 cells was assessed – specifically within the transmigrated part of the cell. Circularity and cell area were monitored to establish a possible link between the shedding of L-selectin and a change in cell shape during TEM.

## 6.2 Experimental Procedure

In order to study the interaction between L-selectin and CaM during TEM, the parallel plate flow chamber assay was used in combination with FRET/FLIM analysis. The parallel plate flow chamber assay is a method developed to study the interaction between leukocytes and endothelial cells under shear stress conditions (7). This method involves culturing endothelial cells on to fibronectin-coated glass coverslips until a monolayer is established. The monolayers are then activated with TNF-α prior to their assembly in to the flow chamber (see Section 2.20 for details of the experimental set-up). Leukocyte suspensions are perfused over the endothelial monolayer using a syringe pump. The flow rate is set at 0.25 ml/min, which corresponds to a shear stress of 1.24 dyn/cm$^2$. This represents a shear stress that is physiologically relevant to post capillary venules, where shear stresses of between 1-5 dyn/cm$^2$ have been measured (459). It should be noted that under this setting, THP-1 cells cannot undergo full TEM. The reason for this is likely to be their size. As HUVEC are plated on fibronectin-coated glass coverslips, transmigrating THP-1 cells have very little space to pass underneath this monolayer. Full TEM is therefore rarely observed. This does however, allow the process of TEM to be explored in detail, which is normally a rapid event when primary monocytes or neutrophils are used (which are much smaller in size than THP-1 cells).  By using the THP-1 cells

expressing L-selectin-GFP and CaM-RFP produced in the previous chapter, FRET/FLIM analysis was used to study the interaction between the two at different times during TEM, which provided information about when the interaction was occurring and enabled the deciphering of the regulation of shedding of L-selectin during TEM.

As CaM binding to L-selectin is important for inhibiting L-selectin shedding, it was of interest to determine if mutating the cytosolic tail of L-selectin affected the rate of shedding of L-selectin and if this could be linked to the dissociation of CaM. A Western blotting method was developed in the Ivetic lab to measure L-selectin shedding in THP-1 cells undergoing TEM over time. This involved culturing HUVEC cells in six well plates to form monolayers. The HUVECs were then activated and THP-1 cells were placed on top and incubated for a specified amount of time. Cell lysates were then produced and prepared for Western blotting. Full-length and cleaved (occasionally referred to as the "stump") L-selectin-GFP was analysed by anti-GFP immunoblotting. By comparing cell lines expressing wildtype and mutant L-selectin-GFP, it was possible to assess if the cytoplasmic tail of L-selectin was contributing to the shedding event during TEM.

Previous work in the Ivetic lab demonstrated a role for L-selectin shedding in regulating cell shape change during TEM. For this reason the protrusion dynamics, cell area and circularity of THP-1 cells expressing the different forms of L-selectin were assessed during recruitment. Cells were scored as having zero, one, two or multiple protrusions, with circularity and cell area calculated by drawing around the cell perimeter, including any protrusions. ImageJ software was used to carry out the analysis.

## 6.3 Results

### 6.3.1 Monitoring the biochemical interaction between CaM and L-selectin in THP-1 cells following co-culture with activated endothelial cells

The interaction between CaM and L-selectin-GFP mutants in resting cells was previously assessed using the GFPTrap assay (Section 5.3.6). It was decided to

use this same assay to assess if the presence of an activated HUVEC monolayer affected the interaction between CaM and L-selectin. This also provides an alternative experimental procedure to FRET/FLIM analysis for monitoring the CaM/L-selectin interaction. If the experimental data is supportive of the FRET/FLIM observation, it would clearly strengthen the observations made with this method.

The experiment was performed with $2 \times 10^6$ THP-1 cells co-cultured with a monolayer of TNF-activated HUVEC for five minutes. This time point was chosen as it corresponded to the early time point of the FRET/FLIM analysis (Section 6.3.2). This would allow direct comparison between the FRET/FLIM analysis and the GFPTrap assay results.

Initial experiments were carried out using the manufacturer's protocol for lysis and wash buffers (see Section 2.23) and the experimental details were as described previously (see Section 2.23.2). The results showed that CaM was co-precipitated with wildtype L-selectin-GFP and all the L-selectin mutations tested (Figure 6.1A), with the greatest amount of co-precipitated CaM being observed in the lane corresponding to THP-1 cells expressing ΔM-N-L-selectin-GFP (Figure 6.1A lane 6). However, a band corresponding to CaM was also co-precipitated with THP-1 cells expressing GFP protein alone (Figure 6.1A lane 1), as was observed with the GFPTrap assay carried out with resting THP-1 cells (Section 5.3.6, Figure 5.14). As explained previously (see Section 5.3.6), 1 % ovalbumin was added to the lysis and wash buffers to block any non-specific interactions between CaM and the GFPTrap beads. As was observed previously, CaM was no longer co-precipitated in THP-1 cells expressing GFP with the presence of ovalbumin (Figure 6.1C lane 1). However, the addition of ovalbumin also affected the interaction between L-selectin and CaM, with very little CaM visible on the western blot with any of the L-selectin-GFP cell lines tested (Figure 6.1C lanes 2-6). As the bands were so faint, analysis was not possible. The experiment could be repeated with an increase in the number of THP-1 cells collected to produce the lysate in an effort to co-precipitate a larger quantity of CaM.
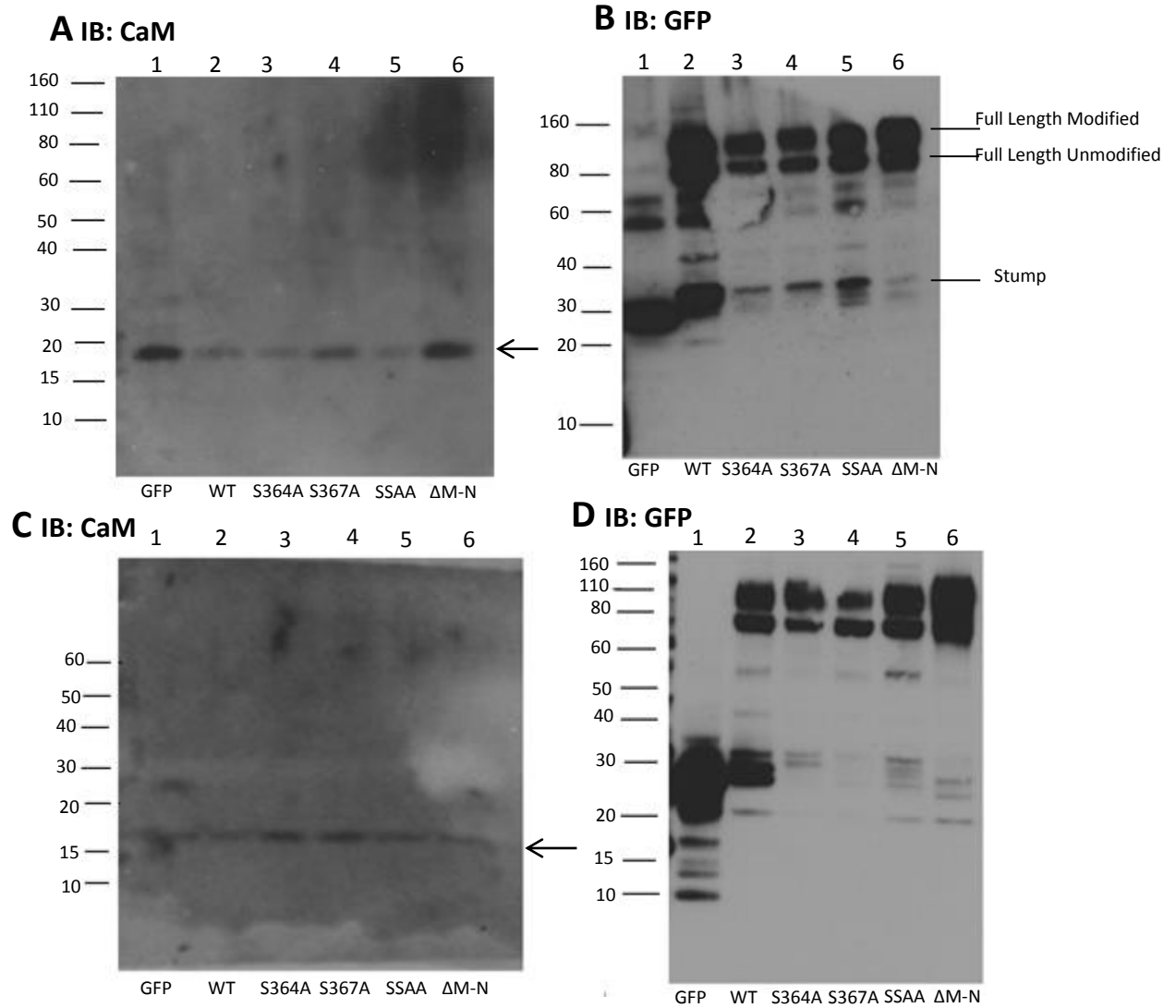
**Figure 6.1: GFPTrap assay with THP-1 cells co-cultured with activated HUVECs.** GFPTrap immunoprecipitation assay was carried out as previously described (Section 5.3.6) except THP-1 cells were incubated with TNF-activated HUVEC monolayers for five minutes prior to cell lysis. Western blot analysis was carried out with anti-CaM (A) and anti-GFP antibody (B). The experiment was repeated with 1 % ovalbumin in the lysis and wash buffers and Western blots were analysed with anti-CaM (C) and anti-GFP antibodies (D). The arrow shows endogenous CaM.

## 6.3.2 Monitoring the interaction between wildtype L-selectin-GFP and CaM-RFP during TEM using FRET/FLIM analysis

Since biochemical analysis of the interaction between L-selectin and CaM in THP-1 cells were co-cultured with TNF-activated HUVEC was unsuccessful, the parallel plate flow chamber was used to assess the interaction. This assay allows the capture of THP-1 cells undergoing the initial stages of recruitment and TEM, where pseudopods of adherent THP-1 cells begin to protrude beneath the HUVEC monolayer. THP-1 cells were perfused over activated HUVEC monolayers for a fixed period of time. Two different time points were chosen for analysis, an early time point of six minutes and a late time point of twenty five minutes. These time points were selected as it was previously observed that L-selectin shedding peaked at approximately twenty minutes following incubation with TNF-activated HUVECs (Karolina Rzeniewicz, unpublished data). This meant that at six minutes L-selectin would be predominantly uncleaved, whereas maximal shedding would have occurred by twenty five minutes. Studying the interaction between L-selectin and CaM within a given cell enables one to specifically address the dynamics of the interaction during TEM.

The FRET efficiency between CaM-RFP and L-selectin-GFP was measured at two thin optical sections to better understand the subcellular distribution of the interaction. In other words, the interaction between the two chimeric proteins was analysed specifically within the non-transmigrated and transmigrated part of the cell (Figure 6.2A). By measuring FRET in both locations the effect of TEM on the interaction between L-selectin and CaM could be assessed. After dis-assembly of the parallel plate flow chamber, the specimen was rapidly fixed in 4% paraformaldehyde followed by permeabilisation and staining with phalliodin-Alexa633 (see Section 2.21.2 in Materials and Methods for experimental procedure). Phalloidin binds to actin filaments (F-actin) within both cell types. More importantly, it was used as a marker to determine where the optical sections were taken: specifically above and below the HUVEC monolayer. All of the FRET measurements were taken by Dr Maddy Parsons at the Randall Division of Biophysics and Molecular Biology (KCL).

After six minutes of perfusion, the interaction between L-selectin-GFP and CaM-RFP was assessed in both the transmigrated (base) and the non-transmigrated (top) parts of the cell (Figure 6.2B). The FRET efficiency was found to be similar within both these sub-cellular domains (7.01±0.91% in the non-transmigrated part and 8.14±0.68% in the transmigrated part of the cell, Figure 6.2D). When the FRET efficiency was analysed at twenty five minutes (Figure 6.2C), little change within the non-transmigrated part of the cell had occurred between the two time points (6.61±0.47% and 7.01±0.91% respectively, Figure 6.2D). This suggested that CaM-RFP/L-selectin-GFP interaction was sustained over time and it was likely that shedding was not taking place in this sub-cellular domain. In contrast, the FRET efficiency between CaM-RFP/L-selectin-GFP in the transmigrated part of the cell changed dramatically by twenty five minutes compared to six minutes TEM (2.84±0.53% compared to 8.14±0.68%, Figure 6.2D). This suggested that CaM-RFP was no longer bound to L-selectin-GFP and that shedding had likely taken place, specifically in this sub-cellular domain.
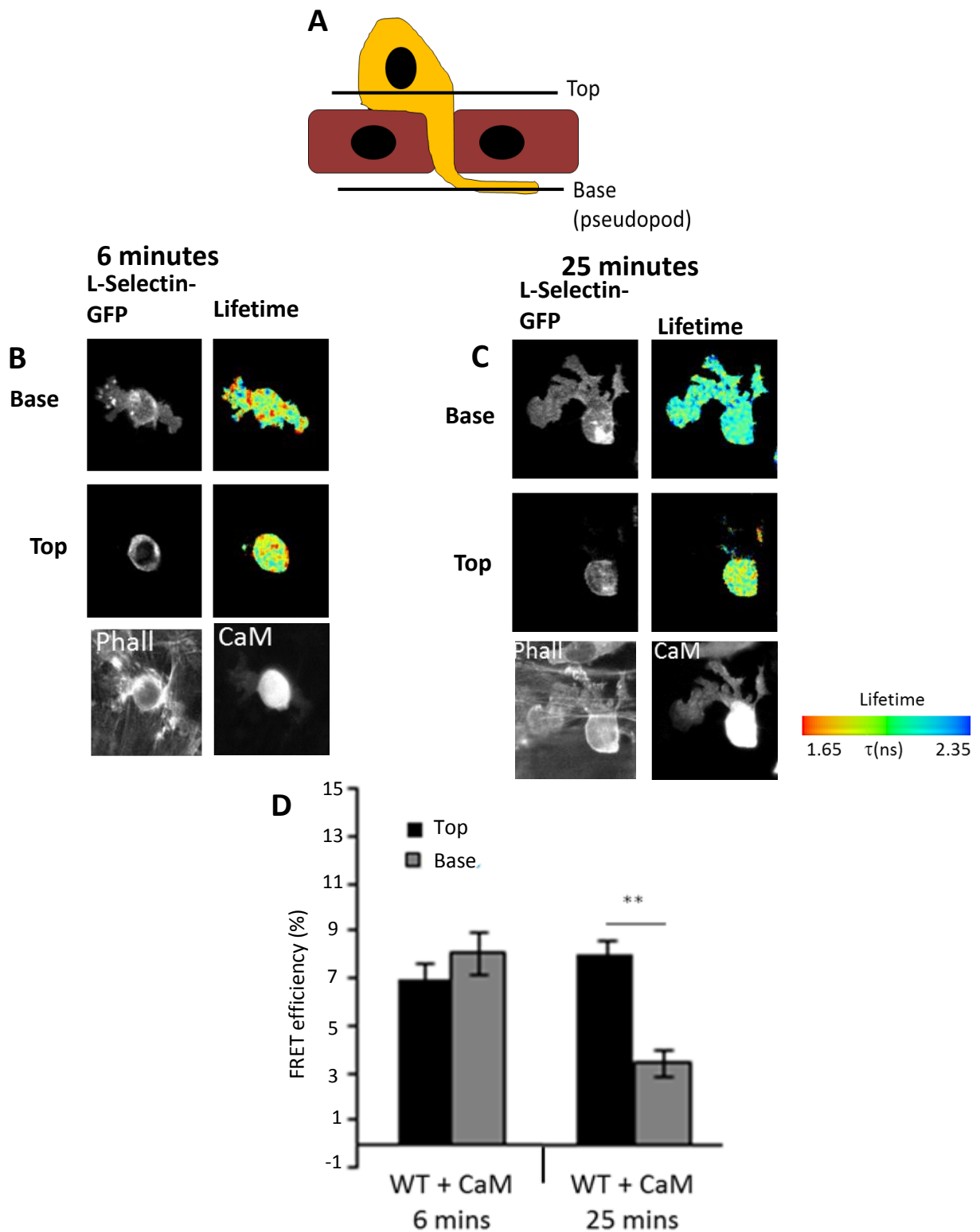
**Figure 6.2: Interaction between wildtype L-selectin and CaM during TEM.** THP-1 cells co-expressing wildtype L-selectin-GFP and CaM-RFP were perfused over TNF-activated HUVEC monolayers for either 6 min or 25 min, fixed with 4 % PFA and processed for FRET analysis. Images of the transmigrated (top) and non-transmigrated (base) parts of the cell (A) were produced after six minutes of flow (B) and twenty five minutes of flow (C). The left panel in (B) and (C) shows confocal images of L-selectin-GFP, the right panels show the lifetime fluorescence of GFP shown by a pseudo-colour scale, the bottom left panel shows the phalloidin-Alexa633 staining and the bottom right panel shows CaM-RFP (RFP image taken by fluorescence microscopy). (D) The FRET efficiency between L-selectin-GFP and CaM-RFP during TEM was measured at each time point and the difference between the results in the top and base of the cell was compared. Results are an average of three experiments with 10-15 cells measured for each experiment; error bars represent SEM. Statistical significance was assessed using a two-tailed unpaired Student's T test. **=p<0.01. All FRET analysis was performed by Dr Maddy Parsons, KCL.

### 6.3.3 Monitoring CaM/L-selectin interaction in the ΔM-N Sheddase Resistant Mutant THP-1 cell line during TEM

The interaction between the sheddase resistant mutant ΔM-N-L-selectin and CaM was assessed using the same method as above, with the FRET efficiency at the same time points measured and compared to the results observed with cells expressing wildtype L-selectin-GFP. The interaction was studied in this mutant to assess if blocking shedding affected the interaction with CaM, especially as CaM plays a role in regulating shedding.

At the six minute time point, the FRET efficiency was very low in both the transmigrated and non-transmigrated parts of the cell, both being significantly lower than that observed with wildtype L-selectin-GFP cells (Figure 6.3A, B and E). This suggested that ΔM-N-L-selectin-GFP and CaM-RFP were not interacting with one another. In contrast, after twenty five minutes of flow, the FRET efficiency increased in both the transmigrating and the non-transmigrating parts of the cell compared to that observed at six minutes TEM (Figure 6.3D and F), suggesting that at this later time point CaM-RFP was capable of interacting with ΔM-N-L-selectin-GFP throughout the entire cell. The FRET efficiency at twenty five minutes in the transmigrated and non-transmigrated parts of the cell was compared between the wildtype and ΔM-N cell lines (Figure 6.3C and D). The results showed that the FRET efficiency in the non-transmigrated part of the cell was similar in both cell lines (6.61±0.53% for wildtype and 5.52±0.53% for ΔM-N cells, Figure 6.3F). However, the FRET efficiency in the transmigrated part of the cell of ΔM-N was significantly higher than that observed with wildtype cells (5.15±0.52% versus 2.83±0.47%, Figure 6.3F). It is tempting to suggest at this point that the differences in binding observed between the cell lines suggest that the cytoplasmic tail is regulated differently between the wildtype and ΔM-N cell lines. One possibility is that serine phosphorylation of the tail could be differently regulated in the ΔM-N sheddase-resistant mutant.
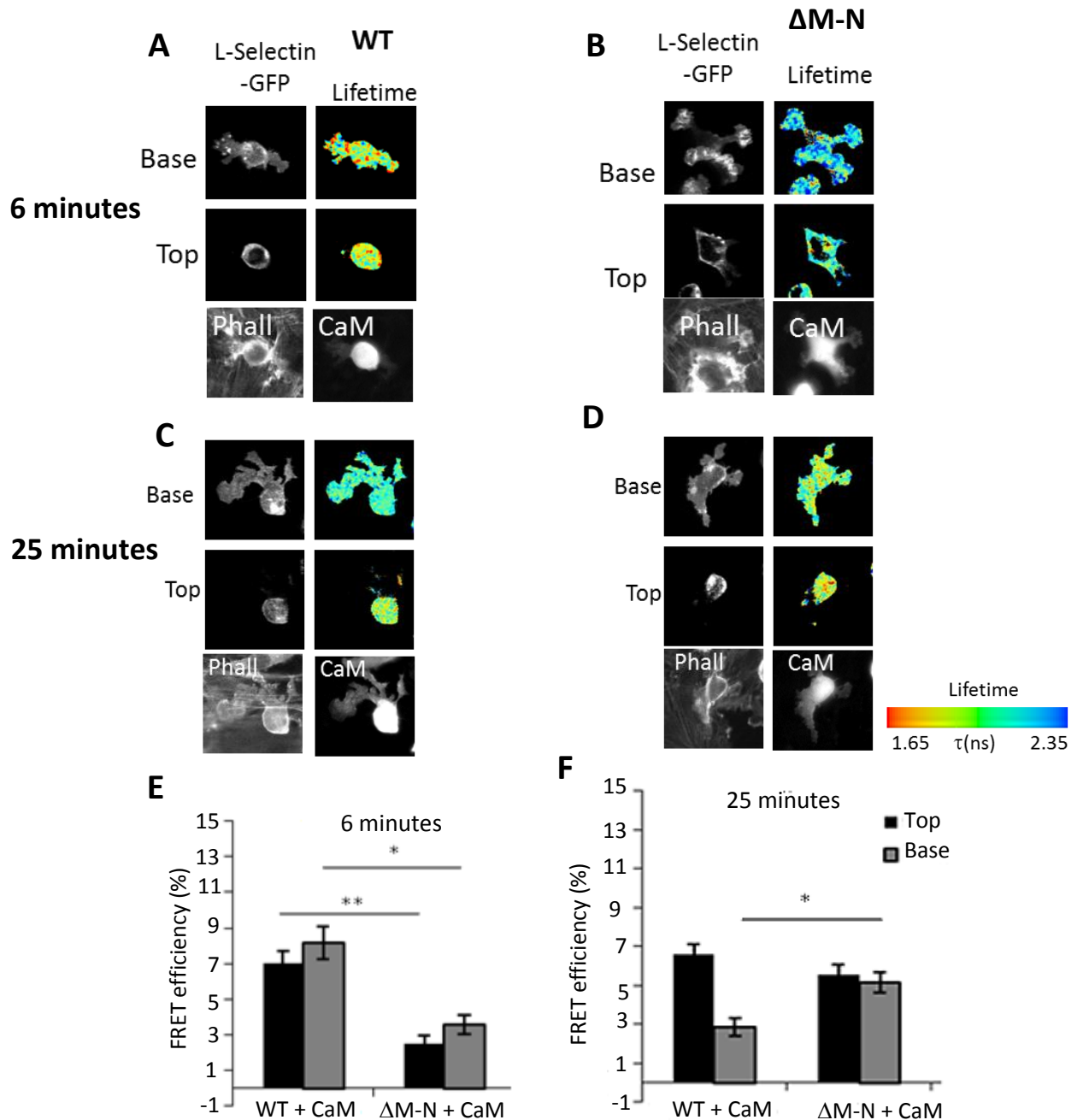
**Figure 6.3: Comparing the Interaction between L-selectin and CaM in wildtype and ΔM-N THP-1 cells.** THP-1 cells expressing L-selectin-GFP and CaM-RFP were perfused over activated HUVEC monolayers for either 6 min or 25 min and fixed with 4 % PFA to be processed for FRET analysis. Images showing the FRET efficiency between L-selectin-GFP and CaM-RFP in the transmigrated (top) and non-transmigrated part of the cell after six minutes of flow for wildtype (A) and ΔM-N (B) and twenty five minutes of flow for wildtype (C) and ΔM-N (D). The left panel in (A-D) shows confocal images of L-selectin-GFP, the right panels show the lifetime fluorescence of GFP shown by a pseudo-colour scale, the bottom left panel shows the phalloidin-Alexa633 staining and the bottom right panel shows CaM-RFP (RFP image taken by fluorescence microscopy). (E) The FRET efficiency between L-selectin-GFP and CaM-RFP during TEM was measured after 6 minutes of flow in cells expressing wildtype and ΔM-N-L-selectin-GFP and (F) the same analysis was carried out after 25 minutes of flow, with a comparison made between the cell lines. Results are an average of three experiments with 10-15 cells measured for each experiment; error bars represent SEM. Statistical significance was assessed using a two-tailed unpaired Student's T test. *=$p<0.05$, **=$p<0.01$. All FRET analysis was performed by Dr Maddy Parsons, KCL.

## 6.3.4 Monitoring CaM/L-selectin interaction in serine-to-alanine mutant THP-1 cell lines undergoing TEM

It was hypothesised that phosphorylation of serine residues within the cytosolic tail of L-selectin were responsible for the dissociation of CaM during TEM, which led to L-selectin cleavage. In the previous chapters (Chapter 4 and 5) the interaction was studied using biophysical and biochemical techniques, with conflicting results observed. To test if phosphorylation had an effect on the interaction during TEM under flow, serine residues within the tail of L-selectin were mutated to alanines, so phosphorylation would be blocked. The interaction between L-selectin and CaM was then assessed as above, by FRET/FLIM analysis, to investigate if blocking phosphorylation of either one or both serine residues affected the sub-cellular distribution of the interaction seen with wildtype L-selectin-GFP THP-1 cells during TEM under flow conditions.

The FRET efficiency of cells expressing S364A-L-selectin-GFP was measured in the non-transmigrated and transmigrated parts of the cell after six minutes of flow (Figure 6.4B) and then compared to the results observed with cells expressing wildtype L-selectin-GFP (Figure 6.4A). The comparison revealed that the FRET efficiencies were very similar in all parts of the cell for both cell lines (Figure 6.4E), showing the S364A mutation had no effect on the ability of CaM-RFP to bind to L-selectin-GFP after six minutes of flow.

Comparison between the FRET efficiency measured for cells expressing S367A-L-selectin-GFP (Figure 6.4C) and wildtype L-selectin-GFP after six minutes of recruitment (Figure 6.4A) revealed the FRET efficiency in the non-transmigrated part of the cell was similar in both cell lines. However, the FRET efficiency in the transmigrated part of the cell was significantly lower in cells expressing S367A-L-selectin-GFP (Figure 6.4E). This shows that there is a reduction in the interaction between CaM-RFP and L-selectin-GFP in the transmigrated part of the cell with this mutation, possibly leading to L-selectin shedding.
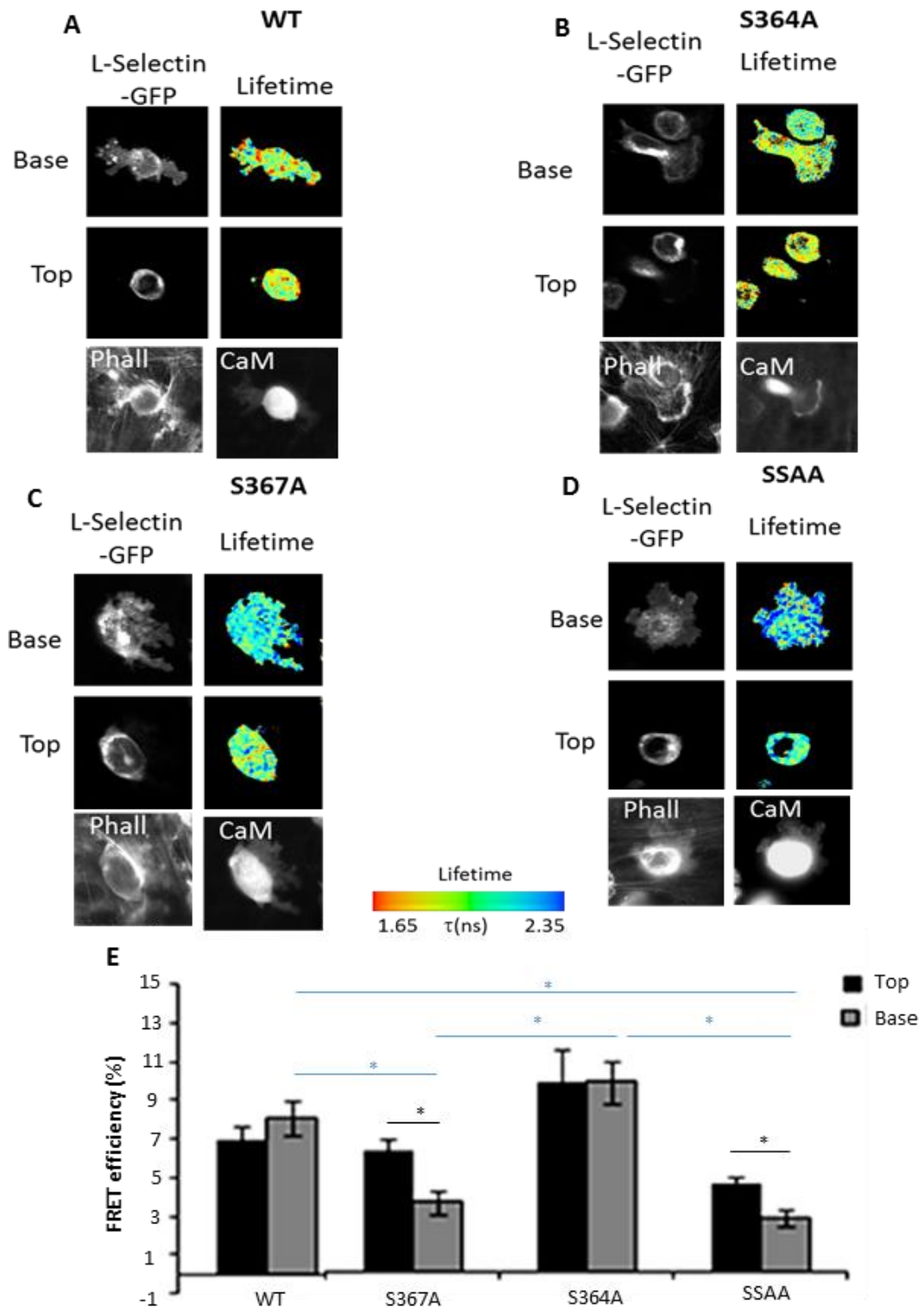
**Figure 6.4: Comparing the FRET efficiencies between L-selectin-GFP and CaM-RFP during TEM in wildtype and mutant cell lines after six minutes of flow.** THP-1 cells expressing L-selectin-GFP and CaM-RFP were perfused for 6 min over HUVEC monolayers activated with TNF-α and then fixed with 4 % PFA. Images showing the FRET efficiency between L-selectin-GFP and CaM-RFP in the transmigrated (top) and non-transmigrated (base) part of the cell after six minutes of TEM for wildtype (A), S364A (B), S367A (C) and SSAA (D). The left panel shows images of L-selectin-GFP, the right panels show the lifetime fluorescence of GFP shown by a pseudo-colour scale, the bottom left panel shows the phalloidin-Alexa633 staining and the bottom right panel shows CaM-RFP (RFP image taken by fluorescence microscopy). (E) Summary of the FRET efficiency between L-selectin-GFP and CaM-RFP during TEM for cells expressing wildtype, S364A-, S367A- and SSAA-L-selectin-

GFP. Results show the average of three experiments with 10-15 cells measured each time, with error bars representing SEM. To test statistical significance between the top and base within each cell line was assessed using an unpaired, two-tailed Student's T test (black lines). Statistical significance of the differences between the cell lines in the top or base (blue lines) of the cells was assessed using one-way Anova, followed by Tukey's post-hoc test. *=p<0.05. All FRET analysis was carried out by Dr Maddy Parsons, KCL.

The same analysis was undertaken using cells expressing SSAA-L-selectin-GFP (Figure 6.4D). Comparison to wildtype L-selectin-GFP showed that the FRET efficiency in the transmigrated part of the cell was significantly lower in cells expressing SSAA-L-selectin-GFP (Figure 6.4E), similarly to cells expressing S367A-L-selectin-GFP. Interestingly, the FRET efficiency was also significantly lower in the non-transmigrated part of the cell with the SSAA mutation. This result implies the SSAA mutation reduces CaM binding in all subcellular locations after six minutes of flow. Whether this may have something to do with binding of this mutant tail of L-selectin to the inner leaflet of the plasma membrane, as discussed in Section 5.4.2, is currently not known.

The FRET efficiency in the different cell lines was then assessed after twenty five minutes of recruitment. As for the results at six minutes, the results with the L-selectin-GFP mutants were compared those found with wildtype-L-selectin-GFP. Analysis of cells expressing S364A-L-selectin-GFP (Figure 6.5B) showed that the FRET efficiency in the non-transmigrated part of the cell was significantly higher than that of cells expressing wildtype-L-selectin-GFP (6.61±0.53% for wildtype cells versus 11.99±1.08% for S364A cells, Figure 6.5E). In the transmigrated part of the cell there was also a significant difference in the FRET efficiency between the cell lines, with a much higher FRET efficiency observed with cells expressing S364A-L-selectin-GFP (2.83±0.47% for wildtype versus 7.56±1.37% for S364A, Figure 6.5E). This showed that the interaction between CaM-RFP and L-selectin-GFP was maintained in all parts of the cell when S364 was mutated to alanine. This is in contrast to wildtype L-selectin-GFP cells, where the interaction was lost in the transmigrated part of the cell at the twenty five minute time point. This further implies that the S364A mutation will block the shedding of L-selectin in the transmigrated part of the cell, and implies that the L-selectin tail is phosphorylated differently in the transmigrated part of the tail versus the non-transmigrated part.

At twenty five minutes, comparison between the wildtype (Figure 6.5A) and S367A-L-selectin-GFP (Figure 6.5C) cell lines showed that both cell lines had a similar level of FRET efficiency in the non-transmigrated part of the cell (6.61±0.53% and 4.6±0.57% respectively, Figure 6.5E) and the transmigrated part of the cell (2.83±0.47% and 2.21±0.70% respectively, Figure 6.5E). These results reveal that the S367A mutation had no effect on the sub-cellular distribution of the CaM-RFP/L-selectin-GFP interaction after twenty five minutes of flow.

The FRET efficiency after twenty five minutes of flow was compared between wildtype (Figure 6.5A) and SSAA-L-selectin-GFP (Figure 6.5D) cell lines. The results indicated that there was no difference in the FRET efficiency in the non-transmigrated part of the cell in either cell line (6.61±0.53% for wildtype and 6.45±0.60% for SSAA-L-selectin-GFP, Figure 6.5E). In the transmigrated part of the cell, the FRET efficiency was significantly higher in cells expressing SSAA-L-selectin-GFP compared to cells expressing wildtype L-selectin-GFP (Figure 6.5E). This is likely due to the presence of the S364A mutation, blocking the dissociation of CaM-RFP in the transmigrated part of the cell.

Taken together, this data suggests that blocking phosphorylation of S364 by alanine mutation inhibited the loss of interaction between L-selectin-GFP and CaM-RFP in the transmigrated part of the cell after twenty five minutes of recruitment. It is therefore likely that the shedding of L-selectin was also blocked. Mutating S367 to alanine also affected the interaction between L-selectin-GFP and CaM-RFP, with the interaction being disrupted in the transmigrated part of the cell at the six minute time point (possibly through binding to phosphatidyl serine (PS)). This suggests it is likely that phosphorylation of the tail of L-selectin plays an important role in regulating the interaction between L-selectin and CaM during TEM.
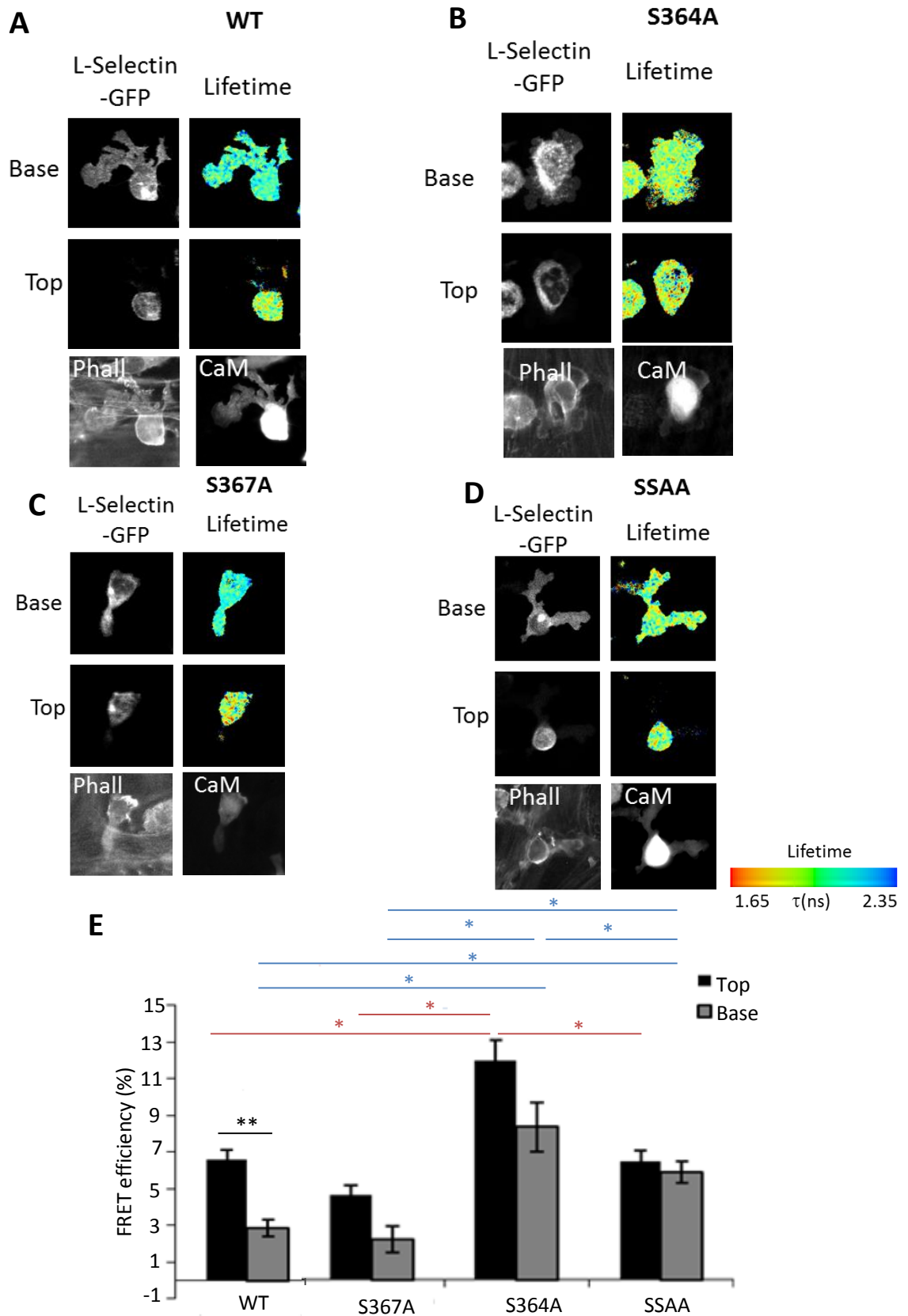
**Figure 6.5: Comparing the FRET efficiencies between L-selectin-GFP and CaM-RFP during TEM in wildtype and mutant cell lines after twenty five minutes of flow.** THP-1 cells expressing L-selectin-GFP and CaM-RFP were perfused over TNF-α activated HUVEC monolayers for 25 min and fixed with 4 % PFA ready for FRET/FLIM analysis. Images showing the FRET efficiency between L-selectin-GFP and CaM-RFP in the transmigrated (top) and non-transmigrated (base) part of the cell after twenty five minutes of TEM for wildtype (A), S364A (B), S367A (C) and SSAA (D). The right panel shows images of L-selectin-GFP, the right

panel shows the lifetime fluorescence of GFP shown by a pseudo-colour scale, the bottom left panel shows the phalloidin-Alexa633 staining and the bottom right panel shows CaM-RFP (RFP image taken by fluorescence microscopy). (E) Summary of the FRET efficiency between L-selectin-GFP and CaM-RFP during TEM for wildtype, S364A, S367A and SSAA. Results show the average of three experiments with 10-15 cells measured each time. Error bars represent SEM. To test statistical significance between the top and base within each cell line was assessed using an unpaired two-tailed Student's T test (black lines). Statistical significance of the differences between the cell lines in the top (red lines) or base (blue lines) of the cells was assessed using one-way Anova, followed by Tukey's post-hoc test. *=p<0.05, **=p<0.001. All FRET analysis was carried out by Dr Maddy Parsons, KCL.

## 6.3.5 Co-Culturing of THP-1 cells with activated HUVEC monolayers to assess the shedding of L-selectin

The analysis of the interaction between CaM-RFP and L-selectin-GFP using FRET/FLIM analysis showed that the S364A mutation blocked the dissociation of CaM from L-selectin during TEM. It is therefore possible that L-selectin shedding would also be blocked by the S364A mutation, as CaM has been shown to bind to L-selectin and inhibit its shedding from the cell surface (215). To test if this was the case, shedding of L-selectin was visualised by Western blot analysis. By using an anti-GFP antibody all bands corresponding to the different cleavage products of L-selectin could be observed as the GFP tag would still be present at the C-terminal. As it is not practically possible to perform Western blot analysis on THP-1 cells under flow conditions, a static assay was developed to overcome this. HUVEC monolayers were grown to confluence in fibronectin-coated six well plates and THP-1 cells were co-cultured with activated monolayers for zero, five, ten, twenty, thirty or sixty minutes. Lysates were prepared from bound and unbound THP-1 cells and used in Western blots to assess the GFP signals derived from full length and cleaved (known as the stump) L-selectin (Figure 6.6). More importantly, this allowed one to closely monitor L-selectin shedding over time. Previous experiments had shown that the anti-GFP antibody did not recognise any components of the HUVEC lysate (Karolina Rzeniewicz, unpublished data), so any signal detected by the anti-GFP antibody would be derived exclusively from the THP-1 cell lysate. THP-1 cells expressing wildtype, S364A- or S367A-L-selectin-GFP were co-cultured with HUVEC monolayers to assess the effect of these mutations on shedding of L-selectin.
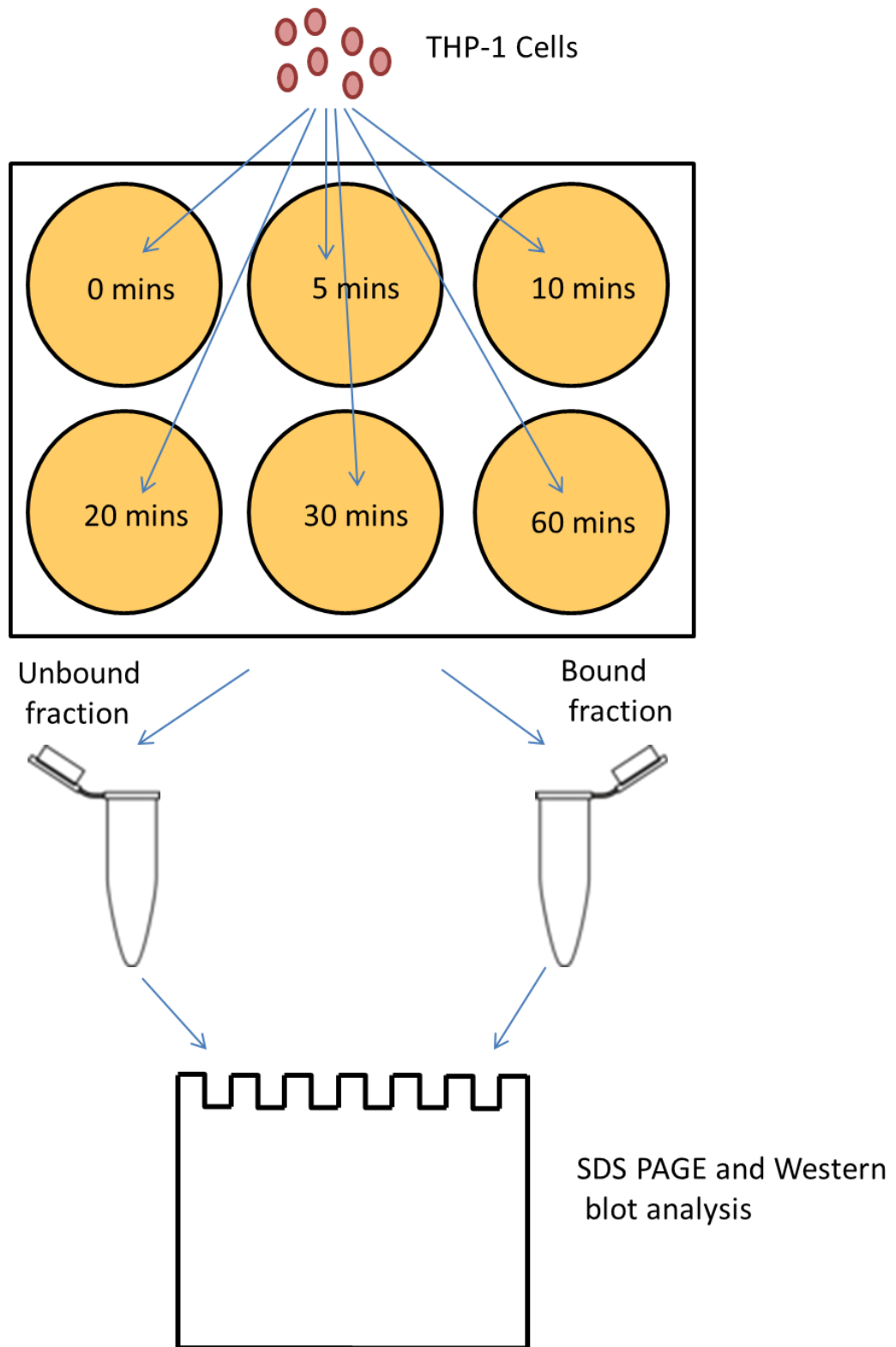
**Figure 6.6: Schematic of THP-1 cell co-culture with TNF-α activated HUVEC experiment.** HUVEC cells were grown in fibronectin-coated six well dishes until confluent. The HUVEC cells were then activated with TNF-α and 0.75 x10$^6$ THP-1 cells were placed in each well of the dish. The THP-1 cells were then incubated with the HUVEC monolayer for the time indicated in each well, after which point the unbound and bound fractions were collected and cell lysates were produced. the cell lysates were then analysed by Western blot, with anti-GFP antibody used to visualise L-selectin-GFP.

261

Analysis of the unbound and bound fractions of THP-1 cells expressing wildtype L-selectin-GFP at the different time points showed that a majority of the cells were bound after five minutes of incubation, with only faint bands corresponding to L-selectin-GFP observed in the unbound fraction after this time point (Figure 6.7A, Left Panel). As maximal THP-1 cell binding to activated HUVEC monolayers was achieved by five minutes of co-culture, all other time points were compared to this as a base line value. In other words, shedding of L-selectin was calculated from a start time of 5 minutes. Signals derived from both the full length and the stump of L-selectin (Figure 6.7A, Right Panel) were assessed at each time point by densitometric analysis (see Materials and Methods, Section 2.16.3).

The results for THP-1 cells expressing wildtype L-selectin-GFP showed that the levels of full length L-selectin did not significantly change over time (Figure 6.7B). The levels of the stump of L-selectin-GFP did increase slightly between five and ten minutes. The level then remained similar between ten and twenty minutes before decreasing between twenty and sixty minutes (Figure 6.7C). However, these changes were not quite significant due to variation between the experiments (one-way Anova p=0.054). It was possible that the downward trend in stump levels observed between twenty and sixty minutes was a result of the stump being cleared from the plasma membrane and degraded (e.g. via an endocytic pathway). This suggested that a majority of shedding occurred between five and twenty minutes, after which time the rate of shedding decreased, possibly returning to basal levels. Since these experiments were performed, members of the Ivetic lab had realised that the anti-GFP antibody used in these experiments had lost their specificity over time. Therefore caution is needed with the interpretation of these results.
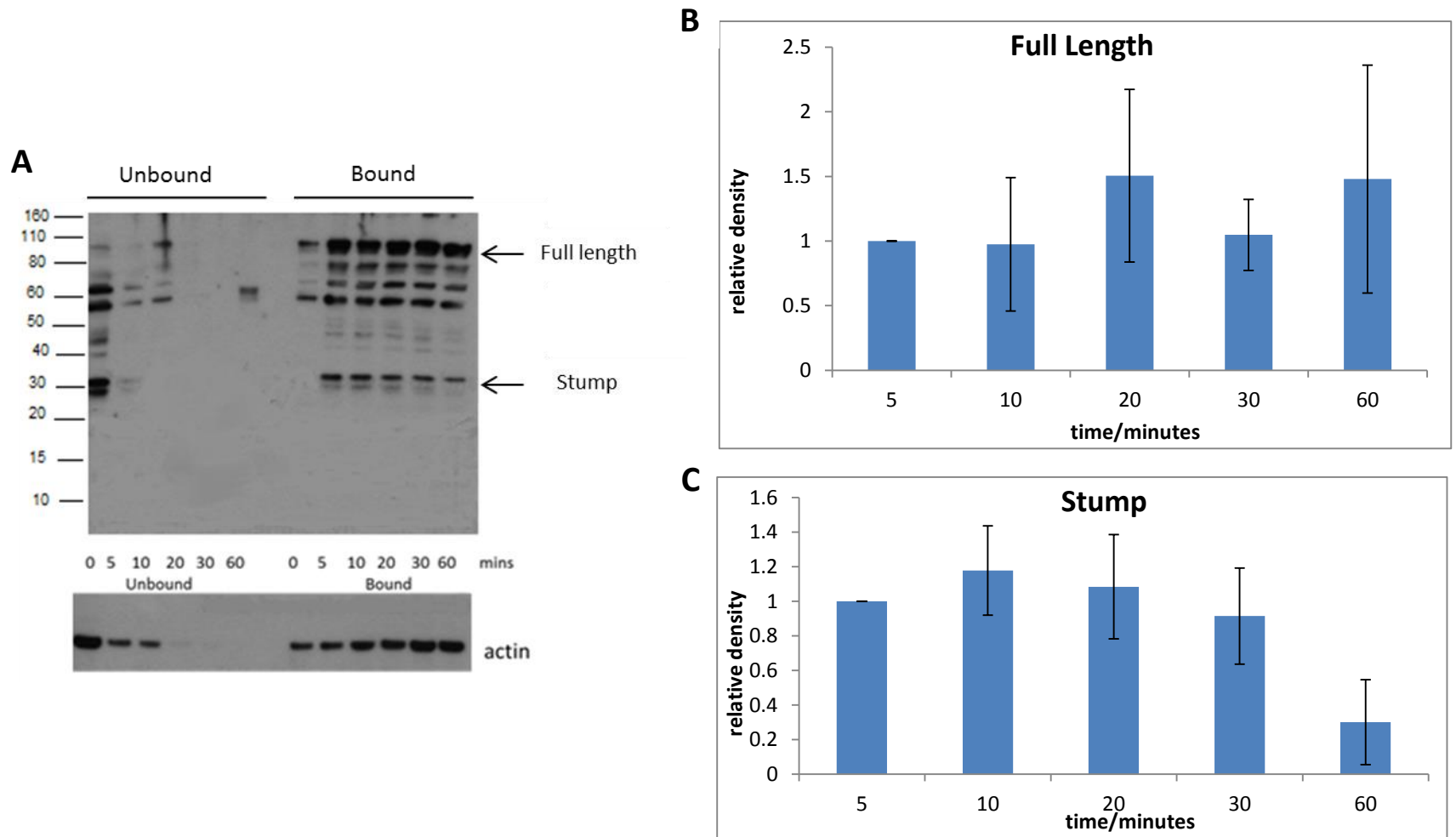
**Figure 6.7: Co-Culture of wildtype L-selectin THP-1 cells with TNF-α activated HUVECs.** (A) Western blot analysis of the levels of L-selectin after co-culture with HUVECs for increasing lengths of time (0 to 60 minutes). The unbound and bound fractions were collected and cell lysates were produced. Western blots were probed with anti-GFP antibody to visualise the different forms of L-selectin. The level of actin at each time point was also assessed for the use as a loading control. Western blot is representative of three independent experiments. Levels of full length (B) and the stump (C) of L-selectin were analysed using densitometric analysis, with actin used as a loading control and all other time points compared relative to five minutes. Results shown are the mean of three experiments with error bars showing the standard deviation. A One-way Annova was used to assess statistical significance.

With the cell line expressing S364A-L-selectin-GFP it was observed that bands corresponding to L-selectin-GFP were visible in the unbound fraction at later time points compared to wildtype L-selectin-GFP cells, with faint bands remaining visible at sixty minutes (Figure 6.8A, Left Panel). As the number of cells added to each well was carefully calculated using a hemocytometer, this suggested that the S364A-L-selectin-GFP cells may bind less efficiently to the HUVEC monolayer than wildtype L-selectin cells. It is possible that this less efficient binding of cells with this mutant may be a result of fewer THP-1 cell protrusions being produced (see Section 6.4.3 for a discussion of this possibility). The L-selectin-GFP signal was similar in all the unbound fractions after ten minutes. For this reason the ten minute time point was used for the base line value of L-selectin-GFP to which all other time points would be compared. As with the wildtype L-selectin-GFP cells, the levels of full length and stump of L-selectin-GFP (Figure 6.8A, Right Panel) were assessed using densitometric analysis.

The levels of full length L-selectin did not change over time with cells expressing S364A-L-selectin-GFP (Figure 6.8B), similarly to the observation made with cells expressing wildtype L-selectin-GFP. Analysis of the level of L-selectin stump formation in cells expressing S364A-L-selectin-GFP showed there was little change in the levels of the stump over time (Figure 6.8C). This was a variation from the change in stump levels observed with THP-1 cells expressing wildtype L-selectin-GFP, which showed a slight increase between five and ten minutes and a decrease in formation of the stump after twenty minutes. As the level of the stump did not change with the S364A-L-selectin-GFP cell line, this suggested that mutation of S364 (to block selective phosphorylation at this site) reduced the extent of L-selectin shedding upon cell activation observed in THP-1 cells expressing wildtype L-selectin-GFP.

THP-1 cells expressing S367A-L-selectin-GFP were also analysed under similar conditions. Western blot analysis revealed that L-selectin-GFP was detected in the unbound fraction after five minutes of co-culture with HUVEC (Figure 6.9A, Left panel), suggesting a good proportion of THP-1 cells remained unbound at this time point. As with S364A-L-selectin-GFP cells, this may be because fewer

protrusions are produced with these cells, meaning they are easier to dissociate from the membrane (Section 6.3.6.3.5). After ten minutes the anti-GFP signal in the unbound fraction had decreased. This indicated that a majority of the THP-1 cells had bound to the HUVEC monolayer by this time point. Based on this, it was decided that the ten minute time point would be used as the baseline level of L-selectin-GFP to which all other time points could be compared. Densitometric analysis was used to compare the changes in the protein levels of full length and the stump of L-selectin-GFP during co-culture with activated HUVEC monolayer (Figure 6.9A, Right Panel). The results showed that the levels of full length L-selectin tended to increase as the time the cells were co-cultured with HUVECs progressed, with the anti-GFP signal at sixty minutes being significantly higher than that at five and ten minutes (Figure 6.9B). The trend in increase in the level of full length L-selectin observed with THP-1 cells expressing S367A-L-selectin-GFP was potentially different from the results observed with wildtype L-selectin-GFP, but, due to the large error bars produced by variation in the experiments, it was unclear if this was significant. The level of the stump with cells expressing S367A-L-selectin-GFP tended to increase up to twenty minutes, followed by a decrease between twenty and sixty minutes, although this was not significant, again due to the variation between experiments (Figure 6.9C). This trend was very similar to that observed with wildtype L-selectin-GFP. Taken together these results imply that the rate of shedding of S367A-L-selectin-GFP followed a similar trend to that observed with wildtype L-selectin-GFP, but due to the variation between the experiments, and the quality of the anti-GFP antibody, it was unclear if this mutation did have an effect on the rate of shedding.
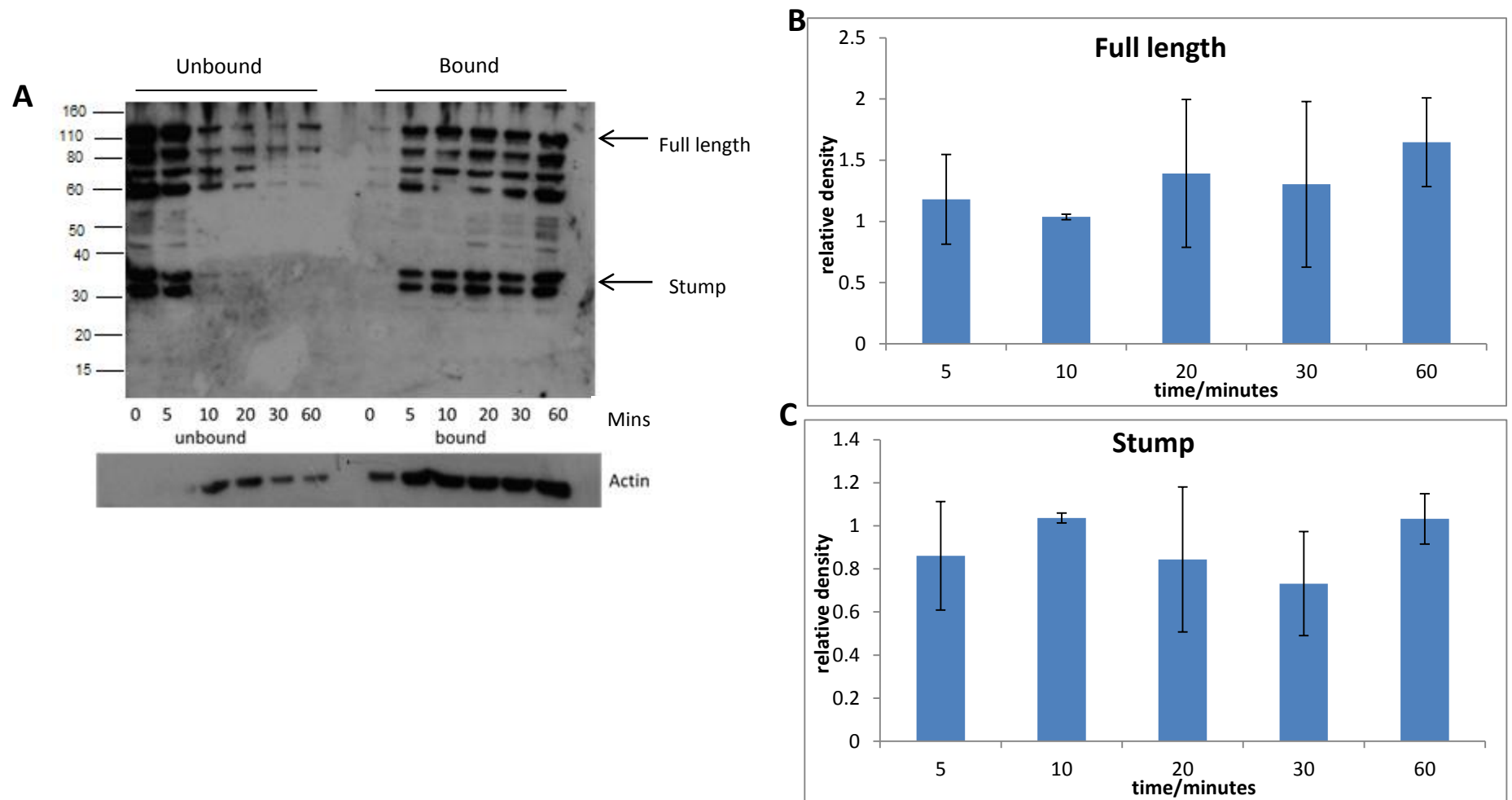
**Figure 6.8: Co-Culture of S364A-L-selectin-GFP THP-1 cells with activated HUVECs.** (A) A Western blot representing the levels of full length and the stump of L-selectin-GFP after co-culture with HUVECs for increasing lengths of time, from 0 to 60 minutes. At each time point the unbound and bound fractions were collected and cell lysates were produced. The Western Blot was probed with anti-GFP antibody to assess the levels of L-selectin-GFP and the level of actin was assessed to use as a loading control. The levels of full length (B) and the stump (C) of L-selectin were assessed using densitometric analysis with actin used as a loading control to normalise variation. The levels of both full length and the stump of L-selectin in the bound fraction at all the time points were compared to the levels at ten minutes, where the majority of THP-1 cells bound to the endothelium. Results shown are the mean of three experiments with error bars showing the standard deviation. Statistical analysis was carried out using a one-way Anova.

266
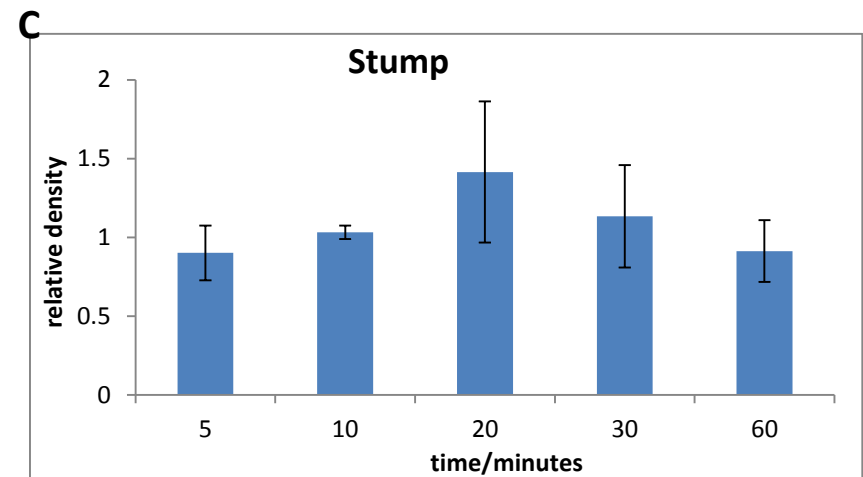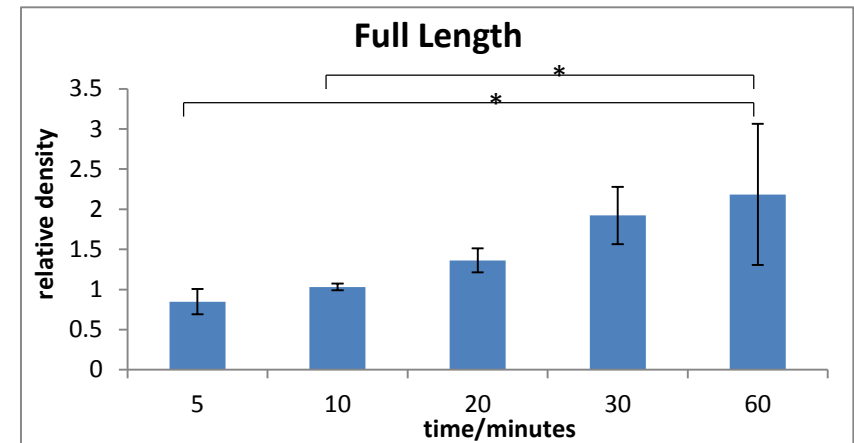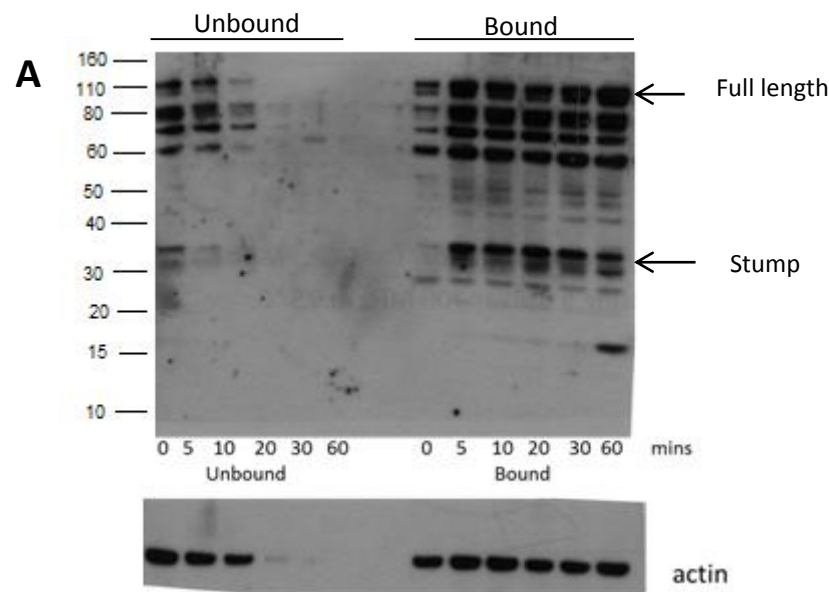
**Figure 6.9: Co-Culture of S367A-L-selectin-GFP THP-1 cells with activated HUVECs.** THP-1 cells expressing S367A-L-selectin-GFP were after co-cultured with HUVECs for increasing lengths of time (0 to 60 minutes). The unbound and bound cells were then collected and cell lysates were produced. The levels of L-selectin-GFP were analysed by Western blot (A). The blot is representative of three independent experiments. Levels of full length (B) and the stump (C) of L-selectin were analysed by densitometric analysis using actin as a loading control and comparing the levels at all other time points to those at ten minutes. Results shown are the mean of three experiments with error bars showing the standard deviation. Statistical significance was analysed using one-way Anova followed by Tukey's post-hoc test. * represents results that are significantly different, $p < 0.05$.

267

### 6.3.6 Analysing the role of the L-selectin tail in regulating cell morphological changes during TEM under flow conditions.

Once leukocytes exit the circulation and enter the surrounding microenvironment, directionality becomes an important determinant in how efficiently they undergo chemotaxis towards an inflammatory insult. Chemokines are released by stromal cells surrounding a site of inflammation and act as essential soluble guidance cues for leukocyte migration towards any given inflammatory insult (460,461). Glycans, such as heparan sulphate proteoglycans (HSPGs) that decorate extracellular matrix proteins, provide an appropriate scaffold for chemokine immobilisation (153). These immobilised chemokines will provide a gradient that can be sensed by the emigrated leukocyte (462,463). The receptors for chemokines are located at the cell's leading edge (463-466), which facilitates directional migration. Previous reports have shown that antibody or ligand-induced clustering of L-selectin promotes the surface expression of chemokine receptors (208,209,467,468). This suggests that L-selectin engagement is a pre-requisite for chemokine expression in some leukocytes. Another report showed that clustering of L-selectin on naïve T-cells increases cell responsiveness to chemokines *in vivo*, but does not affect the overall expression of the chemokine receptor at the cell surface (208). Interestingly, blocking the shedding of L-selectin in mice through the generation of a "sheddase-resistant" L-selectin knock-in mutation dramatically affected chemotaxis (123), although the mechanism underlying this observation is not fully understood. Although these reports would suggest that shedding forms an important mechanism in sensing chemokine gradients and possibly directionality, collectively they are disjointed – as these studies are derived from different research labs that ask rather specific questions. In respect of this thesis chapter, it was of interest to understand: (a) whether L-selectin shedding contributes to cell shape change during TEM, and (b) whether the cytoplasmic tail of L-selectin is a key regulatory domain of such responses.

Wide field fluorescence time-lapse microscopy of THP-1 cells undergoing TEM under flow conditions revealed distinct morphological changes as recruitment progressed towards eventual TEM. To assess if mutating L-selectin affected cell shape change during TEM, three different parameters were measured during recruitment:

(i)     Cell area

(ii)     Cell circularity

(iii)    Protrusion number

These characteristics were chosen as they provide information about the dynamic nature of the cells during TEM. By measuring cell area, information about how far the cell spreads during TEM could be obtained. The circularity provides information about how polarised the cell becomes during TEM. The number of protrusions provides information about the cell's "invasiveness" (i.e. the more pseudopods that protrude beneath the endothelium, the more invasive the cell is) and priming directionality of migration during chemotaxis; one protrusion would show clear directionality whereas multiple protrusions would show a lack of directionality. Digital videos obtained during each flow assay were analysed to monitor these parameters at an early time point of seven minutes, a middle time point of fifteen minutes and a late time point of twenty five minutes to determine how they changed over time.

### 6.3.6.1 Analysis of Cell Area

The area of the cell was measured using ImageJ software to draw around the perimeter of the cell, including the protrusions, and calculating the area of the shape produced (Figure 6.10). Cells expressing mutated forms of L-selectin were directly compared to cells expressing wildtype L-selectin-GFP to decipher whether mutating L-selectin affected the area of the cell during recruitment.
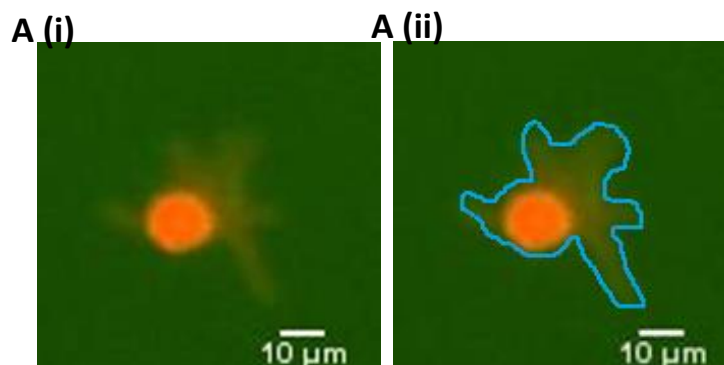


**Figure 6.10: Analysis of cell area.** Images of cells from the flow chamber assay were opened with ImageJ for the measurement of the cell area. A (i) shows the initial image and A (ii) shows the image with the outline of the cell shown in blue.

When the area of cells expressing ΔM-N-L-selectin-GFP were compared to those expressing wildtype L-selectin-GFP, the results showed that there was no significant difference in cell area between these cell lines after seven minutes of recruitment (Figure 6.11A). However, after fifteen minutes, cells expressing ΔM-N-L-selectin-GFP were significantly larger in area than those expressing wildtype L-selectin-GFP (with a cell area of 1088±21.1 arbitrary units (AU) for ΔM-N versus a cell area of 984±47.9 AU for wildtype, Figure 6.11B). This difference became more significant by twenty five minutes (Figure 6.11C). This highlights the fact that as recruitment of THP-1 cells progressed, cells expressing the sheddase-resistant form of L-selectin become larger in area, implying they had spread further.
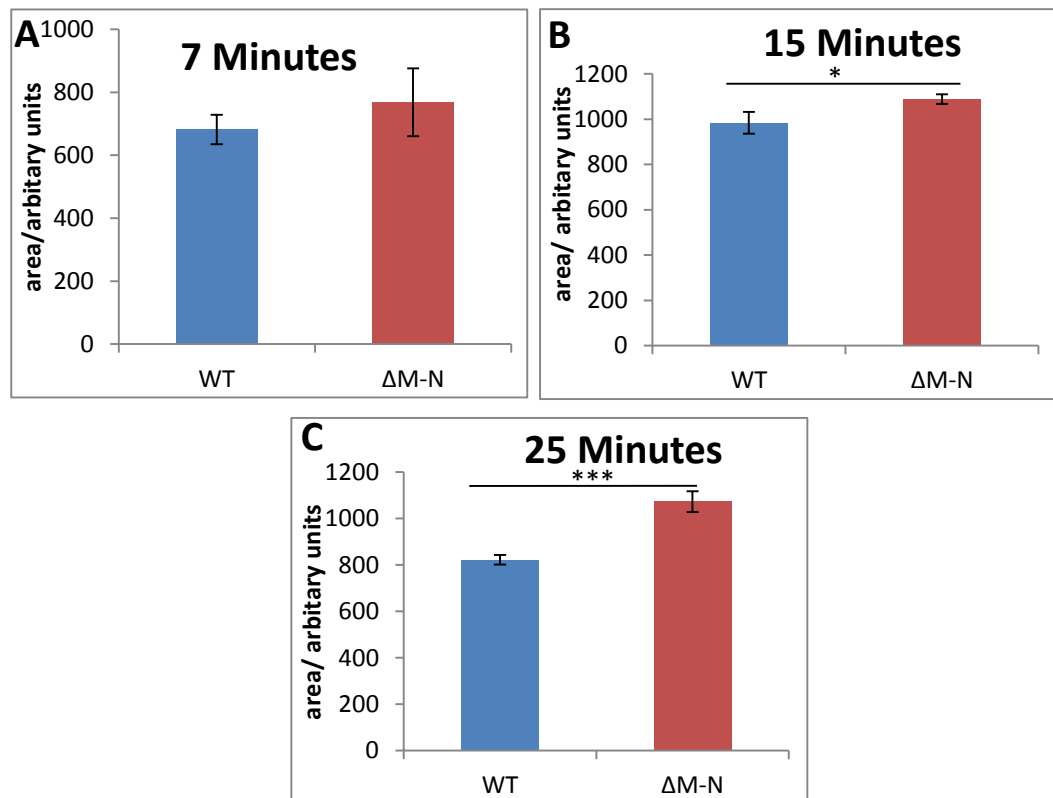


**Figure 6.11: Cell area of THP-1 cells expressing either wildtype or ΔM-N-L-selectin-GFP during TEM under flow conditions.** The cell area was calculated using ImageJ for THP-1 cell lines expressing either wildtype or ΔM-N-L-selectin-GFP undergoing recruitment at seven minutes (A), fifteen minutes (B) and twenty five minutes (C). For each experiment three fields of view were analysed and between 10 and 40 cells per field of view were measured. Results shown are the mean of three experiments with standard deviation as error bars. An independent two-tailed Student's t test was used to assess statistical significance. *=p<0.05, ***=p<0.005.

Cells expressing the S364A mutant form of L-selectin-GFP were compared to cells expressing wildtype L-selectin-GFP to decipher if this mutant affected the area of the cell during recruitment. After seven minutes recruitment cells expressing S364A-L-selectin-GFP were significantly larger in area than those expressing wildtype L-selectin-GFP (an area of 833±48 AU for S364A compared to an area of 681±46.3 AU for wildtype, Figure 6.12A)). However, after fifteen (Figure 6.12B) and twenty five minutes (Figure 6.12C) of recruitment there was no significant difference between the area of cells expressing S364A-L-selectin-GFP and wildtype L-selectin-GFP. This suggested that at early stages of recruitment THP-1 cells expressing S364A-L-selctin-GFP were more spread than those expressing wildtype L-selectin-GFP. However, at later stages of TEM both cell lines were spread to a similar extent.
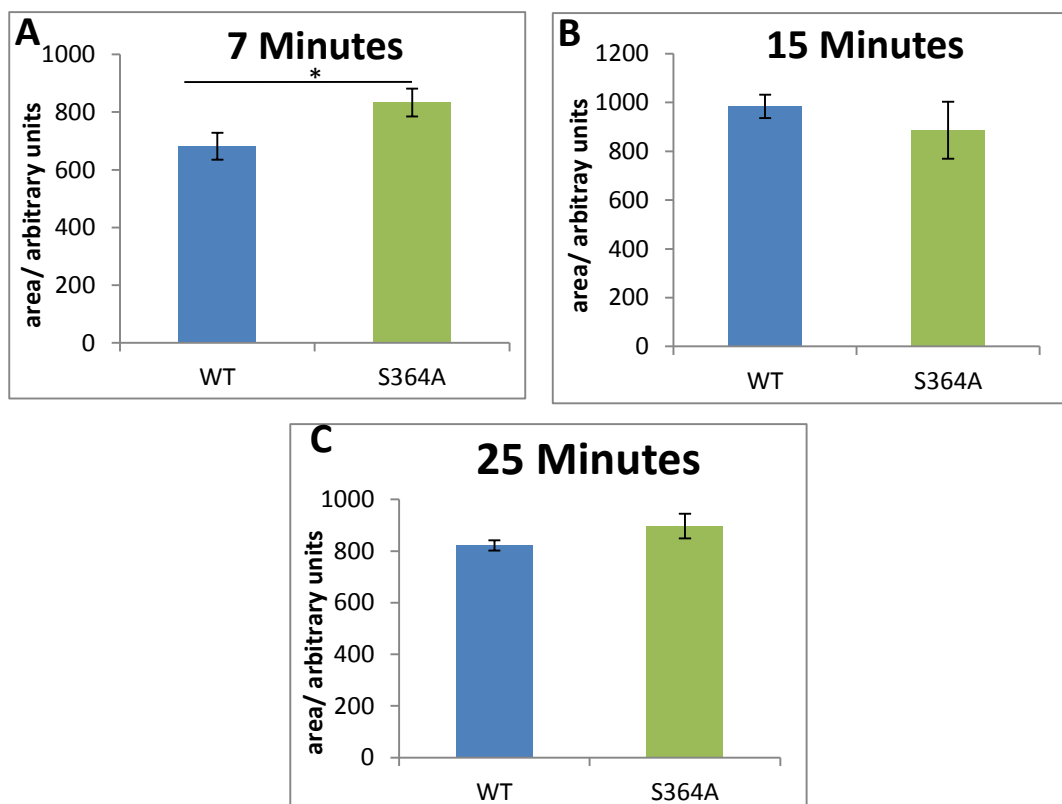


**Figure 6.12: Cell area of THP-1 cells expressing either wildtype or S364A-L-selectin-GFP during TEM under flow.** ImageJ software was used to calculate the cell area of THP-1 cell lines expressing either wildtype or S364A-L-selectin-GFP undergoing TEM at seven minutes (A), fifteen minutes (B) and twenty five minutes (C). Three fields of view were analysed for each experiment, with between 10 and 40 cells per field of view were measured. Results shown are the mean of three independent experiments with error bars representing the standard deviation. An independent two-tailed Student's t test was used to assess statistical significance. *=p<0.05.

Next, the area of THP-1 cells expressing S367A-L-selectin-GFP was compared to wildtype L-selectin-GFP cells. After seven minutes of flow, cells expressing wildtype L-selectin-GFP had a significantly greater area than those expressing S367A-L-selectin-GFP (an area of 681±46.3 AU and 536±21.4 AU respectively, Figure 6.13A). This difference became more significant after fifteen minutes of TEM (Figure 6.13B). However, after twenty five minutes of flow both cell lines had a similar area (821±20.11 AU for wildtype and 759±46.6 AU for S367A, Figure 6.13C). This would suggest that at early stages of recruitment cells expressing S367A-L-selectin-GFP were smaller than wildtype L-selectin-GFP and therefore less spread. Interestingly, as TEM progressed both cell lines were equally spread.
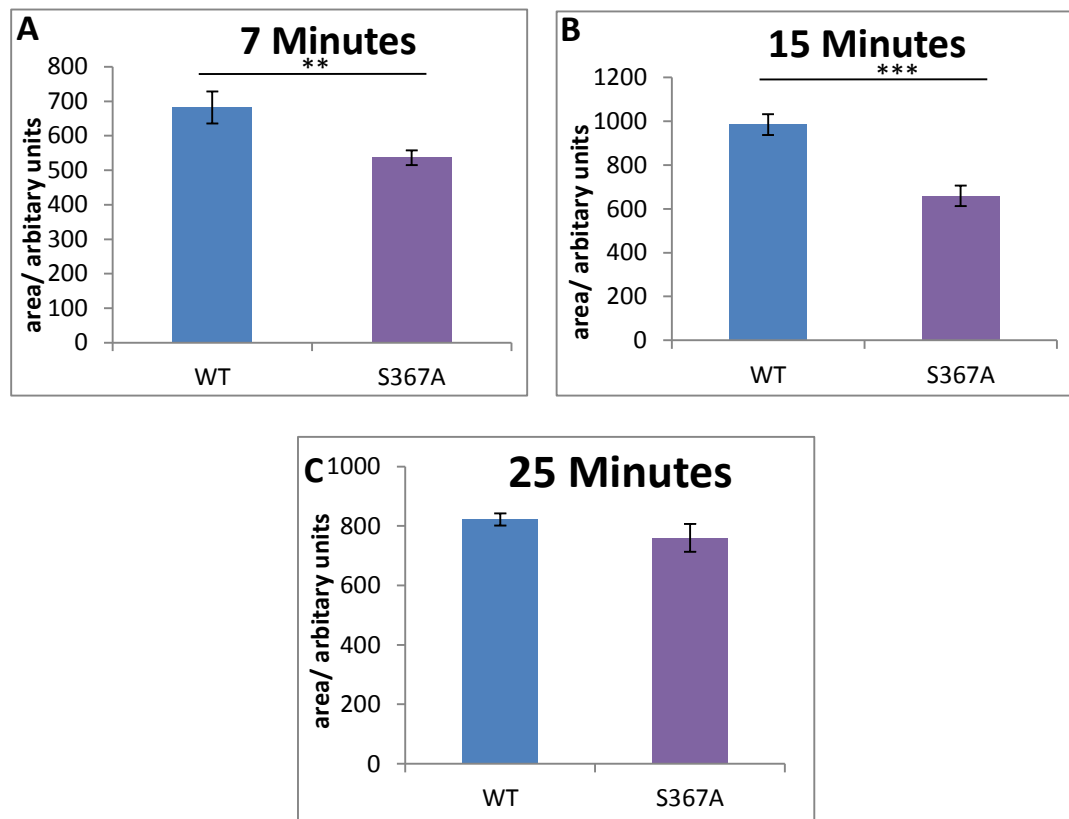


**Figure 6.13: Cell area of THP-1 cells expressing either wildtype or S367A-L-selectin-GFP during TEM under flow conditions.** The cell area of THP-1 cell lines expressing either wildtype or S367A-L-selectin-GFP undergoing TEM at seven minutes (A), fifteen minutes (B) and twenty five minutes (C) was calculated using ImageJ. For each experiment three fields of view were analysed and between 10 and 40 cells per field of view were measured. Results shown are the mean of three experiments with standard deviation as error bars. An independent two-tailed Student's t test was used to assess statistical significance. *=p<0.05, ***=p<0.005.

Cells expressing SSAA-L-selectin-GFP were next compared to cells expressing wildtype L-selectin-GFP cells during TEM. After seven minutes of flow, cells expressing wildtype L-selectin-GFP had a significantly greater area than cells expressing SSAA-L-selectin-GFP (681±46.3 AU and 488±54.3 AU respectively, Figure 6.14A). The same result was also observed after fifteen minutes (Figure 6.14B). Analysis after twenty five minutes of TEM revealed that the cell area of both cell lines was similar (Figure 6.14C). This analysis suggests that at early stages of recruitment cells expressing SSAA-L-selectin-GFP spread less than wildtype L-selectin-GFP cells, but at the later stages of recruitment both cell lines spread to a similar degree. The phenotype displayed by the SSAA L-selectin-GFP-expressing cells was most similar to the S367A-expressing cells.



**Figure 6.14: Cell area of THP-1 cells expressing either wildtype or SSAA-L-selectin-GFP during TEM under flow conditions.** During TEM the cell area was calculated at seven minutes (A), fifteen minutes (B) and twenty five minutes (C) for THP-1 cell lines expressing either wildtype or SSAA-L-selectin-GFP using ImageJ software. For each experiment three fields of view were analysed and between 10 and 40 cells per field of view were measured. Results shown are the average of three experiments with standard deviation as error bars. An independent two-tailed Student's t test was used to assess statistical significance. *=p<0.05, ***=p<0.005.

The change in cell area over time was analysed in the different cell lines to assess how cell spreading altered during the progression of recruitment. Cells expressing wildtype L-selectin-GFP increased in area significantly between seven and fifteen minutes, but the area significantly decreased between fifteen and twenty five minutes (Figure 6.15A). This suggested that between seven and fifteen minutes the cells were spreading and sending out protrusions, but between fifteen and twenty five minutes the protrusions were being retracted, leading to a decrease in the spread area. From these results, it seems that the altered CaM/L-selectin interaction, and therefore shedding, could be a driver for these observed changes in spreading.

THP-1 cells expressing ΔM-N-L-selectin-GFP had the same pattern of change in cell area as wildtype L-selectin-GFP cells between seven and fifteen minutes, with an increase in the cell area observed. However, between fifteen and twenty five minutes the cell area of ΔM-N-L-selectin-GFP cells did not change (Figure 6.15B), showing that the protrusions were not retracted, as they appear to be with cells expressing wildtype L-selectin-GFP.

Analysis of the cell area of THP-1 cells expressing S364A-L-selectin-GFP showed that there was no change in cell area as time progressed (Figure 6.15C). This shows a clear difference from the results observed with wildtype L-selectin-GFP cells, where the cell area fluctuated over time.

Both S367A-L-selectin-GFP (Figure 6.15D) and SSAA-L-selectin-GFP (Figure 6.15E) were smaller in area than wildtype L-selectin-GFP cells at seven minutes. The cell area significantly increased between seven and fifteen minutes, but not to the same extent as wildtype L-selectin-GFP cells. Between fifteen and twenty five minutes, the spread area of the S367A-L-selectin-GFP and SSAA-L-selectin-GFP cell lines showed a slight increase, with a cell area similar to that seen in wildtype L-selectin-GFP cells at this time point. This data suggested that S367A- and SSAA-L-selectin-GFP cells spread at a slower rate than wildtype L-selectin cells and did not spread as far during the TEM. It also suggests that the overall phenotype of the SSAA L-selectin was most similar to S367A, and not S364A.
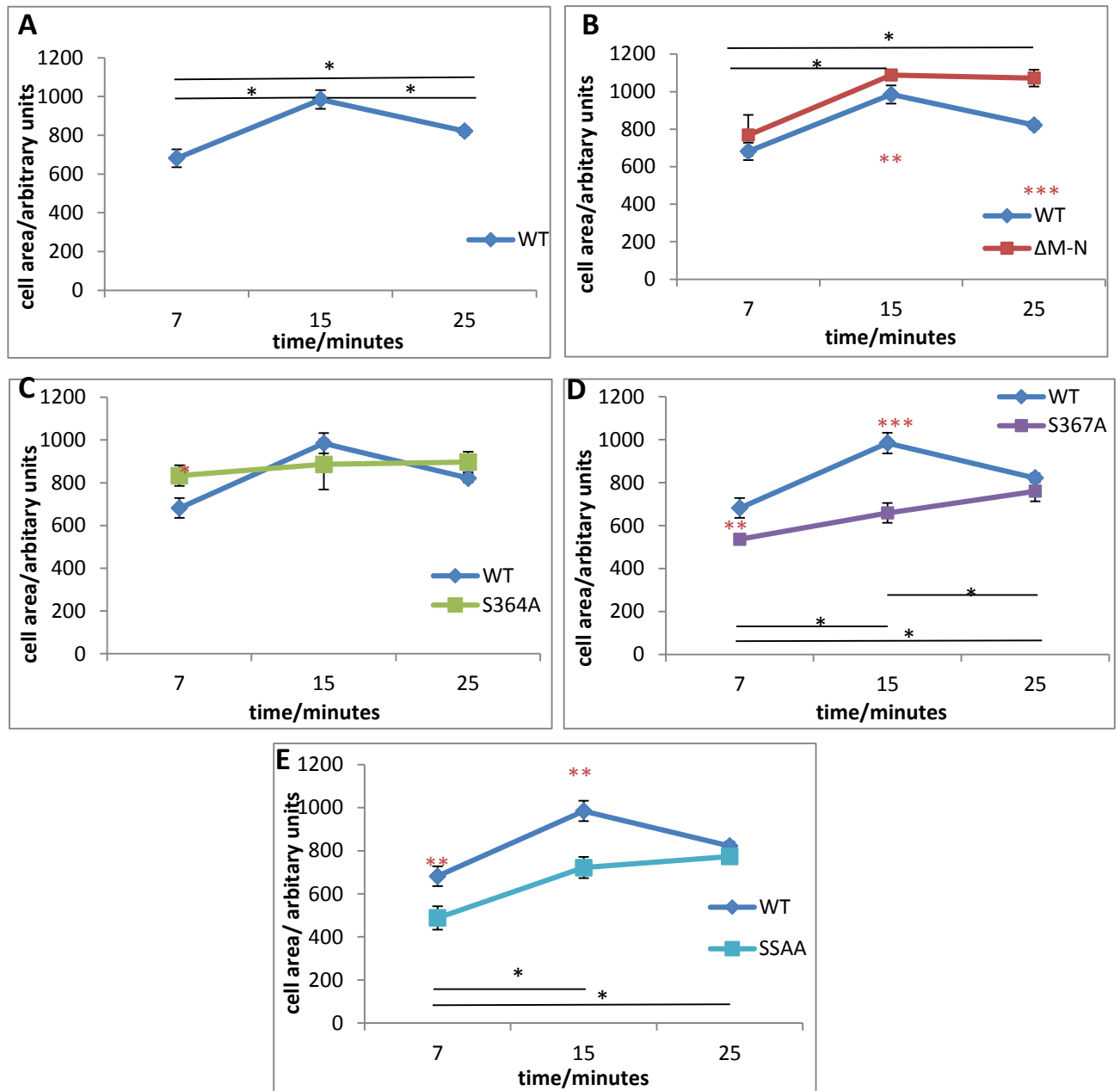
**Figure 6.15: Analysis of the change in cell area during TEM under flow conditions.** (A) The area of THP-1 cells expressing wildtype L-selectin-GFP was analysed over time during recruitment. The change in cell area over time was then analysed for each of the mutant cell lines and compared to the results for cells expressing wildtype L-selectin-GFP ((B) shows the results for ΔM-N, (C) shows the results for S364A, (D) shows the results for S367A and (E) shows the results for SSAA). For each experiment three fields of view were analysed and between 10 and 40 cells per field of view were measured. Results shown are the mean of three experiments with standard deviation as error bars. Statistical significance between the cell area at each time point was assessed for each cell line using a One-way Annova followed by Tukey's post hoc test (shown in black) and an independent two-tailed Student's t test was used to assess statistical significance between wildtype and mutant cell lines at each time point (shown in red). *=$p<0.05$, **=$p<0.01$, ***=$p<0.005$.

### 6.3.6.2 Analysis of Cell Circularity

The circularity of the THP-1 cells during recruitment was assessed using the same images as above, with ImageJ software used for the calculation of circularity. Circularity was assessed to decipher whether there was a link between the changes in cell area observed above and a decrease in circularity, suggesting the cells were sending out protrusions and becoming more polarised – rather than adopting a "fried egg" morphology. Circularity was calculated using the formula: $4\pi\left(area \div perimeter^2\right)$ and was measured on a scale between zero and one, with one being a perfect circle and the number decreasing towards zero as the shape becomes more elongated. As with cell area, the circularity was assessed after seven, fifteen and twenty five minutes of recruitment in the different cell lines, with each mutant being compared to the results for cell expressing wildtype L-selectin-GFP. Moreover, changes in circularity will allow monitoring of dynamic changes in circularity over time between cell lines.

The results comparing the circularity of cells expressing ΔM-N-L-selectin-GFP to those expressing wildtype L-selectin-GFP showed that there was no significant difference in the circularity between the different cell lines after seven (Figure 6.16A), fifteen (Figure 6.16B) and twenty five minutes (Figure 6.16C) of recruitment. This suggested that both cell lines became polarised following binding to the endothelium.
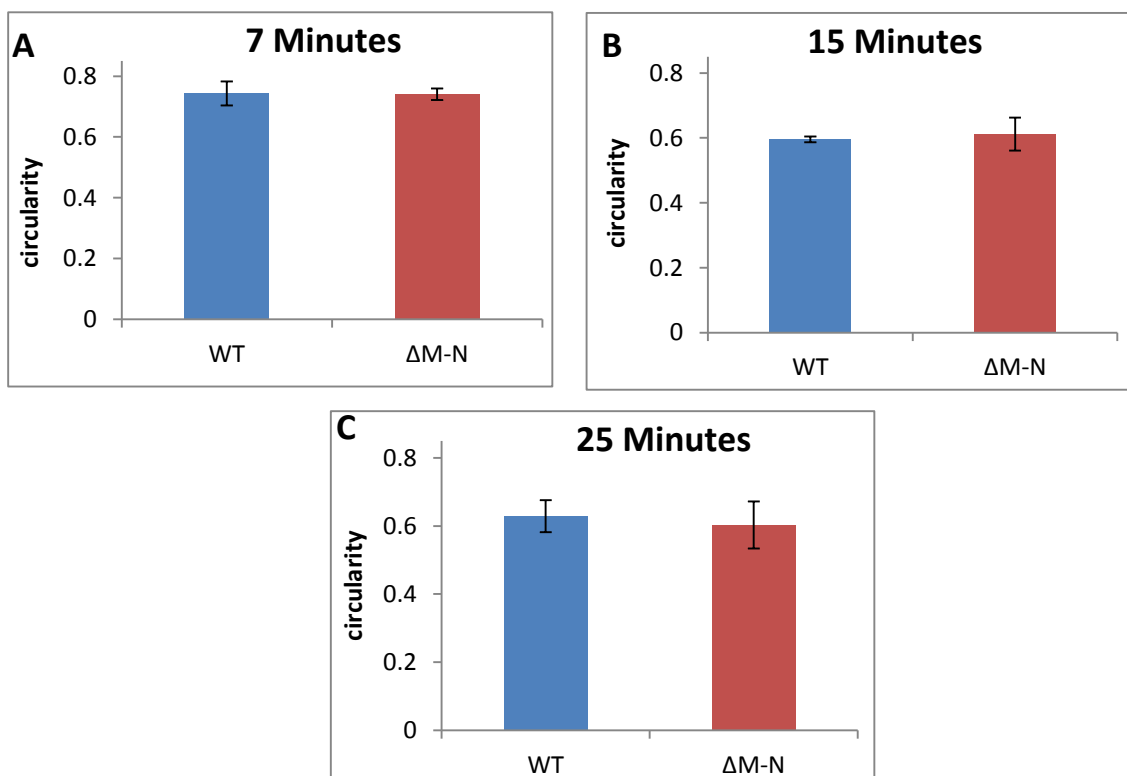
**Figure 6.16: Circularity of THP-1 cells expressing either wildtype or ΔM-N-L-selectin-GFP during recruitment under flow.** The circularity was calculated using ImageJ for THP-1 cell lines expressing either wildtype or ΔM-N-L-selectin-GFP undergoing recruitment at seven minutes (A), fifteen minutes (B) and twenty five minutes (C). For each experiment three fields of view were analysed and between 10 and 40 cells per field of view were measured. Results shown are the mean of three experiments with standard deviation as error bars. An independent two-tailed Student's t test was used to assess statistical significance.

The circularity of cells expressing S364A-L-selectin-GFP was compared to cells expressing wildtype L-selectin-GFP. The results showed that at seven minutes there was no significant difference in the circularity of the cell lines (Figure 6.17A). After fifteen minutes of recruitment, cells expressing S364A-L-selectin-GFP tended to remain more circular than those expressing wildtype L-selectin-GFP, but this was not significant (Figure 6.17B). This was also the case after twenty five minutes of flow (Figure 6.17C). Altogether, these results imply that there was little difference in the circularity between these cell lines, though cell expressing S364A-L-selectin-GFP tended to be more circular as TEM progressed.
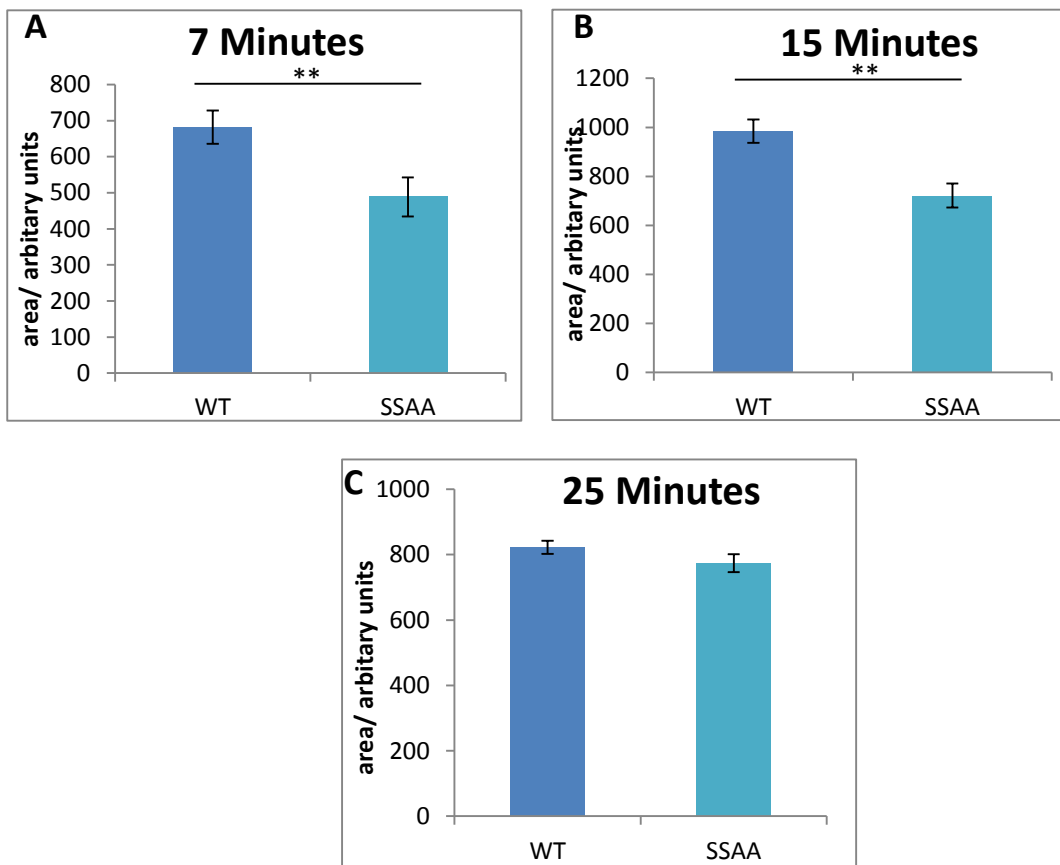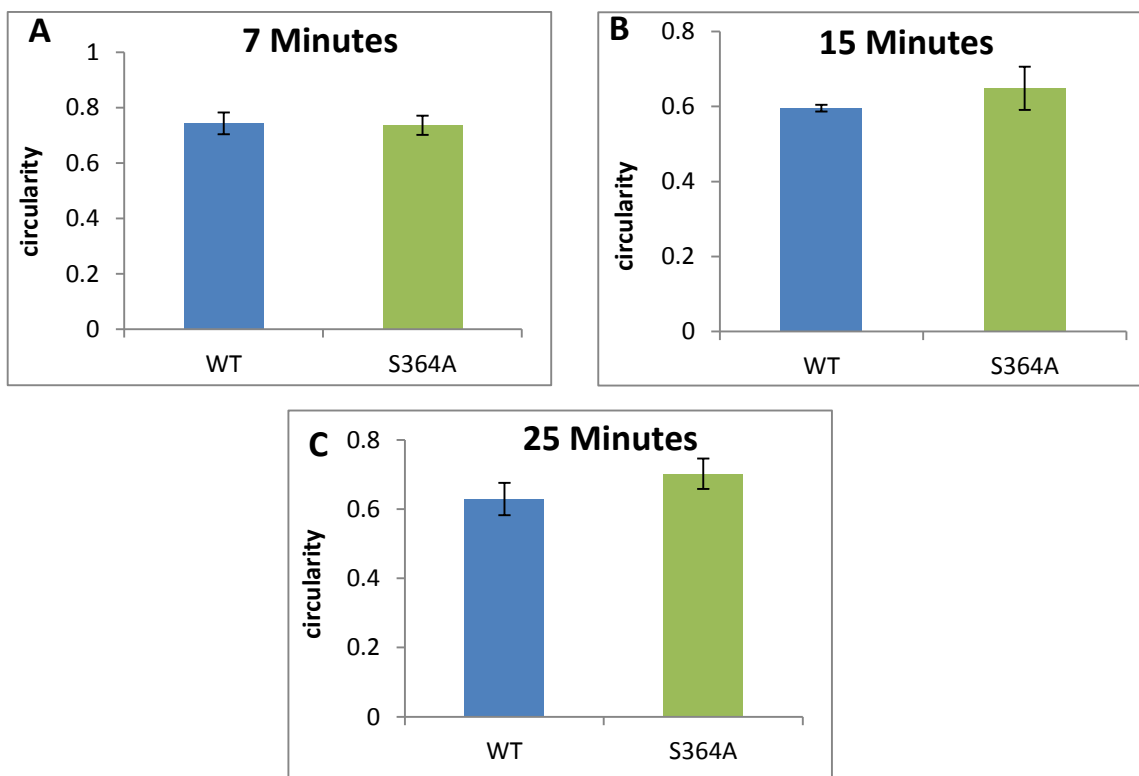


**Figure 6.17: Circularity of THP-1 cells expressing either wildtype or S364A-L-selectin-GFP during TEM under flow conditions.** ImageJ software was used to calculate the circularity of THP-1 cell lines expressing either wildtype or S364A-L-selectin-GFP undergoing TEM at seven minutes (A), fifteen minutes (B) and twenty five minutes (C). For each independent experiment three fields of view were analysed and between 10 and 40 cells per field of view were measured. Results shown are the mean of three experiments with error bars representing the standard deviation. An independent two-tailed Student's t test was used to assess statistical significance.

277

When the circularity of cells expressing S367A-L-selectin-GFP was compared to cells expressing wildtype L-selectin-GFP the results showed that after seven minutes of recruitment S367A-L-selectin-GFP cells were significantly more circular in nature than wildtype L-selectin-GFP cells ($0.814\pm0.012$ versus $0.734\pm0.040$, Figure 6.18A). S367A-L-selectin-GFP cells were also significantly more circular than wildtype L-selectin-GFP cells after fifteen (Figure 6.18B) and twenty five minutes (Figure 6.18C) of recruitment. This shows that cells expressing S367A-L-selectin-GFP generally lacked the ability to become elongated during TEM.
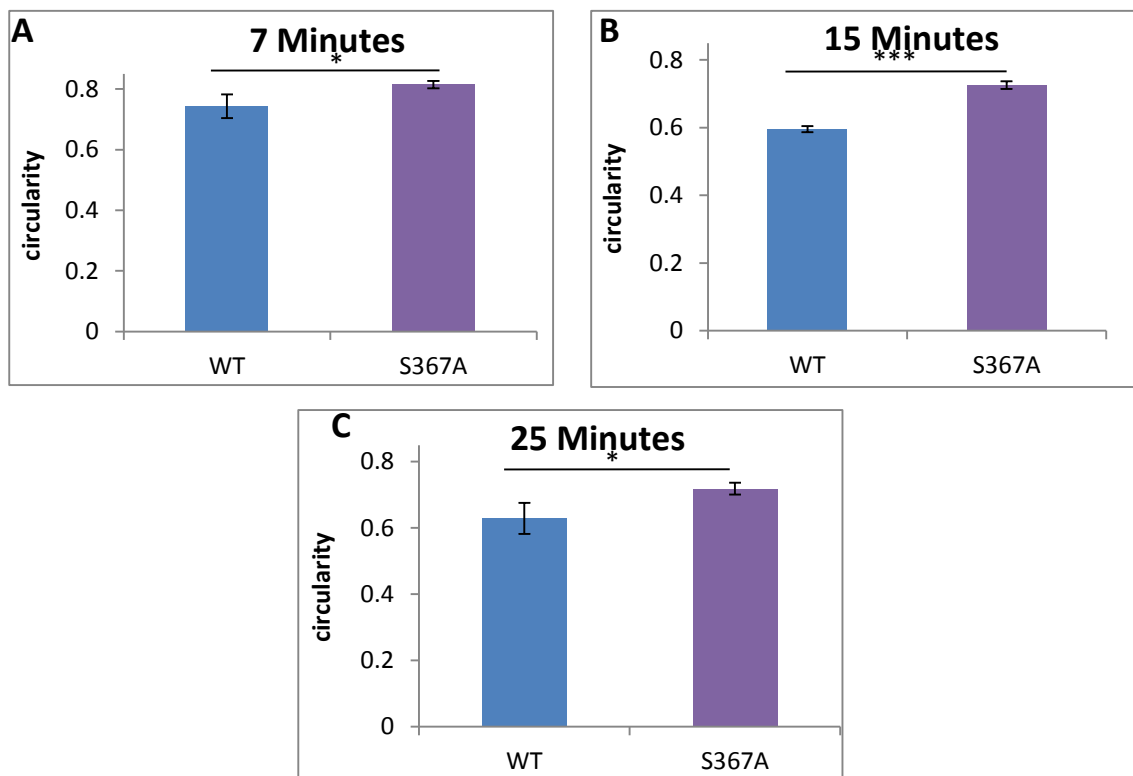


**Figure 6.18: Circularity of THP-1 cells expressing either wildtype or S367A-L-selectin-GFP during TEM under flow.** The circularity of THP-1 cell lines expressing either wildtype or S367A-L-selectin-GFP was calculated using ImageJ after seven minutes (A), fifteen minutes (B) and twenty five minutes (C) of flow. Three fields of view were analysed for each experiment, with between 10 and 40 cells per field of view being measured. Results shown are the mean of three experiments with standard deviation as error bars. An independent two-tailed Student's t test was used to assess statistical significance. *=$p<0.05$, ***=$p<0.005$.

The same analysis as above was carried with cells expressing SSAA-L-selectin-GFP. When the circularity of these cells was compared to that of cells expressing wildtype L-selectin-GFP, after seven minutes of recruitment there was no significant difference in the circularity of either cell line (Figure 6.19A). The results after fifteen minutes of recruitment showed the circularity of cells expressing SSAA-L-selectin-GFP was significantly greater than that of cells expressing wildtype L-selectin-GFP ($0.703\pm0.015$ for SSAA compared to $0.596\pm0.009$ for wildtype, Figure 6.19B). This was also observed after twenty five minutes of recruitment ($0.714\pm0.023$ versus $0.629\pm0.047$, Figure 6.19C). These results showed that during recruitment, cells expressing SSAA-L-selectin-GFP were more circular and less spread than cells expressing wildtype L-selectin-GFP. As with the cell area results, the circularity phenotype of the SSAA L-selectin-expressing cells sided with the S367A L-selectin-expressing cells.
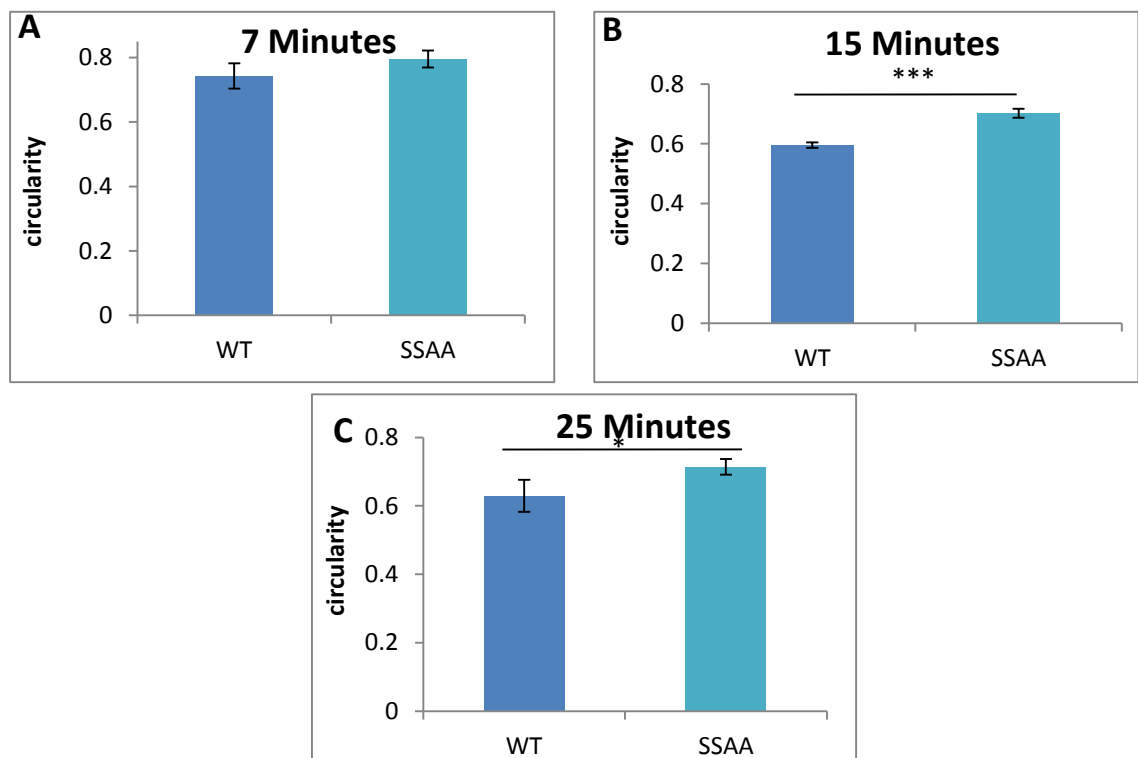


**Figure 6.19: Circularity of THP-1 cells expressing either wildtype or SSAA-L-selectin-GFP during recruitment under flow conditions.** The circularity of cells was calculated using ImageJ for THP-1 cell lines expressing either wildtype or SSAA-L-selectin-GFP undergoing recruitment at seven minutes (A), fifteen minutes (B) and twenty five minutes (C). For each experiment three fields of view were analysed and between 10 and 40 cells per field of view were measured. Results shown are the means of three experiments with standard deviation as error bars. An independent two-tailed Student's t test was used to assess statistical significance. *=$p<0.05$, ***=$p<0.005$.

As with cell area (Figure 6.15), the circularity over time was assessed for each cell line to analyse how it changed as recruitment progressed. The circularity of cells expressing wildtype L-selectin-GFP decreased between seven and fifteen minutes of recruitment. After twenty five minutes of recruitment the circularity remained significantly less than that observed at seven minutes (Figure 6.20A).

Cells expressing ΔM-N-L-selectin-GFP showed a similar dynamic profile of circularity change during recruitment as wildtype L-selectin-GFP, with the circularity decreasing between seven and fifteen minutes and remaining low (approx. 0.6) between fifteen and twenty five minutes (Figure 6.20B).

The results for cells expressing S364A-L-selectin-GFP showed no significant difference in the circularity of the cells between the time points analysed (Figure 6.20C). Analysis of cells expressing S367A-L-selectin-GFP revealed that the circularity decreased between seven and fifteen minutes, but to a lesser extent than wildtype-L-selectin-GFP cells (Figure 6.20D). A similar result was also observed with the SSAA-L-selectin-GFP cell line (Figure 6.20E). These results show that with wildtype L-selectin-GFP cells, as recruitment proceeds, the cells become less circular. However, mutating L-selectin affected this, with the mutants S367A- and SSAA-L-selectin-GFP, remaining more circular than wildtype cells and the S364A-L-selectin-GFP mutant causing no change in the circularity as recruitment progressed.
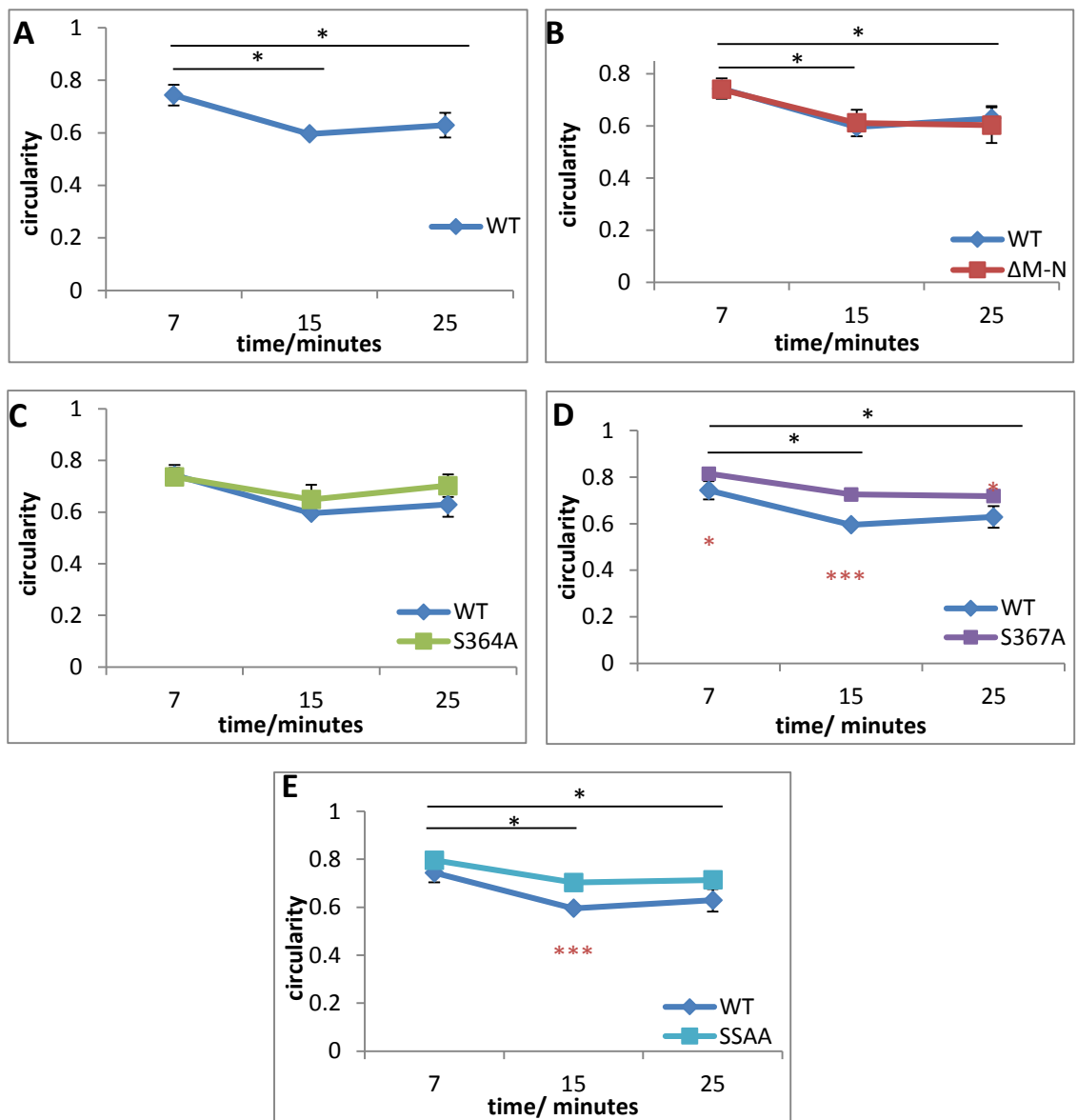
**Figure 6.20: Analysis of the change in cell circularity during THP-1 recruitment under flow conditions.** (A) The circularity of cells expressing wildtype L-selectin-GFP was analysed over time during recruitment. The change in cell circularity over time was then analysed for each of the mutant cell lines and compared to the results for cells expressing wildtype L-selectin-GFP ((B) shows the results for ΔM-N, (C) shows the results for S364A, (D) shows the results for S367A and (E) shows the results for SSAA). For each experiment three fields of view were analysed and between 10 and 40 cells per field of view were measured. Results shown are the mean of three experiments with standard deviation as error bars. Statistical significance between the cell circularity at each time point was assessed for each cell line using a One-way Annova followed by Tukey's post hoc test (indicated by black lines). An independent two-tailed Student's t test was used to assess statistical significance between wildtype and mutant cell lines at each time point (shown in red). *=p<0.05, **=p<0.01, ***=p<0.005.

When the results for cell area and circularity were analysed together, there was a strong correlation between the two parameters, with an increase in cell area causing a decrease in circularity (Figure 6.21). This correlation was apparent across all the cell lines studied. This showed that as cell area increased during recruitment the cells became more elongated, suggesting that the cells were spreading and becoming more polarised.
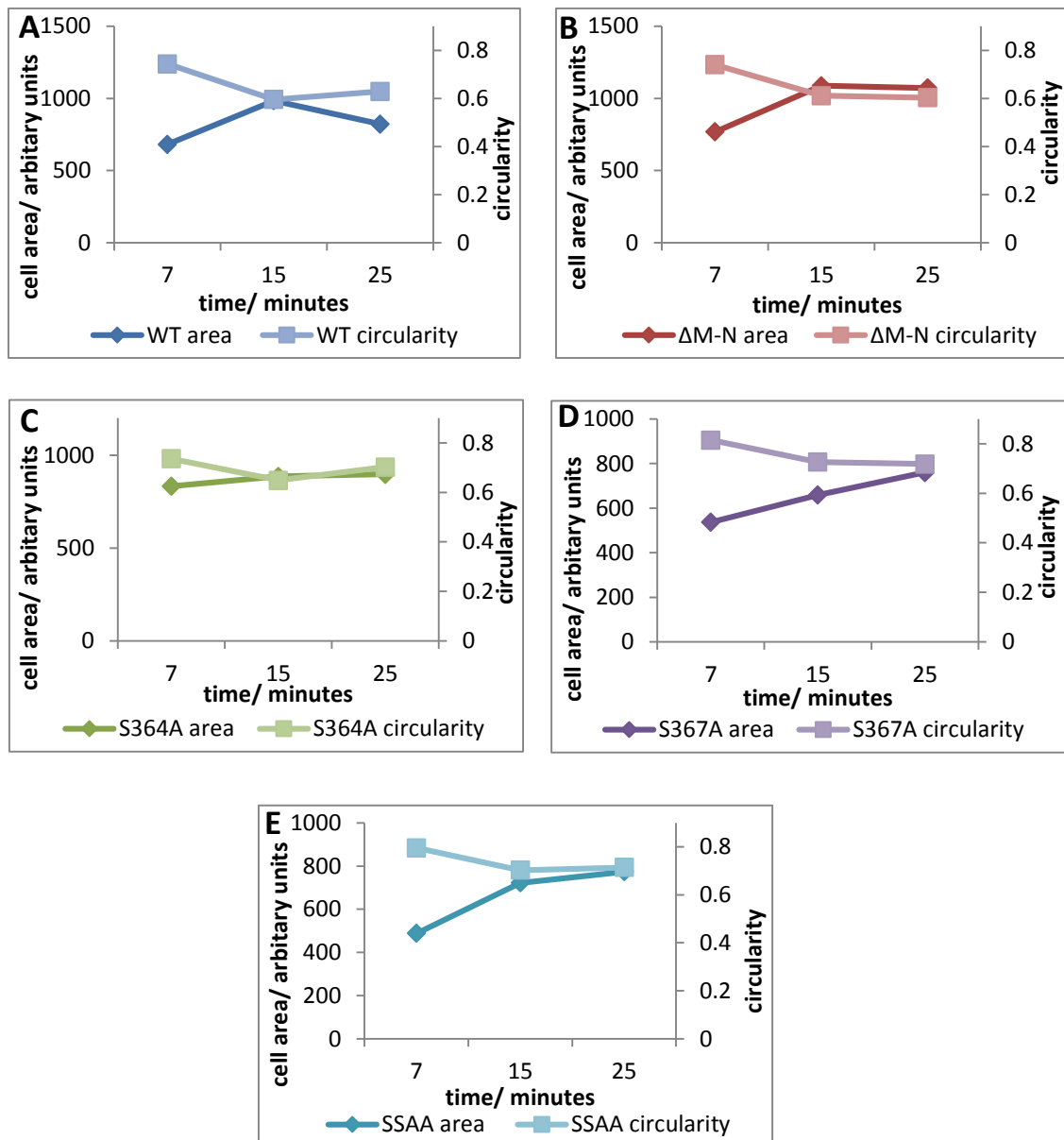


**Figure 6.21: Comparison of the changes in cell area and circularity of THP-1 cells during recruitment under flow.** The changes cell area and circularity during recruitment was compared for THP-1 cells expressing wildtype L-selectin-GFP (A), ΔM-N-L-selectin-GFP (B), S364A-L-selectin-GFP (C), S367A-L-selectin-GFP (D) and SSAA-L-selectin-GFP (E). For each experiment three fields of view were analysed and between 10 and 40 cells per field of view were measured. Results shown are the mean of three experiments.

### 6.3.6.3 Analysis of Protrusion Dynamics

Analysis of the spread cell area and circularity during recruitment indicated that, as TEM progressed, the THP-1 cells spread and became more polarised, suggesting the cells were extending protrusions beneath the monolayer. As the spread area and circularity in some cell lines would change over time (Figure 6.21), this suggested that the protrusions were extending and retracting over time. To assess if these changes were in fact due to dynamic changes in protrusions during recruitment, the number of protrusions emanating from each cell was analysed over time. Mutating the cytosolic tail of L-selectin-GFP or blocking shedding of L-selectin-GFP significantly altered the extent of cell spreading during TEM under flow conditions (Section 6.3.6.1). For this reason, analysis of protrusion dynamics was carried out on cells expressing wildtype L-selectin-GFP, with the results compared to those found with each of the L-selectin-GFP mutants. The number of protrusions was analysed at time points similar to those indicated before. The cells were categorized as having zero, one, two or multiple protrusions (Figure 6.22), with the percentage of cells with each number of protrusions recorded at each time point.
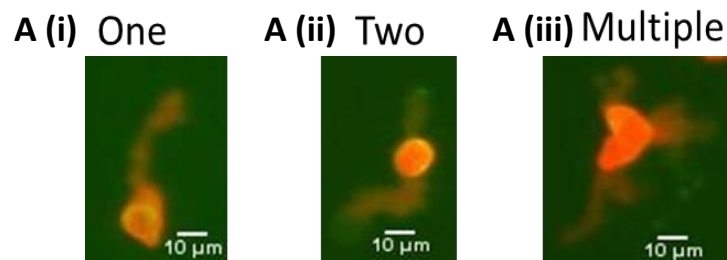


**Figure 6.22: Examples of Protrusion numbers.** Images of cells from the flow chamber assay showing examples of cells scored as having one protrusion (A (i)), two protrusions (A (ii)) and multiple protrusions (A (iii)).

Previously in the lab THP-1 cells transduced with GFP protein were analysed as a control, to ensure the presence of GFP did not affect the protrusion dynamics. The results for GFP and wildtype L-selectin-GFP cells were compared at seven and fifteen minutes. At the earlier time point both cell lines had similar percentages of cells with one or multiple protrusions, but a significantly greater percentage of wildtype L-

selectin-GFP cells had two protrusions (Figure 6.23A). After fifteen minutes of recruitment there was no significant difference in the protrusion dynamics between either of the cell lines (Figure 6.23B). These results show that cells expressing wildtype L-selectin-GFP tend to have a greater number of protrusions at the earlier time point than GFP cells, suggesting they possibly display a more invasive phenotype. As time progressed this effect was diminished, as shown by the decrease in cells classified as having multiple protrusions (analysis was undertaken by Karolina Rzeniewicz, PhD Thesis December 2013).
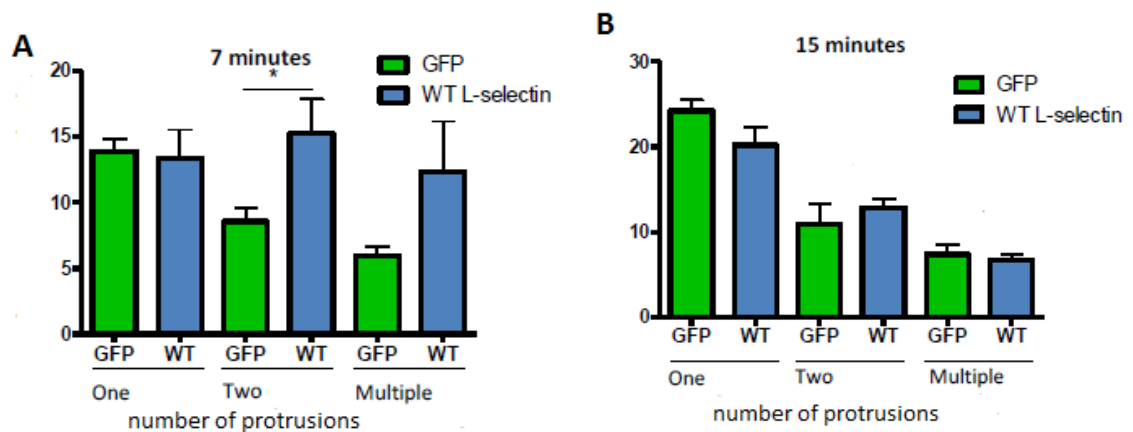


**Figure 6.23: Analysis of protrusion dynamics in THP-1 cells during recruitment under flow conditions.** THP-1 cell protrusion numbers were analysed as cells were recruited to TNF-α-activated HUVEC monolayers. Analysis was undertaken at seven minutes (A) and fifteen minutes (B) with results for cells expressing GFP and those expressing wildtype L-selectin-GFP compared. Results represent the mean of three independent experiments, with three fields of view analysed for each experiment. Error bars represent SEM. Statistical analysis was assessed using two-tailed unpaired Student's T test, *=p<0.05.Experiments and analysis were carried out by Karolina Rzeniewicz, PhD Thesis.

The cell lines analysed in this report were transduced with both L-selectin-GFP and CaM-RFP. In order to be able to compare the L-selectin-GFP mutant with wildtype L-selectin-GFP cell lines, the protrusion dynamics were first assessed in THP-1 cells expressing wildtype L-selectin-GFP and CaM-RFP (referred to hereafter as wildtype L-selectin-GFP). The results were analysed in two ways, firstly cells were scored as having zero, one, two or multiple protrusions at seven, fifteen or twenty five minutes (Figure 6.24A-C). In addition, cells possessing a specific protrusion number were grouped in to a single category over time (Figure 6.25A-D). This allowed analysis of the protrusion number that was most common at each time point as well as assessing how the number of cells with a given number of protrusions changed as recruitment progressed. The same method of analysis was then used for the L-selectin-GFP mutant cell lines to allow direct comparison between the mutant and wildtype cells.

One protrusion was the most prevalent phenotype at seven minutes (Figure 6.24A). At fifteen minutes the percentage of cells with one protrusion remained significantly higher than those with zero, one, two or multiple protrusions (Figure 6.24B), as was the case at twenty five minutes (Figure 6.24C).
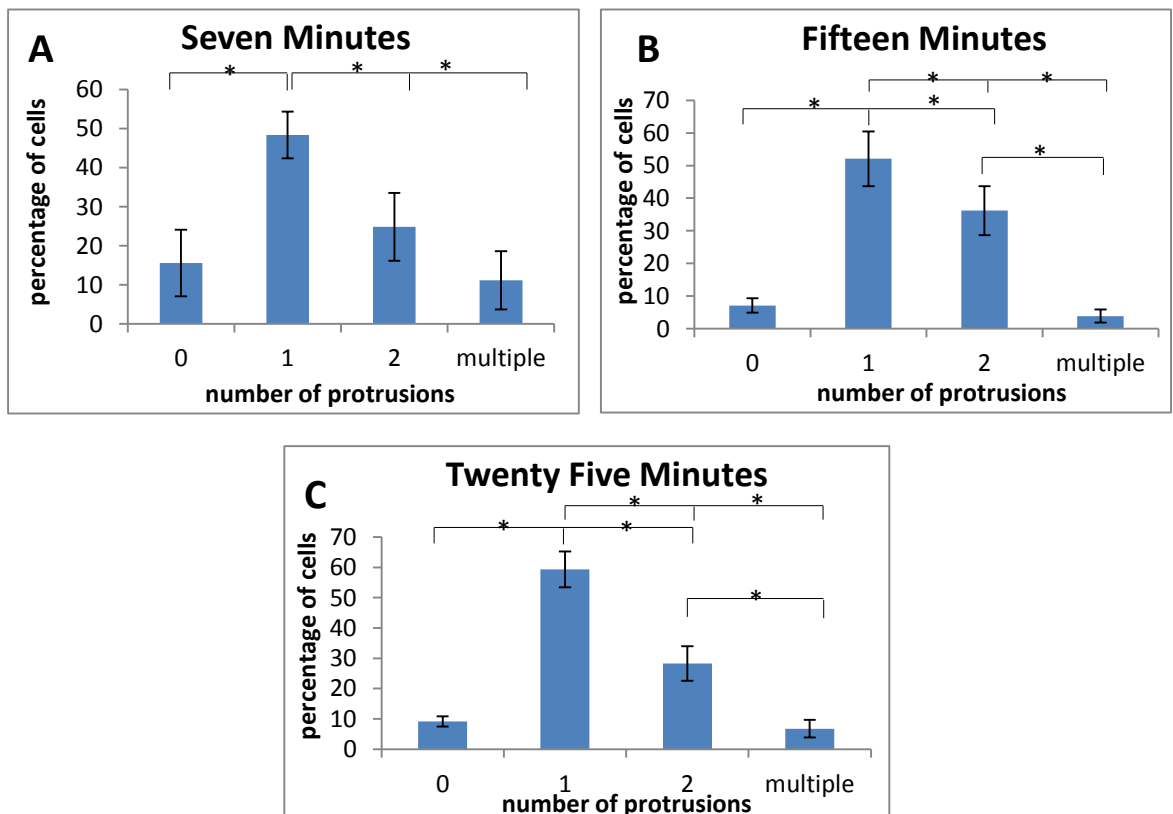
**Figure 6.24: Analysis of THP-1 protrusion numbers during TEM with cells expressing wildtype L-selectin-GFP.** Time-lapse microscopy was used to produce movies of THP-1 cells expressing wildtype L-selectin-GFP undergoing TEM. Analysis of protrusion dynamics was carried by scoring cells as having zero, one, two or multiple protrusions at seven (A), fifteen (B) and twenty five (C) minutes. Results represent the mean of three experiments, with three fields of view studied for each experiment and 20-100 cells analysed for each field of view. Error bars represent standard deviation. Statistically significant differences were assessed using One-Way Annova with Tukey's post-hoc test. *=p<0.05.

Next, cells were categorised on the basis of protrusion number over time. The results showed that the percentage of cells with zero protrusions tended to decrease over time, but this was not significant (Figure 6.25A). The percentage of cells extending a single protrusion tended to increase over time, but once again not significantly (Figure 6.25B). Similarly, there was no significant change in the percentage of cells with two protrusions over time (Figure 6.25C). Analysis of the percentage of cells with multiple protrusions at each time point showed that the percentage of this phenotype tended to decrease as time progressed, but this was not significant (Figure 6.25D). Together, these results showed that, as time progressed, cells with zero and multiple protrusions tended to decrease while the percentage of cells with a single protrusion tended to increase.

These results correlate with the results observed for cell area and circularity, with the number of cells protruding increasing between seven and fifteen minutes, corresponding with an increase in area and a decrease in circularity. Between fifteen and twenty five minutes, when cell area decreased and circularity increased (Figure 6.21), the number of protrusions produced by each cell likely decreased.
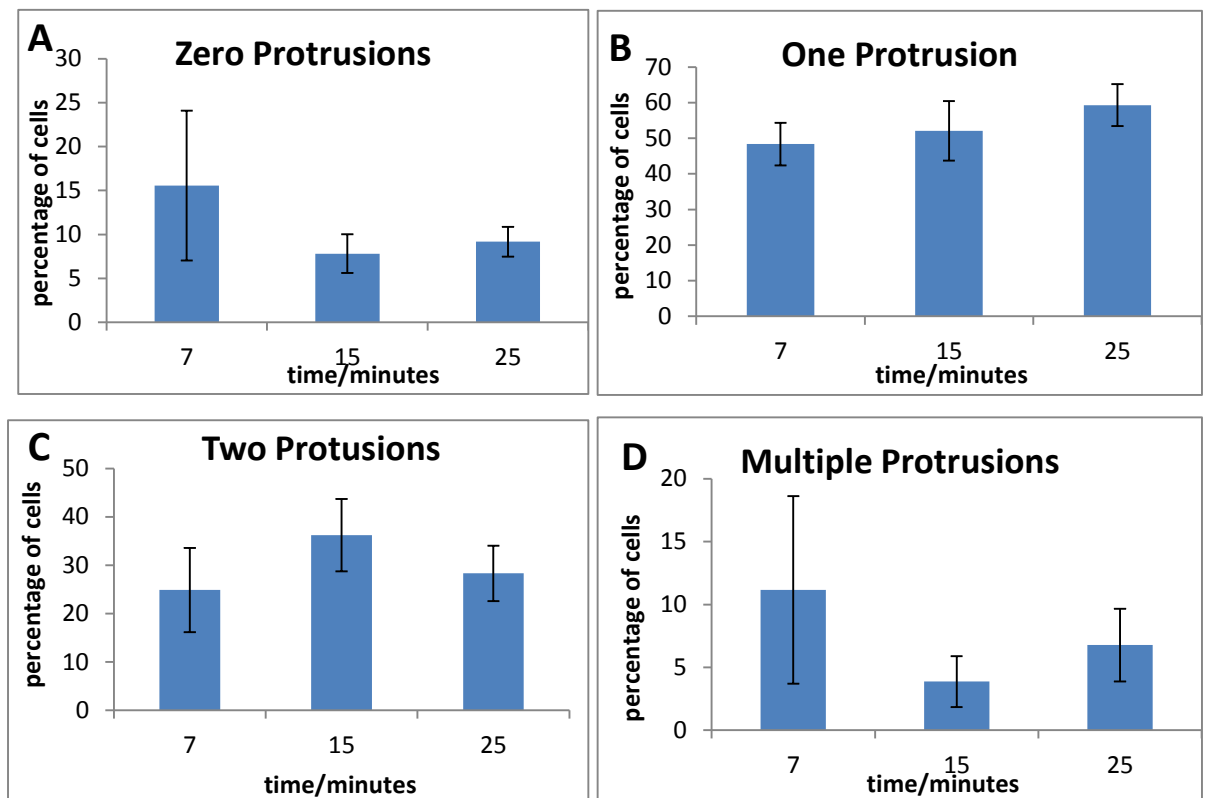
**Figure 6.25: Analysis of Protrusion Dynamics of THP-1 cells expressing wildtype L-selectin-GFP during TEM under flow conditions.** The percentage of cells with zero (A), one (B), two (C) or multiple (D) protrusions was analysed as TEM progressed. Results are the mean of three experiments with error bars showing the standard deviation. For each experiment three fields of view were analysed with 20-100 cells characterised per field of view. Statistical analysis was undertaken using one-way Anova.

### 6.3.6.3.2 Analysis of Protrusion Numbers of cells expressing ΔM-N-L-selectin-GFP

The same analysis of protrusion dynamics was carried out using the sheddase resistant THP-1 cell line expressing ΔM-N-L-selectin-GFP. At seven minutes the percentage of cells with each protrusion number was similar (Figure 6.26A). After fifteen minutes of recruitment a majority of cells produced one protrusion, with two protrusions being the next most common phenotype (Figure 6.26B). At twenty five minutes there are very few cells with no protrusions. The percentage of cells with one, two or multiple protrusions were similar at this time point (Figure 6.26C).

The change in the protrusion number of ΔM-N-L-selectin-GFP cells was assessed over time. The results showed that the percentage of cells with zero protrusions significantly decreased as time progressed (from 23.9±9.1% at seven minutes to 6±3.9% at twenty five minutes, Figure 6.26D). There was no change in the percentage of cells with one protrusion at the different time points (Figure 6.26E).

Cells expressing ΔM-N-L-selectin-GFP with two protrusions increased significantly between seven and fifteen minutes (Figure 6.26F)and the percentage of cells with multiple protrusions tended to increase as time progressed, but not significantly (Figure 6.26G).

### *6.3.6.3.3 Comparison of Protrusion Dynamics of Wildtype and ΔM-N-L-selectin-GFP*

Comparison between cells expressing wildtype and ΔM-N-L-selectin-GFP revealed that at seven minutes there were no significant differences in the percentages of cells with any of the protrusion numbers (Figure 6.26A). After fifteen minutes of recruitment there were significantly more cells with multiple protrusions in the ΔM-N-L-selectin-GFP cell line compared to wildtype cells (16.6±2.5% and 3.9±2.0% respectively, Figure 6.26B), which persisted at twenty five minutes (Figure 6.26C).

These results show that as TEM progressed cells expressing ΔM-N-L-selectin-GFP had a greater number of cells with multiple protrusions compared to cells expressing wildtype L-selectin-GFP. This was interesting, as it correlated with ΔM-N-L-selectin-GFP cells having a significantly larger cell area at fifteen and twenty five minutes compared to wildtype L-selectin-GFP cells (Figure 6.11). It is therefore likely that the difference in cell area is a result of ΔM-N-L-selectin-GFP cells sending out a greater number of protrusions.
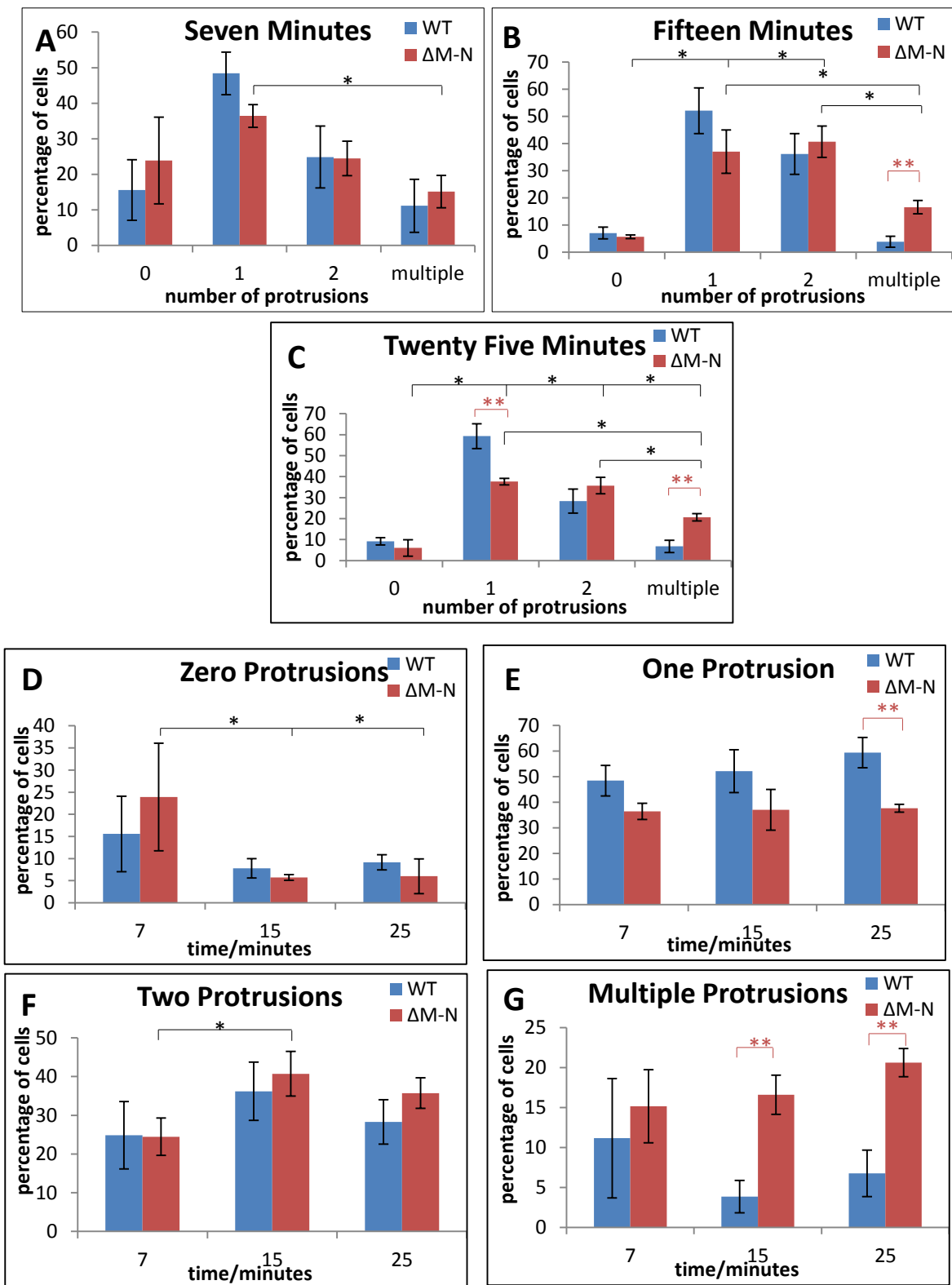
**Figure 6.26: Analysis of THP-1 protrusion dynamics during TEM with cells expressing ΔM-N L-selectin-GFP, with a comparison between the mutant and wildtype results.** Time-lapse microscopy was used to produce movies of THP-1 cells, expressing either wildtype or ΔM-N L-selectin-GFP, undergoing TEM. Analysis of protrusion dynamics was carried out at seven, fifteen and twenty five minutes, with cells scored for having no, one, two or multiple protrusions for both cell lines. Data was summarised by assessing the percentage of cells with each phenotype at seven (A), fifteen (B) and twenty five (C) minutes. The change in the percentage of cells with each protrusion number over time was also assessed (D-G). Results represent the mean of three experiments, with three fields of view studied for each experiment and 20-100 cells analysed for

each field of view. Error bars represent standard deviation of three experiments. Statistically significant differences within the ΔM-N cell line were assessed using One-Way Anova with Tukey's post-hoc test (represented by the black lines). Statistical differences between wildtype and ΔM-N cell lines at each point were assessed using an independent, two-tailed Student's T test (red lines), *=p<0.05, **=p<0.01.

### 6.3.6.3.4 Analysis of Protrusion Dynamics of cells expressing S364A-L-selectin-GFP

The protrusion dynamics of the cell line expressing the L-selectin mutant S364A-L-selectin-GFP was also assessed as above. The results showed that at seven minutes the percentage of cells with one protrusion was significantly higher than other protrusion numbers (Figure 6.27A). The percentage of cells with multiple protrusions was also significantly lower than those with either zero or two protrusions. This distribution of protrusion numbers was conserved at fifteen (Figure 6.27B) and twenty five minutes (Figure 6.27C).

When the change in the percentage of cells carrying a specific protrusion number was analysed over time, the results showed that as time progressed there was no change in the percentage of cells with zero (Figure 6.27D), one (Figure 6.27E), two (Figure 6.27F) or multiple protrusions (Figure 6.27G). This directly correlated with the results observed for both cell area and circularity with this cell line, where there was no change as time progressed (Sections 6.3.61 and 6.3.6.2). This provides further evidence that changes in cell area and circularity is a result of the changes in protrusion number.

### 6.3.6.3.5 Comparison of Protrusion Dynamics of Wildtype and S364A-L-selectin-GFP

Given that the number of cells with each protrusion did not change as recruitment progressed, it was of interest how this compared to cells expressing wildtype L-selectin-GFP. The percentage of cells with zero protrusions was significantly higher at fifteen  and twenty five minutes for cells expressing S364A-L- compared to cells expressing selectin-GFP wildtype L-selectin-GFP (Figure 6.27D). As TEM progressed, cells expressing wildtype L-selectin-GFP tended to have a larger proportion of cells with one protrusion compared to cells expressing S364A-L-selectin-GFP, with a significant difference observed at twenty five minutes (Figure 6.27E). The percentage of cells with two protrusions was similar for both cell lines at every time point (Figure 6.27F). Comparison of the percentage of cells with multiple protrusions at each time

point revealed that the percentage of cells was similar in both cell lines at seven minutes and twenty five minutes. At fifteen minutes the percentage of cells with multiple protrusions was significantly higher with cells expressing S364A-L-selectin-GFP (Figure 6.27G). These results confirm that mutating the residue S364 to alanine blocked the change in protrusion dynamics over time, compared to cells expressing wildtype L-selectin-GFP.
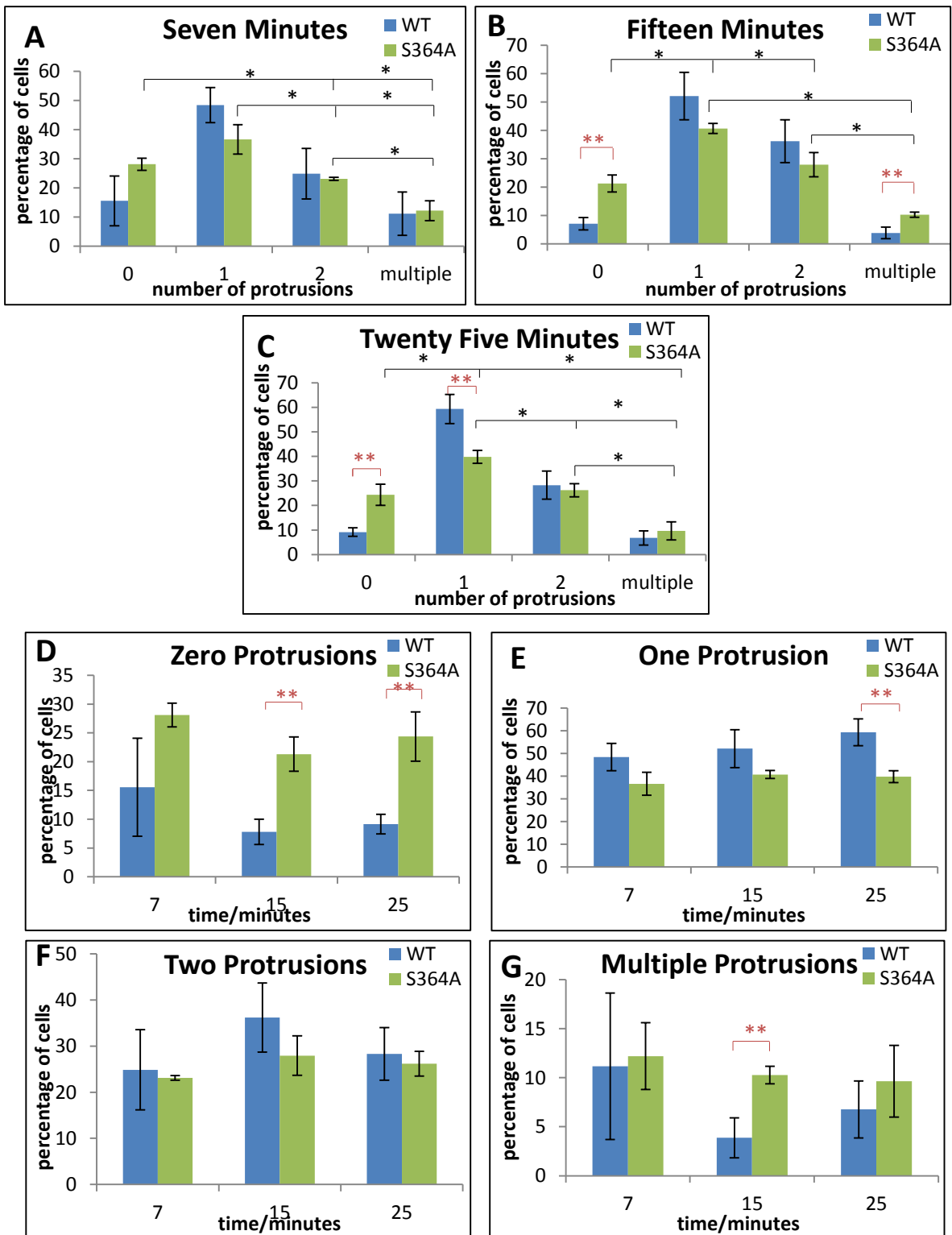
**Figure 6.27: Analysis of THP-1 protrusion dynamics during TEM with cells expressing S364A L-selectin-GFP, with a comparison between the mutant and wildtype results.** Movies of THP-1 cells, expressing either wildtype or S364A L-selectin-GFP, undergoing TEM were produced by time-lapse microscopy. Analysis of protrusion dynamics was carried out at seven (A), fifteen (B) and twenty five minutes (C), with cells scored for having no, one, two or multiple protrusions for both cell lines. The change in the percentage of cells with each protrusion number over time was also assessed (D-G). Results represent the mean of three experiments, with three fields of view studied for each experiment and 20-100 cells analysed for each field of view and error bars representing the standard deviation. Statistically significant differences within the S364A cell line was assessed using One-Way Anova with Tukey's post-hoc test (represented by black lines). Statistical differences between wildtype and S364A cell lines at each point were assessed using a Student's T test (red lines),*=p<0.05, **=p<0.01.

### *6.3.6.3.6 Analysis of Protrusion Number of Cells Expressing S367A-L-selectin-GFP*

The S367A L-selectin-GFP mutant cell line was analysed to assess the effect of this mutant on protrusion dynamics. The results showed that at all time points analysed a majority of the cells had either zero or one protrusion, with very few having multiple protrusions (Figure 6.28A-C).

The change in protrusion dynamics of S367A-L-selectin-GFP cells was analysed over time. The results showed that the number of cells with zero protrusions decreased between seven and fifteen minutes significantly (from 38.9±5.3% to 24.4±3.4%, Figure 6.28D). The percentage of cells with one protrusion increased between seven and fifteen minutes, with the percentage of cells at fifteen and twenty five minutes being significantly higher than that at seven minutes (Figure 6.28E). As time progressed there was no change in the percentage of cells with two (Figure 6.28F) or multiple protrusions (Figure 6.28G).

### *6.3.6.3.7 Comparison of Protrusion Numbers of Wildtype and S367A-L-selectin-GFP*

When comparing wildtype and S367A-L-selectin-GFP cell lines, the results showed that the percentage of cells with zero protrusions was significantly higher with the S367A-L-selectin-GFP cell line compared to wildtype L-selectin-GFP cells at all the time points analysed (Figure 6.28D). In contrast, wildtype L-selectin-GFP cells had a higher percentage of cells with two protrusions compared to S367A-L-selectin-GFP, with a significant difference observed at fifteen and twenty five minutes (Figure 6.28F). The percentage of cells with multiple protrusions tended to be higher with wildtype L-selectin-GFP cells than S367A-L-selectin-GFP cells, but this was only significant at twenty five minutes (Figure 6.28G).

These results show that mutating residue S367 to alanine reduces the number of protrusions the THP-1 cells produce during recruitment and this inhibition of protrusion formation becomes more apparent as TEM progressed. The fact that cells expressing S367A-L-selectin-GFP produce fewer protrusions was consistent with them being more circular and smaller in area than wildtype L-selectin-GFP (Figures 6.13 and 6.18).
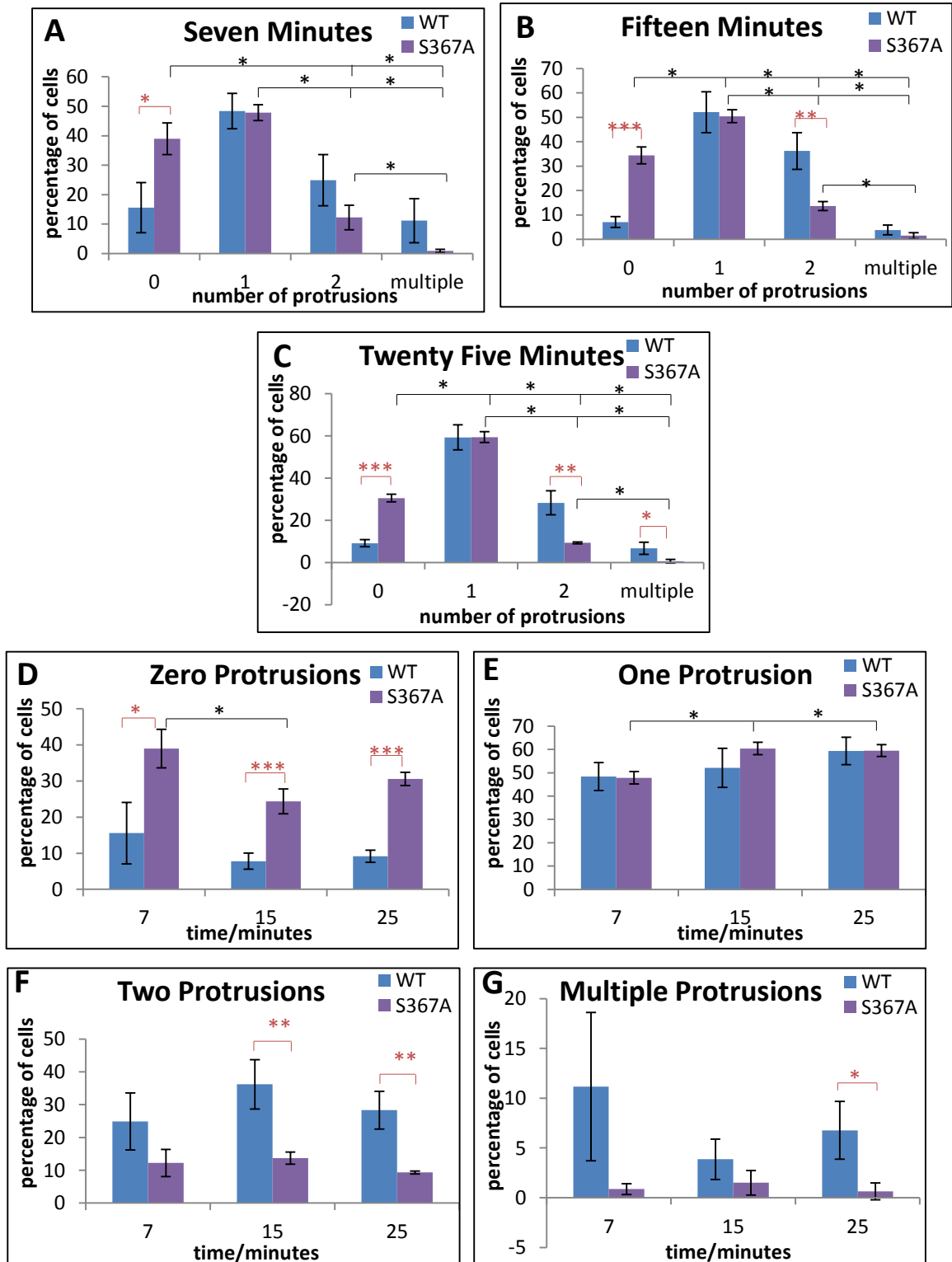
**Figure 6.28: Analysis of THP-1 protrusion dynamics during TEM with cells expressing S367A L-selectin-GFP, with a comparison between the mutant and wildtype results.** Time-lapse microscopy was used to produce movies of THP-1 cells undergoing TEM, expressing either wildtype or S367A L-selectin-GFP. Analysis of protrusion dynamics was carried out by scoring cells as having zero, one, two or multiple protrusions for both cell lines. Data was summarised by assessing the percentage of cells with each phenotype at seven (A), fifteen (B) and twenty five (C) minutes. The change in the percentage of cells with each protrusion number over time was also assessed (D-G). Results represent the mean of three experiments, with three fields of view studied for each experiment and 20-100 cells analysed for each field of view. Error bars represent standard deviation. Statistically significant differences within the S367A cell line were assessed using One-Way Anova with Tukey's post-hoc test (black lines). Statistical differences between wildtype and S367A cell lines at each point were assessed using a Student's T test (red lines), *=$p<0.05$, **=$p<0.01$, ***=$p<0.005$.

### 6.3.6.3.8 Analysis of Protrusion Dynamics of Cell Expressing SSAA-L-selectin-GFP

The protrusion dynamics of cells expressing the double serine to alanine mutation of L-selectin (SSAA) was also assessed. After seven minutes of recruitment, a majority of the cells had zero or one protrusion, with very few cells with two or multiple protrusions (Figure 6.29A). The results at fifteen minutes showed that a majority of the cells had one protrusion, very few had multiple protrusions and a similar percentage had either zero or two protrusions (22.4±1.3% and 24.9±1.2% respectively, Figure 6.29B). At twenty five minutes the results were similar to that observed at fifteen minutes (Figure 6.29C).

How the percentage of cells with each protrusion number changed over time was also assessed. The results showed that the percentage of cells not protruding decreased over time (Figure 6.29D). The percentage of cells with one protrusion increased significantly between seven and fifteen minutes (from 51.0±3.6% to 59.2±0.36%, Figure 6.29E). For both two (Figure 6.29F) and multiple (Figure 6.29G) protrusions the percentage of cells increased between seven and fifteen minutes and then remained the same between fifteen and twenty five minutes. In general these results showed that the percentage of cells with zero protrusions decreased over time and the percentage of cells with two or multiple protrusions increased.

### 6.3.6.3.9 Comparison of Protrusion Numbers of Wildtype and SSAA-L-selectin-GFP

Comparison between cells expressing wildtype and SSAA-L-selectin-GFP showed that at seven minutes more SSAA-L-selectin-GFP cells were not protruding compared to wildtype L-selectin-GFP cells, but this was just under statistical

significance (p=0.0507, Figure 6.29A). The results for all other protrusion numbers at seven minutes were similar for both wildtype and SSAA-L-selectin-GFP cell lines. This pattern was also observed at fifteen (Figure 6.29B) and twenty five minutes (Figure 6.29C). These results show that the SSAA-L-selectin-GFP mutant leads to an increase in the number of cells not protruding at all the time points studied.

Once again these results correlate with the analysis of the cell area and circularity, with SSAA-L-selectin-GFP cells being smaller in size, more circular and having fewer cells protruding than wildtype L-selectin-GFP cells. This provides further evidence that the changes in cell area and circularity observed during TEM is a result of the cells sending out protrusions.
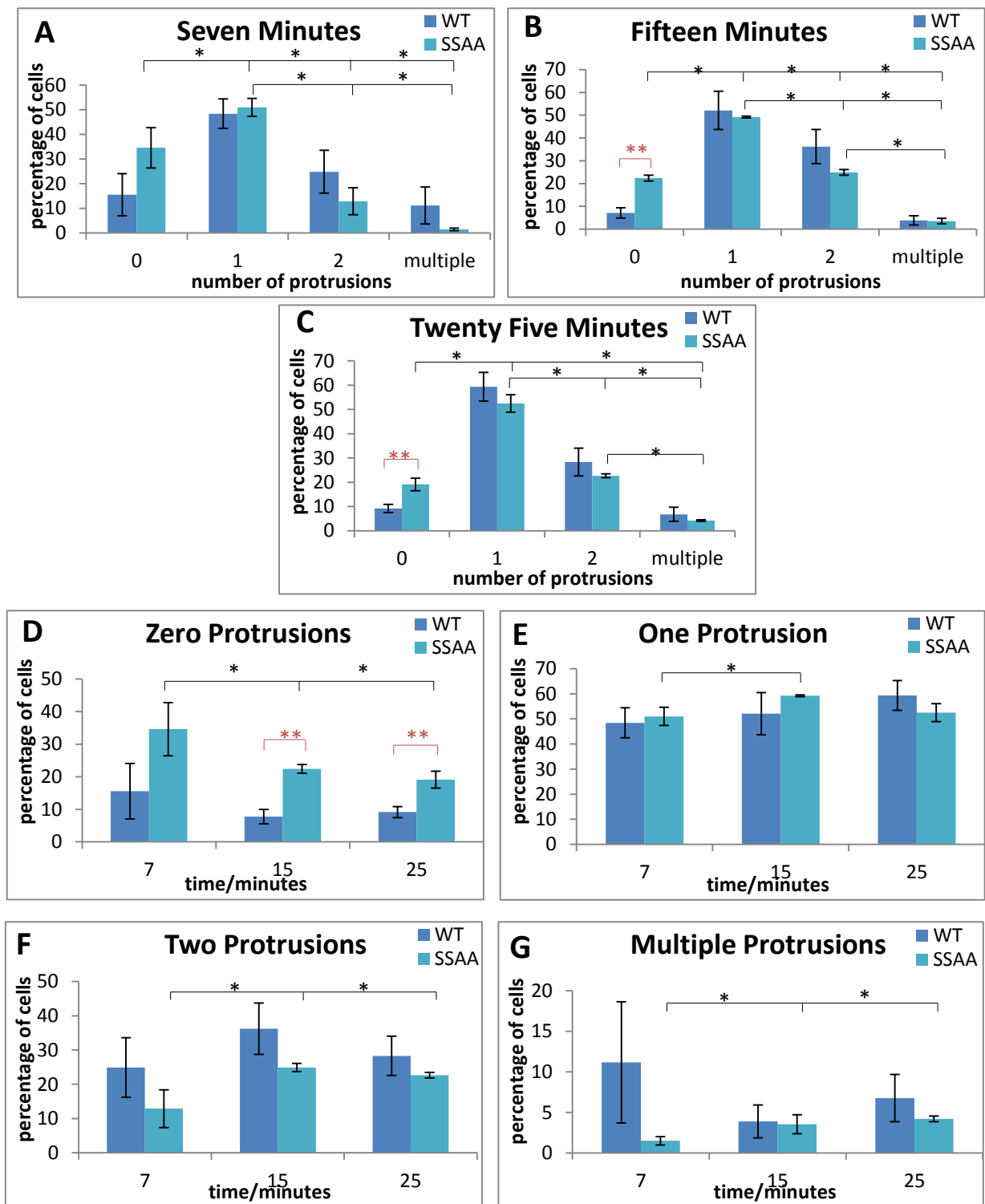
**Figure 6.29: Analysis of THP-1 protrusion dynamics during TEM with cells expressing SSAA L-selectin-GFP, with a comparison between the mutant and wildtype results.** Time-lapse microscopy was used to produce movies of THP-1 cells, expressing either wildtype or SSAA L-selectin-GFP, whilst undergoing TEM. Analysis of protrusion dynamics was carried out at seven (A), fifteen (B) and twenty five (C) minutes, with cells scored for having no, one, two or multiple protrusions for both cell lines. The change in the percentage of cells with each protrusion number over time was also assessed (D-G). Results represent the mean of three experiments, with three fields of view studied for each experiment and 20-100 cells analysed for each field of view. Error bars represent standard deviation. Statistically significant differences within the SSAA cell line was assessed using One-Way Anova with Tukey's post-hoc test (black lines). Statistical differences between wildtype and SSAA cell lines at each point were assessed using an independent two-tailed Student's T test (red lines), *=p<0.05, **=p<0.01.

## 6.4 Discussion

In the previous chapters the interaction between CaM and L-selectin was studied *in vitro* using biophysical and biochemical techniques, and subsequently in resting THP-1 cell lines. Experiments in this chapter focussed on the CaM/L-selectin interaction when THP-1 cells were co-cultured with HUVECs, either under static or flow conditions. Using FRET/FLIM approaches enabled direct assessment of interaction during TEM.

### 6.4.1 Loss of interaction between L-selectin and CaM in transmigrated pseudopods of THP-1 cells

Analysis of the interaction between wildtype L-selectin-GFP and CaM-RFP during TEM by FRET/FLIM showed that the interaction was detected in all parts of the cell at early time points, but the interaction was exclusively lost in the transmigrated part of the cell at later time points (Section 6.3.2). This suggested that L-selectin was shed in the transmigrated part of the cell at this time, but not in the non-transmigrated part of the cell. This led to the question of why a polarity in cleavage of L-selectin occurred. It was possible that L-selectin was retained in the non-transmigrated part of the cell to allow it to play a role in secondary tethering (see Section 1.2.1). Secondary tethering is thought to be important for amplifying the accumulation of leukocytes to the endothelium. It has been shown that blocking L-selectin with a function blocking antibody causes a loss of secondary tethering (469-472). Alon et al (1996) (469) found that L-selectin-dependent secondary tethering accounted for 70% of the accumulated neutrophils on P- and E-selectin. Secondary tethering has also been observed *in vivo* (318), with L-selectin deficient mice lacking secondary tethering (318), again showing the role of L-selectin in this process.

It has previously been thought that L-selectin was only responsible for the initial capture of leukocytes from the blood flow and then was quickly shed once cells had firmly adhered to the endothelium (97,127). The results here suggested that L-selectin remained bound to CaM up to six minutes after capture, so was therefore presumably still in its full length form. The images taken at six minutes clearly showed that the cell had begun to transmigrate, with clear protrusions observed under the HUVEC monolayer. The fact that L-selectin is un-cleaved at this point allows it to play a role in cellular processes during TEM. L-selectin has been shown to bind to several

proteins in the extracellular matrix and basement membrane such as heparan sulphate proteoglycans (Section 1.3.5.2) (HSPGs)(153). It is possible that L-selectin binding to these "sub-endothelial" ligands is required for the directional migration of the leukocyte towards the inflammatory insult. A Previous study using an elaborate *in vivo* chemotaxis model demonstrated that L-selectin-deficient leukocytes accumulate on the endothelial surface at the same rate as wildtype cells, but undergo less emigration (130). The study also showed that L-selectin-deficient leukocytes failed to chemotax towards a soluble chemokine (130). The fact that L-selectin remains intact six minutes after capture suggests that it could play a role in signalling to promote directed cell migration, or at least during TEM.

## 6.4.2 Phosphorylation of S364 promotes the dissociation of CaM specifically within the non-transmigrated part of the cell

The FRET efficiency results for the serine-to-alanine mutants showed that when S364 was mutated to S364A, CaM failed to dissociate within the transmigrated part of the cell, suggesting that it is possible that phosphorylation of this residue was responsible for the dissociation of CaM seen in wildtype L-selectin-GFP cells (Figure 6.30). It has been shown that activation of PKC isozymes by either PMA or chemoattractant receptors resulted in an increase in phosphorylation of L-selectin (95) and that the phosphorylation occurred at the serine residues, as the responses were blocked by the SSAA mutation (95). Further analysis revealed the PKC isozymes θ and ι were responsible for the phosphorylation (214). It is therefore likely that L-selectin is phosphorylated after cell activation and this could be responsible for CaM dissociation.



298
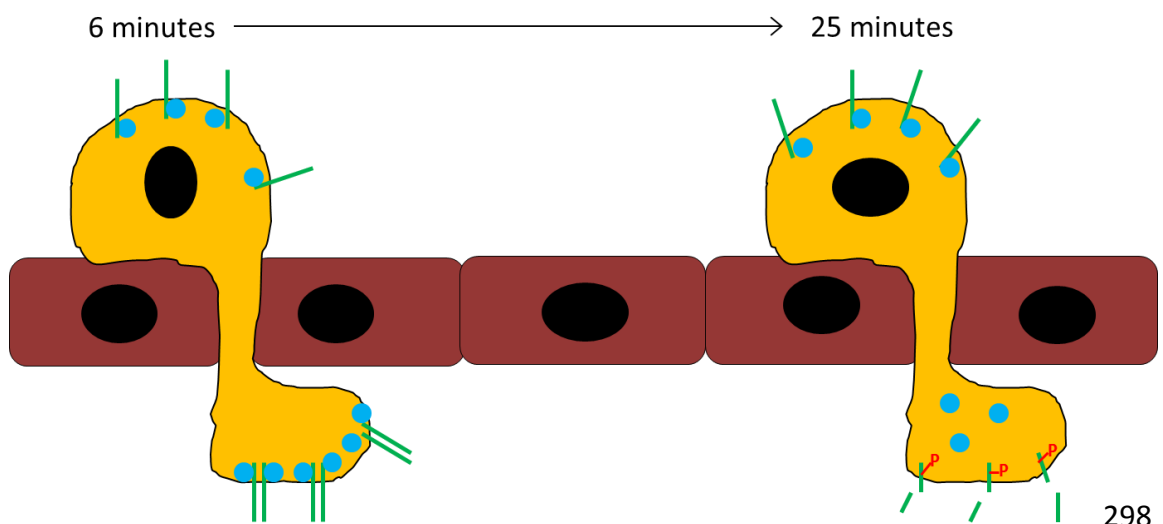
**Figure 6.30: Potential mechanism of L-selectin shedding in monocytes undergoing TEM.** After six minutes of TEM, CaM (blue circle) was bound to the tail of L-selectin (green line) in both the transmigrated and non-transmigrated parts of the cell and therefore L-selectin was protected from extracellular cleavage. At twenty five minutes residue S364 was phosphorylated (red P) in the transmigrated part of the cell only leading to CaM dissociation in this subcellular region and shedding of L-selectin. The fact that L-selectin remains intact in the non-transmigrated part of the cell allows it to play a potential role in secondary tethering of leukocytes.

Cells expressing wildtype L-selectin-GFP and the S367A-L-selectin-GFP mutation had a similar profile of interaction with CaM-RFP at twenty five minutes. However, at six minutes the interaction between S367A-L-selectin-GFP and CaM-RFP was also lost in the transmigrated part of the cell, unlike wildtype L-selectin-GFP cells. This could be because blocking the phosphorylation of S367 promotes the phosphorylation of S364, leading to a decrease in the interaction between CaM and L-selectin. Using anti-phospho-serine antibodies to study the phosphorylation state of the cytosolic tail of L-selectin after activation may help provide information about whether mutating one serine to alanine affects the phosphorylation state of the other. The role of other binding partners of L-selectin must also be taken into account. The ERM proteins may be important in enabling CaM to interact with L-selectin and the S367A mutation could affect the ERM interaction and as a result the CaM is no longer able to interact with L-selectin.

As explained in the previous chapter (Section 5.3.7), CaM and L-selectin do not interact with one another in resting THP-1 cells, possibly due to the tail of L-selectin interacting with PS in the plasma membrane. It is possible that phosphorylation of S367 is responsible for dissociation of L-selectin from the plasma membrane. It is predicted that the interaction between the plasma membrane and L-selectin is due to electrostatic interactions between positive amino acids in the cytosolic tail of L-selectin and negatively charged PS in the plasma membrane. It is therefore probable that the addition of the negatively charged phosphate group to S367 will interrupt this charge-charge interaction. This may explain why the FRET efficiency between L-selectin-S367A-GFP and CaM-RFP is much lower in the transmigrated part of the cell at six minutes compared to wildtype L-selectin-GFP cells. It is possible that at the early time point L-selectin is still interacting with the plasma membrane in the S367A mutated cells and as a result CaM-RFP is not able to interact with L-selectin. This may also

explain why the FRET efficiency in resting THP-1 cells was much higher with the S364A mutation (Figure 5.15). It is possible that when phosphorylation of S364 is blocked by the alanine mutation it promotes phosphorylation of S367. This could mean that L-selectin is no longer able to interact with PS in the plasma membrane and therefore CaM binding is observed in the S364A mutant in resting cells. Again, phospho-specific antibodies would prove to be an invaluable resource in deciphering the subcellular distribution of S364 and S367 phosphorylation during TEM.

It is plausible that phosphorylation of the two serine residues regulate L-selectin differently, with phosphorylation of S367 occurring early after cell activation, causing interruption of the interaction between L-selectin and the plasma membrane and allowing CaM to bind to L-selectin and protect it from shedding. At a later time point, between six and twenty five minutes after recruitment, S364 is phosphorylated, causing CaM dissociation from L-selectin and therefore L-selectin cleavage. (Figure 6.31). By producing cell lines with one serine residue mutated to alanine and the other mutated to aspartate to mimic phosphorylation (e.g. S364A/S367D or S364D/S367A mutants, where one residue mimics phosphorylation and phosphorylation of the other residue is blocked) it may be possible to assess the role of phosphorylation of each residue individually without the complication of not knowing the phosphorylation status of the other serine residue. This will provide clear evidence of the role of phosphorylation of each residue and enable one to decipher the difference between the two. One will need to consider the structural constraints a double alanine/aspartate mutant may make on the cytoplasmic tail, so caution should be taken with this approach.
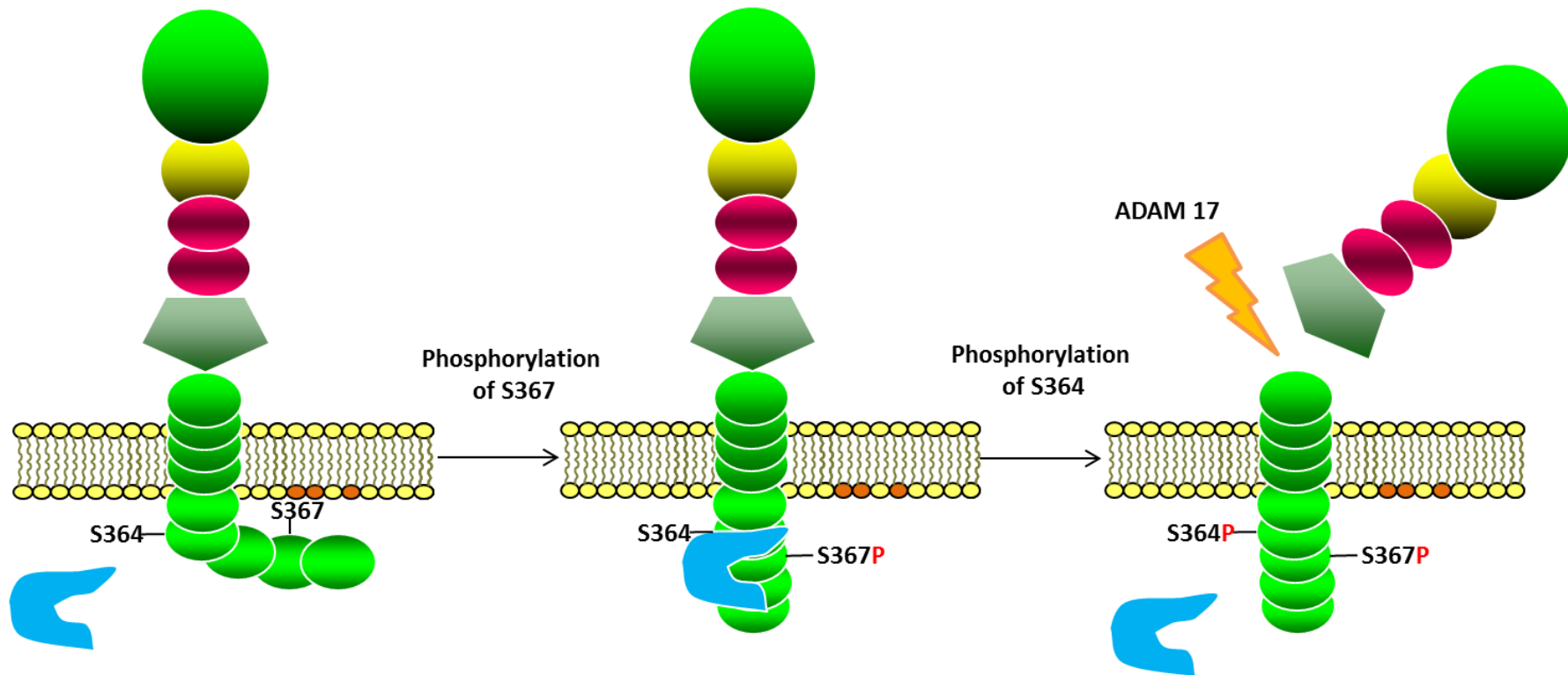
**Figure 6.31: The possible role of phosphorylation of different serine residues in the cytosolic tail of L-selectin.** It is hypothesised that phosphorylation of the serine residues play a role in regulating L-selectin function. One possibility is that in resting THP-1 cells both serine residues are unphosphorylated and the tail of L-selectin interacts with PS (shown in orange) in the plasma membrane, meaning CaM (shown in blue) is not able to interact with L-selectin. Early after cell activation, S367 is phosphorylated by PKC isozymes. This means the interaction between L-selectin and PS in the plasma membrane is disrupted and CaM is able to bind to L-selectin and protect it from shedding. At a later point of TEM, phosphorylation also occurs at residue S364. This leads to CaM dissociation and L-selectin is cleaved by ADAM 17 at the extracellular cleavage site.

The FRET efficiency results for SSAA at twenty five minutes are similar to those of S364A at the same time point, with CaM interacting with L-selectin in all parts of the cell. This was consistent with phosphorylation of S364 being responsible the dissociation of CaM in the transmigrated part of the cell. However, at six minutes little to no interaction between CaM and SSAA-L-selectin was observed. This may support the hypothesis that phosphorylation of S367 is required to disrupt the tail of L-selectin interacting with the plasma membrane and allow CaM binding at the early time point. It is also possible that this mutation affects the association of the other binding partners of L-selectin and this in turn may affect the interaction of CaM. Studying the interaction between this mutant and the other partners, such as moesin, may provide information as to why CaM binding was altered with this mutation.

The sheddase-resistant mutant ΔM-N-L-selectin-GFP had a similar profile of interaction as the SSAA-L-selectin-GFP mutant, with no interaction observed at six minutes and interaction in all subcellular locations of the cell at twenty five minutes. As with SSAA this may be due to this mutation affecting the dynamic phosphorylation/dephosphorylation of the tail. As this form of L-selectin cannot be shed, it is susceptible to continual phosphorylation/dephosphorylation and this dysregulation of phosphorylation may lead to the differences in CaM binding observed here.

The results above suggest that the phosphorylation state of the tail at particular stages of TEM may be important in regulating CaM binding and, if this was affected, it could alter CaM binding. The limitation of the FRET/FLIM analysis here was that it only allows analysis of the interaction at very specific time points, with the cells being fixed at a certain time after the start of the flow chamber assay. This only provides information of the interaction at that particular time point. It was possible that CaM dissociates and re-associates several times during TEM. One possible way of monitoring the interaction continuously during TEM is to use real time FRET, where the FRET efficiency is measured as the experiment progresses. Real time FRET would also give vital clues as to whether the interaction was influenced by protrusions, if the protrusions themselves had an influence on the interaction, or both. Currently, this technique is rare and is under development in only very few labs around the world and is discussed in more detail in Section 7.6.

Since writing this thesis, Dr Angela Rey Gallardo from the Ivetic lab has confirmed that phospho-mimic serine-to-aspartate mutagenesis of the cytoplasmic serines confirmed that the S364D-GFP mutant blocked interaction with CaM-RFP at both six and twenty five minutes. In contrast, binding of CaM-RFP to the S367D-GFP mutant behaved similarly to wild type L-selectin. Lastly, the SSDD-GFP mutant blocked interaction to a similar extent as S364D. This provides further evidence that phosphorylation of S364 is important in regulating the interaction between L-selectin and CaM.

## 6.4.3 Shedding is compromised in serine-to-alanine mutants when THP-1 cells are co-cultured with HUVEC

Co-culturing THP-1 cells with HUVEC monolayers revealed that in cells expressing wildtype L-selectin, the maximal level of stump formation of L-selectin was seen at around ten minutes, suggesting that the highest level of shedding occurred at this time. When S364 is mutated to alanine there was no significant difference in the levels of stump at any of the time points, suggesting there was no peak time of shedding. The S367A mutant had a similar profile of stump formation at the different time points as wildtype L-selectin cells, with peak shedding possibly occurring between ten and twenty minutes, but due to the fact that large error bars were produced it was not possible the make firm conclusions. In fact, the results from this assay were disappointing due to the variable detection of the anti-GFP antibody. Several contaminating bands were also visible between full length L-selectin-GFP and the stump making analysis of the results difficult. An alternative antibody has recently been purchased, which provides a clearer signal. These experiments can now be repeated with the new antibody in the hope that clearer results are produced. Due to the limitations of this method and the fact that different baselines had to be used, it was not possible to undertake direct comparison between the different cell lines. This meant that the trend in protein level changes was compared to assess if there was a difference. This was not ideal and in the future the assay could be modified, possibly by lowering the number of THP-1 cells used in the assay so the same baseline can be used for all cell lines.

Although the anti-GFP antibody used in these experiments lacked specificity for L-selectin-GFP, one interesting observation from this assay was the fact that GFP signal was observed in the unbound fraction after incubation with the HUVEC monolayer increased when the serine residues in the L-selectin cytosolic tail were mutated to alanine, with the S364A-L-selectin-GFP cells having the strongest signal in the unbound fraction (Figure 6.8). This suggested that the serine to alanine mutations led to the THP-1 cells not binding as effectively to the HUVEC monolayer compared to wildtype cells. It is possible that this binding deficiency could be linked to an inability of the cells to send protrusions beneath the HUVEC monolayer. Analysis of the protrusion dynamics revealed that cells expressing S367A-L-selectin-GFP sent out fewer protrusions, with a greater proportion of cells not protruding, compared to wildtype L-selectin-GFP cells (Figure 6.28). This could result in the cells being more easily removed from the HUVEC monolayer, during wash steps. The results for cells expressing S364A-L-selectin-GFP showed that the protrusion dynamics did not change as TEM progressed (Figure 6.27) and the same was true for cell area (Figure 6.12). This suggests that although these cells did send out protrusions, they are smaller in size than wildtype L-selectin-GFP cells and may not have protruded as far under the monolayer. As a result of this S364A-L-selectin-GFP cells may be removed from the HUVEC monolayer more readily than wildtype L-selectin-GFP cells and may explain why a greater number of cells were found in the unbound fraction. Clearly, more work is required to optimise this technique before any firm conclusions can be made.

### 6.4.4 Mutating the tail of L-selectin affects the size, shape and number of protrusions of the cell during TEM

The analysis of the cell area, circularity and protrusion number during TEM showed that these factors were affected by mutation of L-selectin, with S367A- and SSAA-L-selectin-GFP cells being in general, smaller, more circular and producing fewer protrusions than wildtype and ΔM-N-L-selectin-GFP cells being larger and producing more protrusions. S364A-L-selectin-GFP cells were similar to wildtype at early time points, but as TEM progressed this similarity was lost.

Protrusions have been observed in several different leukocytes following cell capture (473). The function of these protrusions is not entirely clear but it is thought that they play a crucial role in TEM. They are thought to be produced as leukocytes remain on the apical surface of the endothelium and patrol the local environment until a suitable place for diapedesis is found (473). Once on the basolateral surface, it is thought that they search for an area in the basement membrane permissive for migration towards the extravascular space (473). It is also possible that the protrusions detect subendothelial chemokines to direct leukocyte chemotaxis (474). It has been shown that the integrin LFA-1 is responsible for the movement of the invasive protrusions in lymphocytes and it has been shown to interact with its ligand ICAM-1 on the luminal surface of the endothelial and basolateral surface (474). As the adhesion between these protrusions and the endothelium must be strong to resist the shear flow in the vessel it is expected that this process is integrin-dependent and not selectin-dependent. This leads to the question as to why mutations in L-selectin affect the size and number of these protrusions. The fact that inhibiting the shedding of L-selectin leads to an increase in the number of protrusions suggests that extracellular cleavage of L-selectin may play an important role in limiting the number of protrusions. Results have suggested that cleavage of L-selectin is required for directional migration towards a chemokine in the mouse cremaster (123,475). This implies that the multiple protrusion phenotype could be responsible for the loss of directional migration (Figure 6.32). The reason S367A- and SSAA-L-selectin-GFP cell lines do not protrude to the same extent as wildtype L-selectin-GFP cells remains unclear. It is possible that other binding partners of L-selectin, such as moesin or ezrin, may play a role in regulating protrusion dynamics in correlation with L-selectin shedding. It is possible that these mutations affect moesin/ezrin interacting with L-selectin and as a result protrusion formation is affected. Further research is required to prove if this is the case. Another possibility to take into consideration is the importance of dynamic changes in phosphorylation of L-selectin as TEM progresses. Phosphorylation of S367 may be required for enhancing the production of protrusions. Further research is required fully understand the role of S367 in regulating protrusion dynamics.
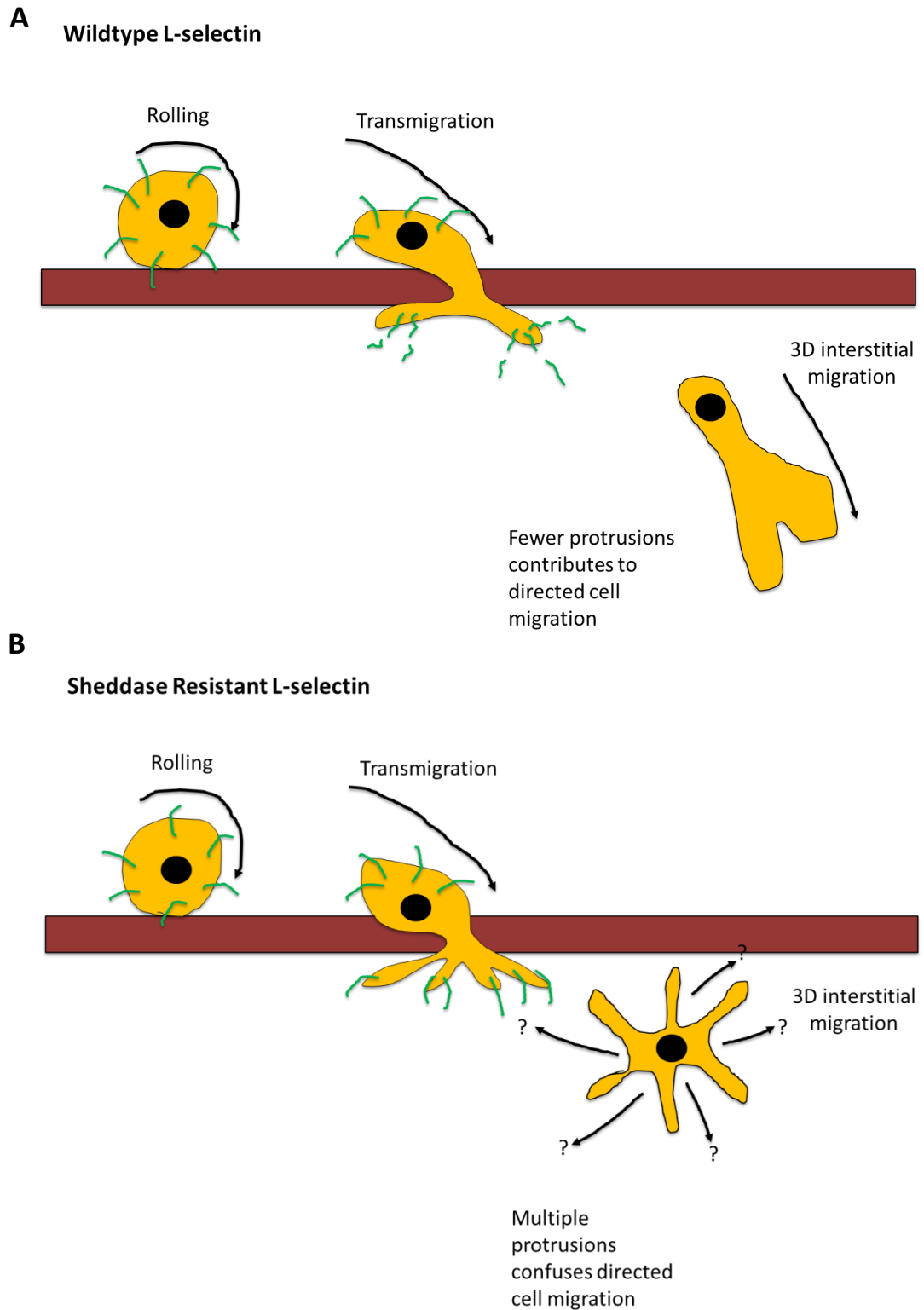
**Figure 6.32: Shedding of L-selectin may limit the number of protrusions produced during TEM.** (A) In leukocytes expressing wildtype L-selectin (shown in green), as cells transmigrate L-selectin is cleaved from the surface, leading to few protrusions and cells undergo directional migration. (B) When L-selectin shedding is blocked, cells produce multiple protrusions, which leads to a reduction in directional migration.

# Chapter 7: Discussion

The purpose of this thesis was to investigate the interaction between L-selectin and its binding partners moesin and CaM and in doing so decipher the mechanisms regulating the interactions. As this was an interdisciplinary PhD, both biophysical and cell biological methods were utilised to gain further insight into the interaction. To this end, recombinant proteins were produced as described in Chapter 3, with the proteins produced used to study the interaction with L-selectin cytosolic tail peptides using biophysical techniques such as ITC, NMR and MST (Chapter 4). In conjunction with this THP-1 cells were engineered to express L-selectin-GFP and CaM-RFP/moesin-RFP (as described in Chapter 5) and this allowed the analysis of the interaction in intact cells and during TEM (Chapter 6).

The main findings of the biophysical analysis are: i) CaM interacts with wildtype L-selectin cytosolic tail peptide in the presence and absence of calcium, though the binding mechanisms may differ, and ii) neither phosphorylation nor alanine mutation of serine residues in the cytosolic tail of L-selectin affect the interaction between the two molecules. The cell biological results also provide some interesting results, namely: i) CaM dissociates from L-selectin specifically in the transmigrated part of the cell as TEM progresses, suggesting L-selectin is cleaved only in this part of the cell, ii) blocking the phosphorylation of S364 by mutating it to alanine inhibits the dissociation of CaM in the transmigrated part of the cell during TEM and iii) mutating serine residues within L-selectin affects the protrusion dynamics of the cell as TEM progresses. These results are summarised in Table 7.1.

As previously explained (Section 1.3.7.3) CaM has been implicated in protecting L-selectin from shedding, with phosphorylation of serine residues 364 and 367 predicted to regulate CaM binding to L-selectin. The biophysical data here does not support this theory, whereas the cell biological data does suggest phosphorylation of S364 is responsible for the dissociation of CaM from L-selectin. This discrepancy highlights the importance of studying proteins in the correct context. In the case of transmembrane proteins the role of the plasma membrane should be taken into account.

| | ITC 20°C, ApoCaM | ITC 20°C, CaM-Ca | ITC 10°C, CaM-Ca | MST | GFP-Trap Assay | FRET/FLIM analysis in resting cells | FRET/FLIM analysis during TEM | | | |
|---|---|---|---|---|---|---|---|---|---|---|
| | | | | | | | 6 Minutes | | 25 Minutes | |
| | | | | | | | Non-transmigrated part of the cell | Transmigrated part of the cell | Non-transmigrated part of the cell | Transmigrated part of the cell |
| Wildtype | Binding observed | Binding observed | Binding observed | Binding observed | Binding observed | No binding observed | Binding observed | Binding observed | Binding observed | No binding observed |
| S364A | Binding observed | Not able to measure binding | Binding observed | Binding observed | Binding observed-to a lesser extent than wildtype | Binding observed | FRET similar to wildtype, suggesting binding | FRET similar to wildtype, suggesting binding | FRET similar to wildtype, suggesting binding | FRET significantly greater than wildtype, suggesting binding |
| S367A | Binding observed | Binding observed | Binding observed | Binding observed | Binding observed- to a lesser extent than wildtype | No significant difference to wildtype, suggesting no binding | FRET similar to wildtype, suggesting binding | FRET significantly less than wildtype, suggesting no binding | FRET similar to wildtype, suggesting binding | FRET similar to wildtype, suggesting no binding |
| SSAA | ND | ND | ND | ND | Binding observed- to a lesser extent than wildtype | Binding observed | FRET significantly less than wildtype, suggesting no binding | FRET significantly less than wildtype, suggesting no binding | FRET similar to wildtype, suggesting binding | FRET significantly greater than wildtype, suggesting binding |
| ΔM-N | ND | ND | ND | ND | Binding observed | No significant difference to wildtype, suggesting no binding | FRET significantly less than wildtype, suggesting no binding | FRET significantly less than wildtype, suggesting no binding | FRET similar to wildtype, suggesting binding | FRET significantly greater than wildtype, suggesting binding |

**Table 7.1: Summary of the interaction between L-selectin and CaM studied using different methodologies.** A comparison of the results from the different methods used to study the interaction between L-selectin and CaM, including biophysical, biochemical and in vivo methods, highlighting the differences observed with these methods. ND= Not Done, showing experiments that were not carried out.

## 7.1 What leads to the interaction between CaM and L-selectin upon THP-1 binding to activated endothelial cells?

The results in Section 5.3.7 of this thesis show that the L-selectin/CaM interaction is not observed in resting cells (analysed in poly-L-lysine-bound cells), most likely due to the tail of L-selectin interacting with the inner leaflet of the plasma membrane. The interaction is then present in all parts of the cell once recruitment to the endothelial monolayer has occurred, showing the association must occur at some point after adhesion to the activated endothelium. Possible mechanisms allowing CaM interaction upon activation are shown in Figure 5.16. A tempting hypothesis is that binding of ERMs causes the dissociation of L-selectin tail from the plasma membrane and allows CaM binding, which has been shown to occur *in vitro* (223). To test if this is the case in THP-1 cells, the FRET/FLIM between L-selectin-GFP and moesin/ezrin-RFP can be assessed in resting cells and after six minutes of flow. It would be expected that the interaction between L-selectin-GFP and moesin/ezrin-GFP would be lacking in resting cells but present after 6 minutes of recruitment if ERMs are responsible for desorbing the tail of L-selectin from the plasma membrane upon cell activation.

It is also plausible that S367 phosphorylation is required for the dissociation of L-selectin from the plasma membrane at early stages of recruitment (Figure 6.31). This is highlighted by the fact that S367A-L-selectin-GFP and CaM-RFP did not interact in the transmigrated part of the cell after six minutes of flow (Figure 6.4), suggesting S367 phosphorylation maybe required for the CaM binding in the transmigrated part of the cell. This could be supported by the FRET/FLIM results in resting cells (Figure 5.15), where the interaction between CaM-RFP and S364A-L-selectin-GFP observed may be a result of this alanine mutation promoting the phosphorylation of S367 and therefore dissociation of L-selectin from the plasma membrane, allowing CaM to bind.

One cannot formally exclude that phosphorylation of one of the serine residues is dramatically affected by blocking the phosphorylation of the other. For example, S364 may be hyper-phosphorylated in the S367A mutant and this could be responsible for blocking CaM binding to L-selectin in the transmigrated part of the cell. To test if this is the case, experiments could be undertaken using L-selectin embedded into liposomes enriched with different types of phospholipids, similar to the experiments

carried out by Deng *et al* (2011) (216), except using the serine to alanine or serine to aspartate (as a phosphomimetic mutation) mutants of L-selectin and assessing if the interaction between the L-selectin cytosolic tail and the liposome is affected by any of these mutations.

## 7.2 How is polarisation of L-selectin shedding controlled?

The mechanism controlling the location of CaM dissociation and therefore L-selectin shedding in the transmigrated part of the cell remains unclear. It is possible that ligation of L-selectin with ECM ligands activates signalling pathways, leading to the phosphorylation of L-selectin and therefore CaM dissociation, as described below in more detail (Section 7.4). It is also possible that ADAM17, the metalloprotease responsible for cleaving L-selectin (details in Section 1.3.4), is localised to specific parts of the cell during TEM. It has been shown that ADAM17 expression increases in T-cells stimulated with PMA (476), however, the location of the expression during TEM has not been investigated. It would be interesting to observe if an increase ADAM17 surface expression correlates with the location of L-selectin shedding during TEM.

ADAM17 has been shown to be associated with lipid rafts (101,477), with the thought that this compartmentalisation is a possible method of restricting its activity. Analysis has revealed that the proportion of the ADAM17 substrate TNF-α in the lipid raft increased when cells are treated with metalloprotease inhibitors (477), suggesting TNF-α relocated to the lipid raft in preparation for ADAM17 cleavage. It is possible that L-selectin clustering promotes its movement to lipid rafts (discussed in more detail in Section 7.4) to facilitate its cleavage by ADAM17. Interestingly, the disruption of lipid rafts by depleting cholesterol increases ADAM17-dependent cleavage of TNF-α and its receptors (477), as well as interleukin-6 receptor (IL-6R) (478), showing that the presence of lipid rafts provides an environment for the control of the location of shedding. This provides a possible method of regulation for limiting shedding to the transmigrated part of the cell, with specific signals activated upon diapedesis leading to L-selectin relocation to lipid rafts exclusively in that part of the cell.

It is possible that activation of p38 mitogen-activated protein kinase (MAPK) plays a role in regulating L-selectin shedding. p38 has been shown to be activated by L-selectin clustering (193) and this leads to the shedding of L-selectin (96,479). Analysis

of the mechanism behind this revealed that p38 phosphorylates the tail of ADAM17, which increases its surface expression (6). This could mean that ADAM17 activity is limited to the transmigrated part of the cell by the activation of p38 only occurring in this location.

## 7.3 The importance of the polarisation of L-selectin shedding: Is there a direct link to regulating protrusions?

The fact that CaM dissociated from L-selectin in the transmigrated part of the cell raised the question why polarisation of shedding occurs. The intact L-selectin on the non-transmigrated part of the cell may play a role in secondary tethering, which is thought to enhance the recruitment of leukocytes to the endothelium. The importance of L-selectin-dependent secondary tethering is discussed in Section 6.4.1. Interestingly, L-selectin-dependent secondary tethering has been observed in atherosclerotic plaques and has therefore been implicated in recruiting more leukocytes to the plaques and therefore enhancing the development of the disease (318). It would therefore be interesting to understand the mechanism behind the protection of L-selectin shedding in the non-transmigrated part of the cell as inducing the shedding of L-selectin at this location may be a possible therapeutic target for protecting against the development of atherosclerosis.

When L-selectin is shed, levels of soluble L-selectin (sL-selectin) are detectable in the blood (480), with such increases observed in many disease states, including type I diabetes (481), myocardial ischemia during angina (482) and systemic lupus erythematous (483). sL-selectin still retains its ligand binding capability (480) and is hypothesised to act as a repressor of leukocyte tethering by competing with ligands. The results here suggest that L-selectin is shed below the endothelium during TEM and this raises the question as to how it can be detected in the blood. One possibility is that endothelial cells transport sL-selectin from the abluminal to luminal side by retrograde transcytosis (463). Several different cytokines have been shown to be transported in this manner by endothelial cells so they can be presented to leukocytes. These include interleukin-8 (Il-8) (484), chemokine C-C motif ligand 2 (CCL2) (485,486) and chemokine C-X-C motif ligand 10 (CXCL10) (486), with cargo vesicles containing caveolin implicated in the process (484,486,487). Interestingly, heparan sulphate (HS)

has been shown to be important in the transcytosis of Il-8, with the C-terminal of this molecule shown to interact with HS (484). When this interaction is blocked, Il-8 is not present on the luminal surface of the endothelium (484). As explained in Section 1.3.5.2 L-selectin is capable of binding to HS presented on proteoglycans. It is therefore possible that sL-selectin interacting with HS facilitates its transportation to the luminal surface so it can act to inhibit the recruitment of further leukocytes.

Limiting the shedding of L-selectin to the transmigrated part of the cell will mean that the stump of L-selectin is only generated in this part of the cell. As stated in Section 1.3.4 it is possible the stump acts as a signalling molecule to activate different signalling pathways from full length L-selectin. The activation of L-selectin stump-specific signalling pathways in the transmigrated part of the cell implies that they might be important for the directional migration. This was assessed *in vivo* by placing a KC-coated agarose cube on the surface of the cremaster a specific distance from a post capillary venule and leukocyte migration towards the chemoattractant was assessed in wildtype, L-selectin KO, and sheddase-resistant mice (123,130). The results showed the lack of stump formation blocked chemotactic migration (123,130). It is possible that p38 MAPK is involved in the formation of the stump for chemotaxis. As stated above (Section 7.2), p38 has been implicated in L-selectin shedding and when p38 is inhibited emigration and chemotaxis is blocked (488). This provides further evidence that shedding of L-selectin and therefore stump formation is important for chemotaxis.

Analysis of cell protrusion number suggested that shedding of L-selectin is required for limiting the number of protrusions as TEM progresses (Section 6.4.4). Signalling through the formation of the stump may be responsible for reducing the number of protrusions and therefore promoting chemotaxis as stated above. It remains unclear the reason why cells expressing S367A had fewer protrusions than wildtype cells. It is possible that this mutation leads to hyper-phosphorylation of S364, leading to CaM dissociation and L-selectin shedding, potentially reducing the number of protrusions. It is also possible that serine to alanine mutations affect the binding of other partners to L-selectin. A likely candidate is the ERM family of proteins via their interaction with cell division control protein 42 (Cdc42). It has been shown that Cdc42 is a regulator in the formation of invasive filopodia in T-cells at the apical endothelial surface (489). Cdc42 is a member of the RhoGTPase family, which have been shown to

regulate cytoskeletal dynamics. When T-cells were treated with an inhibitor of Cdc42, the cells were able to arrest on HUVECs, but did not crawl or undergo TEM and no invasive filopodia were observed (489), showing the importance of Cdc42 activity in the formation of protrusions and their role in diapedesis. It has previously been shown that ERMs can regulate the activity of RhoGTPases (Section 1.5.2). Dbl is a RhoGEF which activates Cdc42. It has been shown that ezrin binds to Dbl and recruits it to lipid rafts and this leads to activation of Cdc42 at these sites (281). The expression of a dominant negative form of ezrin led to a reduction in Cdc42 activity and inhibited cell migration in MDA-MB-231 cell line (281). This shows that ezrin may play a role in protrusion formation in these cells via Cdc42 activation. It is therefore possible a similar mechanism exists in the THP-1 cell line. It is plausible that ERM interaction with L-selectin is required for the formation of protrusions and L-selectin shedding limits this process. Unearthing the effect of the serine to alanine mutations on the ERM/L-selectin interaction during TEM may provide evidence that ERMs are responsible for controlling protrusion number of THP-1 cells during TEM.

## 7.4 Is there a link between L-selectin shedding and clustering?

It has been shown that L-selectin exists as a monomer in the plasma membrane (490) and   cross-linking of L-selectin with antibody (6) or using multivalent ligands (114,180) causes shedding of L-selectin. It is hypothesised that this is due to the clustering of L-selectin. As it was observed in this thesis that CaM only dissociates from L-selectin in the transmigrated part of the cell and it is therefore likely L-selectin is only shed in this location, it was of interest to determine if this correlated with the clustering of L-selectin. Previously in the lab the clustering of L-selectin has been investigated using THP-1 cells transduced with L-selectin-GFP and L-selectin-RFP, so FRET/FLIM analysis could be undertaken to observe where and when L-selectin clustered during TEM. Interestingly, the results showed that L-selectin was only clustered in the transmigrated part of the cell after fifteen minutes of recruitment (Karolina Rzeniewicz, unpublished data), correlating with the location of the predicted shedding of L-selectin. It would therefore be plausible to predict that clustering of L-selectin is a prerequisite for the shedding of L-selectin. The mechanism behind this remains unclear, though membrane location may be important. It has been shown that

cross-linking of L-selectin in Jurkat cells relocates it to lipid rafts (450,491). It is possible that tyrosine phosphorylation of the cytosolic tail of L-selectin may act as a signal for the movement of L-selectin to the lipid rafts as a study revealed that L-selectin located in lipid rafts is tyrosine phosphorylated (450). To test the importance of tyrosine phosphorylation, cells expressing a tyrosine to alanine mutated form of L-selectin could be generated and the location of the adhesion molecule could be assessed after cell activation to observe if this mutation blocks the translocation of L-selectin to lipid rafts. As described in Section 7.2 ADAM17 is located in lipid rafts and therefore L-selectin re-localisation to the lipid raft may be required for shedding.

As described in Section 1.3.5.3 multivalent ligands have been shown to cause the shedding of L-selectin through the clustering of L-selectin, with a distance of 17-35 Å between the ligands required for the induction of shedding. HSPGs have been suggested as potential ligands for L-selectin in the ECM (see Section 1.3.5.2 for details). The HS side chains of HSPGs range from 50 to 150 saccharides in length and are only sulphated at particular sections, normally 2-8 saccharides in length (492). These highly sulphated regions, designated S domains, are uniformly distributed along the chain and are separated by non-sulphated regions 16-18 saccharides in length (493), which equates to approximately 17 Å between each S domain (494). It may be the case that the S domains of HSPGs are responsible for clustering L-selectin and causing the shedding of L-selectin. This provides an interesting hypothesis for the regulation of L-selectin shedding in the transmigrated part of the cell, summarised in Figure 7.1. Clustering of L-selectin by multivalent ligands in the ECM causes the re-localisation of L-selectin to lipid rafts and activates signalling pathways. After a time L-selectin is phosphorylated on residue S364 causing CaM dissociation and L-selectin shedding.
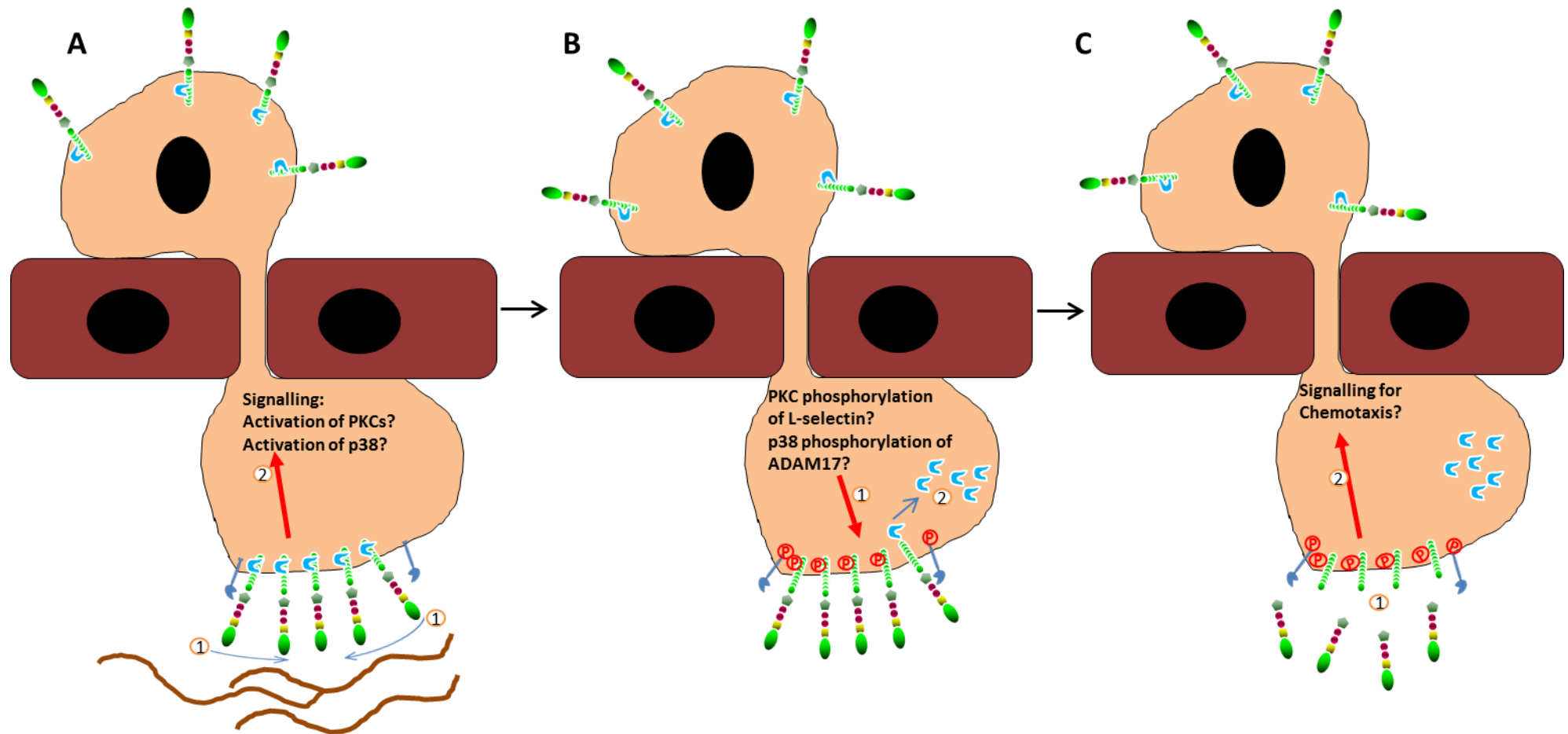
**Figure 7.1: Model of clustering of L-selectin inducing shedding.** (A) Once the leukocyte has begun transmigration, L-selectin encounters multivalent ligands, such as HSPGs, in the ECM which cause L-selectin to cluster (①). It is likely that this activates signalling pathways in the cell, such as PKC and p38 activation (②). At this time CaM (shown in blue) is bound to the tail of L-selectin, protecting it from shedding. (B) Activation of p38 and PKC may result in the phosphorylation of ADAM17 (by p38) and L-selectin (by PKCs)(①, leading to the activation of ADAM17and the dissociation of CaM from L-selectin (②). (C) Once CaM has dissociated L-selectin and ADAM17 is activated, L-selectin is shed (①), with the remaining stump potentially regulating chemotaxis (②).

315

Interestingly, clustering of L-selectin is also thought to be important for initialising signalling pathways, as highlighted by Killock *et al* (2009)(3). As described in Section 1.3.6 the Ras pathway is activated by L-selectin cross-linking via Sos/Grb (197), with Sos shown to interact with ERMs (282) and CaM interacting with k-Ras (286). It is therefore plausible that clustering of L-selectin results in activation of the Ras pathway by bring k-Ras and Sos into close proximity (Figure 7.2). It is possible that clustering of L-selectin induces its shedding via the activation of this signalling pathway. Ras signalling has been shown to activate the enzyme Rac-1 in lymphocytes (495), with k-Ras specifically shown to be able to activate Rac-1 (Figure 7.2, 1)(496). In turn Rac-1 is capable of activating phospholipase C (PLC) β2 and γ2 (Figure 7.2, 2)(497), both of which are expressed in leukocytes (498,499). PLCs produces diacylglycerol (DAG) (Figure 7.2, 3), which in turn is capable of activating conventional and novel PKCs (Figure 7.2, 4)(500), such as PKCθ, which has been shown to interact with and phosphorylate L-selectin (Figure 7.2, 5, details in Section 1.3.7.2). It is therefore conceivable that Ras activation leads to the activation of PKC, which in turn phosphorylates L-selectin causing CaM dissociation and shedding (Figure 7.2, 6). As stated in Section 7.2, L-selectin clustering also activates p38, which phosphorylates and activates ADAM17. The Ras/Rac pathway is also capable of activating p38 (Figure 7.2, 7) (501). It is therefore possible that PKCs and p38, activated by Ras signalling, act in unison to shed L-selectin following clustering (Figure 7.2).
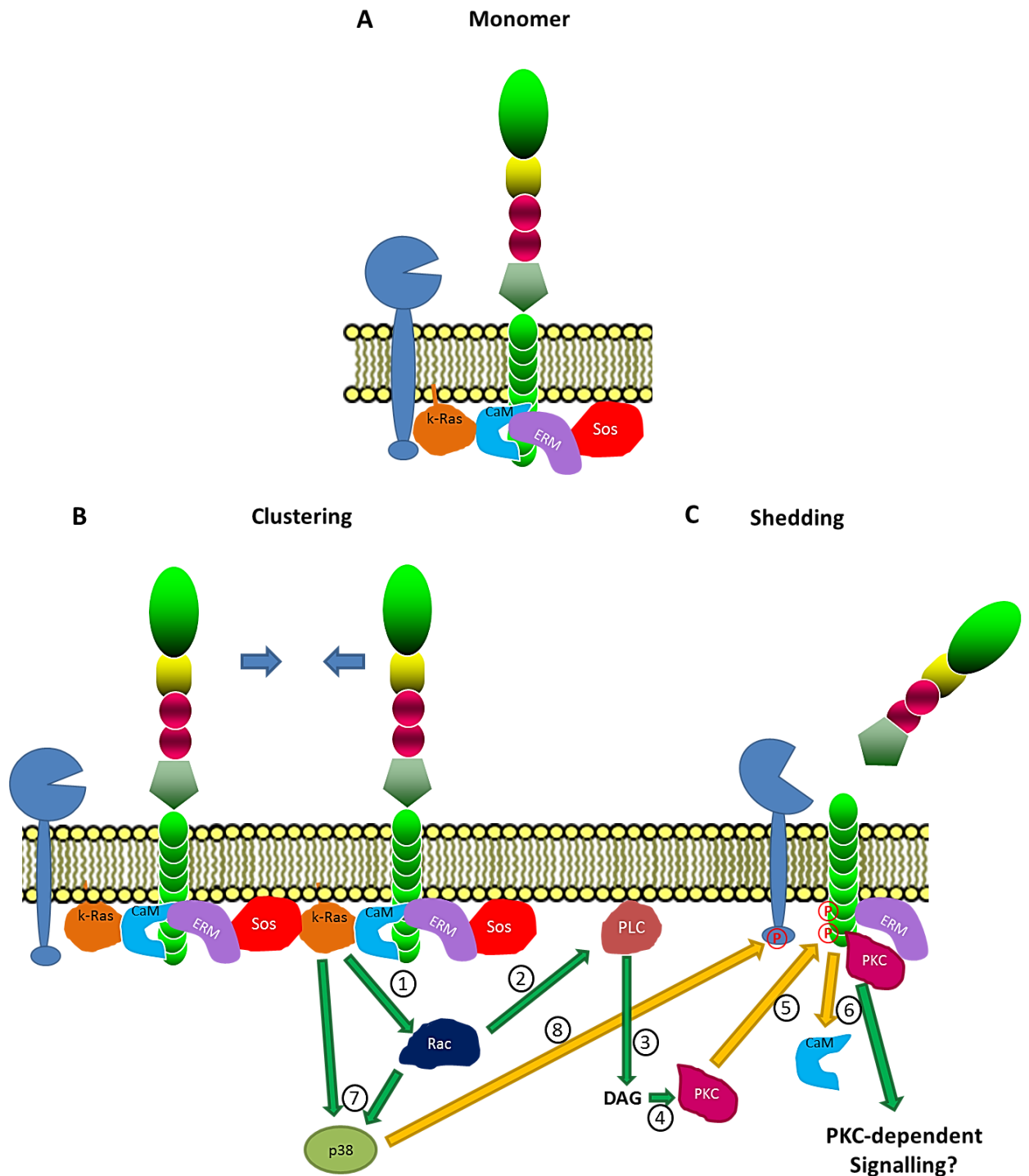
**Figure 7.2: Activation of the Ras signalling pathway following clustering of L-selectin.** It is proposed that in its monomeric form L-selectin interacts with CaM and ERM in a trimeric complex. It has been shown that CaM is able to interact with k-Ras and ERM interacts with Sos. Clustering of L-selectin may result in the activation of the Ras signalling pathway by bring k-Ras and Sos into close proximity of each other. This could potentially activate PKCs, via Rac activation of PLC (1-4), which could result in the phosphorylation of the cytosolic tail of L-selectin (5). This would result in the dissociation of CaM from L-selectin (6), meaning the adhesion molecule would be shed. At the same time Ras/Rac signalling may also activate p38 MAPK (7), which has been shown to phosphorylate and activate ADAM17 (8), enabling it to cleave L-selectin. PKCs may interact with the stump of L-selectin, inducing PKC-dependent signalling events. Figure modified from Killock, D. J., and Ivetic, A. (2010) The cytoplasmic domains of TNF-a-converting enzyme (TACE/ADAM17) and L-selectin are regulated differently by p38 MAPK and PKC to promote ectodomain shedding. Biochemical Journal 428, 293-304 (6).

## 7.5 The importance of L-selectin cytosolic tail modification in regulating leukocyte activity

The results in this thesis highlight the importance of modifications to the cytosolic tail of L-selectin in regulating leukocyte function. Phosphorylation of serine residues plays a role in regulating CaM binding (Section 6.3.4) and controlling the invasiveness of the leukocyte by regulating the protrusion dynamics (Section 6.3.6.3). It is worth noting that in this thesis the role of serine phosphorylation is investigated by mutating the residues to alanine and thereby blocking phosphorylation. This means that one can only presume that the resulting phenotypes are due to the inhibition of phosphorylation. However, it is not possible to discern if the alanine mutations are interfering with L-selectin activity independently of blocking phosphorylation. For this reason studies should be carried out using alanine to aspartate mutations to act as phosphomimetics, so results with both mutations can be analysed together to provide clearer information. In the Ivetic lab experiments with cell lines co-expressing CaM-RFP with L-selectin S364D-GFP or S367D-GFP have been undertaken. Results have revealed that the S364D mutation blocks CaM interaction with L-selectin in all parts of the cell at all time points assessed during the flow chamber assay (Dr Angela Rey, unpublished data). This correlates with the fact that when phosphorylation of S364 is blocked by alanine mutation, CaM dissociation is inhibited. In contrast, the S367D mutant does not affect binding to CaM, and is in fact indistinguishable from the FRET profiles of wildtype L-selectin (Dr Angela Rey, unpublished data) at early and late time points. Where the S367A mutant showed reduced binding to CaM, the S367D had restored this level of interaction to wildtype levels. These results would favour the idea that phosphorylation of S367 is actually dissociating the L-selectin tail from the plasma membrane. There is however, one drawback to using phosphomimetic mutants as they cannot be dephosphorylated. The data in this thesis hints at the fact that dynamic phosphorylation/dephosphorylation of the L-selectin cytosolic tail may be important for the correct regulation of activity, as highlighted by results with the ΔM-N-L-selectin mutant (Section 6.4.2). The ideal situation would be to monitor the phosphorylation state of L-selectin in real time as TEM progresses. The generation of phospho-specific antibodies to detect the phosphorylated species at S364 or S367 in primary

transmigrating monocytes would help complement the molecular mechanism uncovered so far.

## 7.6 Concluding Remarks

The results in this thesis reveal the complexity of the regulation of L-selectin interacting with its binding partners, with the interactions varying depending upon the activation status of the cell. Due to experimental limitations it was not possible to pinpoint the exact moment of CaM association/dissociation from L-selectin during TEM in real time. One possible way of following the dynamic interaction between L-selectin and its binding partners during TEM would be to carry out real-time FRET. Technology has been developed in order to a acquire high speed FLIM data and has been used to analyse FRET efficiency in pituitary cells plated on coverslips and placed in a chamber with media (502). However, with moving objects spurious signals are generated (503), so using this method in conjunction with the parallel plate flow chamber would not be possible. A previous study was able to assess the activity of RhoA in T-cells during crawling and transmigration on HUVEC monolayers using real-time FRET (504). It is possible that the same method could be employed to assess the interaction of L-selectin with its binding partners. It is worth noting however, that flow was not used in the above experiment, so therefore it will have to be assessed if this technique can be used to measure the real-time FRET with the parallel plate flow chamber assay.

This thesis focuses on the role of L-selectin and its binding partners during TEM. It is likely however, that L-selectin works in conjunction with other adhesion molecules to regulate cell activity. An example of this has been highlighted by work in the Ivetic lab. It was revealed that the cross-linking of other adhesion molecules, namely CD43 and PECAM-1 led to the clustering of L-selectin (Karolina Rzeniewicz, unpublished data). This would suggest there is a signalling event linking the different adhesion molecules, though the mechanism behind this remains unclear. It will be important to decipher the signals that link the adhesion molecules, and understand how signals converge to regulate the process of recruitment, as this may provide novel targets for therapeutics. This would be particularly useful in understanding under acute and chronic inflammatory settings.

The results provided in this thesis show the effect of blocking the phosphorylation of serine residues in the cytosolic tail of L-selectin expressed in a monocytic cell line. The next step would be to assess the effect these mutations have on leukocyte activity in an animal model. This could be investigated using lentivirus to deliver wildtype L-selectin-GFP and mutated L-selectin-RFP into the bone marrow of L-selectin knockout mice. It would then be possible to assess the response of the different leukocytes to an inflammatory insult. The response to acute inflammation could be assessed by injecting zymosan into the peritoneal cavity to induce peritonitis. The number of neutrophils and monocytes recruited to the peritoneum could then be assessed 48-72hrs after injection and the number of GFP-positive and RFP-positive cells could be compared to decipher if the mutation had an effect on leukocyte recruitment. It would also be interesting to assess if mutating L-selectin has an effect on chronic inflammation, such as the development of atherosclerosis. A similar method above could be used to analyse this, except L-selectin/ApoE double knockout mice could be transduced with the lentivirus. The mice would then be fed a high fat diet to induce the development of atherosclerotic plaques and the recruitment of the different leukocytes to the plaques could then be assessed. This would allow one to observe if the mutations that effect leukocyte TEM in the parallel plate flow chamber have an effect on *in vivo* acute and chronic inflammation.

# References

1. Fehon, R. G., McClatchey, A. I., and Bretscher, A. (2010) Organizing the cell cortex: the role of ERM proteins. *Nat Rev Mol Cell Biol* **11**, 276-287
2. Feig, A. L. (2007) Applications of isothermal titration calorimetry in RNA biochemistry and biophysics. *Biopolymers* **87**, 293-301
3. Killock, D. J., Parsons, M., Zarrouk, M., Ameer-Beg, S. M., Ridley, A. J., Haskard, D. O., Zvelebil, M., and Ivetic, A. (2009) In Vitro and in Vivo Characterization of Molecular Interactions between Calmodulin, Ezrin/Radixin/Moesin, and L-selectin. *Journal of Biological Chemistry* **284**, 8833-8845
4. Johansson, M. W., and Mosher, D. F. (2013) Integrin activation states and eosinophil recruitment in asthma. *Frontiers in Pharmacology* **4**
5. Orbay, H., Hong, H., Zhang, Y., and Cai, W. (2013) Positron emission tomography imaging of atherosclerosis. *Theranostics* **3**, 894-902
6. Killock, D. J., and Ivetic, A. (2010) The cytoplasmic domains of TNF−a-converting enzyme (TACE/ADAM17) and L-selectin are regulated differently by p38 MAPK and PKC to promote ectodomain shedding. *Biochemical Journal* **428**, 293-304
7. Wiese, G., Barthel, S. R., and Dimitroff, C. J. (2009) Analysis of physiologic E-selectin-mediated leukocyte rolling on microvascular endothelium. *Journal of visualized experiments : JoVE*
8. Xiao, L., Liu, Y., and Wang, N. (2014) New paradigms in inflammatory signaling in vascular endothelial cells. *American journal of physiology. Heart and circulatory physiology* **306**, H317-325
9. Szekanecz, Z., and Koch, A. E. (2004) Vascular endothelium and immune responses: implications for inflammation and angiogenesis. *Rheumatic diseases clinics of North America* **30**, 97-114
10. Ley, K., Laudanna, C., Cybulsky, M. I., and Nourshargh, S. (2007) Getting to the site of inflammation: the leukocyte adhesion cascade updated. *Nat Rev Immunol* **7**, 678-689
11. Mai, J., Virtue, A., Shen, J., Wang, H., and Yang, X. F. (2013) An evolving new paradigm: endothelial cells--conditional innate immune cells. *Journal of hematology & oncology* **6**, 61
12. Lopez-Dee, Z., Pidcock, K., and Gutierrez, L. S. (2011) Thrombospondin-1: Multiple Paths to Inflammation. *Mediators of Inflammation* **2011**
13. Alberts B, J. A., Lewis J, Raff M, Roberts K, Walter P. (2002) *Molecular Biology of the Cell*, 4th ed., Garland Science, New York
14. Murphy K, T. P., Walport M. (2007) *Immunobiology*, 7th ed., Garland Science, New York
15. Libby, P., Ridker, P. M., and Hansson, G. r. K. (2009) Inflammation in Atherosclerosis: From Pathophysiology to Practice. *Journal of the American College of Cardiology* **54**, 2129-2138
16. Sperandio, M., Smith, M. L., Forlow, S. B., Olson, T. S., Xia, L., McEver, R. P., and Ley, K. (2003) P-selectin Glycoprotein Ligand-1 Mediates L-Selectin-dependent Leukocyte Rolling in Venules. *The Journal of Experimental Medicine* **197**, 1355-1363
17. Brady, H. R., Spertini, O., Jimenez, W., Brenner, B. M., Marsden, P. A., and Tedder, T. F. (1992) Neutrophils, monocytes, and lymphocytes bind to cytokine-

activated kidney glomerular endothelial cells through L-selectin (LAM-1) in vitro. *Journal of immunology (Baltimore, Md. : 1950)* **149**, 2437-2444

18. Spertini, O., Luscinskas, F. W., Gimbrone, M. A., Jr., and Tedder, T. F. (1992) Monocyte attachment to activated human vascular endothelium in vitro is mediated by leukocyte adhesion molecule-1 (L-selectin) under nonstatic conditions. *J Exp Med* **175**, 1789-1792

19. Spertini, O., Luscinskas, F. W., Kansas, G. S., Munro, J. M., Griffin, J. D., Gimbrone, M. A., Jr., and Tedder, T. F. (1991) Leukocyte adhesion molecule-1 (LAM-1, L-selectin) interacts with an inducible endothelial cell ligand to support leukocyte adhesion. *Journal of immunology (Baltimore, Md. : 1950)* **147**, 2565-2573

20. Alon, R., Hammer, D. A., and Springer, T. A. (1995) Lifetime of the P-selectin-carbohydrate bond and its response to tensile force in hydrodynamic flow. *Nature* **374**, 539-542

21. Ley, K., Gaehtgens, P., Fennie, C., Singer, M. S., Lasky, L. A., and Rosen, S. D. (1991) Lectin-like cell adhesion molecule 1 mediates leukocyte rolling in mesenteric venules in vivo. *Blood* **77**, 2553-2555

22. von Andrian, U. H., Chambers, J. D., Berg, E. L., Michie, S. A., Brown, D. A., Karolak, D., Ramezani, L., Berger, E. M., Arfors, K. E., and Butcher, E. C. (1993) L-selectin mediates neutrophil rolling in inflamed venules through sialyl LewisX-dependent and -independent recognition pathways. *Blood* **82**, 182-191

23. von Andrian, U. H., Chambers, J. D., McEvoy, L. M., Bargatze, R. F., Arfors, K. E., and Butcher, E. C. (1991) Two-step model of leukocyte-endothelial cell interaction in inflammation: distinct roles for LECAM-1 and the leukocyte beta 2 integrins in vivo. *Proceedings of the National Academy of Sciences of the United States of America* **88**, 7538-7542

24. Arbones, M. L., Ord, D. C., Ley, K., Ratech, H., Maynard-Curry, C., Otten, G., Capon, D. J., and Tedder, T. F. (1994) Lymphocyte homing and leukocyte rolling and migration are impaired in L-selectin-deficient mice. *Immunity* **1**, 247-260

25. Abbassi, O., Lane, C. L., Krater, S., Kishimoto, T. K., Anderson, D. C., McIntire, L. V., and Smith, C. W. (1991) Canine neutrophil margination mediated by lectin adhesion molecule-1 in vitro. *Journal of immunology (Baltimore, Md. : 1950)* **147**, 2107-2115

26. Luscinskas, F. W., Kansas, G. S., Ding, H., Pizcueta, P., Schleiffenbaum, B. E., Tedder, T. F., and Gimbrone, M. A., Jr. (1994) Monocyte rolling, arrest and spreading on IL-4-activated vascular endothelium under flow is mediated via sequential action of L-selectin, beta 1-integrins, and beta 2-integrins. *J Cell Biol* **125**, 1417-1427

27. McEver, R. P., and Cummings, R. D. (1997) Perspectives series: cell adhesion in vascular biology. Role of PSGL-1 binding to selectins in leukocyte recruitment. *J Clin Invest* **100**, 485-491

28. Walcheck, B., Moore, K. L., McEver, R. P., and Kishimoto, T. K. (1996) Neutrophil-neutrophil interactions under hydrodynamic shear stress involve L-selectin and PSGL-1. A mechanism that amplifies initial leukocyte accumulation of P-selectin in vitro. *J Clin Invest* **98**, 1081-1087

29. Sperandio, M., Smith, M. L., Forlow, S. B., Olson, T. S., Xia, L., McEver, R. P., and Ley, K. (2003) P-selectin glycoprotein ligand-1 mediates L-selectin-dependent leukocyte rolling in venules. *J Exp Med* **197**, 1355-1363

30. da Costa Martins, P., García-Vallejo, J.-J., van Thienen, J. V., Fernandez-Borja, M., van Gils, J. M., Beckers, C., Horrevoets, A. J., Hordijk, P. L., and Zwaginga, J.-J. (2007) P-Selectin Glycoprotein Ligand-1 Is Expressed on Endothelial Cells and Mediates Monocyte Adhesion to Activated Endothelium. *Arteriosclerosis, thrombosis, and vascular biology* **27**, 1023-1029

31. Kansas, G. S. (1996) Selectins and their ligands: current concepts and controversies. *Blood* **88**, 3259-3287

32. Wang, H.-B., Wang, J.-T., Zhang, L., Geng, Z. H., Xu, W.-L., Xu, T., Huo, Y., Zhu, X., Plow, E. F., Chen, M., and Geng, J.-G. (2007) P-selectin primes leukocyte integrin activation during inflammation. *Nat Immunol* **8**, 882-892

33. McEver, R. P., Beckstead, J. H., Moore, K. L., Marshall-Carlson, L., and Bainton, D. F. (1989) GMP-140, a platelet alpha-granule membrane protein, is also synthesized by vascular endothelial cells and is localized in Weibel-Palade bodies. *J Clin Invest* **84**, 92-99

34. Berman, C. L., Yeo, E. L., Wencel-Drake, J. D., Furie, B. C., Ginsberg, M. H., and Furie, B. (1986) A platelet alpha granule membrane protein that is associated with the plasma membrane after activation. Characterization and subcellular localization of platelet activation-dependent granule-external membrane protein. *J Clin Invest* **78**, 130-137

35. Bevilacqua, M. P., Stengelin, S., Gimbrone, M. A., Jr., and Seed, B. (1989) Endothelial leukocyte adhesion molecule 1: an inducible receptor for neutrophils related to complement regulatory proteins and lectins. *Science* **243**, 1160-1165

36. Haraldsen, G., Kvale, D., Lien, B., Farstad, I. N., and Brandtzaeg, P. (1996) Cytokine-regulated expression of E-selectin, intercellular adhesion molecule-1 (ICAM-1), and vascular cell adhesion molecule-1 (VCAM-1) in human microvascular endothelial cells. *Journal of immunology (Baltimore, Md. : 1950)* **156**, 2558-2565

37. Hidalgo, A. s., Peired, A. J., Wild, M. K., Vestweber, D., and Frenette, P. S. (2007) Complete Identification of E-Selectin Ligands on Neutrophils Reveals Distinct Functions of PSGL-1, ESL-1, and CD44. *Immunity* **26**, 477-489

38. Abbassi, O., Kishimoto, T. K., McIntire, L. V., Anderson, D. C., and Smith, C. W. (1993) E-selectin supports neutrophil rolling in vitro under conditions of flow. *J Clin Invest* **92**, 2719-2730

39. Lawrence, M. B., and Springer, T. A. (1993) Neutrophils roll on E-selectin. *Journal of immunology (Baltimore, Md. : 1950)* **151**, 6338-6346

40. Olofsson, A. M., Arfors, K. E., Ramezani, L., Wolitzky, B. A., Butcher, E. C., and von Andrian, U. H. (1994) E-selectin mediates leukocyte rolling in interleukin-1-treated rabbit mesentery venules. *Blood* **84**, 2749-2758

41. Lawrence, M. B., Kansas, G. S., Kunkel, E. J., and Ley, K. (1997) Threshold levels of fluid shear promote leukocyte adhesion through selectins (CD62L,P,E). *J Cell Biol* **136**, 717-727

42. Finger, E. B., Puri, K. D., Alon, R., Lawrence, M. B., von Andrian, U. H., and Springer, T. A. (1996) Adhesion through L-selectin requires a threshold hydrodynamic shear. *Nature* **379**, 266-269

43. Sokurenko, E. V., Vogel, V., and Thomas, W. E. (2008) Catch-bond mechanism of force-enhanced adhesion: counterintuitive, elusive, but ... widespread? *Cell host & microbe* **4**, 314-323

44. Kunkel, E. J., and Ley, K. (1996) Distinct phenotype of E-selectin-deficient mice. E-selectin is required for slow leukocyte rolling in vivo. *Circulation research* **79**, 1196-1204

45. Chesnutt, B. C., Smith, D. F., Raffler, N. A., Smith, M. L., White, E. J., and Ley, K. (2006) Induction of LFA-1-dependent neutrophil rolling on ICAM-1 by engagement of E-selectin. *Microcirculation (New York, N.Y. : 1994)* **13**, 99-109

46. Kadono, T., Venturi, G. M., Steeber, D. A., and Tedder, T. F. (2002) Leukocyte rolling velocities and migration are optimized by cooperative L-selectin and intercellular adhesion molecule-1 functions. *Journal of immunology (Baltimore, Md. : 1950)* **169**, 4542-4550

47. Dunne, J. L., Ballantyne, C. M., Beaudet, A. L., and Ley, K. (2002) Control of leukocyte rolling velocity in TNF-alpha-induced inflammation by LFA-1 and Mac-1. *Blood* **99**, 336-341

48. Berlin, C., Bargatze, R. F., Campbell, J. J., von Andrian, U. H., Szabo, M. C., Hasslen, S. R., Nelson, R. D., Berg, E. L., Erlandsen, S. L., and Butcher, E. C. (1995) alpha 4 integrins mediate lymphocyte attachment and rolling under physiologic flow. *Cell* **80**, 413-422

49. Chan, J. R., Hyduk, S. J., and Cybulsky, M. I. (2001) Chemoattractants induce a rapid and transient upregulation of monocyte alpha4 integrin affinity for vascular cell adhesion molecule 1 which mediates arrest: an early step in the process of emigration. *J Exp Med* **193**, 1149-1158

50. Shamri, R., Grabovsky, V., Gauguet, J. M., Feigelson, S., Manevich, E., Kolanus, W., Robinson, M. K., Staunton, D. E., von Andrian, U. H., and Alon, R. (2005) Lymphocyte arrest requires instantaneous induction of an extended LFA-1 conformation mediated by endothelium-bound chemokines. *Nat Immunol* **6**, 497-506

51. Constantin, G., Majeed, M., Giagulli, C., Piccio, L., Kim, J. Y., Butcher, E. C., and Laudanna, C. (2000) Chemokines trigger immediate beta2 integrin affinity and mobility changes: differential regulation and roles in lymphocyte arrest under flow. *Immunity* **13**, 759-769

52. Hyduk, S. J., Chan, J. R., Duffy, S. T., Chen, M., Peterson, M. D., Waddell, T. K., Digby, G. C., Szaszi, K., Kapus, A., and Cybulsky, M. I. (2007) Phospholipase C, calcium, and calmodulin are critical for alpha4beta1 integrin affinity up-regulation and monocyte arrest triggered by chemoattractants. *Blood* **109**, 176-184

53. Tadokoro, S., Shattil, S. J., Eto, K., Tai, V., Liddington, R. C., de Pereda, J. M., Ginsberg, M. H., and Calderwood, D. A. (2003) Talin binding to integrin beta tails: a final common step in integrin activation. *Science* **302**, 103-106

54. Wegener, K. L., Partridge, A. W., Han, J., Pickford, A. R., Liddington, R. C., Ginsberg, M. H., and Campbell, I. D. (2007) Structural basis of integrin activation by talin. *Cell* **128**, 171-182

55. Giagulli, C., Ottoboni, L., Caveggion, E., Rossi, B., Lowell, C., Constantin, G., Laudanna, C., and Berton, G. (2006) The Src Family Kinases Hck and Fgr Are Dispensable for Inside-Out, Chemoattractant-Induced Signaling Regulating B2 Integrin Affinity and Valency in Neutrophils, but Are Required for B2 Integrin-Mediated Outside-In Signaling Involved in Sustained Adhesion. *The Journal of Immunology* **177**, 604-611

56. Schenkel, A. R., Mamdouh, Z., and Muller, W. A. (2004) Locomotion of monocytes on endothelium is a critical step during extravasation. *Nat Immunol* **5**, 393-400

57. Phillipson, M., Heit, B., Colarusso, P., Liu, L., Ballantyne, C. M., and Kubes, P. (2006) Intraluminal crawling of neutrophils to emigration sites: a molecularly distinct process from adhesion in the recruitment cascade. *J Exp Med* **203**, 2569-2575

58. Millan, J., and Ridley, A. J. (2005) Rho GTPases and leucocyte-induced endothelial remodelling. *The Biochemical journal* **385**, 329-337

59. Del Maschio, A., Zanetti, A., Corada, M., Rival, Y., Ruco, L., Lampugnani, M. G., and Dejana, E. (1996) Polymorphonuclear leukocyte adhesion triggers the disorganization of endothelial cell-to-cell adherens junctions. *The Journal of Cell Biology* **135**, 497-510

60. Vestweber, D. (2002) Regulation of endothelial cell contacts during leukocyte extravasation. *Curr Opin Cell Biol* **14**, 587-593

61. William A, M. (2003) Leukocyte-endothelial-cell interactions in leukocyte transmigration and the inflammatory response. *Trends in Immunology* **24**, 326-333

62. Dietmar, V. (2002) Regulation of endothelial cell contacts during leukocyte extravasation. *Current Opinion in Cell Biology* **14**, 587-593

63. Bonecchi, R. (2008) Transmigration at the borders: Recycling and trafficking of adhesion molecules. *Cell adhesion & migration* **2**, 55-56

64. Ebnet, K., Suzuki, A., Ohno, S., and Vestweber, D. (2004) Junctional adhesion molecules (JAMs): more molecules with dual functions? *Journal of cell science* **117**, 19-29

65. Carman, C. V., and Springer, T. A. (2004) A transmigratory cup in leukocyte diapedesis both through individual vascular endothelial cells and between them. *The Journal of Cell Biology* **167**, 377-388

66. Dvorak, A. M., and Feng, D. (2001) The Vesiculo-Vacuolar Organelle (VVO): A New Endothelial Cell Permeability Organelle. *Journal of Histochemistry & Cytochemistry* **49**, 419-431

67. Millan, J., Hewlett, L., Glyn, M., Toomre, D., Clark, P., and Ridley, A. J. (2006) Lymphocyte transcellular migration occurs through recruitment of endothelial ICAM-1 to caveola- and F-actin-rich domains. *Nature cell biology* **8**, 113-123

68. Hallmann, R., Horn, N., Selg, M., Wendler, O., Pausch, F., and Sorokin, L. M. (2005) Expression and Function of Laminins in the Embryonic and Mature Vasculature. *Physiological Reviews* **85**, 979-1000

69. Wang, S., Voisin, M.-B., Larbi, K. Y., Dangerfield, J., Scheiermann, C., Tran, M., Maxwell, P. H., Sorokin, L., and Nourshargh, S. (2006) Venular basement membranes contain specific matrix protein low expression regions that act as exit points for emigrating neutrophils. *The Journal of Experimental Medicine* **203**, 1519-1532

70. Dangerfield, J., Larbi, K. Y., Huang, M. T., Dewar, A., and Nourshargh, S. (2002) PECAM-1 (CD31) homophilic interaction up-regulates alpha6beta1 on transmigrated neutrophils in vivo and plays a functional role in the ability of alpha6 integrins to mediate leukocyte migration through the perivascular basement membrane. *J Exp Med* **196**, 1201-1211

71. Stoolman, L. M., and Rosen, S. D. (1983) Possible role for cell-surface carbohydrate-binding molecules in lymphocyte recirculation. *J Cell Biol* **96**, 722-729

72. Rosen, S. D., Chi, S. I., True, D. D., Singer, M. S., and Yednock, T. A. (1989) Intravenously injected sialidase inactivates attachment sites for lymphocytes on high endothelial venules. *Journal of immunology (Baltimore, Md. : 1950)* **142**, 1895-1902

73. Bevilacqua, M. P., and Nelson, R. M. (1993) Selectins. *J Clin Invest* **91**, 379-387

74. Graves, B. J., Crowther, R. L., Chandran, C., Rumberger, J. M., Li, S., Huang, K. S., Presky, D. H., Familletti, P. C., Wolitzky, B. A., and Burns, D. K. (1994) Insight into E-selectin/ligand interaction from the crystal structure and mutagenesis of the lec/EGF domains. *Nature* **367**, 532-538

75. Pigott, R., Needham, L. A., Edwards, R. M., Walker, C., and Power, C. (1991) Structural and functional studies of the endothelial activation antigen endothelial leucocyte adhesion molecule-1 using a panel of monoclonal antibodies. *Journal of immunology (Baltimore, Md. : 1950)* **147**, 130-135

76. Kansas, G. S., Saunders, K. B., Ley, K., Zakrzewicz, A., Gibson, R. M., Furie, B. C., Furie, B., and Tedder, T. F. (1994) A role for the epidermal growth factor-like domain of P-selectin in ligand recognition and cell adhesion. *J Cell Biol* **124**, 609-618

77. Jutila, M. A., Watts, G., Walcheck, B., and Kansas, G. S. (1992) Characterization of a functionally important and evolutionarily well-conserved epitope mapped to the short consensus repeats of E-selectin and L-selectin. *J Exp Med* **175**, 1565-1573

78. Bruehl, R. E., Springer, T. A., and Bainton, D. F. (1996) Quantitation of L-selectin distribution on human leukocyte microvilli by immunogold labeling and electron microscopy. *The journal of histochemistry and cytochemistry : official journal of the Histochemistry Society* **44**, 835-844

79. Sackstein, R. (2010) *Functional Glycomics*, Academic Press, USA

80. Zak, I., Lewandowska, E., and Gnyp, W. (2000) Selectin glycoprotein ligands. *Acta biochimica Polonica* **47**, 393-412

81. Varki, A. (1994) Selectin ligands. *Proceedings of the National Academy of Sciences of the United States of America* **91**, 7390-7397

82. van Zante, A., and Rosen, S. D. (2003) Sulphated endothelial ligands for L-selectin in lymphocyte homing and inflammation. *Biochemical Society transactions* **31**, 313-317

83. Lawrence, M. B. (1999) Selectin-carbohydrate interactions in shear flow. *Current opinion in chemical biology* **3**, 659-664

84. Dang, X., Raffler, N. A., and Ley, K. (2009) Transcriptional regulation of mouse L-selectin. *Biochimica et biophysica acta* **1789**, 146-152

85. Lou, Y., Lu, X., and Dang, X. (2012) FOXO1 Up-Regulates Human L-selectin Expression Through Binding to a Consensus FOXO1 Motif. *Gene regulation and systems biology* **6**, 139-149

86. Kerdiles, Y. M., Beisner, D. R., Tinoco, R., Dejean, A. S., Castrillon, D. H., DePinho, R. A., and Hedrick, S. M. (2009) Foxo1 links homing and survival of naive T cells by regulating L-selectin, CCR7 and interleukin 7 receptor. *Nat Immunol* **10**, 176-184

87. Fabre, S., Carrette, F., Chen, J., Lang, V., Semichon, M., Denoyelle, C., Lazar, V., Cagnard, N., Dubart-Kupperschmitt, A., Mangeney, M., Fruman, D. A., and

Bismuth, G. (2008) FOXO1 regulates L-Selectin and a network of human T cell homing molecules downstream of phosphatidylinositol 3-kinase. *Journal of immunology (Baltimore, Md. : 1950)* **181**, 2980-2989

88. Dengler, H. S., Baracho, G. V., Omori, S. A., Bruckner, S., Arden, K. C., Castrillon, D. H., DePinho, R. A., and Rickert, R. C. (2008) Distinct functions for the transcription factor Foxo1 at various stages of B cell differentiation. *Nat Immunol* **9**, 1388-1398

89. Chao, C. C., Jensen, R., and Dailey, M. O. (1997) Mechanisms of L-selectin regulation by activated T cells. *Journal of immunology (Baltimore, Md. : 1950)* **159**, 1686-1694

90. Kaldjian, E. P., and Stoolman, L. M. (1995) Regulation of L-selectin mRNA in Jurkat cells. Opposing influences of calcium- and protein kinase C-dependent signaling pathways. *Journal of immunology (Baltimore, Md. : 1950)* **154**, 4351-4362

91. Evans, S. S., Collea, R. P., Appenheimer, M. M., and Gollnick, S. O. (1993) Interferon-alpha induces the expression of the L-selectin homing receptor in human B lymphoid cells. *J Cell Biol* **123**, 1889-1898

92. Hebeda, C. B., Teixeira, S. A., Muscara, M. N., Vinolo, M. A., Curi, R., de Mello, S. B., and Farsky, S. H. (2008) In vivo blockade of Ca(+2)-dependent nitric oxide synthases impairs expressions of L-selectin and PECAM-1. *Biochemical and biophysical research communications* **377**, 694-698

93. Kittipatarin, C., Li, W., Durum, S. K., and Khaled, A. R. (2010) Cdc25A-driven proliferation regulates CD62L levels and lymphocyte movement in response to interleukin-7. *Experimental hematology* **38**, 1143-1156

94. Jung, T. M., and Dailey, M. O. (1990) Rapid modulation of homing receptors (gp90MEL-14) induced by activators of protein kinase C. Receptor shedding due to accelerated proteolytic cleavage at the cell surface. *Journal of immunology (Baltimore, Md. : 1950)* **144**, 3130-3136

95. Haribabu, B., Steeber, D. A., Ali, H., Richardson, R. M., Snyderman, R., and Tedder, T. F. (1997) Chemoattractant Receptor-induced Phosphorylation of L-selectin. *Journal of Biological Chemistry* **272**, 13961-13965

96. Lee, D., Schultz, J. B., Knauf, P. A., and King, M. R. (2007) Mechanical Shedding of L-selectin from the Neutrophil Surface during Rolling on Sialyl Lewis x under Flow. *Journal of Biological Chemistry* **282**, 4812-4820

97. Kishimoto, T. K., Jutila, M. A., and Butcher, E. C. (1990) Identification of a human peripheral lymph node homing receptor: a rapidly down-regulated adhesion molecule. *Proceedings of the National Academy of Sciences of the United States of America* **87**, 2244-2248

98. Zhao, L.-C., Edgar, J. B., and Dailey, M. O. (2001) Characterization of the Rapid Proteolytic Shedding of Murine L-Selectin. *Developmental Immunology* **8**, 267-277

99. Peschon, J. J., Slack, J. L., Reddy, P., Stocking, K. L., Sunnarborg, S. W., Lee, D. C., Russell, W. E., Castner, B. J., Johnson, R. S., Fitzner, J. N., Boyce, R. W., Nelson, N., Kozlosky, C. J., Wolfson, M. F., Rauch, C. T., Cerretti, D. P., Paxton, R. J., March, C. J., and Black, R. A. (1998) An Essential Role for Ectodomain Shedding in Mammalian Development. *Science* **282**, 1281-1284

100. Scheller, J., Chalaris, A., Garbers, C., and Rose-John, S. (2011) ADAM17: a molecular switch to control inflammation and tissue regeneration. *Trends Immunol* **32**, 380-387

101. Dreymueller, D., Pruessmeyer, J., Groth, E., and Ludwig, A. (2012) The role of ADAM-mediated shedding in vascular biology. *Eur J Cell Biol* **91**, 472-485

102. Arribas, J., and Esselens, C. (2009) ADAM17 as a therapeutic target in multiple diseases. *Current pharmaceutical design* **15**, 2319-2335

103. Brou, C., Logeat, F., Gupta, N., Bessia, C., LeBail, O., Doedens, J. R., Cumano, A., Roux, P., Black, R. A., and Israel, A. (2000) A novel proteolytic cleavage involved in Notch signaling: the role of the disintegrin-metalloprotease TACE. *Molecular cell* **5**, 207-216

104. Tsakadze, N. L., Sithu, S. D., Sen, U., English, W. R., Murphy, G., and D'Souza, S. E. (2006) Tumor necrosis factor-alpha-converting enzyme (TACE/ADAM-17) mediates the ectodomain cleavage of intercellular adhesion molecule-1 (ICAM-1). *The Journal of biological chemistry* **281**, 3157-3164

105. Garton, K. J., Gough, P. J., Philalay, J., Wille, P. T., Blobel, C. P., Whitehead, R. H., Dempsey, P. J., and Raines, E. W. (2003) Stimulated shedding of vascular cell adhesion molecule 1 (VCAM-1) is mediated by tumor necrosis factor-alpha-converting enzyme (ADAM 17). *The Journal of biological chemistry* **278**, 37459-37464

106. Soond, S. M., Everson, B., Riches, D. W. H., and Murphy, G. (2005) ERK-mediated phosphorylation of Thr735 in TNFα-converting enzyme and its potential role in TACE protein trafficking. *Journal of cell science* **118**, 2371-2380

107. Xu, P., and Derynck, R. (2010) Direct Activation of TACE-Mediated Ectodomain Shedding by p38 MAP Kinase Regulates EGF Receptor-Dependent Cell Proliferation. *Molecular cell* **37**, 551-566

108. Willems, S. H., Tape, C. J., Stanley, P. L., Taylor, N. A., Mills, I. G., Neal, D. E., McCafferty, J., and Murphy, G. (2010) Thiol isomerases negatively regulate the cellular shedding activity of ADAM17. *Biochemical Journal* **428**, 439-450

109. Dusterhoft, S., Jung, S., Hung, C. W., Tholey, A., Sonnichsen, F. D., Grotzinger, J., and Lorenzen, I. (2013) Membrane-proximal domain of a disintegrin and metalloprotease-17 represents the putative molecular switch of its shedding activity operated by protein-disulfide isomerase. *J Am Chem Soc* **135**, 5776-5781

110. Long, C., Wang, Y., Herrera, A. H., Horiuchi, K., and Walcheck, B. (2010) In vivo role of leukocyte ADAM17 in the inflammatory and host responses during E. coli-mediated peritonitis. *Journal of leukocyte biology* **87**, 1097-1101

111. Arndt, P. G., Strahan, B., Wang, Y., Long, C., Horiuchi, K., and Walcheck, B. (2011) Leukocyte ADAM17 regulates acute pulmonary inflammation. *PLoS One* **6**, e19938

112. Menghini, R., Fiorentino, L., Casagrande, V., Lauro, R., and Federici, M. (2013) The role of ADAM17 in metabolic inflammation. *Atherosclerosis* **228**, 12-17

113. Tang, J., Zarbock, A., Gomez, I., Wilson, C. L., Lefort, C. T., Stadtmann, A., Bell, B., Huang, L. C., Ley, K., and Raines, E. W. (2011) Adam17-dependent shedding limits early neutrophil influx but does not alter early monocyte recruitment to inflammatory sites. *Blood* **118**, 786-794

114. Smalley, D. M., and Ley, K. (2005) L-selectin: mechanisms and physiological significance of ectodomain cleavage. *Journal of Cellular and Molecular Medicine* **9**, 255-266

115. Kahn, J., Ingraham, R. H., Shirley, F., Migaki, G. I., and Kishimoto, T. K. (1994) Membrane proximal cleavage of L-selectin: identification of the cleavage site

and a 6-kD transmembrane peptide fragment of L-selectin. *The Journal of Cell Biology* **125**, 461-470

116. Stoddart, J. H., Jasuja, R. R., Sikorski, M. A., von Andrian, U. H., and Mier, J. W. (1996) Protease-resistant L-selectin mutants. Down-modulation by cross-linking but not cellular activation. *The Journal of Immunology* **157**, 5653-5659

117. Migaki, G. I., Kahn, J., and Kishimoto, T. K. (1995) Mutational analysis of the membrane-proximal cleavage site of L-selectin: relaxed sequence specificity surrounding the cleavage site. *The Journal of Experimental Medicine* **182**, 549-557

118. Zhao, L., Shey, M., Farnsworth, M., and Dailey, M. O. (2001) Regulation of membrane metalloproteolytic cleavage of L-selectin (CD62l) by the epidermal growth factor domain. *The Journal of biological chemistry* **276**, 30631-30640

119. Chen, A., Engel, P., and Tedder, T. F. (1995) Structural requirements regulate endoproteolytic release of the L-selectin (CD62L) adhesion receptor from the cell surface of leukocytes. *The Journal of Experimental Medicine* **182**, 519-530

120. Alexander, S. R., Kishimoto, T. K., and Walcheck, B. (2000) Effects of selective protein kinase C inhibitors on the proteolytic down-regulation of L-selectin from chemoattractant-activated neutrophils. *Journal of leukocyte biology* **67**, 415-422

121. Feehan, C., Darlak, K., Kahn, J., Walcheck, B., Spatola, A. F., and Kishimoto, T. K. (1996) Shedding of the Lymphocyte L-Selectin Adhesion Molecule Is Inhibited by a Hydroxamic Acid-based Protease Inhibitor. *Journal of Biological Chemistry* **271**, 7019-7024

122. Walcheck, B., Kahn, J., Fisher, J. M., Wang, B. B., Fisk, R. S., Payan, D. G., Feehan, C., Betageri, R., Darlak, K., Spatola, A. F., and Kishimoto, T. K. (1996) Neutrophil rolling altered by inhibition of L-selectin shedding in vitro. *Nature* **380**, 720-723

123. Venturi, G. M., Tu, L., Kadono, T., Khan, A. I., Fujimoto, Y., Oshel, P., Bock, C. B., Miller, A. S., Albrecht, R. M., Kubes, P., Steeber, D. A., and Tedder, T. F. (2003) Leukocyte Migration Is Regulated by L-Selectin Endoproteolytic Release. *Immunity* **19**, 713-724

124. Galkina, E., Tanousis, K., Preece, G., Tolaini, M., Kioussis, D., Florey, O., Haskard, D. O., Tedder, T. F., and Ager, A. (2003) L-Selectin Shedding Does Not Regulate Constitutive T Cell Trafficking but Controls the Migration Pathways of Antigen-activated T Lymphocytes. *The Journal of Experimental Medicine* **198**, 1323-1335

125. Tu, L., Poe, J. C., Kadono, T., Venturi, G. M., Bullard, D. C., Tedder, T. F., and Steeber, D. A. (2002) A Functional Role for Circulating Mouse L-Selectin in Regulating Leukocyte/Endothelial Cell Interactions In Vivo. *The Journal of Immunology* **169**, 2034-2043

126. Hafezi-Moghadam, A., Thomas, K. L., Prorock, A. J., Huo, Y., and Ley, K. (2001) L-Selectin Shedding Regulates Leukocyte Recruitment. *The Journal of Experimental Medicine* **193**, 863-872

127. Zhao, L. C., Edgar, J. B., and Dailey, M. O. (2001) Characterization of the rapid proteolytic shedding of murine L-selectin. *Dev Immunol* **8**, 267-277

128. Reiss, K., Maretzky, T., Ludwig, A., Tousseyn, T., de Strooper, B., Hartmann, D., and Saftig, P. (2005) ADAM10 cleavage of N-cadherin and regulation of cell-cell adhesion and beta-catenin nuclear signalling. *Embo j* **24**, 742-752

129. Okamoto, I., Kawano, Y., Murakami, D., Sasayama, T., Araki, N., Miki, T., Wong, A. J., and Saya, H. (2001) Proteolytic release of CD44 intracellular domain and its role in the CD44 signaling pathway. *J Cell Biol* **155**, 755-762

130. Hickey, M. J., Forster, M., Mitchell, D., Kaur, J., De Caigny, C., and Kubes, P. (2000) L-selectin facilitates emigration and extravascular locomotion of leukocytes during acute inflammatory responses in vivo. *Journal of immunology (Baltimore, Md. : 1950)* **165**, 7164-7170

131. Zarbock, A., and Rossaint, J. (2013) L-selectin shedding by NSAIDs: old friends in new dresses. *European journal of immunology* **43**, 50-54

132. Herrera-Garcia, A., Dominguez-Luis, M., Arce-Franco, M., Lopez-Fernandez, J., Feria, M., Barreiro, O., Sanchez-Madrid, F., and Diaz-Gonzalez, F. (2013) In vivo modulation of the inflammatory response by nonsteroidal antiinflammatory drug-related compounds that trigger L-selectin shedding. *European journal of immunology* **43**, 55-64

133. Diaz-Gonzalez, F., and Sanchez-Madrid, F. (1998) Inhibition of leukocyte adhesion: an alternative mechanism of action for anti-inflammatory drugs. *Immunology today* **19**, 169-172

134. Gomez-Gaviro, M. V., Dominguez-Jimenez, C., Carretero, J. M., Sabando, P., Gonzalez-Alvaro, I., Sanchez-Madrid, F., and Diaz-Gonzalez, F. (2000) Down-regulation of L-selectin expression in neutrophils by nonsteroidal anti-inflammatory drugs: role of intracellular ATP concentration. *Blood* **96**, 3592-3600

135. Dominguez-Luis, M., Herrera-Garcia, A., Arce-Franco, M., Armas-Gonzalez, E., Rodriguez-Pardo, M., Lorenzo-Diaz, F., Feria, M., Cadenas, S., Sanchez-Madrid, F., and Diaz-Gonzalez, F. (2013) Superoxide anion mediates the L-selectin down-regulation induced by non-steroidal anti-inflammatory drugs in human neutrophils. *Biochemical pharmacology* **85**, 245-256

136. Uchimura, K., Kadomatsu, K., El-Fasakhany, F. M., Singer, M. S., Izawa, M., Kannagi, R., Takeda, N., Rosen, S. D., and Muramatsu, T. (2004) N-acetylglucosamine 6-O-sulfotransferase-1 regulates expression of L-selectin ligands and lymphocyte homing. *The Journal of biological chemistry* **279**, 35001-35008

137. Xiao, B., Tong, C., Jia, X., Guo, R., Lu, S., Zhang, Y., McEver, R. P., Zhu, C., and Long, M. (2012) Tyrosine replacement of PSGL-1 reduces association kinetics with P- and L-selectin on the cell membrane. *Biophysical journal* **103**, 777-785

138. Martinez, M., Joffraud, M., Giraud, S., Baisse, B., Bernimoulin, M. P., Schapira, M., and Spertini, O. (2005) Regulation of PSGL-1 interactions with L-selectin, P-selectin, and E-selectin: role of human fucosyltransferase-IV and -VII. *The Journal of biological chemistry* **280**, 5378-5390

139. Leppanen, A., Yago, T., Otto, V. I., McEver, R. P., and Cummings, R. D. (2003) Model glycosulfopeptides from P-selectin glycoprotein ligand-1 require tyrosine sulfation and a core 2-branched O-glycan to bind to L-selectin. *The Journal of biological chemistry* **278**, 26391-26400

140. Ramachandran, V., Nollert, M. U., Qiu, H., Liu, W. J., Cummings, R. D., Zhu, C., and McEver, R. P. (1999) Tyrosine replacement in P-selectin glycoprotein ligand-1 affects distinct kinetic and mechanical properties of bonds with P- and L-selectin. *Proceedings of the National Academy of Sciences of the United States of America* **96**, 13771-13776

141. Imai, Y., Lasky, L. A., and Rosen, S. D. (1993) Sulphation requirement for GlyCAM-1, an endothelial ligand for L-selectin. *Nature* **361**, 555-557

142. Nicholson, M. W., Barclay, A. N., Singer, M. S., Rosen, S. D., and van der Merwe, P. A. (1998) Affinity and kinetic analysis of L-selectin (CD62L) binding to glycosylation-dependent cell-adhesion molecule-1. *The Journal of biological chemistry* **273**, 763-770

143. Hwang, S. T., Singer, M. S., Giblin, P. A., Yednock, T. A., Bacon, K. B., Simon, S. I., and Rosen, S. D. (1996) GlyCAM-1, a physiologic ligand for L-selectin, activates beta 2 integrins on naive peripheral lymphocytes. *J Exp Med* **184**, 1343-1348

144. Suguri, T., Kikuta, A., Iwagaki, H., Yoshino, T., Tanaka, N., and Orita, K. (1996) Increased plasma GlyCAM-1, a mouse L-selectin ligand, in response to an inflammatory stimulus. *Journal of leukocyte biology* **60**, 593-597

145. Kobayashi, M., Hoshino, H., Masumoto, J., Fukushima, M., Suzawa, K., Kageyama, S., Suzuki, M., Ohtani, H., Fukuda, M., and Nakayama, J. (2009) GlcNAc6ST-1-mediated decoration of MAdCAM-1 protein with L-selectin ligand carbohydrates directs disease activity of ulcerative colitis. *Inflammatory bowel diseases* **15**, 697-706

146. Berg, E. L., McEvoy, L. M., Berlin, C., Bargatze, R. F., and Butcher, E. C. (1993) L-selectin-mediated lymphocyte rolling on MAdCAM-1. *Nature* **366**, 695-698

147. Satomaa, T., Renkonen, O., Helin, J., Kirveskari, J., Makitie, A., and Renkonen, R. (2002) O-glycans on human high endothelial CD34 putatively participating in L-selectin recognition. *Blood* **99**, 2609-2611

148. Hernandez Mir, G., Helin, J., Skarp, K. P., Cummings, R. D., Makitie, A., Renkonen, R., and Leppanen, A. (2009) Glycoforms of human endothelial CD34 that bind L-selectin carry sulfated sialyl Lewis x capped O- and N-glycans. *Blood* **114**, 733-741

149. McEvoy, L. M., Sun, H., Frelinger, J. G., and Butcher, E. C. (1997) Anti-CD43 inhibition of T cell homing. *J Exp Med* **185**, 1493-1498

150. McEvoy, L. M., Jutila, M. A., Tsao, P. S., Cooke, J. P., and Butcher, E. C. (1997) Anti-CD43 inhibits monocyte-endothelial adhesion in inflammation and atherogenesis. *Blood* **90**, 3587-3594

151. Stockton, B. M., Cheng, G., Manjunath, N., Ardman, B., and von Andrian, U. H. (1998) Negative regulation of T cell homing by CD43. *Immunity* **8**, 373-381

152. Fieger, C. B., Sassetti, C. M., and Rosen, S. D. (2003) Endoglycan, a member of the CD34 family, functions as an L-selectin ligand through modification with tyrosine sulfation and sialyl Lewis x. *The Journal of biological chemistry* **278**, 27390-27398

153. Celie, J. W., Beelen, R. H., and van den Born, J. (2009) Heparan sulfate proteoglycans in extravasation: assisting leukocyte guidance. *Frontiers in bioscience (Landmark edition)* **14**, 4932-4949

154. Yen, W. Y., Cai, B., Zeng, M., Tarbell, J. M., and Fu, B. M. (2012) Quantification of the endothelial surface glycocalyx on rat and mouse blood vessels. *Microvascular research* **83**, 337-346

155. Constantinescu, A. A., Vink, H., and Spaan, J. A. (2003) Endothelial cell glycocalyx modulates immobilization of leukocytes at the endothelial surface. *Arteriosclerosis, thrombosis, and vascular biology* **23**, 1541-1547

156. Celie, J. W., Keuning, E. D., Beelen, R. H., Drager, A. M., Zweegman, S., Kessler, F. L., Soininen, R., and van den Born, J. (2005) Identification of L-selectin

binding heparan sulfates attached to collagen type XVIII. *The Journal of biological chemistry* **280**, 26965-26973

157. Watanabe, N., Kawashima, H., Li, Y. F., and Miyasaka, M. (1999) Identification and characterization of ligands for L-selectin in the kidney. III. Characterization of L-selectin reactive heparan sulfate proteoglycans. *Journal of biochemistry* **125**, 826-831

158. Li, Y. F., Kawashima, H., Watanabe, N., and Miyasaka, M. (1999) Identification and characterization of ligands for L-selectin in the kidney. II. Expression of chondroitin sulfate and heparan sulfate proteoglycans reactive with L-selectin. *FEBS Lett* **444**, 201-205

159. Giuffre, L., Cordey, A. S., Monai, N., Tardy, Y., Schapira, M., and Spertini, O. (1997) Monocyte adhesion to activated aortic endothelium: role of L-selectin and heparan sulfate proteoglycans. *J Cell Biol* **136**, 945-956

160. Wang, L., Fuster, M., Sriramarao, P., and Esko, J. D. (2005) Endothelial heparan sulfate deficiency impairs L-selectin- and chemokine-mediated neutrophil trafficking during inflammatory responses. *Nat Immunol* **6**, 902-910

161. Kawashima, H., Hirose, M., Hirose, J., Nagakubo, D., Plaas, A. H., and Miyasaka, M. (2000) Binding of a large chondroitin sulfate/dermatan sulfate proteoglycan, versican, to L-selectin, P-selectin, and CD44. *The Journal of biological chemistry* **275**, 35448-35456

162. Kitaya, K., and Yasuo, T. (2009) Dermatan sulfate proteoglycan biglycan as a potential selectin L/CD44 ligand involved in selective recruitment of peripheral blood CD16(-) natural killer cells into human endometrium. *Journal of leukocyte biology* **85**, 391-400

163. Suzuki, Y., Toda, Y., Tamatani, T., Watanabe, T., Suzuki, T., Nakao, T., Murase, K., Kiso, M., Hasegawa, A., Tadanoaritomi, K., Ishizuka, I., and Miyasaka, M. (1993) Sulfated Glycolipids Are Ligands for a Lymphocyte Homing Receptor, L-Selectin (LECAM-1), Binding Epitope in Sulfated Sugar Chain. *Biochemical and Biophysical Research Communications* **190**, 426-434

164. Ogawa, D., Shikata, K., Honke, K., Sato, S., Matsuda, M., Nagase, R., Tone, A., Okada, S., Usui, H., Wada, J., Miyasaka, M., Kawashima, H., Suzuki, Y., Suzuki, T., Taniguchi, N., Hirahara, Y., Tadano-Aritomi, K., Ishizuka, I., Tedder, T. F., and Makino, H. (2004) Cerebroside Sulfotransferase Deficiency Ameliorates L-selectin-dependent Monocyte Infiltration in the Kidney after Ureteral Obstruction. *Journal of Biological Chemistry* **279**, 2085-2090

165. Cahalon, L., Lider, O., Schor, H., Avron, A., Gilat, D., Hershkoviz, R., Margalit, R., Eshel, A., Shoseyev, O., and Cohen, I. R. (1997) Heparin disaccharides inhibit tumor necrosis factor-alpha production by macrophages and arrest immune inflammation in rodents. *International immunology* **9**, 1517-1522

166. Hershkoviz, R., Schor, H., Ariel, A., Hecht, I., Cohen, I. R., Lider, O., and Cahalon, L. (2000) Disaccharides generated from heparan sulphate or heparin modulate chemokine-induced T-cell adhesion to extracellular matrix. *Immunology* **99**, 87-93

167. Dallas, M. R., Chen, S. H., Streppel, M. M., Sharma, S., Maitra, A., and Konstantopoulos, K. (2012) Sialofucosylated podocalyxin is a functional E- and L-selectin ligand expressed by metastatic pancreatic cancer cells. *American journal of physiology. Cell physiology* **303**, C616-624

168. Thomas, S. N., Schnaar, R. L., and Konstantopoulos, K. (2009) Podocalyxin-like protein is an E-/L-selectin ligand on colon carcinoma cells: comparative

biochemical properties of selectin ligands in host and tumor cells. *American journal of physiology. Cell physiology* **296**, C505-513

169. Sassetti, C., Tangemann, K., Singer, M. S., Kershaw, D. B., and Rosen, S. D. (1998) Identification of podocalyxin-like protein as a high endothelial venule ligand for L-selectin: parallels to CD34. *J Exp Med* **187**, 1965-1975

170. Kerr, S. C., Fieger, C. B., Snapp, K. R., and Rosen, S. D. (2008) Endoglycan, a member of the CD34 family of sialomucins, is a ligand for the vascular selectins. *Journal of immunology (Baltimore, Md. : 1950)* **181**, 1480-1490

171. Kanda, H., Tanaka, T., Matsumoto, M., Umemoto, E., Ebisuno, Y., Kinoshita, M., Noda, M., Kannagi, R., Hirata, T., Murai, T., Fukuda, M., and Miyasaka, M. (2004) Endomucin, a sialomucin expressed in high endothelial venules, supports L-selectin-mediated rolling. *International immunology* **16**, 1265-1274

172. Samulowitz, U., Kuhn, A., Brachtendorf, G., Nawroth, R., Braun, A., Bankfalvi, A., Bocker, W., and Vestweber, D. (2002) Human endomucin: distribution pattern, expression on high endothelial venules, and decoration with the MECA-79 epitope. *The American journal of pathology* **160**, 1669-1681

173. Hemmerich, S., Butcher, E. C., and Rosen, S. D. (1994) Sulfation-dependent recognition of high endothelial venules (HEV)-ligands by L-selectin and MECA 79, and adhesion-blocking monoclonal antibody. *J Exp Med* **180**, 2219-2226

174. Hoke, D., Mebius, R. E., Dybdal, N., Dowbenko, D., Gribling, P., Kyle, C., Baumhueter, S., and Watson, S. R. (1995) Selective modulation of the expression of L-selectin ligands by an immune response. *Current biology : CB* **5**, 670-678

175. Harms, G., Kraft, R., Grelle, G., Volz, B., Dernedde, J., and Tauber, R. (2001) Identification of nucleolin as a new L-selectin ligand. *The Biochemical journal* **360**, 531-538

176. Zollner, O., Lenter, M. C., Blanks, J. E., Borges, E., Steegmaier, M., Zerwes, H. G., and Vestweber, D. (1997) L-selectin from human, but not from mouse neutrophils binds directly to E-selectin. *J Cell Biol* **136**, 707-716

177. Kawashima, H., Watanabe, N., Hirose, M., Sun, X., Atarashi, K., Kimura, T., Shikata, K., Matsuda, M., Ogawa, D., Heljasvaara, R., Rehn, M., Pihlajaniemi, T., and Miyasaka, M. (2003) Collagen XVIII, a basement membrane heparan sulfate proteoglycan, interacts with L-selectin and monocyte chemoattractant protein-1. *The Journal of biological chemistry* **278**, 13069-13076

178. Kawashima, H., Li, Y. F., Watanabe, N., Hirose, J., Hirose, M., and Miyasaka, M. (1999) Identification and characterization of ligands for L-selectin in the kidney. I. Versican, a large chondroitin sulfate proteoglycan, is a ligand for L-selectin. *International immunology* **11**, 393-405

179. Jin, C., Ekwall, A. K., Bylund, J., Bjorkman, L., Estrella, R. P., Whitelock, J. M., Eisler, T., Bokarewa, M., and Karlsson, N. G. (2012) Human synovial lubricin expresses sialyl Lewis x determinant and has L-selectin ligand activity. *The Journal of biological chemistry* **287**, 35922-35933

180. Mowery, P., Yang, Z. Q., Gordon, E. J., Dwir, O., Spencer, A. G., Alon, R., and Kiessling, L. L. (2004) Synthetic glycoprotein mimics inhibit L-selectin-mediated rolling and promote L-selectin shedding. *Chemistry & biology* **11**, 725-732

181. Sanders, W. J., Gordon, E. J., Dwir, O., Beck, P. J., Alon, R., and Kiessling, L. L. (1999) Inhibition of L-selectin-mediated leukocyte rolling by synthetic glycoprotein mimics. *The Journal of biological chemistry* **274**, 5271-5278

182. Liu, S., and Kiick, K. (2011) Architecture effects on L-selectin shedding induced by polypeptide-based multivalent ligands. *Polymer chemistry* **2**, 1513-1522

183. Crockett-Torabi, E., Sulenbarger, B., Smith, C. W., and Fantone, J. C. (1995) Activation of human neutrophils through L-selectin and Mac-1 molecules. *The Journal of Immunology* **154**, 2291-2302

184. Waddell, T. K., Fialkow, L., Chan, C. K., Kishimoto, T. K., and Downey, G. P. (1994) Potentiation of the oxidative burst of human neutrophils. A signaling role for L-selectin. *Journal of Biological Chemistry* **269**, 18485-18491

185. Laudanna, C., Constantin, G., Baron, P., Scarpini, E., Scarlato, G., Cabrini, G., Dechecchi, C., Rossi, F., Cassatella, M. A., and Berton, G. (1994) Sulfatides trigger increase of cytosolic free calcium and enhanced expression of tumor necrosis factor-alpha and interleukin-8 mRNA in human neutrophils. Evidence for a role of L-selectin as a signaling molecule.

186. Green, C. E., Pearson, D. N., Camphausen, R. T., Staunton, D. E., and Simon, S. I. (2004) Shear-Dependent Capping of L-Selectin and P-Selectin Glycoprotein Ligand 1 by E-Selectin Signals Activation of High-Avidity β2-Integrin on Neutrophils. *the Journal of Immunology* **172**, 7780-7790

187. Giblin, P. A., Hwang, S. T., Katsumoto, T. R., and Rosen, S. D. (1997) Ligation of L-selectin on T lymphocytes activates beta1 integrins and promotes adhesion to fibronectin. *The Journal of Immunology* **159**, 3498-3507

188. Simon, S. I., Burns, A. R., Taylor, A. D., Gopalan, P. K., Lynam, E. B., Sklar, L. A., and Smith, C. W. (1995) L-selectin (CD62L) cross-linking signals neutrophil adhesive functions via the Mac-1 (CD11b/CD18) β2-integrin. *Journal of Immunology* **155**, 1502-1514

189. Zarbock, A., Lowell, C. A., and Ley, K. (2007) Spleen tyrosine kinase Syk is necessary for E-selectin-induced alpha(L)beta(2) integrin-mediated rolling on intercellular adhesion molecule-1. *Immunity* **26**, 773-783

190. Kuwano, Y., Spelten, O., Zhang, H., Ley, K., and Zarbock, A. (2010) Rolling on E- or P-selectin induces the extended but not high-affinity conformation of LFA-1 in neutrophils. *Blood* **116**, 617-624

191. Stadtmann, A., Germena, G., Block, H., Boras, M., Rossaint, J., Sundd, P., Lefort, C., Fisher, C. I., Buscher, K., Gelschefarth, B., Urzainqui, A., Gerke, V., Ley, K., and Zarbock, A. (2013) The PSGL-1-L-selectin signaling complex regulates neutrophil adhesion under flow. *J Exp Med* **210**, 2171-2180

192. Waddell, T. K., Fialkow, L., Chi Kin, C., Takashi Kei, K., and Downey, G. P. (1995) Signaling functions of L-selectin. Enhancement of tyrosine phosphorylation and activation of MAP kinase. *Journal of Biological Chemistry* **270**, 15403-15411

193. Smolen, J. E., Petersen, T. K., Koch, C., O'Keefe, S. J., Hanlon, W. A., Seo, S., Pearson, D., Fossett, M. C., and Simon, S. I. (2000) L-selectin signaling of neutrophil adhesion and degranulation involves p38 mitogen-activated protein kinase. *Journal of Biological Chemistry* **275**, 15876-15884

194. Turutin, D. V., Kubareva, E. A., Pushkareva, M. A., Ullrich, V., and Sud'ina, G. F. (2003) Activation of NF-kappa B transcription factor in human neutrophils by sulphatides and L-selectin cross-linking. *FEBS Lett* **536**, 241-245

195. Udalova, I. A., Knight, J. C., Vidal, V., Nedospasov, S. A., and Kwiatkowski, D. (1998) Complex NF-κB interactions at the distal tumor necrosis factor promoter region in human monocytes. *Journal of Biological Chemistry* **273**, 21178-21186

196. Fujiie, S., Hieshima, K., Izawa, D., Nakayama, T., Fujisawa, R., Ohyanagi, H., and Yoshie, O. (2001) Proinflammatory cytokines induce liver and activation-

regulated chemokine/macrophage inflammatory protein-3α/CCL20 in mucosal epithelial cells through NK-κB. *International immunology* **13**, 1255-1263

197. Brenner, B., Gulbins, E., Schlottmann, K., Koppenhoefer, U., Busch, G. L., Walzog, B., Steinhausen, M., Coggeshall, K. M., Linderkamp, O., and Lang, F. (1996) l-Selectin activates the Ras pathway via the tyrosine kinase p56lck. *Proc. Natl. Acad. Sci.* **93**, 15376-15381

198. Barkhausen, T., Krettek, C., and Griensven, M. v. (2005) L-selectin: Adhesion, signalling and its importance in pathologic posttraumatic endotoxemia and non-septic inflammation. *Experimental and Toxicologic Pathology* **57**, 39-52

199. Brenner, B., Gulbins, E., Busch, G. L., Koppenhoefer, U., Lang, F., and Linderkamp, O. (1997) L-selectin regulates actin polymerisation via activation of the small G-protein Rac2. *Biochemical and Biophysical Research Communications* **231**, 802-807

200. Brenner, B., Weinmann, S., Grassmé, H., Lang, F., Linderkamp, O., and Gulbins, E. (1997) L-selectin activates JNK via src-like tyrosine kinases and the small G-protein Rac. *Immunology* **92**, 214-219

201. Brenner, B. C., Kadel, S., Grigorovich, S., and Linderkamp, O. (2002) Mechanisms of L-selectin-induced activation of the nuclear factor of activated T lymphocytes (NFAT). *Biochemical and Biophysical Research Communications* **291**, 237-244

202. Chen, C., Cui, L., Shang, X., and Zeng, X. (2010) NFAT regulates CSF-1 gene transcription triggered by L-selectin crosslinking. *Biocell : official journal of the Sociedades Latinoamericanas de Microscopia Electronica ... et. al* **34**, 57-63

203. Brenner, B., Grassmé, H. U. C., Müller, C., Lang, F., Speer, C. P., and Gulbins, E. (1998) L-selectin stimulates the neutral sphingomyelinase and induces release of ceramide. *Experimental Cell Research* **243**, 123-128

204. Schütze, S., Machleidt, T., and Krönke, M. (1994) The role of diacylglycerol and ceramide in tumor necrosis factor and interleukin-1 signal transduction. *Journal of leukocyte biology* **56**, 533-541

205. Kolesnick, R., and Golde, D. W. (1994) The sphingomyelin pathway in tumor necrosis factor and interleukin-1 signaling. *Cell* **77**, 325-328

206. Schutze, S., Potthoff, K., Machleidt, T., Berkovic, D., Wiegmann, K., and Kronke, M. (1992) TNF activates NF-kappa B by phosphatidylcholine-specific phospholipase C-induced "acidic" sphingomyelin breakdown. *Cell* **71**, 765-776

207. Machleidt, T., Wiegmann, K., Henkel, T., Schutze, S., Baeuerle, P., and Kronke, M. (1994) Sphingomyelinase activates proteolytic I kappa B-alpha degradation in a cell-free system. *The Journal of biological chemistry* **269**, 13760-13765

208. Ding, Z., Issekutz, T. B., Downey, G. P., and Waddell, T. K. (2003) L-selectin stimulation enhances functional expression of surface CXCR4 in lymphocytes: implications for cellular activation during adhesion and migration. *Blood* **101**, 4245-4252

209. Perfilyeva, Y. V., Kustova, E. A., Urazalieva, N. T., Baisheva, S. A., Aubakirova, A. T., Tleulieva, R. T., Belyaev, N. N., and Zakiryanova, G. K. (2012) Effects of L-selectin stimulation of the expression of chemokine receptor CXCR4 on NK cells of healthy donors and tumor patients. *Bulletin of experimental biology and medicine* **153**, 86-88

210. Subramanian, H., Grailer, J. J., Ohlrich, K. C., Rymaszewski, A. L., Loppnow, J. J., Kodera, M., Conway, R. M., and Steeber, D. A. (2012) Signaling through L-selectin mediates enhanced chemotaxis of lymphocyte subsets to secondary

lymphoid tissue chemokine. *Journal of immunology (Baltimore, Md. : 1950)* **188**, 3223-3236

211. Ivetic, A., Ridley Anne. (2004) The Telling tail of L-selectin. *biochemical soceity transactions* **32**, 1118-1121

212. Dwir, O., Kansas, G. S., and Alon, R. (2001) Cytoplasmic anchorage of L-selectin controls leukocyte capture and rolling by increasing the mechanical stability of the selectin tether. *The Journal of Cell Biology* **155**, 145-156

213. Pavalko, F. M., Walker, D. M., Graham, L., Goheen, M., Doerschuk, C. M., and Kansas, G. S. (1995) The cytoplasmic domain of L-selectin interacts with cytoskeletal proteins via alpha-actinin: receptor positioning in microvilli does not require interaction with alpha-actinin. *J Cell Biol* **129**, 1155-1164

214. Kilian, K., Dernedde, J., Mueller, E.-C., Bahr, I., and Tauber, R. (2004) The Interaction of Protein Kinase C Isozymes alpha, iota, and theta¸ with the Cytoplasmic Domain of L-selectin Is Modulated by Phosphorylation of the Receptor. *Journal of Biological Chemistry* **279**, 34472-34480

215. Kahn, J., Walcheck, B., Migaki, G. I., Jutila, M. A., and Kishimoto, T. K. (1998) Calmodulin Regulates L-Selectin Adhesion Molecule Expression and Function through a Protease-Dependent Mechanism. *Cell* **92**, 809-818

216. Deng, W., Srinivasan, S., Zheng, X., Putkey, J. A., and Li, R. (2011) Interaction of Calmodulin with l-Selectin at the Membrane Interface: Implication on the Regulation of l-Selectin Shedding. *Journal of Molecular Biology* **411**, 220-233

217. Wong, M.-X., Harbour, S. N., Wee, J. L., Lau, L.-M., Andrews, R. K., and Jackson, D. E. (2004) Proteolytic cleavage of platelet endothelial cell adhesion molecule-1 (PECAM-1/CD31) is regulated by a calmodulin-binding motif. *FEBS Letters* **568**, 70-78

218. Lai, Z. W., Lew, R. A., Yarski, M. A., Mu, F.-T., Andrews, R. K., and Smith, A. I. (2009) The Identification of a Calmodulin-Binding Domain within the Cytoplasmic Tail of Angiotensin-Converting Enzyme-2. *Endocrinology* **150**, 2376-2381

219. Mo, X., Nguyen, N. X., Mu, F. T., Yang, W., Luo, S. Z., Fan, H., Andrews, R. K., Berndt, M. C., and Li, R. (2010) Transmembrane and trans-subunit regulation of ectodomain shedding of platelet glycoprotein Ibalpha. *The Journal of biological chemistry* **285**, 32096-32104

220. Andrews, R. K., Munday, A. D., Mitchell, C. A., and Berndt, M. C. (2001) Interaction of calmodulin with the cytoplasmic domain of the platelet membrane glycoprotein Ib-IX-V complex. *Blood* **98**, 681-687

221. Andrews, R. K., Suzuki-Inoue, K., Shen, Y., Tulasne, D., Watson, S. P., and Berndt, M. C. (2002) Interaction of calmodulin with the cytoplasmic domain of platelet glycoprotein VI. *Blood* **99**, 4219-4221

222. Dewitz, C., Moller-Hackbarth, K., Schweigert, O., Reiss, K., Chalaris, A., Scheller, J., and Rose-John, S. (2014) T-cell immunoglobulin and mucin domain 2 (TIM-2) is a target of ADAM10-mediated ectodomain shedding. *The FEBS journal* **281**, 157-174

223. Deng, W., Cho, S., and Li, R. (2013) FERM Domain of Moesin Desorbs the Basic-Rich Cytoplasmic Domain of l-Selectin from the Anionic Membrane Surface. *J Mol Biol* **425**, 3549-3562

224. Ivetic, A., Deka, J., Ridley, A., and Ager, A. (2002) The Cytoplasmic Tail of L-selectin Interacts with Members of the Ezrin-Radixin-Moesin (ERM) Family of Proteins. *the Journal of Biological Chemistry* **277**, 2321-2329

225. Ivetic, A., Florey, O., Deka, J., Haskard, D. O., Ager, A., and Ridley, A. J. (2004) Mutagenesis of the Ezrin-Radixin-Moesin Binding Domain of L-selectin Tail Affects Shedding, Microvillar Positioning, and Leukocyte Tethering. *the Journal of Biological Chemistry* **279**, 33263-33272

226. Crivici, A., and Ikura, M. (1995) Molecular and Structural Basis of Target Recognition by Calmodulin. *Annu. Rev. Biophys. Biomol. Struct.* **24**, 85-116

227. Babu, Y. S., Sack, J. S., Greenhough, T. J., Bugg, C. E., Means, A. R., and Cook, W. J. (1985) Three-dimensional structure of calmodulin. *Nature* **315**, 37-40

228. Kretsinger, R. H., Rudnick, S. E., and Weissman, L. J. (1986) Crystal structure of calmodulin. *Journal of Inorganic Biochemistry* **28**, 289-302

229. Chattopadhyaya, R., Meador, W. E., Means, A. R., and Quiocho, F. A. (1992) Calmodulin structure refined at 1.7 Ã… resolution. *Journal of Molecular Biology* **228**, 1177-1192

230. Barbato, G., Ikura, M., Kay, L. E., Pastor, R. W., and Bax, A. (1992) Backbone dynamics of calmodulin studied by nitrogen-15 relaxation using inverse detected two-dimensional NMR spectroscopy: the central helix is flexible. *Biochemistry* **31**, 5269-5278

231. Hennessey, J. P., Manavalan, P., Johnson, W. C., Malencik, D. A., Anderson, S. R., Schimerlik, M. I., and Shalitin, Y. (1987) Conformational transitions of calmodulin as studied by vacuum-UV CD. *Biopolymers* **26**, 561-571

232. Chin, D., and Means, A. R. (2000) Calmodulin: a prototypical calcium sensor. *Trends Cell Biol* **10**, 322-328

233. Zhang, M., Abrams, C., Wang, L., Gizzi, A., He, L., Lin, R., Chen, Y., Loll, P. J., Pascal, J. M., and Zhang, J. F. (2012) Structural basis for calmodulin as a dynamic calcium sensor. *Structure* **20**, 911-923

234. Tidow, H., and Nissen, P. (2013) Structural diversity of calmodulin binding to its target sites. *The FEBS journal* **280**, 5551-5565

235. Blumenthal, D. K., Krebs, E. G., and Anthony R. Means, P. M. C. (1987) [10] Preparation and properties of the calmodulin-binding domain of skeletal muscle myosin light chain kinase. in *Methods in Enzymology*, Academic Press. pp 115-126

236. Ye, Q., Li, X., Wong, A., Wei, Q., and Jia, Z. (2005) Structure of Calmodulin Bound to a Calcineurin Peptide: A New Way of Making an Old Binding Model. *Biochemistry* **45**, 738-745

237. Vorherr, T., James, P., Krebs, J., Enyedi, A., McCormick, D. J., Penniston, J. T., and Carafoli, E. (1990) Interaction of calmodulin with the calmodulin binding domain of the plasma membrane calcium pump. *Biochemistry* **29**, 355-365

238. Vorherr, T., Knoepfel, L., Hofmann, F., Mollner, S., Pfeuffer, T., and Carafoli, E. (1993) The calmodulin binding domain of nitric oxide synthase and adenylyl cyclase. *Biochemistry* **32**, 6081-6088

239. Rodriguez-Castaneda, F., Maestre-Martinez, M., Coudevylle, N., Dimova, K., Junge, H., Lipstein, N., Lee, D., Becker, S., Brose, N., Jahn, O., Carlomagno, T., and Griesinger, C. (2010) Modular architecture of Munc13/calmodulin complexes: dual regulation by Ca2+ and possible function in short-term synaptic plasticity. *EMBO J* **29**, 680-691

240. Drum, C. L., Yan, S. Z., Bard, J., Shen, Y. Q., Lu, D., Soelaiman, S., Grabarek, Z., Bohm, A., and Tang, W. J. (2002) Structural basis for the activation of anthrax adenylyl cyclase exotoxin by calmodulin. *Nature* **415**, 396-402

241. Schumacher, M. A., Crum, M., and Miller, M. C. (2004) Crystal structures of apocalmodulin and an apocalmodulin/SK potassium channel gating domain complex. *Structure* **12**, 849-860

242. Chagot, B., and Chazin, W. J. (2011) Solution NMR Structure of Apo-Calmodulin in Complex with the IQ Motif of Human Cardiac Sodium Channel NaV1.5. *Journal of Molecular Biology* **406**, 106-119

243. Alexander, K. A., Wakim, B. T., Doyle, G. S., Walsh, K. A., and Storm, D. R. (1988) Identification and characterization of the calmodulin-binding domain of neuromodulin, a neurospecific calmodulin-binding protein. *Journal of Biological Chemistry* **263**, 7544-7549

244. Tanaka, T., Kadowaki, K., Lazarides, E., and Sobue, K. (1991) Ca2(+)-dependent regulation of the spectrin/actin interaction by calmodulin and protein 4.1. *Journal of Biological Chemistry* **266**, 1134-1140

245. Nunomura, W., Takakuwa, Y., Parra, M., Conboy, J. G., and Mohandas, N. (2000) Ca2+-dependent and Ca2+-independent Calmodulin Binding Sites in Erythrocyte Protein 4.1. *Journal of Biological Chemistry* **275**, 6360-6367

246. Meador, W. E., Means, A. R., and Quiocho, F. A. (1992) Target enzyme recognition by calmodulin: 2.4 A structure of a calmodulin-peptide complex. *Science* **257**, 1251-1255

247. Ikura, M., Clore, G. M., Gronenborn, A. M., Zhu, G., Klee, C. B., and Bax, A. (1992) Solution structure of a calmodulin-target peptide complex by multidimensional NMR. *Science* **256**, 632-638

248. Meador, W. E., Means, A. R., and Quiocho, F. A. (1993) Modulation of calmodulin plasticity in molecular recognition on the basis of x-ray structures. *Science* **262**, 1718-1721

249. Osawa, M., Tokumitsu, H., Swindells, M. B., Kurihara, H., Orita, M., Shibanuma, T., Furuya, T., and Ikura, M. (1999) A novel target recognition revealed by calmodulin in complex with Ca2+-calmodulin-dependent kinase kinase. *Nat Struct Biol* **6**, 819-824

250. Contessa, G. M., Orsale, M., Melino, S., Torre, V., Paci, M., Desideri, A., and Cicero, D. O. (2005) Structure of calmodulin complexed with an olfactory CNG channel fragment and role of the central linker: residual dipolar couplings to evaluate calmodulin binding modes outside the kinase family. *Journal of biomolecular NMR* **31**, 185-199

251. Simonovic, M., Zhang, Z., Cianci, C. D., Steitz, T. A., and Morrow, J. S. (2006) Structure of the calmodulin alphaII-spectrin complex provides insight into the regulation of cell plasticity. *The Journal of biological chemistry* **281**, 34333-34340

252. Ogura, K., Kumeta, H., Takahasi, K., Kobashigawa, Y., Yoshida, R., Itoh, H., Yazawa, M., and Inagaki, F. (2012) Solution structures of yeast Saccharomyces cerevisiae calmodulin in calcium- and target peptide-bound states reveal similarities and differences to vertebrate calmodulin. *Genes to cells : devoted to molecular & cellular mechanisms* **17**, 159-172

253. Ataman, Z. A., Gakhar, L., Sorensen, B. R., Hell, J. W., and Shea, M. A. (2007) The NMDA receptor NR1 C1 region bound to calmodulin: structural insights into functional differences between homologous domains. *Structure* **15**, 1603-1617

254. Juranic, N., Atanasova, E., Filoteo, A. G., Macura, S., Prendergast, F. G., Penniston, J. T., and Strehler, E. E. (2010) Calmodulin wraps around its binding

domain in the plasma membrane Ca2+ pump anchored by a novel 18-1 motif. *The Journal of biological chemistry* **285**, 4015-4024

255. Halling, D. B., Georgiou, D. K., Black, D. J., Yang, G., Fallon, J. L., Quiocho, F. A., Pedersen, S. E., and Hamilton, S. L. (2009) Determinants in CaV1 channels that regulate the Ca2+ sensitivity of bound calmodulin. *The Journal of biological chemistry* **284**, 20041-20051

256. Lau, S. Y., Procko, E., and Gaudet, R. (2012) Distinct properties of Ca2+-calmodulin binding to N- and C-terminal regulatory regions of the TRPV1 channel. *The Journal of general physiology* **140**, 541-555

257. Maximciuc, A. A., Putkey, J. A., Shamoo, Y., and Mackenzie, K. R. (2006) Complex of calmodulin with a ryanodine receptor target reveals a novel, flexible binding mode. *Structure* **14**, 1547-1556

258. Fallon, J. L., Halling, D. B., Hamilton, S. L., and Quiocho, F. A. (2005) Structure of calmodulin bound to the hydrophobic IQ domain of the cardiac Ca(v)1.2 calcium channel. *Structure* **13**, 1881-1886

259. Pearson, M. A., Reczek, D., Bretscher, A., and Karplus, P. A. (2000) Structure of the ERM Protein Moesin Reveals the FERM Domain Fold Masked by an Extended Actin Binding Tail Domain. *Cell* **101**, 259-270

260. Neisch, A. L., and Fehon, R. G. (2011) Ezrin, Radixin and Moesin: key regulators of membrane-cortex interactions and signaling. *Curr Opin Cell Biol* **23**, 377-382

261. Jayaraman, B., and Nicholson, L. K. (2007) Thermodynamic Dissection of the Ezrin FERM/CERMAD Interface. *Biochemistry* **46**, 12174-12189

262. Matsui, T., Maeda, M., Doi, Y., Yonemura, S., Amano, M., Kaibuchi, K., Tsukita, S., and Tsukita, S. (1998) Rho-kinase phosphorylates COOH-terminal threonines of ezrin/radixin/moesin (ERM) proteins and regulates their head-to-tail association. *J Cell Biol* **140**, 647-657

263. Ng, T., Parsons, M., Hughes, W. E., Monypenny, J., Zicha, D., Gautreau, A., Arpin, M., Gschmeissner, S., Verveer, P. J., Bastiaens, P. I., and Parker, P. J. (2001) Ezrin is a downstream effector of trafficking PKC-integrin complexes involved in the control of cell motility. *Embo j* **20**, 2723-2741

264. Maniti, O., Khalifat, N., Goggia, K., Dalonneau, F., Guerin, C., Blanchoin, L., Ramos, L., and Picart, C. (2012) Binding of moesin and ezrin to membranes containing phosphatidylinositol (4,5) bisphosphate: a comparative study of the affinity constants and conformational changes. *Biochimica et biophysica acta* **1818**, 2839-2849

265. Doi, Y., Itoh, M., Yonemura, S., Ishihara, S., Takano, H., Noda, T., Tsukita, S., and Tsukita, S. (1999) Normal Development of Mice and Unimpaired Cell Adhesion/Cell Motility/Actin-based Cytoskeleton without Compensatory Up-regulation of Ezrin or Radixin in Moesin Gene Knockout. *Journal of Biological Chemistry* **274**, 2315-2321

266. Saotome, I., Curto, M., and McClatchey, A. I. (2004) Ezrin Is Essential for Epithelial Organization and Villus Morphogenesis in the Developing Intestine. *Developmental Cell* **6**, 855-864

267. Bonilha, V. L., Rayborn, M. E., Saotome, I., McClatchey, A. I., and Hollyfield, J. G. (2006) Microvilli defects in retinas of ezrin knockout mice. *Experimental eye research* **82**, 720-729

268. Hashimoto, S., Amaya, F., Matsuyama, H., Ueno, H., Kikuchi, S., Tanaka, M., Watanabe, Y., Ebina, M., Ishizaka, A., Tsukita, S., and Hashimoto, S. (2008) Dysregulation of lung injury and repair in moesin-deficient mice treated with

intratracheal bleomycin. *American journal of physiology. Lung cellular and molecular physiology* **295**, L566-574

269. Hirata, T., Nomachi, A., Tohya, K., Miyasaka, M., Tsukita, S., Watanabe, T., and Narumiya, S. (2012) Moesin-deficient mice reveal a non-redundant role for moesin in lymphocyte homeostasis. *International immunology* **24**, 705-717

270. Edwards, S. D., and Keep, N. H. (2001) The 2.7 Ã… Crystal Structure of the Activated FERM Domain of Moesin: An Analysis of Structural Changes on Activation. *Biochemistry* **40**, 7061-7068

271. Mori, T., Kitano, K., Terawaki, S.-i., Maesaki, R., Fukami, Y., and Hakoshima, T. (2008) Structural Basis for CD44 Recognition by ERM Proteins. *Journal of Biological Chemistry* **283**, 29602-29612

272. Cannon, J. L., Mody, P. D., Blaine, K. M., Chen, E. J., Nelson, A. D., Sayles, L. J., Moore, T. V., Clay, B. S., Dulin, N. O., Shilling, R. A., Burkhardt, J. K., and Sperling, A. I. (2011) CD43 interaction with ezrin-radixin-moesin (ERM) proteins regulates T-cell trafficking and CD43 phosphorylation. *Molecular biology of the cell* **22**, 954-963

273. Hamada, K., Shimizu, T., Yonemura, S., Tsukita, S., Tsukita, S., and Hakoshima, T. (2003) Structural basis of adhesion-molecule recognition by ERM proteins revealed by the crystal structure of the radixin/ICAM-2 complex. *EMBO J* **22**, 502-514

274. Takai, Y., Kitano, K., Terawaki, S.-i., Maesaki, R., and Hakoshima, T. (2007) Structural basis of PSGL-1 binding to ERM proteins. *Genes to Cells* **12**, 1329-1338

275. Spertini, C., Baisse, B., and Spertini, O. (2012) Ezrin-radixin-moesin-binding sequence of PSGL-1 glycoprotein regulates leukocyte rolling on selectins and activation of extracellular signal-regulated kinases. *The Journal of biological chemistry* **287**, 10693-10702

276. Snapp, K. R. (2002) Attachment of the PSGL-1 cytoplasmic domain to the actin cytoskeleton is essential for leukocyte rolling on P-selectin. *Blood* **99**, 4494-4502

277. Reczek, D., Berryman, M., and Bretscher, A. (1997) Identification of EBP50: A PDZ-containing Phosphoprotein that Associates with Members of the Ezrin-Radixin-Moesin Family. *the Journal of Cell Biology* **139**, 169-179

278. Takahashi, K., Sasaki, T., Mammoto, A., Hotta, I., Takaishi, K., Imamura, H., Nakano, K., Kodama, A., and Takai, Y. (1998) Interaction of radixin with Rho small G protein GDP/GTP exchange protein Dbl. *Oncogene* **16**, 3279-3284

279. Takahashi, K., Sasaki, T., Mammoto, A., Takaishi, K., Kameyama, T., Tsukita, S., and Takai, Y. (1997) Direct interaction of the Rho GDP dissociation inhibitor with ezrin/radixin/moesin initiates the activation of the Rho small G protein. *The Journal of biological chemistry* **272**, 23371-23375

280. Ivetic, A., and Ridley, A. J. (2004) Ezrin/radixin/moesin proteins and Rho GTPase signalling in leucocytes. *Immunology* **112**, 165-176

281. Prag, S., Parsons, M., Keppler, M. D., Ameer-Beg, S. M., Barber, P., Hunt, J., Beavil, A. J., Calvert, R., Arpin, M., Vojnovic, B., and Ng, T. (2007) Activated ezrin promotes cell migration through recruitment of the GEF Dbl to lipid rafts and preferential downstream activation of Cdc42. *Molecular biology of the cell* **18**, 2935-2948

282. Orian-Rousseau, V., Morrison, H., Matzke, A., Kastilan, T., Pace, G., Herrlich, P., and Ponta, H. (2007) Hepatocyte Growth Factor-induced Ras Activation

Requires ERM Proteins Linked to Both CD44v6 and F-Actin. *Molecular biology of the cell* **18**, 76-83

283. Chen, E. J., Shaffer, M. H., Williamson, E. K., Huang, Y., and Burkhardt, J. K. (2013) Ezrin and moesin are required for efficient T cell adhesion and homing to lymphoid organs. *PLoS One* **8**, e52368

284. Liu, Y., Belkina, N. V., Park, C., Nambiar, R., Loughhead, S. M., Patino-Lopez, G., Ben-Aissa, K., Hao, J. J., Kruhlak, M. J., Qi, H., von Andrian, U. H., Kehrl, J. H., Tyska, M. J., and Shaw, S. (2012) Constitutively active ezrin increases membrane tension, slows migration, and impedes endothelial transmigration of lymphocytes in vivo in mice. *Blood* **119**, 445-453

285. Yoshinaga-Ohara, N., Takahashi, A., Uchiyama, T., and Sasada, M. (2002) Spatiotemporal Regulation of Moesin Phosphorylation and Rear Release by Rho and Serine/Threonine Phosphatase during Neutrophil Migration. *Experimental Cell Research* **278**, 112-122

286. Villalonga, P., López-Alcalá, C., Bosch, M., Chiloeches, A., Rocamora, N., Gil, J., Marais, R., Marshall, C. J., Bachs, O., and Agell, N. (2001) Calmodulin Binds to K-Ras, but Not to H- or N-Ras, and Modulates Its Downstream Signaling. *Molecular and cellular biology* **21**, 7345-7354

287. Jalkanen, S., and Salmi, M. (2001) Lymphocytes: Recirculation. in *eLS*, John Wiley & Sons, Ltd. pp

288. Jutila, M. A., Rott, L., Berg, E. L., and Butcher, E. C. (1989) Function and regulation of the neutrophil MEL-14 antigen in vivo: comparison with LFA-1 and MAC-1. *Journal of immunology (Baltimore, Md. : 1950)* **143**, 3318-3324

289. Lewinsohn, D. M., Bargatze, R. F., and Butcher, E. C. (1987) Leukocyte-endothelial cell recognition: evidence of a common molecular mechanism shared by neutrophils, lymphocytes, and other leukocytes. *Journal of immunology (Baltimore, Md. : 1950)* **138**, 4313-4321

290. Mulligan, M. S., Watson, S. R., Fennie, C., and Ward, P. A. (1993) Protective effects of selectin chimeras in neutrophil-mediated lung injury. *Journal of immunology (Baltimore, Md. : 1950)* **151**, 6410-6417

291. Tedder, T. F., Steeber, D. A., and Pizcueta, P. (1995) L-selectin-deficient mice have impaired leukocyte recruitment into inflammatory sites. *J Exp Med* **181**, 2259-2264

292. Eriksson, E. E. (2011) Intravital Microscopy on Atherosclerosis in Apolipoprotein E Deficient Mice Establishes Microvessels as Major Entry Pathways for Leukocytes to Advanced Lesions / Clinical Perspective. *Circulation* **124**, 2129-2138

293. Ball, C. J., Reiffel, A. J., Chintalapani, S., Kim, M., Spector, J. A., and King, M. R. (2013) Hydrogen sulfide reduces neutrophil recruitment in hind-limb ischemia-reperfusion injury in an L-selectin and ADAM-17-dependent manner. *Plastic and reconstructive surgery* **131**, 487-497

294. Mudter, J., Wirtz, S., Galle, P. R., and Neurath, M. F. (2002) A new model of chronic colitis in SCID mice induced by adoptive transfer of CD62L+ CD4+ T cells: insights into the regulatory role of interleukin-6 on apoptosis. *Pathobiology : journal of immunopathology, molecular and cellular biology* **70**, 170-176

295. Tang, M. L., Hale, L. P., Steeber, D. A., and Tedder, T. F. (1997) L-selectin is involved in lymphocyte migration to sites of inflammation in the skin: delayed

rejection of allografts in L-selectin-deficient mice. *Journal of immunology (Baltimore, Md. : 1950)* **158**, 5191-5199

296. Yang, X. D., Michie, S. A., Tisch, R., Karin, N., Steinman, L., and McDevitt, H. O. (1994) A predominant role of integrin alpha 4 in the spontaneous development of autoimmune diabetes in nonobese diabetic mice. *Proceedings of the National Academy of Sciences of the United States of America* **91**, 12604-12608

297. McMurray, R. W. (1996) Adhesion molecules in autoimmune disease. *Seminars in arthritis and rheumatism* **25**, 215-233

298. Laubli, H., and Borsig, L. (2010) Selectins promote tumor metastasis. *Seminars in cancer biology* **20**, 169-177

299. Borsig, L., Wong, R., Hynes, R. O., Varki, N. M., and Varki, A. (2002) Synergistic effects of L- and P-selectin in facilitating tumor metastasis can involve non-mucin ligands and implicate leukocytes as enhancers of metastasis. *Proceedings of the National Academy of Sciences* **99**, 2193-2198

300. Läubli, H., Stevenson, J. L., Varki, A., Varki, N. M., and Borsig, L. (2006) L-selectin facilitation of metastasis involves temporal induction of Fut7-dependent ligands at sites of tumor cell arrest. *Cancer Research* **66**, 1536-1542

301. Evani, S. J., Prabhu, R. G., Gnanaruban, V., Finol, E. A., and Ramasubramanian, A. K. (2013) Monocytes mediate metastatic breast tumor cell adhesion to endothelium under flow. *FASEB journal : official publication of the Federation of American Societies for Experimental Biology* **27**, 3017-3029

302. Ross, R. (1993) The pathogenesis of atherosclerosis: a perspective for the 1990s. *Nature* **362**, 801-809

303. Ross, R. (1999) Atherosclerosis — An Inflammatory Disease. *New England Journal of Medicine* **340**, 115-126

304. Libby, P., Ridker, P. M., and Maseri, A. (2002) Inflammation and Atherosclerosis. *Circulation* **105**, 1135-1143

305. Dal Secco, D., Paron, J. A., de Oliveira, S. H., Ferreira, S. H., Silva, J. S., and Cunha Fde, Q. (2003) Neutrophil migration in inflammation: nitric oxide inhibits rolling, adhesion and induces apoptosis. *Nitric oxide : biology and chemistry / official journal of the Nitric Oxide Society* **9**, 153-164

306. Kubes, P., Suzuki, M., and Granger, D. N. (1991) Nitric oxide: an endogenous modulator of leukocyte adhesion. *Proceedings of the National Academy of Sciences of the United States of America* **88**, 4651-4655

307. Swirski, F. K., and Nahrendorf, M. (2013) Leukocyte behavior in atherosclerosis, myocardial infarction, and heart failure. *Science* **339**, 161-166

308. Gerrity, R. G. (1981) The role of the monocyte in atherogenesis: I. Transition of blood-borne monocytes into foam cells in fatty lesions. *The American journal of pathology* **103**, 181-190

309. Gerrity, R. G. (1981) The role of the monocyte in atherogenesis: II. Migration of foam cells from atherosclerotic lesions. *The American journal of pathology* **103**, 191-200

310. Hansson, G. K., Libby, P., Schonbeck, U., and Yan, Z. Q. (2002) Innate and adaptive immunity in the pathogenesis of atherosclerosis. *Circulation research* **91**, 281-291

311. Moore, K. J., and Tabas, I. (2011) Macrophages in the pathogenesis of atherosclerosis. *Cell* **145**, 341-355

312. van Gils, J. M., Derby, M. C., Fernandes, L. R., Ramkhelawon, B., Ray, T. D., Rayner, K. J., Parathath, S., Distel, E., Feig, J. L., Alvarez-Leite, J. I., Rayner, A. J.,

McDonald, T. O., O'Brien, K. D., Stuart, L. M., Fisher, E. A., Lacy-Hulbert, A., and Moore, K. J. (2012) The neuroimmune guidance cue netrin-1 promotes atherosclerosis by inhibiting the emigration of macrophages from plaques. *Nat Immunol* **13**, 136-143

313. Andersson, J., Libby, P., and Hansson, G. K. (2010) Adaptive immunity and atherosclerosis. *Clinical Immunology* **134**, 33-46

314. Lahoute, C., Herbin, O., Mallat, Z., and Tedgui, A. (2011) Adaptive immunity in atherosclerosis: mechanisms and future therapeutic targets. *Nature reviews. Cardiology* **8**, 348-358

315. Peoples, G. E., Blotnick, S., Takahashi, K., Freeman, M. R., Klagsbrun, M., and Eberlein, T. J. (1995) T lymphocytes that infiltrate tumors and atherosclerotic plaques produce heparin-binding epidermal growth factor-like growth factor and basic fibroblast growth factor: a potential pathologic role. *Proceedings of the National Academy of Sciences of the United States of America* **92**, 6547-6551

316. Kaartinen, M., van der Wal, A. C., van der Loos, C. M., Piek, J. J., Koch, K. T., Becker, A. E., and Kovanen, P. T. (1998) Mast cell infiltration in acute coronary syndromes: implications for plaque rupture. *J Am Coll Cardiol* **32**, 606-612

317. Takaya, N., Yuan, C., Chu, B., Saam, T., Polissar, N. L., Jarvik, G. P., Isaac, C., McDonough, J., Natiello, C., Small, R., Ferguson, M. S., and Hatsukami, T. S. (2005) Presence of intraplaque hemorrhage stimulates progression of carotid atherosclerotic plaques: a high-resolution magnetic resonance imaging study. *Circulation* **111**, 2768-2775

318. Eriksson, E. E., Xie, X., Werr, J., Thoren, P., and Lindbom, L. (2001) Importance of primary capture and L-selectin-dependent secondary capture in leukocyte accumulation in inflammation and atherosclerosis in vivo. *J Exp Med* **194**, 205-218

319. Galkina, E., Kadl, A., Sanders, J., Varughese, D., Sarembock, I. J., and Ley, K. (2006) Lymphocyte recruitment into the aortic wall before and during development of atherosclerosis is partially L-selectin dependent. *J Exp Med* **203**, 1273-1282

320. Rozenberg, I., Sluka, S. H., Mocharla, P., Hallenberg, A., Rotzius, P., Boren, J., Krankel, N., Landmesser, U., Borsig, L., Luscher, T. F., Eriksson, E. E., and Tanner, F. C. (2011) Deletion of L-selectin increases atherosclerosis development in ApoE-/- mice. *PLoS One* **6**, e21675

321. Carlos, T. M., and Harlan, J. M. (1994) Leukocyte-endothelial adhesion molecules. *Blood* **84**, 2068-2101

322. Seekamp, A., van Griensven, M., Dhondt, E., Diefenbeck, M., Demeyer, I., Vundelinckx, G., Haas, N., Schaechinger, U., Wolowicka, L., Rammelt, S., Stroobants, J., Marzi, I., Brambrink, A. M., Dziurdzik, P., Gasiorowski, J., Redl, H., Beckert, M., and Khan-Boluki, J. (2004) The effect of anti-L-selectin (aselizumab) in multiple traumatized patients--results of a phase II clinical trial. *Critical care medicine* **32**, 2021-2028

323. Ulbrich, H., Eriksson, E. E., and Lindbom, L. (2003) Leukocyte and endothelial cell adhesion molecules as targets for therapeutic interventions in inflammatory disease. *Trends in Pharmacological Sciences* **24**, 640-647

324. Aydt, E., and Wolff, G. (2002) Development of synthetic pan-selectin antagonists: A new treatment strategy for chronic inflammation in asthma.

*Pathobiology : journal of immunopathology, molecular and cellular biology* **70**, 297-301

325. Boehncke, W. H., and Schön, M. P. (2003) Interfering with leukocyte rolling - A promising therapeutic approach in inflammatory skin disorders? *Trends in Pharmacological Sciences* **24**, 49-52

326. Hicks, A. E., Nolan, S. L., Ridger, V. C., Hellewell, P. G., and Norman, K. E. (2003) Recombinant P-selectin glycoprotein ligand-1 directly inhibits leukocyte rolling by all 3 selectins in vivo: complete inhibition of rolling is not required for anti-inflammatory effect. *Blood* **101**, 3249-3256

327. Hayward, R., and Lefer, A. M. (1999) Acute mesenteric ischemia and reperfusion: protective effects of recombinant soluble P-selectin glycoprotein ligand-1. *Shock (Augusta, Ga.)* **12**, 201-207

328. Scalia, R., Armstead, V. E., Minchenko, A. G., and Lefer, A. M. (1999) Essential role of P-selectin in the initiation of the inflammatory response induced by hemorrhage and reinfusion. *J Exp Med* **189**, 931-938

329. Scalia, R., Hayward, R., Armstead, V. E., Minchenko, A. G., and Lefer, A. M. (1999) Effect of recombinant soluble P-selectin glycoprotein ligand-1 on leukocyte-endothelium interaction in vivo. Role in rat traumatic shock. *Circulation research* **84**, 93-102

330. Barthel, S. R., Gavino, J. D., Descheny, L., and Dimitroff, C. J. (2007) Targeting selectins and selectin ligands in inflammation and cancer. *Expert opinion on therapeutic targets* **11**, 1473-1491

331. Borsig, L. (2007) Antimetastatic activities of modified heparins: selectin inhibition by heparin attenuates metastasis. *Seminars in thrombosis and hemostasis* **33**, 540-546

332. Gasteiger E., H. C., Gattiker A., Duvaud S., Wilkins M.R., Appel R.D., Bairoch A.,. (2005) Protein Identification ana Analysis Tools on the Expasy Server. in *The Proteomics Protocols Handbook* (Walker, J. M. ed.), Humana Press, New Jersey. pp 571-607

333. Velázquez-Campoy, A., Ohtaka, H., Nezami, A., Muzammil, S., and Freire, E. (2001) Isothermal Titration Calorimetry. in *Current Protocols in Cell Biology*, John Wiley & Sons, Inc. pp

334. Pierce, M. M., Raman, C. S., and Nall, B. T. (1999) Isothermal Titration Calorimetry of Protein-Protein Interactions. *Methods* **19**, 213-221

335. Leavitt, S., and Freire, E. (2001) Direct measurement of protein binding energetics by isothermal titration calorimetry. *Current Opinion in Structural Biology* **11**, 560-566

336. Breukels, V., Konijnenberg, A., Nabuurs, S. M., Doreleijers, J. F., Kovalevskaya, N. V., and Vuister, G. W. (2011) Overview on the use of NMR to examine protein structure. *Current protocols in protein science / editorial board, John E. Coligan ... [et al.]* **Chapter 17**, Unit17 15

337. Keeler, J. (2002) Chapter 7: Two-Dimensional NMR. Cambridge

338. Ishida, H., Nakashima, K., Kumaki, Y., Nakata, M., Hikichi, K., and Yazawa, M. *1H, 15N and 13C resonance assignments of yeast Saccharomyces cerevisiae calmodulin in the Ca2+-free state*, J Biomol NMR. 2002 Aug;23(4):323-4.

339. Ikura, M., Kay, L. E., and Bax, A. (1990) A novel approach for sequential assignment of 1H, 13C, and 15N spectra of proteins: heteronuclear triple-resonance three-dimensional NMR spectroscopy. Application to calmodulin. *Biochemistry* **29**, 4659-4667

340. Martino, L., Pennell, S., Kelly, G., Bui, T. T. T., Kotik-Kogan, O., Smerdon, S. J., Drake, A. F., Curry, S., and Conte, M. R. (2012) Analysis of the interaction with the hepatitis C virus mRNA reveals an alternative mode of RNA recognition by the human La protein. *Nucleic Acids Research* **40**, 1381-1394

341. Bulheller, B. M., Rodger, A., and Hirst, J. D. (2007) Circular and linear dichroism of proteins. *Physical chemistry chemical physics : PCCP* **9**, 2020-2035

342. Whitmore, L., and Wallace, B. A. (2008) Protein secondary structure analyses from circular dichroism spectroscopy: methods and reference databases. *Biopolymers* **89**, 392-400

343. Kelly, S. M., Jess, T. J., and Price, N. C. (2005) How to study proteins by circular dichroism. *Biochimica et biophysica acta* **1751**, 119-139

344. Jerabek-Willemsen, M., Wienken, C. J., Braun, D., Baaske, P., and Duhr, S. (2011) Molecular interaction studies using microscale thermophoresis. *Assay and drug development technologies* **9**, 342-353

345. Wienken, C. J., Baaske, P., Rothbauer, U., Braun, D., and Duhr, S. (2010) Protein-binding assays in biological liquids using microscale thermophoresis. *Nature communications* **1**, 100

346. Griesbach, J. (2011) Determination of thermodynamic parameters ΔG and ΔH of a small molecule binding to p38 using MST. in *Protein-small molecule interaction analysis*, http://www.nanotemper-technologies.com/uploads/media/Application_Note_NT004_-_Determination_of_thermodynamic_parameters_V002_01.pdf

347. Davanloo, P., Rosenberg, A. H., Dunn, J. J., and Studier, F. W. (1984) Cloning and expression of the gene for bacteriophage T7 RNA polymerase. *Proceedings of the National Academy of Sciences of the United States of America* **81**, 2035-2039

348. Graslund, S., Nordlund, P., Weigelt, J., Hallberg, B. M., Bray, J., Gileadi, O., Knapp, S., Oppermann, U., Arrowsmith, C., Hui, R., Ming, J., dhe-Paganon, S., Park, H. W., Savchenko, A., Yee, A., Edwards, A., Vincentelli, R., Cambillau, C., Kim, R., Kim, S. H., Rao, Z., Shi, Y., Terwilliger, T. C., Kim, C. Y., Hung, L. W., Waldo, G. S., Peleg, Y., Albeck, S., Unger, T., Dym, O., Prilusky, J., Sussman, J. L., Stevens, R. C., Lesley, S. A., Wilson, I. A., Joachimiak, A., Collart, F., Dementieva, I., Donnelly, M. I., Eschenfeldt, W. H., Kim, Y., Stols, L., Wu, R., Zhou, M., Burley, S. K., Emtage, J. S., Sauder, J. M., Thompson, D., Bain, K., Luz, J., Gheyi, T., Zhang, F., Atwell, S., Almo, S. C., Bonanno, J. B., Fiser, A., Swaminathan, S., Studier, F. W., Chance, M. R., Sali, A., Acton, T. B., Xiao, R., Zhao, L., Ma, L. C., Hunt, J. F., Tong, L., Cunningham, K., Inouye, M., Anderson, S., Janjua, H., Shastry, R., Ho, C. K., Wang, D., Wang, H., Jiang, M., Montelione, G. T., Stuart, D. I., Owens, R. J., Daenke, S., Schutz, A., Heinemann, U., Yokoyama, S., Bussow, K., and Gunsalus, K. C. (2008) Protein production and purification. *Nature methods* **5**, 135-146

349. Jayaraj, R., and Smooker, P. M. (2009) So you Need a Protein-A Guide to the Production of Recombinant Proteins. *Open Veterinary Science Journal* **3**, 28-34

350. Hayashi, N., Matsubara, M., Takasaki, A., Titani, K., and Taniguchi, H. (1998) An Expression System of Rat Calmodulin Using T7 Phage Promoter inEscherichia coli. *Protein Expression and Purification* **12**, 25-28

351. Jim Hartnett, J. G. a. M. R. S. (2006) the single step competent cells- efficient cloning and high protein yields. Promega Corporation

352. Grodberg, J., and Dunn, J. J. (1988) ompT encodes the Escherichia coli outer membrane protease that cleaves T7 RNA polymerase during purification. *Journal of bacteriology* **170**, 1245-1253

353. Studier, F. W. (1991) Use of bacteriophage T7 lysozyme to improve an inducible T7 expression system. *J Mol Biol* **219**, 37-44

354. Robert Novy, D. D., Keith Yaeger and Robert Mierendorf. (2001) Overcoming the codon bias of E. coli for enhanced protein expression. in *inNovations*, Novagen

355. (2003) Rosetta™ 2(DE3) Competent Cells for enhanced coverage of codon bias in E. coli. in *inNovations*, Novagen

356. Walls, D., and Loughran, S. (2011) Tagging Recombinant Proteins to Enhance Solubility and Aid Purification. in *Protein Chromatography* (Walls, D., and Loughran, S. T. eds.), Humana Press. pp 151-175

357. Hunt, I. (2005) From gene to protein: a review of new and enabling technologies for multi-parallel protein expression. *Protein Expr Purif* **40**, 1-22

358. Kaplan, W., Husler, P., Klump, H., Erhardt, J., Sluis-Cremer, N., and Dirr, H. (1997) Conformational stability of pGEX-expressed Schistosoma japonicum glutathione S-transferase: a detoxification enzyme and fusion-protein affinity tag. *Protein science : a publication of the Protein Society* **6**, 399-406

359. Zhou, P., Lugovskoy, A. A., and Wagner, G. (2001) A solubility-enhancement tag (SET) for NMR studies of poorly behaving proteins. *Journal of biomolecular NMR* **20**, 11-14

360. Manjasetty, B. A., Turnbull, A. P., Panjikar, S., Bussow, K., and Chance, M. R. (2008) Automated technologies and novel techniques to accelerate protein crystallography for structural genomics. *Proteomics* **8**, 612-625

361. Kim, K. I., Park, S. C., Kang, S. H., Cheong, G. W., and Chung, C. H. (1999) Selective degradation of unfolded proteins by the self-compartmentalizing HtrA protease, a periplasmic heat shock protein in Escherichia coli. *J Mol Biol* **294**, 1363-1374

362. Truscott, K. N., Bezawork-Geleta, A., and Dougan, D. A. (2011) Unfolded protein responses in bacteria and mitochondria: A central role for the ClpXP machine. *IUBMB Life* **63**, 955-963

363. Phan, J., Zdanov, A., Evdokimov, A. G., Tropea, J. E., Peters, H. K., Kapust, R. B., Li, M., Wlodawer, A., and Waugh, D. S. (2002) Structural Basis for the Substrate Specificity of Tobacco Etch Virus Protease. *Journal of Biological Chemistry* **277**, 50564-50572

364. Li, H., and Villalobo, A. (2002) Evidence for the direct interaction between calmodulin and the human epidermal growth factor receptor. *Biochem. J.* **362**, 499-505

365. Ikura, M., Hiraoki, T., Hikichi, K., Mikuni, T., Yazawa, M., and Yagi, K. (1983) Nuclear magnetic resonance studies on calmodulin: calcium-induced conformational change. *Biochemistry* **22**, 2573-2579

366. Zhang, Y., Li, Z., Sacks, D. B., and Ames, J. B. (2012) Structural Basis for Ca2+-induced Activation and Dimerization of Estrogen Receptor α by Calmodulin. *Journal of Biological Chemistry* **287**, 9336-9344

367. Stewart A. Frankel, L. A. L. (1993) SOLUBILIZATION OF PROTEIN AFTER BACTERIAL EXPRESSION USING SARKOSYL. Albert Einstein College of Medicine of Yeshiva University, Bronx, NY., USA

368. Tao, H., Liu, W., Simmons, B. N., Harris, H. K., Cox, T. C., and Massiah, M. A. (2010) Purifying natively folded proteins from inclusion bodies using sarkosyl, Triton X-100, and CHAPS. *BioTechniques* **48**, 61-64

369. Mendoza, J. A., Dulin, P., and Warren, T. (2000) The lower hydrolysis of ATP by the stress protein GroEL is a major factor responsible for the diminished chaperonin activity at low temperature. *Cryobiology* **41**, 319-323

370. Ferrer, M., Chernikova, T. N., Yakimov, M. M., Golyshin, P. N., and Timmis, K. N. (2003) Chaperonins govern growth of Escherichia coli at low temperatures. *Nat Biotech* **21**, 1266-1267

371. Takai, Y., Kitano, K., Terawaki, S., Maesaki, R., and Hakoshima, T. (2008) Structural basis of the cytoplasmic tail of adhesion molecule CD43 and its binding to ERM proteins. *J Mol Biol* **381**, 634-644

372. Barreiro, O., Yanez-Mo, M., Serrador, J. M., Montoya, M. C., Vicente-Manzanares, M., Tejedor, R., Furthmayr, H., and Sanchez-Madrid, F. (2002) Dynamic interaction of VCAM-1 and ICAM-1 with moesin and ezrin in a novel endothelial docking structure for adherent leukocytes. *J Cell Biol* **157**, 1233-1245

373. Serrador, J. M., Alonso-Lebrero, J. L., del Pozo, M. A., Furthmayr, H., Schwartz-Albiez, R., Calvo, J., Lozano, F., and Sanchez-Madrid, F. (1997) Moesin interacts with the cytoplasmic region of intercellular adhesion molecule-3 and is redistributed to the uropod of T lymphocytes during cell polarization. *J Cell Biol* **138**, 1409-1423

374. Tsutomu, K. (1978) Theory of chromatography of rigid molecules on hydroxyapatite columns with small loads : IV. Estimation of the adsorption energy of nucleoside polyphosphates. *Journal of Chromatography A* **151**, 95-112

375. Tsutomu, K. (1978) Theory of chromatography on hydroxyapatite columns with small loads : V. Determination of the adsorption energy of the ε-amino group of poly-l-lysine and the manner of adsorption of the molecule. *Journal of Chromatography A* **157**, 7-42

376. Kawasaki, T., Takahashi, S., and Ideda, K. (1985) Hydroxyapatite high-performance liquid chromatography: column performance for proteins. *European Journal of Biochemistry* **152**, 361-371

377. Gorbunoff, M. J., and Timasheff, S. N. (1984) The interaction of proteins with hydroxyapatite: III. Mechanism. *Analytical Biochemistry* **136**, 440-445

378. Marina J, G. (1984) The interaction of proteins with hydroxyapatite: I. Role of protein charge and structure. *Analytical Biochemistry* **136**, 425-432

379. Marina J, G. (1984) The interaction of proteins with hydroxyapatite: II. Role of acidic and basic groups. *Analytical Biochemistry* **136**, 433-439

380. Murby, M., Uhlén, M., and Ståhl, S. (1996) Upstream Strategies to Minimize Proteolytic Degradation upon Recombinant Production inEscherichia coli. *Protein Expression and Purification* **7**, 129-136

381. Neidigh, J. W., Fesinmeyer, R. M., and Andersen, N. H. (2002) Designing a 20-residue protein. *Nat Struct Biol* **9**, 425-430

382. Neidigh, J. W., Fesinmeyer, R. M., Prickett, K. S., and Andersen, N. H. (2001) Exendin-4 and Glucagon-like-peptide-1: NMR Structural Comparisons in the Solution and Micelle-Associated States†. *Biochemistry* **40**, 13188-13200

383. Herman, R. E., Badders, D., Fuller, M., Makienko, E. G., Houston, M. E., Quay, S. C., and Johnson, P. H. (2007) The Trp Cage Motif as a Scaffold for the Display of

a Randomized Peptide Library on Bacteriophage T7. *Journal of Biological Chemistry* **282**, 9813-9824

384. Ikura, M., Hiraoki, T., Hikichi, K., Mikuni, T., Yazawa, M., and Yagi, K. (1983) Nuclear magnetic resonance studies on calmodulin: spectral assignments in the calcium-free state. *Biochemistry* **22**, 2568-2572

385. Gaberc-Porekar, V., Menart, V., Jevsevar, S., Vidensek, A., and Stalc, A. (1999) Histidines in affinity tags and surface clusters for immobilized metal-ion affinity chromatography of trimeric tumor necrosis factor alpha. *Journal of chromatography. A* **852**, 117-128

386. Klock, H. E., Koesema, E. J., Knuth, M. W., and Lesley, S. A. (2008) Combining the polymerase incomplete primer extension method for cloning and mutagenesis with microscreening to accelerate structural genomics efforts. *Proteins* **71**, 982-994

387. Persechini, A., Gansz, K. J., and Paresi, R. J. (1996) Activation of Myosin Light Chain Kinase and Nitric Oxide Synthase Activities by Engineered Calmodulins with Duplicated or Exchanged EF Hand Pairs†. *Biochemistry* **35**, 224-228

388. Freyer, M. W., and Lewis, E. A. (2008) Isothermal titration calorimetry: experimental design, data analysis, and probing macromolecule/ligand binding and kinetic interactions. *Methods in cell biology* **84**, 79-113

389. McDonnell, J. M. (2001) Surface plasmon resonance: towards an understanding of the mechanisms of biological molecular recognition. *Current opinion in chemical biology* **5**, 572-577

390. Magde, D., Elson, E. L., and Webb, W. W. (1974) Fluorescence correlation spectroscopy. II. An experimental realization. *Biopolymers* **13**, 29-61

391. Phizicky, E. M., and Fields, S. (1995) Protein-protein interactions: methods for detection and analysis. *Microbiological reviews* **59**, 94-123

392. Behnen, P., Davis, E., Delaney, E., Frohm, B., Bauer, M., Cedervall, T., O'Connell, D., Akerfeldt, K. S., and Linse, S. (2012) Calcium-dependent interaction of calmodulin with human 80S ribosomes and polyribosomes. *Biochemistry* **51**, 6718-6727

393. Lu, Y., Kwan, A. H., Jeffries, C. M., Guss, J. M., and Trewhella, J. (2012) The motif of human cardiac myosin-binding protein C is required for its Ca2+-dependent interaction with calmodulin. *The Journal of biological chemistry* **287**, 31596-31607

394. Bronowska, A. K. (2011) Thermodynamics - Interaction Studies - Solids, Liquids and Gases. in *Thermodynamics of Ligand-Protein Interactions: Implications for Molecular Design* (Pirajan, D. J. C. M. ed.

395. Elshorst, B., Hennig, M., Försterling, H., Diener, A., Maurer, M., Schulte, P., Schwalbe, H., Griesinger, C., Krebs, J., Schmid, H., Vorherr, T., and Carafoli, E. (1999) NMR Solution Structure of a Complex of Calmodulin with a Binding Peptide of the Ca2+ Pump†,‡. *Biochemistry* **38**, 12320-12332

396. Gifford, J. L., Ishida, H., and Vogel, H. J. (2012) Structural Insights into Calmodulin-regulated L-selectin Ectodomain Shedding. *Journal of Biological Chemistry* **287**, 26513-26527

397. Wintrode, P. L., and Privalov, P. L. (1997) Energetics of target peptide recognition by calmodulin: A calorimetric study. *Journal of Molecular Biology* **266**, 1050-1062

398. Chou, D. K., Krishnamurthy, R., Randolph, T. W., Carpenter, J. F., and Manning, M. C. (2005) Effects of Tween 20 and Tween 80 on the stability of Albutropin during agitation. *Journal of pharmaceutical sciences* **94**, 1368-1381

399. Law, S. L., and Shih, C. L. (1999) Adsorption of calcitonin to glass. *Drug development and industrial pharmacy* **25**, 253-256

400. Prevost, M., Jacquemotte, F., Oberg, K. A., Staelens, D., Devreese, B., and Van Beeumen, J. (2000) Conformational variability of the synthetic peptide 129-141 of the mouse prion protein. *Journal of biomolecular structure & dynamics* **18**, 237-248

401. Hugonin, L., Barth, A., Gräslund, A., and Perálvarez-Marín, A. (2008) Secondary structure transitions and aggregation induced in dynorphin neuropeptides by the detergent sodium dodecyl sulfate. *Biochimica et Biophysica Acta (BBA) - Biomembranes* **1778**, 2580-2587

402. Bozzi, M., Di Stasio, E., Cicero, D. O., Giardina, B., Paci, M., and Brancaccio, A. (2004) The effect of an ionic detergent on the natively unfolded beta-dystroglycan ectodomain and on its interaction with alpha-dystroglycan. *Protein science : a publication of the Protein Society* **13**, 2437-2445

403. Kwan, A. H., Mobli, M., Gooley, P. R., King, G. F., and Mackay, J. P. (2011) Macromolecular NMR spectroscopy for the non-spectroscopist. *FEBS Journal* **278**, 687-703

404. Kelly, A. E., Ou, H. D., Withers, R., and Dötsch, V. (2002) Low-Conductivity Buffers for High-Sensitivity NMR Measurements. *Journal of the American Chemical Society* **124**, 12013-12019

405. Bellucci, M., Zambelli, B., Musiani, F., Turano, P., and Ciurli, S. (2009) Helicobacter pylori UreE, a urease accessory protein: specific Ni2+- and Zn2+-binding properties and interaction with its cognate UreG. *Biochemical Journal* **422**, 91-100

406. Huang, D., Zhao, T., Xu, W., Yang, T., and Cremer, P. S. (2013) Sensing Small Molecule Interactions with Lipid Membranes by Local pH Modulation. *Analytical Chemistry* **85**, 10240-10248

407. Umenaga, Y., Paku, K. S., In, Y., Ishida, T., and Tomoo, K. (2011) Identification and function of the second eIF4E-binding region in N-terminal domain of eIF4G: comparison with eIF4E-binding protein. *Biochemical and biophysical research communications* **414**, 462-467

408. Besançon, W., and Wagner, R. (1999) Characterization of transient RNA-RNA interactions important for the facilitated structure formation of bacterial ribosomal 16S RNA. *Nucleic Acids Research* **27**, 4353-4362

409. Technologies, N. (2013) Comparison of Interactions Measured with MST and other Methods. NanoTemper Technologies

410. Radhakrishnan, A., Stein, A., Jahn, R., and Fasshauer, D. (2009) The Ca2+ affinity of synaptotagmin 1 is markedly increased by a specific interaction of its C2B domain with phosphatidylinositol 4,5-bisphosphate. *The Journal of biological chemistry* **284**, 25749-25760

411. van den Bogaart, G., Meyenberg, K., Diederichsen, U., and Jahn, R. (2012) Phosphatidylinositol 4,5-bisphosphate increases Ca2+ affinity of synaptotagmin-1 by 40-fold. *The Journal of biological chemistry* **287**, 16447-16453

412. Bayer, H., Essig, K., Stanzel, S., Frank, M., Gildersleeve, J. C., Berger, M. R., and Voss, C. (2012) Evaluation of riproximin binding properties reveals a novel

mechanism for cellular targeting. *The Journal of biological chemistry* **287**, 35873-35886

413. Seidel, S. A. I., Dijkman, P. M., Lea, W. A., van den Bogaart, G., Jerabek-Willemsen, M., Lazic, A., Joseph, J. S., Srinivasan, P., Baaske, P., Simeonov, A., Katritch, I., Melo, F. A., Ladbury, J. E., Schreiber, G., Watts, A., Braun, D., and Duhr, S. (2013) Microscale thermophoresis quantifies biomolecular interactions under previously challenging conditions. *Methods* **59**, 301-315

414. Matala, E., Alexander, S. R., Kishimoto, T. K., and Walcheck, B. (2001) The Cytoplasmic Domain of L-Selectin Participates in Regulating L-Selectin Endoproteolysis. *The Journal of Immunology* **167**, 1617-1623

415. Wang, C., Chung, Ben C., Yan, H., Lee, S.-Y., and Pitt, Geoffrey S. (2012) Crystal Structure of the Ternary Complex of a NaV C-Terminal Domain, a Fibroblast Growth Factor Homologous Factor, and Calmodulin. *Structure* **20**, 1167-1176

416. Samal, A. B., Ghanam, R. H., Fernandez, T. F., Monroe, E. B., and Saad, J. S. (2011) NMR, Biophysical, and Biochemical Studies Reveal the Minimal Calmodulin Binding Domain of the HIV-1 Matrix Protein. *Journal of Biological Chemistry* **286**, 33533-33543

417. Deng, W., Putkey, J. A., and Li, R. (2013) Calmodulin Adopts an Extended Conformation when Interacting with L-Selectin in Membranes. *PLoS ONE* **8**, e62861

418. Calalb, M. B., Kincaid, R. L., and Soderling, T. R. (1990) Phosphorylation of calcineurin: Effect on calmodulin binding. *Biochemical and Biophysical Research Communications* **172**, 551-556

419. Luscinskas, F. W., Ding, H., Tan, P., Cumming, D., Tedder, T. F., and Gerritsen, M. E. (1996) L- and P-selectins, but not CD49d (VLA-4) integrins, mediate monocyte initial attachment to TNF-alpha-activated vascular endothelium under flow in vitro. *Journal of immunology (Baltimore, Md. : 1950)* **157**, 326-335

420. León, B., and Ardavín, C. (2008) Monocyte migration to inflamed skin and lymph nodes is differentially controlled by L-selectin and PSGL-1. *Blood* **111**, 3126-3130

421. Shikata, K., Suzuki, Y., Wada, J., Hirata, K., Matsuda, M., Kawashima, H., Suzuki, T., Iizuka, M., Makino, H., and Miyasaka, M. (1999) L-selectin and its ligands mediate infiltration of mononuclear cells into kidney interstitium after ureteric obstruction. *The Journal of pathology* **188**, 93-99

422. Pizcueta, P., and Luscinskas, F. W. (1994) Monoclonal antibody blockade of L-selectin inhibits mononuclear leukocyte recruitment to inflammatory sites in vivo. *The American journal of pathology* **145**, 461-469

423. Grober, J. S., Bowen, B. L., Ebling, H., Athey, B., Thompson, C. B., Fox, D. A., and Stoolman, L. M. (1993) Monocyte-endothelial adhesion in chronic rheumatoid arthritis. In situ detection of selectin and integrin-dependent interactions. *J Clin Invest* **91**, 2609-2619

424. Park, F. (2007) Lentiviral vectors: are they the future of animal transgenesis? *Physiological Genomics* **31**, 159-173

425. Trono, D. (2000) Lentiviral vectors: turning a deadly foe into a therapeutic agent. *Gene therapy* **7**, 20-23

426. Koya, R. C., Weber, J. S., Kasahara, N., Lau, R., Villacres, M. C., Levine, A. M., and Stripecke, R. (2004) Making dendritic cells from the inside out: lentiviral vector-mediated gene delivery of granulocyte-macrophage colony-stimulating factor

and interleukin 4 into CD14+ monocytes generates dendritic cells in vitro. *Human gene therapy* **15**, 733-748

427. Prieto, J., Eklund, A., and Patarroyo, M. (1994) Regulated expression of integrins and other adhesion molecules during differentiation of monocytes into macrophages. *Cellular immunology* **156**, 191-211

428. Cheng, P.-C. (2006) The Contrast Formation in Optical Microscopy. in *Handbook Of Biological Confocal Microscopy* (Pawley, J. B. ed.), Springer US. pp 162-206

429. Helms, V. (2008) Fluorescence Resonance Energy Transfer. in *Prinicples of Computational Cell Biology*, Wiley-VCH, Weinheim. pp 202

430. Bastiaens, P. I. H., and Squire, A. (1999) Fluorescence lifetime imaging microscopy: spatial resolution of biochemical processes in the cell. *Trends in Cell Biology* **9**, 48-52

431. Gadella Jr, T. W. J., Jovin, T. M., and Clegg, R. M. (1993) Fluorescence lifetime imaging microscopy (FLIM): Spatial resolution of microstructures on the nanosecond time scale. *Biophysical Chemistry* **48**, 221-239

432. Lakowicz, J. R., Szmacinski, H., Nowaczyk, K., Berndt, K. W., and Johnson, M. (1992) Fluorescence lifetime imaging. *Analytical Biochemistry* **202**, 316-330

433. Clegg, R. M. (2009) Chapter 1 Förster resonance energy transfer—FRET what is it, why do it, and how it's done. in *Laboratory Techniques in Biochemistry and Molecular Biology* (Gadella, T. W. J. ed.), Elsevier. pp 1-57

434. Oida, T., Sako, Y., and Kusumi, A. (1993) Fluorescence lifetime imaging microscopy (flimscopy). Methodology development and application to studies of endosome fusion in single cells. *Biophysical journal* **64**, 676-685

435. Szmacinski, H., Lakowicz, J. R., and Johnson, M. L. (1994) [30] Fluorescence lifetime imaging microscopy: Homodyne technique using high-speed gated image intensifier. in *Methods in Enzymology* (Michael L. Johnson, L. B. ed.), Academic Press. pp 723-748

436. Delenda, C. (2004) Lentiviral vectors: optimization of packaging, transduction and gene expression. *The Journal of Gene Medicine* **6**, S125-S138

437. Zufferey, R., Dull, T., Mandel, R. J., Bukovsky, A., Quiroz, D., Naldini, L., and Trono, D. (1998) Self-inactivating lentivirus vector for safe and efficient in vivo gene delivery. *J Virol* **72**, 9873-9880

438. Pluta, K., and Kacprzak, M. M. (2009) Use of HIV as a gene transfer vector. *Acta biochimica Polonica* **56**, 531-595

439. Pestonjamasp, K., Amieva, M. R., Strassel, C. P., Nauseef, W. M., Furthmayr, H., and Luna, E. J. (1995) Moesin, ezrin, and p205 are actin-binding proteins associated with neutrophil plasma membranes. *Molecular biology of the cell* **6**, 247-259

440. Iontcheva, I., Amar, S., Zawawi, K. H., Kantarci, A., and Van Dyke, T. E. (2004) Role for Moesin in Lipopolysaccharide-Stimulated Signal Transduction. *Infection and Immunity* **72**, 2312-2320

441. Takai, Y., Kitano, K., Terawaki, S.-i., Maesaki, R., and Hakoshima, T. (2008) Structural Basis of the Cytoplasmic Tail of Adhesion Molecule CD43 and Its Binding to ERM Proteins. *Journal of Molecular Biology* **381**, 634-644

442. Sanchez-Madrid, F., and del Pozo, M. A. (1999) Leukocyte polarization in cell migration and immune interactions. *Embo j* **18**, 501-511

443. Lee, J. H., Katakai, T., Hara, T., Gonda, H., Sugai, M., and Shimizu, A. (2004) Roles of p-ERM and Rho-ROCK signaling in lymphocyte polarity and uropod formation. *J Cell Biol* **167**, 327-337

444. Mazia, D., Schatten, G., and Sale, W. (1975) Adhesion of cells to surfaces coated with polylysine. Applications to electron microscopy. *The Journal of Cell Biology* **66**, 198-200

445. Gottfried, E. L. (1967) Lipids of human leukocytes: relation to cell type. *Journal of Lipid Research* **8**, 321-327

446. Zachowski, A. (1993) Phospholipids in animal eukaryotic membranes: transverse asymmetry and movement. *The Biochemical journal* **294 ( Pt 1)**, 1-14

447. Vance, J. E., and Steenbergen, R. (2005) Metabolism and functions of phosphatidylserine. *Progress in lipid research* **44**, 207-234

448. Vermes, I., Haanen, C., Steffens-Nakken, H., and Reutellingsperger, C. (1995) A novel assay for apoptosis Flow cytometric detection of phosphatidylserine expression on early apoptotic cells using fluorescein labelled Annexin V. *Journal of Immunological Methods* **184**, 39-51

449. Boon, J. M., Lambert, T. N., Sisson, A. L., Davis, A. P., and Smith, B. D. (2003) Facilitated phosphatidylserine (PS) flip-flop and thrombin activation using a synthetic PS scramblase. *J Am Chem Soc* **125**, 8195-8201

450. Phong, M. C., Gutwein, P., Kadel, S., Hexel, K., Altevogt, P., Linderkamp, O., and Brenner, B. (2003) Molecular mechanisms of L-selectin-induced co-localization in rafts and shedding [corrected]. *Biochemical and biophysical research communications* **300**, 563-569

451. Campanero, M. R., Pulido, R., Alonso, J. L., Pivel, J. P., Pimentel-Muinos, F. X., Fresno, M., and Sanchez-Madrid, F. (1991) Down-regulation by tumor necrosis factor-alpha of neutrophil cell surface expression of the sialophorin CD43 and the hyaluronate receptor CD44 through a proteolytic mechanism. *European journal of immunology* **21**, 3045-3048

452. Buhrer, C., Berlin, C., Thiele, H. G., and Hamann, A. (1990) Lymphocyte activation and expression of the human leucocyte-endothelial cell adhesion molecule 1 (Leu-8/TQ1 antigen). *Immunology* **71**, 442-448

453. Elliott, J. I., Surprenant, A., Marelli-Berg, F. M., Cooper, J. C., Cassady-Cain, R. L., Wooding, C., Linton, K., Alexander, D. R., and Higgins, C. F. (2005) Membrane phosphatidylserine distribution as a non-apoptotic signalling mechanism in lymphocytes. *Nature cell biology* **7**, 808-816

454. Foster, J. G., Carter, E., Kilty, I., MacKenzie, A. B., and Ward, S. G. (2013) Mitochondrial superoxide generation enhances P2X7R-mediated loss of cell surface CD62L on naive human CD4+ T lymphocytes. *Journal of immunology (Baltimore, Md. : 1950)* **190**, 1551-1559

455. Scheuplein, F., Schwarz, N., Adriouch, S., Krebs, C., Bannas, P., Rissiek, B., Seman, M., Haag, F., and Koch-Nolte, F. (2009) NAD+ and ATP released from injured cells induce P2X7-dependent shedding of CD62L and externalization of phosphatidylserine by murine T cells. *Journal of immunology (Baltimore, Md. : 1950)* **182**, 2898-2908

456. Yeung, T., Gilbert, G. E., Shi, J., Silvius, J., Kapus, A., and Grinstein, S. (2008) Membrane phosphatidylserine regulates surface charge and protein localization. *Science* **319**, 210-213

457. Labasi, J. M., Petrushova, N., Donovan, C., McCurdy, S., Lira, P., Payette, M. M., Brissette, W., Wicks, J. R., Audoly, L., and Gabel, C. A. (2002) Absence of the P2X7 receptor alters leukocyte function and attenuates an inflammatory response. *Journal of immunology (Baltimore, Md. : 1950)* **168**, 6436-6445

458. Walcheck, B., Alexander, S. R., St Hill, C. A., and Matala, E. (2003) ADAM-17-independent shedding of L-selectin. *Journal of leukocyte biology* **74**, 389-394

459. Lawrence, M. B., and Springer, T. A. (1991) Leukocytes roll on a selectin at physiologic flow rates: distinction from and prerequisite for adhesion through integrins. *Cell* **65**, 859-873

460. D'Apuzzo, M., Rolink, A., Loetscher, M., Hoxie, J. A., Clark-Lewis, I., Melchers, F., Baggiolini, M., and Moser, B. (1997) The chemokine SDF-1, stromal cell-derived factor 1, attracts early stage B cell precursors via the chemokine receptor CXCR4. *European journal of immunology* **27**, 1788-1793

461. Bleul, C. C., Fuhlbrigge, R. C., Casasnovas, J. M., Aiuti, A., and Springer, T. A. (1996) A highly efficacious lymphocyte chemoattractant, stromal cell-derived factor 1 (SDF-1). *J Exp Med* **184**, 1101-1109

462. Tanaka, Y., Adams, D. H., and Shaw, S. (1993) Proteoglycans on endothelial cells present adhesion-inducing cytokines to leukocytes. *Immunology today* **14**, 111-115

463. Middleton, J., Patterson, A. M., Gardner, L., Schmutz, C., and Ashton, B. A. (2002) Leukocyte extravasation: chemokine transport and presentation by the endothelium. *Blood* **100**, 3853-3860

464. Singer, I. I., Scott, S., Kawka, D. W., Chin, J., Daugherty, B. L., DeMartino, J. A., DiSalvo, J., Gould, S. L., Lineberger, J. E., Malkowitz, L., Miller, M. D., Mitnaul, L., Siciliano, S. J., Staruch, M. J., Williams, H. R., Zweerink, H. J., and Springer, M. S. (2001) CCR5, CXCR4, and CD4 Are Clustered and Closely Apposed on Microvilli of Human Macrophages and T Cells. *Journal of Virology* **75**, 3779-3790

465. Nieto, M., Frade, J. M., Sancho, D., Mellado, M., Martinez, A. C., and Sanchez-Madrid, F. (1997) Polarization of chemokine receptors to the leading edge during lymphocyte chemotaxis. *J Exp Med* **186**, 153-158

466. Vicente-Manzanares, M., Montoya, M. C., Mellado, M., Frade, J. M., del Pozo, M. A., Nieto, M., de Landazuri, M. O., Martinez, A. C., and Sanchez-Madrid, F. (1998) The chemokine SDF-1alpha triggers a chemotactic response and induces cell polarization in human B lymphocytes. *European journal of immunology* **28**, 2197-2207

467. Yamada, M., Kubo, H., Kobayashi, S., Ishizawa, K., He, M., Suzuki, T., Fujino, N., Kunishima, H., Hatta, M., Nishimaki, K., Aoyagi, T., Tokuda, K., Kitagawa, M., Yano, H., Tamamura, H., Fujii, N., and Kaku, M. (2011) The increase in surface CXCR4 expression on lung extravascular neutrophils and its effects on neutrophils during endotoxin-induced lung injury. *Cellular & molecular immunology* **8**, 305-314

468. Duchesneau, P., Gallagher, E., Walcheck, B., and Waddell, T. K. (2007) Up-regulation of leukocyte CXCR4 expression by sulfatide: an L-selectin-dependent pathway on CD4+ T cells. *European journal of immunology* **37**, 2949-2960

469. Alon, R., Fuhlbrigge, R. C., Finger, E. B., and Springer, T. A. (1996) Interactions through L-selectin between leukocytes and adherent leukocytes nucleate rolling adhesions on selectins and VCAM-1 in shear flow. *The Journal of Cell Biology* **135**, 849-865

470. Bargatze, R. F., Kurk, S., Butcher, E. C., and Jutila, M. A. (1994) Neutrophils roll on adherent neutrophils bound to cytokine-induced endothelial cells via L-selectin on the rolling cells. *The Journal of Experimental Medicine* **180**, 1785-1792

471. Lim, Y.-C., Snapp, K., Kansas, G. S., Camphausen, R., Ding, H., and Luscinskas, F. W. (1998) Important Contributions of P-Selectin Glycoprotein Ligand-1-Mediated Secondary Capture to Human Monocyte Adhesion to P-Selectin, E-Selectin, and TNF-α-Activated Endothelium Under Flow In Vitro. *The Journal of Immunology* **161**, 2501-2508

472. Walcheck, B., Moore, K. L., McEver, R. P., and Kishimoto, T. K. (1996) Neutrophil-neutrophil interactions under hydrodynamic shear stress involve L-selectin and PSGL-1. A mechanism that amplifies initial leukocyte accumulation of P-selectin in vitro. *The Journal of Clinical Investigation* **98**, 1081-1087

473. Carman, C. V. (2009) Mechanisms for transcellular diapedesis: probing and pathfinding by 'invadosome-like protrusions'. *Journal of cell science* **122**, 3025-3035

474. Alon, R., and Shulman, Z. (2011) Chemokine triggered integrin activation and actin remodeling events guiding lymphocyte migration across vascular barriers. *Exp Cell Res* **317**, 632-641

475. Khan, A. I., and Kubes, P. (2003) L-selectin: an emerging player in chemokine function. *Microcirculation (New York, N.Y. : 1994)* **10**, 351-358

476. Ebsen, H., Schroder, A., Kabelitz, D., and Janssen, O. (2013) Differential surface expression of ADAM10 and ADAM17 on human T lymphocytes and tumor cells. *PLoS One* **8**, e76853

477. Tellier, E., Canault, M., Rebsomen, L., Bonardo, B., Juhan-Vague, I., Nalbone, G., and Peiretti, F. (2006) The shedding activity of ADAM17 is sequestered in lipid rafts. *Exp Cell Res* **312**, 3969-3980

478. Matthews, V., Schuster, B., Schütze, S., Bussmeyer, I., Ludwig, A., Hundhausen, C., Sadowski, T., Saftig, P., Hartmann, D., Kallen, K.-J., and Rose-John, S. (2003) Cellular Cholesterol Depletion Triggers Shedding of the Human Interleukin-6 Receptor by ADAM10 and ADAM17 (TACE). *Journal of Biological Chemistry* **278**, 38829-38839

479. Rizoli, S. B., Rotstein, O. D., and Kapus, A. (1999) Cell Volume-dependent Regulation of L-selectin Shedding in Neutrophils: A ROLE FOR p38 MITOGEN-ACTIVATED PROTEIN KINASE. *Journal of Biological Chemistry* **274**, 22072-22080

480. Schleiffenbaum, B., Spertini, O., and Tedder, T. F. (1992) Soluble L-selectin is present in human plasma at high levels and retains functional activity. *J Cell Biol* **119**, 229-238

481. Kretowski, A., Gillespie, K. M., Bingley, P. J., and Kinalska, I. (2000) Soluble L-selectin levels in type I diabetes mellitus: a surrogate marker for disease activity? *Immunology* **99**, 320-325

482. Siminiak, T., Smielecki, J., Dye, J. F., Balinski, M., El-Gendi, H., Wysocki, H., and Sheridan, D. J. (1998) Increased release of the soluble form of the adhesion molecules L-selectin and ICAM-1 but not E-selectin during attacks of angina pectoris. *Heart and vessels* **13**, 189-194

483. Font, J., Pizcueta, P., Ramos-Casals, M., Cervera, R., Garcia-Carrasco, M., Navarro, M., Ingelmo, M., and Engel, P. (2000) Increased serum levels of soluble L-selectin (CD62L) in patients with active systemic lupus erythematosus (SLE). *Clinical and experimental immunology* **119**, 169-174

484. Middleton, J., Neil, S., Wintle, J., Clark-Lewis, I., Moore, H., Lam, C., Auer, M., Hub, E., and Rot, A. (1997) Transcytosis and Surface Presentation of IL-8 by Venular Endothelial Cells. *Cell* **91**, 385-395

485. Ge, S., Song, L., Serwanski, D. R., Kuziel, W. A., and Pachter, J. S. (2008) Transcellular transport of CCL2 across brain microvascular endothelial cells. *Journal of neurochemistry* **104**, 1219-1232

486. Mordelet, E., Davies, H. A., Hillyer, P., Romero, I. A., and Male, D. (2007) Chemokine transport across human vascular endothelial cells. *Endothelium : journal of endothelial cell research* **14**, 7-15

487. Simionescu, M., Gafencu, A., and Antohe, F. (2002) Transcytosis of plasma macromolecules in endothelial cells: a cell biological survey. *Microscopy research and technique* **57**, 269-288

488. Cara, D. C., Kaur, J., Forster, M., McCafferty, D. M., and Kubes, P. (2001) Role of p38 mitogen-activated protein kinase in chemokine-induced emigration and chemotaxis in vivo. *Journal of immunology (Baltimore, Md. : 1950)* **167**, 6552-6558

489. Shulman, Z., Shinder, V., Klein, E., Grabovsky, V., Yeger, O., Geron, E., Montresor, A., Bolomini-Vittori, M., Feigelson, S. W., Kirchhausen, T., Laudanna, C., Shakhar, G., and Alon, R. (2009) Lymphocyte Crawling and Transendothelial Migration Require Chemokine Triggering of High-Affinity LFA-1 Integrin. *Immunity* **30**, 384-396

490. Srinivasan, S., Deng, W., and Li, R. (2011) L-selectin transmembrane and cytoplasmic domains are monomeric in membranes. *Biochimica et Biophysica Acta (BBA) - Biomembranes* **1808**, 1709-1715

491. Abbal, C., Lambelet, M., Bertaggia, D., Gerbex, C., Martinez, M., Arcaro, A., Schapira, M., and Spertini, O. (2006) Lipid raft adhesion receptors and Syk regulate selectin-dependent rolling under flow conditions. *Blood* **108**, 3352-3359

492. Gallagher, J. T. (2006) Multiprotein signalling complexes: regional assembly on heparan sulphate. *Biochemical Society transactions* **34**, 438-441

493. Bame, K. J., Venkatesan, I., Stelling, H. D., and Tumova, S. (2000) The spacing of S-domains on HS glycosaminoglycans determines whether the chain is a substrate for intracellular heparanases. *Glycobiology* **10**, 715-726

494. Mulloy, B., and Forster, M. J. (2000) Conformation and dynamics of heparin and heparan sulfate. *Glycobiology* **10**, 1147-1156

495. Genot, E., Reif, K., Beach, S., Kramer, I., and Cantrell, D. (1998) p21ras initiates Rac-1 but not phosphatidyl inositol 3 kinase/PKB, mediated signaling pathways in T lymphocytes. *Oncogene* **17**, 1731-1738

496. Walsh, A. B., and Bar-Sagi, D. (2001) Differential Activation of the Rac Pathway by Ha-Ras and K-Ras. *Journal of Biological Chemistry* **276**, 15609-15615

497. Harden, T. K., Hicks, S. N., and Sondek, J. (2009) Phospholipase C isozymes as effectors of Ras superfamily GTPases. *Journal of Lipid Research* **50**, S243-S248

498. Rebecchi, M. J., and Pentyala, S. N. (2000) Structure, function, and control of phosphoinositide-specific phospholipase C. *Physiol Rev* **80**, 1291-1335

499. Hempel, W. M., Schatzman, R. C., and DeFranco, A. L. (1992) Tyrosine phosphorylation of phospholipase C-gamma 2 upon cross-linking of membrane Ig on murine B lymphocytes. *Journal of immunology (Baltimore, Md. : 1950)* **148**, 3021-3027

500. Idris, I., Gray, S., and Donnelly, R. (2001) Protein kinase C activation: isozyme-specific effects on metabolism and cardiovascular complications in diabetes. *Diabetologia* **44**, 659-673

501.  Li, C., Hu, Y., Sturm, G., Wick, G., and Xu, Q. (2000) Ras/Rac-Dependent activation of p38 mitogen-activated protein kinases in smooth muscle cells stimulated by cyclic strain stress. *Arteriosclerosis, thrombosis, and vascular biology* **20**, E1-9

502.  Elangovan, M., Day, R. N., and Periasamy, A. (2002) Nanosecond fluorescence resonance energy transfer-fluorescence lifetime imaging microscopy to localize the protein interactions in a single living cell. *Journal of microscopy* **205**, 3-14

503.  Elson, D. S., Munro, I., Requejo-Isidro, J., McGinty, J., Dunsby, C., Galletly, N., Stamp, G. W., Neil, M. A. A., Lever, M. J., Kellett, P. A., Dymoke-Bradshaw, A., Hares, J., and French, P. M. W. (2004) Real-time time-domain fluorescence lifetime imaging including single-shot acquisition with a segmented optical image intensifier. *New Journal of Physics* **6**, 180

504.  Heasman, S. J., Carlin, L. M., Cox, S., Ng, T., and Ridley, A. J. (2010) Coordinated RhoA signaling at the leading edge and uropod is required for T cell transendothelial migration. *J Cell Biol* **190**, 553-563